Improvement of the numerical efficiency of SWAN

SBW Waddenzee

A. J. van der Westhuysen, G. Ph. van Vledder and I. Wenneker

Prepared for:
Rijkswaterstaat Waterdienst

Improvement of the numerical efficiency of SWAN

SBW Waddenzee

A. J. van der Westhuysen, G. Ph. van Vledder and
I. Wenneker

Report

July 2008

H5107.46/A2114

Client	Rijkswaterstaat Waterdienst
Title	Improvement of the numerical efficiency of SWAN

Abstract

The spectral wind wave model SWAN (Booij et al. 1999) plays a key role in the estimation of the Hydraulic Boundary Conditions (HBC) for the primary sea defences of the Netherlands. Since some uncertainty remains with respect to the reliability of the wind wave model SWAN for application to the geographically complex area of the Wadden Sea, a number of activities have been initiated under the project 'SBW-Waddenzee' to devise a strategy for the improvement of the model. In this regard, hindcast studies carried out with SWAN for the Amelander Zeegat in the Wadden Sea have shown that significant computational times are required to achieve results with the desired levels of numerical accuracy. This has prompted investigations into ways of reducing the computational time of SWAN.

In the present study, various methods for reducing the simulation time of SWAN have been evaluated and refined, to facilitate the efficient execution of large numbers of SWAN simulations (possibly in combination with parallel computing) during the HBC computations. The methods evaluated here include the following: the Dynamical Deactivation Method (DDM), the Multigrid (MG) method, deactivating the action limiter and quadruplet interaction in the surf zone, improving the efficiency of the DIA quadruplet interaction term, and batch run organization using the so-called *hotfile* functionality of SWAN. These methods were all evaluated using the same set of eight field cases (featuring the Amelander Zeegat, the Eems-Dollard, Petten and Lake Sloten), and the same evaluation criteria, taking into account the total CPU time, iteration behaviour and mean convergence errors. This study has shown the DDM and batch run approaches to be the most successful techniques, both yielding reductions in total simulation time for Wadden Sea applications in the order of 31-35% with respect to the default SWAN model. The use of these methods affect model outcomes, which for the significant wave height and mean period can locally reach 1.5% and 5% respectively with respect to the converged results of a standard SWAN simulation. These errors are considered acceptable. For the mean direction and directional spreading, these errors can locally exceed 5^{o} and 5% respectively. These errors can be unacceptably large, and require further work to minimise. Based on these results, the DDM and batch run methods are recommended for application to the HBC computations. The remaining numerical methods proved to be less effective, often leading to unacceptable increases in simulation time, poor iteration behaviour or large model errors.

References	RWS Waterdienst overeenkomst WD-4968/4500121262 Raamovereenkomst WD-4924 betreffende 'Specialistische adviezen van de Stichting Deltares t.b.v. het Ministerie van Verkeer en Waterstaat'

Ver	Author	Date	Remarks	Review	Approved by
1	A. J. vd Westhuysen et al.	June 2008	Draft	J. Groeneweg	
2	A. J. vd Westhuysen et al.	July 2008	Final	M. Zijlema	M. R. A. v Gent
3	A. J. vd Westhuysen G. Ph. v Vledder and I. Wenneker	July 2008	Final, with minor corrections	M. Zijlema	M. R. A. v Gent

Project number	H5107.46/A2114
Keywords	SBW Waddenzee, SWAN, numerical efficiency, DDM, Multigrid, Triplet
Number of pages	126
Classification	None
Status	Final

Summary

General

In compliance with the Dutch Flood Defences Act ('Wet op de Waterkering, 1995'), the primary coastal structures must be monitored every five years (2001, 2006, 2011, etc.) for the required level of protection. This assessment is based on the Hydraulic Boundary Conditions (HBC) and the Safety Assessment Regulation (VTV: Voorschrift op Toetsen op Veiligheid). These HBC are derived every five years and approved by the Minister of Transport, Public Works and Water Management. The spectral wind wave model SWAN (Booij et al. 1999) plays a key role in the estimation of these HBC. Since some uncertainty remains about the reliability of SWAN for application to the geographically complex area of the Wadden Sea, a number of activities have been initiated under the project 'SBW-Waddenzee' to improve the model.

Problem statement

In the context of the SBW-Waddenzee project, hindcast and sensitivity studies carried out with SWAN for the Amelander Zeegat in the Wadden Sea (WL 2006; Royal Haskoning 2006, 2007; Alkyon, 2007a,b; WL & Alkyon 2007a) have shown that significant computational times are required (for the latter study, approximately 2.5 hours per simulation on a 3.4 GHz Pentium processor with 1.0 GB RAM) to achieve results with the desired levels of numerical accuracy. The computation of the complete HBC with SWAN, which includes a great number of environmental conditions and a model domain of the entire Wadden Sea, would therefore result in a substantial total computational time. This finding has led to a drive towards exploring ways to reduce the computational time required by SWAN. The most commonly-used technique for this is parallel computing, which is already available in SWAN. However, a number of other methods exist for further reducing simulation times of SWAN by improving the numerical efficiency of the model. In this study, a number of these methods are evaluated in terms of their influence on the simulation time and accuracy of the model.

Study aim

The aim of the present study is to evaluate and develop methods for improving the numerical efficiency of SWAN simulations, to be applied alongside parallel computing facilities in the execution of large numbers of SWAN simulations during the HBC computations. Based on a wide range of field cases and objective evaluation criteria of computational speed and model accuracy, optimal techniques for reducing the simulation time of SWAN are identified.

Approach

This study involved the evaluation of various techniques for improving the computational efficiency of SWAN, by which the simulation time of the model can be reduced. The following five methods, two of which have been developed within the framework of SBW-Waddenzee, were considered in this study:

- *The Multigrid (MG) approach (WL & Alkyon 2007b):* SWAN simulations are first computed on a computational grid with a reduced resolution to obtain a first estimate of the simulation result. This solution is subsequently used as the initial guess in the iteration procedure on the full resolution computational grid. In this

way, the full resolution simulation phase should require fewer iterations, reducing the total computational time.

- *The Dynamic Deactivation Method (DDM) (WL 2007):* Computational time is saved by not updating (i.e. deactivating) computational grid points at which the SWAN model has already reached a converged solution. During the course of a simulation, a progressively larger number of grid points become converged and are deactivated. Since the model equations are not computed at these deactivated grid points, large savings in computational time can result. The combination of this method with the Multigrid approach was also investigated.

- *Deactivation of action limiter and quadruplet interaction in the surf zone (Van der Westhuysen 2007):* The numerical solution procedure of SWAN can become instable through the influence of the nonlinear quadruplet interaction term. The so-called *action limiter* is therefore used to stabilise the model by slowing down the solution procedure. As a result, the action limiter can delay the convergence of SWAN, in particular in the surf zone where large changes in the wave field occur. However, here the quadruplet interaction term, and hence action limiting, appears to be relatively unimportant. With the investigated numerical approach, simulation speed is enhanced by deactivating the action limiter (and with it quadruplet interactions) in the surf zone.

- *Efficiency in calculating the nonlinear quadruplet interaction term:* The nonlinear quadruplet interaction term, computed with the Discrete Interaction Approximation (DIA), is responsible for about 50% of the computational time of SWAN. Two options for improving the efficiency of the DIA are investigated. Firstly, time can be saved by omitting all bi-linear interpolation steps during the computation of nonlinear transfer of wave energy (so-called IQUAD=8 option in SWAN). A second method of improving the efficiency of computing the DIA is the so-called Triplet method (Van Vledder 2005c). With this method, time-consuming elements of the DIA are pre-computed outside the actual simulation, and hence can significantly speed up the computation of the DIA.

- *Batch run organization:* The total simulation time of SWAN can be reduced by taking advantage of the fact that in batch calculations of wave climates (e.g. during the HBC calculations), sequential simulation conditions can be sorted such that conditions change only gradually from one simulation to the next. Here the so-called *hotfile* functionality of SWAN can be used in order to use the converged results of a particular simulated condition as the initial guess for the next simulation condition in sequence. This can lead to a reduction in the number of iterations required, and hence in a reduction of the total simulation time.

These five numerical techniques were evaluated for a diverse set of eight field cases: (a) one storm in the Amelander Zeegat and one in the Eems-Dollard, each featuring three storm instants (flood, slack and ebb), one case for the western Dutch coast near Petten and (c) one case for Lake Sloten. The five numerical methods were evaluated and compared for these validation cases, using the methodology developed in WL & Alkyon (2007b) as basis. Following this methodology, the reduction in simulation time, the iteration behaviour and the impact on model accuracy were quantified for each combination of numerical method and test case.

Conclusions

Detailed conclusions drawn from the results of this investigation have been provided at the end of Sections 4 to 9. From these, the following main conclusions can be drawn:

- Of the investigated numerical methods, only the DDM technique and batch run organization (with *hotfile* and increments in wind speed) proved to realise consistent savings in total CPU time relative to the standard SWAN (31-35% with respect to the default SWAN model for the Wadden Sea field cases). These methods are both compatible with the OpenMP parallel computing facilities in SWAN, which afford an additional significant increase in computational speed.

- The application of the DDM and batch run methods results in increased model errors. For the significant wave height and mean period these can locally reach 1.5% and 5% respectively with respect to the results of a fully-converged standard SWAN simulation, which is considered acceptable. However, in the mean direction and directional spreading these errors can locally exceed 5^o and 5% respectively, which can be unacceptably high. In the case of the batch run organization, an increase to the numerical precision of the *hotfiles*, as proposed by WL (2008), may reduce these errors.

- The convergence criteria applied in the present study, namely the curvature-based criteria proposed by Zijlema and Van der Westhuysen (2005) extended to include also the curvature of the mean period, yielded generally well-converged results of significant wave height and period. The integral parameters of mean direction and directional spreading failed to converge in a number of cases, leading to convergence errors of up to 5^o and 5% respectively relative to the fully-converged results.

Recommendations

Based on the results of this study and the general conclusions drawn in Section 11, the following main recommendations are made:

- On the strength of their positive performance in the present evaluation, it is recommended to apply the DDM technique and batch run organization (with *hotfile* and increments in wind speed) to reduce the computational time of SWAN simulations during the HBC computations. It is recommended to apply these methods for improved efficiency in combination with parallel computing, to obtain further gains in computational speed.

- The curvature-based criteria proposed by Zijlema and Van der Westhuysen (2005) extended to include also the curvature of the mean period, yielded generally well-converged simulation results in the present study. It is recommended to apply these convergence criteria to SWAN simulation studies in general. In addition, in the light of remaining large convergence errors in the parameters of mean direction and directional spreading, it is recommended to investigate the inclusion of directional parameters in these convergence criteria and also in the deactivation criteria of the DDM.

Contents

List of Tables

List of Figures

List of Symbols

Symbol	Unit	Description
α_{BJ}	-	Proportionality coefficient for surf breaking (ALPHA in SWAN)
α_{EB}	-	Proportionality coefficient for triad interaction (TRFAC in SWAN)
θ	^{o}	Wave direction
δ	var	Convergence difference (for batch run investigation)
Δ	var	Convergence error at a given grid index *m*
η	var	Mean convergence difference (for batch run investigation)
γ	-	Peak enhancement factor of the JONSWAP spectrum
γ_{BJ}	-	Breaker parameter for surf breaking (GAMMA in SWAN)
λ	-	Scaling factor for DIA quadruplet expression
μ	var	Mean convergence error
σ	rad/s	Instrinsic radian frequency
a	m	Wave amplitude
C_H	-	Maximum allowable curvature of H_{m0} in convergence criterium
C_T	-	Maximum allowable curvature of T_{m01} in convergence criterium
C_{JON}	m^2s^{-3}	Proportionality coefficient for bottom friction (CFJON in SWAN)
d	m	Water depth
Dir	^{o}N	Mean wave direction (Nautical convention)
Dspr	^{o}	Directional spreading
E	var	Relative gain in accuracy
f	Hz	Wave frequency
H_{m0}	m	Significant wave height
k	rad/m	Wave number
N_{iter}	-	Number of iterations used by a simulation
NAP	m	Dutch national levelling datum
m	-	Index for geographical location
M	-	Total number of geographical locations
$P_{B,m}$	var	Integral parameters produced by benchmark run
$P_{C,m}$	var	Integral parameters produced by control run
$P_{R,m}$	var	Integral parameters produced by reference run
Rx, Ry	-	Grid reduction factors in x,y space
$R\sigma$, $R\theta$	-	Grid reduction factors in σ,θ space
T_{cpu}	min	Total CPU required by a simulation
T_{m01}	s	Mean absolute wave period (=(m0/m1))
$T_{m-1,0}$	s	Mean absolute wave period (=(m-1/m0))
U_{10}	m/s	Wind speed at a height of 10 m
U_{dir}	^{o}N	Wind direction (Nautical convention)

1 Introduction

1.1 SBW project background and problem statement

In compliance with the Dutch Flood Defences Act ('Wet op de Waterkering, 1995'), the primary coastal structures must be monitored every five years (2001, 2006, 2011, etc.) for the required level of protection. This assessment is based on the Hydraulic Boundary Conditions (HBC) and the Safety Assessment Regulation (VTV: Voorschrift op Toetsen op Veiligheid). These HBC are derived every five years and approved by the Minister of Transport, Public Works and Water Management.

The HBC are used to subject the sea defences to a stepwise assessment ranging from 'simple' to 'advanced' tests. During these assessments so-called 'knowledge vacuums' (kennisleemtes) are encountered. The result may be that the assessment cannot be completed and sections of the sea defence are labelled 'geen oordeel' (no judgement; safety level unknown), which is an undesirable situation. Another possibility may be that sea defences are erroneously pass or fail the assessment.

Because of this problem of a 'knowledge vacuum' with respect to the assessment of the safety of flood defences, the overall SBW ('Strength and Loading of Water Defenses' (SBW: Sterkte en Belasting Waterkeringen)) project has the following general objective:

'To fill the most important knowlegde vacuums in order to achieve a better estimate of the safety against flooding of the primary flood defences.'

As part of this larger project, the subproject SBW-Waddenzee was started in 2006. The starting point is the observation that there is uncertainty concerning the quality of the HBC which are an important input into the assessment, in particular those for the Wadden Sea. This is because they were obtained from an inconsistent set of measurements and design values (WL 2002), while for the rest of the Dutch coast (the closed Holland Coast and the Zeeland Delta) they have been determined with a probabilistic method, in which offshore wave statistics are transformed to nearshore locations, For the latter the wave model SWAN (Booij et al. 1999) has been applied. There is insufficient confidence in the wave model SWAN (initially mainly regarding the swell penetration) to use it to obtain reliable boundary conditions in the Wadden Sea at present. In addition to initially recognized problems with respect to swell penetration, the subproject sets out to determine the general suitability of SWAN in the Wadden Sea and to specify the improvements required to produce reliable HBC in the Wadden Sea.

The objective of the SBW-Waddenzee project is therefore to

'Verify and where possible improve the quality of the models and methods so that in 2011 and beyond better HBC can be calculated.'

The path toward meeting this objective is laid out in a Plan of Action which describes a step by step approach of performing hindcasts of storm events in the Wadden Sea and other relevant areas, analysis of the results, and sensitivity and uncertainty analyses. Despite recent and ongoing measurement campaigns in the Dutch part of the Wadden Sea, the storm events are scarce, and information about the performance of the wave model in relevant areas is highly valued.

1.2 Problem statement of present study

In the context of the SBW-Waddenzee project, hindcast and sensitivity studies carried out with SWAN for the Amelander Zeegat in the Wadden Sea (WL 2006; Royal Haskoning 2006, 2007; Alkyon, 2007a,b; WL & Alkyon 2007a) have shown that significant computational times are required (for the latter study, approximately 2.5 hours per simulation on a 3.4 GHz Pentium processor with 1.0 GB RAM) to achieve results with the desired levels of numerical accuracy. The computation of the complete HBC with SWAN, which includes a great number of environmental conditions and a model domain of the entire Wadden Sea, would therefore result in a substantial total computational time. This finding has led to a drive towards exploring ways to reduce the computational time required by SWAN, a number of which are evaluated and compared in the present study.

1.3 Methods for reducing computational time

When aiming to reduce the large simulation times involved in computing the HBC with SWAN, a number of options are available. The most widely-used and best developed method for speeding up numerical models such as SWAN is to apply parallel computing. Such parallel computing facilities have been implemented in SWAN by Campbell et al. (2002) and Zijlema (2005), with which it is possible to run simulations on respectively shared-memory and distributed-memory parallel computers. The main advantage of parallel computing over any other method for reducing simulation time is that there is no loss of accuracy in the model results. Also, parallel implementations with good scaling characteristics (such as the distributed-memory approach) allow multiple increases in simulation speed by incorporating multiple processors. The main disadvantage of parallel computing is that it requires special parallel computing facilities, which are not always available.

On the other hand, a number of possibilities exist for speeding up SWAN simulations by either improving the efficiency of the model itself (by removing redundant operations), or by efficiently setting up the sequential simulations comprising an HBC computation. Such methods, a selection of which is presented below, can be applied independently of parallel computing facilities and hence do not require specialised computer facilities. Nonetheless, it is desirable that these methods would also be able to function in combination with the parallel computing facilities of SWAN. In this way, the gain in speed by parallel computing on a given number of processors can be further enhanced by the improved simulation efficiency of SWAN afforded by such methods. This is the optimal combination for speeding up SWAN envisaged for the HBC computations. However, as opposed to the use of parallel computing, the application of methods for improved efficiency of numerical models typically suffers from two drawbacks. Firstly, these methods are usually *not scalable*. In other words, an increase in speed (30%, say) cannot be multiplied by repeated application of the given method. Secondly, there is typically a *loss in model accuracy* involved. The latter implies that it must be evaluated whether the loss in accuracy incurred by applying a given numerical method is acceptable, and whether it is in proportion to the possible gain in computational speed afforded by that method.

In this regard, three novel methods for reducing the computational time required by SWAN have recently been developed, two of which within the framework of SBW-Waddenzee. In the first of these, reported in WL (2007), the computational time per iteration is reduced by dynamically deactivating computational grid points that have

already converged. This implementation is known as the Dynamical Deactivation Method (DDM). In the second approach, described in WL & Alkyon (2007b), the total number of iterations is reduced by first performing the simulation on a computationally cheap coarse grid, and subsequently using this estimate as the initial guess on the detailed computational grid. This method is known as the Multigrid (MG) technique. The third approach, proposed by Van der Westhuysen (2007), is to deactivate the action limiter, and with it the quadruplet interaction term, in the surf zone once a threshold Ursell number (a measure of the nonlinearity and dispersion) has been reached. Deactivating the action limiter in this region, where fast changes in the spectrum occur, has been shown to reduce the number of iterations required for convergence. Based on evaluations on a limited set of test cases, these three approaches have shown promising results. These implementations are potentially useful for reducing total computational time of SWAN, for example for the computation of the HBC. However, additional testing of these methods is required in order to optimize them and to evaluate their general performance for a wider range of cases.

In addition to these three new numerical functionalities in SWAN, other less intrusive methods of reducing the total simulation time of a batch of SWAN simulations exist. It is well known that the quadruplet interaction term, using the DIA approximation, is the most computationally intensive source term in SWAN. Sensitivity tests with the quadruplet term deactivated shows that the DIA is responsible for approximately 50% of the total simulation time of SWAN[1]. In this regard, reduction in the time spent in calculating the DIA source term can lead to significant gains in computational speed. In recent versions of SWAN, the computation of the DIA has been simplified so that during each interaction, the distribution of transferred energy amongst spectral bins are not done by means of interpolation (default), but by assigning the interaction contribution to the nearest neighouring bin. This option, activated by setting IQUAD=8 in the mode input, has been used to speed up SWAN simulations for the HR computations for the Holland coast (Royal Haskoning & WL 2005). However, Alkyon (2005a) has shown that, when this setting is applied to one-dimensional wave growth situations, it systematically affects the results of computed wave parameters by up to 5%. Therefore, the influence of this setting on simulation results in the Wadden Sea will need to be checked. A second method of improving the efficiency of computing the DIA is the so-called Triplet method (Van Vledder 2005c). This method computes the nonlinear transfer rate in each spectral bin as the finite sum of weighted triple products of energy densities at discrete spectral bins. These can be pre-computed outside the actual simulation, and hence can significantly speed up the computation of the DIA.

Finally, the total simulation time of SWAN can also be reduced by taking advantage of the fact that in batch calculations of wave climates, sequential simulation conditions can be sorted such that conditions change only gradually from one simulation to the next. Here the so-called *hotfile* functionality of SWAN can be used in order to use the converged results of a particular simulated condition as the initial guess for the next simulation condition in sequence. This method therefore appears to be a good candidate for application to the Wadden Sea. However, the impacts on model accuracy of using the *hotfile* as an initial condition instead of the default second-generation first guess are uncertain. Therefore, the advantages in terms of reduced simulation time and the potential disadvantages in terms of loss of model accuracy should be investigated for Wadden Sea applications.

1. *This result is a revision of the timing estimates of the DIA presented in WL (2007). Investigation showed that the CPU timing reported in WL (2007) is distorted, since the timing function in SWAN consumes non-negligible amounts of CPU time itself. This is discussed in Section 3.5.2 of the present report.*

1.4 Study aim

The aim of the present study is to evaluate and develop methods for improving the numerical efficiency of SWAN simulations, to be applied alongside parallel computing facilities in the execution of large numbers of SWAN simulations during the HBC computations. Based on a wide range of field cases and objective evaluation criteria of computational speed and model accuracy, optimal techniques for reducing the simulation time of SWAN are identified.

1.5 Approach

This study involved the evaluation and comparison of various techniques for reducing the simulation time of SWAN. The numerical methods for the improvement of the efficiency of SWAN reviewed above were systematically evaluated, using the same range of field cases and the same evaluation criteria. These numerical techniques were studied in three groups, according to their respective approaches to reducing simulation time, namely novel numerical implementations, the improvement of the efficiency of the DIA and batch run organization. The methodology for evaluating each of these groups of methods is presented below.

1.5.1 Evaluation of the DDM, Multigrid and action limiter deactivation

In WL (2007) and WL & Alkyon (2007b), the DDM and Multigrid implementations in SWAN have been tested separately for a limited number of conditions and for a limited range of parameter settings. Likewise, Van der Westhuysen (2007) presents favourable results for the deactivation of the action limiter and quadruplet interaction in the surf zone, considering selected cases. In this first group of evaluations, these methods were tested, for a wider range of cases, and for additional parameter settings. In addition, it was also investigated to what extent these three methods for speeding up SWAN can be combined to take advantage of their individual capabilities, and to test the benefits of their interaction. In the evaluations described in WL (2007) and WL & Alkyon (2007b), the NW storms of 9 February 2006 and 16 December 2005, occurring in the Amelander Zeetgat, were considered. In the present study, the collection of test cases was extended to also include the Eastern Wadden Sea (the Eems-Dollard) and simpler field cases, such as the western Dutch coast near Petten and Lake Sloten. In total, eight test conditions were defined: (a) one storm in the Amelander Zeegat (different to those considered by WL (2007) and WL & Alkyon (2007b)) and one in the Eems-Dollard, each featuring three storm instants (flood, slack and ebb), one case for the western Dutch coast near Petten and (c) one case for Lake Sloten. The geographical locations of these field cases are presented in Figure 1.1.

The Multigrid method was evaluated for this extended set of eight validation cases, using the methodology developed in WL & Alkyon (2007b) as basis. With this methodology, the reduction in simulation time, the influence on iteration behaviour and the impact on model accuracy were quantified. The Multigrid method was optimised with respect to the choice of dimensions in which the resolution of the computational grid used in the initial guess simulation is reduced. Likewise, the DDM method was evaluated for this extended set of validation cases, using the methodology developed in WL & Alkyon (2007b) as basis. The DDM method was optimised with respect to the regime for deactivating and (periodically) reactivating grid points. The effectiveness of

deactivating the action limiter and quadruplet interactions in the surf zone, proposed by Van der Westhuysen (2007), was investigated for a number of thresholds for the Ursell number.

In addition to optimising and verifying the DDM, Multigrid and action limit deactivation methods individually, the performance of a combined Multigrid-DDM model was also investigated (a combination with the deactivation of the action limiter was not considered, since this method proved less successful in the individual evaluations). In WL (2007) it was found that, especially in regions with strong wave-current interaction, the performance of the DDM approach was impeded by an insufficient initial guess of the final solution (so-called second-generation 'first guess'). In a combined Multigrid-DDM application, the Multigrid approach was used to obtain an improved initial guess on a coarse grid, after which the DDM method was applied to the final simulation on the full resolution grid. The performance of this combined model was evaluated for the eight selected field cases, again using the methodology developed in WL & Alkyon (2007b).

In order to verify whether these numerical techniques for improving the efficiency of SWAN would be effective in combination with parallel computing, the simulations were conducted using an OpenMP compilation (Campbell et al. 2002) of the SWAN source code, run on dual core computers (see Section 3.6).

1.5.2 Efficiency of the DIA source term

In this second group of evaluations, two methods of improving the efficiency of computing the DIA source term were tested. Firstly, the application of the computationally faster nearest-neighbour version of the DIA (model setting IQUAD=8) was investigated. Using the same set of eight test cases (Amelander Zeegat, Eems-Dollard, Petten, Lake Sloten) listed in Section 1.5.1, the simulation results produced by the model version with the nearest-neighbour DIA was compared to those produced by the default model. The analysis of the model results was done using the methodology developed in WL & Alkyon (2007b). Using this methodology, an evaluation was made of the speed-up achieved by the nearest-neighbour DIA setting and the influence of this setting on model accuracy.

Secondly, the application of the Triplet method to the DIA was considered. The Triplet method can either be applied to the default version of the DIA, or to the nearest neighbour (IQUAD=8) version. Therefore, the application of the Triplet method was investigated in two ways, namely (a) a comparison between the results produced using the Triplet version of the standard DIA and those by the default model, and (b) comparison between the results produced using the Triplet version of the nearest-neighbour DIA (IQUAD=8) and those by the default model. This analysis was done on the same eight field cases listed in Section 1.5.1, again using the methodology developed in WL & Alkyon (2007b).

1.5.3 Batch file organization

In this third and final group of evaluations, it was investigated whether, when computing a large number of simulations in batch mode for the Amelander Zeegat, the total simulation time can be reduced by making use of the *hotfile* functionality. The two most efficient ways of applying *hotfiles* to save computational time appears to be to arrange sequential runs so that either (a) mean wind and (offshore) wave directions belonging to a storm condition are held constant and the wind speed and offshore significant wave height are incrementally increased through all classes in the computational climate, or

(b) the wind speed and the (offshore) significant wave height are held constant as the mean wind and offshore wave direction systematically sweep through all directional bins comprising the climate.

For both these options, the benefit in terms of total simulation time and gain (or loss) in accuracy was evaluated for one selected field case of the Amelander Zeegat. For this one field case, a synthetic wind and wave climate, comprising six wind speeds and nine directions, was compiled. These individual conditions in the climate were run in batch mode without the use of a *hotfile* (the reference runs), and subsequently with *hotfiles* (the control runs). The gain in simulation time was computed over the total series of simulations, and a total error measure was defined, denoting the difference in model outcomes averaged over all the simulation results. In order to verify whether this technique would be effective in combination with parallel computing, the simulations were also conducted using an OpenMP compilation of the SWAN source code.

Finally, the results of the groups of tests described in Sections 1.5.1, 1.5.2 and 1.5.3 were considered collectively, in order to identify the most promising methods for reducing the computational time of SWAN in the HBC computations for the Wadden Sea.

1.6 Project team

This study was carried out by A. J. van der Westhuysen and I. Wenneker of Deltares (under project H5107.46) and G. Ph. van Vledder of Alkyon (under project A2114). The internal quality assurance was conducted by Jacco Groeneweg of Deltares. The external review of this study was carried out by M. Zijlema of Delft University of Technology.

1.7 Report structure

This report is structured as follows: Section 2 presents the test cases and model setup considered in the present evaluation. Section 3 gives details on the model settings and evaluation criteria used. Subsequently, Sections 4 to 7 present the first group of numerical methods, namely the evaluation of the Multigrid, the DDM, the deactivation of action limiting in the surf zone, and the combination of these methods. Section 8 presents the second group of evaluations, namely on the efficiency of the DIA. Section 9 presents the final group of tests, namely the batch file organization. Section 10 collects these results in a global evaluation and discussion of these results. Sections 11 and 12 close this report with conclusions and recommendations.

2 Test cases and model setup

2.1 Introduction

This section describes the selection of test cases for the evaluation of the numerical techniques intended for speeding up SWAN, as presented in Section 1. The collection of test cases used in this evaluation features eight field cases, which have all been considered previously in hindcast studies, so that existing SWAN model setups could be used.

The set of test cases firstly contains three cases in the Amelander Zeegat, with three storm instants featuring different flow conditions (flood, slack and ebb); secondly, three cases in the Eems-Dollard (flood, slack and ebb); thirdly, one case for the western Dutch Coast near Petten and finally one case in Lake Sloten. The first six cases were selected to verify the conclusions regarding the performance of the DDM and MG methods in the Amelander Zeegat drawn by WL (2007) and WL & Alkyon (2007b). These also serve as a good basis for evaluating the performance of the remaining numerical methods presented in Section 1. The last two cases were added to assess the performance of the proposed numerical methods for relatively simple geographical situations. To distinguish between the different model runs the following coding convention is applied:

[area]_[date&time]_[numerics]

in which the terms between square brackets indicate the geographical region and the SWAN domain (e.g. computational grid) used, the date and time of the hindcast instant, and the numerical settings, respectively. The coding for the area and hindcast instant is presented in this section, whereas, the coding for the numerical settings is presented in Sections 4 to 9 for each particular type of simulation.

2.2 Amelander Zeegat

Three instants recorded in the Amelander Zeegat during the WNW storm of 2 January 2005 are considered. These cases have been hindcast by Alkyon (2007a).

- 2 Jan. 2005, 10:00 hours (U_{10} = 19.96 m/s, U_{dir} = 277°) (flood)
- 2 Jan. 2005, 12:00 hours (U_{10} = 17.82 m/s, U_{dir} = 277°) (slack)
- 2 Jan. 2005, 17:00 hours (U_{10} = 16.28 m/s, U_{dir} = 276°) (ebb)

The coding for the various model runs is as follows:

azg3a_20050102_1000
azg3a_20050102_1200
azg3a_20050102_1700

Figure 2.1 (upper panel) shows the computational grid AZG3A for the Amelander Zeegat. For clarity every fifth grid line is drawn. In the lower panel the average grid size is shown, defined as the square root of the area of each grid cell. It can be seen that the finest geographical resolution is found in the central part of the tidal inlet. The bathymetry of the Amelander Zeegat is shown in Figure 2.2. Included in this figure are

the locations of three test points which will be used in the subsequent chapters for the analysis of the convergence behaviour of SWAN.

2.3 Eems-Dollard

Three instants recorded in the Eems-Dollard during the NW storm of 1 November 2006 are considered. These cases have been hindcast by Alkyon (2008).

- 1 Nov. 2006, 3:00 hours. U_{10}=20.8 m/s, U_{dir}=320° (flood)
- 1 Nov. 2006, 6:30 hours, U_{10}=20.0 m/s, U_{dir}=340° (slack)
- 1 Nov. 2006, 9:30 hours, U_{10}=17.0 m/s, U_{dir}=345° (ebb)

The coding for the various model runs is as follows:

eems3a_20061101_0300
eems3a_20061101_0630
eems3a_20061101_0930

Figure 2.3 (upper panel) shows the computational grid Eems3a for the Eems-Dollard estuary. For convenience every fifth grid line is drawn. The grid Eems3a is derived from grid Eems3 which is used in Alkyon (2008). The only difference between the grids Eems3 and Eems3a is that the former extend further to the west such that it also includes part of the Wadden Sea south of the island of Ameland. The average grid size is shown in the lower panel, defined as the square root of the area of each grid cell. The bathymetry of the eastern part of the Wadden Sea and Eems-Dollard estuary is shown in Figure 2.4. Included in this figure are the locations of three test points, to be used for the analysis of convergence behaviour.

2.4 Petten

One storm instant recorded at Petten is considered, previously investigated by Alkyon (2004):

- 1 Jan. 1995, 10:00 hours, U_{10}=25 m/s, U_{dir}=329°. No currents.

The base code for the various model runs is as follows:

p_20050101_1000

Figure 2.5 (upper panels) show the computational grid for the North Sea area around the Petten measurement site (upper left), and zoomed in to the surf zone (upper right). The lower panels of Figure 2.5 show the average size of the grid cells, at these two scales. Cell sizes decrease from the North Sea side towards the land. Figure 2.6 shows the bathymetry of the Petten grid and the location of three test points, to be used in the analysis of convergence behaviour. These test points coincide with the locations of wave observation buoys and wave gauges in the Petten transect.

2.5 Lake Sloten

One storm instant recorded in the shallow Lake Sloten is considered, previously investigated by Bottema (2007):

- 27 October 2002, averaged conditions over 15-16 hours (Case SLE). This is a depth-limited situation (H_{m0}/d=0.43 at SL29), with a wind speed of 21.4 m/s with a direction of 252°N. No currents.

The basic run code for the Lake Sloten runs is:

sle_20021027_1500

For this field case, a regular computational grid with a cell size of 10 m was used (not shown). Figure 2.7 shows the bathymetry of the Lake Sloten. It can be seen that the depth is rather constant at a level of NAP -2.1 m. The locations of three test points for the analysis of iteration behaviour are indicated, the third of which is at the location of the observation station SL29.

2.6 Changes to model setup required by Multigrid method

As mentioned in the introduction to this section, the eight field cases selected here originate from existing hindcast studies, so that existing SWAN model setups could be used. However, while setting up the computations for the Multigrid method in our dedicated SWAN version, a number of problems were encountered which necessitated adaptations to two of these field case setups.

The first problem consisted of insufficient virtual memory to perform the computations on the original grid for the Eems-Dollard. This grid (Eems3, see Alkyon 2008) was designed to fit on a Windows PC with 2 Gb internal memory. Problems arose when testing this grid using a Multigrid setting with reduced spectral resolution. Evidently, the conversion of all spectra from a reduced spectral resolution to the full spectral resolution required more internal memory than available. To overcome this problem, the grid for the Eems-Dollard was reduced in size such that it works for the Multigrid settings using a reduced spectral resolution. The reduction consisted of shifting the western boundary from Ameland to Schiermonnikoog, resulting in the grid Eems3A presented in Section 2.3 above.

The second problem encountered while setting up the Multigrid simulations was the specifications of the boundary conditions for the Eems-Dollard and Petten field case area using segments. For some reason, the Multigrid setting with a reduced geographical resolution was not able to treat the segments properly. Despite efforts to solve this problem, another approach was followed to specify the boundary conditions along the edges of the computational domain for these two areas. This approach consists of two steps: In the first step, a simulation was performed using 10 iterations, without invoking the Multigrid option, and using segments to specify the boundary. Two-dimensional spectra were output to all grid points along the boundary of the computational domain. These 2D spectra were subsequently used as the boundary condition. This treatment of the boundary enabled the application of the Multigrid implementation in SWAN, with negligible influence on the results of the simulation.

3 Model settings and simulation types

In this study, various numerical implementations for reducing the computational time of SWAN are investigated. These numerical settings are considered as variations to a basic model setup, which is detailed below.

3.1 Model physics

The computations were performed in third-generation mode, using the SWAN model version 40.51A. For wind-wave generation, the setting WESTH was used, which features the combination of wind input and saturation-based whitecapping proposed by Van der Westhuysen et al. (2007). Quadruplet interactions are modelled used the Discrete Interaction Approximation of Hasselmann et al. (1985). Wind fields were modelled as spatially uniform. The shallow source terms include triad interaction according to Eldeberky (1996) using α_{EB} = 0.05 and CUTFR = 2.5, surf breaking according to Battjes and Janssen (1978) using α_{BJ} = 1 and γ_{BJ} = 0.73. Bottom friction is modelled according to the JONSWAP formulation with C_{JON} = 0.067 (Hasselmann et al. 1973). These settings are activated by the following user commands:

```
BREAKING alpha=1. gamma=0.73
FRICTION JONSWAP cfjon=0.067
TRIAD trfac=0.05 cutfr=2.5
GEN3 WESTH
```

These settings agree with those used in the recent hindcast studies of WL (2006), Royal Haskoning (2006, 2007), WL & Alkyon (2007a). One exception to these settings is for the Petten field case, for which the friction coefficient was adapted to C_{JON} = 0.038, to account for the local swell conditions. Details of the grid setup for the various field cases are given in Alkyon (2004, 2007a, 2008) and Bottema (2007).

3.2 Convergence criteria

The convergence criteria selected for this study are based on the curvature criterion proposed by Zijlema and Van der Westhuysen (2005). In Alkyon (2007b) it was proposed to extend these criteria to also include the curvature of the iteration curve of the mean period. This was required especially in cases featuring wave-current interaction, for which the convergence of the mean period can be slower than that of the wave height. Therefore, the criterion of Zijlema and Van der Westhuysen (2005), as extended with the mean period, was applied with a maximum curvature of both the significant wave height and mean period of $C_H = C_T$ = 0.001. This option is activated with the following command:

```
NUM STOPC  0.000  0.010  0.001  99  STAT mxitst=80 alfa=0.001
```

The inclusion of the mean period in the convergence criteria was accomplished through an alteration to the subroutine SWSTPC (see WL 2007). A small degree of under-relaxation (alfa=0.001) was applied to reduce small amplitude oscillations that sometimes appeared in the iteration signals. For the Eems-Dollard cases, a somewhat

higher degree of under-relaxation (alfa=0.002) was necessary to sufficiently reduce these iteration oscillations.

3.3 Simulation types

In Section 1, a number of numerical methods for reducing the simulation time of SWAN were presented. In order to compare these methods objectively for each field case, they have been evaluated here using the structure developed by WL & Alkyon (2007b). For each field case, three types of simulations were carried out. Firstly, a benchmark run was carried out using 80 iterations to obtain an estimate of the converged solution. Secondly, a reference run was conducted, using selected convergence criteria, to determine the so-called convergence error of the default model (the difference between its solution at the end of the iteration process and the benchmark solution). Third, a simulation was carried out with the given method for numerical speed-up (e.g DDM, MG, efficiency of the DIA). The control runs use the same convergence criteria as the reference runs to assess the effect of applying the initial guess. Table 3.1 below summarizes these three types of simulations. Examples of the SWAN input files used are included in Appendix A.

Code	Description
B	Benchmark run, continued up to 80 iterations
R	Reference run, using convergence criteria
C	Control run, applying the numerical technique, and convergence criteria

Table 3.1: Run codes for the various types of simulations conducted.

3.4 Reference run results

As reference of the performance of the default version of SWAN, this section presents the reference run simulation results for the eight field cases, as found for the settings of model physics and numerics presented in Sections 3.1 and 3.2. Included in these figures are rectangular demarcations over which the average model error was computed, for the comparison of the various numerical techniques tested (see Section 3.5 below). For each field case, this evaluation region is located over the area of primary interest for the given simulation, such as in the tidal inlets (Wadden Sea cases) or the surf zone (Petten).

3.4.1 Amelander Zeegat

For the Amelander Zeegat, three cases during the storm of 2 January 2005 (flood, ebb and slack) were hindcast. Figures 3.1 to 3.9 present the results for the input current and water level fields, and the wave parameters of significant wave height H_{m0}, mean spectral period $T_{m-1,0}$, mean wave direction *Dir* and directional spreading Dspr. The current and water level fields were computed by the WAQUA model on the 'Kuststrook fijn' model. Figures 3.1-3.3 show the flow fields and wave parameters for 2 January 2005 at 10:00 (flood) with a strong current going into the Wadden Sea. Figures 3.4-3.6 show the situation for 2 January 2005 at 12:00, around slack tide. The ebb situation of 2 January 2005 at 17:00 is shown in Figures 3.7-3.9. Also shown in these figures is the rectangular region over which model errors were computed (Section 3.5). For these field cases, this evaluation area is located over the tidal inlet where strong wave

breaking and wave-current interaction is found, which was the focus area in the study of Alkyon (2007a).

The offshore wave conditions in the Amelander Zeegat for the three hindcast moments (flood, ebb and slack) are very similar. At all three storm instants, these offshore waves are strongly dissipated on the ebb-tidal delta, resulting in a rapid decrease of both the significant wave height H_{m0} and spectral period $T_{m-1,0}$. In the Wadden Sea, the waves are relatively small and determined by the local wind and depth. The main differences between the three hindcast situations are found in the amount of penetration of low frequency wave energy in the main tidal channel into the Wadden Sea. This can be seen in the geographical variation of the spectral period $T_{m-1,0}$, which shows a yellow tongue pointing southwards. For the flood situation (Fig. 3.2, lower panel) this yellow area ends at the south western tip of Ameland. For the slack tide situation (Fig. 3.5) this area extends well to the south of the tidal inlet. For the ebb situation (Fig. 3.8) this area exists in the main tidal channel, where the waves encounter an opposing current.

Figures 3.3 (flood), 3.6 (slack) and 3.9 (ebb) present the geographical variation of the mean wave direction and directional spreading, from which the effects of refraction can be seen. Variations in the mean wave direction are visible around the southern island tips bordering the tidal inlet. The bottom panels of these figures show the effect of refraction along the northern edges of the island, where all waves turn toward to coast normal, leading to a reduction of the directional spreading. High values ($>50^o$) of the directional spreading are visible in the tidal channels, in the tidal inlet, but also further into the Wadden Sea. This is due to the fact that relatively long waves refract out of the channels where they mix with relative shorter waves propagating more or less in the direction of the wind.

3.4.2 Eems-Dollard estuary

For the eastern part of the Wadden Sea, namely the Eems-Dollard estuary, also three cases were hindcast. The geographical distribution of the significant wave height H_{m0}, mean spectral period $T_{m-1,0}$, mean wave direction *Dir* and the directional spreading, current speed and direction and water levels are given in the Figures 3.10 to 3.18. The set-up and order of the figures is the same as for the Amelander Zeegat. The three cases refer to a situation with a strong flood situation (Figure 3.10), slack tide (Figure 3.13) and a strong ebb current (Figure 3.16). Also shown in these figures is the retangular region over which model errors were computed. Here the evaluation area is located over the tidal inlet with pronounced tidal channel, which was the focus area in the studty of Alkyon (2008).

The geographical variation of significant wave height H_{m0} and spectral period $T_{m-1,0}$ shows that for all three events the wave height is strongly dissipated on the ebb tidal delta, except for the main tidal channel towards the Eems-Dollard estuary, which shows slightly higher values of the significant wave height compared to the surrounding tidal flat. This small increase is also due to local wave growth in the relatively deep tidal channel. The geographical variation of the spectral period $T_{m-1,0}$ clearly shows that relatively long waves are able to propagate to the northern tip of Groningen and well into the Eems-Dollard estuary. The green colours behind the Wadden islands point to local wave growth. For the ebb situation (Figure 3.17) a clearly defined strip of relatively long waves occurs in the main tidal channel towards the Eems-Dollard estuary.

The variation of the mean direction (upper panels in the Figures 3.12, 3.15 and 3.18) is the strongest along the edges of the tidal channels. Similar to the Amelander Zeegat,

the directional spreading reduces north of the Wadden islands (lower panel in the Figures 3.12, 3.15 and 3.18). The highest values of the directional spreading occur behind the island and along the tidal channels.

3.4.3 Petten

For the Petten area the geographical variation of the significant wave height H_{m0} and spectral period $T_{m-1,0}$ is given in Figure 3.19. The results for the mean wave direction *Dir* and directional spreading *Dspr* are given in Figure 3.20. The rectangular evaluation area for model accuracy (Section 3.5) is located along the surf zone. The significant wave height (upper panels of Fig. 3.19) gradually decreases as the waves encounter the shallow areas in front of the coast. The strong dissipative effects of the ebb-tidal delta west of the Marsdiep are also clearly visible. The variation of the spectral period $T_{m-1,0}$ (lower panels of Fig. 3.19) shows that it remains more or less constant towards the coast. Only around the Marsdiep the spectral period decreases, and the wave field becomes dominated by locally generated waves. The variation of the mean wave direction (upper panels Fig. 3.20) clearly shows the effect of refraction, turning the waves towards the coast normal. The effect on the directional spreading (lower panels Fig. 3.20) shows a decrease consistent with the effects of refraction. Only in the Marsdiep the directional spreading increases considerably due to refraction effects around the shallow sand banks.

3.4.4 Lake Sloten

For Lake Sloten the geographical variation of the significant wave height H_{m0} and spectral period $T_{m-1,0}$ is given in Figure 3.21. The results for the mean wave direction *Dir* and directional spreading *Dspr* are given in Figure 3.22. The rectangular evaluation area for model accuracy is located over the second half on the lake, and includes the second and third test points (compare Figure 2.7). Figure 3.21 shows a situation of fetch-limited wave growth with gradually increasing wave heights and periods along the main axis of the lake. Only at the downwind part of the lake, the wave height decreases again. The mean wave direction (upper panel of Fig. 3.22) agrees more or less with the wind direction along the central axis of the lake, but it deviates along the sides of the lake. This behaviour is a typical example of wave-growth in a narrow fetch situation. The directional spreading (lower panel Fig. 3.22) shows that at the begin of the fetch, the highest directional spreading occurs, diminishing with fetch.

3.5 Evaluation criteria

The effectiveness of the various numerical speed-up techniques was evaluated in a number of ways. Firstly, the iteration behaviour of a number of integral parameters was studied to assess how the particular numerical technique influences the iteration behaviour. Secondly, it was investigated whether the application of the given numerical technique reduces the number of iterations of the control run, and hence the overall simulation time. Thirdly, the accuracy of the result of the control run was assessed by comparing the convergence error of the control run with that of the reference run. Details on these methods are given below.

3.5.1 Iteration behaviour

The iteration behaviour of the SWAN computation was investigated by inspection of the percentage of accepted points per iteration. In addition, the evolution of the significant

wave height H_{m0}, the spectral period $T_{m-1,0}$, the mean direction *Dir* and the directional spreading *Dspr* was obtained from the 2D spectra that were output every iteration at the test points defined for each field case above (see Figures 2.2, 2.4, 2.6 and 2.7).

3.5.2 Simulation speed

An important evaluation parameter in this study is the total CPU time spent by SWAN during a particular simulation. In this study, the CPU time has not been measured using the internal timing routines in SWAN. This is because it was found that the timing calls made to the processor seem to, in itself, consume considerable amounts of the total CPU time (between 15% and 50%). Therefore, the procedure calls to these timing routines have been switched off at the compilation of the SWAN source code. Instead of using these timing routines of SWAN, in the present study the CPU time has been estimated by subtracting the start time of the run as given at the top of the SWAN PRINT file from the date stamp of the PRINT file itself. This method of timing proved to be well reproducible, and to be accurate to within one minute.

3.5.3 Accuracy

The accuracy of applying the various numerical techniques is investigated by a qualitative and a quantitative comparison of the spatial distributions of the errors in the four integral wave parameters with respect to the benchmark results, found with the tested numerical technique and the reference run. Firstly, spatial plots are made of the differences between the converged results of respectively the control and reference runs and the benchmark results. These are respectively defined at every geographical grid point *m* as

$$\Delta\left(P_{C,m}\right)=\frac{P_{C,m}-P_{B,m}}{P_{B,m}}\times 100\% \quad \text{and} \quad \Delta\left(P_{R,m}\right)=\frac{P_{R,m}-P_{B,m}}{P_{B,m}}\times 100\% \qquad (3.1)$$

for the significant wave height H_{m0}, the spectral period $T_{m-1,0}$ and the directional spreading *Dspr*, and

$$\Delta\left(P_{C,m}\right)=\left|P_{C,m}-P_{B,m}\right| \quad \text{and} \quad \Delta\left(P_{R,m}\right)=\left|P_{R,m}-P_{B,m}\right| \qquad (3.2)$$

for the mean period *Dir* (properly accounting for directional periodicity). Here $P_{C,m}$ is any of the four integral parameters produced by the control run at a geographical location *m*, $P_{R,m}$ is the corresponding parameter produced by the reference run, $P_{B,m}$ is the corresponding parameter of the benchmark run, and Δ is the difference in result at that location, expressed as a percentage or an absolute difference. In the reference run, the difference Δ represents the error due to non-convergence. In the control runs of the various numerical methods, these differences represent both the error due to non-convergence, as well as any error incurred due to the application of the particular numerical method. In the following, the quantity Δ will be referred to simply as the convergence error.

A quantitative measure of the average convergence error is computed as the absolute value of the error Δ of each parameter value, averaged over a rectangular box positioned in each computational area (see Section 3.4). For the control run, and parameter *P* being the wave height, wave period or directional spreading, this is computed as

$$\mu\left(P_C\right)=\frac{1}{M}\sum_{m=1}^{M}\left|\Delta\left(P_{C,m}\right)\right|=\frac{1}{M}\sum_{m=1}^{M}\frac{\left|P_{C,m}-P_{B,m}\right|}{P_{B,m}}\times 100\% \tag{3.3}$$

and similarly for the reference run as

$$\mu\left(P_R\right)=\frac{1}{M}\sum_{m=1}^{M}\left|\Delta\left(P_{R,m}\right)\right|=\frac{1}{M}\sum_{m=1}^{M}\frac{\left|P_{R,m}-P_{B,m}\right|}{P_{B,m}}\times 100\% \tag{3.4}$$

counting over all of the *M* points located inside the rectangle defined over the tidal inlet. For the control run, and parameter *P* being the wave direction, the mean convergence error is computed as

$$\mu\left(P_C\right)=\frac{1}{M}\sum_{m=1}^{M}\left|\Delta\left(P_{C,m}\right)\right|=\frac{1}{M}\sum_{m=1}^{M}\left|P_{C,m}-P_{B,m}\right| \tag{3.5}$$

and similarly for the reference run as

$$\mu\left(P_R\right)=\frac{1}{M}\sum_{m=1}^{M}\left|\Delta\left(P_{R,m}\right)\right|=\frac{1}{M}\sum_{m=1}^{M}\left|P_{R,m}-P_{B,m}\right| \tag{3.6}$$

making sure that directional periodicity is properly accounted for.

3.6 Parallel computing and computers used

In Section 1, it was explained that it is desirable to test the effectiveness of the investigated numerical techniques in combination with the parallel computing facilities of SWAN. The majority of the computations in this study were therefore performed with a 32-bit dual-core executable of SWAN version 4051A, obtained with the OpenMP compilation option (Campbell et al. 2002). In this way, it was possible to test the operation of the DDM, Multigrid and the remaining numerical techniques in a parallel computing environment. It was verified that the application of dual-core parallel computing itself results in a reduction of the total computational time by about 45% relative to the serial computing mode of SWAN. We note that all comparative results concerning the timing of all simulations presented in this study, except those of Section 8, are relative to this dual-core executable of SWAN 40.51A, referred to here as the standard model version.

The simulations presented in Section 4 were run on a dual-core processor Intel®Core™ 2 CPU, T7600, with 2.33 GHz clock speed, and 2 Gb RAM, under the supervision of Alkyon. The simulations presented in Sections 5 to 7 and 9, were run on the Hydrax cluster nodes at Deltares, each featuring a dual-core AMD Athlon64 processor model 4000+, with a 2.4 GHz clock speed and 4.0 Gb RAM. In order to obtain an equal comparison of all simulation times, the simulations of Section 4 were repeated on the Hydrax cluster of Deltares.

The only exception to these parallel mode computations is for Section 8. Since the Triplet method, investigated in this section, is not currently compatible with parallel

computing facilities, all simulations in this section were carried out in the serial mode of SWAN. These were conducted on a single processor on the Hydrax cluster of Deltares.

4 Multigrid approach

4.1 Introduction

The Multigrid approach aims to reduce the total number of iterations required by SWAN for convergence by starting the iteration process with an improved estimate of the final solution. The basic idea pursued is that the solution obtained on a given computational grid can be approximated well by simulation on a coarser grid, while this coarse-grid computation can be completed in a fraction of the time required on the original grid. Since this coarse grid run would be computed using the same third-generation model physics as the detailed grid run, it would provide a better starting point for the iteration process than the default 'first guess' of SWAN that is based on second-generation physics. The strategy followed is to start the simulation on a grid with a reduced resolution (initial guess run phase), iterate up to a desired level of accuracy, copy the results onto the required final resolution, and continue the simulation up to convergence (full resolution run phase). Since computation on the reduced grid is faster than on the original grid, and since a good initial guess from the coarse run should reduce the required number of iterations on the original resolution grid, the combined time required for the two simulations should be less than when iterating on the detailed grid only.

This multigrid approach, which is related to a larger family of multigrid methods (e.g. Ferziger and Perić 2002), was originally proposed by Van Vledder (2005b). In WL & Alkyon (2007b) the Multigrid approach was implemented in SWAN and tested for a number of field cases in the Amelander Zeegat with and without the presence of currents. In the latter study, a number of alternatives for reducing the computational grid resolution of the initial estimate simulation were investigated, namely reductions in geographical space, spectral space, and in both geographical and spectral spaces. Based on these investigations, a number of promising Multigrid options were proposed for further studies. These options are the use of a reduced geographical resolution with a factor 2 in both x and y dimensions, a reduced spectral resolution with a factor 2 in both frequency and direction, and the combination of using a reduced resolution in both geographical and spectral spaces, each with a factor 2. In the present study, these Multigrid combinations were tested on a wider range of field cases, namely those presented in Section 2 featuring the Eems-Dollard, Petten, Lake Sloten, and the Amelander Zeegat (three other cases than those considered by WL & Alkyon (2007b)).

This section is structured as follows: Section 4.2 presents the test setup and coding conventions applied in this investigation. The simulation results and analysis are presented in Sections 4.3 to 4.5. Section 4.6 presents a discussion on the results, followed by conclusions and recommendations in Sections 4.7 and 4.8.

4.2 Test setup and coding conventions

Using the methodology described in Section 3.3, the performance of each Multigrid option was assessed as follows: Firstly, a benchmark run was performed with the default SWAN model, using a fixed number of 80 iterations. The results of these simulations are considered to represent the converged solution of SWAN. Secondly, a reference run was performed with the default SWAN model, using the convergence criteria described in Section 3.2. Thirdly, each Multigrid option was tested in turn in a control run. These control runs were performed using the same convergence criteria

used in the reference run (Section 3.2), and are applied to both the initial guess and the full resolution run phases. In this regard, it is noted that WL & Alkyon (2007b) found that the results of the Multigrid method are not very sensitive to the choice of convergence criteria for the initial guess run phase. The effectiveness of each Multigrid simulation was assessed on the basis of the iteration behaviour, the total run time and the accuracy of the results, using the criteria described in Section 3.5.

For each of the eight cases described in Section 3, three Multigrid settings were tested. The first featured a reduced spatial resolution in *x* and *y* dimensions, the second a reduced spectral resolution in frequencies and directions, and the third a reduced resolution in both the spatial and spectral dimensions. The reduction factor in all cases was 2, which was found to be optimal by WL & Alkyon (2007b). Table 4.1 presents the coding convention used to distinguish between the various simulations and Multigrid settings applied in this investigation.

Run code	Description
Bx1y1d1s1	Benchmark run, full spatial and spectral resolution, 80 iterations
Rx1y1d1s1	Reference run, full spatial and spectral resolution, convergence criteria
Cx2y2d1s1	Control run with a reduced spatial resolution, convergence criteria
Cx1y1d2s2	Control run with a reduced spectral resolution, convergence criteria
Cx2y2d2s2	Control run with a reduced spatial and spectral resolution, convergence criteria

Table 4.1 Coding convention of the applied model settings to investigate the Multigrid method.

As mentioned in Section 2.6, while setting up the computations for the Multigrid method in our dedicated SWAN version, a number of problems were encountered which necessitated adaptations to two of the four field case setups. Firstly, the memory usage of SWAN is increased when interpolating spectra from a coarse grid resolution to the required full resolution. Secondly, an error occurs when boundary conditions are specified as segments. Details on how these problems were circumvented in the present study were given in Section 2.6. In addition, it is noted that the so-called *test S1D* and *S2D* output files of SWAN are incomplete when using the Multigrid setting with reduced spectral resolution. When this Multigrid option is used, metadata (header information) is only given for the initial guess run phase, and not for the full resolution run phase. It is stressed that these identified implementation shortcomings did not affect the outcomes of this investigation.

4.3 Influence on simulation time

The influence of the Multigrid method on the simulation times of the eight investigated field cases is summarized in the Tables 4.2 to 4.4. For each test case, consisting of a hindcast situation and a Multigrid option, results are shown of the number of iterations (N_{iter}) for the reference and the control runs and an estimation of the required CPU time (T_{cpu}). The latter was determined using the method described in Section 3.5.2. Also indicated is the ratio (in percentage) between the total simulation time of a particular Multigrid option and its corresponding reference run (hence values <100% denote a reduction in simulation time). The number of iterations of the control run is split in two numbers. The first number is the number of iterations of the initial guess run phase using a reduced geographical and/or spectral resolution. The second number is the number of iterations required for the full resolution run phase. Due to the reduced

resolution, the time spent per iteration during the initial guess phase is significantly less than during the full resolution run phase.

Run code	AZG3a 10:00 (flood)		AZG3a 12:00 (slack)		AZG3a 17:00 (ebb)	
	N_{iter}	T_{cpu} [min (% ref)]	N_{iter}	T_{cpu} [min (% ref)]	N_{iter}	T_{cpu} [min (% ref)]
Bx1y1d1s1	80	126	80	131	80	128
Rx1y1d1s1	41	66	46	76	37	60
Cx2y2d1s1	42/40	84 (127%)	59/40	92 (121%)	41/63	120 (200%)
Cx1y1d2s2	80/53	125 (189%)	80/54	90 (118%)	80/20	70 (117%)
Cx2y2d2s2	80/63	111 (168%)	80/64	113 (149%)	80/71	118 (197%)

Table 4.2 Number of iterations and CPU time (in minutes, including % of reference run time) for three storm instants on 2 January 2005 in the Amelander Zeegat for the Multigrid simulations.

Run code	Eems3a 3:00 (flood)		Eems3a 6:30 (slack)		Eems3a 9:30 (ebb)	
	N_{iter}	T_{cpu} [min (% ref)]	N_{iter}	T_{cpu} [min (% ref)]	N_{iter}	T_{cpu} [min (% ref)]
Bx1y1d1s1	80	208	80	210	80	208
Rx1y1d1s1	43	113	44	113	46	120
Cx2y2d1s1	69/71	236 (209%)	54/48	163 (144%)	80/60	229 (191%)
Cx1y1d2s2	80/80	271 (240%)	80/66	234 (207%)	80/72	228 (190%)
Cx2y2d2s2	80/80	227 (201%)	80/74	212 (188%)	80/76	216 (180%)

Table 4.3 Number of iterations and CPU time (in minutes, including % of reference run time) for three storm instants on 1 November 2006 in the Eems-Dollard for the Multigrid simulations.

Run code	Petten		Lake Sloten	
	N_{iter}	T_{cpu} [min (% ref)]	N_{iter}	T_{cpu} [min (% ref)]
Bx1y1d1s1	80	148	80	109
Rx1y1d1s1	30	57	30	42
Cx2y2d1s1	41/13	47 (83%)	32/13	30 (71%)
Cx1y1d2s2	80/19	83 (146%)	32/13	32 (76%)
Cx2y2d2s2	80/18	49 (86%)	35/15	26 (62%)

Table 4.4 Number of iterations and CPU time (in minutes, including % of reference run time) for one storm instant at Petten and in Lake Sloten for the Multigrid simulations.

The results in Tables 4.2 to 4.4 indicate that in general the Multigrid method does not lead to faster SWAN computations. The only exceptions are for the Lake Sloten case (all control runs) and for the Petten field case with the control run Cx2y2d1s1. These results are less favorable than those obtained in WL & Alkyon (2007b), where it was found that the Multigrid method produces a general gain in speed of 10% to 20%. The main reason for these differing results is that in the present study the convergence criteria were set stricter than in WL & Alkyon (2007b), since now also information on the convergence behaviour of the spectral period is taken into account (Section 3.2). Evidently, these stricter convergence criteria necessitate the (computationally expensive) full resolution grid phase to perform more iterations relative to the reference run than in WL & Alkyon (2007b), making the Multigrid simulations conducted here relatively more time-consuming. This issue is further discussed in Section 4.6.

Regarding the various field cases, the Multigrid method performs the best for the Lake Sloten and Petten field cases, although not always faster than the reference run. The Multigrid method performs unsatisfactorily for the Amelander Zeegat and for the Eems-Dollard. These differences in behaviour may be due to the fact that the Petten and Lake Sloten are relatively simple physical situations, i.e. without complex wave systems, currents and a complicated bathymetry.

The effectiveness of the Multigrid method in situations with currents shows that for the Amelander Zeegat the best results (i.e. requiring the least computational time) are found for the slack tide situations, whereas for the flood and ebb situations the results are worse, but mutually comparable. For the flood situation, the best results are found for the Multigrid option with reduced geographical resolution (control run Cx2y2d1s1), whereas for the ebb situation the best results are found for the reduced spectral resolution (Cx1y1d2s2). For the Eems-Dollard, the best results are found for the situation around slack tide.

Considering that the Multigrid method generally leads to longer simulation times than the reference run, no clear best Multigrid setting can be identified. For the Amelander Zeegat, the Multigrid options with reduced geographical (Cx2y2d1s1) or spectral resolution (Cx1y1d2s2) can be considered to perform relatively better than the option with a reduction in all dimensions, although nowhere achieving reduced simulation times. For the Eems-Dollard, the Multigrid option with reduced geographical resolution (Cx2y2d1s1) gives the shortest run times for the situation around slack tide (although still longer than for the reference run), whereas for all other cases no clear best method exists. For Petten, the best results are obtained for the Multigrid option with reduced geographical resolution (Cx2y2d1s1), and for Lake Sloten the best results are found with reductions in all dimensions (Cx2y2d2s2). For both of these control runs, a time saving with respect to the reference run is achieved. The results discussed here suggest a slight preference for the Multigrid option with reduced geographical resolution (control run Cx2y2d1s1) when considering total simulation times.

4.4 Iteration behaviour

The iteration behaviour of SWAN using the various Multigrid options was investigated by visualising the percentage of accepted points (i.e. the percentage of wet grid points at which the convergence criteria are met) and the variation of the four integral wave parameters of the significant wave height H_{m0}, the spectral period $T_{m-1,0}$, the mean wave direction *Dir* and the directional spreading *Dspr*. These were considered for the benchmark run, the reference run and the control runs (both the initial geuss and full resolution parts). The iteration behaviour of these four integral parameters were obtained from the SWAN output as described in Section 3.5.1, and were investigated in three test points per area (see Section 2).

Figure 4.1 shows the iteration behaviour for the Amelander Zeegat storm of 2 January 2005 at 10:00 (flood), using the Multigrid setting with reduced geographical resolution (Cx2y2d1s1). The results are shown for test point 1, located on the edge of the ebb tidal delta. The upper left-hand panel shows the percentage of accepted points for the benchmark run (thin line), the reference run (thick line, and the last point marked with a black dot), the initial guess run (dash-dot line) and the full resolution control run (dashed line). The upper right-hand panel shows the location of the test points per geographical area. The rectangle that is used for the computation of the simulation errors is also

indicated. The lower four panels show the iteration behaviour of the four integral wave parameters. The end points of the initial guess runs and corresponding control runs are marked with a diamond and square, respectively. The line with the results of the full resolution control run starts where the line with the results of the initial guess ends. This is to indicate that the full resolution run phase continues from where the initial guess run phase ends off. In addition, this superposition allows the investigation of differences between the coarse grid solution and the first iteration result on the full resolution grid. These include the difference in discretisation error made on the coarse and full resolution grids, and possible interpolation errors made during the conversion of the wave field from the coarse grid to the full resolution grid.

The top left-hand panel of Figure 4.1 shows that for the control run Cx2y2d1s1 the initial guess run phase has a similar rate of grid point acceptance as the reference run. By contrast, the full resolution control run has a slightly faster rate of grid point convergence than the reference run until 96% convergence is reached. This demonstrates the benefit of starting the iteration process with the Multigrid initial guess, as opposed to the second-generation first guess of the default model (reference run). Inspection of the lower four panels shows differences in the integral parameter values between the converged results of the initial guess run and the reference run. These differences are presumably due to the difference in discretisation error in the coarse and full resolution grids. These are rapidly decreased in the first 10 iterations of the subsequent full resolution control run. The full resolution simulation, using the convergence criteria of Section 3.2, can be seen to converge well, unlike the results in WL & Alkyon (2007b), which were often not properly converged. However, the full resolution control run phase can be seen to use about the same number of iterations as the reference run. Figure 4.2 shows the corresponding iteration behaviour of the wave parameters in test point 3, situated well into the Wadden Sea where young waves develop over strong ambient current. In general, the iteration behaviour is similar to that of test point 1, including good convergence of the full resolution run phase. The only exception is found in the mean wave direction, which has not even converged in the benchmark run, not even after 80 iterations.

Figures 4.3 and 4.4 show the iteration behaviour for the same storm instant and test points as above, but with the Multigrid option with reduced spectral resolution (control run Cx1y1d2s2). It can be seen that the initial guess run displays poor convergence behaviour compared to the reference run (top left-hand corner), resulting from small amplitude oscillations in the integral parameters H_{m0} and T_{m01} (also seen in $T_{m-1,0}$), which are not present, or less severe, in the reference run. As a result, the initial guess simulation uses the maximum imposed number of 80 iterations. Had it not been for these oscillations, the initial guess run would probably have been converged after half as many iterations. Similar findings were found for the Multigrid option with a reduced resolution in both geographical and spectral space (control run Cx2y2d2s2). This is illustrated in the Figures 4.5 and 4.6 for the test points 1 and 3.

For the Eems-Dollard, the situation around slack tide (1 November 2006 at 6:30) is selected to illustrate the convergence behaviour of the Multigrid method. Figures 4.7 and 4.8 show the iteration behaviour of the Multigrid run with a reduced geographical resolution (control run Cx2y2d1s1) for test point 1 (North Sea side of the ebb tidal delta) and test point 3 (in the Eems-Dollard near Eemshaven). The results again show that the coarse grid initial guess produces somewhat different solutions than the reference run due to discretisation errors, but that the subsequent detailed grid phase quickly modifies the parameter values to values that are close to the results obtained with the benchmark run. Figures 4.9 and 4.10 present the results of the Multigrid option with a

reduced spectral resolution (control run Cx1y1d2s2). As found for the control run Cx1y1d2s2 above (Figures 4.3 and 4.4), the initial guess run never meets the convergence criteria, due to oscillations in the solution for the wave height and wave period. The full resolution phase of the control run converges to values that are close to those of the benchmark run, but only after 66 iterations. A remarkable feature is the fact that the percentage of accepted points of the full resolution control run initially converges faster than those of the reference run, but slows down after about 30 iterations. Figures 4.11 and 4.12 show the results for the Multigrid setting with a reduced resolution in both geographical and spectral space (Cx2y2d2s2). The results are very similar to those of the Multigrid run with only a reduced spectral resolution (Cx1y1d2s2).

For the Petten field case, results are shown in the Figures 4.13 to 4.15 for test point 2, located in the surf zone, for all three Multigrid options. The results for the reduced geographical resolution (control run Cx2y2d1s1, Figure 4.13) show that the initial guess has converged, but also that the solutions for the wave parameters of the benchmark run starts showing small amplitude oscillations after 20 iterations. These oscillations are noticeable in all four integral wave parameters. Nonetheless, the control run converges in 20 iterations. It can also be seen that for this situation the start values of the full resolution control run phase are close to the end results of the initial guess run phase. This indicates that the interpolation errors are small and that geographical discretisation effects play a minor role. This might be related to the fact that the geometry for this case is relatively simple. Figures 4.14 and 4.15 show the corresponding results for both Multigrid options that include a reduced spectral resolution (control runs Cx1y1d2s2 and Cx2y2d2s2). The results indicate that, as found above for these Multigrid settings, the initial guess run has not converged. Again small amplitude oscillations in the iteration behaviour appear to be responsible for this poor convergence behaviour. Despite this, the parameter values seem to have converged in general. It is also found that the full resolution control run phase quickly (within 15 iterations) reaches a solution of the parameter values that is close to that of the benchmark run.

Figures 4.16 to 4.19 present the iteration behaviour found for Lake Sloten for the Multigrid method with either a reduced geographical resolution (Cx2y2d1s1) or a reduced spectral resolution (Cx1y1d2s2). Results are shown for test point 1 at the upwind lake edge and test point 3 at the observation station SL29. The results in Figures 4.16 and 4.17 show that, for the control run Cx2y2d1s1, the initial guess run phase produces an almost equal solution to that of the reference run. Even the number of iterations is almost equal. This would suggest that the coarser geographical resolution of the setting Cx2y2d1s1 is already sufficient to resolve the gradients in the underlying model physics. Since only one Lake Sloten case was considered, it is not possible to determine the generality of this result. The full resolution run phase continues from this good initial estimate, reducing the remaining differences with respect to the benchmark results further, and converges after only 13 iterations.

Figures 4.18 and 4.19 show the corresponding results at test points 1 and 3 when applying the Multigrid setting with a reduced spectral resolution (Cx1y1d2s2). It can be seen that the initial guess run phase produces results that are within 10% or 1^{o} of the results of the reference run. Thanks to the good starting point afforded by the initial guess, the full resolution run phase again requires only 13 iterations to converge to a solution close to that of the benchmark run (see also Table 4.4). We note that for this Lake Sloten field case the model has not converged at test point 1 yet (neither in the reference nor benchmark runs), so that these results should be treated with caution. The slow convergence is probably related to the fact that at test point 1 only a few

upwind grid points exist, so that here the model is only weakly forced to its final solution. Nonetheless, the grid points at which this problem occurs are evidently limited, so that in the reference run the convergence criteria still consider the overall model to be sufficiently converged after 30 iterations.

4.5 Convergence error

The third aspect of the evaluation of the Multigrid method is the magnitude of the convergence errors found with this approach relative to that found for the reference run. These mean convergence errors have been computed as described in Section 3.5.3, namely the absolute value of the difference between the converged result of the investigated simulation (reference or control) and the benchmark result, averaged over a given evaluation area. These results are summarized in the Tables 4.5 to 4.8 and discussed in the paragraphs below.

Run code	$\mu(H_{m0})$ [%]	$\mu(T_{m-1,0})$ [%]	$\mu(\mathrm{Dir})$ [^{0}]	$\mu(\mathrm{Dspr})$ [%]
Rx1y1d1s1	0.15	0.23	0.39	0.67
Cx2y2d1s1	0.21	0.27	0.54	0.69
Cx1y1d2s2	0.36	1.00	0.76	1.14
Cx2y2d2s2	0.29	0.98	0.69	0.63

Table 4.5 Average differences in wave parameters for three storm instants on 2 January 2005 in the Amelander Zeegat for the Multigrid simulations. Computed as the mean of $\mu(.)$ for each parameter over the three storm instants.

Run code	$\mu(H_{m0})$ [%]	$\mu(T_{m-1,0})$ [%]	$\mu(\mathrm{Dir})$ [^{0}]	$\mu(\mathrm{Dspr})$ [%]
Rx1y1d1s1	0.20	0.25	0.42	0.81
Cx2y2d1s1	0.18	0.26	0.37	0.52
Cx1y1d2s2	0.24	0.64	0.29	0.59
Cx2y2d2s2	0.16	0.65	0.29	0.44

Table 4.6 Average differences in wave parameters for three storm instants on 1 November 2006 in the Eems-Dollard for the Multigrid simulations. Computed as the mean of $\mu(.)$ for each parameter over the three storm instants.

Run code	$\mu(H_{m0})$ [%]	$\mu(T_{m-1,0})$ [%]	$\mu(\mathrm{Dir})$ [^{0}]	$\mu(\mathrm{Dspr})$ [%]
Rx1y1d1s1	0.11	0.18	0.24	0.50
Cx2y2d1s1	0.19	0.48	0.30	0.60
Cx1y1d2s2	0.25	0.84	0.41	0.76
Cx2y2d2s2	0.29	1.08	0.51	1.11

Table 4.7 Average differences in wave parameters for one storm instant at Petten for the Multigrid simulations.

Run code	$\mu(H_{m0})$ [%]	$\mu(T_{m-1,0})$ [%]	$\mu(\mathrm{Dir})$ [^{0}]	$\mu(\mathrm{Dspr})$ [%]
Rx1y1d1s1	0.63	0.58	0.59	1.11
Cx2y2d1s1	0.22	0.25	0.15	0.38
Cx1y1s2d2	0.58	1.05	0.44	0.55
Cx2y2d2s2	0.49	0.88	0.33	0.62

Table 4.8 Average differences in wave parameters for one storm instant in Lake Sloten for the Multigrid simulations.

Tables 4.5 to 4.8 show that in many cases the Multigrid method produces results with comparable overall accuracy to the reference run (within the rectangular evaluation areas). For the Amelander Zeegat (Table 4.5), the Multigrid setting with reduced geographical resolution (Cx2y2d1s1) gives the best results for H_{m0} and $T_{m-1,0}$, yielding model errors that are close to those obtained with the reference run. Regarding the directional parameters, all model errors produced by the Multigrid method are comparable to those found with the reference run, with no setting consistently yielding the lowest errors. For the Eems-Dollard (Table 4.6), all Multigrid options yield generally similar convergence error results for all four wave parameters as the reference run. For the Petten area (Table 4.7), the Multigrid option with reduced geographical resolution (Cx2y2d1s1) gives similar model errors as the reference run, but the other Multigrid options yield less accurate results. For Lake Sloten (Table 4.8), the Multigrid option with reduced geographical resolution (Cx2y2d1s1) yields model errors of about half those of the reference run.

The summary results presented in the Tables 4.5 to 4.8 provide a single quantitative assessment of the relative accuracy of the various Multigrid options. However, by using a single number (parameter μ), some relevant information on the spatial variation of the prediction error is lost. Therefore, we next consider the spatial distributions of the convergence errors for selected Multigrid simulations, defined as the difference between the outcomes of the reference and control runs and those of the benchmark results. These are computed with Equations (3.1) and (3.2). For consistency, results will be shown for the same situations for which the convergence behaviour was presented above.

Figures 4.20 and 4.21 present results for the Amelander Zeegat for the situation on 2 January 2005 at 10:00 (flood), for the Multigrid setting with reduced geographical resolution (Cx2y2d1s1). The upper panels of these figures show the convergence errors of the reference run in terms of the significant wave height H_{m0}, spectral period $T_{m-1,0}$, mean direction *Dir* (its absolute value) and directional spreading *Dspr*. The lower panels show the corresponding model errors for the control run. Included in all these panels are the evaluation area (rectangle) and, for reference and comparison, the average error μ in this area, as considered above. Note that, according to the definitions (3.3) to (3.6) the parameter μ represents the average of the *absolute value* of the error, and not the simple average of the error values in the evaluation area. The upper panels of Figures 4.20 and 4.21 indicate that in the reference run the largest errors in the wave height are found over the ebb tidal delta and along the tidal channel southwest of Ameland. For the control run, relatively large errors also occur at the leeward side of Ameland in a situation where initial wave growth occurs. For the spectral period, a similar pattern occurs as for the wave height, but the magnitude of the errors is slightly higher. Large errors also occur on the shallow areas along the Frisian coast. In both cases, and for both parameters, the errors are more or less evenly distributed in the

computational domain. The errors in predicted mean wave direction (Figure 4.21) are generally small (less than 1^o), but at some locations relatively large errors occur (larger than 5°). Such large errors occur in the shallow area in the western part of the Amelander Zeegat. For the control run such areas with relatively large errors also occur at the lee-side of Ameland and Terschelling. The error in directional spreading is evenly distributed in the computational domain, except for a few areas where this error is more than 5%. These areas coincide with the areas in the errors of the mean wave direction.

The results for the same storm condition, but for the Multigrid option with reduced spectral resolution (Cx1y1d2s2) are shown in the Figures 4.22 and 4.23. For the wave height similar results are found as for the Multigrid option with reduced geographical resolution considered above. For the spectral period, the errors in the control run are relatively large (up to 5%) along the northern coastal strip along the Wadden islands, whereas in the Wadden Sea the errors are much lower (nearly equal to zero). The results for the mean wave directions are generally smaller (error less than 0.5^o) for the control run than for the reference run. The errors in directional spreading are generally close to zero, but relatively high (up to 5%) just north of Terschelling. The Figures 4.24 and 4.25 present the corresponding results for the Multigrid option with both a reduction in geographical and spectral resolution (Cx2y2d2s2). The results are similar to those presented in the Figures 4.22 and 4.23 (Multigrid option with reduced spectral resolution). It appears that, also for this case, the reduction in spectral resolution in the initial guess run phase is responsible for the relatively large errors along the Northern strip of the Wadden islands. The reason for this behaviour is not yet known and might be found by a detailed analysis of the spectral evolution at locations with relatively high errors.

For the Eems-Dollard field case, results are presented for the storm instant of 1 November 2006 at 6:30 (slack) for all three investigated Multigrid settings. Figures 4.26 and 4.27 present the result for the Multigrid setting with reduced geographical resolution (Cx2y2d1s1). For the significant wave height H_{m0} the errors for the reference run are generally close to zero, but they are relatively high (up to 5%) in some areas in the tidal inlets between the Wadden islands and also along the access channel towards the Eemshaven. For the control run, the area south of the island of Juist contains relatively large errors (up to 5%). Such an increase in error at the lee-side of an island was also found behind the island of Terschelling, but on a much smaller spatial scale. The origin of these errors is not known at present, but could again be found by detailed analysis of the spectral evolution is this region. The error in spectral period for the reference run is concentrated in small areas along channels in the tidal inlet. For the control run, the error in the tidal inlets become smaller compared to the reference run, but again behind the island of Juist a large area with errors of up to 5% occur. In the reference run, the convergence errors in mean wave direction are generally very small ($<0.5^o$), except for a few regions in the tidal channels between the Wadden islands. These errors are possibly caused by refraction effects which weakly turn the wave directions, such that many iterations are needed to obtain converged results. For the control run, a large area with error in mean direction of at least 5^o is found south of the island of Juist. The errors in directional spreading for the reference run are generally small. For the control run, however, a region with relatively high error (up to 5%) is again found behind the islands of Juist and Schiermonnikoog.

Figures 4.28 and 4.29 present results for the same conditions, but now using the Multigrid setting of reduced spectral resolution (Cx1y1d2s2). For the significant wave height, overall errors are smaller for the control run than for the reference run. North of the German Wadden islands, some areas appear with somewhat higher errors (up

to 1.5%). For the spectral period, the results of the control run show a large area north of the Wadden islands with errors of up to 3%, as was found above for the Amelander Zeegat. In the Wadden Sea, however, these errors are close to zero (differences less than 1%), in contrast to the reference run result in some areas. The errors in the mean wave direction of the control run are much smaller than for the reference run. However, in the control run, a few regions with relatively high errors (up to 3^o) occur just north of the island of Borkum. Regarding the error in the directional spreading, the results of the reference run show many areas with an underestimation of the directional spreading. For the control run, the parameter μ has decreased, but now the directional spreading is over-predicted in many areas just north of the Wadden islands and the shallow areas between these islands.

Figures 4.30 and 4.31 present the results for the Multigrid option with a reduced resolution in geographical and spectral space (Cx2y2d2s2). For the significant wave height H_{m0} and spectral period $T_{m-1,0}$ the results are very similar to the results of the Multigrid setting with only a reduced spectral resolution (Cx1y1d2s2). The most striking differences are an increase in error south of the island Juist for the significant wave height, and an increase in error in the spectral period on the northern coastlines of the Wadden islands, as found above. For the mean wave direction and directional spreading relatively high errors (respectively $>5^o$ and up to 5%) are found in areas south of the island Juist. The directional spreading is also over-predicted up 2% north of the Wadden islands and the shallow areas between these areas.

For the Petten field case, results of all investigated Multigrid options are shown in the Figures 4.32 to 4.37. Here the errors in significant wave height and spectral period of the reference run are significantly lower than for the Amelander Zeegat and the Eems-Dollard (Figures 4.32 and 4.33). The Multigrid option with reduced geographical resolution (Cx2y2d1s1) can be seen to yield similarly small prediction errors. For the mean wave direction and directional spreading, the errors are also smaller than for the Wadden Sea areas. Applying the Multigrid setting Cx2y2d1s1 yields similar (small) errors in these parameters as the reference run.

Figures 4.34 and 4.35 show the results for the Multigrid option with a reduced spectral resolution (Cx1y1d2s2). The average error in significant wave height increases by about a factor two compared to that of the control run Cx2y2d1s1, but it is still rather small. This increase in average error is also found for the spectral period. For the control run the error in wave height and wave period slightly increases in the area west of the rectangle. For the mean wave direction and directional spreading, the control run produces average errors that are about twice as high as for the reference run, but these errors are still rather small. The corresponding results of the Multigrid option with a reduced resolution in geographical and spectral space (Cx2y2d2s2) are very similar to the results obtained with the Multigrid option using only a reduced spectral resolution. The main differences are that somewhat higher errors are found for the significant wave height H_{m0} and spectral period $T_{m-1,0}$. For the latter, the average error doubles to about 1%.

Figures 4.38 to 4.41 present the results for the Lake Sloten for the Multigrid setting with either a reduced geographical resolution (Cx2y2d1s1) or a reduced spectral resolution (Cx1y1d2s2). The top panels of Figures 4.38 and 4.39 show that for the reference run, the errors in significant wave height (H_{m0}) and spectral period ($T_{m-1,0}$) is negative (up to -5%) at the very start of the fetch (measured along the main axis of the Lake Sloten, starting at the south-westerly corner) and that these errors reduce to about 0.5-1% at the end of the fetch. For the mean wave direction and directional spreading the results

of the reference run also show relatively large errors at the beginning of the fetch. Towards the centre of the lake, the mean direction has errors of 0.5-1.5^{o}, whereas in large parts the directional spreading has errors in the range 1.5-2.5%. For the control run Cx2y2d1s1 (Figures 4.38 and 4.39, bottom panels), comparable spatial patterns of model error to those of the reference run are found, but with the average magnitude approximately halved. This is particularly an improvement for the directional spreading.

The results of the Multigrid option with reduced spectral resolution (Cx1y1d2s2, Figures 4.40 and 4.41) show that the model error has a stripy pattern, with alternating bands of a certain error range. However, for the significant wave height H_{m0} the errors are at most 1% and the average error is half of that value. For the spectral period, the errors are somewhat higher (up to 2.5%). Figure 4.41 shows that for this Multigrid setting the errors in mean direction remain approximately similar to that of the control run, and the errors in directional spreading change to a slight underprediction (-0.5%) relative to the benchmark result.

4.6 Discussion

In this study, the Multigrid implementation in SWAN of WL & Alkyon (2007b) was tested for eight field conditions, and three settings for the reduction of the computational grid resolution. The performance of the Multigrid method was assessed on the basis of three criteria, namely the gain in computational speed, changes to the iteration behaviour and changes to model accuracy. The results of the present simulations show that only for a few cases a small gain in speed is achieved with the Multigrid method, whereas in most cases this numerical approach leads to much longer simulation times. Regarding model outcomes, the Multigrid method was found to produce similar accuracy to the default model (reference runs), with some notable exceptions of relatively large errors.

The results of the present study are less favorable than those obtained in WL & Alkyon (2007), where it was found that the Multigrid method produces a gain in speed of 10% to 20%. The main reason for this difference is the fact that in the present study the convergence criteria were set stricter, since here also information on the convergence behaviour of the spectral period is taken into account (as recommended by Alkyon (2007b)). In WL & Alkyon (2007), the results of the full resolution run phase, and in particular the mean period, often did not properly converge (see e.g. their Figures 3.1 to 3.6). The stricter convergence criteria applied in the present study have forced the full resolution run phase to perform more iterations than under similar conditions in the simulations of WL & Alkyon (2007). Hence, the total run time of the Multigrid simulation is relatively longer in the present study. Although the stricter convergence criteria are also applied to the initial guess part of the Multigrid computation, it evidently does not lead to a better starting point for the full resolution phase, in which case iterations would be saved. This holds especially for the Multigrid options with a reduced spectral resolution (control runs Cx1y1d2s2 and Cx2y2d2s2).

The experience gained with the Multigrid method in this study revealed some shortcomings that make it difficult to judge at present whether this method should be further developed. Based on the results of Tables 4.2 to 4.8 it can be concluded that the Multigrid method, in its present form, only provides a speed-up for the simpler Petten and Lake Sloten cases, and not for the more complex Wadden Sea cases. However, some sensitivity testing showed that some modifications to the Multigrid method may improve its performance such that it might speed up SWAN computations in general.

The most salient problem found in this investigation is that, when applying reductions in spectral space (control runs Cx1y1d2s2 and Cx2y2d2s2), the initial guess run phase does not converge and hence consumes the maximum number of iterations. Inspection of the results indicated that, for these simulations, SWAN is not able to converge due to the presence of small amplitude oscillations in the solutions for the significant wave height H_{m0} and spectral period $T_{m-1,0}$ (as shown in the convergence plots) and probably also in the spectral period T_{m01} which is used to assess the convergence behaviour. It therefore appears that the application of the reduced spectral resolution deteriorates the iteration behaviour, and hence delays convergence. Such oscillations can be suppressed by applying under-relaxation (Zijlema and Van der Westhuysen 2005). In the computations carried out here, the amount of under-relaxation was set to 0.001 for the Amelander Zeegat, Petten and Lake Sloten cases, and to 0.002 for the Eems-Dollard (Section 3.2). It appears that this amount of under-relaxation is insufficient to suppress the oscillations induced by the reduction in spectral resolution. Trial computations with a higher amount of under-relaxation indicate that these oscillations can be eliminated, so that the number of iterations in the initial guess run phase can be halved. However, this does not always lead to a significant reduction in number of iterations of the full resolution run phase. Further tests should indicate which amount of under-relaxation gives the largest reduction in number of iteration, but also whether application of such an optimal value lead to an overall speed-up of SWAN computations.

Finally, one of the aims of the present study is to investigate whether the Multigrid method can be applied in combination with the DDM approach (to be considered in Section 5), in order to improve the accuracy of the latter. Analysis of the convergence errors of the DDM by WL (2007) showed that this method can produce relatively large convergence errors in regions where strong currents are present. This was found to be due to the slow convergence of SWAN in these regions, since the default second-generation first guess of SWAN, as used in the DDM, appears not to model wave-current interaction with sufficient accuracy. In this regard, the application of the Multigrid method could provide an improved initial guess of the wave field, properly including the influence of current, which may improve the performance (accuracy) of the DDM technique. On the basis of the results of the various Multigrid options, summarized in Tables 4.2 to 4.8, no Multigrid setting can be considered as being particularly promising, especially regarding Wadden Sea applications. However, the option using a reduced geographical resolution (Cx2y2d1s1) was seen to produce generally more encouraging results than those using a reduced spectral resolution, particularly also in the light of the discussion in the previous paragraph. Therefore, the option with reduced geographical resolution is regarded as the most suitable candidate for combining with the DDM. The combination of these two numerical methods is considered in Section 7.

4.7 Conclusions

The following conclusions can be formulated with respect to the application of the Multigrid method for the eight conditions:

- The Multigrid method produces generally longer simulation times than the default SWAN model (reference runs), with generally comparable accuracy. Whereas the performance of the Multigrid method is good for the simpler Petten and Lake Sloten cases, it is unsatisfactory for the complex geographical areas such as the Amelander Zeegat and Eems-Dollard.

- Although the Multigrid method in its present form cannot be considered to be successful in reducing the simulation times of SWAN in general, it may still prove effective in combination with the DDM technique (to be evaluated in Section 5). Considering overall model performance and accuracy, the best Multigrid option for this purpose appears to be the reduction in spatial resolution (Cx2y2d1s1).

- Application of the Multigrid option with reduced spectral resolution often causes oscillations in the iteration behaviour, the presence of which prevents SWAN from converging to within the required level of accuracy. This behaviour negatively affects the application of the Multigrid option.

- The Multigrid setting with reduced spectral resolution produces consistent errors in the mean period (up to 2.5%) along the northern coastlines of the Wadden Islands (Amelander Zeegat and Eems-Dollard field cases). The Multigrid setting with reduced geographical resolution produces consistent errors in H_{m0} (5%), $T_{m-1,0}$ (5%), *Dir* (>5^{o}) and *Dspr* (5%) directly downwind of the island of Juist in the Eems-Dollard field case. The origin of these inaccuracies is not known at present.

4.8 Recommendations

From the results of this study, and the subsequent discussion and conclusions, the following is recommended:

- On the basis of the present results it is not recommended to apply the Multigrid method in SWAN for HBC computations

- Although the Multigrid method in its present form does not provide positive results, it should be investigated whether it can complement the performance of the DDM method, by harnessing the improved initial guess in cases with currents. This will be investigated in Section 7.

- Investigate whether the application of stronger under-relaxation than considered in this study may improve the iteration behaviour of the initial guess run phase for Multigrid reductions in spectral space such that overall simulation times can be reduced.

- Only when carrying out the previous two recommendations leads to positive results, attention should be given to the implementation problems like the treatment of boundary conditions, memory usage and layout of test files (see Sections 2.6 and 4.2).

5 Dynamic Deactivation Method (DDM)

5.1 Introduction

In this section, the effectivity of the Dynamic Deactivation Method (DDM) in decreasing the total computational time of SWAN is investigated. As presented in WL (2007), the basic premise of the DDM, first proposed by Van Vledder (2005a), is to reduce the total simulation time of SWAN by deactivating computational grid points as they become converged, based on given criteria. Since typically towards the end of a simulation only a small percentage of unconverged grid points remain, this method eliminates costly and unnecessary computing time spent on the converged grid points comprising the rest of the model domain.

WL (2007) investigated the performance of this method for the Amelander Zeegat region, including flood, slack and ebb conditions. WL (2007) concludes that the performance of the DDM is critically dependent on the criteria applied to determine the deactivation of a particular grid point, and on the underlying iteration behaviour of the model. The latter, in turn, depends on the physical situation modelled, such as wave-following flood or wave-opposing ebb currents in the Amelander Zeegat. In addition, periodic reactivation of the entire computational grid proved important for communicating upwave changes in wave field to down-wave grid points that have already been deactivated on the basis of their convergence. Based on the Amelander Zeegat cases investigated, WL (2007) recommends the application of deactivation criteria based on the curvature-based convergence criteria proposed by Zijlema and Van der Westhuysen (2005), extended to include also the curvature of the mean period T_{m01}. In addition, a reactivation schedule is recommended in which the entire computational domain remains active during the first five iterations, whereafter it is reactivated every five iterations. Deactivation can take place during the intervening iterations.

In the present investigation, the recommendations of WL (2007) are evaluated for the extended set of eight field cases presented in Section 2, and variations on the reactivation schedule are investigated. As will be shown, the periodic reactivation (updating) of the entire computational grid temporarily reduces the level of model convergence. Hence, longer intervals between reactivation might be needed for all grid points to adjust to the updated computational domain, in order to satisfy the convergence criteria. On the other hand, reactivation was found to be beneficial to the accuracy of results, so that longer periods of reactivation may improve the overall accuracy of the approach. These variations to the application of the DDM are investigated in the sections below. Section 5.2 presents the test setup and coding convention of the simulations considered. Sections 5.3 to 5.6 present the performance of the various model configurations tested, which is discussed in Section 5.7. Section 5.8 closes with the conclusions drawn from these investigations.

5.2 Test setup and coding convention

Based on the definitions given in Section 3.3, three types of simulations were applied in the investigation of the DDM technique, namely benchmark, reference and control runs (see Tabel 5.1). Three different settings of the DDM approach were applied in three variants of the control run. Based on the recommendation of WL (2007), all DDM simulations in the control run featured deactivation criteria based on the convergence curvature-based convergence criteria proposed by Zijlema and Van der Westhuysen (2005), extended to include also the curvature of the mean period T_{m01}. These also correspond to the overall convergence criteria applied in this study (Section 3.2).

Run code	Description
B_r00_d00	Benchmark run, continued up to 80 iterations
R_r00_d00	Reference run, using convergence criteria
C_r05_d01	DDM run, with refreshment interval of 5 iterations
C_r10_d01	DDM run, with refreshment interval of 10 iterations
C_r10_d05	DDM run, refresh every 10 iterations, for 5 iterations

Table 5.1 Coding convention of the applied model settings to investigate the DDM.

The three types of control runs vary with respect to the reactivation schedule discussed in Section 5.1. The first variant of the control run (code C_r05_d01) features the reactivation scheme recommended by WL (2007), namely a fully activated domain during the first 5 iterations, followed by reactivation of the entire computational domain every 5 iterations. In the second control run variant (code C_r10_d01), the interval of reactivation is increased to 10 iterations, again with the entire domain active during the first five iterations. The third control run variant (code C_r10_d05) investigates a prolonged reactivation of the computational domain: the domain is reactivated every 10 iterations, and remains activated everywhere for 5 iterations. These reactivation schemes are visualized in Table 5.2 below

Run code	Iteration																									
	1	2	3	4	5	6	7	8	9	10	11	12	13	14	15	16	17	18	19	20	21	22	23	24	25	...
C_r05_d01	■	■	■	■	■					■					■					■					■	
C_r10_d01	■	■	■	■	■					■										■						
C_r10_d05	■	■	■	■	■					■	■	■	■	■						■	■	■	■	■		

Table 5.2 Reactivation schedule of the DDM applied in the various control runs. Shaded blocks indicate iterations during which the entire computational domain is considered (activated).

These settings of the DDM were invoked by extending the input command in the subroutine SWREAD, contained in the source code swanpre1.ftn, to the following:

```
!
! ================================================
!
!   DDM [freshfr] [freshdur]
!
! ================================================
!
      IF (KEYWIS('DDM')) THEN                                          40.DDM
          IDDM = 1                                                     40.DDM
          CALL ININTG('FRESHFR',FRESHFR,'STA',5)                       40.DDM
          CALL ININTG('FRESHDUR',FRESHDUR,'STA',1)                     40.DDM
          WRITE(PRINTF,*)'DDM routine: FRESHFR=',FRESHFR,              40.DDM
     &                               'FRESHDUR=',FRESHDUR              40.DDM
         GOTO 100                                                      40.DDM
      ENDIF                                                            40.DDM
```

in which the parameter [freshfr] gives the reactivation interval in number of iterations (default value 5), and the parameter [freshdur] gives the number of iterations that the computational domain is reactivated (default value 1). The command for the reactivation of computational grid points (at the top of the subroutine SWCOMP in the source code swancom1.ftn) has correspondingly been adapted:

```
!---       Control the number of inactive geo points for this iteration   40.DDM
           IF ((ITER.LE.5).OR.(MOD(ITER,FRESHFR).LT.FRESHDUR)) THEN
              SLEEP(:)=.FALSE.
           ENDIF
```

which results in the reactivation schedule presented in Tabel 5.2 above.

5.3 Grid point deactivation patterns

Figures 5.1 to 5.9 illustrate the deactivation of the computational grids for the various field cases for selected storm instants and DDM settings. Figures 5.1 to 5.3 present the geographical distribution of active computational grid points (blue dots) in the simulation of the Amelander Zeegat field case of 2 January 2005 at 10:00 (flood). Figure 5.1 shows these results for the control run C_r05_d01 (reactivation every 5 iterations) at selected iteration levels just before reactivation. It can be seen that the number of active grid points gradually decreases during the simulation. At iteration 9, a large part of the computational domain is still active, but parts of the Wadden Sea interior have been deactivated. After 14 iterations, the active region has been reduced to the surf zones on the North Sea side of the barrier islands and the mainland coast, in the tidal inlet, and less than half of the grid points in the Wadden Sea interior. In Figures 3.2 and 3.3 it can be seen that these are the locations with the strongest variations in wave condtions. This trend is continued, so that after 34 iterations, only a small percentage of grid points remain. This behaviour agrees with the findings of WL (2007) for similar cases.

This result can be contrasted to that of the control run C_r10_d01 (reactivation every 10 iterations). Up to 14 iterations the results are identical to those discussed above. However, at iteration 19, fewer grid points are active than for the run C_r05_d01 (Figure 5.1). This is due to not reactivating the domain at iteration 15 (see Table 5.2). By contrast, at iteration 24 (after reactivation at iteration 20), the present case has more active grid points than run C_r05_d01. This alternating pattern is repeated for iterations 29 and 34. The corresponding results for the control run C_r10_d05 (reactivation every 10 iterations, remaining active for 5 iterations) is presented in Figure 5.3. Interestingly, this run has a very similar activation pattern to run C_r10_d01 for iterations 19 and 29,

despite the prolonged reactivation periods, including iterations 14, 24 and 34 (compare with Figure 5.2).

Figure 5.4 presents a comparative overview of the deactivation behaviour of these three control runs for all three Amerlander Zeegat cases. This figure presents the percentage of active grid points in the computational domain[2]. All three DDM settings tend towards a reduction in the percentage of grid points, but at different speeds due to the differing reactivation schedules. The top panel of Figure 5.4 shows that run C_r05_d01 generally has more active grid points than run C_r10_d01 due to the frequent reactivation (bringing the percentage of active points back to the maximum). However, after 9 iterations of deactivation of grid points, the reactivation in run C_r10_d01 appears to affect more grid points locally in iteration space than in run C_r05_d01 (between iterations 21-24, 31-34, and so on), as seen Figure 5.2 above. Run C_r10_d05 displays strong drops in the percentage of active points after each prolonged period of forced activity, suggesting that these reactivation periods promote convergence (and hence grid point deactivation). Also apparent in this graph is that the control run C_r05_d01, featuring frequent reactivations, continues for the most iterations of the three runs. This issue is discussed in Section 5.5 below. The remaining panels of Figure 5.4 presents the results for the remaining two storm instants (slack and ebb), which show similar results to those desribed above.

Figure 5.5 presents an example of the geographical distribution of grid point deactivation for the Eems-Dollard field case (1 November 2006 at 03:00, flood). The results are shown for the control run C_r05_d01 (reactivation every 5 iterations). As found for the Amelander Zeegat above, the number of active grid points gradually reduces during the simulation (between regular reactivation steps). For the Eems-Dollard field case, the first region to be deactivated is again the Wadden Sea interior (iteration 9). Thereafter, by iteration 19, the region offshore of the barrier island surf zone has been deactivated. Subsequently, by iterations 29 to 39 only the sheltered regions (behind islands and up the estuary toward Delfzijl) are active, where young wave fields are found. Figure 5.6 presents an overview of the deactivation activity for all the investigated Eems-Dollard control runs and storm instants. Comparison with Figure 5.4 confirms that for the Eems-Dollard the DDM displays similar alternating behaviour as in the Amelander Zeegat.

Figures 5.7 and 5.8 present the spatial patterns of grid point deactivation for the less complex Petten and Lake Sloten field cases. Figure 5.7 shows that for the Petten field case the active computational domain is quickly (after 19 iterations) reduced to only the narrow coastal strip including the surf zone and the Marsdiep tidal inlet (which is outside the area of interest in the present study). Figure 5.8 presents the deactivation pattern for Lake Sloten. It can be seen that the deactivation of grid points starts over the downwind region, and gradually spreads in the upwind direction towards the younger part of the wave field at the start of the fetch. Figure 5.9 summarizes the deactivation behaviour of the DDM for these two field cases, which shows similar behaviour to that of the regions discussed above (compare Figures 5.4 and 5.6).

2. *From this total the percentage of permanently inactive dry points is subtracted, so that the total does not always reach 100%.*

5.4 Efficiency

Tables 5.3 to 5.5 summarise the total CPU time and number of iterations for each of the DDM simulations investigated. These results show that application of the DDM technique succeeds in significantly reducing the total simulation time of SWAN for all but one simulation. The reduction in simulation time afforded by the DDM varies with the reactivation settings applied, with the C_r10_d01 control run yielding the greatest saving (average of about 50%), and the C_r05_d01 and C_r10_d05 control runs somewhat less (about 35% on average).

Inspecting the results in more detail, for example for the Amelander Zeegat field case, it can be seen that the C_r05_d01 control runs use significantly more iterations than their corresponding reference runs. This implies that a large number of quick iterations are executed during the simulation, in agreement with the small number of active grid points, as seen in Figure 5.1. By contrast, fewer iterations are used in the C_r10_d01 and C_r10_d05 control runs, suggesting better iteration behaviour. In Section 5.5 it will be shown that this difference in iteration behaviour is related to the frequent reactivations applied in the C_r05_d01 runs. Comparison of the total CPU time at the three tidal instants of the Amelander Zeegat field case reveals that the simulations at slack tide appear to have marginal reductions in CPU time due to the DDM than the other instants. This suggests that the slight drop in performance of the DDM is related to the presence of the strong currents in the simulation domain in these cases, in agreement with WL (2007).

Run code	AZG3a 10:00 (flood)		AZG3a 12:00 (slack)		AZG3a 17:00 (ebb)	
	N_{iter}	T_{cpu} [min (% ref)]	N_{iter}	T_{cpu} [min (% ref)]	N_{iter}	T_{cpu} [min (% ref)]
B_r00_d00	80	126	80	132	80	129
R_r00_d00	41	65	46	76	37	60
C_r05_d01	63	41 (63%)	59	44 (58%)	54	39 (65%)
C_r10_d01	37	28 (43%)	38	31 (41%)	37	28 (47%)
C_r10_d05	37	40 (62%)	38	43 (57%)	37	41 (68%)

Table 5.3 Number of iterations and CPU time of the DDM simulations for three storm instants on 2 January 2005 in the Amelander Zeegat.

Run code	Eems3a 3:00 (flood)		Eems3a 6:30 (slack)		Eems3a 9:30 (ebb)	
	N_{iter}	T_{cpu} [min (% ref)]	N_{iter}	T_{cpu} [min (% ref)]	N_{iter}	T_{cpu} [min (% ref)]
B_r00_d00	80	208	80	210	80	208
R_r00_d00	43	114	43	115	46	120
C_r05_d01	64	80 (70%)	59	81 (70%)	69	86 (72%)
C_r10_d01	39	54 (47%)	39	56 (49%)	47	62 (52%)
C_r10_d05	39	69 (61%)	39	71 (62%)	47	84 (70%)

Table 5.4 Number of iterations and CPU time of the DDM simulations for three storm instants on 1 November 2006 in the Eems-Dollard.

Run code	Petten		Lake Sloten	
	N_{iter}	T_{cpu} [min (% ref)]	N_{iter}	T_{cpu} [min (% ref)]
B_r00_d00	80	148	80	109
R_r00_d00	30	57	30	41
C_r05_d01	53	44 (77%)	79	50 (122%)
C_r10_d01	28	29 (51%)	39	27 (66%)
C_r10_d05	37	48 (84%)	34	35 (85%)

Table 5.5 Number of iterations and CPU time of the DDM simulations for one storm instant at Petten and in Lake Sloten.

The performance of the DDM in the Eems-Dollard field case is comparable, though somewhat less positive than for the Amelander Zeegat. It is interesting to find that the DDM shows the least reduction in simulation time in the simpler field cases of Petten and Lake Sloten, and even an increase in one case. This suggests that the least promising performance of the DDM (least gains in speed) is found for such relatively simple geometries without current.

5.5 Iteration behaviour

Figures 5.10 to 5.38 present the iteration behaviour of the DDM simulations of the various field cases. Figures 5.10 to 5.18 show this iteration behaviour for the Amelander Zeegat, for the storm instant of 2 January 2005 at 10:00 (flood). Figures 5.10 to 5.12 present these results for the control run C_r05_d01 at three output (test) points. The lower four panels of these figures show that all three test points are deactivated for the first time somewhat before convergence is reached. This can be seen by the departure of their iteration curves from those of the reference run. Test point 3 (Wadden Sea interior) can be seen to deactivate the earliest of the three. Nonetheless, all three test points are regularly reactivated, so that they still approximate the iteration curve of the reference run reasonably well. It can be seen, however, that the control run performs significantly more iterations than the reference run.

The upper left-hand panel in Figures 5.10 to 5.12 presents the progress of the percentage of accepted grid points during the simulation. It can be seen that the percentage of accepted grid points of the control run is consistently below that of the reference run. Also, this plot of accepted points strongly oscillates. Both these results are related to the reactivation of the computational grid every 5 iterations. Upon reactivation of the total computational domain, the updating of formerly deactivated grid points with information from surrounding grid points can cause large changes in wave parameters. As a result, significant numbers of grid points formerly considered converged and deactivated may not be assessed as converged any longer. This results in substantial drops in the percentage of converged points at intervals of 5 iterations (in the case of C_r05_d01). After this drop, the percentage of converged points can be seen to rise fast in subsequent iterations. However, since the interval to the next reactivation is only five iterations, it is possible that the next reactivation is reached (and hence another drop in overall convergence) before the overall convergence criteria are met. In this way, the point of run termination can be postponed, perhaps unnecessarily, until much later than the reference run.

This unwanted behaviour can be addressed by increasing the intervals between reactivation of the computational grid, such as done in the control run C_r10_d01 (from every 5 iterations to every 10 iterations). Figures 5.13 to 5.15 present the iteration behaviour for this DDM setting. The top left-hand panel of these figures shows the progression of accepted points for this DDM setting, which differs significantly from that discussed above. The drops in the percentage of accepted points following each reactivation step (every 10 iterations) are very pronounced. In subsequent iterations, however, the percentage of accepted points rises sharply, at times surpassing that of the reference run. Finally, this control run is able to reach the required level for run termination significantly sooner than for the control run C_r05_d01 considered above. However, the four lower panels of Figures 5.13 to 5.15 show that the iteration behaviour of the integral parameters features more abrupt corrections at each reactivation step than for the option C_r05_d01, removing them further from those of the reference run. This can lead to the iteration evolution of these parameters not following closely enough on the reference run (e.g. H_{m0} in Figure 5.14) or even overshooting this evolution (e.g. H_{m0} in Figure 5.15). In Section 5.6 it will be shown that these mismatches can lead to significant convergence errors relative to those of the reference run.

Figures 5.16 to 5.18 present an example of the behaviour of the third DDM setting (C_r10_d05), in which the reactivation every tenth iteration is sustained for five iterations. With this setting, it is intended to allow the wave field more iterations to adjust after reactivation, thereby improving the iteration behaviour and hence the accuracy. The top panel of these figures shows that the progression of converged points is smoother than for the run C_r10_d01, although still strongly variable. Drops in the percentage of accepted points are found both at the start and end of reactivation periods, as the wave field adapts itself. However, globally the convergence is fast, and convergence is reached earlier than in the reference run. The lower panels of Figures 5.16 to 5.18 shows that the iteration behaviour of the control run benefits from the prolonged periods of reactivation, now following that of the reference run better than the other investigated DDM options (compare H_{m0} in Figures 5.11, 5.14 and 5.17).

Strong differences between the three control runs can also be seen when considering the results over the tidal cycle of the Amelander Zeegat. Above the results for the flood condition was discussed. Figures 5.19 to 5.21 and 5.22 to 5.24 present the iteration behaviour for slack and ebb storm instants, at test point 3. At this output location, the young wave field is strongly affected by tidal currents ranging between 0.5 and 1.5 m/s, causing slow variation in the wave field (see also discussion in WL (2007)). Comparison of the results of the three DDM options for this output location over the tidal cycle shows that the control run C_r10_d05, with prolonged reactivation is the most successful in following the iteration behaviour of the reference run.

The iteration behaviour of the Eems-Dollard field case resembles that of the Amelander Zeegat presented above. Figures 5.25 to 5.32 give an overview of these results for the C_r05_d01 and C_r10_d05 control runs. In Section 5.6 the control run C_r10_d01 will be shown to yield unfavourable model accuracy. Therefore, for economy, the iteration behaviour of this setting has not been included in the following. Figures 5.25 to 5.30 present the iteration behaviour of the selected two control runs for the storm instant of 1 November 2006 at 03:00 (flood) at three output locations. The top left-hand panels of these figures show similar progression of the percentage of accepted points as found for the Amelander Zeegat. More rapid, but less smooth behaviour is found for control run C_r10_d05 (Figure 5.28) than for control run C_r05_d01 (Figure 5.25). As found for the Amelander Zeegat, the iteration behaviour of the run C_r10_d05 follows that of the reference run more closely than the control run C_r05_d01, in particular for test

location 3 where convergence is slow (compare Figures 5.27 and 5.30). Figures 5.31 and 5.32 confirm these differences at test location 3 for the ebb condition of 1 November 2006 at 09:30.

Figures 5.33 to 5.36 present the iteration behaviour of the DDM for the Petten field case for the control runs C_r05_d01 and C_r10_d05. The top left-hand panels of these figures show the progression of accepted points to be similar to those found for the field case presented above, with the control run C_r10_d05 producing the better results in terms of number of iterations and differences with the reference run. In Section 5.3 it was shown that during DDM simulations the active computational domain is soon reduced to only the surf zone. Figures 5.33 and 5.35 show the iteration behaviour at the test point 1 in the offshore. Here convergence is indeed reached fast (at least for significant wave height and mean period), so that the performance of the C_r05_d01 and C_r10_d05 runs are quite similar. However, at test point 3 in the surf zone the convergence is slow. Here the control run C_r10_d05 displays better iteration behaviour than control run C_r05_d01 (compare Figures 5.34 and 5.36).

Finally, Figures 5.37 and 5.38 present the iteration behaviour of the DDM found for the Lake Sloten field case. The top left-hand panels of these figures show that the progression of converged points is poor for both control runs. Control run C_r05_d01 displays significant drops in the percentage of converged points during reactivation steps, and as a result only terminates the simulation at 79 iterations. As seen in Table 5.5, this even results in an increase in simulation time relative to the control run. Control run C_r10_d05 does terminate in approximately the same number of iterations as the reference run, but the number of accepted points falls very strongly during reactivation cycles in the process. A likely cause of this behaviour is the fact that, for this field case, the downwind grid points are deactivated before the upwind points (refer Figure 5.8). As a result, during the reactivation steps, large parts of the computational grid need to be updated to upwind changes. This situation is principally different from the case where only the surf zone remains active, such as in the Petten field case. Figures 5.37 and 5.38 also show that the control run C_r10_d05 produces better iteration behaviour at test location 3 (measurement station SL29) than control run C_r05_d01, in agreement with the results of the other field cases considered

5.6 Convergence error

In this section, the influence of the DDM technique on the model accuracy is presented, as expressed in terms of convergence error. Tables 5.6 to 5.9 compare the convergence errors of the investigated control runs with the reference runs for all cases considered. These mean convergence errors have been computed as described in Section 3.5.3, namely the absolute value of the difference between the converged result of the investigated simulation (reference or control) and the benchmark result, averaged over the evaluation area. In addition to having been averaged over the evaluation area, to create an overview, the convergence errors for the Amelander Zeegat and Eems-Dollard cases have also been averaged over the tidal cycle (flood, slack and ebb). However, these tidal instants are considered separately in the discussion below.

Run code	$\mu(H_{m0})$ [%]	$\mu(T_{m-1,0})$ [%]	$\mu(\mathrm{Dir})$ [^{0}]	$\mu(\mathrm{Dspr})$ [%]
R_r00_d00	0.147	0.228	0.392	0.674
C_r05_d01	0.292	0.430	1.039	1.561
C_r10_d01	0.588	0.895	1.639	2.813
C_r10_d05	0.293	0.478	1.014	1.584

Table 5.6 Average differences in wave parameters for the DDM method for three storm instants on 2 January 2005 in the Amelander Zeegat. Computed as the mean of μ(.) for each parameter over the three storm instants.

Run code	$\mu(H_{m0})$ [%]	$\mu(T_{m-1,0})$ [%]	$\mu(\mathrm{Dir})$ [^{0}]	$\mu(\mathrm{Dspr})$ [%]
R_r00_d00	0.201	0.248	0.424	0.809
C_r05_d01	0.425	0.455	0.991	1.566
C_r10_d01	1.290	1.210	2.103	3.033
C_r10_d05	0.560	0.598	1.203	1.774

Table 5.7 Average differences in wave parameters for the DDM method for three storm instants on 1 November 2006 in the Eems-Dollard. Computed as the mean of μ(.) for each parameter over the three storm instants.

Run code	$\mu(H_{m0})$ [%]	$\mu(T_{m-1,0})$ [%]	$\mu(\mathrm{Dir})$ [^{0}]	$\mu(\mathrm{Dspr})$ [%]
R_r00_d00	0.118	0.249	0.301	0.566
C_r05_d01	0.175	0.522	0.503	0.678
C_r10_d01	0.468	1.352	0.792	2.112
C_r10_d05	0.140	0.373	0.381	0.619

Table 5.8 Average differences in wave parameters for the DDM method for one storm instant at Petten.

Run code	$\mu(H_{m0})$ [%]	$\mu(T_{m-1,0})$ [%]	$\mu(\mathrm{Dir})$ [^{0}]	$\mu(\mathrm{Dspr})$ [%]
R_r00_d00	0.632	0.579	0.586	1.106
C_r05_d01	0.553	0.513	0.658	0.950
C_r10_d01	1.413	1.183	1.562	1.441
C_r10_d05	0.886	0.724	0.837	1.281

Table 5.9 Average differences in wave parameters for the DDM method for one storm instant in Lake Sloten.

From these tables it can be seen that the application of the DDM technique in the control runs generally results in larger convergence errors (differences in results with respect to the benchmark runs) than for the reference runs. It can also be seen that these convergence errors depend on the type of field case considered, and also varies strongly with the DDM settings applied, as suggested by the results in Section 5.5 above. For the complex field cases of the Amelander Zeegat and the Eems-Dollard, the control runs C_r05_d01 and C_r10_d05 perform rather similarly, and produce about a doubling of the convergence error of the reference run. For the Petten and Lake Sloten cases, these DDM settings produce convergence errors of the same order as those of the reference runs. By contrast, the control run C_r10_d01, with less frequent reactivation, typically yields 4-5 times larger convergence errors than the reference run.

Figures 5.39 to 5.56 present examples of the spatial distribution of the convergence errors given above. Figures 5.39 to 5.44 present the distribution of these errors for the Amelander Zeegat storm instant of 2 January 2005 at 10:00 (flood), the same condition as presented in detail in Section 5.5. Figures 5.39 and 5.40 show that in the control run C_r05_d01 the increases in the convergence errors in the significant wave height, mean period, mean direction and spreading are restricted to the Wadden Sea interior. The error in the significant wave height is similar to that of the reference run (1.5%) in the tidal inlet, but increases for various locations in the Wadden Sea interior (to again 1.5%). Errors in the mean period increase gradually toward the mainland coast, reaching values of 5%. The strongest increases in convergence error are found for the directional spreading, showing errors exceeding 5% over large regions, and the mean direction, which have isolated errors exceeding 5^o. The results of the control run C_r10_d01 are similar in pattern to those for C_r05_d01, but greater in magnitude (Figures 5.41 and 5.42). For this case, the convergence error in the directional spreading exceeds 5% over the greater part of the Wadden Sea interior, and large errors in the mean direction ($>5^o$) and period (>5%) are widespread in this region. For the mean period, notable increases in convergence error now also extend to the ebb tidal delta. Figures 5.43 and 5.44 present the corresponding results for the control run C_r10_d05. These can be seen to agree well in terms of pattern and magnitude with those of control run C_r05_d01 presented above.

An indication of the influence of the tidal cycle and currents on the convergence errors of the DDM is obtained by considering the addition storm instants of 12:00 (slack) and 17:00 (ebb) during the 2 January 2005 storm in the Amelander Zeegat. Figures 5.45 to 5.48 present these results for the control run C_r10_d05. Comparison with Figures 5.43 and 5.44 shows that the increase in the convergence error for significant wave height and mean period are lower than found for the investigated flood instant. For the ebb storm instant, the convergence error in the directional spreading, and in particular in the mean direction, can be seen to reduce by the same degree as during flood (compare Figures 5.44 and 5.48). These results therefore suggest an influence of the tidal instant on the accuracy of the DDM, in agreement with WL (2007).

Figures 5.49 to 5.52 present the convergence errors for the Eems-Dollard field case for the 03:00 (flood) and 09:30 (ebb) instants of the storm of 1 November 2006. The results are presented for the control run C_r10_d05, which closely resemble those of C_r05_d01. Figures 5.49 and 5.50 show the results at the flood instant, which display increases in the convergence error for the mean period in the Wadden Sea interior of up to 5% in places, and local increases of up to more than 5^o and 5% in mean direction and especially directional spreading. Figures 5.51 and 5.52 show similar, but less intense increases in the convergence error of the mean period, mean direction and directional spreading for the ebb storm instant. These results can be considered to generally resemble those of the Amelander Zeegat.

Figures 5.53 and 5.54 present the convergence errors for the Petten field case of 1 January 1995 at 10:00, as obtained by the control run C_r10_d05. These figures show that the small convergence errors of the reference run are well reproduced by this DDM setting, as was seen in Table 5.8. It is noted that the control run C_r05_d01 achieves similar good results (not shown). Finally, Figures 5.55 and 5.56 present the convergence errors for the Lake Sloten field case of 27 October 2002, for the control run simulation C_r10_d05. Figure 5.55 shows some increase in the convergence error of the mean period, in particular towards the downwind shoreline of the lake. Likewise, Figure 5.56 shows small increases in the convergence error of the mean direction and

directional spreading. It is noted that the convergence error for the control run C_r05_d01, not included in the figures, have similar spatial distributions to those shown, but a somewhat smaller magnitude in general (as reflected in Table 5.9).

5.7 Discussion

In the sections above the performance of the DDM was investigated for a number of different test cases, using three settings for the regular reactivation of the computational grid. It was found that the performance of the DDM, in terms of computational time, iteration behaviour and accuracy strongly depends on the choice of these reactivation criteria. The DDM option of C_r05_d01 (reactivation of the computational grid every 5 iterations) proved to produce a high number of iterations, since the frequent reactivation reduces the rate at which grid points are considered to be converged by the overall convergence criteria. This high number of iterations, although performed fast, may be considered as unwanted model behaviour. Increasing the interval between reactivation steps (control run C_r10_d01) proved not to be an effective solution, since this setting leads to a large increase in convergence errors. By contrast, prolonging the period over which the reactivation takes place (C_r10_d05), proved successful in reducing the number of iterations used before the overall convergence criteria are satisfied. This setting of the DDM produced convergence errors of similar magnitude as with reactivation interval of 5 iterations (C_r05_d01), and is on average slightly faster for the cases considered.

The DDM, with the setting C_r10_d05, produces total simulation times that are consistently lower (about 35% in the Wadden Sea) than those of the reference run for the test cases considered. This method therefore appears to be a good candidate for reducing the computational time of SWAN. The cost for this increased speed is a doubling – on average – of the convergence error of the reference run. For the significant wave height and mean period these convergence errors appear to be acceptable. However, the convergence errors in the mean direction and directional spreading can exceed 5^{o} and 5% respectively in the Wadden Sea interior. These errors represent the weakest aspect of the current DDM implementation, which, due to the lack of inclusion of deactivation criteria based on directional parameters, fails to resolve the often slow convergence of these parameters.

5.8 Conclusions

In this section, the effectiveness of the Dynamical Deactivation Method (DDM) in the reduction of the CPU times of SWAN simulations was evaluated. The method was evaluated for a wide range of field test cases, including the Amelander Zeegat, the Eems-Dollard, the Dutch coast near Petten and Lake Sloten. A number of settings for the DDM were considered, all related to the sequence of regular reactivation of the computational gird. Based on the results of this investigation, the following can be concluded:

- The DDM technique succeeds in significantly reducing the total CPU time of SWAN for the wide range of field test cases considered, with an acceptable increase in model error relative to the standard model version.

- The effectiveness of this method depends strongly on the settings applied for reactivation of the computational gird, and to some degree on the physical

conditions modelled. From the variations studied, the most effective setting is a reactivation of the computational grid every ten iterations, sustained for 5 iterations (control run C_r10_d05).

- Using the setting proposed above, simulation times in the Wadden Sea are reduced by about 35% on average, with an average doubling of the convergence error. For the significant wave height and mean period, these convergence errors are found to reach up to respectively 1.5% and 5%, which appears to be acceptable. However, the convergence errors in the mean direction and directional spreading can become large, exceeding 5^{o} and 5% respectively in the Wadden Sea interior. These inaccuracies will require further development work to resolve.

6 Deactivation of the action limiter and quadruplet interaction in the surf zone

6.1 Introduction

In the surf zone, the processes of triad interaction and depth-induced breaking are typically dominant. Triad interactions transfer energy from the spectral peak towards higher and lower frequencies, creating characteristic shallow water spectra featuring a series of harmonics. Depth-induced breaking causes a high rate of energy dissipation, resulting in large energy losses over short spatial scales. Van der Westhuysen (2007) shows that the action limiter, used in SWAN to stabilize the iteration behaviour, can greatly increase the number of iterations required for model convergence in these shallow water regions. This happens because the action limiter has been developed for deep water application, with an f^{-5} shape, in close agreement to the high-frequency equilibrium shape of the frequency spectrum in deep water. As a result, only small changes in the action at high frequencies are allowed per iteration, slowing down the formation of higher harmonics and the rapid loss of energy through depth-induced breaking in the surf zone.

Van der Westhuysen (2007) shows that it can be beneficial to the convergence speed of SWAN, and hence to the total required simulation time, to deactivate the action limiter in the surf zone. This implies that the quadruplet interaction term, which the limiter is designed to stabilise, should also be deactivated in the surf zone. Van der Westhuysen (2007) recommends to use the Ursell number as a robust criterion for the deactivation of both the quadruplet term and the action limiter in the surf zone. Based on a limited dataset, Van der Westhuysen proposes to deactivate these model components where the Ursell number exceeds a value of 0.10. It is noted that the other nonlinear term, that of triad interactions, does not require the action limiter for stabilisation. This term is therefore not deactivated together with the action limiter.

In the present section, the above-mentioned recommendation of Van der Westhuysen (2007) for the reduction of simulation time of SWAN is investigated. The influence of the deactivation of the action limiter and quadruplet interaction on model performance is investigated for the eight field cases presented in Section 2. Since preliminary results indicated that the outcomes of this method depend strongly on the applied Ursell number limit, and since no clear guideline exist for its choice, a range of values for this limit is investigated. As done in the preceding sections, the impact on model performance is expressed in terms of the influence on the total simulation time, the iteration behaviour and the effect on the model outcomes. Section 6.2 presents the simulations conducted in this investigation. The simulation results and analysis are presented in Sections 6.3 to 6.6. Section 6.7 closes with conclusions.

6.2 Test setup and coding convention

Based on the definitions given in Section 3.3, three types of simulations were defined for investigating the deactivation of the limiter in the surf zone, namely benchmark, reference and control runs (see Tabel 6.1). In the control runs three different values of the Ursell number were used for the deactivation of the action limiter and quadruplet interactions, namely Ursell = 0.10, 0.15 and 0.20. It is noted that 0.10, suggested by Van der Westhuysen (2007), was not selected as the centre value in this series since

initial investigations showed that for this value the influence of this numerical technique can already extend far outside the surf zone (see Section 6.3 below). The Ursell number is given by the ratio of the relative amplitude, *a*/*d*, of the wave field (as a measure of its nonlinearity) to the square of its dimensionless depth, $(kd)^2$, (as a measure of its dispersion), and is computed in SWAN as follows:

$$Ur = \frac{(a/d)}{(kd)^2} \approx \frac{g}{8\sqrt{2}\pi^2}\frac{H_{m0}T_{m01}^2}{d^2} \tag{6.1}$$

In the surf zone the nonlinearity typically increases and the amount of dispersion decreases moving towards the shore. Therefore, the lower the value of the Ursell number limit is set, the greater the area over which the action limiter and quadruplet interaction will be deactivated. Hence, for the selected simulations in Table 6.1, the greatest impact of the investigated technique is found for the lowest Ursell number limit of 0.10 (run C_urs_010).

Run code	Description
B_urs_000	Benchmark run, continued up to 80 iterations
R_urs_000	Reference run, using convergence criteria
C_urs_010	Quadruplets deactivated at Ursell = 0.10
C_urs_015	Quadruplets deactivated at Ursell = 0.15
C_urs_020	Quadruplets deactivated at Ursell = 0.20

Table 6.1 Coding convention of the applied model settings to investigate the deactivation of the action limiter and quadruplet interaction in the surf zone.

6.3 Regions of activity

As an illustration of the working of the deactivation of the action limiter and quadruplet interactions in the surf zone, Figure 6.1 presents, for the four geographical regions considered, the areas over which the deactivation is invoked for the Ursell number limit of 0.10 (control run type C_urs_010). In this figure, the geographical areas over which the limiter is deactivated are shaded in blue.

In agreement with results shown by Van der Westhuysen (2007), the most clearly defined areas where the action limiter and quadruplets are deactivated are the regions leading up to and including the various surf zones in the model field cases, where higher Ursell numbers are found. For the Eems-Dollard field case, this region even extends all the way to the offshore model boundary. These regions decrease in size as higher values for the Ursell number limit is taken (results not shown). It is also striking to see that, in the case of the Amelander Zeegat, the region over which the Ursell number exceeds 0.10 also includes the Wadden Sea interior to some degree. In the case of Lake Sloten, the region where the limiter is deactivated is limited to the down-wind bank of the lake.

6.4 Timing

Tables 6.2 to 6.4 present an overview of the total simulation time required by the various simulations conducted here, including the three types of control runs with the Ursell number limit at 0.10, 0.15 and 0.20. These total CPU times have been estimated

using the technique described in Section 3.5.2. Given the results presented by Van der Westhuysen (2007), it could be expected that the application of the Ursell limiter would lead to reduced simulation times relative to the reference runs. Tables 6.2 to 6.4 show that this not the case in any of the investigated field cases. In fact, the method rather leads to an increase in total simulation time. In this regard, a clear pattern is that the lower the Ursell number limit (larger areas of deactivation), the larger increases in total simulation time. For the Amelander Zeegat and Eems-Dollard cases, no clear trend in simulation time changes with respect to tidal phase (flood, slack or ebb tide) can be seen. For the Lake Sloten case, for which the Ursell number is generally low (young waves and no clear surf zone), the simulation time was not affected. Hence, from the point of view of reducing the simulation time of SWAN, this method does not seem to be successful. These results therefore raise the question of why, despite apparently speeding up convergence in the surf zone, the total CPU can be increased. This issue is addressed in Section 6.5 below.

Run code	AZG3a 10:00 (flood)		AZG3a 12:00 (slack)		AZG3a 17:00 (ebb)	
	N_{iter}	T_{cpu} [min (% ref)]	N_{iter}	T_{cpu} [min (% ref)]	N_{iter}	T_{cpu} [min (% ref)]
B_urs_000	80	126	80	132	80	128
R_urs_000	41	66	46	76	37	60
C_urs_010	64	96 (145%)	73	114 (150%)	56	86 (143%)
C_urs_015	53	81 (123%)	66	106 (139%)	46	72 (120%)
C_urs_020	47	74 (112%)	53	86 (113%)	44	70 (117%)

Table 6.2 Number of iterations and CPU time for the deactivation of the action limiter for three storm instants on 2 January 2005 in the Amelander Zeegat.

Run code	Eems3a 3:00 (flood)		Eems3a 6:30 (slack)		Eems3a 9:30 (ebb)	
	N_{iter}	T_{cpu} [min (% ref)]	N_{iter}	T_{cpu} [min (% ref)]	N_{iter}	T_{cpu} [min (% ref)]
B_urs_000	80	211	80	209	80	209
R_urs_000	43	114	43	114	47	122
C_urs_010	70	174 (153%)	48	120 (105%)	59	147 (120%)
C_urs_015	52	133 (117%)	46	118 (104%)	49	125 (102%)
C_urs_020	56	144 (126%)	50	129 (113%)	51	130 (107%)

Table 6.3 Number of iterations and CPU time for the deactivation of the action limiter for three storm instants on 1 November 2006 in the Eems-Dollard.

Run code	Petten		Lake Sloten	
	N_{iter}	T_{cpu} [min (% ref)]	N_{iter}	T_{cpu} [min (% ref)]
B_urs_000	80	148	80	110
R_urs_000	30	56	30	41
C_urs_010	34	59 (105%)	30	41 (100%)
C_urs_015	34	62 (111%)	30	41 (100%)
C_urs_020	32	59 (105%)	30	41 (100%)

Table 6.4 Number of iterations and CPU time for the deactivation of the action limiter for one storm instant at Petten and in Lake Sloten.

6.5 Iteration behaviour

Figures 6.2 to 6.7 present the iteration behaviour in the Amelander Zeegat for the storm instant of 2 January 2005 at 10:00 (flood), at three different test (observation) points, for two different control runs (C_urs_010 and C_urs_020). The three test points differ strongly in terms of geographical location, and hence in terms of physical processes modelled (see Figure 2.2). It can be seen that for the test points 1 (directly behind the ebb tidal delta, e.g. Figure 6.2) and 2 (tidal channel, e.g. Figure 6.3) the iteration behaviour of the control run differs markedly from that of the reference run, whereas they are similar for the test point 3 (Wadden Sea interior, e.g. Figure 6.4). These differences are the greatest for the lowest Ursell limit of 0.10 (Figures 6.2-6.4), and smallest for the Ursell limit at 0.20 (Figures 6.5-6.7). In the case of the Ursell limit at 0.10 (C_urs_010), the converged mean direction at the test output location 1 differs by 4^o from that of the reference run, the directional spreading is reduced by 1.5^o and the significant wave height by about 3% (Figure 6.2). In essence, both the reference and control runs can be seen to converge well. Hence, given the differences in the converged results, more iterations are required by the control run to reach convergence from the common initial guess value. These differences in model behaviour, in particular the decrease in the directional spreading, can directly be related to the deactivation of quadruplet interactions in the surf zone, which is known to increase this parameter (e.g. Van Vledder 2006). The results at test point 2, also affected by the deactivation of the action limiter and quadruplet interactions, show similar but smaller differences with respect to the reference run. By contrast, the iteration behaviour at test point 3 in the Wadden Sea interior differs only marginally from that of the reference run. For the remaining investigated storm instants of the Amelander Zeegat, 2 January 2005 at 12:00 (slack) and 2 January 2005 at 17:00 (ebb), the changes to the iteration behaviour is similar in character to those described above.

Figure 6.8 to 6.13 show the iteration behaviour of the Eems-Dollard model case for the storm instant of 1 November 2006 at 3:00 (flood), at three different test points, for two different control runs (C_urs_010 and C_urs_020). These results largely resemble those presented for the Amelander Zeegat above. As seen for in the Amelander Zeegat, the three test points differ strongly in terms of physical processes modelled (Figure 2.2). For the test points 1 (offshore mouth tidal channel, e.g. Figure 6.8) and 2 (tidal channel, e.g. Figure 6.9) the iteration behaviour of the control run differs markedly from that of the reference run, whereas they are quite similar for the test point 3 (at the Eemshaven, e.g. Figure 6.10). These differences are the greatest for the lowest Ursell limit of 0.10 (Figures 6.8-6.10), and smallest for the Ursell limit at 0.20 (Figures 6.11-6.13). It is noted that for test point 3, the results of neither the reference nor the control runs are converged. For the remaining investigated storm instants, 1 November 2006 at 6:30 (slack) and 1 November 2006 at 9:30 (ebb), the changes to the iteration behaviour is similar in character to those described above.

Figures 6.14 to 6.16 present the iteration behaviour of the Petten field case at three test points namely 1 (offshore), 2 (outer surf zone) and 3 (inner surf zone). The Petten field case, which features a simple beach bathymetry, may be expected to show the best results for the present numerical technique. Indeed the top left-hand panel of Figures 6.14 to 6.16 show that the percentage accepted points of the control run closely matches, and sometimes even exceeds that of the reference run. Figure 6.14 shows that the offshore test location 1 converges fast, and that the iteration behaviour of the control run is only slightly different. By contrast, test point 3 (Figures 6.16) converges significantly slower. Here the deactivation of the action limiter in the control run can be

seen to speed up the convergence of the mean period $T_{m-1,0}$, in agreement with the findings of Van der Westhuysen (2007). However, the iteration behaviour and the converged levels of all integral parameters are significantly altered, presumably due to the deactivation of quadruplet interaction. As a result, the overall simulation time is not reduced. As found for the other field cases above, an increase in the Ursell limit to 0.20 decreases the differences between the iteration behaviour of the control and reference runs (results not shown).

Figure 6.17 presents the influence of the action limiter deactivation on the iteration behaviour of the Lake Sloten field case. It was seen in Figure 6.1 above that this field case features such low Ursell numbers that, even for the lowest Ursell number limit, the action limiter deactivation only affects the other fringes of the computational domain. As a result, Figure 6.17 shows that for this lowest Ursell limit (C_urs_010) the iteration behaviour of the control run cannot be distinguished from that of the reference run.

6.6 Convergence error

Tables 6.5 to 6.8 compare the convergence errors of the investigated control runs with the reference runs for all cases considered. These mean convergence errors have been computed as described in Section 3.5.3, namely the absolute value of the difference between the converged result of the investigated simulation (reference or control) and the benchmark result, averaged over a given evaluation area. In addition to having been averaged over the evaluation area, to create an overview, the convergence errors for the Amelander Zeegat and Eems-Dollard cases have also been averaged over the tidal cycle (flood, slack and ebb).

As suggested by considering the iteration behaviour presented in Section 6.5, the use of an Ursell number limit on the application of the action limiter and quadruplet interactions yields clear differences in model outcomes relative to the benchmark results. Since in Section 6.5 the benchmark, reference and control run results were all shown to be generally well-converged, the differences in outcomes shown in Tables 6.5 to 6.8 suggest that the applied technique has changed the modelled physics of SWAN (the source term balance). For the Amelander Zeegat, the Eems-Dollard and Petten, the largest mean changes to the model outcomes are found for the lowest setting of the Ursell number limit, namely 0.10 (C_urs_010), and reduces going towards a limit of 0.20 (C_urs_020). These convergence errors become particularly significant for the directional spreading. For the Lake Sloten field case, for which the Ursell number is generally low, the selected Ursell limits are too high to have any meaningful influence on the results.

Run code	$\mu(H_{m0})$ [%]	$\mu(T_{m-1,0})$ [%]	$\mu(\mathrm{Dir})$ [^{0}]	$\mu(\mathrm{Dspr})$ [%]
R_urs_000	0.147	0.228	0.392	0.674
C_urs_010	0.665	1.007	1.179	3.434
C_urs_015	0.443	0.535	0.660	1.975
C_urs_020	0.249	0.353	0.442	1.135

Table 6.5 Average differences in wave parameters for the deactivation of the action limiter for three storm instants on 2 January 2005 in the Amelander Zeegat. Computed as the mean of $\mu(.)$ for each parameter over the three storm instants.

Run code	$\mu(H_{m0})$ [%]	$\mu(T_{m-1,0})$ [%]	$\mu(\mathrm{Dir})$ [^{0}]	$\mu(\mathrm{Dspr})$ [%]
R_urs_000	0.201	0.248	0.424	0.809
C_urs_010	0.606	1.083	1.142	4.135
C_urs_015	0.458	0.712	0.786	2.265
C_urs_020	0.336	0.513	0.534	1.467

Table 6.6 Average differences in wave parameters for the deactivation of the action limiter for three storm instants on 1 November 2006 in the Eems-Dollard. Computed as the mean of $\mu(.)$ for each parameter over the three storm instants.

Run code	$\mu(H_{m0})$ [%]	$\mu(T_{m-1,0})$ [%]	$\mu(\mathrm{Dir})$ [^{0}]	$\mu(\mathrm{Dspr})$ [%]
R_urs_000	0.118	0.249	0.301	0.566
C_urs_010	0.485	1.536	1.514	13.217
C_urs_015	0.280	0.519	0.555	5.067
C_urs_020	0.170	0.255	0.350	2.364

Table 6.7 Average differences in wave parameters for the deactivation of the action limiter for one storm instant at Petten.

Run code	$\mu(H_{m0})$ [%]	$\mu(T_{m-1,0})$ [%]	$\mu(\mathrm{Dir})$ [^{0}]	$\mu(\mathrm{Dspr})$ [%]
R_urs_000	0.632	0.579	0.586	1.106
C_urs_010	0.636	0.598	0.583	1.237
C_urs_015	0.632	0.579	0.586	1.106
C_urs_020	0.632	0.579	0.586	1.106

Table 6.8 Average differences in wave parameters for the deactivation of the action limiter for one storm instant in Lake Sloten.

Figures 6.18 to 6.29 present the geographical distribution of the convergence errors of the investigated simulations. Figures 6.18 to 6.21 show the convergence errors of the Amelander Zeegat for the storm instant of 2 January 2005 at 10:00 (flood) with respect to the significant wave height, mean period, mean direction and directional spreading. Figures 6.18 and 6.19 show that for the Ursell number setting of 0.10 (C_urs_010), all four presented parameters are affected in a broad region along the North Sea shoreline of the barrier islands and a thin strip along the mainland coast of Friesland. This geographical region corresponds to that presented in Figure 6.1, showing the primary region of activity of this numerical method. As was seen in Table 6.5 above, the largest influence is felt in the directional spreading, which is strongly reduced in this region.

In addition to the activity of the Ursell-based limiting in the surf zone (the intended application area), it can be seen that for an Ursell number limit of 0.10 the results of the Wadden Sea interior behind the Amelander Zeegat are also affected. The significant wave height and mean period results are somewhat lower than the benchmark result, suggesting that wave growth has been slightly retarded here (See also Figure 6.4). In addition, the directional spreading has been reduced by a small degree over this region. These results are presumably due to the deactivation of quadruplet interactions in some areas. Figures 6.20 and 6.21 show that the observed model errors with respect to the benchmark results are significantly reduced when applying an Ursell limit setting of 0.20 instead of 0.10. Along the North Sea coast of the barrier islands the differences in

model outcomes with respect to the reference run are much smaller than for an Ursell limit of 0.10, and the results in the Wadden Sea interior are now identical to that of the reference run. For the remaining investigated storm instants of the Amelander Zeegat, 2 January 2005 at 12:00 (slack) and 2 January 2005 at 17:00 (ebb), the convergence errors of the control runs are similar in character and magnitude as those described above.

Figures 6.22 to 6.25 compare the convergence errors for the Eems-Dollard for the storm instant of 1 November 2006 at 3:00 (flood). Figures 6.22 to 6.23 present these results for the control run with an Ursell number limit at 0.10 (run C_urs_010). These figures show an overall increase in convergence errors, with similar patterns to those found in the Amelander Zeegat above. The most salient increases in the error are found on the North Sea coast of the barrier islands, for the mean wave period, mean direction and the directional spreading. As for the Amelander Zeegat, the directional spreading is strongly reduced over a large area in this region. The mean period is reduced over an equally widespread area, but by smaller amount. The convergence errors in the mean wave direction are increased more locally, but by up to 5^{o}. In the tidal channel, relatively smaller increases in the convergence error in the significant wave height are found. Figures 6.24 to 6.25 show that the observed model errors with respect to the benchmark results are significantly reduced when applying an Ursell limit of 0.20 instead of 0.10 (not shown). For the remaining investigated storm instants, namely 6:30 (slack) and 9:30 (ebb), convergence errors of comparable magnitude to those described above are found (results not shown).

Figures 6.26 and 6.27 present the convergence errors for the Petten field case found for the control run with an Ursell limit of 0.10 (run C_urs_010). It can be seen that all integral parameters are affected over a broad region along the coast, corresponding to the region of influence of the action limiter deactivation as shown in Figure 6.1. The influence of the directional spreading and mean wave period are particularly widespread. Large changes in the mean direction are found towards the north of the modelled region. These convergence errors reduce for the control runs with higher Ursell limit values (results not shown). For Lake Sloten, Figures 6.28 and 6.29 show that only slight changes (mostly increases in the convergence errors are found along the downwind banks of the lake.

6.7 Conclusions

In this section, the deactivation of the action limiter in the surf zone, and with it the quadruplet interaction term, was investigated as a means of reducing the simulation time of SWAN. This numerical technique was investigated for the full range of field cases defined in Section 2, and for various Ursell number limits for the initiating the deactivation. From the findings presented in this section, the following conclusions can be drawn:

- The investigated numerical technique of deactivating the action limiter and quadruplet interactions in the surf zone results in consistently longer simulation times than the reference run. In fact, the lower the Ursell number limit is chosen (greater influence of the method), the longer the simulation times tend to become.

- Application of the Ursell number limit does not seem to lead to better converged solutions in the test points considered. In fact, the omission of quadruplet

interactions appears to result in narrower directional spreading, and changes in the significant wave height, the mean period and the mean direction.

- Since both the simulation speed and model accuracy relative to the reference run is deteriorated by the use of the Ursell number limiter, it is not recommended to apply this approach for reducing the simulation time of SWAN in HBC computations.

7 Combination of Multigrid and DDM methods

7.1 Introduction

In Sections 4 to 6, three methods were investigated that are intended for the reduction of the computational time of SWAN, namely the Multigrid method, the DDM and the deactivation of the action limiter (and quadruplet interactions) in the surf zone. In the present section, it is investigated whether these methods can be combined to yield greater savings in computational time than found for these methods individually.

Regarding the Multigrid method, WL & Alkyon (2007b) concluded that this method is able to reduce the computational time of SWAN, by providing a computationally cheap initial estimate of the final solution on a computational grid with reduced resolution. In the present study, this finding has been reassessed using a larger set of field test cases and stricter convergence criteria (seen Section 3.2). In Section 4 of the present report it was found that, when using these stricter convergence criteria, the Multigrid method produces less positive results than found by WL & Alkyon (2007b), typically leading to increases in total simulation time. It therefore appears not desirable to apply the Multigrid method, in its present form, to speed up simulations - at least not on its own.

Regarding the DDM technique, both WL (2007) and Section 5 of the present study showed this method to be effective in reducing the simulation times of SWAN. However, analyses of the convergence errors of the DDM (see especially WL (2007)) have shown that this method can produce relatively large convergence errors in regions where strong currents are present. This was found to be due to the slow convergence of SWAN in these regions, for which the investigated criteria for the deactivation of computational grid points are less successful. With regard to this aspect, the DDM may benefit from being combined with the Multigrid method. The default second-generation first guess of SWAN, as used in the DDM, computes wave-current interaction with insufficient accuracy. Therefore, a large number of iterations are spent on correcting for the influence of currents in the subsequent third-generation iteration steps (see WL 2007).

In this regard, the application of the Multigrid method could provide an improved initial guess of the wave field, properly including the influence of current, which may improve the performance (accuracy) of the DDM technique. The combined model will therefore compute an initial guess simulation using the MG method, after which a full resolution run is started, for which the DDM is activated. Based on the conclusions of Section 4, only the Multigrid setting with reduced resolution in geographical space (Cx2y2d1s1) was considered suitable for this purpose. The Multigrid method with this setting was combined with the most successful DDM setting found in Section 5, namely reactivation of the computational grid every 10 iterations, sustained for 5 iterations.

At the start of this study, it was intended to also include in this combined numerical method the numerical technique investigated in Section 6, namely the deactivation of the action limiter in the surf zone. However, the results for this method presented in Section 6 showed improvement neither in simulation speed nor in model accuracy for this numerical technique. This method was therefore not considered in the combined method investigated here.

The structure of this section is the following: Section 7.2 presents the test setup and coding convention of the simulations considered. Sections 7.3 to 7.5 present the performance of the combined MG-DDM method, which is discussed in Section 7.6. Section 7.7 closes with the conclusions drawn from this investigation.

7.2 Test setup and coding convention

Table 7.1 presents the coding convention applied in this investigation. Based on the definitions given in Section 3.3, three types of simulations were applied, namely benchmark, reference and control runs. As discussed in the introduction, only one control run type is investigated in the present section, namely the combination of the Multigrid setting Cx2y2d1d1 (for the initial guess) with the DDM setting C_r10_d05. The run coding is comprised here as follows: C[multigrid setting]_[DDM setting]. Therefore, the resulting combined method has the run code C2211_105. As in Section 5, the DDM component of the control run featured deactivation criteria based on the convergence curvature-based convergence criteria proposed by Zijlema and Van der Westhuysen (2005), extended to include the curvature of the mean period T_{m01}.

Run code	Description
B1111_00	Benchmark run, continued up to 80 iterations
R1111_00	Reference run, using convergence criteria
C2211_105	Multigrid run with Cx2y2d1s1, DDM run with C_r10_d05, using convergence criteria

Table 7.1 Coding convention of the applied model settings to investigate the combination of the Multigrid and DDM methods.

7.3 Timing

Tables 7.2 to 7.4 below present an overview of the gain or loss in computational speed of the combined MG-DDM simulations relative to the reference run (standard SWAN), and the comparative number of iterations used. As in Section 4, the number of iterations of the initial guess and full resolution run phases are reported separately. For comparison, the results of the stand-alone DDM control run C_r10_d05, taken from Tables 5.3 to 5.5, have been included in these tables. It can be seen in these tables that the combined MG-DDM method is not able to consistently reduce the total CPU time of the investigated field cases. For the Wadden Sea field cases a general increase in simulation times are found (by up to 147% of the reference run), with the exception of one Amelander Zeegat case (2 January 2005 at 12:00, slack). By contrast, for the field cases with simpler geographical situations, namely Petten and Lake Sloten, the simulation times are found to be reduced. This result qualitatively agrees with that found with the stand-alone Multigrid simulations (Section 4). When comparing the MG-DDM results with the favourable performance of the stand-alone DDM included in these tables, the results of the Wadden Sea can be seen to be significantly worsened by the MG-DDM combination, and those of the Petten and Lake Sloten cases to be improved. Inspection of the tidal cycle in the Amelander Zeegat and the Eems-Dollard reveals that the changes in simulation times at slack are relatively more favourable than those at flood or ebb.

Run code	AZG3a 10:00 (flood)		AZG3a 12:00 (slack)		AZG3a 17:00 (ebb)	
	N_{iter}	T_{cpu} [min (% ref)]	N_{iter}	T_{cpu} [min (% ref)]	N_{iter}	T_{cpu} [min (% ref)]
B1111_000	80	126	80	132	80	129
R1111_000	41	65	46	76	37	60
C2211_105	42/47	66 (102%)	59/39	65 (86%)	41/58	73 (122%)
C_r10_d05*	37	40 (62%)	38	43 (57%)	37	41 (68%)

*Table 7.2 Number of iterations and CPU time for the combined MG-DDM method for three storm instants on 2 January 2005 in the Amelander Zeegat. *Stand-alone DDM control run (see Table 5.3).*

Run code	Eems3a 3:00 (flood)		Eems3a 6:30 (slack)		Eems3a 9:30 (ebb)	
	N_{iter}	T_{cpu} [min (% ref)]	N_{iter}	T_{cpu} [min (% ref)]	N_{iter}	T_{cpu} [min (% ref)]
B1111_000	80	208	80	210	80	208
R1111_000	43	114	43	115	46	120
C2211_105	70/77	168 (147%)	54/57	131 (114%)	80/67	159 (133%)
C_r10_d05*	39	69 (61%)	39	71 (62%)	47	84 (70%)

*Table 7.3 Number of iterations and CPU time for the combined MG-DDM method for three storm instants on 1 November 2006 in the Eems-Dollard. *Stand-alone DDM control run (see Table 5.4).*

Run code	Petten		Lake Sloten	
	N_{iter}	T_{cpu} [min (% ref)]	N_{iter}	T_{cpu} [min (% ref)]
B1111_000	80	140	80	109
R1111_000	30	57	30	41
C2211_105	41/17	43 (75%)	32/17	27 (66%)
C_r10_d05*	37	48 (84%)	34	35 (85%)

*Table 7.4 Number of iterations and CPU time for the combined MG-DDM method for one storm instant at Petten and in Lake Sloten. *Stand-alone DDM control run (see Table 5.5).*

7.4 Iteration behaviour

Figures 7.1 to 7.14 present examples of the iteration behaviour of the combined MG-DDM method for the various investigated field cases. Figures 7.1 to 7.3 present the iteration behaviour found for the Amelander Zeegat case of 2 January 2005 at 10:00 (flood) at three output locations. As in Section 4, these figures show the iteration behaviour of both the initial guess and full resolution phases of the control run. The top left-hand panel of these figures show the percentage of converged points. The initial guess phase can be seen to fulfil the convergence criteria at a similar rate as the reference run. The subsequent full resolution run phase does not exceed this rate of converged point acceptance, and again features the regular drops in accepted points during reactivation steps seen in Section 5. Hence, in terms of convergence speed, the full resolution run does not appear to benefit from the initial guess phase. In fact, comparison with Figure 5.16 shows that the number of iterations that the DDM requires for convergence has increased, explaining the increase in simulation time seen by comparing the C2211_105 and C_r10_d05 control run results in Table 7.2.

The lower panels of Figures 7.1 to 7.3 present the iteration behaviour of the integral parameters for this simulation. It can be seen that, at all output locations, the parameters of the initial guess run converge to values that are quite far removed from the converged values of the reference run, and often to not improve much on the second-generation first guess of the reference run. As a result, the subsequent DDM phase on the full resolution computational grid needs to make significant adjustments to the wave field before reaching convergence at values close to those of the reference run, comparable to the full resolution run behaviour in the stand-alone MG (see Section 4). This behaviour should be contrasted to that found for the stand-alone DDM, presented in Figures 5.16 to 5.18 and discussed above. By comparison of these figures with Figures 7.1 to 7.3 it can be seen that the MG initial guess unfortunately does not seem to contribute towards providing an improved starting position for the DDM at any of the test output locations.

To investigate the influence of the tidal cycle on these findings, Figures 7.4 and 7.5 show the corresponding iteration behaviour at 12:00 (slack) and 17:00 (ebb) for the test location 3 featuring a young local wave field exposed to the tidal current. Comparison of Figure 7.4 with Figure 5.21 (slack tide) shows that in the MG-DDM simulation the rate of compliance with the convergence criteria has increased in the DDM full resolution phase with respect to the stand-alone DDM (top left-hand panel). However, comparison of the iteration behaviour between these figures (note the different scales) shows that for the significant wave height and mean period the initial guess has not contributed towards providing an improved starting value for the full resolution DDM run phase. This behaviour is also found for the ebb case (2 January 2005 at 17:00). Comparison of Figures 7.5 and 5.24 (noting again the different scales) shows that the MG initial guess does not improve on the second-generation first guess of SWAN used in the stand-alone DDM, requiring a strong correction, and more iterations from the DDM than when applied stand-alone.

Figures 7.6 to 7.10 present examples of the iteration behaviour found in the Eems-Dollard field case. Figures 7.6 to 7.8 present the results at three test points for the storm instant of 1 November 2006 03:00 (flood). The upper left-hand panel of these figures show that percentage accepted point falls behind those of the reference run, in particular towards the end of the simulation. The progression of accepted points of the subsequent full resolution run with the DDM is poor. Comparison with Figure 5.30 (stand-alone DDM) shows that the percentage accepted points increase faster initially, but towards the end of the simulation performance deteriorates. Inspection of the iteration curves of the integral parameters shows that in a number of cases the MG initial estimate does indeed provide a favourable starting position to the DDM full resolution run phase. In some cases this appears to result in faster convergence of the full resolution run phase (e.g. curves of H_{m0} and $T_{m-1,0}$ in Figures 7.6 and 7.7). However, counter-examples are also found, such as the curve of H_{m0} at test point 3 (Figure 7.8). Here the significant wave height, despite having a starting value on the level of convergence, performs an excursion of about 5% before converging again to approximately the starting level. This suggests that here the underlying wave spectrum provided by the MG initial guess was still significantly removed from the converged solution unlike, perhaps, the case in Figure 7.6.

Figures 7.9 and 7.10 present the iteration behaviour of test point 3 (young wave field in strong ambient current) for the two remaining storm instants, namely 06:30 (slack) and 09:30 (ebb). The upper left-hand panels of these figures show that the slack and ebb tide cases have better performance (in terms of excepted points) than the flood case,

but it can still be considered poor relative to the stand-alone DDM (compare Figures 7.10 and 5.32). The lower four panels in these figures show no clear differences for these tidal instants with respect to the flood case. At both slack and ebb the initial guess run fails to produce results close to the converged solution, requiring many iterations in the full resolution DDM run phase.

The exception to these fairly negative results is found in the Petten and Lake Sloten field cases. Figures 7.11 and 7.12 present the iteration behaviour for the Petten field case for 1 January 1995 at 10:00, at the test points 1 and 3 respectively. The upper left-hand panels of these figures show fast convergence of both the initial guess and the full resolution DDM run phases in terms of percentage accepted points. The iteration behaviour presented in the lower four panels also show positive results. The initial guess provides a good starting position in all integral parameters, so that the full resolution run phase requires relatively few (17) iterations for convergence. This results in a shorter total simulation time than the stand-alone DDM. Hence, for this case the DDM method clearly benefits from the starting position offered by the Multigrid initial guess. Figures 7.13 and 7.14 present the iteration behaviour for the Lake Sloten field case for 27 October 2002 at 15:00, at the test points 1 and 3 respectively. These results show similar good performance as found for the Petten case. The initial guess run displays similar convergence speed, in terms of number of iterations, as the reference run (upper left-hand panels). From this initial run phase a good starting condition is obtained for all integral parameters, with the possible exception of the directional spreading at test point 1. This leads to fast convergence of the subsequent full resolution DDM run phase (17 iterations), to values close to the benchmark result.

7.5 Convergence error

Tables 7.5 to 7.8 below compare the convergence errors of the investigated control and reference runs for all cases considered. These mean convergence errors have been computed as described in Section 3.5.3, namely the absolute value of the difference between the converged result of the investigated simulation (reference or control) and the benchmark result, averaged over a given evaluation area. In addition to having been averaged over the evaluation area, to create an overview, the convergence errors for the Amelander Zeegat and Eems-Dollard cases have also been averaged over the tidal cycle (flood, slack and ebb). For comparison, these tables also include the results of the stand-alone DDM control run C_r10_d05, taken from Tables 5.6 to 5.9.

Run code	$\mu(H_{m0})$ [%]	$\mu(T_{m-1,0})$ [%]	$\mu(\mathrm{Dir})$ [^{0}]	$\mu(\mathrm{Dspr})$ [%]
R1111_000	0.147	0.228	0.392	0.674
C2211_105	0.261	0.361	1.001	1.247
C_r10_d05*	0.293	0.478	1.014	1.584

*Table 7.5 Average differences in wave parameters for the combined MG-DDM method for three storm instants on 2 January 2005 in the Amelander Zeegat. Computed as the mean of $\mu(.)$ for each parameter over the three storm instants. *Stand-alone DDM control run (see Table 5.6).*

Run code	$\mu(H_{m0})$ [%]	$\mu(T_{m-1,0})$ [%]	$\mu(\mathrm{Dir})$ [^{0}]	$\mu(\mathrm{Dspr})$ [%]
R1111_000	0.201	0.248	0.424	0.809
C2211_105	0.340	0.540	0.735	1.238
C_r10_d05*	0.560	0.598	1.203	1.774

*Table 7.6 Average differences in wave parameters for the combined MG-DDM method for three storm instants on 1 November 2006 in the Eems-Dollard. Computed as the mean of $\mu(.)$ for each parameter over the three storm instants. *Stand-alone DDM control run (see Table 5.7).*

Run code	$\mu(H_{m0})$ [%]	$\mu(T_{m-1,0})$ [%]	$\mu(\mathrm{Dir})$ [^{0}]	$\mu(\mathrm{Dspr})$ [%]
R1111_000	0.118	0.249	0.301	0.566
C2211_105	0.173	0.259	0.290	0.582
C_r10_d05*	0.140	0.373	0.381	0.619

*Table 7.7 Average differences in wave parameters for the combined MG-DDM method for one storm instant at Petten. *Stand-alone DDM control run (see Table 5.8).*

Run code	$\mu(H_{m0})$ [%]	$\mu(T_{m-1,0})$ [%]	$\mu(\mathrm{Dir})$ [^{0}]	$\mu(\mathrm{Dspr})$ [%]
R1111_000	0.632	0.579	0.586	1.106
C2211_105	0.274	0.312	0.197	0.490
C_r10_d05*	0.886	0.724	0.837	1.281

*Table 7.8 Average differences in wave parameters for the combined MG-DDM method for one storm instant in Lake Sloten. *Stand-alone DDM control run (see Table 5.9).*

Tables 7.5 to 7.8 show that the convergence errors for the combined MG-DDM method are consistently relatively low. For the Amelander Zeegat and Eems-Dollard cases, the relatively small convergence errors of the reference runs have been doubled, and for the Petten field case these errors are comparable to those of the reference run. For the Lake Sloten case, the convergence errors of the reference run have approximately been halved. Comparison with the DDM results included from Tables 5.6 to 5.8 shows that for the Amelander Zeegat, Eems-Dollard and Petten cases the convergence errors of the combined MG-DDM method are slightly, but consistently smaller than those of the stand-alone DDM. In this regard, the best result is found for the Lake Sloten case. The average model errors found with the DDM (being somewhat greater than those of the reference run) have been more than halved with the MG-DDM combination.

Figures 7.15 to 7.22 present examples of the spatial distribution of the convergence errors, as summarized in Tables 7.5 and 7.8 above. Shown in these figures are the convergence errors for the Amelander Zeegat case of 2 January 2005 at 10:00 (flood, Figures 7.15 and 7.16), the Eems-Dollard case of 1 November 2006 at 03:00 (flood, Figures 7.17 and 7.18), the Petten storm of 1 January 1995 at 10:00 (Figures 7.19 and 7.20), and for the Lake Sloten case of 27 October 2002 at 15:00 (Figures 7.21 and 7.22). Comparison of these figures with the results of Section 5 (Figures 5.43 to 5.56) shows that the patterns of the convergence errors are generally similar to those obtained with the stand-alone DDM: the Petten case shows no appreciable increases in convergence error in the control run, whereas in the Wadden Sea cases the errors are primarily found in the young wave fields in the Wadden Sea interior. As in the case of the stand-alone DDM, the largest convergence errors are found for the flood and ebb storm instants in the Amelander Zeegat and the Eems-Dollard (results not shown).

These results suggest that, regarding the influence of currents on the DDM reported by WL (2007), no significant improvement in model accuracy is obtained in the Wadden Sea when applying the Multigrid initial guess as a starting condition. An exception is found for the Lake Sloten field case (simple geometry, no currents). Comparison between Figures 7.21 and 7.22 (MG-DDM) and Figures 5.55 and 5.56 (DDM) shows that for this field case a notable improvement in accuracy is obtained with the MG-DDM combination, as was also seen in Table 7.8.

7.6 Discussion

In the present section it was investigated whether the combination of the Multigrid and DDM methods could lead to gains in computational speed or accuracy relative to these methods being applied individually. The premise of this approach was to apply the initial estimate of the Multigrid method to provide a well-converged starting position for the DDM simulation, in order to improve the latter's performance in situations of slow convergence (such as in ambient current). If this initial estimate would be closer to the converged result than that of the second-generation first guess, the DDM could yield faster simulation times and improved accuracy.

However, the simulation results of this section have shown that, in general, the Multigrid method does not yield a better first estimate of the converged wave field than the default second-generation first guess of SWAN. As a result, the DDM, applied in the subsequent full resolution run phase, typically requires more iterations (and hence longer simulation time) to reach convergence than when applied stand-alone. These results are most clearly seen or Wadden Sea cases, and found both in situations with and without current. For the flood and ebb situations with strong tidal currents, no significant improvement in model error was found relative to the stand-alone DDM results. Hence, the application of the Multigrid initial guess does not appear to improve the performance of the DDM in ambient current either in terms of speed or in accuracy. The only exceptions to these unsatisfactory results were found for Petten and Lake Sloten field cases, with simpler geometries and no ambient current.

From the iteration behaviour results of the combined MG-DDM method it appears important that the Multigrid component provides an accurate initial estimate in terms of the total wave spectrum, not just in terms of a select integral parameter such as the significant wave height. Based on the successful application in the Petten and Lake Sloten field cases, it appears that the Multigrid initial guess is able to produce such accurate spectra for relatively simple situations. This implies that, in addition to the conclusions drawn in Section 4, further development efforts of the Multigrid method should take into account the details of the spectra produced by the initial guess, particularly in more complex field cases such as the Wadden Sea.

7.7 Conclusions

In the present section, it was investigated whether the combination of the Multigrid (MG) and DDM methods, investigated individually in Sections 4 and 5, could lead to gains in computational speed or accuracy relative to the stand-alone application of these methods, and ultimately the default SWAN model. This combined MG-DDM method was investigated for the full range of field cases defined in Section 2, using the most successful settings for each individual method, as determined in Sections 4 and 5. From the findings presented in this section, the following conclusions can be drawn:

- The addition of the MG method to the DDM technique does not generally improve the performance of the DDM approach. In most cases investigated, the convergence errors reduce slightly relative to those found for the stand-alone DDM, but remain of the same order, whereas the simulation times increase strongly.

- From the iteration behaviour results of the combined MG-DDM method it appears to be important that the Multigrid component provides an accurate initial estimate in terms of the total wave spectrum, not just in terms of select integral parameters.

- The combined MG-DDM method yields improved results over the stand-alone DDM method only for the Petten and Lake Sloten field cases. This suggests that the MG-DDM combination is the most successful for field cases with simple geometries and physical conditions.

8 Efficiency of the DIA term

8.1 Introduction

The DIA (Discrete Interaction Approximation) is a way to compute the quadruplet wave-wave interactions. In the activity described in this chapter, two methods of improving the efficiency of computing the DIA source term will be investigated. Firstly, the application of the computationally faster nearest-neighbour version of the DIA (model setting IQUAD=8) will be investigated. Using the same set of eight test cases (Amelander Zeegat, Petten, Eems-Dollard and Lake Sloten) defined in Chapter 2, the simulation results produced by the model version with the nearest-neighbour DIA will be compared to those produced by the default model (model setting IQUAD=2). An evaluation will be made of the speed-up achieved by the nearest-neighbour DIA setting and the influence of this setting on model accuracy.

Secondly, the application of the Triplet method (Van Vledder 2005c) to the DIA will be considered. The Triplet method has been implemented by Gerbrant van Vledder in a dedicated version of SWAN, based on SWAN version 40.51A. The Triplet method can either be applied to the default version of the DIA (IQUAD=2), or to the nearest-neighbour (IQUAD=8) version. Therefore, the application of the Triplet method will be investigated in two ways, namely (a) a comparison between the results produced using the Triplet version of the standard DIA and those by the default method to compute the standard DIA, and (b) comparison between the results produced using the Triplet version of the nearest-neighbour DIA (IQUAD=8) and those by the default method to compute the standard DIA (IQUAD=2).

8.2 Test setup, coding convention and executables

For each of the eight field cases considered in Chapter 2, five model runs are executed:

- The benchmark run, carried out with the default model settings (e.g., the default version of the DIA (IQUAD=2) and default computation of the DIA) and continued up to 80 iterations.
- The reference run, carried out with the default model settings (e.g. the default version of the DIA (IQUAD=2) and default computation of the DIA) and using the convergence criteria as given in Section 3.2.
- A control run, carried out with the nearest-neighbour version of the DIA (IQUAD=8) and default computation of the DIA, and using convergence criteria.
- A control run, carried out with the Triplet method applied to the default version of the DIA (IQUAD=2), and using convergence criteria.
- A control run, carried out with the Triplet method applied to the nearest-neighbour version of the DIA (IQUAD=8), and using convergence criteria.

These five different model settings are summarized in Table 8.1.

Run code	Description
B_iq2_std	Benchmark run, continued up to 80 iterations
R_iq2_std	Reference run, iquad=2, default method to compute DIA
C_iq8_std	Control run, iquad=8, default method to compute DIA
C_iq2_tri	Control run, iquad=2, Triplet method to compute DIA
C_iq8_tri	Control run, iquad=8, Triplet method to compute DIA

Table 8.1 Coding convention of the applied model settings to investigate the efficiency of the DIA.

As mentioned before, the application of the Triplet method will be investigated in two ways, namely (a) a comparison between the results produced using the Triplet version of the standard DIA and those by the default method to compute the standard DIA, and (b) comparison between the results produced using the Triplet version of the nearest-neighbour DIA (IQUAD=8) and those by the default method to compute the standard DIA (IQUAD=2). In terms of run codes this means for (a) a comparison between C_iq2_tri and R_iq2_std, and for (b) a comparison between C_iq8_tri and R_iq2_std.

Concerning the applied executables, the following is noted:

- Application of the Triplet method requires some additional preprocessing. At present, this preprocessing needs to be executed outside SWAN, resulting in a Triplets database containing weights and indices, see also Van Vledder (2005c). The size of this database depends on the number of frequency and directional bins, and (primarily) on the selected DIA version (IQUAD=2 or IQUAD=8). The size of the database is therefore independent of the number of geographical grid points in the computational domain. For the selected spectral resolution, the size of the database is in the order of 0.6 MB for IQUAD=8 and 11 MB for IQUAD=2. Generation of this database is fairly trivial to do, and does not take much time from the user. The required CPU time to generate a database is small, typically in the order of 10 seconds. If the Triplet method turns out to be a useful functionality for SWAN, it may at some later stage be incorporated in the operational SWAN source code.

- All computations described in this chapter have been performed with a dedicated version of SWAN 40.51A, in which the Triplet method has been implemented by Gerbrant van Vledder. In its present implementation, the Triplet method does not consider interactions in a specific directional sector. Therefore, it can only compute the nonlinear transfer rate per iteration and not per sweep. Consequently, its implementation is equivalent to using the DIA with SWAN option IQUAD=3. The present implementation is also not suited (yet) for parallel computations based on OpenMP (as used in Sections 4 to 7), and therefore the simulations were done in single processor mode. The SWAN code has been compiled on a Linux operation system for running on a single processor. It has been verified that this executable gives identical results as SWAN version 40.51A on Linux for the default method to compute the DIA.

8.3 Timing

The number of iterations and CPU time are given in Tables 8.2 to 8.4 below.

Run code	AZG3a 10:00 (flood)		AZG3a 12:00 (slack)		AZG3a 17:00 (ebb)	
	N_{iter}	T_{cpu} [min (%ref)]	N_{iter}	T_{cpu} [min (%ref)]	N_{iter}	T_{cpu} [min (%ref)]
B_iq2_std	80	232	80	242	80	233
R_iq2_std	41	120	46	139	37	109
C_iq8_std	45	117 (98%)	51	138 (99%)	47	123 (113%)
C_iq2_tri	37	453 (378%)	50	662 (476%)	41	512 (470%)
C_iq8_tri	44	219 (183%)	53	276 (199%)	46	231 (212%)

Table 8.2 Number of iterations and CPU time for quadruplet investigation for three storm instants on 2 January 2005 in the Amelander Zeegat.

Run code	Eems3a 3:00 (flood)		Eems3a 6:30 (slack)		Eems3a 9:30 (ebb)	
	N_{iter}	T_{cpu} [min (%ref)]	N_{iter}	T_{cpu} [min (%ref)]	N_{iter}	T_{cpu} [min (%ref)]
B_iq2_std	80	381	80	378	80	380
R_iq2_std	43	205	44	209	46	218
C_iq8_std	48	206 (100%)	41	174 (83%)	41	173 (79%)
C_iq2_tri	54	1109 (541%)	45	921 (441%)	51	1071 (491%)
C_iq8_tri	50	408 (199%)	48	390 (187%)	44	355 (163%)

Table 8.3 Number of iterations and CPU time for quadruplet investigation for three storm instants on 1 November 2006 in the Eems-Dollard.

Run code	Petten		Lake Sloten	
	N_{iter}	T_{cpu} [min (%ref)]	N_{iter}	T_{cpu} [min (%ref)]
B_iq2_std	80	406	80	198
R_iq2_std	30	152	30	74
C_iq8_std	42	193 (127%)	35	75 (101%)
C_iq2_tri	37	706 (464%)	31	417 (564%)
C_iq8_tri	48	294 (193%)	34	151 (204%)

Table 8.4 Number of iterations and CPU time for quadruplet investigation for one storm instant at Petten and in Lake Sloten.

The most salient result from these tables is that the present implementation of the Triplet method leads to a significant increase in the CPU time. The increase is roughly a factor 5 for IQUAD=2 and a factor 2 for IQUAD=8. An increase in the CPU time is contrary to our expectations, since a decrease was expected. The reason for this is discussed further in Section 8.7.

The content of Tables 8.2 to 8.4, discarding the Triplet method results, is presented in Figure 8.1. The four upper images show the CPU time as function of the number of iterations, displayed per field case and per DIA version. To facilitate interpretation of the four upper images, a least-squares fit of all data per figure is included. Please note that

the least-squares fit has no other meaning than merely serving as an aid to the reader by indicating the trend of the data. Also note that in the four upper images the benchmark results, with N_{iter} = 80, are included. The lower image displays the CPU time of the reference runs (R_iq2_std) versus the CPU time of the corresponding control runs (C_iq8_std). In the lower image, the benchmark result is not included, because of lack of corresponding control run data, i.e. data obtained with an 80 iterations run with setting IQUAD=8.

Continuing the discussion on the content of Tables 8.2 to 8.4 (again discarding the Triplet method results) and Figure 8.1:

- For four out of the eight field cases, the required CPU time to reach convergence for the nearest-neighbour version of the DIA (IQUAD=8) and for the default version of the DIA (IQUAD=2) are virtually the same. For two cases (Eems – 6:30 and 9:30 hours), the model setting IQUAD=8 leads to a faster simulation, and for the remaining cases (Petten and AZG – 17:00 hours) the model setting IQUAD=2 leads to a faster simulation.

- The ratio of CPU time per iteration for IQUAD=8 and CPU time per iteration for IQUAD=2 varies between 0.87 (for Petten) and 0.90 (for AZG, Sloten and Eems). In other words, the model setting IQUAD=8 is, per iteration, about 11% to 15% faster. The CPU time per iteration is computed by taking the average of the CPU time per iteration for all runs for a given field case and a given DIA version (i.e., a given value of IQUAD).

- The number of SWAN iterations required to reach convergence is different for the two studied versions of the DIA. For IQUAD=8, for 6 out of 8 field cases more SWAN iterations are required to reach convergence. In some instances (AZG3a, 17:00 hours (ebb) and Petten) this difference is significant, leading also to a higher CPU time.

These findings can be summarized as follows. Though application of the more efficient nearest-neighbour version of the DIA (IQUAD=8) is, per iteration, 11% to 15% faster than the default version of the DIA (IQUAD=2), this does not always lead to a reduction in the total CPU time. This is due to the fact that, often, for IQUAD=8 more iterations are required to reach convergence than for IQUAD=2. The iteration behaviour will be addressed in more detail in Section 8.5.

8.4 Consistency check

The Triplet method aims at efficient computation of the operations involved in the computation of the DIA, but it is not a new DIA method. In other words, it is a reformulation of existing DIA methods. Therefore, for a given DIA version (i.e. given value of IQUAD), the wave fields obtained in a simulation performed with the Triplet method and a simulation performed with the default method for DIA computation should be identical. This will be referred to as the DIA-Triplet consistency requirement. For a given field case and with reference to the coding convention in Table 8.1, the wave field computed in run R_iq2_std should be identical to that of run C_iq2_tri, and the wave field computed in run C_iq8_std should be identical to that of run C_iq8_tri.

This DIA-Triplet consistency is, however, not satisfied with the present implementation of the Triplet method. This can be deduced from the fact that the number of required

iterations in Tables 8.2 to 8.4 is different for corresponding runs. Furthermore, it has been verified that the wave fields for corresponding runs are different, as described in Section 8.6 below. The difference in results can be attributed to the different sweep mechanism used and a slightly different interpolation procedure. For the IQUAD=2 simulation, in which the DIA is computed per sweep, this difference is partly due to the fact that the Triplet method is used per iteration. Use of the Triplet method per iteration which is similar to applying the DIA with IQUAD=3. However, the IQUAD=8 simulations compute the source terms per iteration, both for the DIA and the Triplet method. For these cases also difference in results are found. These differences originate from a slightly different interpolation procedure of interacting spectral bins.

Since the present implementation of the Triplet method in SWAN suffers from both an unacceptable increase in CPU time (see Section 8.3) and a lack of DIA-Triplet consistency, results obtained with the Triplet method will get limited attention in the discussion in Sections 8.5 and 8.6. Hence, the focus will be on the results obtained with the default computation of the DIA. This means that we restrict ourselves in these sections mainly to the results of three model settings: the benchmark run results (B_iq2_std), the reference run results (R_iq2_std) and the control run results (C_iq8_std).

8.5 Iteration behaviour

The iteration behaviour for all eight field cases has been investigated in three test locations. This is discussed below.

Amelander Zeegat – 2 Jan. 2005: 10:00 (flood), 12:00 (slack) and 17:00 hours (ebb)

Figures 8.2 to 8.6 show examples of the iteration behaviour. The results show that the iteration behaviours in locations 1 (Figures 8.2 and 8.4) and 2 (Figures 8.3 and 8.5) are, for a given storm moment and model variant, rather similar. The iteration behaviour in location 3 (Figure 8.6) is for all three storm moments rather similar. As a consequence, not all iteration behaviour figures are included in this report. The following can be observed:

- The iteration behaviour of the wave parameters at a given location for the reference runs and the corresponding control runs differs significantly. Related to this are the very large differences between the converged reference and control run results. The differences can, in the test locations studied, go up to 6 cm (wave height), 0.1 s (wave period), 5^o (wave direction) and 1^o (directional spreading).

- The percentage of converged points shows for all reference and corresponding control runs a fairly identical behaviour.

- At 17:00 hours, the iteration behaviour of the wave period of the control run shows a slightly oscillatory behaviour in location 3 (Figure 8.6). Related to this, note that, at 17:00 hours, the control run needs significantly more iterations (47) than the reference run (37).

Eems-Dollard – 1 Nov. 2006: 3:00 (flood), 6:30 (slack) and 9:30 hours (ebb)

Figures 8.7 (location 3, at 3:00 hours), 8.8 (location 1, at 6:30 hours) and 8.9 (location 2, at 9:30 hours) depict samples of the iteration behaviour. Only the most relevant figures showing the iteration behaviour are included in this report. The following can be seen:

- The iteration behaviour of the wave parameters at a given location for the reference runs and the corresponding control runs differs significantly. Related to this are the very large differences between the converged reference and control run results. The differences in the test locations can go up to 10 cm (wave height), 0.3 s (wave period), 20^o (wave direction) and 3^o (directional spreading).

- The behaviour of the percentage of converged points is significantly different for the reference and corresponding control run at storm moments 6:30 and 9:30 hours.

Petten – 1 Jan. 1995: 10:00 hours

Figures 8.10 to 8.12 depict the iteration behaviour in the three test locations. The following can be observed:

- There are differences between the converged reference and control runs results, though not as dramatic as observed for the Amelander Zeegat and Eems field cases. In particular, at the most shallow location (test location 3) the differences are relatively small. The reason is that other physical processes dominate over quadruplet interaction.

- The behaviour of the percentage of converged points deviates somewhat for the reference and the control run. In particular, it shows somewhat erratic behaviour in the case of the latter. Related to this, the control run requires significantly more iterations (42) than the reference run (30).

Lake Sloten – 27 Oct. 2002: 15-16 hours

Figures 8.13 to 8.15 depict the iteration behaviour in the three test locations. The following can be seen:

- The control run and reference run are not fully converged: the iteration curves clearly have not reached a constant value yet. This holds in particular for the upwind banks (location 1), and becomes less in the downwind direction (locations 2 and 3).

- The behaviour of the percentage of converged points is different for the reference and the control run. The control run needs more iterations (35) than the reference run (30).

- The iteration behaviour of the wave parameters for the reference runs and the corresponding control runs differ significantly for the wave direction (location 1) and directional spreading (locations 1, 2 and 3), but not for the other quantities.

For several field cases, the control runs (IQUAD=8) shows a more wiggly iteration behaviour than the reference runs (IQUAD=2), in particular for the wave period. This is a consequence of the less accurate quadruplet formulation of IQUAD=8. Furthermore, the results suggest that the computed wave fields for the reference and control runs are significantly different. This will be confirmed by showing the convergence errors, as will be done in Section 8.6.

8.6 Convergence errors

The convergence errors for the reference and control runs, as defined in Section 3.5.3, are discussed below for the simulation results obtained in this chapter. The overall results of this section are presented in Tables 8.5 to 8.8 below.

Case	Run code	$\mu(H_{m0})$ [%]	$\mu(T_{m-1,0})$ [%]	$\mu(\mathrm{Dir})$ [^{0}]	$\mu(\mathrm{Dspr})$ [%]
AZG3a – 10:00	R_iq2_std	0.159	0.292	0.407	0.825
AZG3a – 10:00	C_iq8_std	0.604	0.638	1.20	3.02
AZG3a – 10:00	C_iq2_tri	1.29	1.34	1.33	2.47
AZG3a – 10:00	C_iq8_tri	1.64	1.68	1.75	2.22
AZG3a – 12:00	R_iq2_std	0.115	0.198	0.180	0.305
AZG3a – 12:00	C_iq8_std	0.520	0.462	0.946	2.80
AZG3a – 12:00	C_iq2_tri	1.40	1.06	0.884	1.79
AZG3a – 12:00	C_iq8_tri	1.79	1.39	1.45	2.36
AZG3a – 17:00	R_iq2_std	0.166	0.194	0.588	0.894
AZG3a – 17:00	C_iq8_std	1.33	1.33	4.28	5.89
AZG3a – 17:00	C_iq2_tri	1.98	1.53	4.23	4.40
AZG3a – 17:00	C_iq8_tri	2.31	1.70	4.71	5.15
AZG3a – avg time	R_iq2_std	0.148	0.228	0.392	0.675
AZG3a – avg time	C_iq8_std	0.818	0.810	2.14	3.90
AZG3a – avg time	C_iq2_tri	1.56	1.31	2.15	2.89
AZG3a – avg time	C_iq8_tri	1.91	1.59	2.64	3.24

Table 8.5 Average convergence errors for quadruplet investigation for Amelander Zeegat field cases.

Case	Run code	$\mu(H_{m0})$ [%]	$\mu(T_{m-1,0})$ [%]	$\mu(\mathrm{Dir})$ [^{0}]	$\mu(\mathrm{Dspr})$ [%]
Eems3a – 03:00	R_iq2_std	0.213	0.264	0.538	1.18
Eems3a – 03:00	C_iq8_std	1.72	1.63	4.47	5.08
Eems3a – 03:00	C_iq2_tri	2.43	1.98	4.65	4.03
Eems3a – 03:00	C_iq8_tri	2.82	2.41	4.76	4.58
Eems3a – 06:30	R_iq2_std	0.260	0.265	0.369	0.614
Eems3a – 06:30	C_iq8_std	2.89	2.88	6.59	4.72
Eems3a – 06:30	C_iq2_tri	3.22	2.62	6.75	4.99
Eems3a – 06:30	C_iq8_tri	3.36	2.66	6.62	4.44
Eems3a – 09:30	R_iq2_std	0.117	0.201	0.340	0.593
Eems3a – 09:30	C_iq8_std	2.92	2.47	4.50	4.50
Eems3a – 09:30	C_iq2_tri	3.82	2.37	4.78	5.28
Eems3a – 09:30	C_iq8_tri	4.35	2.52	4.62	4.60
Eems3a – avg time	R_iq2_std	0.200	0.243	0.416	0.796
Eems3a – avg time	C_iq8_std	2.51	2.33	5.19	4.77
Eems3a – avg time	C_iq2_tri	3.16	2.32	5.39	4.77
Eems3a – avg time	C_iq8_tri	3.51	2.53	5.33	4.54

Table 8.6 Average convergence errors for quadruplet investigation for Eems-Dollard field cases.

Run code	$\mu(H_{m0})$ [%]	$\mu(T_{m-1,0})$ [%]	$\mu(\mathrm{Dir})$ [^{0}]	$\mu(\mathrm{Dspr})$ [%]
R_iq2_std	0.118	0.249	0.301	0.566
C_iq8_std	0.184	0.590	0.813	1.76
C_iq2_tri	0.501	1.00	0.381	2.08
C_iq8_tri	0.645	1.45	0.914	1.40

Table 8.7 Average convergence errors for quadruplet investigation for Petten field case.

Run code	$\mu(H_{m0})$ [%]	$\mu(T_{m-1,0})$ [%]	$\mu(\mathrm{Dir})$ [^{0}]	$\mu(\mathrm{Dspr})$ [%]
R_iq2_std	0.632	0.579	0.586	1.11
C_iq8_std	0.303	0.116	0.629	3.54
C_iq2_tri	1.64	1.58	0.804	3.57
C_iq8_tri	2.32	1.25	0.786	0.453

Table 8.8 Average convergence errors for quadruplet investigation for Lake Sloten field case.

Amelander Zeegat – 2 Jan. 2005: 10:00 (flood), 12:00 (slack) and 17:00 hours (ebb)

Figures 8.16 to 8.21 contain spatial plots of the convergence errors in the wave height H_{m0}, wave period $T_{m-1,0}$, the mean direction and the directional spreading for three instants obtained with the default method to compute the DIA for both IQUAD=2 and IQUAD=8. Figures 8.22 and 8.23 show two examples of spatial plots of the convergence errors for 12:00 hours obtained with the Triplet method to compute the DIA. In Table 8.5, the average convergence errors in the rectangular box are given.

The following can be observed:

- The convergence errors of the control runs are, in large parts of the computational domain, much larger than those of the reference runs. The magnitude of the convergence errors of the control runs is significant.

- Roughly speaking, the spatial distribution of the control run convergence error is, for a given wave parameter, similar in shape for the three storm moments. The magnitude of the convergence error increases from storm moment 12:00 (slack) to 10:00 (flood), and then to 17:00 hours (ebb).

- The wave height as computed in the control run is in particular overestimated (>2.5%) in the deeper areas, i.e. in the tidal inlet and in the gullies behind Terschelling and Ameland (see Figure 8.16). In the remaining areas, i.e. the North Sea and the more shallow parts in the Wadden Sea, the control run wave height is slightly overestimated (between 0% and 1%). For the ebb condition, it is underestimated (<-1.5%) in some areas near the tidal inlet and near the gully behind Ameland (see Figure 8.20).

- The wave period as computed in the control run is in particular overestimated (>2.5%) in the deeper areas, i.e. in the gullies behind Terschelling and Ameland and north of Ameland in the shadow of the ebb-tidal delta (see Figure 8.16). In the remaining areas, i.e. the North Sea and the more shallow parts in the Wadden Sea, the convergence error in the control run wave period is rather small, and varies between -0.5% and 0.5%. For the ebb condition (17:00 hours, see Figure 8.20), areas with a large underestimation (<-1.5%) as well as an overestimation (>2.5%) can be found near the tidal inlet and near the gully behind Ameland.

- From the figures and the two bullets above, it can be concluded that the control run convergence error for the wave period and wave height has a more or less similar spatial distribution (both in shape and size). The only noticeable differences are:

    - In larger parts of the domain, the control run wave height is slightly overestimated (between 0% and 1%), whereas the control run wave period deviations vary between -0.5% and 0.5% of the reference run wave period.
    - North of Ameland and, for 17:00 hours (ebb), north of Terschelling, a remarkable feature is visible: the areas with a large overestimation of the wave period coincide with the areas with a large underestimation of the wave height, and vice versa. These results suggest the inspection of the shape of the nonlinear source term using the different options. From this result it can be concluded that the application of IQUAD=8 transfers energy faster to low frequencies than using IQUAD=2. This results in too much low frequency energy and less energy that is under active influence of wind.

- The convergence error in the wave direction as computed in the control run is particularly large in the tidal inlet and behind Terschelling on 17:00 hours (ebb), see Figure 8.21.

- The directional wave spreading as computed in the control run is largely underestimated (<-2.5%) behind the islands. On the ebb-tidal delta north of Ameland, there is a shallow area where the directional spreading is largely overestimated (>2.5%). For the ebb condition, the directional spreading in the gully behind Ameland is overestimated.

- The Triplet method results (Figures 8.22 and 8.23) are different from their default counterparts, i.e. Figures 8.18 and 8.19. This means that the DIA-Triplet consistency requirement is not satisfied.

Eems-Dollard – 1 Nov. 2006: 3:00 (flood), 6:30 (slack) and 9:30 hours (ebb)

Figures 8.24 to 8.29 contain spatial plots of the convergence errors in the wave height H_{m0}, wave period $T_{m-1,0}$, the mean direction and the directional spreading for three instants obtained with the default method to compute the DIA for both IQUAD=2 and IQUAD=8. Figures 8.30 and 8.31 show two examples of spatial plots of the convergence errors for 6:30 hours obtained with the Triplet method to compute the DIA. In Table 8.6, the average convergence errors in the rectangular box are given.

The following can be observed:

- The convergence errors of the control runs are, in large parts of the computational domain, much larger than those of the reference runs. The magnitude of the convergence errors of the control runs is significant.

- Roughly speaking, the spatial distribution of the control run convergence error is, for a given wave parameter, similar in shape for the three storm moments. The magnitude of the convergence error for 6:30 (slack) and 9:30 hours (ebb) is more or less similar, while for 3:00 hours (flood) it is, on the overall, somewhat smaller.

- The spatial distribution of the control run convergence errors show large red and dark blue areas very close to each other, i.e. the convergence error is large and changes very rapidly (that is, over small distances).

- The wave height as computed in the control run is in particular overestimated (>5%) in the gullies. In the North Sea part of the domain, where it is also rather deep, the control run wave height is slightly overestimated (between 0% and 1%). It is underestimated (<-1.5%) in some areas close to the gully.

- The wave period as computed in the control run is in particular overestimated (>5%) in the gullies. Also, in some other parts of the domain it is overestimated.

- From the figures and the two bullets above, it can be concluded that the control run convergence error for the wave period and wave height has a more or less similar spatial distribution (both in shape and size). The only noticeable difference is that, in some areas on the ebb-tidal delta, the areas with a large overestimation of the wave period coincide with the areas with a large underestimation of the wave height, and vice versa.

- The convergence error in the wave direction as computed in the control run is very large for all runs (>5^o for a large part of the domain), and in particular for the 6:30 hours (slack) condition.

- The control run convergence error for the directional wave spreading shows particularly steep gradients. It could be said that the directional wave spreading is underestimated (<-2.5%) in large parts of the domain, with several spots in which it is largely overestimated (>5%).

- The Triplet method results (Figures 8.30 and 8.31) are different from their default counterparts, i.e. Figures 8.26 and 8.27. This means that the DIA-Triplet consistency requirement is not satisfied.

Petten – 1 Jan. 1995: 10:00 hours

Figures 8.32 and 8.33 contain spatial plots of the convergence errors in the wave height H_{m0}, wave period $T_{m-1,0}$, the mean direction and the directional spreading obtained with the default method to compute the DIA for both IQUAD=2 and IQUAD=8. Figures 8.34 and 8.35 show two examples of spatial plots of the convergence error obtained with the Triplet method to compute the DIA. In Table 8.7, the average convergence errors in the rectangular box are given.

The following can be observed:

- The convergence errors of the control run are larger than those of the reference runs.

- The wave height as computed in the control run is overestimated (between 0.5% and 1.5%) in the offshore region, while nearshore it is close to the reference run result. This more or less uniform overestimation in the offshore region is suspicious.

- The wave period as computed in the control run is slightly underestimated (between -0.5% and 0%) in the offshore region, while in some parts nearshore it is somewhat more underestimated (between -1% and -0.5%). This more or less uniform underestimation in the offshore region is suspicious.

- The wave direction as computed in the control run is, apart from some little spots within 1^o of the reference run result.

- The directional spreading as computed in the control run is underestimated (<-2.5%) in the offshore region, while nearshore it is closer (between -1% and 2.5%) to the reference run result.

- The Triplet method results (Figures 8.34 and 8.35) are different from their default counterparts, i.e. Figures 8.32 and 8.33. This means that the DIA-Triplet consistency requirement is not satisfied.

Lake Sloten – 27 Oct. 2002: 15-16 hours

Figures 8.36 and 8.37 contain spatial plots of the convergence errors obtained with the default method to compute the DIA. Figures 8.38 and 8.39 show two examples of spatial plots of the convergence error obtained with the Triplet method to compute the DIA. In Table 8.8, the average convergence errors in the rectangular box are given.

The following can be observed:

- The convergence error of the control run is smaller than that of the reference run for the wave height and wave period. For the mean wave direction, the convergence errors of the reference and control runs are similar.
- The directional spreading as computed in the control runs is largely underestimated (<-2.5%).
- The Triplet method results (Figures 8.38 and 8.39) are different from their default counterparts, i.e. Figures 8.36 and 8.37. This means that the DIA-Triplet consistency requirement is not satisfied.

These conclusions should, however, be treated with care, since the control and reference runs are not fully converged yet, in particular over the upwind banks (see also the discussion in Section 8.5).

8.7 Discussion on the Triplet method

The Triplet method consists of a simple algorithm to compute the nonlinear transfer rate between sets of four wave numbers, so-called quadruplets. It is based on the notion that any method for computing these interactions, such as the Discrete Interaction Approximation or the exact WRT method (Van Vledder 2006) can be rewritten in the form:

$$S_{nl,i} = \sum_{j=1}^{N_{T,j}} w_j E_{p(j)} E_{q(j)} E_{r(j)} \ ,$$

where $S_{\mathrm{nl},i}$ is the nonlinear transfer rate a spectral bin *i*. For each bin, the transfer rate can be considered as the sum of $N_{\mathrm{T},j}$ triplet products of energy densities at the spectral bins with indices *p(j)*, *q(j)* and *r(j)*. The first step in the pre-processing of a Triplet application is to generate a set of triplets, of which the indices and weights are stored in a database. The second step is to add the weights of identical triplet products that are assigned to a particular spectral bin *i*. In the third step the frequency and direction indices of the spectral bins were rewritten as a single number. This step requires that integers are declared as 8 byte integers. The last step of the pre-processing is to make a binary database of the triplet indices and weights. The content of this database depends on the spectral resolution, the power of the parametric tail and the underlying computational method. In the present study two basic versions of DIA-based triplets were made: one corresponding to bi-linear interpolation (IQUAD=2) and one corresponding to the nearest bin approach (IQUAD=8). Since the frequency resolution of the field cases is not equal for all cases, different triplet databases were generated.

It is essential to understand that the Triplet method is not a new approximate method to evaluate the nonlinear interactions. It is only a different technique to evaluate all mathematical operations. As such it can be seen as a unified way to compute the nonlinear interactions. A characteristic of the Triplet method is that the number of triplets (pairs of triple products) increases when a more accurate method is used. For instance, the WRT method produces 2 orders of magnitude more sets than the DIA with one configuration. Omitting triplets that do no significantly contribute to the transfer rate in a certain spectral bin may be a means to obtain a setting that is some where in the middle of the DIA and WRT method in terms of accuracy and computational requirements.

The results of applying the Triplet method show that it is much slower than the standard DIA and also much slower than expected from offline tests of the Triplet method. The theoretical gain in computational speed was based on an evaluation of the number of multiplications and additions of the present DIA algorithm. This evaluation showed that the Triplet method requires twice as many basic operations when it is based on the DIA using bi-linear interpolation (IQUAD=2), whereas the number of operations drops by a factor of 20 when the nearest bin approach is used (IQUAD=8). Van Vledder (2005c) showed that the Triplet method becomes relatively more efficient than the standard DIA approach when multiple wave number configuration are used, i.e. the Multiple DIA. This gain in efficiency results from the fact that triple products can be combined for different λ–values.

The extremely long simulation times found with the Triplet method in the present investigation led us to critically review the implementation of this method in SWAN. A number of areas for improvement were identified. The largest improvement may be in shifting the Triplet method to another subroutine in SWAN. At present, the Triplet method is implemented in the subroutine that is normally used for the Xnl method (IQUAD=51). It appears that the performance is reduced drastically because a lot of computing resources are spent on overhead that is related to the Xnl method, but that is not needed for IQUAD=2 and IQUAD=8. The second possibility for improved speed is related to the computational loops employed in computing the Triplet method. In its present form the triplet pre-processing program assumes that the indices with which a spectral bin is represented are frequency and direction respectively, whereas this order is reversed in SWAN. This requires that all spectra need to be reversed before application in the Triplet method. Consequently, the computation of the nonlinear transfer rate must also be reversed. The third possibility for a gain in speed is related to the fact that the Triplet method is based on energy densities, whereas SWAN is defined in terms of action densities. This difference requires the use of a Jacobian term (viz. the intrinsic frequency σ) to convert energy densities into action densities. These transformations were built in in the interface routine between SWAN and the Triplet method. Inspection of the Triplet method revealed that both transformation (loop structure and Jacobian) can be incorporated into the Triplet method. Offline testing showed that optimizing the retrieval of a single spectrum from the large internal spectral array could speed up the performance of the Triplet method. Combining all possible optimization may improve the performance of the Triplet method considerably, especially when IQUAD=8, or a multiple DIA is used.

8.8 Discussion on different results for IQUAD=2 and IQUAD=8

The different results obtained by the various versions of the DIA are due to different methods of obtaining the energy density at the corresponding interaction wave

numbers. Since the DIA contains cubic products of three energy densities, small differences in (interpolated) energy densities quickly lead to relatively large different nonlinear transfer rates. The fact that the DIA with the nearest bin approach (IQUAD=8) produces different results than the standard DIA (IQUAD=2) does not mean that using IQUAD=8 produces wrong results. As discussed by Van Vledder et al. (2000) the DIA has a number of shortcomings and present day third-generation models are calibrated to compensate for the shortcomings of the DIA. Consequently, replacing the DIA with a more accurate method, e.g. the WRT method, may produce better nonlinear transfer rates, but less accurate overall model results, because the model should be recalibrated. By the same token, using the DIA with the nearest bin approach will certainly give different results and the model may need to be recalibrated. In fact both versions of the DIA are crude approximations of the exact nonlinear transfer rates and tuning of the other source terms may compensate for the shortcomings.

Since the differences between the IQUAD=2 and IQUAD=8 results are due to a different way of computing the quadruplets, it seems reasonable to suppose that the differences are larger in areas or conditions where quadruplet-interactions are more prominent, e.g. strongly wind-driven wave fields in the North Sea. As observed, the largest differences in wave height and wave period occur in deeper areas. It is hypothesized that the differences in directional wave spreading and wave direction are more sensitive to the presence of young waves. Young waves typically have a large directional spreading and quadruplets have a strong effect on the directional distribution of waves (Young and Van Vledder, 1993). Application of a different method to compute the quadruplets then affects in particular the young waves, which results in relatively large differences in the directional wave spreading and wave direction.

The results concerning the convergence behaviour in SWAN reveal that the application of the nearest bin approach requires more iterations than the standard DIA method. This behaviour is related to the fact that the nearest bin approach assumes that the energy density in a spectral bin, with a certain bandwidth $\Delta\sigma\Delta\theta$, is constant and not varying linearly. This discretisation effect amplifies local interactions, such that SWAN needs more iterations to converge. Another side effect is that, especially directional variations, are crudely represented. In relatively simple situations, such as fetch-limited growth, applying SWAN with IQUAD=8 may be a option, but in more complicated situations like the Wadden Sea, discretisation errors worsen the performance of the DIA with this option for approximating the nonlinear quadruplet interactions.

8.9 Conclusions

In this section, two methods of improving the efficiency of SWAN by a more efficient computation of the quadruplets by means of the DIA (Discrete Interaction Approximation) have been studied. The first method concerns application of the computationally faster nearest-neighbour version of the DIA (model setting IQUAD=8) instead of the default model (model setting IQUAD=2). The second method concerns application of the Triplet method to the DIA (Van Vledder 2005c). The Triplet method can either be applied to the default version of the DIA (IQUAD=2), or to the nearest-neighbour (IQUAD=8) version. The same set of eight test cases (Amelander Zeegat, Petten, Eems-Dollard and Lake Sloten) as defined in Section 2 have been used to study the efficiency improvement as well as the influence on the accuracy of these methods.

Concerning the Triplet method, the following can be concluded:

- For the present implementation in SWAN the CPU time is much larger (roughly a factor 5 for IQUAD=2 and a factor 2 for IQUAD=8) than for the default method to compute the DIA.

- The present implementation in SWAN lacks DIA-Triplet consistency. DIA-Triplet consistency means that, for a given DIA version (i.e., given value of IQUAD), the wave fields obtained in a simulation performed with the Triplet method and a simulation performed with the default method for DIA computation should be identical.

These deficiencies were not expected at the beginning of the project. Further ways to optimize the implementation of the Triplet method in SWAN were identified that may yield a viable implementation in SWAN. Summarizing, at this moment no useful conclusions concerning application of the Triplet method in SWAN can be drawn, except that use of the Triplet method, in its current state, is not recommended for the HBC computations.

Concerning the model setting IQUAD=8, the following conclusions can be drawn:

- Though application of the more efficient nearest-neighbour version of the DIA (IQUAD=8) is, per iteration, 11% to 15% faster than the default version of the DIA (IQUAD=2), this does not always lead to a reduction in the total CPU time. This is due to the fact that, often, for IQUAD=8 more iterations are required to reach convergence than for IQUAD=2.

- The model setting IQUAD=8 yields a significantly different iteration behaviour and significantly different solution with respect to the default setting IQUAD=2. This holds in particular for areas with complex geometries (tidal inlets and gully systems) and currents such as the Amelander Zeegat and the Eems-Dollard. The differences are more than 5% in large parts of the domain for the wave parameters wave height, wave period and directional spreading, and more than 5^o for the mean wave direction.

- For areas with less complex geometries and no currents such as the western part of the Dutch coast (Petten), the differences are less extreme, but still significant: up to 2.5% overestimation in the wave height, 1% underestimation in the wave period, 1^o in the wave direction and more than 2.5% underestimation in the directional spreading.

- For another area with a reasonable simple geometry and no current, namely Lake Sloten, no decisive conclusions can be drawn, since neither the reference nor the control run have converged.

Summarizing, one should be reluctant to use the nearest-neighbour version of the DIA (IQUAD=8).

9 Batch run organisation

9.1 Introduction

In this section, it is investigated whether the total simulation time can be reduced by making use of the *hotfile* functionality of SWAN. This can be useful when simulating a large number of simulations in batch mode for the Amelander Zeegat such as will be done in the batch computation of the Hydraulic Boundary Conditions (HBC) in the Wadden Sea. The *hotfile* is produced by a SWAN run in stationary mode and contains the wave field state at the final iteration (to be more precise: the action density spectrum in all grid points). The *hotfile* can be used as an initial guess to the wave field of a next SWAN run in the batch sequence, with modified forcings (e.g. wind speed, wind direction, water level) but identical geometry (computational grid). The underlying idea is that this initial guess would be relatively close to the solution of the next SWAN run, so that fewer iterations, hence less CPU time, would be required to achieve convergence.

In the present study, we restrict ourselves to investigate modifications in the wind speed and wind direction in combination with application of the *hotfile* functionality. The following ways of applying *hotfiles* to save computational time by suitable arrangement of sequential runs have been studied:

a) *Increments in wind speed*: mean wind and (offshore) wave directions belonging to a storm condition are held constant and the wind speed and offshore significant wave height are incrementally increased through all classes in the computational climate, or

b) *Increments in wind direction*: the wind speed and the (offshore) significant wave height are held constant as the mean wind and offshore wave direction systematically sweep through all directional bins comprising the climate.

For both these options, the benefit in terms of total simulation time and gain (or loss) in accuracy was evaluated for one selected field case of the Amelander Zeegat. For this one field case, a synthetic wind and wave climate, comprising six wind speeds and nine directions, was compiled. These individual conditions in the climate will be run in batch mode without the use of a *hotfile* (the reference runs), and subsequently with *hotfiles* (the control runs). The gain in simulation time was computed over the total series of simulations, and a total error measure was computed, denoting the difference in model outcomes averaged over all simulation results.

9.2 Setup of test cases and coding convention

9.2.1 Selected test case

The selected test case is based on the Amelander Zeegat field case for the storm instant of 2 January 2005 at 12:00. To achieve the purpose of the work described in this section, the following items are different from the original model setup as discussed in Sections 2 and 3:

Wind conditions

Synthetic wind conditions (wind speeds and wind directions) are considered in the model runs in the present section:

- To investigate the *hotfile* functionality in combination with increments in the wind speed, the following six wind speeds (uniform over the domain) are considered: 15 m/s, 20 m/s, 25 m/s, 30 m/s, 35 m/s and 40 m/s. The wind direction is kept the same (270^{o}N) for all these runs.

- To investigate the *hotfile* functionality in combination with increments in the wind direction, the following nine wind directions (uniform over the domain) are considered: 225^{o}N, 247.5^{o}N, 270^{o}N, 292.5^{o}N, 315^{o}N, 337.5^{o}N, 0^{o}N, 22.5^{o}N and 45^{o}N. This corresponds to the following directions, respectively: southwest, west-southwest, west, west-northwest, northwest, north-northwest, north, north-northeast and northeast. The wind speed is kept the same (25 m/s) for all these runs.

Currents

Currents are excluded in the model runs described in the present study. The motivation for this is that presently there exist no clear guidelines for the inclusion of current fields in the computation of hydraulic boundary conditions. Currents are influenced by the wind condition, which means that different wind conditions would require different current fields. Moreover, the use of different current fields for different wind conditions would make the model results for the present study harder to analyse. To avoid these difficulties, the Amelander Zeegat field case was considered at slack tide (12:00 hours), and currents are excluded in the model runs.

Water level

This issue is related to that of the currents, see the previous bullet. In the absence of currents, the water level is assumed to be uniform. As also done in Section 3.3.2 in WL (2006), the water level in Nes is taken as representative for the computations. At the given time instance, the water level is + 2.07 m NAP.

Offshore wave boundary conditions

For the selected wind conditions, offshore wave boundary conditions need to be specified. They are not known a priori. Obtaining accurate wave boundary conditions for the present computational domain would require additional SWAN computations over a (much) larger domain, in which the present computational domain is nested. This would require a substantial amount of additional work, which is not necessary for the purpose of this study. Approximate offshore wave boundary conditions suffice for the present purpose, since we are concerned with differences between the reference run and control run results. Inaccuracies in the offshore boundary conditions are expected to have a similar impact on the reference and control runs alike. In Section 9.2.3, the computation of the offshore wave boundary conditions is discussed.

9.2.2 Coding convention and batch file organization

In Table 9.1 the coding convention applied in the present chapter is introduced.

Run code	Description
R_k[xx]_270	Reference run for the study in increments in wind speed, keeping the wind direction constant (270^{o}N). No hotfiles
C_k[xx]_270	Control run for the study in increments in wind speed, keeping the wind direction constant (270^{o}N). With hotfiles
R_25_d[yyy]	Reference run for the study in increments in wind direction, keeping the wind speed constant (25 m/s). No hotfiles
C_25_d[yyy]	Control run for the study in increments in wind direction, keeping the wind speed constant (25 m/s). With hotfiles

Table 9.1 Coding convention of the model settings to investigate the efficiency of the use of hotfiles. The string [xx] represents the wind speed, in m/s. The string [yyy] represents the wind direction, in ^{o}N and rounded to whole numbers.

In reference runs, no use is made of *hotfiles*. Therefore, they are stand-alone runs. In control runs, use is made of the *hotfile* functionality. A given control run uses the converged wave field produced in the previous control run as initial guess. The converged wave field of the previous control run is stored in a so-called *hotfile*, which is opened in the next control run. The string [xx] represents the wind speed, in m/s. The following values for [xx] are used: 15, 20, 25, 30, 35 and 40. The string [yyy] represents the wind direction, in ^{o}N and rounded to integer numbers. The following values for [yyy] are used: 225, 247, 270, 292, 315, 337, 0, 22 and 45. Note that the quantity that is incremented is preceded by a letter ('k' for wind speed and 'd' for wind direction) in the code convention. For example, C_25_d270 is a control run in the study for wind direction increments, and C_k25_270 is a control run in the study for wind speed increments; in both runs, the wind speed is 25 m/s and the wind direction is 270^{o}N.

Two of the most promising ways for arranging the computations to save computational time are made:

1. Increments in wind speed
In these runs, the wind speed is increased incrementally from U_{10} = 15 to 40 m/s. The wind direction is kept constant at 270^{o}N. In total, 12 simulations are performed:

- Six reference runs, with the following codes: R_k15_270, R_k20_270, R_k25_270, R_k30_270, R_k35_270 and R_k40_270. These runs are stand-alone runs in which the *hotfile* functionality is not used.

- Six control runs, with the following codes: C_k15_270, C_k20_270, C_k25_270, C_k30_270, C_k35_270 and C_k40_270. The order given here is the order in which the computations are executed. The first run (C_k15_270) creates a *hotfile* (besides the other requested output). The content of this *hotfile*, i.e. the converged wave field of run C_k15_270, is used as an initial guess for the wave

field of the next run (C_k20_270). This run (C_k20_270) creates again a *hotfile*, which is used as an initial guess for the wave field of the next run (C_k25_270), and so on. Note that the first run is the only run that does not start with an initial guess from the *hotfile*. In cases where the *hotfile* is not used, SWAN applies the default second-generation first guess at the first iteration.

2. Increments in wind direction
In these runs, the wind direction is rotated in the clockwise direction from 225^{o}N to 45^{o}N. The wind speed is kept constant at U_{10} = 25 m/s. In total, 18 simulations are performed:

- Nine reference runs, with the following codes: R_25_d225, R_25_d247, R_25_d270, R_25_d292, R_25_d315, R_25_d337, R_25_d000, R_25_d022 and R_25_d045. These runs are stand-alone runs in which the *hotfile* functionality is not used.

- Nine control runs, with the following codes: C_25_d225, C_25_d247, C_25_d270, C_25_d292, C_25_d315, C_25_d337, C_25_d000, C_25_d022 and C_25_d045. The order given here is the order in which the computations are executed. The first run (C_25_d225) creates a *hotfile* (besides the other requested output). The content of this *hotfile*, i.e. the converged wave field of run C_25_d225, is used as an initial guess for the wave field of the next run (C_25_d247). This run (C_25_d247) creates again a *hotfile*, which is used as an initial guess for the wave field of the next run (C_25_d270), and so on. Note that the first run is the only run that does not start with an initial guess from the *hotfile*. As stated above, when the *hotfile* is not used, SWAN applies the default second-generation first guess at the first iteration.

Hence, in total (12 + 18) = 30 simulations are performed.

Some general remarks need to be made:

- Control runs depend on each other, and need to be executed in a suitably chosen order. For example, run C_25_d045 cannot be started before run C_25_d022 is finished; run C_25_d022 cannot be started before run C_25_d000 is finished, and so on. Therefore, control runs need to be executed sequentially. This does not hold for reference runs; these are completely independent of each other, and can be computed sequentially (on the same or different machines) or in parallel (on different machines).

- We have chosen to consider the option of *increasing* the wind speed between sequential runs when studying increments in the wave speed. The reason for following this option, instead of considering decreasing wind speeds, is the following. Generally speaking, the larger the wind speed, the more energy the wave field contains. We expect that SWAN converges faster in a situation that the initial wave field (delivered by the *hotfile* of the previous run) contains too little wave energy than in a situation that the initial wave field contains too much wave energy. This is based on the assumption that wave energy in a SWAN computation is more easily increased with an increase in wind speed than that wave energy is dissipated after a decrease in wind speed. Therefore, we expect that SWAN requires fewer iterations, i.e. less CPU time, when studying positive wind speed increments.

- Reversing the increments in the wind directions is not expected to yield large differences with respect to the presently selected clockwise increments. The choice of domain and the expected wave field does not give any indications that would support such a preference in wind direction increments.

- The converged wave fields computed respectively in runs C_k15_270 and R_k15_270 should be identical, since they are the first runs in the sequence. The difference between these runs is that in a former run a *hotfile* is created, while in the latter not. The same holds for runs C_25_d225 and R_25_d225.

- The wave fields as computed in runs R_25_d270 and R_k25_270 should be identical, since they have identical model input. However, the wave fields as computed in runs C_25_d270 and C_k25_270 may not be identical, since the initial wave fields are different (i.e. the converged wave fields from runs C_25_d247 and C_k20_270 respectively).

9.2.3 Offshore wave boundary conditions

Since synthetic wind conditions are used in the present study, offshore boundary conditions are not directly available from measurements. To obtain approximate boundary conditions at the offshore boundary (which we have chosen to be that part of the model boundary that is located in the North Sea) the following methodology based on empirical finite-depth wave growth curves is chosen.

In Table 9.2, the wave conditions in ELD and SON at 2 Jan. 2005, 12:00 hours, are given (see Tables 3.4 and 3.5 in WL (2006)).

Location	H_{m0} [m]	T_{m01} [s]	γ	Dir [^{0}N]	Dspr [^{0}]
ELD	4.7	7.6	3.3	292	33
SON	5.0	8.0	3.3	301	28

Table 9.2 Wave conditions in ELD and SON, at 2 Jan. 2005, 12:00 hours.

Taking the average of the wave height and wave period in ELD and SON yields the following values: H_{m0} = 4.85 m; T_{m01} = 7.8 s. Using these values and inverting the depth-limited wave growth limits of Young and Verhagen (1996) for the prevalent wind speed (17.82 m/s) yields the following values for the depth: 40.1 m (for the energy limit) and 35.0 m (for the period limit). The average of these two values yields a quantity that is called here the effective depth[3]: 37.5 m. Inserting the six wind speeds and the effective depth in the depth-limited wave growth limits yields values for the wave height and wave period as given in Table 9.3. The boundary condition spectrum is assumed to have a JONSWAP shape, with a peak enhancement of γ = 3.3. The wave direction (Dir) is taken to be equal to the wind direction, though for the storm instant studied here (see Table 9.2), this is not exactly true (prevalent wind direction: 277^{o}N). The directional spreading (Dspr) is taken to be the average of the measured values in ELD and SON: 30.5^o.

3. *Since the wave growth limit formally only holds for wave growth over uniform water depths (which is not the actual situation in the North Sea) and since we have taken some averages, we speak of an 'effective depth'. The effective depth is a representative value for the depth, which contains the made approximations.*

Wind speed [m/s]	H_{m0} [m]	T_{m01} [s]	γ	Dspr [^{0}]
15	4.12	7.67	3.3	30.5
20	5.04	8.24	3.3	30.5
25	5.89	8.72	3.3	30.5
30	6.69	9.12	3.3	30.5
35	7.45	9.48	3.3	30.5
40	8.18	9.80	3.3	30.5

Table 9.3 Applied offshore wave boundary conditions. The wave direction is taken equal to the wind direction.

Summarizing, the wave boundary conditions are assumed to be uniform along the entire offshore boundary, fully described with the wave parameters as given in Table 9.3. At the remaining model boundaries, no boundary conditions are specified. The parts of the model boundary situated in the Wadden Sea are so shallow, that the wave growth limit is quickly reached. On the land boundary, obviously no wave boundary conditions need to be imposed.

9.3 Results

9.3.1 Consistency check

It has been verified, see also Section 9.2.2, that the wave field as computed in the run C_k15_270 is identical to that of run R_k15_270. This is also the case for runs R_k25_270 and R_25_d270.

9.3.2 Efficiency

The number of iterations and CPU time are given in Table 9.4 (increments in wind speed) and Table 9.5 (increments in wind direction).

Run code	N_{iter}	T_{cpu} [min]	Run code	N_{iter}	T_{cpu} [min]
R_k15_270	29	36	C_k15_270	29	36
R_k20_270	29	36	C_k20_270	20	27
R_k25_270	30	37	C_k25_270	18	24
R_k30_270	30	37	C_k30_270	19	25
R_k35_270	33	41	C_k35_270	18	24
R_k40_270	34	41	C_k40_270	16	21
Sum	**185**	**228**	**Sum**	**120**	**157**

Table 9.4 Increments in wind speed: number of iterations and CPU time. Left: reference runs; right: control runs. Last row: summation of the column above.

Run code	N_{iter}	T_{cpu} [min]	Run code	N_{iter}	T_{cpu} [min]
R_25_d225	34	42	C_25_d225	34	42
R_25_d247	33	40	C_25_d247	41	52
R_25_d270	30	37	C_25_d270	30	39
R_25_d292	31	38	C_25_d292	18	24
R_25_d315	43	53	C_25_d315	16	22
R_25_d337	43	52	C_25_d337	18	24
R_25_d000	39	47	C_25_d000	19	25
R_25_d022	32	39	C_25_d022	22	29
R_25_d045	27	33	C_25_d045	20	25
Sum	**312**	**381**	**Sum**	**218**	**282**

Table 9.5 Increments in wind direction: number of iterations and CPU time. Left: reference runs; right: control runs. Last row: summation of the column above.

The following conclusions can be drawn concerning the wave speed increment runs, see Table 9.4:

- Using the *hotfile* functionality results in a reduction in CPU time of 31% and a reduction in required number of iterations of 35%.

- The CPU time per iteration is for the control runs slightly larger than for the reference runs: 1.31 versus 1.23 (minutes per iteration). The reason for this slight increase is twofold:
  - There is more 'additional' overhead in the control runs. Additional overhead in the control run consists of reading a *hotfile* at the beginning of the run and writing a *hotfile* at the end of the run. The additional overhead for the reference run consists of the computation of the second-generation first guess during the first iteration. The latter amount is evidently smaller than the former.
  - The control runs require fewer iterations. As a consequence, the CPU time required for the 'standard' overhead is distributed over fewer iterations. 'Standard' overhead refers to all overhead that is present in both control and reference runs, such as reading all input, initialisation of all arrays and writing the wave field to file for postprocessing.

The following conclusions can be drawn concerning the wave direction increment runs, see Table 9.5:

- Using the *hotfile* functionality results in a reduction in CPU time of 26% and a reduction in required number of iterations of 30%.

- The CPU time per iteration is for the control runs slightly larger than for the reference runs: 1.29 versus 1.22 (minutes per iteration). These values are very close to those found for the wave speed increment runs, see above. The origin for this slight increase is considered to be the same as mentioned above.

9.3.3 Iteration behaviour

The iteration behaviour in three test points (see Section 3.5.1) has been studied in more detail. For each of these test points, the figures for the final run in the wind speed increments (R_k40_270 and C_k40_270, see Figures 9.1 to 9.3) and wind direction increments (R25_d045 and C25_d045, see Figures 9.4 to 9.6) have been added to this report. The following observations can be made:

For the wave speed increment runs:

- The wave parameters of the converged reference and control runs are very close to each other. For most wind conditions, the maximum differences between the reference and control run results are: 0.01 m for the wave height, 0.05 s for the wave period; 0.7^o for the mean wave direction, and 0.2^o for the directional spreading.

- For all wave parameters, the *hotfile* initial guess is closer to the value after convergence than the second-generation first guess. This in combination with a smooth iteration behaviour (i.e. no spurious rapid variations) leads to a faster convergence.

For the wave direction increment runs (Figures 9.4 to 9.6):

- The wave parameters of the converged reference and control runs are less close to each other than for the wave speed increment runs.

- The differences between the reference and control runs in the test points are at most (including the wave direction increment run results not included in this report): 0.03 m for the wave height, 0.05 s for wave period; 5^o for the mean wave direction, and 1^o for the directional spreading.

- In many control runs, the initial guess for the mean wave direction is rather far from its value after convergence. This due to the fact that the mean wave direction is largely influenced by the wind direction: application of a given increment in the wind direction then should lead to, crudely speaking, a similar increment in the mean wave direction. And since the wind direction increments are relatively large, this requires a large adaptation of the wave direction during a SWAN computation.

- The slope of the iteration curve for the quantities wave direction and directional wave spreading, and less predominant for the wave height and wave period, strongly suggest that the control runs have not fully converged yet.

9.3.4 Convergence differences between control run and reference run results

Definitions

Because we have no benchmark results at our disposal, the convergence error as defined in Section 3.5.3 cannot be computed in the present study. We have decided to study what we call the convergence differences between wave parameters obtained in the control and reference runs. Let $P_{C,m}$ be any of the four integral parameters (wave height, wave period, mean wave direction and directional spreading) produced by the

control run at a geographical location *m*, and $P_{R,m}$ is the corresponding parameter produced by the reference run. Spatial plots of the convergence differences are made. The convergence difference is defined at every geographical grid point m as

$$\delta\left(P_m\right)=\frac{P_{C,m}-P_{R,m}}{P_{R,m}}\times 100\% \tag{9.1}$$

for the significant wave height H_{m0}, the spectral period $T_{m-1,0}$ and directional spreading Dspr. For the mean wave direction, the convergence difference is defined as

$$\delta\left(P_m\right)=\left|P_{C,m}-P_{R,m}\right| \tag{9.2}$$

properly accounting for directional periodicity.

A quantitative measure of the average convergence difference is computed as the mean convergence difference of all parameter values in a rectangular box positioned around the tidal inlet (see Figure 2.1). This is computed as

$$\eta\left(P\right)=\frac{1}{M}\sum_{m=1}^{M}\left|\delta\left(P_m\right)\right|=\frac{1}{M}\sum_{m=1}^{M}\frac{\left|P_{C,m}-P_{R,m}\right|}{\left|P_{R,m}\right|}\times 100\% \tag{9.3}$$

for the wave height, wave period and directional spreading, and

$$\eta\left(P\right)=\frac{1}{M}\sum_{m=1}^{M}\left|\delta\left(P_m\right)\right|=\frac{1}{M}\sum_{m=1}^{M}\left|P_{C,m}-P_{R,m}\right| \tag{9.4}$$

for the mean wave direction (ensuring proper accounting for directional periodicity), counting over all of the *M* points located inside the rectangle defined over the tidal inlet.

The definitions used here are similar to those for the convergence error and average convergence error as presented in Section 3.5.3, except that, as mentioned before, no comparison is made with a benchmark run as defined in Section 3.3.

Increments in wind speed

Wind field	$\eta\left(H_{m0}\right)$ [%]	$\eta\left(T_{m-1,0}\right)$ [%]	$\eta\left(\mathrm{Dir}\right)$ [^{0}]	$\eta\left(\mathrm{Dspr}\right)$ [%]
k15_270	0	0	0	0
k20_270	0.978	1.41	0.697	0.872
k25_270	0.311	0.699	0.922	1.20
k30_270	0.537	1.38	1.48	1.62
k35_270	0.251	0.752	1.56	1.65
k40_270	0.257	0.877	1.72	1.83

Table 9.6 Average convergence differences in wave parameters in the study of increments in wave speed.

The spatial distribution of the convergence differences in wave parameters for the runs studying the increments in wind speed are shown in Figures 9.7 to 9.11, considering wind speeds of 20, 25, 30, 35 and 40 m/s. The following conclusions can be drawn from these figures and Table 9.6:

- For runs k25_270, k35_270 and k40_270, the convergence differences for the wave height and wave period are fairly small: (much) smaller than 1% in most grid points. This is, however, not the case for the North Sea part of the domain in the runs with wind field k20_270 and k30_270, where convergence differences of 2.5% to 5% in the wave height, and 1% - 2.5% in the wave period, occur. It has been verified that this is not due to an error in the SWAN input files. The convergence difference in this area is mainly due to lack of convergence of the reference runs, as will be explained below. The convergence difference in this area cannot be explained. Note that the convergence difference virtually disappears on the ebb-tidal delta, where wave breaking significantly changes the wave field. Since the convergence difference is much smaller in the tidal inlet and the Wadden Sea, this suggests that the spurious convergence difference behaviour in the North Sea part of the domain does not hamper the accuracy in the Wadden Sea itself.

- In general, the convergence differences for the mean wave direction and directional spreading increase when the wind speed is increased. Most notably, large differences (>5% for the directional spreading and $>5^{o}$ for the wave direction for wind speeds 30, 35 and 40 m/s) are visible behind the islands and near the mainland coastline. It is noted that this problem may be related to the limited number of decimals used in the *hotfile* of the standard SWAN version, see (WL 2008).

The spurious results for the runs with wind fields k20_270 and k30_270, see the first bullet, are discussed here in more detail. For the corresponding wind fields, benchmark computations (80 iterations) have been performed, without *hotfile* functionality. These will be denoted with run codes B_k20_270 and B_k30_270, following the code convention introduced earlier. The convergence errors, i.e. the difference between the benchmark runs on the one hand, and the reference or control runs on the other, are shown in Figures 9.12 to 9.15. We observe that the wave height and period in the North Sea part of the domain are less well converged in the reference run (Figure 9.12 for k20_270, and Figure 9.14 for k30_270) than in the control run (Figure 9.13 for k20_270, and Figure 9.15 for k30_270). For wind field k20_270, the situation is reversed in the Wadden Sea, where the wave height and period are better converged in the reference run than in the control run. For wind field k30_270, the wave height and period are slightly better converged in the control run than in the reference run. Concerning the mean wave period and directional spreading for these two wind fields, it seems that the control run results are slightly better converged to the benchmark results than the reference run results.

One may wonder whether the convergence differences found here can be considered as acceptably small or not. Or, in other words, whether the accuracy of the control runs in combination with wind speed increments at the end of the batch file sequence (i.e., after possible accumulation of convergence differences) is acceptable or not. Therefore, we have executed a benchmark computation (80 iterations) with a wind speed equal to 40 m/s and a wind direction equal to 270^{o}N (code: B_k40_270), without *hotfile* functionality. The convergence error, i.e. the difference between the benchmark and reference run result (see also Section 3.5.3), is shown in Figure 9.16. Comparing this

figure with Figure 9.11, one finds that the convergence difference (Figure 9.11) and convergence error (Figure 9.16) are rather similar in shape and size. Hence, if one considers the convergence errors of the reference runs as acceptably small, then also the convergence differences of runs R_k40_270 and C_k40_270 should be considered as acceptably small. This warrants the conclusion that application of the *hotfile* functionality in combination with wind speed increments leads, for the present test case, to a reduction in CPU time while maintaining the same level of accuracy.

Increments in wind direction

Wind field	$\eta(H_{m0})$ [%]	$\eta(T_{m-1,0})$ [%]	$\eta(\mathrm{Dir})$ [^{0}]	$\eta(\mathrm{Dspr})$ [%]
25_d225	0	0	0	0
25_d247	0.322	0.548	1.41	0.994
25_d270	0.484	0.666	2.12	1.35
25_d292	0.722	0.815	4.37	2.41
25_d315	0.916	0.975	6.70	3.39
25_d337	0.974	1.03	6.55	4.14
25_d000	0.834	0.989	5.45	3.58
25_d022	0.680	0.739	3.68	2.40
25_d045	0.618	0.727	3.58	2.27

Table 9.7 Average convergence differences in wave parameters in the study of increments in wave direction.

The spatial distribution of the convergence differences in wave parameters for the runs studying the increments in wind direction are shown in Figures 9.17 to 9.20, considering wind directions of 247^{o}N, 315^{o}N, 0^{o}N and 45^{o}N. The following conclusion can be drawn from these figures (including the figures for the other wind direction conditions which are not shown in this report) and Table 9.7:

- The convergence difference for the mean wave direction is unacceptably large for most runs, often (much) more than 5^o. As is well known, the mean wave direction is largely influenced by the wind direction: application of a given increment in the wind direction then should, roughly speaking, lead to a similar increment in the mean wave direction. By studying actual values of the wave direction (not shown in this report), it is concluded that the mean wave direction is not sufficiently adjusted to the new wind direction. In other words, the mean wave direction is not converged. This could already be inferred from the iteration curves in Figures 9.4, 9.5 and 9.6. In other words, we observe that the wave direction is lagging behind the wind direction increments. This is due to the fact that application of a given increment in the wind direction should, roughly speaking, lead to a similar increment in the mean wave direction. And since the wind direction increments are relatively large, this requires a large adaptation of the wave direction during a SWAN computation.

One may wonder whether the convergence differences found here can be considered as acceptably small or not. Or, in other words, whether the accuracy of the control runs in combination with wind direction increments at the end of the batch file sequence (i.e., after possible accumulation of convergence differences) is acceptable or not. Therefore, we have executed a benchmark computation (80 iterations) with a wind speed equal to 25 m/s and a wind direction equal to 45^{o}N (code: B_25d045), without *hotfile* functionality. The convergence error, i.e. the difference between the benchmark and

reference run result (see also Section 3.5.3), is shown in Figure 9.21. Comparing this figure with Figure 9.20, one finds that the convergence differences (Figure 9.20) for the directional spreading and, particularly, the mean wave direction are much larger than the convergence errors (Figure 9.21). In other words, the control run results is much more different from the benchmark result than the reference result is. As mentioned above, what is observed is that the wave direction is lagging behind the wind direction increments. Concluding, application of the *hotfile* functionality in combination with wind direction increments leads to an unacceptable decrease in accuracy, and is therefore not recommended.

9.4 Discussion

As discussed before, application of the *hotfile* functionality in combination with wind speed increments leads, for the present test case, to a reduction in CPU time while maintaining the same level of accuracy. On the other hand, application of the *hotfile* functionality in combination with wind direction increments leads to an unacceptable decrease in accuracy.

The convergence differences for the quantities wave height and wave period are in almost all runs, for both the wind speed and wind direction increments, rather small (typically 1% or less). This demonstrates that the applied convergence criterium performs satisfactorily (see also WL 2007). However, the convergence difference can become much larger for the quantities wave direction and directional spreading (in some runs more than 5^o respectively 5% in large parts of the domain). This is due to the fact that the presently applied convergence criterion takes the wave period and wave height into account, but not other quantities such as the mean wave direction or directional spreading. This issue also received attention in Alkyon (2007b). Note that application of a convergence criterion that includes mean wave direction and/or directional spreading will probably lead to substantially different results concerning the gain in CPU time. In fact, it may be possible that application of wind direction increments in combination with batch runs may be slower than stand-alone runs, given the slow convergence in wave direction and directional spreading in the former.

9.5 Conclusions

It has been investigated whether, when simulating a large number of simulations in batch mode for the Amelander Zeegat, the total simulation time can be reduced by making use of the *hotfile* functionality. The two most logical ways of applying *hotfiles* to save computational time have been studied by applying either increments in wind speed or increments in wind direction. The test case is based on the existing 2 January 2005, 12:00 hours Amelander Zeegat field case. From the results of this investigation, the following can be concluded:

- The gain in CPU time is for both approaches similar: 31% for application of wind speed increments, and 26% for application of wind direction increments.

- Application of the *hotfile* functionality in combination with wind speed increments leads, for the present test case, to a reduction in CPU time while maintaining the same level of accuracy. It can therefore be considered a promising candidate for reducing simulation times in HBC computations.

- Application of the *hotfile* functionality in combination with wind direction increments leads to results that are often far from the reference results. This is due to a poor initial guess with respect to the wave direction, and convergence criteria that do not check on directional properties. Due to this unacceptable decrease in accuracy, it is not recommended to apply this method in HBC calculations.

10 Discussion

The aim of the present study was to investigate ways of reducing the CPU time required by stationary SWAN simulations. Various ways of achieving this goal exist. The most widely-used and best developed method for speeding up a numerical model such as SWAN is to apply parallel computing. Campbell et al. (2002) and Zijlema (2005) implemented such parallel computing facilities in SWAN, with which it is possible to run simulations on respectively shared-memory and distributed memory parallel computers. The main advantage of parallel computing over any other method for reducing simulation time is that there is no loss of accuracy. Also, parallel implementations with good scaling characteristics allow multiple increases in simulation speed by incorporating multiple processors. The main disadvantage of parallel computing is that parallel computing facilities are not always available, limiting the reach of its application.

On the other hand, a number of possibilities exist for the speeding up of SWAN simulations taking serial processing as a point of departure (although not necessarily be limited by it). Such methods may either be focussed on the reduction of the number of iterations performed by the model, or on the reduction of time spent per iteration. Examples of the former investigated in the present study are the Multigrid method, the deactivation of the action limiter (and quadruplet interaction) in the surf zone, and the efficient arrangement of batch runs linked by so-called *hotfiles*. Examples of the latter are the DDM and the nearest neighbour DIA. As such, these approaches aim to either remove unnecessary and costly aspects of the computation (e.g. the DDM), applying efficient approximations of the model physics (e.g. nearest neighbour DIA, with IQUAD=8), or efficient arrangement of simulations (e.g. batch run with *hotfiles*). However, since all these methods affect the simulation to a lesser or greater degree, it is required to assess the possible gain in simulation speed in the light of the degree to which they affect the model outcomes. Also, since these methods aim for higher efficiency of the model, it is desirable to have these methods compatible with parallel computing facilities.

To address these requirements, the numerical techniques investigated in this study were all (except for the quadruplet methods in Section 8) successfully evaluated for a parallel computing environment. In order to provide a balanced view of the performance of the various proposed numerical techniques, both the impacts in simulation speed and model accuracy were considered. In this regard, Figures 10.1 and 10.2 provide a comparative overview of the performance of the numerical techniques investigated in this study, in terms of the impact on total simulation times and the influence on model accuracy. The data presented in these figures was taken from the summary tables of total CPU time and average error in integral parameters presented in Sections 4 to 8.

Figure 10.1 compares the relative change in total CPU time with respect to that of the reference runs for a number of investigated numerical techniques, split out for all eight field test cases considered in this study. The numerical methods shown are the most promising candidates, or the best settings for the investigated methods, identified in each of the Sections 4 to 8. For the approach of action limiter deactivation (Section 6) no best option was identified, so that the results for an Ursell number limit of 0.10 (control run C_urs_010), proposed by Van der Westhuysen (2007), is included for reference. Since the method of batch run organisation (Section 9) was only investigated for a schematised Amelander Zeegat situation, it is not included in this figure, but will be considered in the following discussion. The vertical dashed line at 100% indicates the

CPU time used by the reference run, so that percentages lower than this represent savings in total CPU time. From the numerical methods presented in Figure 10.1, the DDM technique can be seen to produce the lowest overall run times. It consistently produces savings in total simulation time, which for the Amelander Zeegat and Eems-Dollard field cases are in the order of 35%, and for the simpler Petten and Lake Sloten cases about 15%. It is noted that the batch run technique, organised with wind speed increments, similarly showed a saving of 31% for the Amelander Zeegat field situation (not included in the graph).

None of the remaining methods yield consistent time savings relative to the reference run. The nearest neighbour DIA (IQUAD=8) produces notable reductions in CPU time for two field cases, but also yielded increases for two others. Both the Multigrid method on its own and the MG-DDM combination yielded occasional time savings (e.g. for the Petten and Sloten cases), but typically increases simulation times for the complex Wadden Sea cases. For three of these cases, the Multigrid method even produces a doubling of the reference run CPU time. The underlying reasons for the good or unsatisfactory performances have been presented in Sections 4 and 9. It can be summarized by observing that a typical culprit for poor simulation times is that a given method for numerical efficiency can distort the physics of SWAN, thereby requiring more iterations, and hence often longer simulation times (e.g. the deactivation of the action limiter and quadruplet interaction, see Section 6). As was discussed in Section 4, compared to earlier investigations (e.g. WL & Alkyon (2007b), these difficulties have been highlighted in the present study by applying stricter convergence criteria.

Next, a comparison of the changes in model accuracy is given, in order to put the savings in CPU time into perspective. The relative change in model accuracy has been computed as the ratio of the model error $\mu(P_C)$ (control run) to $\mu(P_R)$ (reference run), defined by (3.3) to (3.6), for each field case and numerical technique. These relative changes have subsequently been averaged over the integral parameters H_{m0}, $T_{m-1,0}$, *Dir* and *Dspr*. It is noted that whereas the total simulation speed is a simple measure for comparison, a large amount of detail is lost in attempting to compare the overall changes in model accuracy. Firstly, comparing the averaged model error μ only provides an indication of the change in the reference run accuracy, which in itself is dependent on the convergence criteria applied. Therefore, such results require an additional evaluation of the acceptability of the numerical errors (e.g. due to non-convergence) of the reference run. In this regard, as a second reservation, considering the averaged model error μ can be misleading, since it may obscure high model errors in a particular parameter or over a particular geographical region.

With these reservations in mind, Figure 10.2 gives an impression of the comparative influence on model accuracy found by applying the various numerical techniques for reducing CPU time. As in Figure 10.1, the results are split out over the eight field cases considered, and a vertical dashed line is included to indicate the model error of the reference run (defined as $\mu(P_R)$). In terms of model error, the best overall results are found for the Multigrid method, which yields comparable accuracy to the default model, except at Lake Sloten, where a particularly large error reduction is found. By comparison, great increases in model error are found for the IQUAD=8 approach. However, neither of these methods yielded consistent reductions in computational time (compare Figure 10.1). For the DDM, the most promising approach in terms of computational time, the average model error can be seen to be 2 to 2.5 times that of the default model (reference run) for the complex Wadden Sea cases, and 1.2 for the simpler Petten and Lake Sloten. It was found that in the reference runs, given the applied convergence criteria, the maximum errors in H_{m0}, $T_{m-1,0}$, *Dir* and *Dspr* were

respectively 1.5%, 2.5%, 5^o and 5%, with respect to the benchmark run (result at 80 iterations). For the DDM, these maximum errors in the parameters H_{m0}, $T_{m-1,0}$, *Dir* and *Dspr* increase to respectively 1.5%, 5%, >5^o and >5% (Figures 5.39 to 5.56). These results indicate that at present the DDM yields acceptable errors in the significant wave height and mean period. However, the errors in directional parameters can be unacceptably large, and points the direction towards further development of this method (e.g. by incorporating directional parameters in the deactivation criteria). The second numerical technique that succeeds in reducing total CPU time is batch run organisation with wind speed increments. For this method, the maximum errors in the significant wave height and mean period were found to be 1% (although up to respectively 5% and 2.5% in two cases) in the investigated Amelander Zeegat field case (see Section 9). For the mean direction and directional spreading, the model errors can exceed respectively 5^o and 5% behind the islands and near the mainland coastline.

It can therefore be concluded that the DDM and batch run approaches (with wind speed increments) represent promising ways of reducing the total simulation time of SWAN. At present, these methods provide consistent savings in computational time, with acceptable levels of model error for the parameters of significant wave height and mean period. However, further development is needed to address the observed excessive errors in directional parameters.

11 Conclusions

In the present study, various methods for reducing the simulation time of SWAN were evaluated and refined, to facilitate the efficient execution of large numbers of SWAN simulations to be conducted during the HBC computations. The methods evaluated here include the Dynamical Deactivation Method (DDM), the Multigrid (MG) method, deactivating the action limiter and quadruplet interaction in the surf zone, the efficiency of the DIA quadruplet interaction term, and batch run organization using the so-called *hotfile* functionality of SWAN. These methods were all evaluated using the same set of eight field cases (featuring Amelander Zeegat, Eems-Dollard, Petten and Lake Sloten), and the same evaluation criteria, taking into account the total CPU time, iteration behaviour and mean convergence errors. Detailed conclusions drawn on these results have been provided at the end of Sections 4 and 9. From these, the following general conclusions can be drawn:

- Of the investigated numerical methods, only the DDM technique and batch run organization (with *hotfile* and increments in wind speed) proved to realise consistent savings in total CPU time relative to the standard SWAN (31-35% with respect to the default SWAN model for the Wadden Sea field cases). These methods are both compatible with the OpenMP parallel computing facilities in SWAN, which afford an additional significant increase in computational speed.

- The application of the DDM and batch run methods results in increased model errors. For the significant wave height and mean period these can locally reach 1.5% and 5% respectively with respect to the results of a fully-converged standard SWAN simulation, which is considered acceptable. However, in the mean direction and directional spreading these errors can locally exceed 5^o and 5% respectively, which can be unacceptably high. In the case of the batch run organization, an increase to the numerical precision of the *hotfiles*, as proposed by WL (2008), may reduce these errors.

- The convergence criteria applied in the present study, namely the curvature-based criteria proposed by Zijlema and Van der Westhuysen (2005) extended to include also the curvature of the mean period, yielded generally well-converged results of significant wave height and period. However, the integral parameters of mean direction and directional spreading failed to converge in a number of cases, leading to convergence errors of up to 5^o and 5% respectively with respect to fully-converged results.

- Neither (a) the Multigrid method, (b) a combined MG-DDM approach, (c) deactivation of the action limiter in the surf zone, (d) the nearest-neighbour (IQUAD=8) option for the DIA, (e) the Triplet method for the DIA, nor (f) batch run organization with increments in wind direction appear to be viable options for reducing the simulation times of SWAN in their present state.

- The Multigrid method generally results in longer CPU times than the standard SWAN with comparable accuracy. Application of under-relaxation may speed up these computations, but first tests show the resulting gain in speed to still be unsatisfactory.

- Despite promising trial studies by Van Vledder (2005c), the Triplet method for the DIA, as currently implemented in SWAN, fails to reduce CPU times of SWAN simulations. This appears to be due to the fact that the Triplet implementation was probably not optimally implemented in SWAN. However, a number of improvements were identified that may speed up the Triplet method in SWAN. In addition, it was found that the Triplet method gave slightly different results than the DIA implementation in SWAN.

- A number of the investigated methods for CPU time reduction suffer from large convergence errors in the parameters of mean direction and directional spreading. This appears to be caused by the omission of these parameters in the convergence criteria of SWAN.

12 Recommendations

Based on the results of this study and the general conclusions drawn in Section 11, the following recommendations are made:

- On the strength of their positive performance in the present evaluation, it is recommended to apply the DDM technique and batch run organization (with *hotfile* and increments in wind speed) to reduce the computational time of SWAN simulations. It is recommended to apply these methods for improved efficiency in combination with parallel computing, to obtain further gains in computational speed.

- The curvature-based criteria proposed by Zijlema and Van der Westhuysen (2005) extended to include also the curvature of the mean period, yielded generally well-converged simulation results in the present study. It is recommended to apply these convergence criteria to SWAN simulation studies in general.

- It was found that a number of the investigated methods for CPU time reduction suffer from large convergence errors in the parameters of mean direction and directional spreading. In order to address this shortcoming, it is recommended to investigate the inclusion of directional parameters in the convergence criteria of SWAN and the deactivation criteria of the DDM.

- In the case of the batch run organization, it is recommended to investigate the application of *hotfiles* with a higher numerical precision, as proposed by WL (2008), to reduce the observed model errors.

- From the investigation conducted here, it was found that the Triplet method, although conceptually promising (Van Vledder 2005c) failed to perform satisfactorily due to sub-optimal implementation in the SWAN source code. It is recommended to revise this implementation and to repeat the evaluation of the Triplet method conducted here.

13 References

Alkyon (2004). Period correction SWAN. Alkyon report A1200, October 2004.

Alkyon (2005a). SWAN acceptance tests for RWS RIZA in 2005. New functionalities. Activity report 2. Alkyon report A1477R2R3, November 2005.

Alkyon, (2005b), Analysis SWAN correction. Phase 2, Background correction factos, based on hindcast Petten, Westerschelde and Petten wave flume with SWAN 40.31. Report A1200r3r2, Januari 2005.

Alkyon (2007a). Analysis SWAN hindcast tidal inlet of Ameland: Storms of 8 February 2004 and 2, 8 January 2005. Alkyon report A1725, February 2007.

Alkyon (2007b). Analysis SWAN hindcast tidal inlet of Ameland: Storms of 17 December 2005 and 9 February 2006. Alkyon report A1725, February 2007.

Alkyon (2008). Currents for HR 2011. Alkyon report A2108, July 2008.

Battjes, J. A. and J. P. F. M. Janssen (1978). Energy loss and set-up due to breaking of random waves. Proc. 16th Int. Conf. on Coastal Engineering, 569-588.

Booij, N., R.C. Ris and L.H. Holthuijsen (1999). A third generation wave model for coastal regions, Part I, Model description and validation. J. Geophys. Res., 104, C4, 7649-7666.

Bottema, M. (2007). Measured wind-wave climatology Lake IJssel (NL). Main results for the period 1997-2006. Report RWS RIZA 2007.020, July 2007.

Campbell, T., J.E. Cazes, and W.E. Rogers (2002). Implementation of an Important Wave Model on Parallel Architectures, Proceedings of MTS/IEEE Oceans 2002 Conference, 1509.

Eldeberky, Y. (1996). Nonlinear transformation of wave spectra in the nearshore zone, Ph.D. thesis, Delft University of Technology, Department of Civil Engineering, The Netherlands.

Ferziger, J.H. and M. Perić (2002). Computational Methods for Fluid Dynamics, 3rd Edition, Springer-Verlag, 423 pp.

Hasselmann, K., T.P. Barnett, E. Bouws, H. Carlson, D.E. Cartwright, K. Enke, J.A. Ewing, H. Gienapp, D.E. Hasselmann, P. Kruseman, A. Meerburg, P. Müller, D.J. Olbers, K. Richter, W. Sell and H. Walden, (1973) Measurements of wind-wave growth and swell decay during the Joint North Sea Wave Project (JONSWAP), Dtsch. Hydrogr. Z. Suppl., vol. 12, A8.

Hasselmann, S., K. Hasselmann, J.H. Allender and T.P. Barnett (1985) Computations and parameterizations of the nonlinear energy transfer in a gravity wave spectrum. Part II: Parameterizations of the nonlinear transfer for application in wave models, J. Phys. Oceanogr., 15 (11), 1378-1391.

Royal Haskoning & WL (2005). SWAN berekeningen ten behoeve van HR2006 voor de Hollandse kust (in Dutch). Rapport Royal Haskoning en WL | Delft Hydraulics, 9P8603.A0.

Royal Haskoning (2006). Hindcast tidal inlet of Ameland. Storms 17 December 2005 and 9 February 2006. Royal Haskoning Report 9S2639.A0, December 2006.

Royal Haskoning (2007). Hindcast tidal inlet of Ameland storms January and March 2007. Royal Haskoning Report 9S8833.A0, December 2007.

Van Vledder, G.Ph., T.H.C. herbers, R.E. Jensen , D.T. Resio and B. Tracy, 2000: Modelling of non-linear quadruplet wave-wave interactions in operational wave models. Proc. 27th Int. Conf. on Coastal Engineering, Sydney, Australia, 797-811.

Van Vledder, G. Ph. (2005a). New-processor SWAN. Alkyon Memo A1356ME01, 25 March 2005 (G. Ph. van Vledder).

Van Vledder, G. Ph. (2005b). Numerical wave modelling in Dutch coastal waters. Proc. ICECOAST 2005 Symposium, Höfn, Iceland.

Van Vledder, G. Ph. (2005c). The triplet method for the computation of nonlinear four-wave interactions in discrete spectral wave models, Proc. 5th Int. Symp. on Ocean Wave Measurement and Analysis.

Van Vledder, G. Ph. (2006). The WRT method for the computation of non-linear four-wave interactions in discrete spectral wave models. Coast Eng., 53, 223-242.

Van der Westhuysen, A. J. (2007). Advances in the spectral modelling of wind waves in the nearshore, Ph.D Thesis, Fac. of Civil Engineering, Delft University of Technology.

Van der Westhuysen, A. J, M. Zijlema, and J. A. Battjes (2005). Improvement of the numerics and deep-water physics in an academic version of SWAN. Proc. 29th Int. Conf. Coastal Engineering, ASCE, 855-867.

WL (2002). Kwaliteit randvoorwaardenboek en kwaliteit SWAN (in Dutch). WL | Delft Hydraulics Report H4061, January 2002.

WL (2006). Storm hindcasts Norderneyer Seegat and Amelander Zeegat. WL | Delft Hydraulics Report H4803.11, August 2006.

WL (2007). Reducing the computational time of SWAN by dynamic deactivation of grid points. WL | Delft Hydraulics Report H4918.37, August 2007.

WL (2008). Nonstationary SWAN simulation in the Wadden Sea. WL | Delft Hydraulics Report H4918.46, April 2008.

WL & Alkyon (2007a). Storm hindcast for Wadden Sea, Hindcasts in inlet systems of Ameland and Nordeney and Lunenburg Bay. WL | Delft Hydraulics Report H4918.20, September 2007.

WL & Alkyon (2007b). Evaluation of a multigrid method for the reduction of the computational time of SWAN. WL | Delft Hydraulics Report H4918.38, December 2007.

Young, I.R., and G.Ph. van Vledder, 1993: A review of the central role of nonlinear interactions in wind-wave evolution. Philos. Trans. Royal. Soc. London, Vol. 342, 505-524.

Zijlema, M. (2005). Parallelization of a nearshore wind wave model for distributed memory architectures. In: Parallel Computational Fluid Dynamics, Multidisciplinary Applications, G. Winter, A. Ecer, J. Periaux, N. Satofuka and P. Fox, Eds. Elsevier.

Zijlema, M. and A.J. van der Westhuysen (2005). On convergence behaviour and numerical accuracy in stationary SWAN simulations of nearshore wind wave spectra. Coastal Engng., vol. 52, 237-256.

A SWAN input files

In this appendix, examples are presented of the SWAN input files used in this study. Included are examples for each of the four geographical areas modelled, for the so-called reference runs (see Section 3.3). These input files feature the dummy strings <MULTIGR>, <TRIPLET>, <DDM> and <LIMITER>, used by a governing batch script to invoke the various numerical methods investigated in this study (a last dummy string <QUAD> has already been replaced by the command 'QUAD iquad=2' in these examples).

A.1 Amelander Zeegat

```
$************************************ HEADING ************************************************
$
$
PROJ 'AZG SWAN' 'CL'
$
$      Runid:    'SBW'
$
$
$************************************** MODEL INPUT ***********************************
$MODE NOUPDATE
$SET LEVEL = 1.04
SET MAXERR = 3 NAUT
$ Definitieve rooster en bodem
$
$<MULTIGR>
CGRID CURVI 285 411  EXC -99.00  CIRCLE  36  0.03 1 37
READ  COOR  1. 'grid/azg3a.grd'  IDLA=3 NHEDF=3 FORMAT '(10X,5F12.3)'
$
INP  BOTTOM CURVI 0. 0. 285 411  EXC -99.0
READ BOTTOM 1. 'bottom/azg3a.bot'  IDLA=3 NHEDF=0 FREE
INP  WLEV  CURVI  0. 0. 285 411  EXC -99.0
READ WLEV  1. 'lev/azg3a_20050102_1000.lev' IDLA=1 NHEDF=0 FREE
INP  CUR  CURVI  0. 0. 285 411  EXC -99.0
READ CUR  1. 'cur/azg3a_20050102_1000.cur' IDLA=1 NHEDF=0 FREE
$
$********************************** BOUNDARY CONDITIONS ********************************
BOUNDNEST1 NEST 'bnest/azg3a_20050102_1000_flu.sp3'  OPEN
$
$************************************** PHYSICA ***************************************
WIND 19.96 276.8
$
GEN3 WESTH
TRIAD trfac=0.05 cutfr=2.5
BREAKING 1 0.73
FRICTION JONSWAP CFJON=0.067
$*** Input block for numerics study H5107.46 ***
QUAD iquad=2
$<TRIPLET>
$<DDM>
$<LIMITER>
$********************************** NUMERIEKE PARAMETERS *******************************
NUM STOPC 0.00 0.01 0.001 99 STAT mxitst=80  alfa=0.001
$************************************ NEST ****************************************************
$********************************** DEFINITIE VAN UITVOERPUNTEN *************************
POINTS 'PNT2004'  FILE 'points/buoys_2004.pnt'
POINTS 'PNT2005'  FILE 'points/buoys_2005.pnt'
$
$********************************** DEFINITIE VAN UITVOERRAAIEN**************************
POINTS 'RAY1'  FILE 'rays/geul.pnt'
POINTS 'RAY2'  FILE 'rays/geul_vasteland1.pnt'
POINTS 'RAY3'  FILE 'rays/geul_vasteland2.pnt'
POINTS 'RAY4'  FILE 'rays/ameland_ray.pnt'
POINTS 'RAY5'  FILE 'rays/terschelling_ray.pnt'
POINTS 'RAY6'  FILE 'rays/nevengeul.pnt'
POINTS 'RAY7'  FILE 'rays/boeien_AZG2004.pnt'
POINTS 'RAY8'  FILE 'rays/braai_2006.pnt'
POINTS 'RAY9'  FILE 'rays/ameland.pnt'
POINTS 'RAY10' FILE 'rays/terschelling.pnt'
POINTS 'RAY11' FILE 'rays/kop_ameland2.pnt'
```

```
POINTS 'RAY12' FILE 'rays/kust_100x.pnt'
POINTS 'RAY13' FILE 'rays/kust_100.pnt'
POINTS 'RAY14' FILE 'rays/kust_200.pnt'
POINTS 'RAY15' FILE 'rays/kust_500.pnt'
POINTS 'RAY16' FILE 'rays/kust_1000.pnt'
POINTS 'RAY17' FILE 'rays/kust_2000.pnt'
POINTS 'RAY18' FILE 'rays/kust_3000.pnt'
POINTS 'RAY19' FILE 'rays/kust_5000.pnt'
POINTS 'RAY20' FILE 'rays/nul_nap.pnt'
$ ********************************** BLOCK UITVOER  ************************************
OUTPUT OPTIONS '%' TABLE 16 BLOCK 9 1000 SPEC 8
$ ********************************** TABEL UITVOER ******* ******************************
TABLE  'PNT2004'   HEAD 'table/azg3a_20050102_1000_rx1y1d1s1_flu_b2004.tab' &
   XP YP DEP HS RTP TMM10 TM01 TM02 FSPR DIR DSPR WLENGTH TPS DHSIGN DRTM01 WATLEV WIND VEL
TABLE  'PNT2005'   HEAD 'table/azg3a_20050102_1000_rx1y1d1s1_flu_b2005.tab' &
   XP YP DEP HS RTP TMM10 TM01 TM02 FSPR DIR DSPR WLENGTH TPS DHSIGN DRTM01 WATLEV WIND VEL
TABLE  'RAY1'   HEAD 'table/azg3a_20050102_1000_rx1y1d1s1_flu_ray1.tab'  &
   XP YP DEP HS RTP TMM10 TM01 TM02 FSPR DIR DSPR WLENGTH TPS DHSIGN DRTM01 WATLEV WIND VEL
TABLE  'RAY2'   HEAD 'table/azg3a_20050102_1000_rx1y1d1s1_flu_ray2.tab'  &
   XP YP DEP HS RTP TMM10 TM01 TM02 FSPR DIR DSPR WLENGTH TPS DHSIGN DRTM01 WATLEV WIND VEL
TABLE  'RAY3'   HEAD 'table/azg3a_20050102_1000_rx1y1d1s1_flu_ray3.tab'  &
   XP YP DEP HS RTP TMM10 TM01 TM02 FSPR DIR DSPR WLENGTH TPS DHSIGN DRTM01 WATLEV WIND VEL
TABLE  'RAY4'   HEAD 'table/azg3a_20050102_1000_rx1y1d1s1_flu_ray4.tab'  &
   XP YP DEP HS RTP TMM10 TM01 TM02 FSPR DIR DSPR WLENGTH TPS DHSIGN DRTM01 WATLEV WIND VEL
TABLE  'RAY5'   HEAD 'table/azg3a_20050102_1000_rx1y1d1s1_flu_ray5.tab'  &
   XP YP DEP HS RTP TMM10 TM01 TM02 FSPR DIR DSPR WLENGTH TPS DHSIGN DRTM01 WATLEV WIND VEL
TABLE  'RAY6'   HEAD 'table/azg3a_20050102_1000_rx1y1d1s1_flu_ray6.tab'  &
   XP YP DEP HS RTP TMM10 TM01 TM02 FSPR DIR DSPR WLENGTH TPS DHSIGN DRTM01 WATLEV WIND VEL
TABLE  'RAY7'   HEAD 'table/azg3a_20050102_1000_rx1y1d1s1_flu_ray7.tab'  &
   XP YP DEP HS RTP TMM10 TM01 TM02 FSPR DIR DSPR WLENGTH TPS DHSIGN DRTM01 WATLEV WIND VEL
TABLE  'RAY8'   HEAD 'table/azg3a_20050102_1000_rx1y1d1s1_flu_ray8.tab'  &
   XP YP DEP HS RTP TMM10 TM01 TM02 FSPR DIR DSPR WLENGTH TPS DHSIGN DRTM01 WATLEV WIND VEL
TABLE  'RAY9'   HEAD 'table/azg3a_20050102_1000_rx1y1d1s1_flu_ray9.tab'  &
   XP YP DEP HS RTP TMM10 TM01 TM02 FSPR DIR DSPR WLENGTH TPS DHSIGN DRTM01 WATLEV WIND VEL
TABLE  'RAY10'  HEAD 'table/azg3a_20050102_1000_rx1y1d1s1_flu_ray10.tab'  &
   XP YP DEP HS RTP TMM10 TM01 TM02 FSPR DIR DSPR WLENGTH TPS DHSIGN DRTM01 WATLEV WIND VEL
$TABLE  'RAY11'  HEAD 'table/azg3a_20050102_1000_rx1y1d1s1_flu_ray11.tab'  &
$   XP YP DEP HS RTP TMM10 TM01 TM02 FSPR DIR DSPR WLENGTH TPS DHSIGN DRTM01 WATLEV WIND VEL
$TABLE  'RAY12'  HEAD 'table/azg3a_20050102_1000_rx1y1d1s1_flu_ray12.tab'  &
$   XP YP DEP HS RTP TMM10 TM01 TM02 FSPR DIR DSPR WLENGTH TPS DHSIGN DRTM01 WATLEV WIND VEL
$TABLE  'RAY13'  HEAD 'table/azg3a_20050102_1000_rx1y1d1s1_flu_ray13.tab'  &
$   XP YP DEP HS RTP TMM10 TM01 TM02 FSPR DIR DSPR WLENGTH TPS DHSIGN DRTM01 WATLEV WIND VEL
$TABLE  'RAY14'  HEAD 'table/azg3a_20050102_1000_rx1y1d1s1_flu_ray14.tab'  &
$   XP YP DEP HS RTP TMM10 TM01 TM02 FSPR DIR DSPR WLENGTH TPS DHSIGN DRTM01 WATLEV WIND VEL
$TABLE  'RAY15'  HEAD 'table/azg3a_20050102_1000_rx1y1d1s1_flu_ray15.tab'  &
$   XP YP DEP HS RTP TMM10 TM01 TM02 FSPR DIR DSPR WLENGTH TPS DHSIGN DRTM01 WATLEV WIND VEL
$TABLE  'RAY16'  HEAD 'table/azg3a_20050102_1000_rx1y1d1s1_flu_ray16.tab'  &
$   XP YP DEP HS RTP TMM10 TM01 TM02 FSPR DIR DSPR WLENGTH TPS DHSIGN DRTM01 WATLEV WIND VEL
$TABLE  'RAY17'  HEAD 'table/azg3a_20050102_1000_rx1y1d1s1_flu_ray17.tab'  &
$   XP YP DEP HS RTP TMM10 TM01 TM02 FSPR DIR DSPR WLENGTH TPS DHSIGN DRTM01 WATLEV WIND VEL
$TABLE  'RAY18'  HEAD 'table/azg3a_20050102_1000_rx1y1d1s1_flu_ray18.tab'  &
$   XP YP DEP HS RTP TMM10 TM01 TM02 FSPR DIR DSPR WLENGTH TPS DHSIGN DRTM01 WATLEV WIND VEL
$TABLE  'RAY19'  HEAD 'table/azg3a_20050102_1000_rx1y1d1s1_flu_ray19.tab'  &
$   XP YP DEP HS RTP TMM10 TM01 TM02 FSPR DIR DSPR WLENGTH TPS DHSIGN DRTM01 WATLEV WIND VEL
$TABLE  'RAY20'  HEAD 'table/azg3a_20050102_1000_rx1y1d1s1_flu_ray20.tab'  &
$   XP YP DEP HS RTP TMM10 TM01 TM02 FSPR DIR DSPR WLENGTH TPS DHSIGN DRTM01 WATLEV WIND VEL
$
$ ******************* HOT TAB OUTPUT *********************************
$TABLE 'COMPGRID' HEAD 'hot/azg3a_20050102_1000_rx1y1d1s1_flu_depth.tab' XP YP DEPTH
$TABLE 'COMPGRID' HEAD 'hot/azg3a_20050102_1000_rx1y1d1s1_flu_wind.tab' XP YP WIND
$ ********************************** SP1 UITVOER ***********************************
SPEC 'PNT2004' SPEC1D 'spec1d/azg3a_20050102_1000_rx1y1d1s1_flu_Pnt2004.sp1'
SPEC 'PNT2005' SPEC1D 'spec1d/azg3a_20050102_1000_rx1y1d1s1_flu_Pnt2005.sp1'
SPEC 'PNT2004' SPEC1D REL 'spec1d/azg3a_20050102_1000_rx1y1d1s1_flu_Pnt2004R.sp1'
SPEC 'PNT2005' SPEC1D REL 'spec1d/azg3a_20050102_1000_rx1y1d1s1_flu_Pnt2005R.sp1'
SPEC 'RAY1' SPEC1D 'spec1d/azg3a_20050102_1000_rx1y1d1s1_flu_Ray1.sp1'
SPEC 'RAY2' SPEC1D 'spec1d/azg3a_20050102_1000_rx1y1d1s1_flu_Ray2.sp1'
SPEC 'RAY3' SPEC1D 'spec1d/azg3a_20050102_1000_rx1y1d1s1_flu_Ray3.sp1'
SPEC 'RAY4' SPEC1D 'spec1d/azg3a_20050102_1000_rx1y1d1s1_flu_Ray4.sp1'
SPEC 'RAY5' SPEC1D 'spec1d/azg3a_20050102_1000_rx1y1d1s1_flu_Ray5.sp1'
SPEC 'RAY6' SPEC1D 'spec1d/azg3a_20050102_1000_rx1y1d1s1_flu_Ray6.sp1'
SPEC 'RAY7' SPEC1D 'spec1d/azg3a_20050102_1000_rx1y1d1s1_flu_Ray7.sp1'
SPEC 'RAY8' SPEC1D 'spec1d/azg3a_20050102_1000_rx1y1d1s1_flu_Ray8.sp1'
SPEC 'RAY9' SPEC1D 'spec1d/azg3a_20050102_1000_rx1y1d1s1_flu_Ray9.sp1'
SPEC 'RAY10' SPEC1D 'spec1d/azg3a_20050102_1000_rx1y1d1s1_flu_Ray10.sp1'
$SPEC 'RAY11' SPEC1D 'spec1d/azg3a_20050102_1000_rx1y1d1s1_flu_Ray11.sp1'
$SPEC 'RAY12' SPEC1D 'spec1d/azg3a_20050102_1000_rx1y1d1s1_flu_Ray12.sp1'
$SPEC 'RAY13' SPEC1D 'spec1d/azg3a_20050102_1000_rx1y1d1s1_flu_Ray13.sp1'
$SPEC 'RAY14' SPEC1D 'spec1d/azg3a_20050102_1000_rx1y1d1s1_flu_Ray14.sp1'
$SPEC 'RAY15' SPEC1D 'spec1d/azg3a_20050102_1000_rx1y1d1s1_flu_Ray15.sp1'
$SPEC 'RAY16' SPEC1D 'spec1d/azg3a_20050102_1000_rx1y1d1s1_flu_Ray16.sp1'
```

```
$SPEC 'RAY17' SPEC1D 'spec1d/azg3a_20050102_1000_rx1y1d1s1_flu_Ray17.sp1'
$SPEC 'RAY18' SPEC1D 'spec1d/azg3a_20050102_1000_rx1y1d1s1_flu_Ray18.sp1'
$SPEC 'RAY19' SPEC1D 'spec1d/azg3a_20050102_1000_rx1y1d1s1_flu_Ray19.sp1'
$SPEC 'RAY20' SPEC1D 'spec1d/azg3a_20050102_1000_rx1y1d1s1_flu_Ray20.sp1'
$ ********************************** SP2 UITVOER ****************************************
SPEC 'PNT2004' SPEC2D 'spec2d/azg3a_20050102_1000_rx1y1d1s1_flu_Pnt2004.sp2'
SPEC 'PNT2005' SPEC2D 'spec2d/azg3a_20050102_1000_rx1y1d1s1_flu_Pnt2005.sp2'
SPEC 'PNT2004' SPEC2D REL 'spec2d/azg3a_20050102_1000_rx1y1d1s1_flu_Pnt2004R.sp2'
SPEC 'PNT2005' SPEC2D REL 'spec2d/azg3a_20050102_1000_rx1y1d1s1_flu_Pnt2005R.sp2'
$SPEC 'RAY1' SPEC2D 'spec2d/azg3a_20050102_1000_rx1y1d1s1_flu_Ray1.sp2'
$SPEC 'RAY2' SPEC2D 'spec2d/azg3a_20050102_1000_rx1y1d1s1_flu_Ray2.sp2'
$SPEC 'RAY3' SPEC2D 'spec2d/azg3a_20050102_1000_rx1y1d1s1_flu_Ray3.sp2'
$SPEC 'RAY4' SPEC2D 'spec2d/azg3a_20050102_1000_rx1y1d1s1_flu_Ray4.sp2'
$SPEC 'RAY5' SPEC2D 'spec2d/azg3a_20050102_1000_rx1y1d1s1_flu_Ray5.sp2'
$SPEC 'RAY6' SPEC2D 'spec2d/azg3a_20050102_1000_rx1y1d1s1_flu_Ray6.sp2'
$SPEC 'RAY7' SPEC2D 'spec2d/azg3a_20050102_1000_rx1y1d1s1_flu_Ray7.sp2'
$SPEC 'RAY8' SPEC2D 'spec1d/azg3a_20050102_1000_rx1y1d1s1_flu_Ray8.sp2'
$SPEC 'RAY9' SPEC2D 'spec1d/azg3a_20050102_1000_rx1y1d1s1_flu_Ray9.sp2'
$SPEC 'RAY10' SPEC2D 'spec2d/azg3a_20050102_1000_rx1y1d1s1_flu_Ray10.sp2'
$SPEC 'RAY11' SPEC2D 'spec2d/azg3a_20050102_1000_rx1y1d1s1_flu_Ray11.sp2'
$SPEC 'RAY12' SPEC2D 'spec2d/azg3a_20050102_1000_rx1y1d1s1_flu_Ray12.sp2'
$SPEC 'RAY13' SPEC2D 'spec2d/azg3a_20050102_1000_rx1y1d1s1_flu_Ray13.sp2'
$SPEC 'RAY14' SPEC2D 'spec2d/azg3a_20050102_1000_rx1y1d1s1_flu_Ray14.sp2'
$SPEC 'RAY15' SPEC2D 'spec2d/azg3a_20050102_1000_rx1y1d1s1_flu_Ray15.sp2'
$SPEC 'RAY16' SPEC2D 'spec2d/azg3a_20050102_1000_rx1y1d1s1_flu_Ray16.sp2'
$SPEC 'RAY17' SPEC2D 'spec2d/azg3a_20050102_1000_rx1y1d1s1_flu_Ray17.sp2'
$SPEC 'RAY18' SPEC2D 'spec2d/azg3a_20050102_1000_rx1y1d1s1_flu_Ray18.sp2'
$SPEC 'RAY19' SPEC2D 'spec2d/azg3a_20050102_1000_rx1y1d1s1_flu_Ray19.sp2'
$SPEC 'RAY20' SPEC2D 'spec2d/azg3a_20050102_1000_rx1y1d1s1_flu_Ray20.sp2'
$ ********************************** SP2 Nest UITVOER ***********************************
$SPEC 'NK1A' SPEC2D 'bnest/ak1a_20050102_1000_rx1y1d1s1_flu.sp2'
$SPEC 'NK2A' SPEC2D 'bnest/ak2a_20050102_1000_rx1y1d1s1_flu.sp2'
$SPEC 'NK3A' SPEC2D 'bnest/ak3a_20050102_1000_rx1y1d1s1_flu.sp2'
$SPEC 'NK4A' SPEC2D 'bnest/ak4a_20050102_1000_rx1y1d1s1_flu.sp2'
$SPEC 'NK5A' SPEC2D 'bnest/ak5a_20050102_1000_rx1y1d1s1_flu.sp2'
$
BLOCK 'COMPGRID' NOHEAD  'block/azg3a_20050102_1000_rx1y1d1s1_fluxp.mat' LAY-OUT 3 XP
BLOCK 'COMPGRID' NOHEAD  'block/azg3a_20050102_1000_rx1y1d1s1_fluyp.mat' LAY-OUT 3 YP
BLOCK 'COMPGRID' NOHEAD  'block/azg3a_20050102_1000_rx1y1d1s1_flude.mat' LAY-OUT 3 DEPTH
BLOCK 'COMPGRID' NOHEAD  'block/azg3a_20050102_1000_rx1y1d1s1_fluhs.mat' LAY-OUT 3 HSIGN
BLOCK 'COMPGRID' NOHEAD  'block/azg3a_20050102_1000_rx1y1d1s1_flutp.mat' LAY-OUT 3 TPS
BLOCK 'COMPGRID' NOHEAD  'block/azg3a_20050102_1000_rx1y1d1s1_flut1.mat' LAY-OUT 3 TM01
BLOCK 'COMPGRID' NOHEAD  'block/azg3a_20050102_1000_rx1y1d1s1_flut2.mat' LAY-OUT 3 TM02
BLOCK 'COMPGRID' NOHEAD  'block/azg3a_20050102_1000_rx1y1d1s1_flut0.mat' LAY-OUT 3 TMM10
BLOCK 'COMPGRID' NOHEAD  'block/azg3a_20050102_1000_rx1y1d1s1_fludi.mat' LAY-OUT 3 DIR
BLOCK 'COMPGRID' NOHEAD  'block/azg3a_20050102_1000_rx1y1d1s1_fluds.mat' LAY-OUT 3 DSPR
BLOCK 'COMPGRID' NOHEAD  'block/azg3a_20050102_1000_rx1y1d1s1_flule.mat' LAY-OUT 3 WLEN
BLOCK 'COMPGRID' NOHEAD  'block/azg3a_20050102_1000_rx1y1d1s1_fludh.mat' LAY-OUT 3 DHSIGN
BLOCK 'COMPGRID' NOHEAD  'block/azg3a_20050102_1000_rx1y1d1s1_fludt.mat' LAY-OUT 3 DRTM01
BLOCK 'COMPGRID' NOHEAD  'block/azg3a_20050102_1000_rx1y1d1s1_fluve.mat' LAY-OUT 3 VEL
BLOCK 'COMPGRID' NOHEAD  'block/azg3a_20050102_1000_rx1y1d1s1_fluwl.mat' LAY-OUT 3 WATLEV
BLOCK 'COMPGRID' NOHEAD  'block/azg3a_20050102_1000_rx1y1d1s1_fluwi.mat' LAY-OUT 3 WIND
TEST 1 0 &
POINTS XY &
161240.  613520.  &   $ AZB11
164990.  614010.  &   $ AZB12
167200.  610400.  &   $ AZB21
167610.  610400.  &   $ AZB22
169380.  607320.  &   $ AZB31
169450.  607110.  &   $ AZB32
171340.  604400.  &   $ AZB41
171500.  604250.  &   $ AZB42
174290.  601500.  &   $ AZB51
175600.  600820.  &   $ AZB52
161450.  613500.  &   $ AZB21 (2004)
PAR 'par/azg3a_20050102_1000_rx1y1d1s1_flu.par'  &
S1D 'par/azg3a_20050102_1000_rx1y1d1s1_flu.s1d' &
S2D 'par/azg3a_20050102_1000_rx1y1d1s1_flu.s2d'
COMPUTE
$HOTFILE 'Hot/azg3a_20050102_1000_rx1y1d1s1_flu.hot'
STOP
```

A.2 Eems-Dollard

```
$************************************ HEADING ************************************************
PROJ 'SBW 2008' 'CL'
$
$      Runid:    'SBW'
$
$************************************** MODEL INPUT ******************************************
SET MAXERR = 3 NAUT

$ Definitieve rooster en bodem
$
$<MULTIGR>
$
CGRID CURVI 456 486 EXC -99.000  CIRCLE 36  0.03 1.00 37
READ  COOR  1. 'grid/eems3a.grd' IDLA=3 NHEDF=3 FORMAT '(10x,5F12.3)'
$
INP  BOTTOM CURVI 0. 0. 456 486 EXC -99.00
READ BOTTOM 1. 'bottom/eems3a.dep'  IDLA=3 NHEDF=0 FREE

INP  WLEV  CURVI  0. 0. 456 486  EXC -99.0
READ WLEV  1. 'lev/eems3a_20061101_0300.lev' IDLA=3 NHEDF=0 FREE

INP  CUR  CURVI  0. 0. 456 486  EXC -99.0
READ CUR  1. 'cur/eems3a_20061101_0300.cur' IDLA=3 NHEDF=0 FREE
$
$********************************** BOUNDARY CONDITIONS ********************************

$BOU  SHAPE JONSWAP PEAK DSPR DEGR
$BOU  SEGMENT XY  278336.9 649942.3  279920.3 639451.6   CON PAR      5.3 13.3 350 30
$BOU  SEGMENT XY  278336.9 649942.3  202357.6 626193.6   CON PAR      5.3 13.3 350 30
$BOU  SEGMENT XY  202357.6 626193.6  204188.9 612475.2   CON PAR      5.3 13.3 350 30
$
BOUNDNEST1 NEST 'bnest/eems3a_20061101_0300.sp2'  OPEN

$************************************** PHYSICA **********************************************
WIND 20.8 320

GEN3 WESTH
TRIAD    trfac=0.05 cutfr=2.5
BREAKING 1 0.73
FRICTION JONSWAP CFJON=0.067
$*** Input block for numerics study H5107.46 ***
QUAD iquad=2
$<TRIPLET>
$<DDM>
$<LIMITER>
$********************************** NUMERIEKE PARAMETERS *********************************

NUM STOPC 0.00 0.01 0.001 99 STAT mxitst=80  alfa=0.002
$************************************ NEST ***************************************************

$************************************ DEFINITIE VAN UITVOERPUNTEN ************************

POINTS 'WZNL-08'  FILE 'points/WZNL-2008.pnt'
POINTS 'WZD-08'  FILE 'points/WZD-2008.pnt'
POINTS 'WZ-HWL' FILE 'points/WZ-HWLEV.pnt'
$
POINTS 'eems3a'  FILE 'bnest/eems3a.bnd'
$************************************ DEFINITIE VAN UITVOERRAAIEN*************************
CURVE 'curv1' 216647 625432 250 222094 604831
CURVE 'curv2' 230394 630560 250 240407 609228
CURVE 'curv3' 244471 637402 250 264734 593608
CURVE 'curv4' 262654 644224 250 270137 629590
$
$ ********************************** BLOCK UITVOER  ***************************************

OUTPUT OPTIONS '%' TABLE 16 BLOCK 9 1000 SPEC 8

BLOCK 'COMPGRID' NOHEAD 'block/eems3_20061101_0300_rx1y1d1s1xp.mat' XP
BLOCK 'COMPGRID' NOHEAD 'block/eems3_20061101_0300_rx1y1d1s1yp.mat' YP
BLOCK 'COMPGRID' NOHEAD 'block/eems3_20061101_0300_rx1y1d1s1de.mat' DEP
BLOCK 'COMPGRID' NOHEAD 'block/eems3_20061101_0300_rx1y1d1s1hs.mat' HS
BLOCK 'COMPGRID' NOHEAD 'block/eems3_20061101_0300_rx1y1d1s1t0.mat' TMM10
BLOCK 'COMPGRID' NOHEAD 'block/eems3_20061101_0300_rx1y1d1s1rt.mat' RTMM10
BLOCK 'COMPGRID' NOHEAD 'block/eems3_20061101_0300_rx1y1d1s1tp.mat' TPS
BLOCK 'COMPGRID' NOHEAD 'block/eems3_20061101_0300_rx1y1d1s1t1.mat' TM01
BLOCK 'COMPGRID' NOHEAD 'block/eems3_20061101_0300_rx1y1d1s1t2.mat' TM02
```

```
BLOCK 'COMPGRID' NOHEAD 'block/eems3_20061101_0300_rx1y1d1s1di.mat' DIR
BLOCK 'COMPGRID' NOHEAD 'block/eems3_20061101_0300_rx1y1d1s1ds.mat' DSPR
BLOCK 'COMPGRID' NOHEAD 'block/eems3_20061101_0300_rx1y1d1s1le.mat' WLEN
BLOCK 'COMPGRID' NOHEAD 'block/eems3_20061101_0300_rx1y1d1s1wf.mat' FORCE
BLOCK 'COMPGRID' NOHEAD 'block/eems3_20061101_0300_rx1y1d1s1dh.mat' DHSIGN
BLOCK 'COMPGRID' NOHEAD 'block/eems3_20061101_0300_rx1y1d1s1dt.mat' DRTM01
BLOCK 'COMPGRID' NOHEAD 'block/eems3_20061101_0300_rx1y1d1s1wl.mat' WATLEV
BLOCK 'COMPGRID' NOHEAD 'block/eems3_20061101_0300_rx1y1d1s1wi.mat' WIND
BLOCK 'COMPGRID' NOHEAD 'block/eems3_20061101_0300_rx1y1d1s1ve.mat' VEL

$ ********************************** TABEL UITVOER ************************************
TABLE  'WZ-HWL'   HEAD 'table/eems3_20061101_0300_rx1y1d1s1_WZ_HWL.tab' &
       XP YP DEP HS RTP TMM10 TM01 TM02 FSPR DIR DSPR WLENGTH TPS DHSIGN DRTM01 WATLEV WIND VEL
TABLE  'WZNL-08'   HEAD 'table/eems3_20061101_0300_rx1y1d1s1_WZNL08.tab' &
       XP YP DEP HS RTP TMM10 TM01 TM02 FSPR DIR DSPR WLENGTH TPS DHSIGN DRTM01 WATLEV WIND VEL
TABLE  'WZD-08'   HEAD 'table/eems3_20061101_0300_rx1y1d1s1_WZD08.tab' &
       XP YP DEP HS RTP TMM10 TM01 TM02 FSPR DIR DSPR WLENGTH TPS DHSIGN DRTM01 WATLEV WIND VEL
TABLE  'curv1'   HEAD 'table/eems3_20061101_0300_rx1y1d1s1_curv1.tab'  &
       XP YP DEP HS RTP TMM10 TM01 TM02 FSPR DIR DSPR WLENGTH TPS DHSIGN DRTM01 WATLEV WIND VEL
TABLE  'curv2'   HEAD 'table/eems3_20061101_0300_rx1y1d1s1_curv2.tab'  &
       XP YP DEP HS RTP TMM10 TM01 TM02 FSPR DIR DSPR WLENGTH TPS DHSIGN DRTM01 WATLEV WIND VEL
TABLE  'curv3'   HEAD 'table/eems3_20061101_0300_rx1y1d1s1_curv3.tab'  &
       XP YP DEP HS RTP TMM10 TM01 TM02 FSPR DIR DSPR WLENGTH TPS DHSIGN DRTM01 WATLEV WIND VEL
TABLE  'curv4'   HEAD 'table/eems3_20061101_0300_rx1y1d1s1_curv4.tab'  &
       XP YP DEP HS RTP TMM10 TM01 TM02 FSPR DIR DSPR WLENGTH TPS DHSIGN DRTM01 WATLEV WIND VEL

$ ********************************** SP1 UITVOER ***************************************
SPEC 'WZ-HWL' SPEC1D 'spec1d/eems3_20061101_0300_rx1y1d1s1_WZ_HWL.sp1'
SPEC 'WZNL-08' SPEC1D 'spec1d/eems3_20061101_0300_rx1y1d1s1_WZNL08.sp1'
SPEC 'WZD-08' SPEC1D 'spec1d/eems3_20061101_0300_rx1y1d1s1_WZD08.sp1'
SPEC 'curv1' SPEC1D 'spec1d/eems3_20061101_0300_rx1y1d1s1_curv1.sp1'
SPEC 'curv2' SPEC1D 'spec1d/eems3_20061101_0300_rx1y1d1s1_curv2.sp1'
SPEC 'curv3' SPEC1D 'spec1d/eems3_20061101_0300_rx1y1d1s1_curv3.sp1'
SPEC 'curv4' SPEC1D 'spec1d/eems3_20061101_0300_rx1y1d1s1_curv4.sp1'

$ ********************************** SP2 UITVOER ***************************************
SPEC 'WZ-HWL' SPEC2D 'spec2d/eems3_20061101_0300_rx1y1d1s1_WZ_HWL.sp2'
SPEC 'WZNL-08' SPEC2D 'spec2d/eems3_20061101_0300_rx1y1d1s1_WZNL08.sp2'
SPEC 'WZD-08' SPEC2D 'spec2d/eems3_20061101_0300_rx1y1d1s1_WZD08.sp2'
SPEC 'curv1' SPEC2D 'spec2d/eems3_20061101_0300_rx1y1d1s1_curv1.sp2'
SPEC 'curv2' SPEC2D 'spec2d/eems3_20061101_0300_rx1y1d1s1_curv2.sp2'
SPEC 'curv3' SPEC2D 'spec2d/eems3_20061101_0300_rx1y1d1s1_curv3.sp2'
SPEC 'curv4' SPEC2D 'spec2d/eems3_20061101_0300_rx1y1d1s1_curv4.sp2'

$ ******************** TEST UITVOER VOOR MEETLOCATIES ************************************

TEST 1 0 POINTS XY &
225877   608435.  &
200000   602587.  &
195573   615137.  &
238498   639349.  &
237482   621214.  &
219900   626397.  &
229819   626226.  &
240580   614890.  &
243900   612140.  &
245500   609810.  &
206131.89  603968.87  &
235954.72  607937.74  &
251112.20  609883.27  &
258198.82  596420.23  &
206131.89  603968.87  &
235954.72  607937.74  &
251112.20  609883.27  &
258198.82  596420.23  &
206131.89  603968.87  &
235954.72  607937.74  &
251112.20  609883.27  &
258198.82  596420.23  &
206131.89  603968.87  &
235954.72  607937.74  &
251112.20  609883.27  &
258198.82  596420.23  &
PAR 'par/eems3_20061101_0300_rx1y1d1s1.par'  &
S1D 'par/eems3_20061101_0300_rx1y1d1s1.s1d' &
S2D 'par/eems3_20061101_0300_rx1y1d1s1.s2d'

COMPUTE
$HOTFILE 'hot/eems3_20061101_0300_rx1y1d1s1.hot'
STOP
```

A.3 Petten

```
$
$   Deltares & Alkyon
$       PROJECT H5107.46/A2114, Multi Grid First Guess
$   Simulatie : d19950101t1000
$
PROJ 'Bodem A2114' 'kust'
$
SET MAXERR = 3  NAUT
$
$<MULTIGR>
$
CGRID CURVILINEAR 520 374  EXCE -999 -999 CIRCLE 36 0.03 1.00 38
READ  COORD 1. 'grid/petten1.grd' IDLA=3 NHEDF=3 FORMAT '(10X,5F12.3)'
$
INP  BOTTOM CURVILINEAR 0. 0. 520 374 EXCE -99.00
READ BOTTOM 1. 'grid/petten1.dep' IDLA=3 NHEDF=0 FREE
$
$
SET LEVEL = 0.54
$
$ Setting boundary conditions
$BOU  SHAPE JONSWAP PEAK DSPR DEGR
$BOU  SEGMENT XY  86858.6  571311.9  110370.8  562935.9  CON PAR   5.85 9.8 329 30
$BOU  SEGMENT XY  86858.6  571311.9  69811.7  516663.7  CON PAR   5.85 9.8 329 30
$BOU  SEGMENT XY  69811.7  516663.7  100430.7  502756.7  CON PAR   5.85 9.8 329 30
$
BOUNDNEST1 NEST 'bnest\petten1.sp2'  OPEN
$
WIND 25  329
GEN3  WESTH
BREAKING 1. 0.73
FRICTION JONSWAP CFJON=0.038
TRIAD trfac=0.05 cutfr=2.5
$*** Input block for numerics study H5107.46 ***
QUAD iquad=2
$<TRIPLET>
$<DDM>
$<LIMITER>
$********************************** NUMERIEKE PARAMETERS *********************************
NUM STOPC 0.00 0.01 0.001 99 STAT mxitst=80  alfa=0.001
$
$************ OUTPUT REQUESTS ************************
$ raai door meetpunten bij Petten, vanaf de rand
$
CURVE 'rp20' 70680 564000 1000 125980 550880
CURVE 'rp10'  69680 563000 1000 115980 540880
CURVE 'rp5'  67680 561000 1000 106080 531380
CURVE 'rp1'  66780 560100 1000 107030 532330
CURVE 'raai' 66680 560000 1000 106080 531380
CURVE 'rm1'  66580 559900 1000 105130 530430
CURVE 'rm5'  65680 559000 1000 101580 526880
CURVE 'rm10' 63680 557000 1000  96580 521880
CURVE 'rm20' 62680 556000 1000  86580 541880
TABLE  'rp20'     HEAD  'table/p_rx1y1d1s1_rp20.tab'     XP YP DEP HS PER TM01 TM02 RTP DIR DSPR
FSPR DHSIGN TMM10
TABLE  'rp10'     HEAD  'table/p_rx1y1d1s1_rp10.tab'     XP YP DEP HS PER TM01 TM02 RTP DIR DSPR
FSPR DHSIGN TMM10
TABLE  'rp5'      HEAD  'table/p_rx1y1d1s1_rp5.tab'     XP YP DEP HS PER TM01 TM02 RTP DIR DSPR
FSPR DHSIGN  TMM10
TABLE  'rp1'      HEAD  'table/p_rx1y1d1s1_rp1.tab'     XP YP DEP HS PER TM01 TM02 RTP DIR DSPR
FSPR DHSIGN  TMM10
TABLE  'raai'     HEAD  'table/p_rx1y1d1s1_raai.tab'     XP YP DEP HS PER TM01 TM02 RTP DIR DSPR
FSPR DHSIGN TMM10
TABLE  'rm1'      HEAD  'table/p_rx1y1d1s1_rm1.tab'      XP YP DEP HS PER TM01 TM02 RTP DIR DSPR
FSPR DHSIGN TMM10
TABLE  'rm5'      HEAD  'table/p_rx1y1d1s1_rm5.tab'      XP YP DEP HS PER TM01 TM02 RTP DIR DSPR
FSPR DHSIGN TMM10
TABLE  'rm10'     HEAD  'table/p_rx1y1d1s1_rm10.tab'     XP YP DEP HS PER TM01 TM02 RTP DIR DSPR
FSPR DHSIGN TMM10
TABLE  'rm20'     HEAD  'table/p_rx1y1d1s1_rm20.tab'     XP YP DEP HS PER TM01 TM02 RTP DIR DSPR
FSPR DHSIGN TMM10
SPECOUT  'raai'  SPEC1D ABS 'sp1/p_rx1y1d1s1_raai.sp1'
SPECOUT  'raai'  SPEC2D ABS 'sp2/p_rx1y1d1s1_raai.sp2'
$
$ file met meetlocaties
$
POINTS 'locs'  FILE  'points/locs.xyz'
TABLE  'locs'  HEAD 'table/p_rx1y1d1s1_locs.tab'     XP YP DEP HS TMM10 TM01 TM02 TPS DIR DSPR &
```

```
  DHSIGN DRTM01 WIND WLEN
SPECOUT  'locs'  SPEC1D ABS 'sp1/p_rx1y1d1s1_locs.sp1'
SPECOUT  'locs'  SPEC2D ABS 'sp2/p_rx1y1d1s1_locs.sp2'
$
$ Block files voor Matlab
$
BLOCK 'COMPGRID' NOHEAD 'block/p_rx1y1d1s1xp.mat' LAYOUT 3 XP
BLOCK 'COMPGRID' NOHEAD 'block/p_rx1y1d1s1yp.mat' LAYOUT 3 YP
BLOCK 'COMPGRID' NOHEAD 'block/p_rx1y1d1s1de.mat' LAYOUT 3 DEPTH
BLOCK 'COMPGRID' NOHEAD 'block/p_rx1y1d1s1hs.mat' LAYOUT 3 HSIGN
BLOCK 'COMPGRID' NOHEAD 'block/p_rx1y1d1s1di.mat' LAYOUT 3 DIR
BLOCK 'COMPGRID' NOHEAD 'block/p_rx1y1d1s1ds.mat' LAYOUT 3 DSPR
BLOCK 'COMPGRID' NOHEAD 'block/p_rx1y1d1s1tp.mat' LAYOUT 3 TPS
BLOCK 'COMPGRID' NOHEAD 'block/p_rx1y1d1s1t0.mat' LAYOUT 3 TMM10
BLOCK 'COMPGRID' NOHEAD 'block/p_rx1y1d1s1t1.mat' LAYOUT 3 TM01
BLOCK 'COMPGRID' NOHEAD 'block/p_rx1y1d1s1t2.mat' LAYOUT 3 TM02
BLOCK 'COMPGRID' NOHEAD 'block/p_rx1y1d1s1wi.mat' LAYOUT 3 WIND
BLOCK 'COMPGRID' NOHEAD 'block/p_rx1y1d1s1wl.mat' LAYOUT 3 WLEN
BLOCK 'COMPGRID' NOHEAD 'block/p_rx1y1d1s1dh.mat' LAYOUT 3 DHSIGN
BLOCK 'COMPGRID' NOHEAD 'block/p_rx1y1d1s1dt.mat' LAYOUT 3 DRTM01
$
TEST 1 0 &
POINTS XY &
 98981 536444 &
 99003 535832 &
103000 533800 &
102890 533728 &
105230 531990 &
105234 531985 &
105520 531830 &
105650 531746 &
105661 531752 &
105661 531752 &
105377 531886 &
105377 531886 &
105522 531817 &
105522 531817 &
105617 531771 &
PAR 'par/p_rx1y1d1s1.par' &
S1D 'par/p_rx1y1d1s1.s1d' &
S2D 'par/p_rx1y1d1s1.s2d'

COMPUTE
STOP
```

A.4 Lake Sloten

```
$
$   RIZA testcase Slotermeer
$   SWAN Slotermeer 2D
$   Bodem: SLM2003dx10.bot
$   Filename: SL_SLE_basa.swn
$   Uitvoerpt: -
$
$  Start-up Commands ************************************
$  CASEBESCHRIJVING: SLOTERMEER: RIZA-CALIBRATIECASE VOOR SWAN 25/9/2003
$  BETREFT CASE 26/02/2002 14-15 UUR MET
$
$  ZOEK EN VERVANG BLOK
$
$  Case    : wlm29u208dd243
$  meerpeil:  -0.29   m + NAP
$  u10     :   20.800   m/s
$  dd      : 243.000   deg N
$  fmax    :   1.7   Hz
$  Nfreq   : MSC=32
$
$ EINDE ZOEK EN VERVANG BLOK
$
$
PROJECT 'RIZA' 'GGL '
        'SWAN Slotermeer  '
        'Cond&Codes:dx=dy=40m MSC=32,fmax=1.7Hz,fmin=0.08Hz,NTH=36'
        'Level= NAP -0.29 m; u10= 20.800 m/s; Dir_N= 243.000 N, SORDUP'
$
$--------------------------------------------------------------------------
$** MEERPEIL (boven referentienivo is +. Optellen bij bodemnivo=waterdiepte)
$--------------------------------------------------------------------------
```

```
$
SET LEVEL=-0.45  DEPMIN=0.01 MAXMES=200 MAXERR=1 RHO=1000 NAUTICAL
$
$-------------------------------------------------------------------------
$** REKENGRID ***
$rekengrid 40m:
$--------------------------------
$
$<MULTIGR>
$
CGRID  XPC=168800 YPC=545600 ALPC=0. XLENC=4800.,YLENC=4000., MXC=480, &
       MYC=400, CIRCLE  MDC=36 FLOW=0.08 FHIGH=1.8  MSC=33
$-------------------------------------------------------------------------
$** BODEMGRID ***  (beneden referentienivo is +)
$-------------------------------------------------------------------------
INP BOT  XPINP=168800. YPINP=545600. ALPINP=0.0 MXINP=480  MYINP=400 &
         DXINP=10.00 DYINP=10.00 EXCEPTION 0
READ BOT FAC=-0.01 'bottom/SLM2003dx10.bot'  IDLA=1  NHEDF=8  FREE
$
$-------------------------------------------------------------------------
$** BREKINGPARAMETERS & BODEMWRIJVING ***
$-------------------------------------------------------------------------
$
BREAKING CON ALPHA=1.0 GAMMA=0.73
FRICTION  jonswap cfjon = 0.067
$
$-------------------------------------------------------------------------
$** WINDSNELHEID, WINDRICHTING  EN WINDGROEI
$-------------------------------------------------------------------------
$
WIND  VEL=21.4  DIR=252
GEN3 westh
$-------------------------------------------------------------------------
$
$ Triad wisselwerking
$-------------------------------------------------------------------------
$
TRIAD trfac=0.05 cutfr=2.5
$
$*** Input block for numerics study H5107.46 ***
QUAD iquad=2
$<TRIPLET>
$<DDM>
$<LIMITER>
$
$---------------------------------------------------------------
$ REKENPARAMETERS
$---------------------------------------------------------------

NUM STOPC 0.00 0.01 0.001 99 STAT mxitst=80  alfa = 0.001

OUTPUT OPTIONS '%' TABLE 16 BLOCK 9 1000 SPEC 8


$-------------------------------------------------------------------------
$** DEFINITIE UITVOERLOCATIES: FRAMES, KROMMEN EN PUNTEN ***
$ FRAME  'Naam' XPF,  YPF,  ALPF, XFLEN,  YFLEN,  MXF, MYF,  (SCALE)
$ Outputframes 40 m (div.) en 80 en 200 m (spectra)
$-------------------------------------------------------------------------
FRAME 'YFR40' 168800., 545600, .0, 4800., 4000.  120, 100
FRAME 'YFR1'  168800., 545600, .0, 4800., 4000.  60, 50
FRAME 'YFR2'  168800., 545600, .0, 4800., 4000.  24, 20
$
$ ******************* HOT TAB OUTPUT *********************************
$TABLE 'COMPGRID' HEAD 'hot/sl_SLE_rx1y1d1s1_depth.tab' XP YP DEPTH
$TABLE 'COMPGRID' HEAD 'hot/sl_SLE_rx1y1d1s1_wind.tab' XP YP WIND

$---------------------------------------------------------------
BLOCK 'YFR40'  FILE  'block/SL_SLE_rx1y1d1s1xp.mat' LAY-OUT 3 XP
BLOCK 'YFR40'  FILE  'block/SL_SLE_rx1y1d1s1yp.mat' LAY-OUT 3 YP
BLOCK 'YFR40'  FILE  'block/SL_SLE_rx1y1d1s1de.mat' LAY-OUT 3 DEPTH
BLOCK 'YFR40'  FILE  'block/SL_SLE_rx1y1d1s1hs.mat' LAY-OUT 3 HSIGN
BLOCK 'YFR40'  FILE  'block/SL_SLE_rx1y1d1s1t1.mat' LAY-OUT 3 TM01
BLOCK 'YFR40'  FILE  'block/SL_SLE_rx1y1d1s1t2.mat' LAY-OUT 3 TM02
BLOCK 'YFR40'  FILE  'block/SL_SLE_rx1y1d1s1t0.mat' LAY-OUT 3 TMM10
BLOCK 'YFR40'  FILE  'block/SL_SLE_rx1y1d1s1di.mat'  LAY-OUT 3 DIR
BLOCK 'YFR40'  FILE  'block/SL_SLE_rx1y1d1s1dh.mat' LAY-OUT 3 DHSIGN
BLOCK 'YFR40'  FILE  'block/SL_SLE_rx1y1d1s1dt.mat' LAY-OUT 3 DRTM01
BLOCK 'YFR40'  FILE 'block/SL_SLE_rx1y1d1s1tp.mat' LAY-OUT 3 TPS
BLOCK 'YFR40'  FILE 'block/SL_SLE_rx1y1d1s1ds.mat' LAY-OUT 3 DSPR
BLOCK 'YFR40'  FILE 'block/SL_SLE_rx1y1d1s1wl.mat' LAY-OUT 3 WLEN
```

```
BLOCK 'YFR40'  FILE 'block/SL_SLE_rx1y1d1s1qb.mat' LAY-OUT 3 QB

SPEC 'YFR1' SPEC1D ABS 'spec1d/SL_SLE_rx1y1d1s1.sp1'
SPEC 'YFR2' SPEC2D ABS 'spec2d/SL_SLE_rx1y1d1s1.sp2'
$-----------------------------------------------
$   write point/table/spectra output requests
$ extra TABLE zonder header omdat QB anders niet goed geplot wordt
$-----------------------------------------------

POINTS 'SL29' xp=172489 yp=548502
TABLE  'SL29' HEADER 'table/SL_SLE_rx1y1d1s1.tab'   &
  XP YP DEP HS TPS TMM10 TM01 TM02 DIR DSPR   &
  TM02 PER WLEN STEEP QB DHSIGN DRTM01 URMS TRANSP
SPEC 'SL29' SPEC1D ABS 'spec1d/SL_SLE_rx1y1d1s1_SL29.sp1'
SPEC 'SL29' SPEC2D ABS 'spec2d/SL_SLE_rx1y1d1s1_SL29.sp2'

$-------------------------------------------------------------------------
$ TEST-output
$-------------------------------------------------------------------------
TEST 1 0 &
POINTS XY &
    172520.01    548560.00  &
    169520.01    546520.00  &
    169520.01    547280.00  &
    169520.01    548040.00  &
    170040.01    546040.00  &
    170040.01    547280.00  &
    170040.01    548520.00  &
    170560.01    546520.00  &
    170560.01    547520.00  &
    170560.01    548520.00  &
    171040.01    546520.00  &
    171040.01    547760.00  &
    171040.01    549040.00  &
    171560.01    547040.00  &
    171560.01    548040.00  &
    171560.01    549040.00  &
    172040.01    547040.00  &
    172040.01    548040.00  &
    172040.01    549040.00  &
    172520.01    547520.00  &
    172520.01    548280.00  &
    172520.01    549040.00  &
    173040.01    548040.00  &
    173040.01    548520.00  &
    173040.01    549040.00  &
PAR 'par/SL_SLE_rx1y1d1s1.par' &
S1D 'par/SL_SLE_rx1y1d1s1.s1d' &
S2D 'par/SL_SLE_rx1y1d1s1.s2d'
COMPUTE
$
$
$HOTFILE 'hot/SL_SLE_rx1y1d1s1.hot'
$
STOP
```

Figures

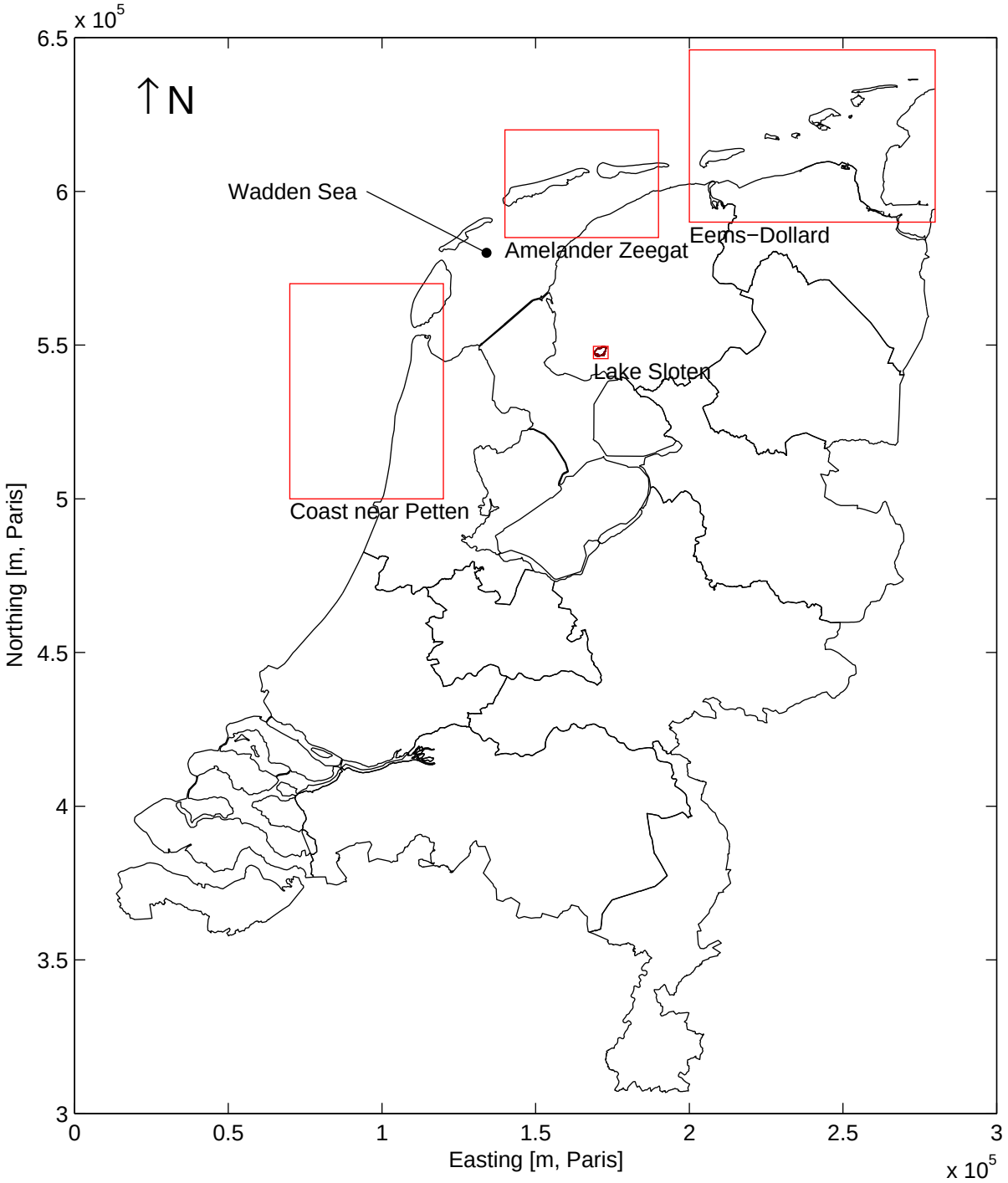

Location of the four field case sites considered in this study		
	Numerical efficiency SWAN	
DELTARES & ALKYON	H5107.46/A2114	Fig. 1.1

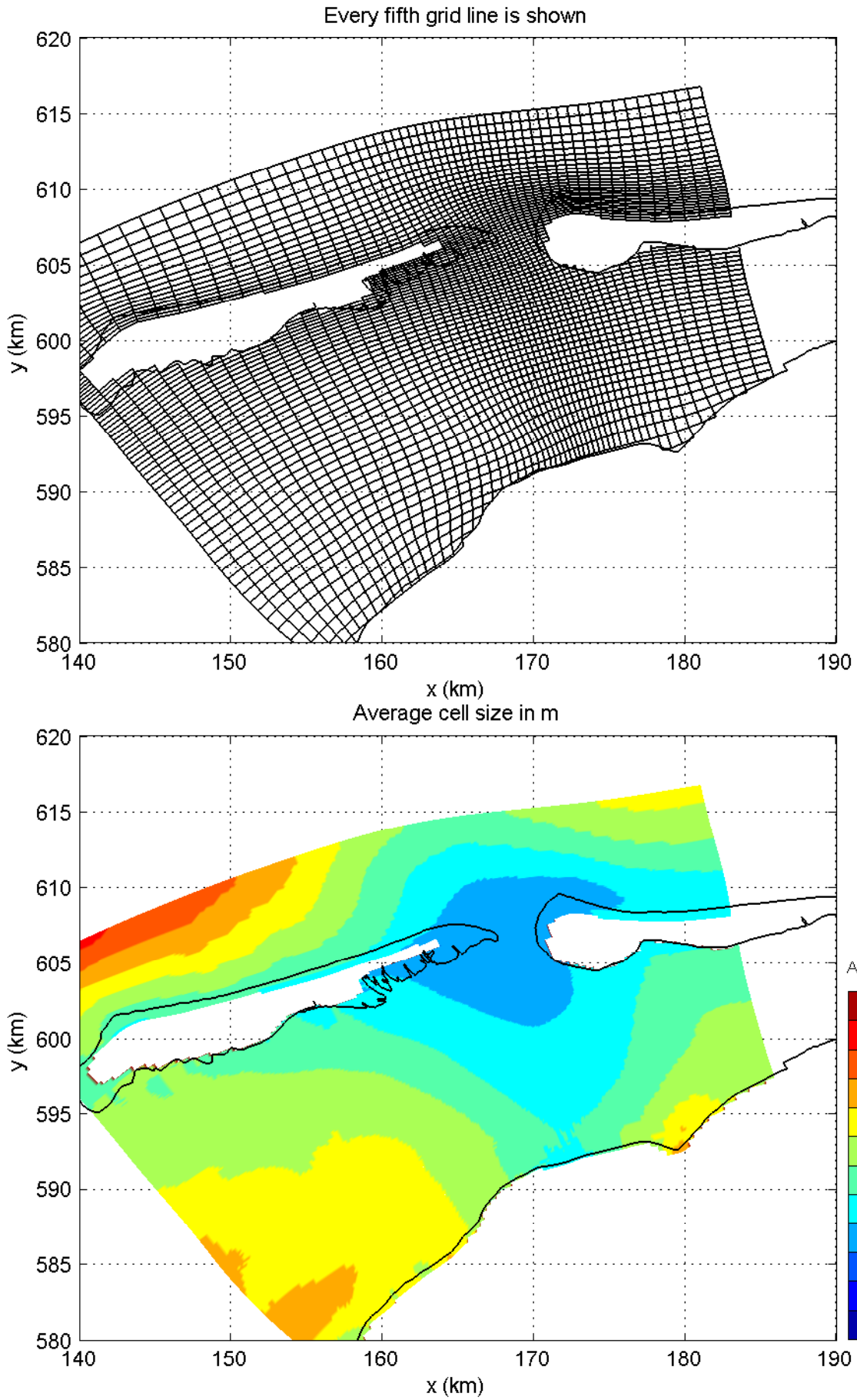

Outline of computational grid of the Amelander Zeegat (upper panel) Average of size of grid cells in m (lower panel)		SWAN 40.51A
		Numerical efficiency SWAN
DELTARES & ALKYON	H5107.46/A2114	Fig. 2.1

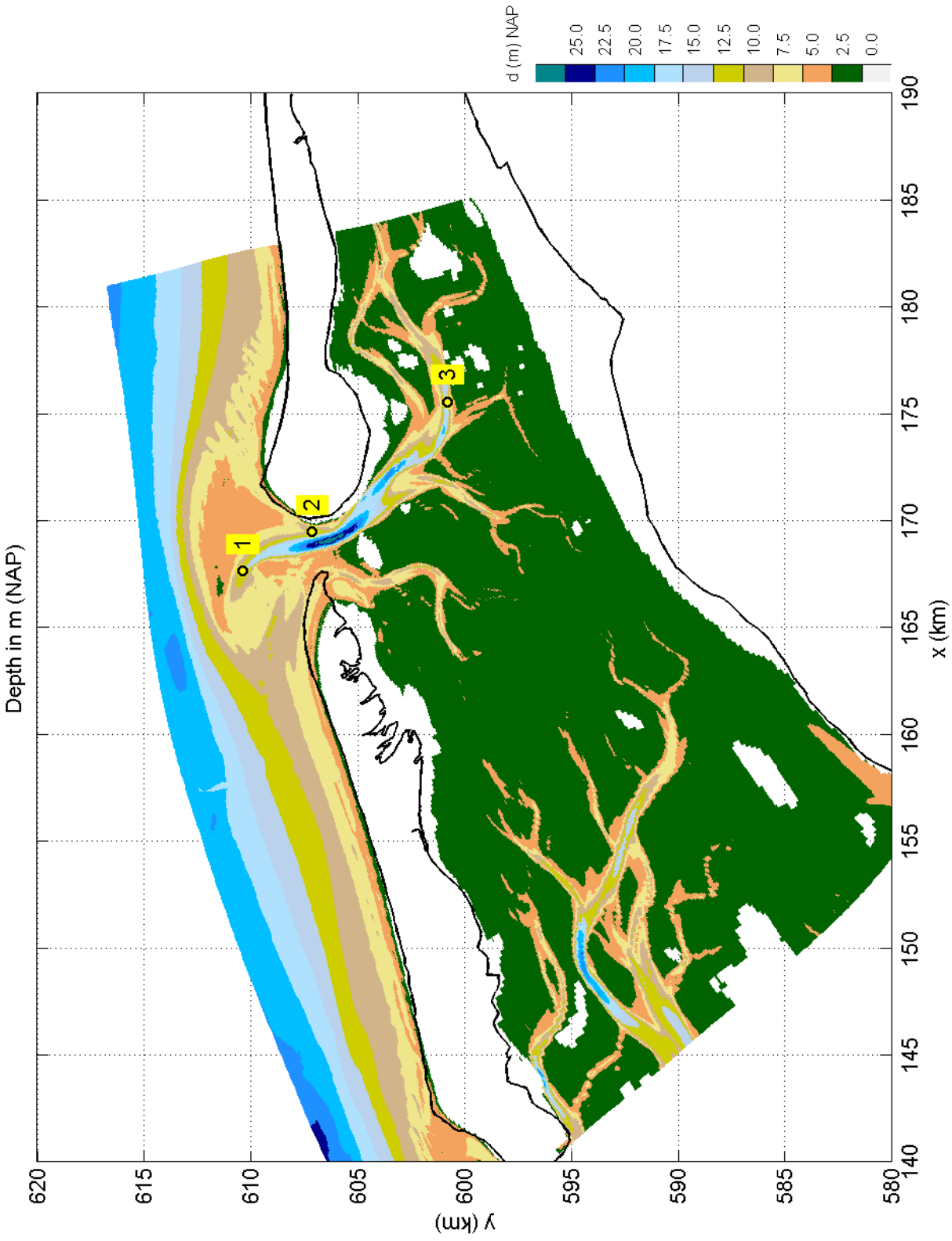

Bathymetry of the Amelander Zeegat and location of test points		SWAN 40.51A
		Numerical efficiency SWAN
DELTARES & ALKYON	H5107.46/A2114	Fig. 2.2

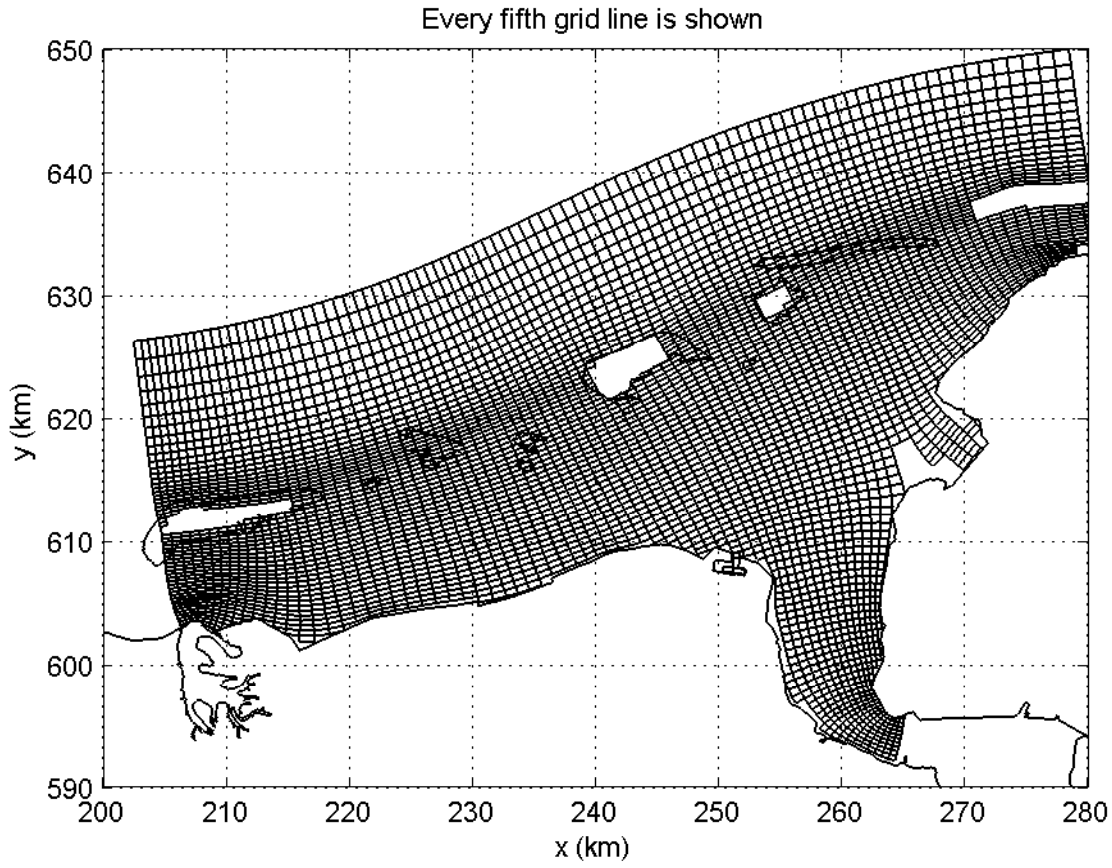

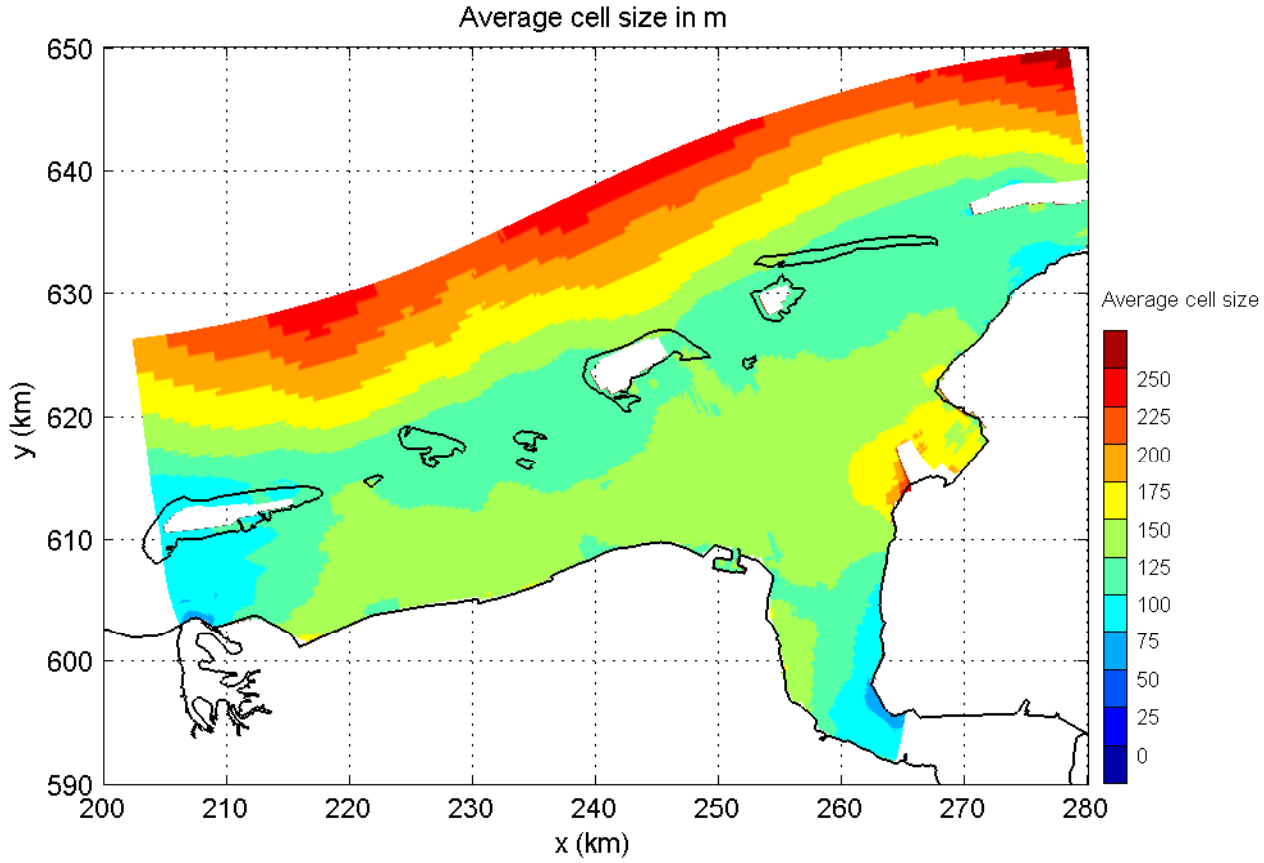

Outline of computational grid of the Eems-Dollard (upper panel) Average of size of grid cells in m (lower panel)		SWAN 40.51A
		Numerical efficiency SWAN
DELTARES & ALKYON	H5107.46/A2114	Fig. 2.3

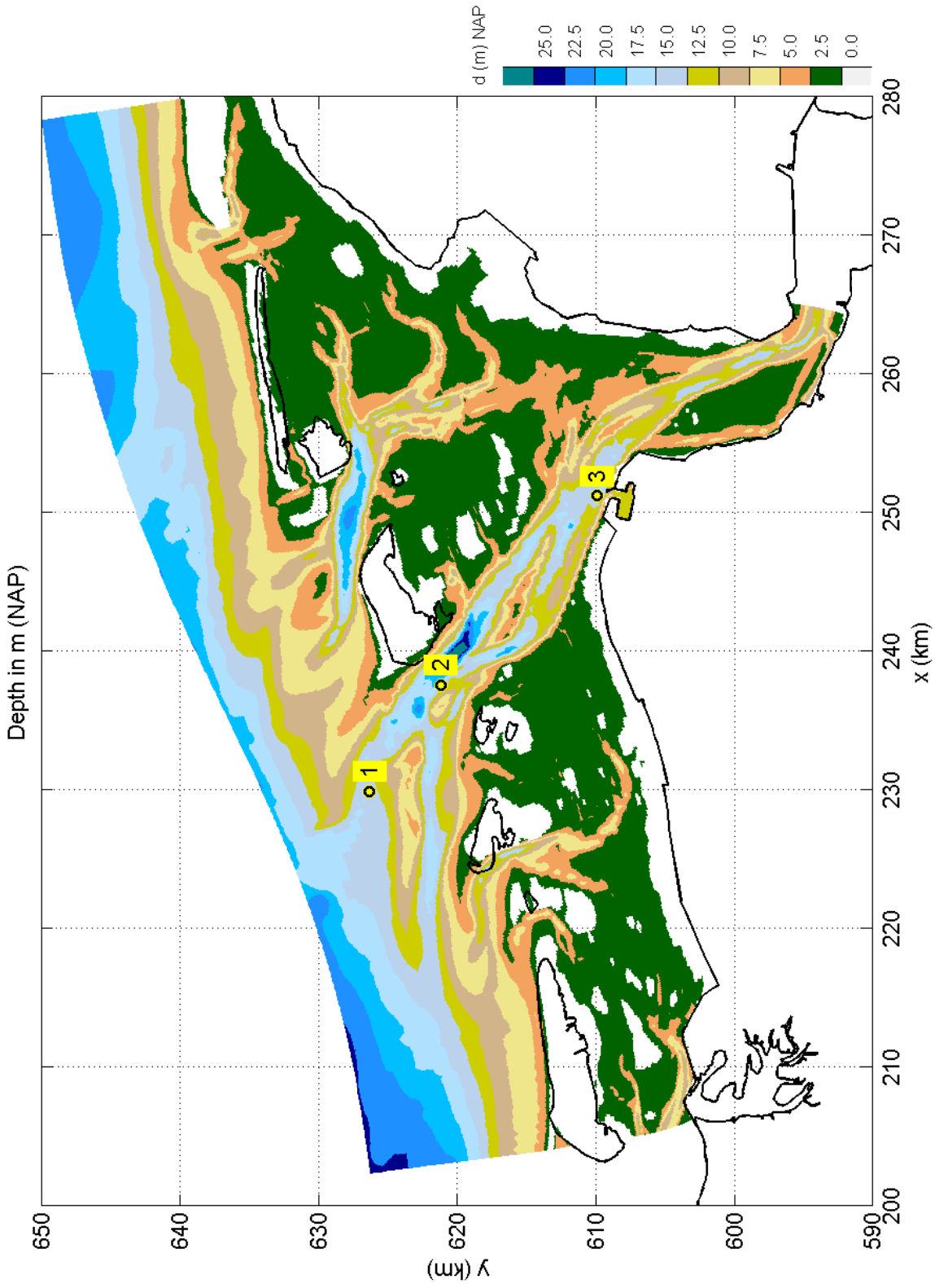

Bathymetry of the Eems-Dollard and location of test points		SWAN 40.51A
		Numerical efficiency SWAN
DELTARES & ALKYON	H5107.46/A2114	Fig. 2.4

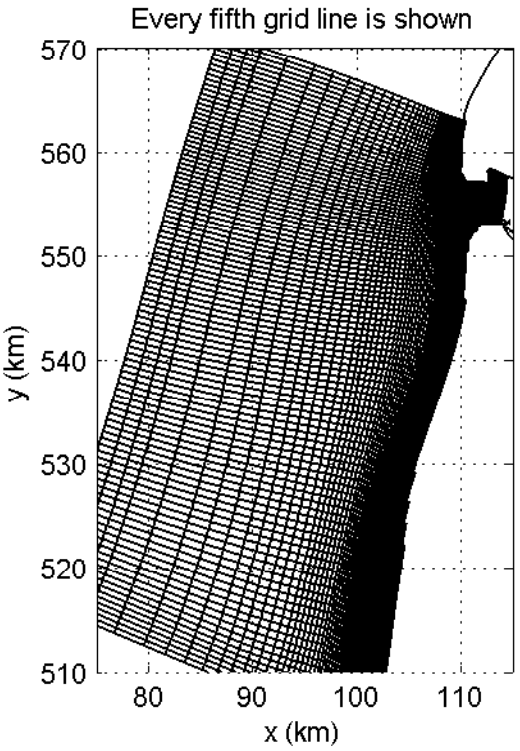

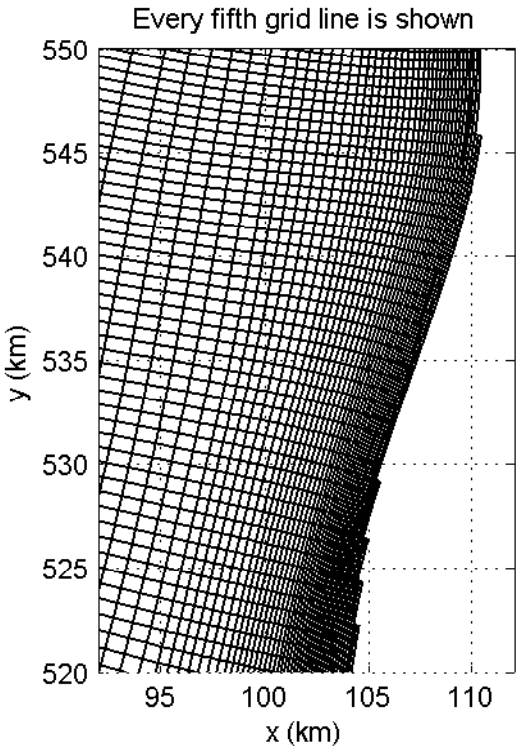

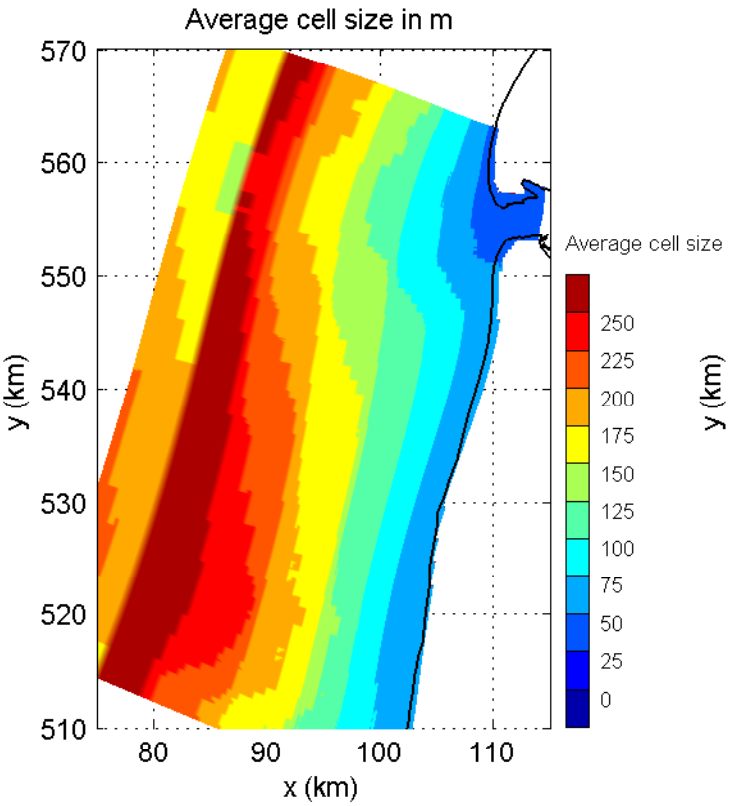

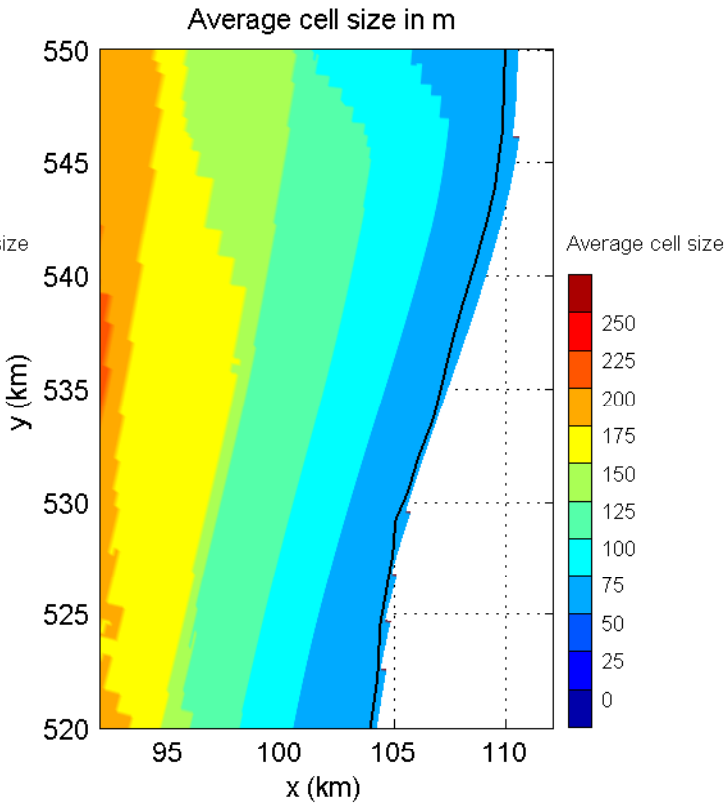

Outline of computational grid for the Petten field case (upper panels) Average of size of grid cells in m (lower panels)		SWAN 40.51A
		Numerical efficiency SWAN
DELTARES & ALKYON	H5107.46/A2114	Fig. 2.5

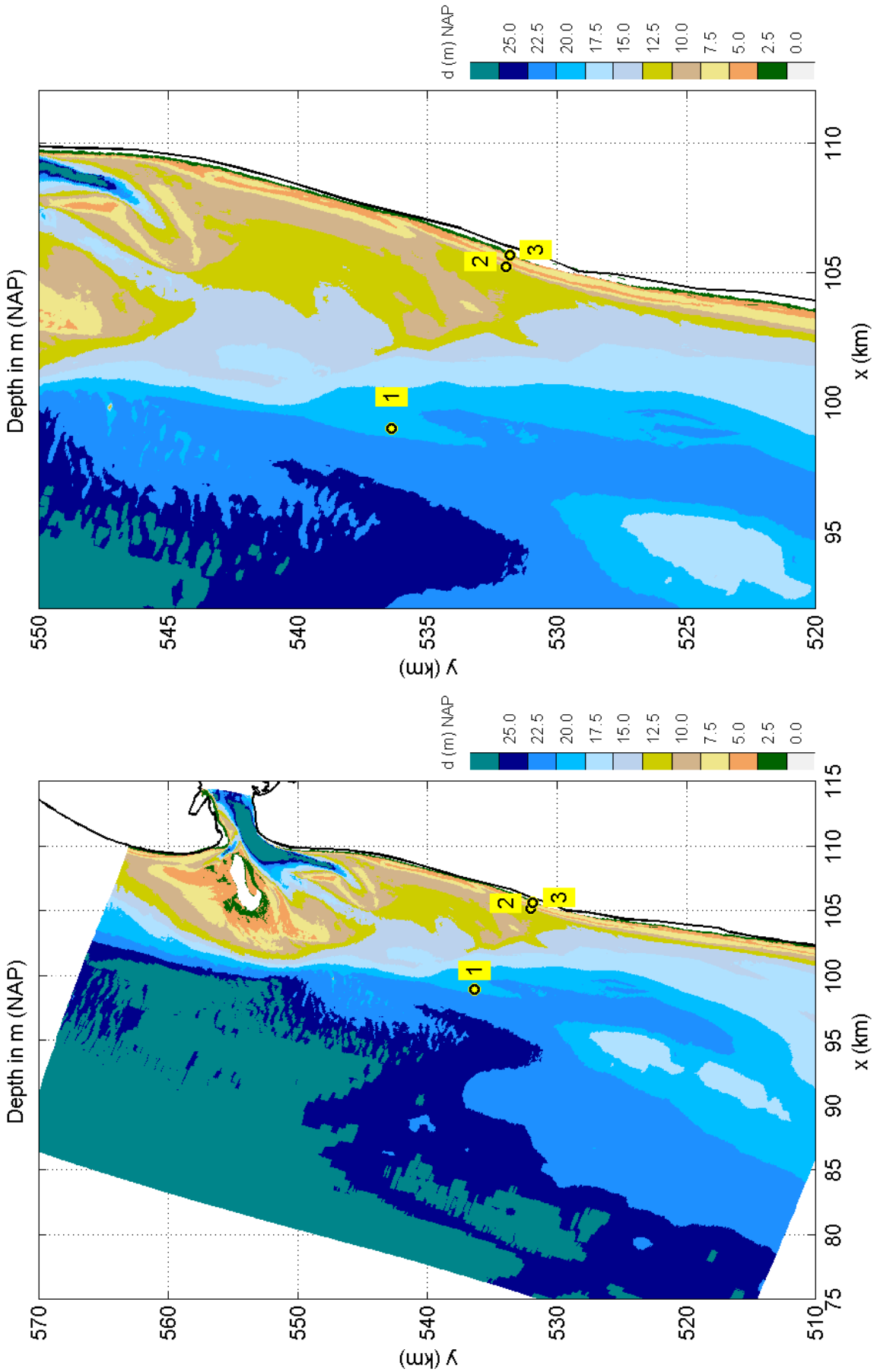

Bathymetry for the Petten field case and location of test points		SWAN 40.51A
		Numerical efficiency SWAN
DELTARES & ALKYON	H5107.46/A2114	Fig. 2.6

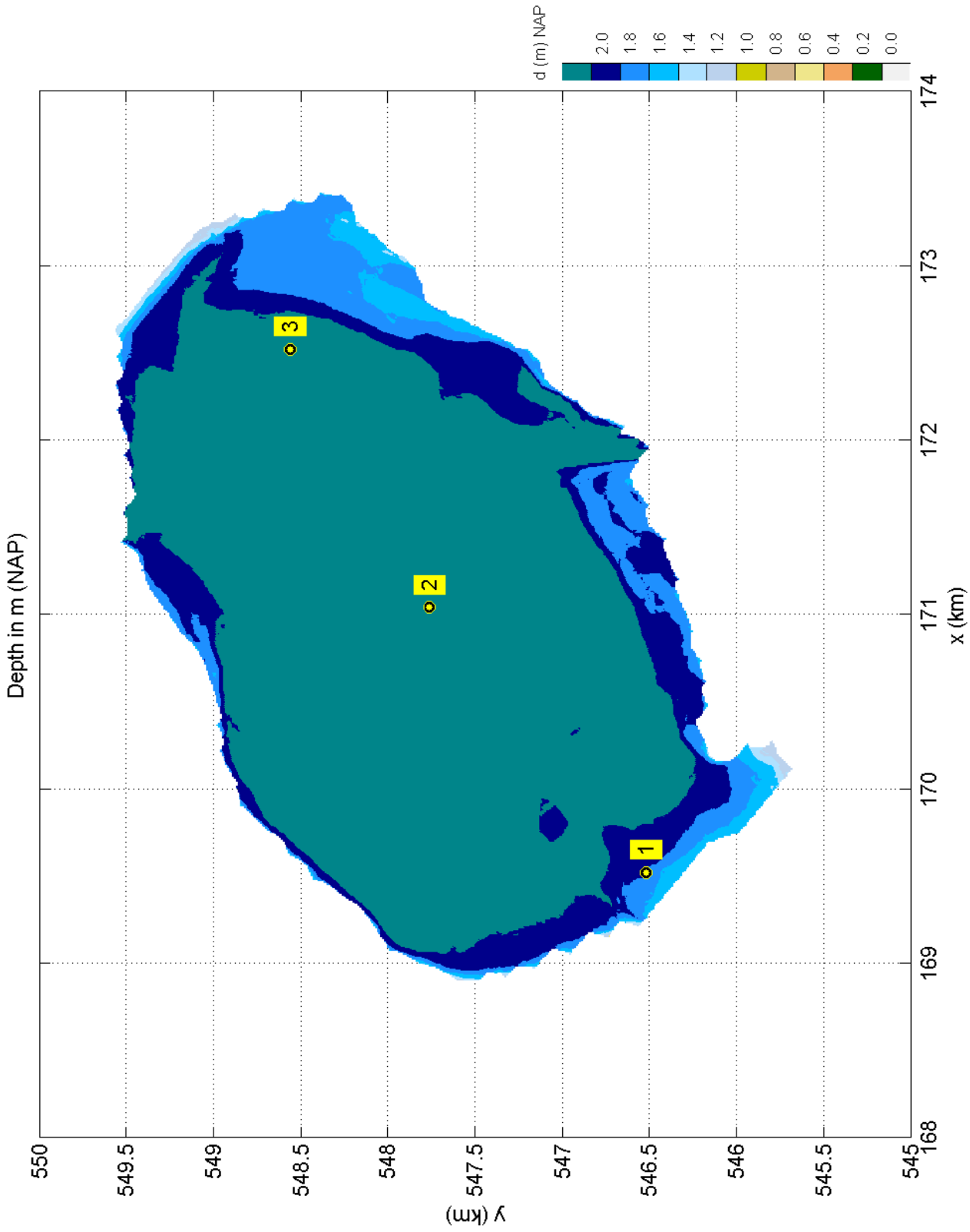

Bathymetry of Lake Sloten and location of test points		SWAN 40.51A
		Numerical efficiency SWAN
DELTARES & ALKYON	H5107.46/A2114	Fig. 2.7

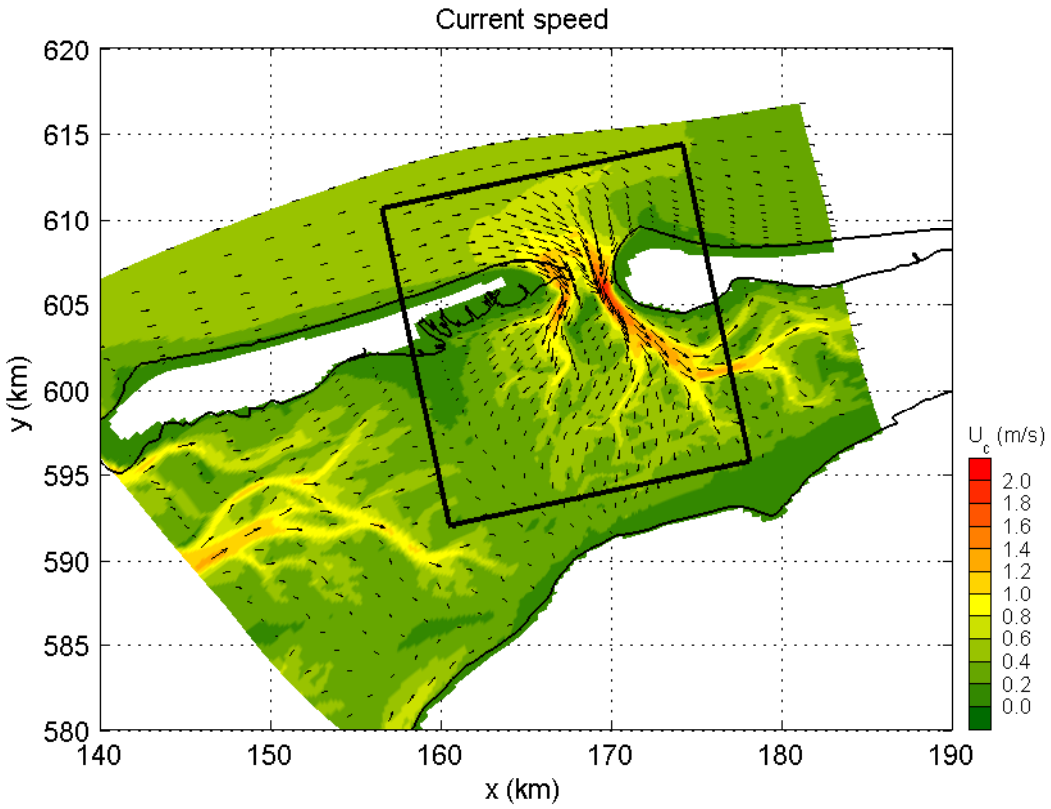

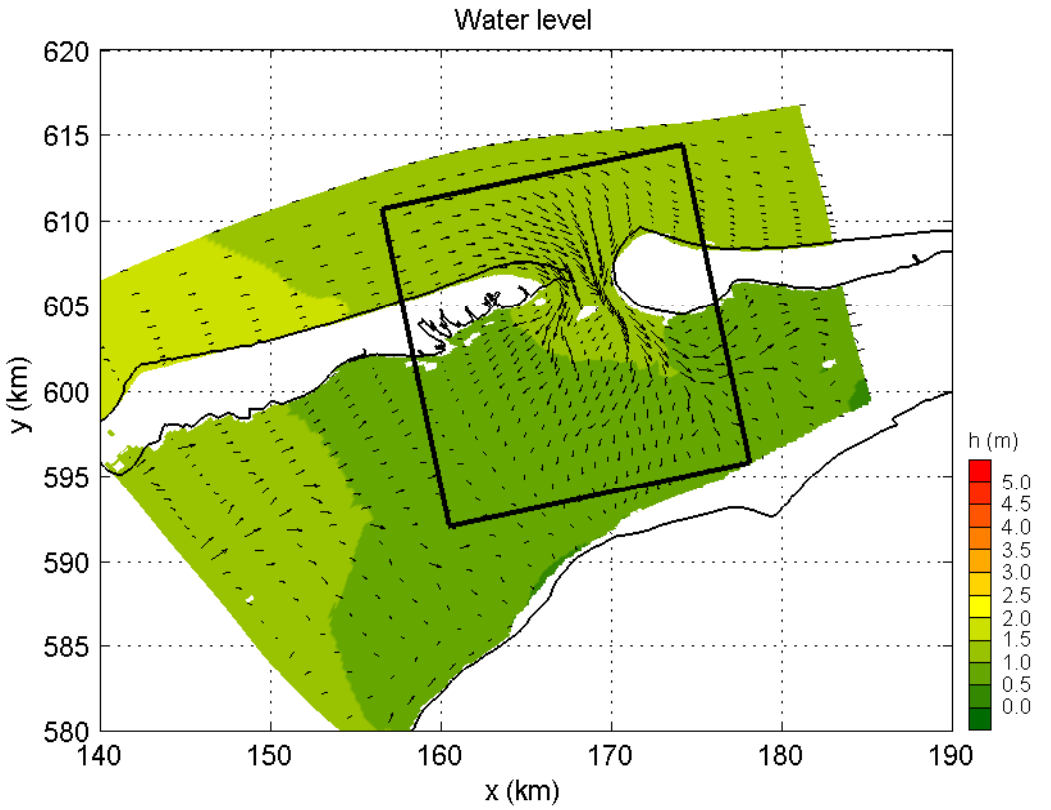

Current speed and direction for 2 Jan. 2005, 10:00 hours in the Amelander Zeegat (flood)		SWAN 40.51A
		Numerical efficiency SWAN
DELTARES & ALKYON	H5107.46/A2214	Fig. 3.1

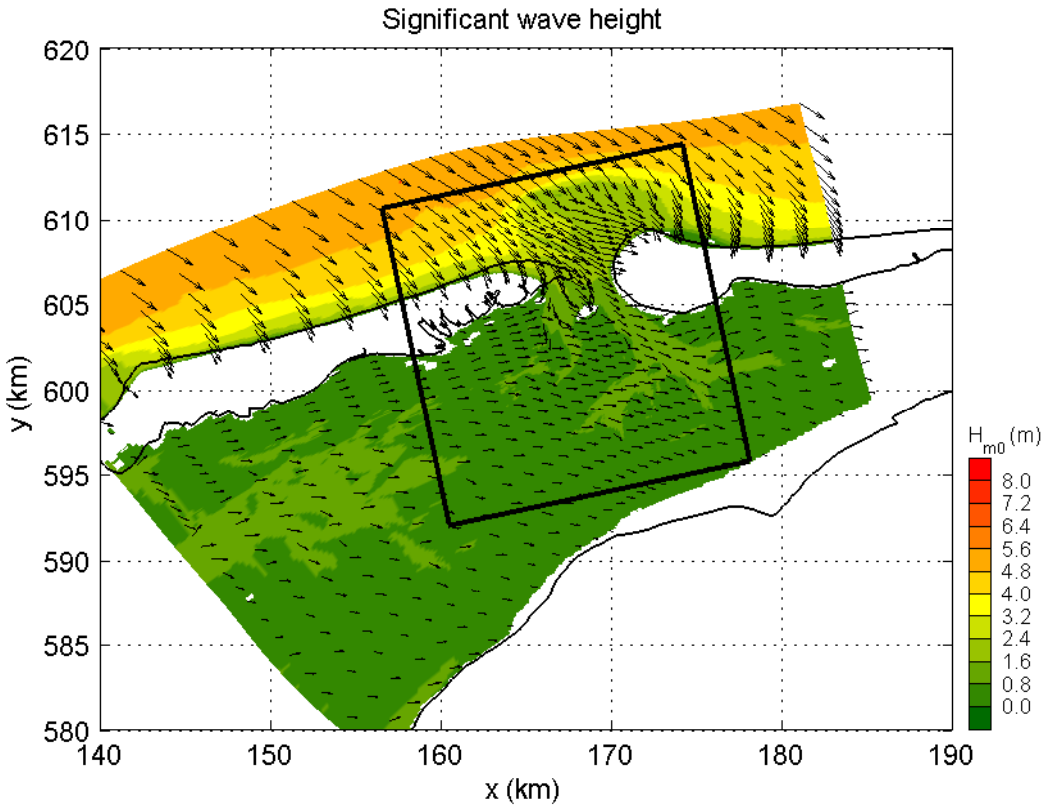

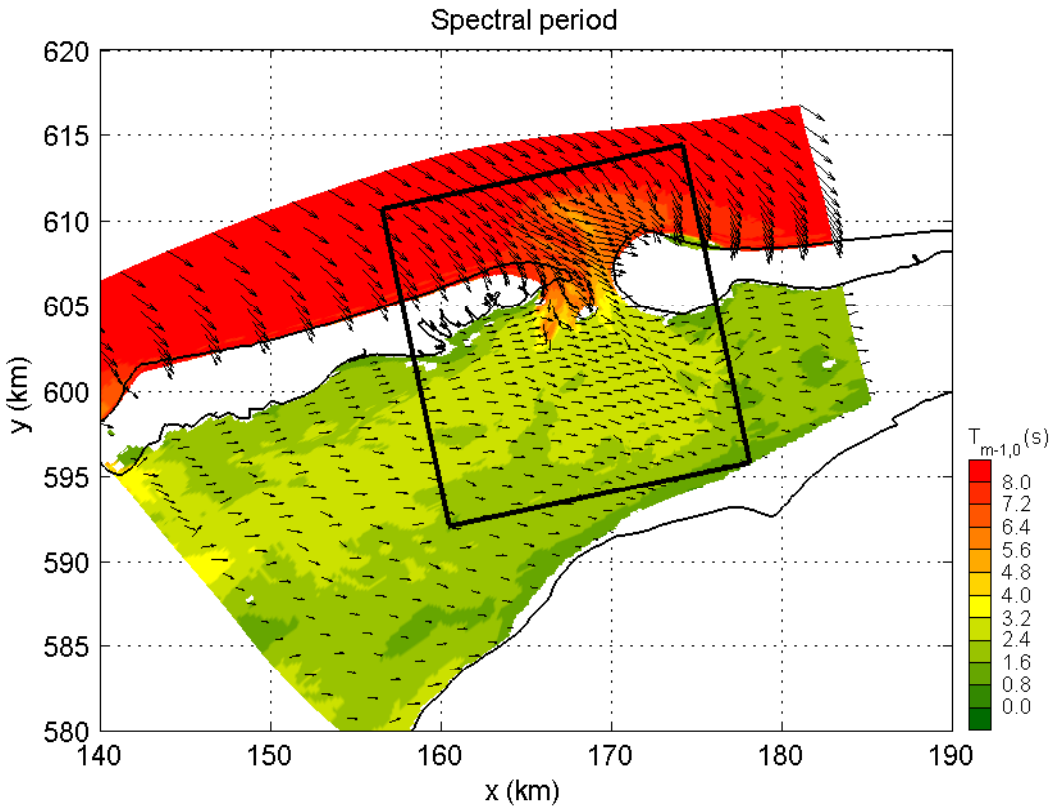

Variation of significant wave height H_{m0} and spectral period $T_{m-1,0}$ in the Amelander Zeegat, Case: AZG3A 2005/1/2 10:00		SWAN 40.51A
		Numerical efficiency SWAN
DELTARES & ALKYON	H5107.46/A2214	Fig. 3.2

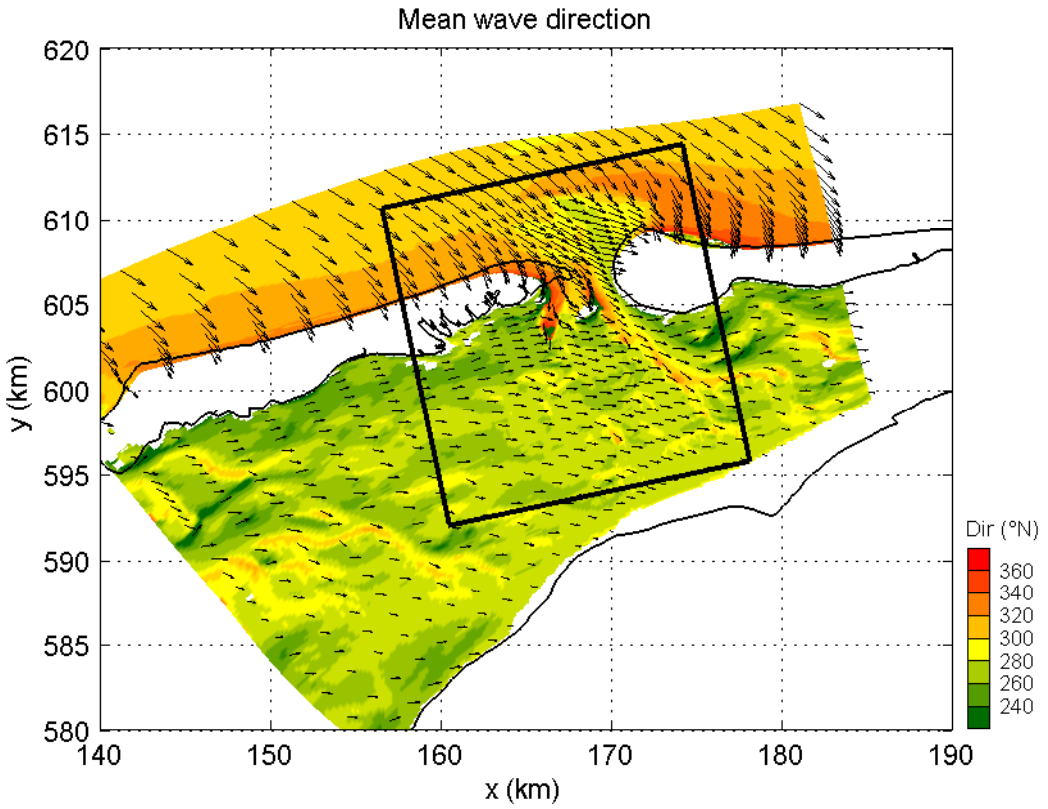

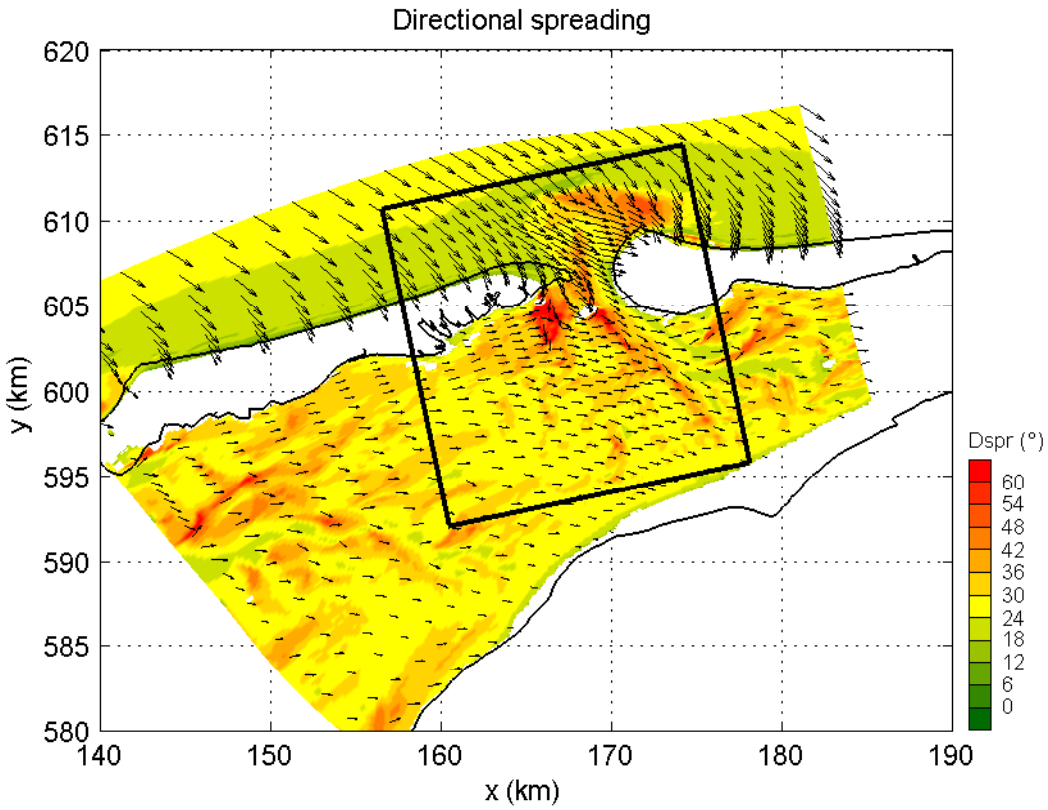

Variation of mean wave direction Dir and directional spreading Dspr in the Amelander Zeegat, Case: AZG3A 2005/1/2 10:00		SWAN 40.51A
	Numerical efficiency SWAN	
DELTARES & ALKYON	H5107.46/A2214	Fig. 3.3

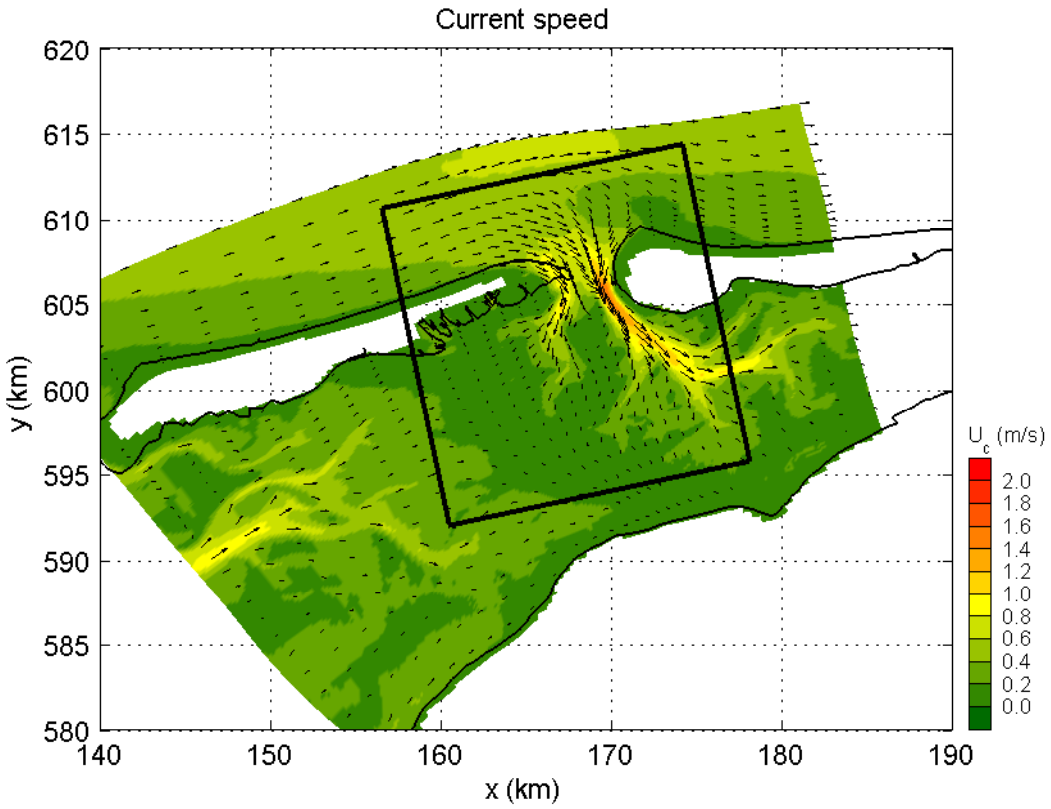

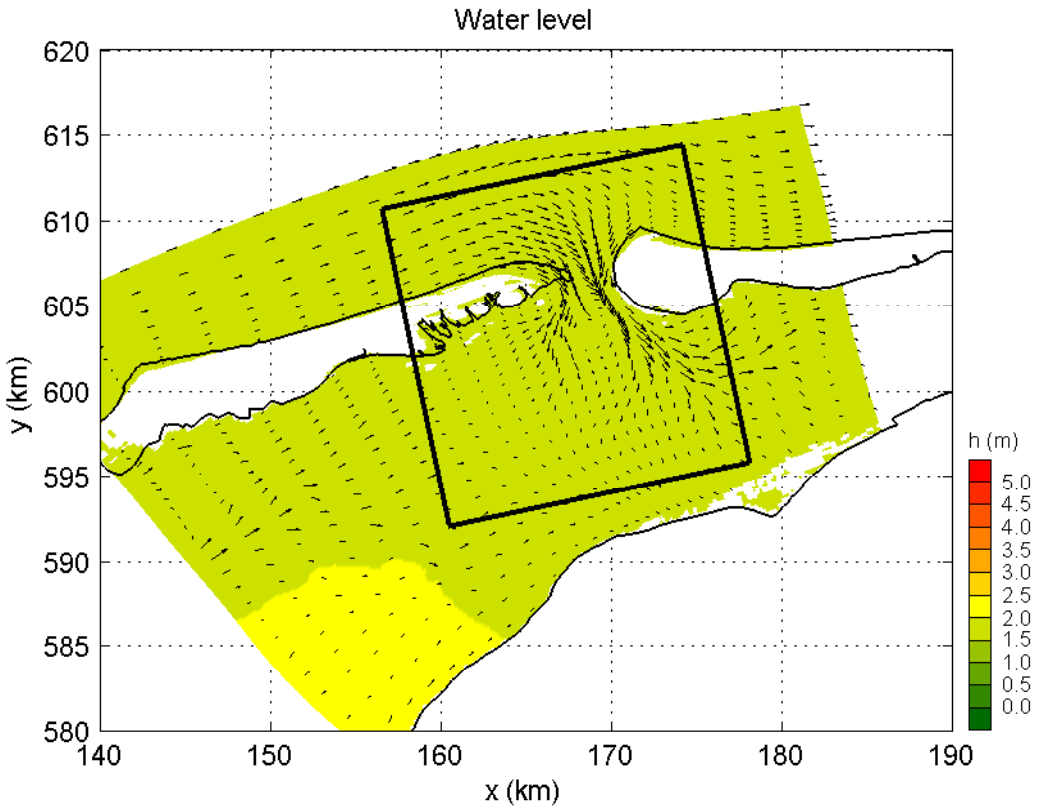

Current speed and direction for 2 Jan. 2005, 12:00 hours in the Amelander Zeegat (slack tide)		SWAN 40.51A
		Numerical efficiency SWAN
DELTARES & ALKYON	H5107.46/A2214	Fig. 3.4

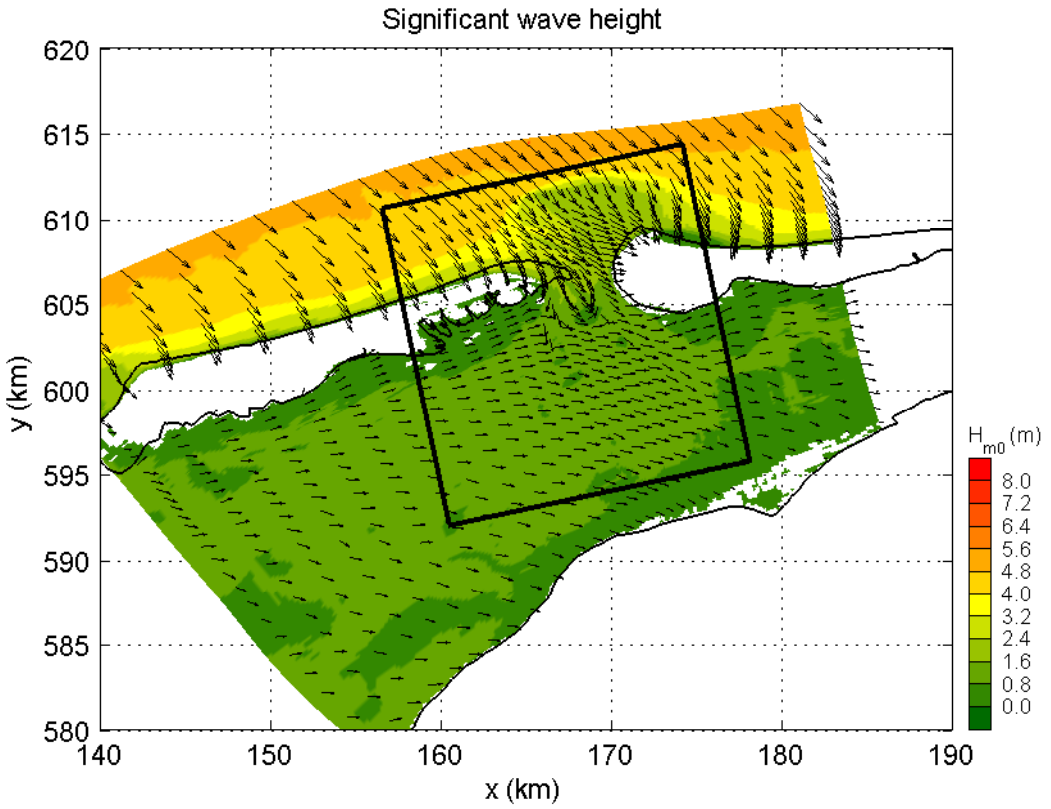

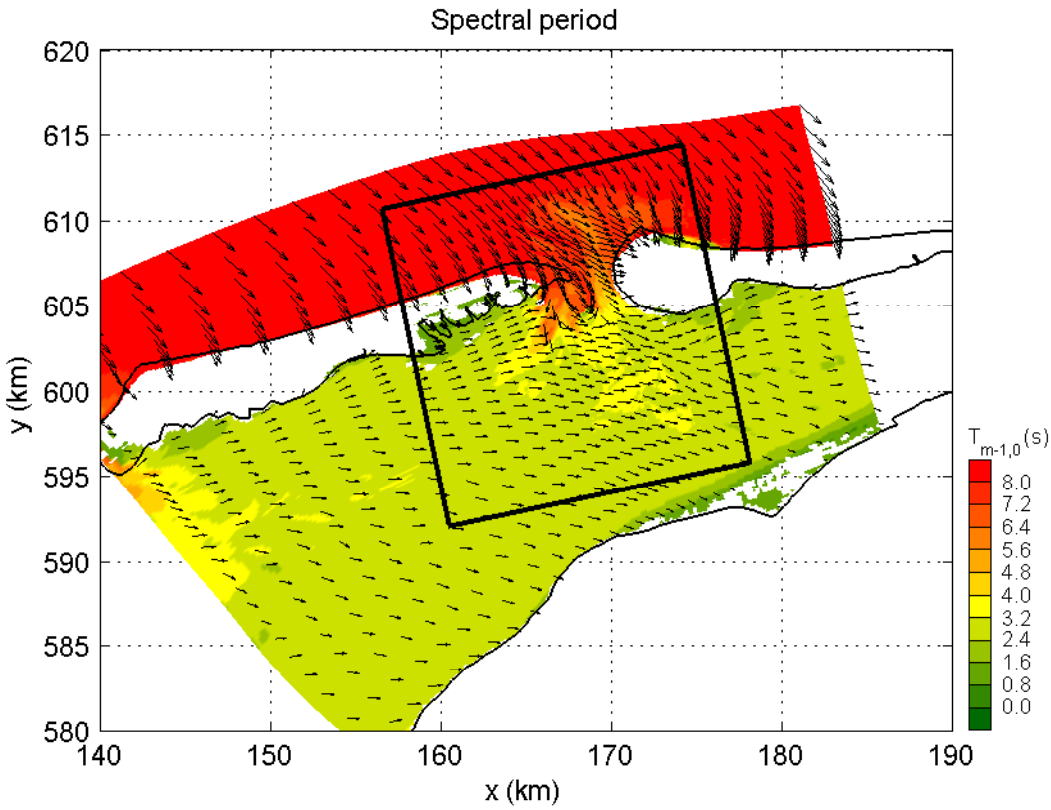

Variation of significant wave height H_{m0} and spectral period $T_{m-1,0}$ in the Amelander Zeegat, Case: AZG3A 2005/1/2 12:00		SWAN 40.51A
		Numerical efficiency SWAN
DELTARES & ALKYON	H5107.46/A2214	Fig. 3.5

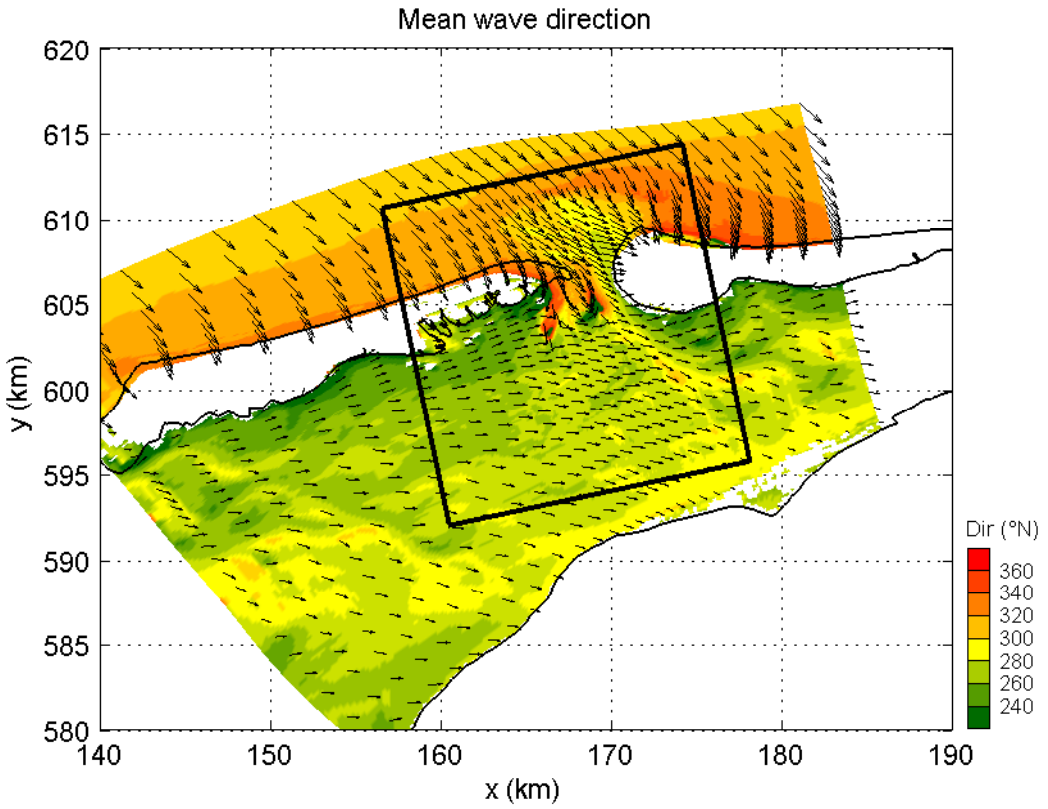

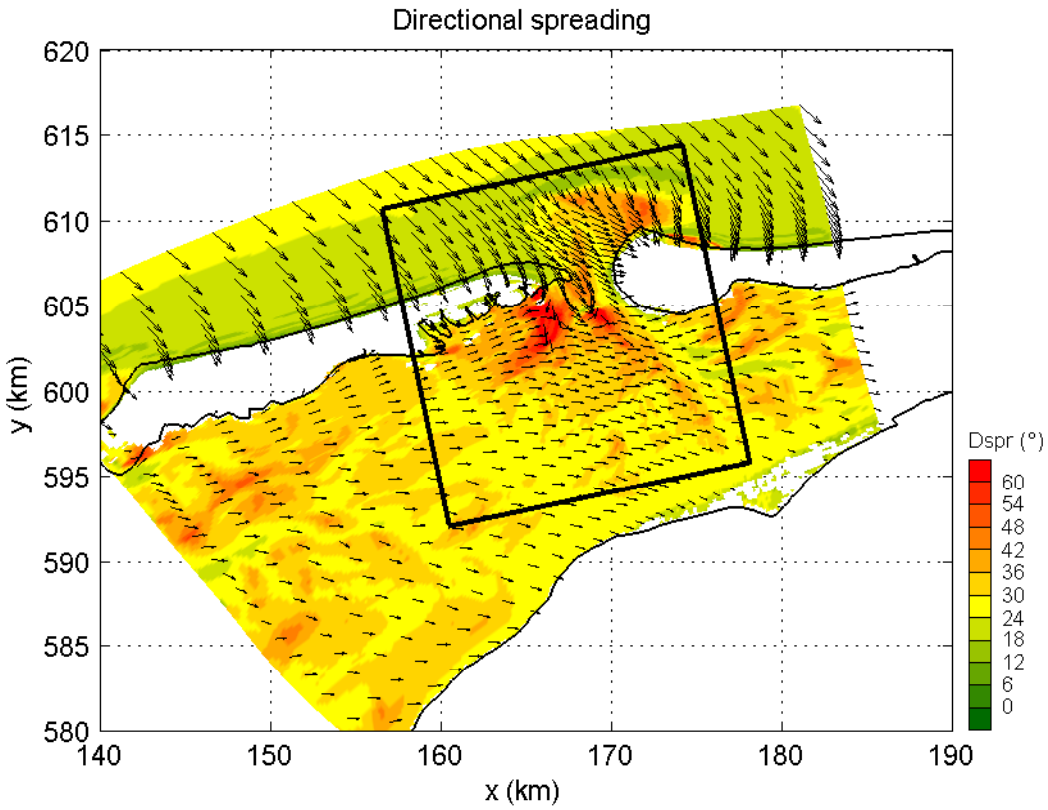

Variation of mean wave direction Dir and directional spreading Dspr in the Amelander Zeegat, Case: AZG3A 2005/1/2 12:00		SWAN 40.51A
	Numerical efficiency SWAN	
DELTARES & ALKYON	H5107.46/A2214	Fig. 3.6

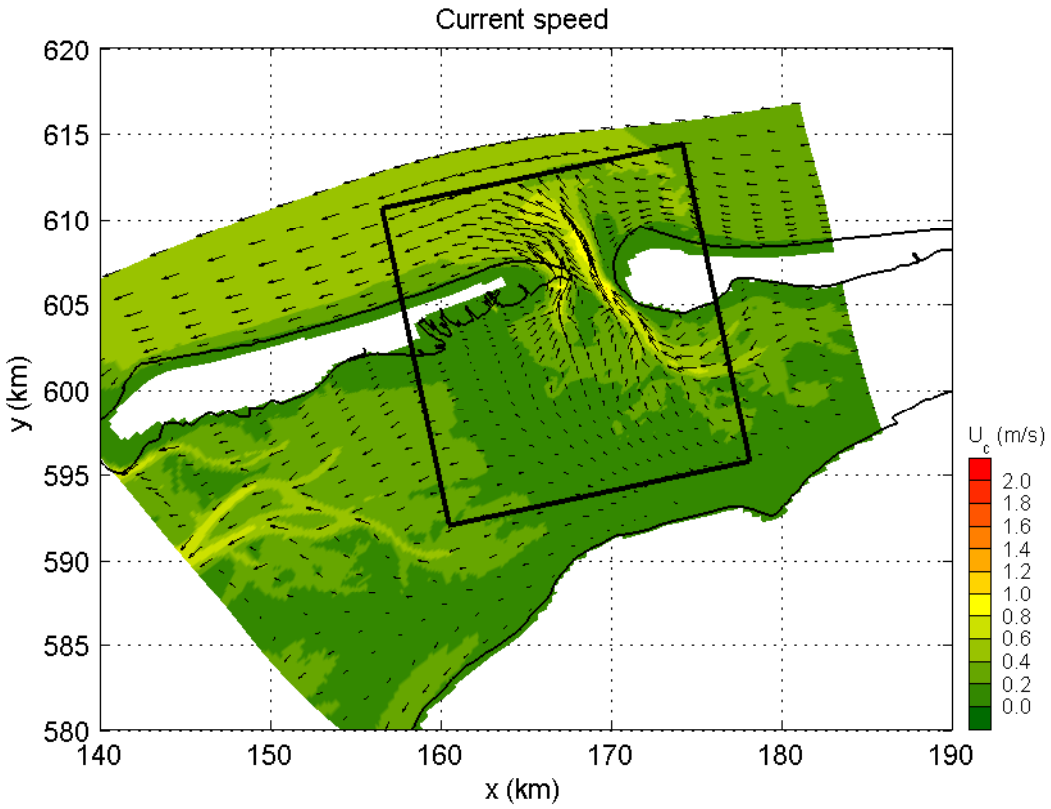

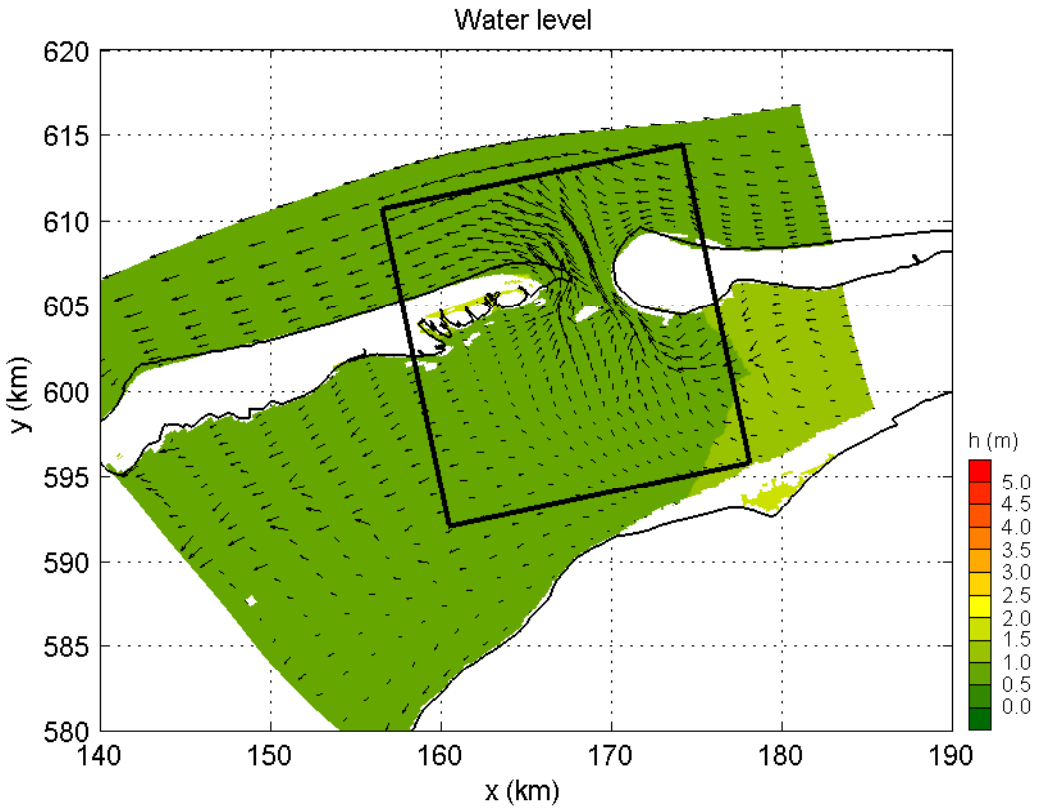

Current speed and direction for 2 Jan. 2005, 17:00 hours in the Amelander Zeegat (ebb)		SWAN 40.51A
		Numerical efficiency SWAN
DELTARES & ALKYON	H5107.46/A2214	Fig. 3.7

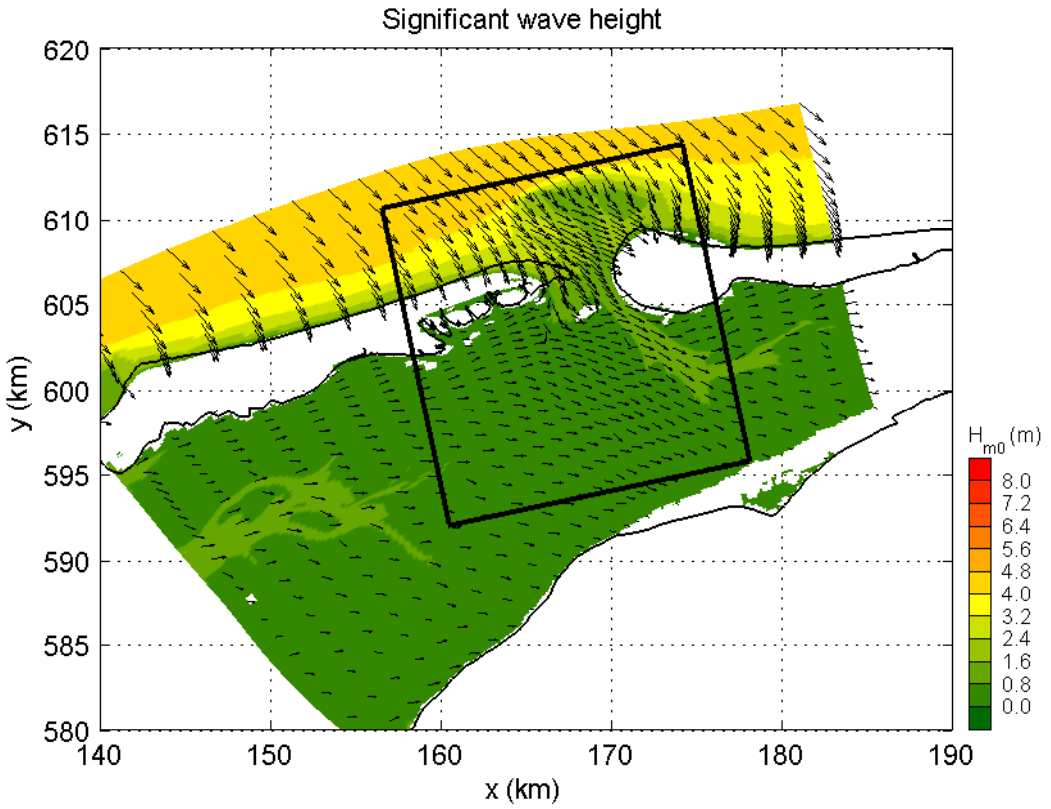

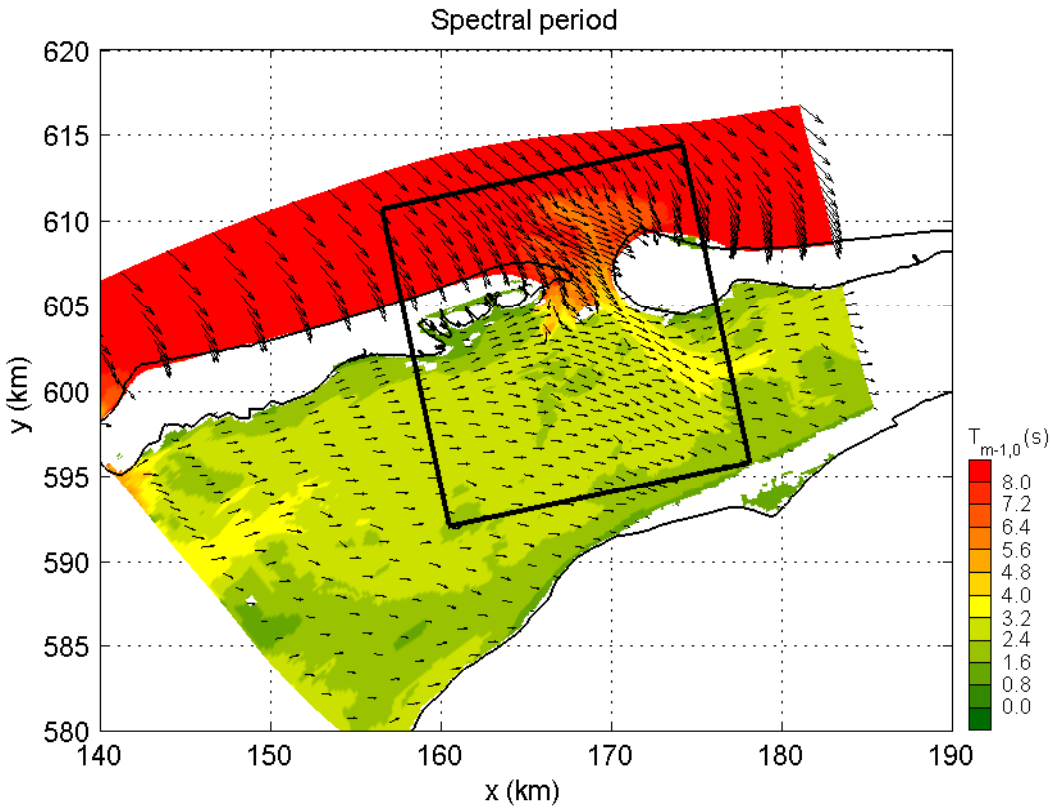

Variation of significant wave height H_{m0} and spectral period $T_{m-1,0}$ in the Amelander Zeegat, Case: AZG3A 2005/1/2 17:00		SWAN 40.51A
		Numerical efficiency SWAN
DELTARES & ALKYON	H5107.46/A2214	Fig. 3.8

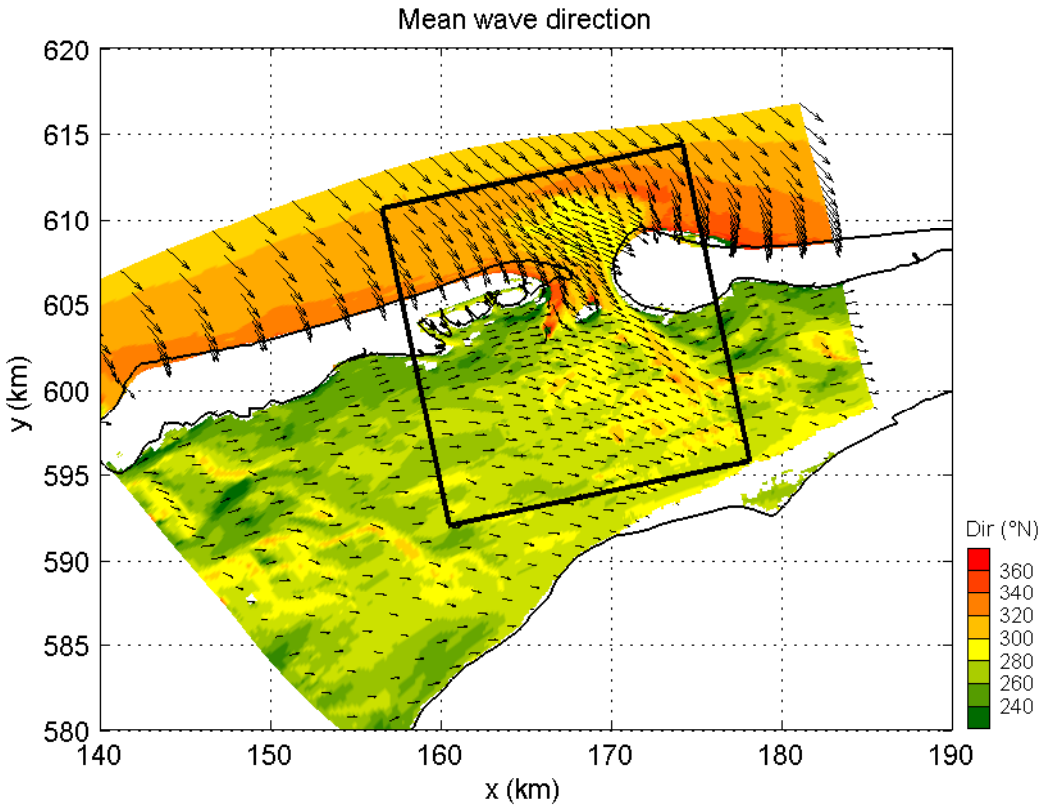

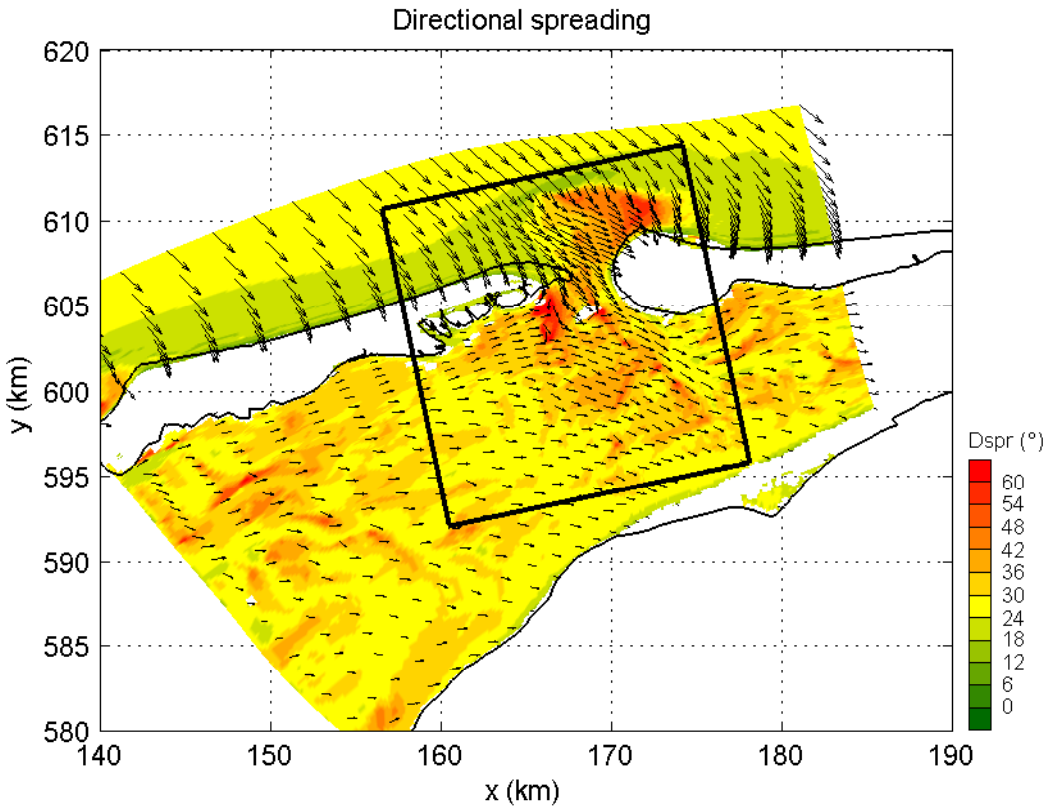

Variation of mean wave direction Dir and directional spreading Dspr in the Amelander Zeegat, Case: AZG3A 2005/1/2 17:00		SWAN 40.51A
	Numerical efficiency SWAN	
DELTARES & ALKYON	H5107.46/A2214	Fig. 3.9

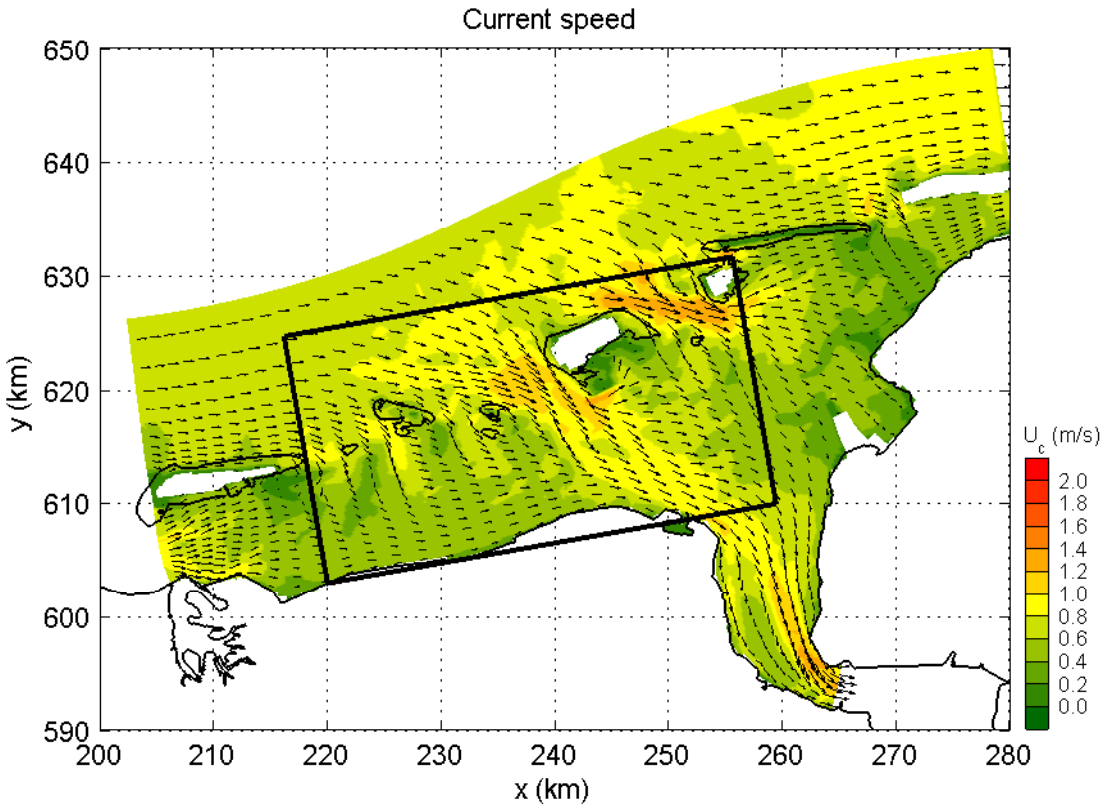

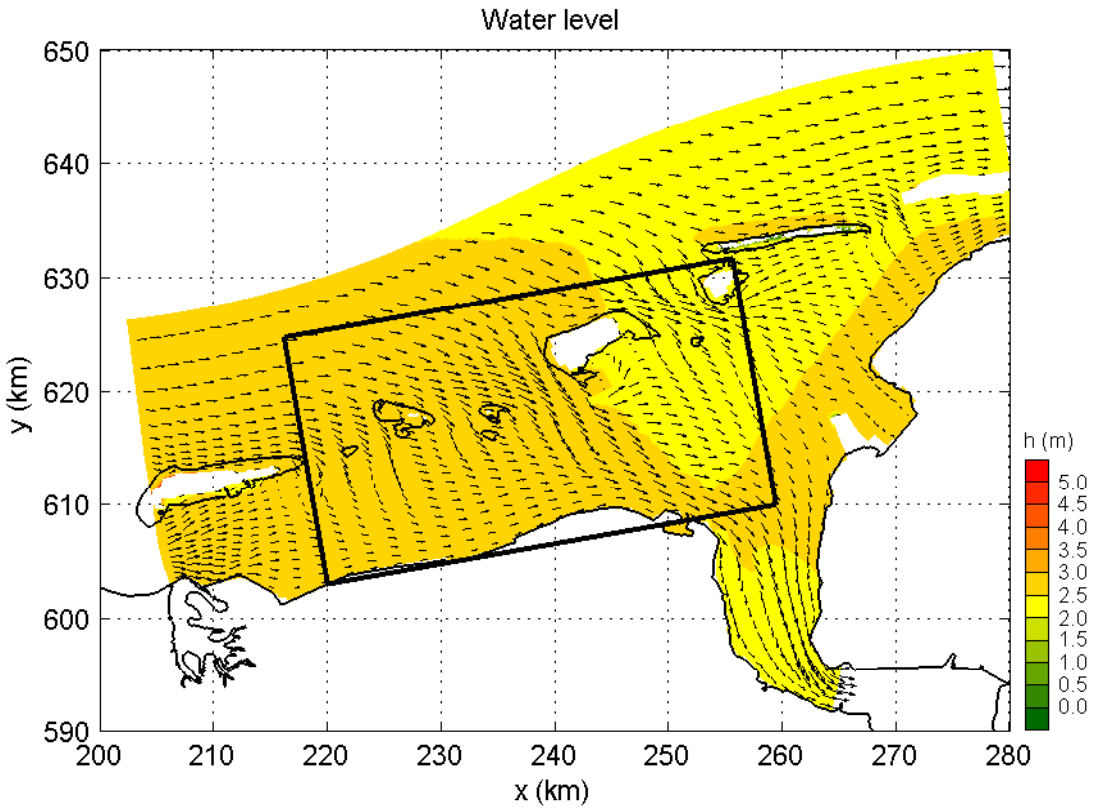

Current speed and direction for 1 Nov. 2006, 03:00 hours in the Eems-Dollard (flood)		SWAN 40.51A
	Numerical efficiency SWAN	
DELTARES & ALKYON	H5107.46/A2214	Fig. 3.10

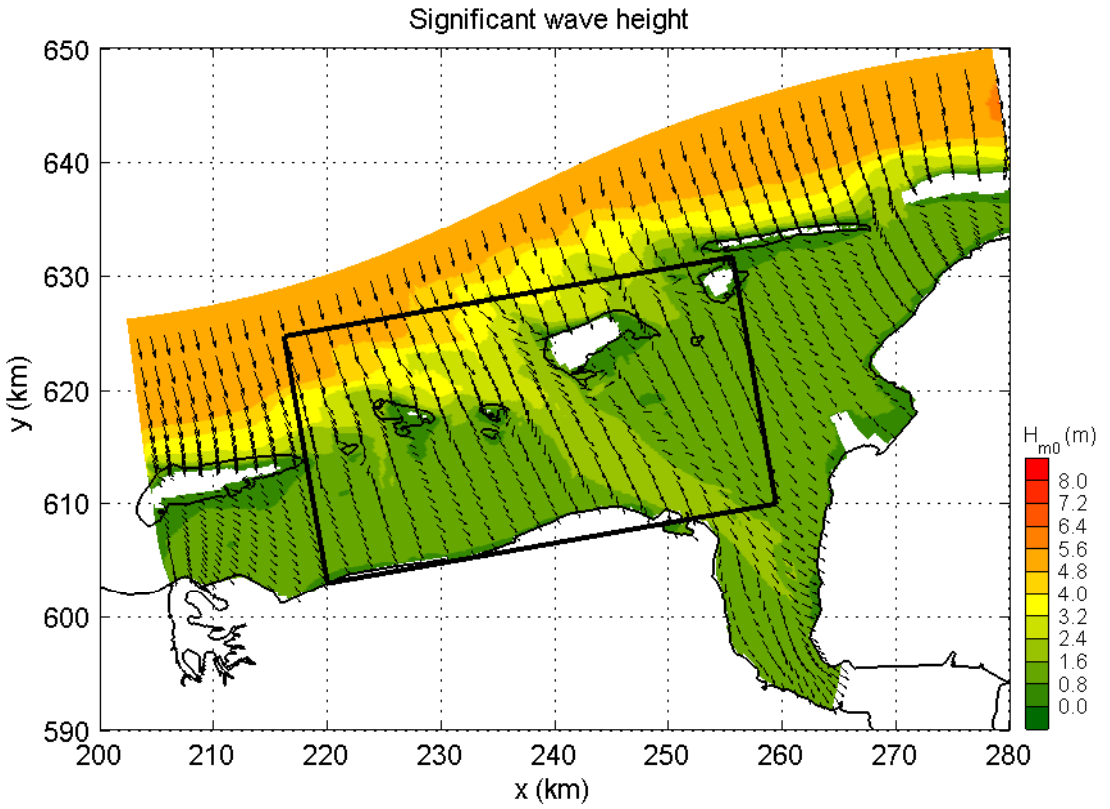

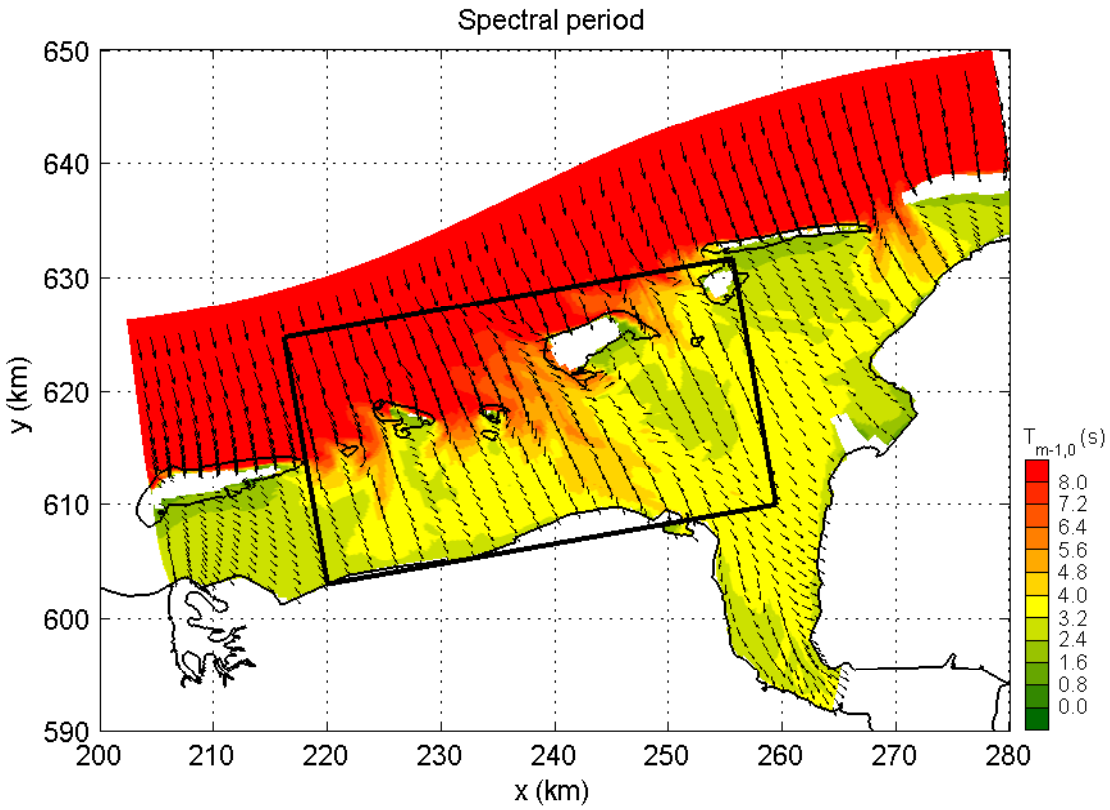

Variation of significant wave height H_{m0} and spectral period $T_{m-1,0}$ in the Eems-Dollard, Case: EEMS3A 2006/11/1 03:00		SWAN 40.51A
		Numerical efficiency SWAN
DELTARES & ALKYON	H5107.46/A2214	Fig. 3.11

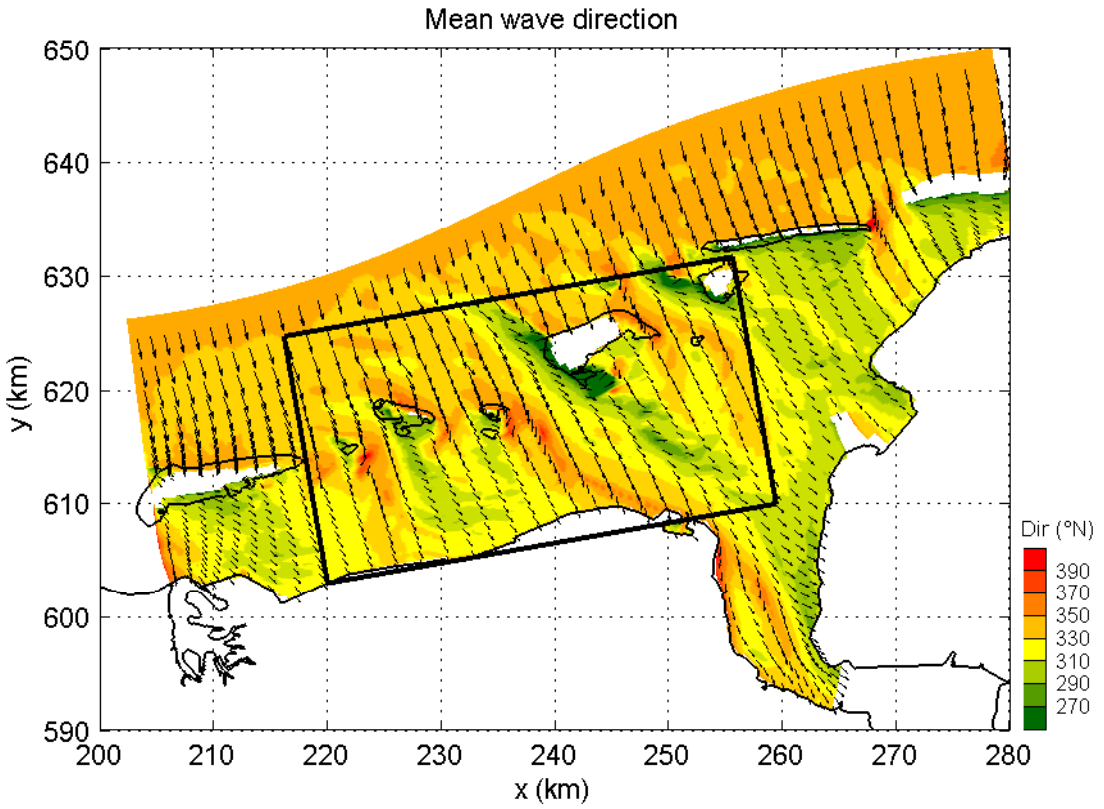

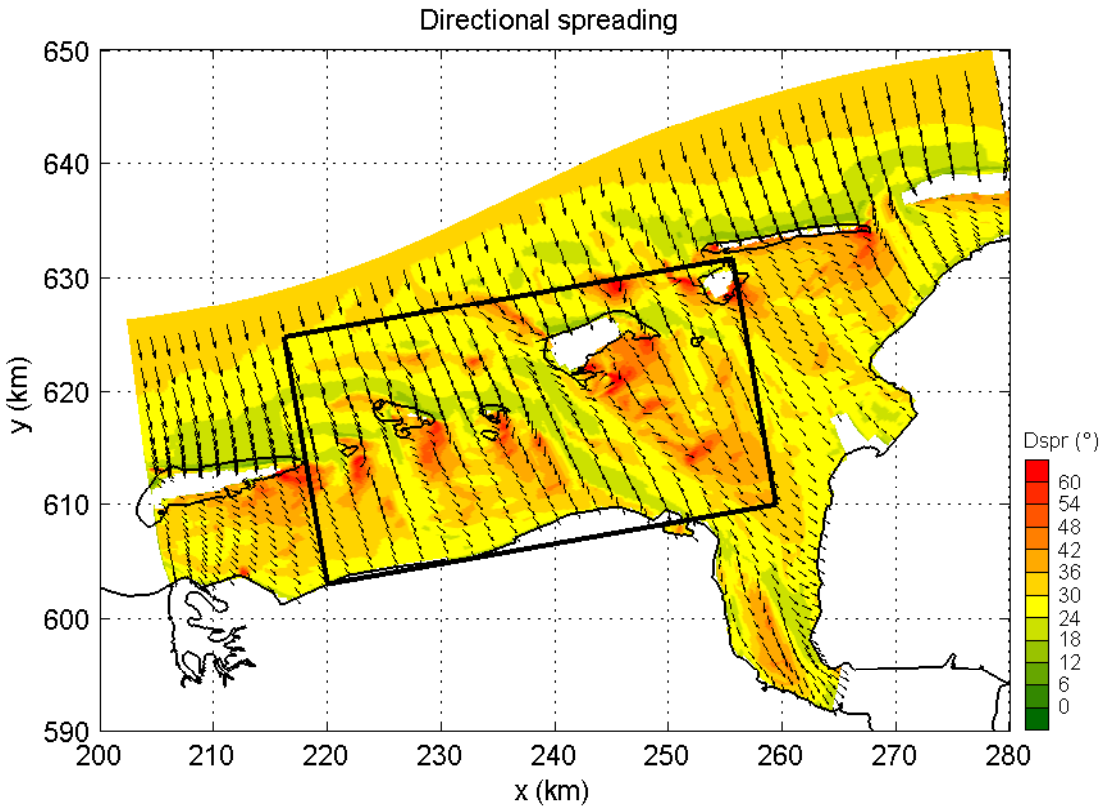

Variation of mean wave direction Dir and directional spreading Dspr in the Eems-Dollard, Case: EEMS3A 2006/11/1 03:00		SWAN 40.51A
		Numerical efficiency SWAN
DELTARES & ALKYON	H5107.46/A2214	Fig. 3.12

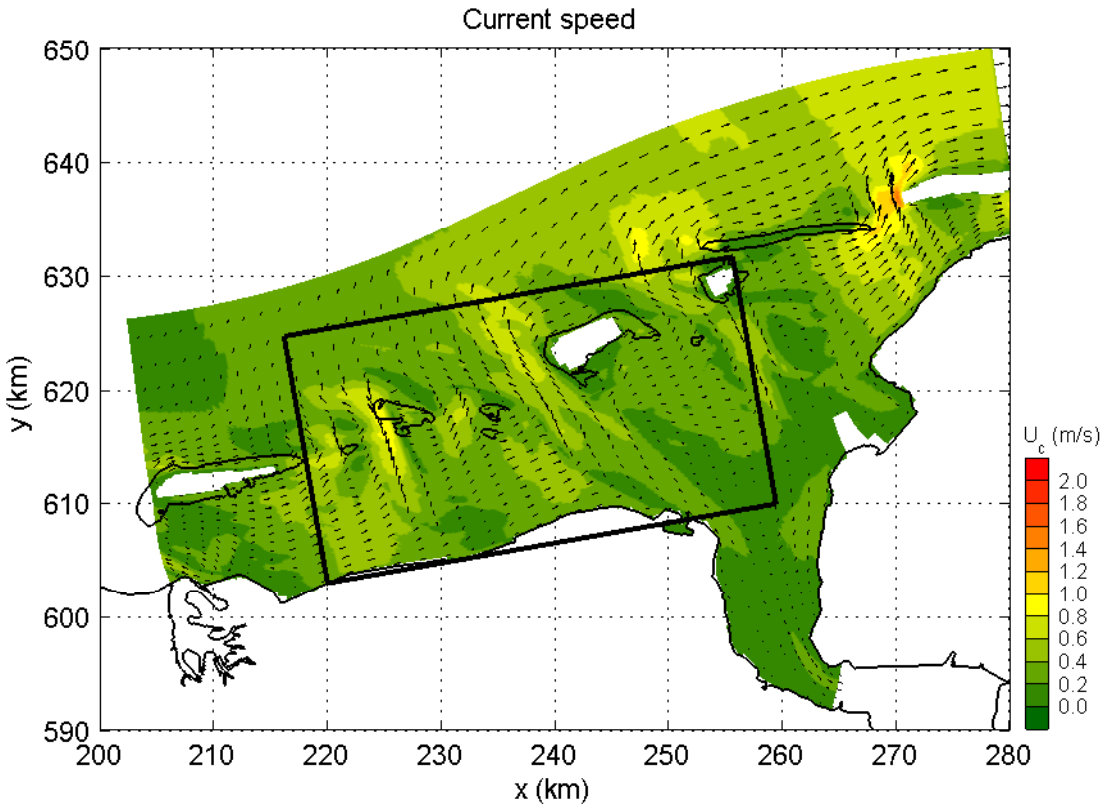

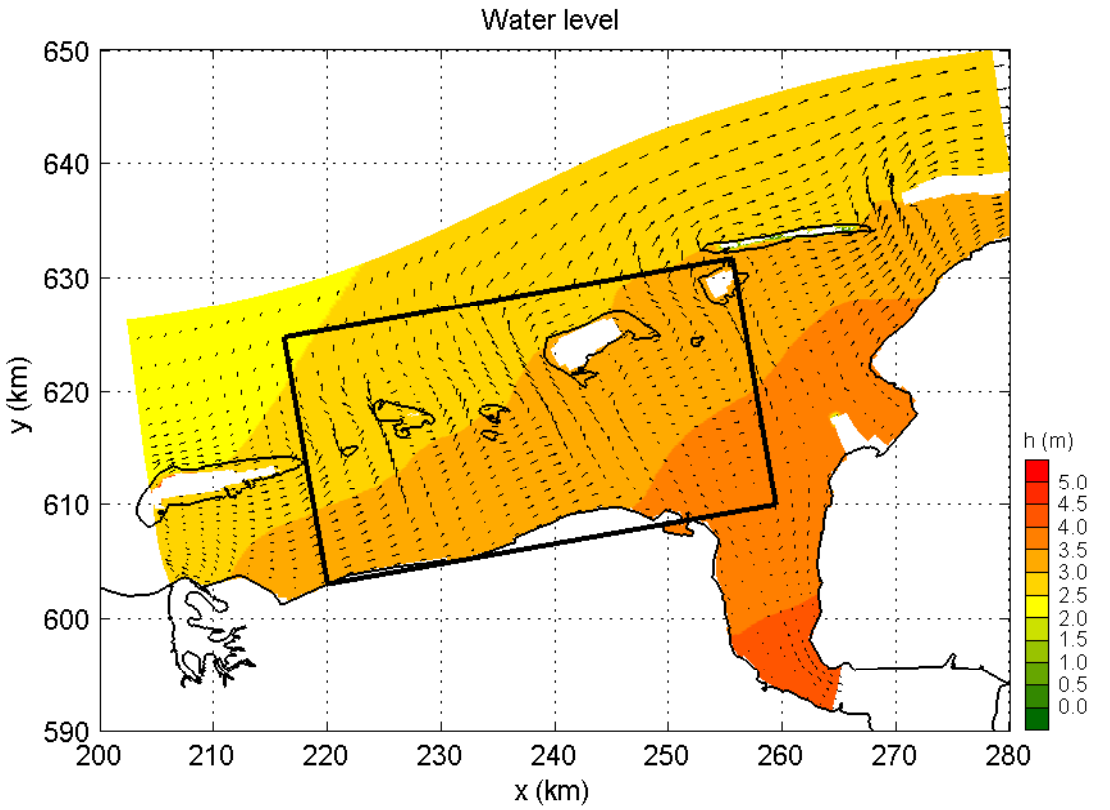

Current speed and direction for 1 Nov. 2006, 06:30 hours in the Eems-Dollard (slack tide)		SWAN 40.51A
	Numerical efficiency SWAN	
DELTARES & ALKYON	H5107.46/A2214	Fig. 3.13

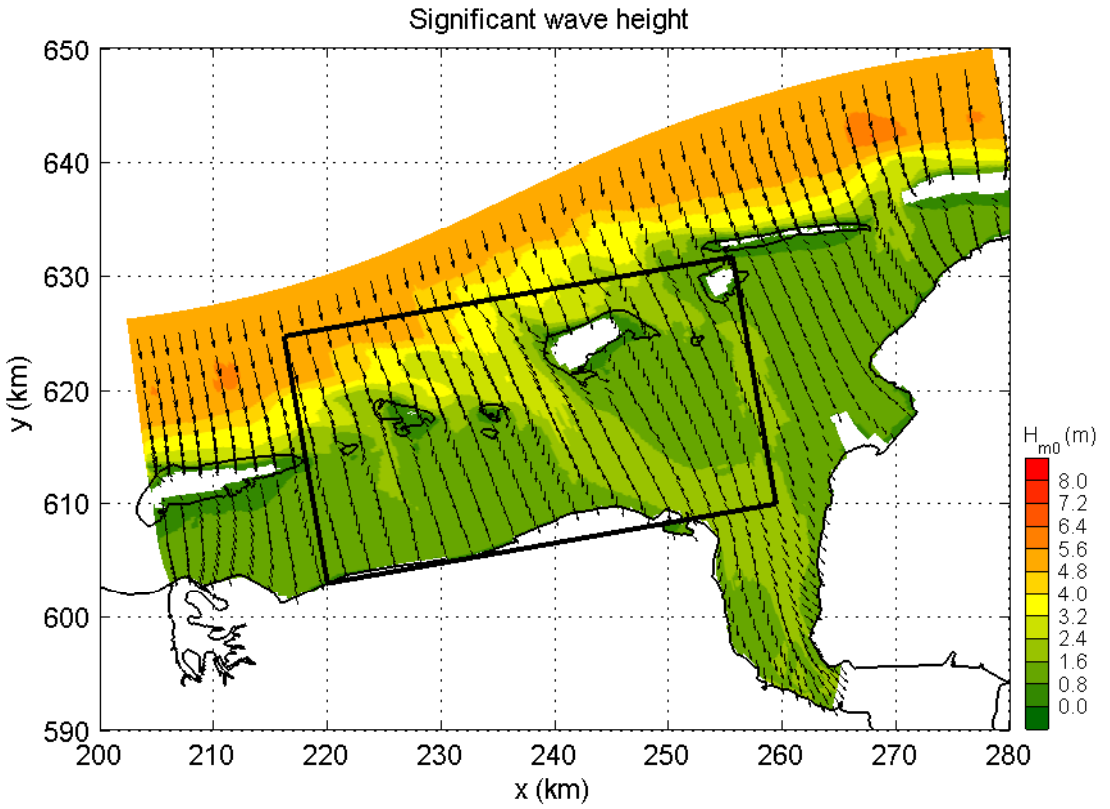

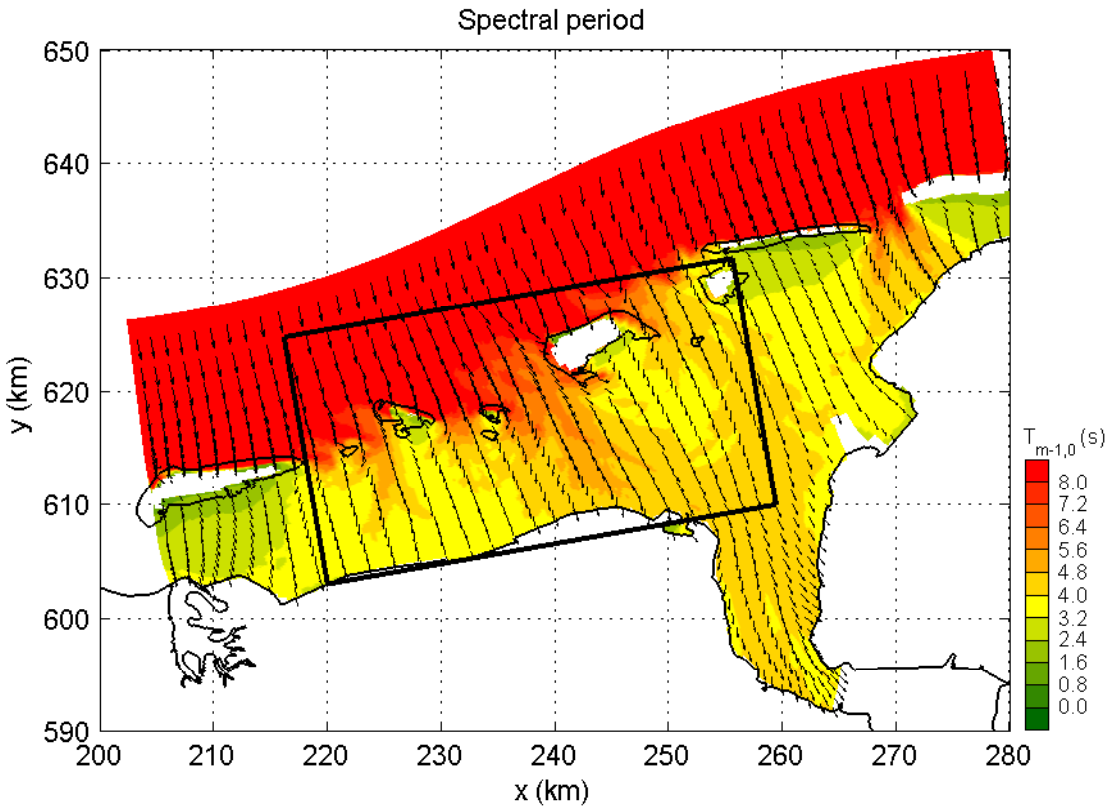

Variation of significant wave height H_{m0} and spectral period $T_{m-1,0}$ in the Eems-Dollard, Case: EEMS3A 2006/11/1 06:30		SWAN 40.51A
		Numerical efficiency SWAN
DELTARES & ALKYON	H5107.46/A2214	Fig. 3.14

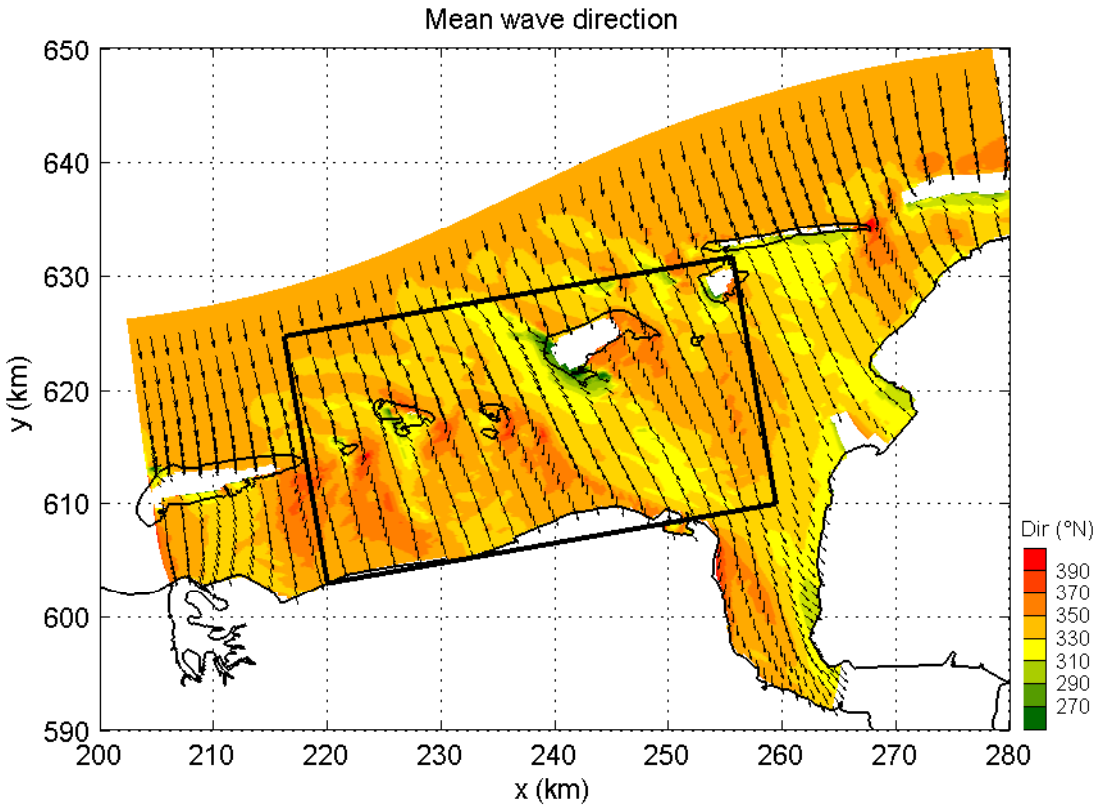

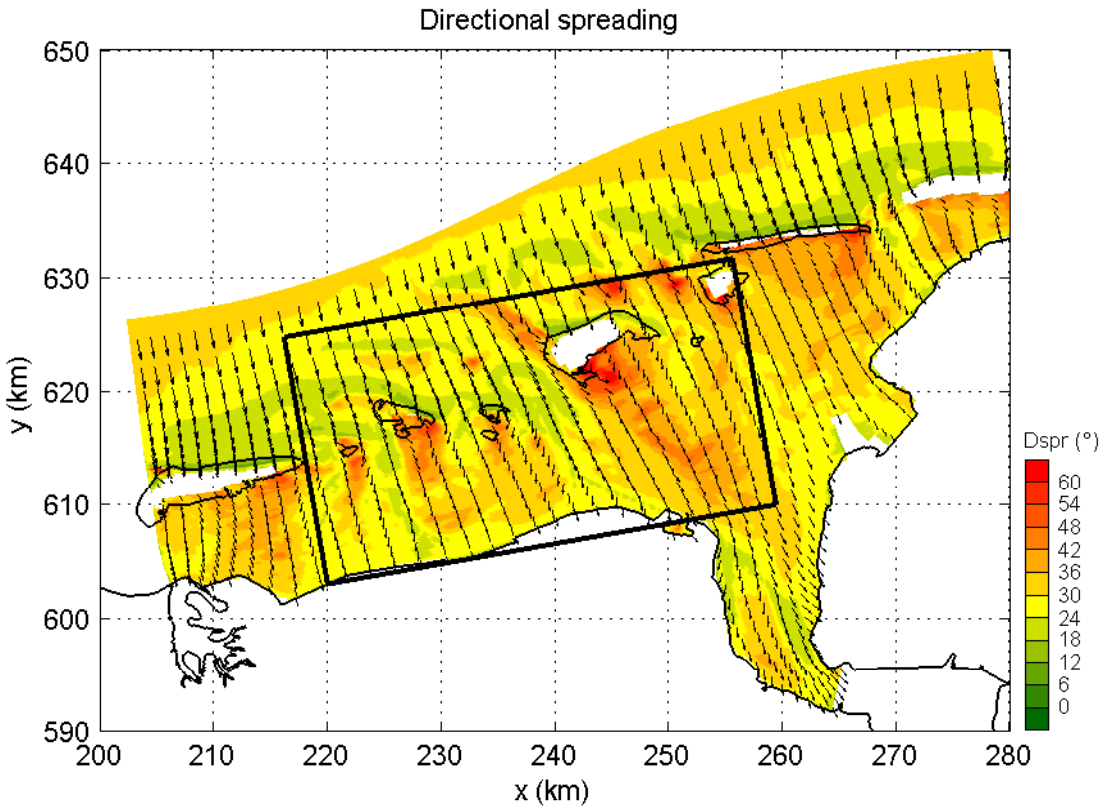

Variation of mean wave direction Dir and directional spreading Dspr in the Eems-Dollard, Case: EEMS3A 2006/11/1 06:30		SWAN 40.51A
		Numerical efficiency SWAN
DELTARES & ALKYON	H5107.46/A2214	Fig. 3.15

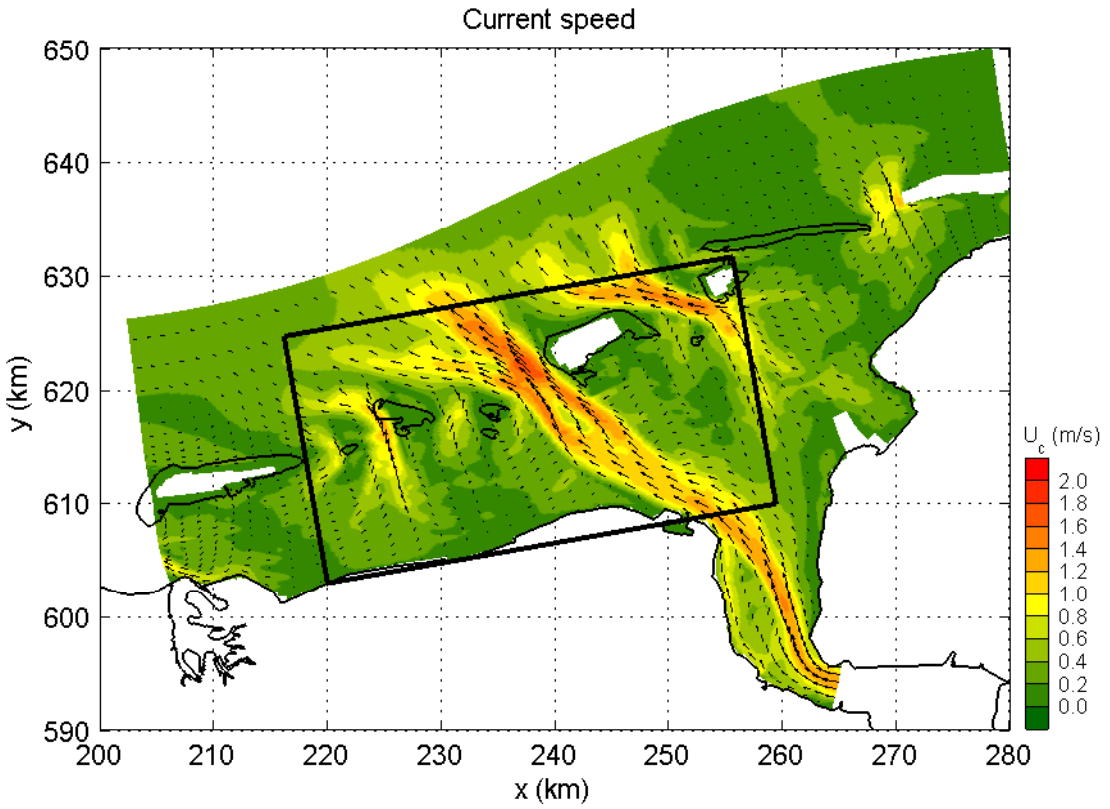

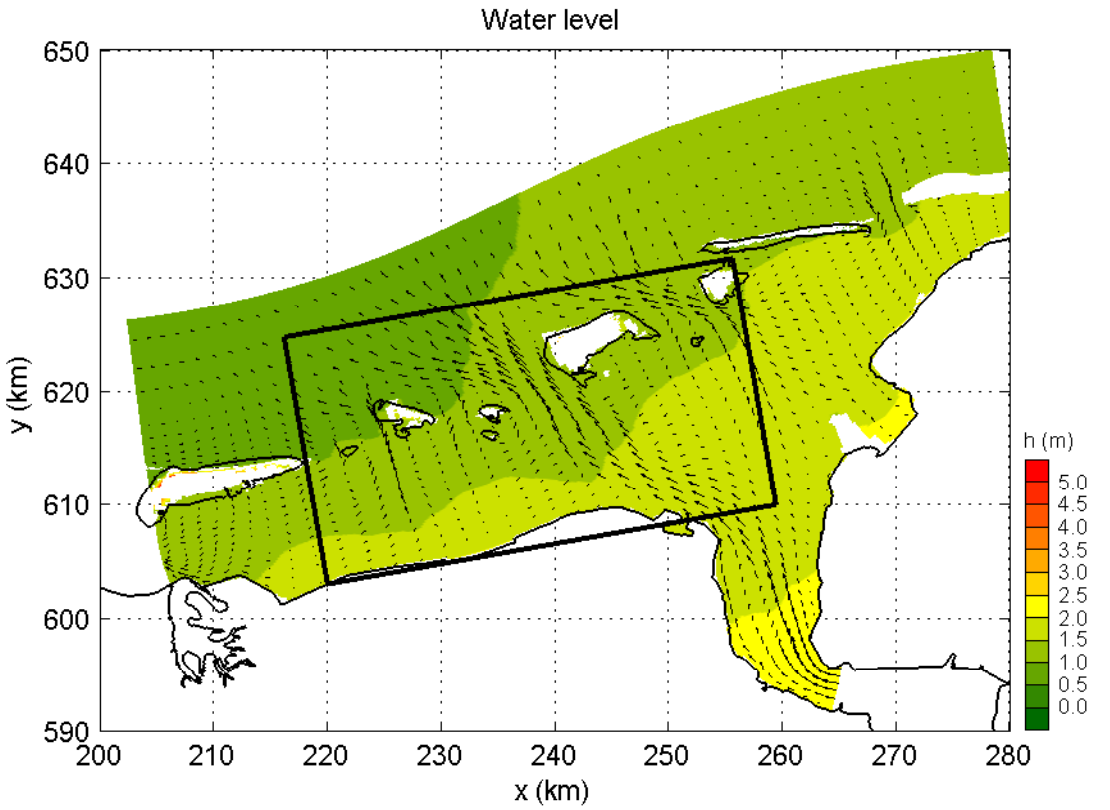

Current speed and direction for 1 Nov. 2006, 09:30 hours in the Eems-Dollard (ebb)		SWAN 40.51A
		Numerical efficiency SWAN
DELTARES & ALKYON	H5107.46/A2214	Fig. 3.16

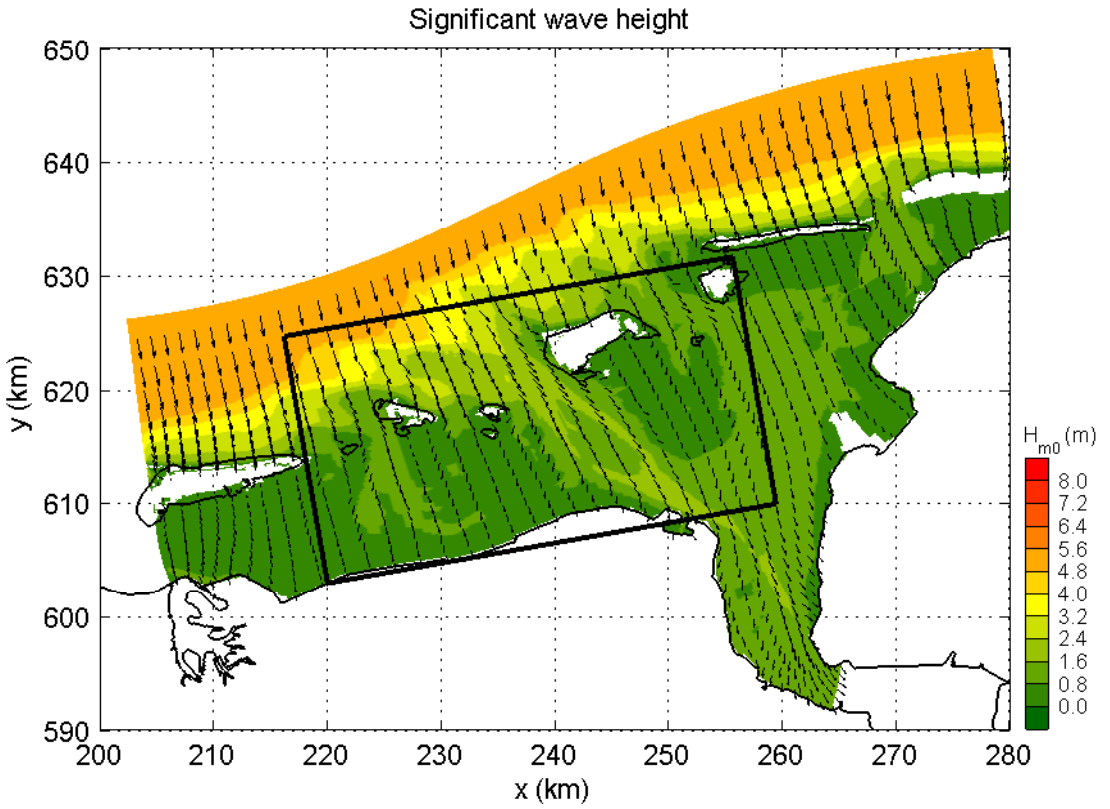

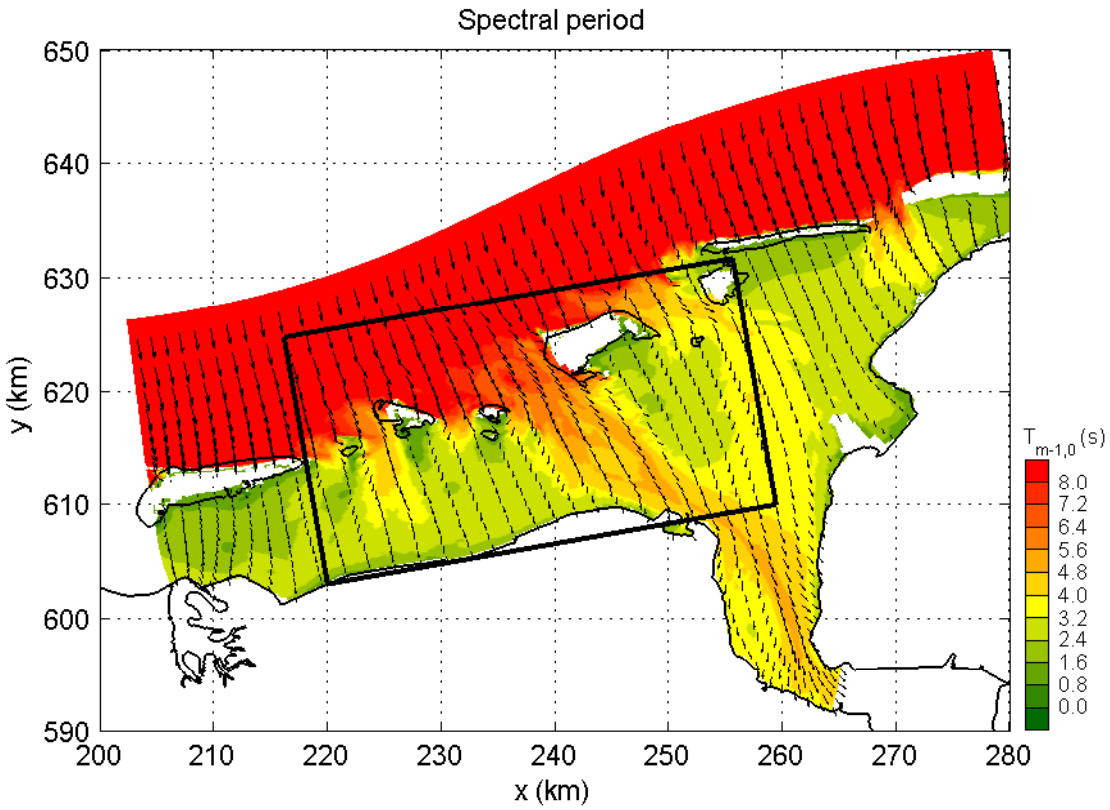

Variation of significant wave height H_{m0} and spectral period $T_{m-1,0}$ in the Eems-Dollard, Case: EEMS3A 2006/11/1 09:30		SWAN 40.51A
		Numerical efficiency SWAN
DELTARES & ALKYON	H5107.46/A2214	Fig. 3.17

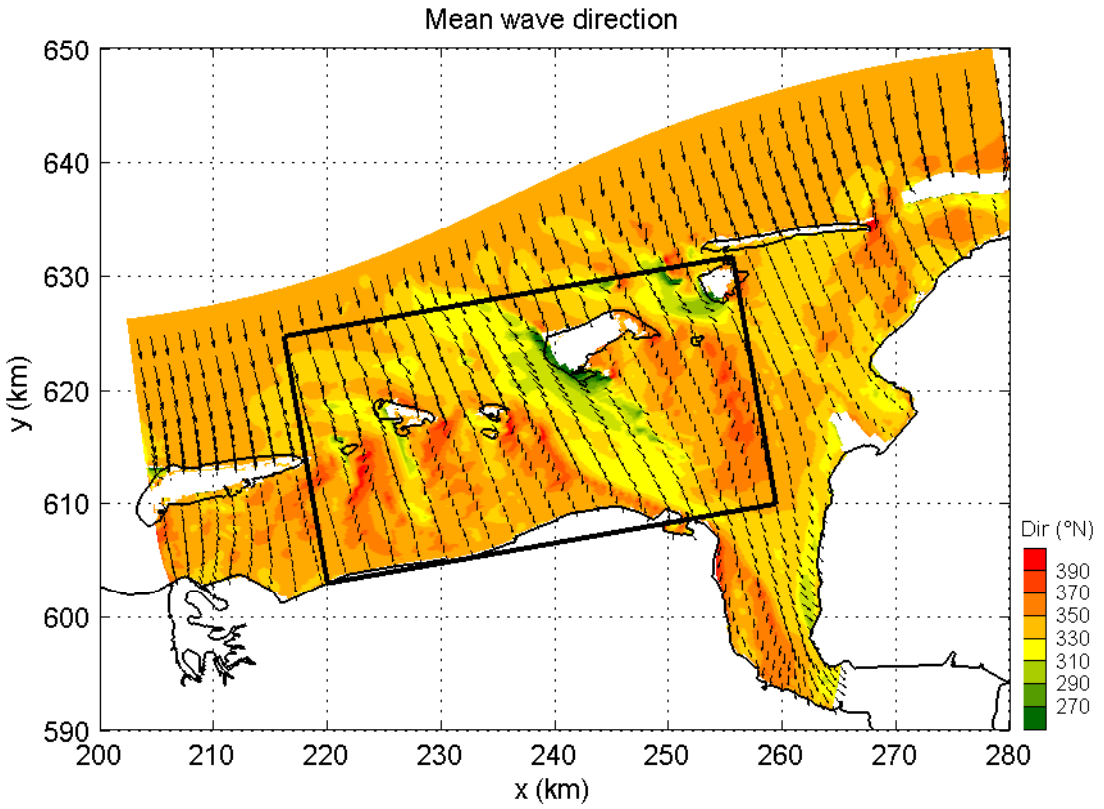

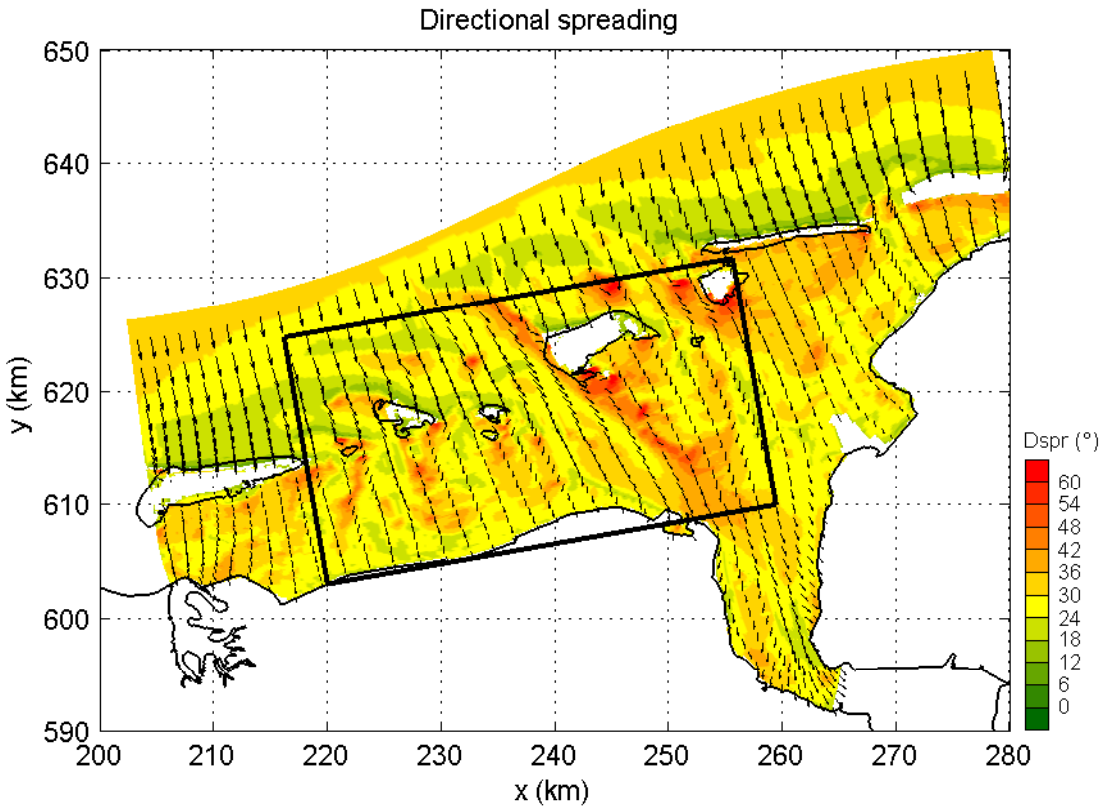

Variation of mean wave direction Dir and directional spreading Dspr in the Eems-Dollard, Case: EEMS3A 2006/11/1 09:30		SWAN 40.51A
		Numerical efficiency SWAN
DELTARES & ALKYON	H5107.46/A2214	Fig. 3.18

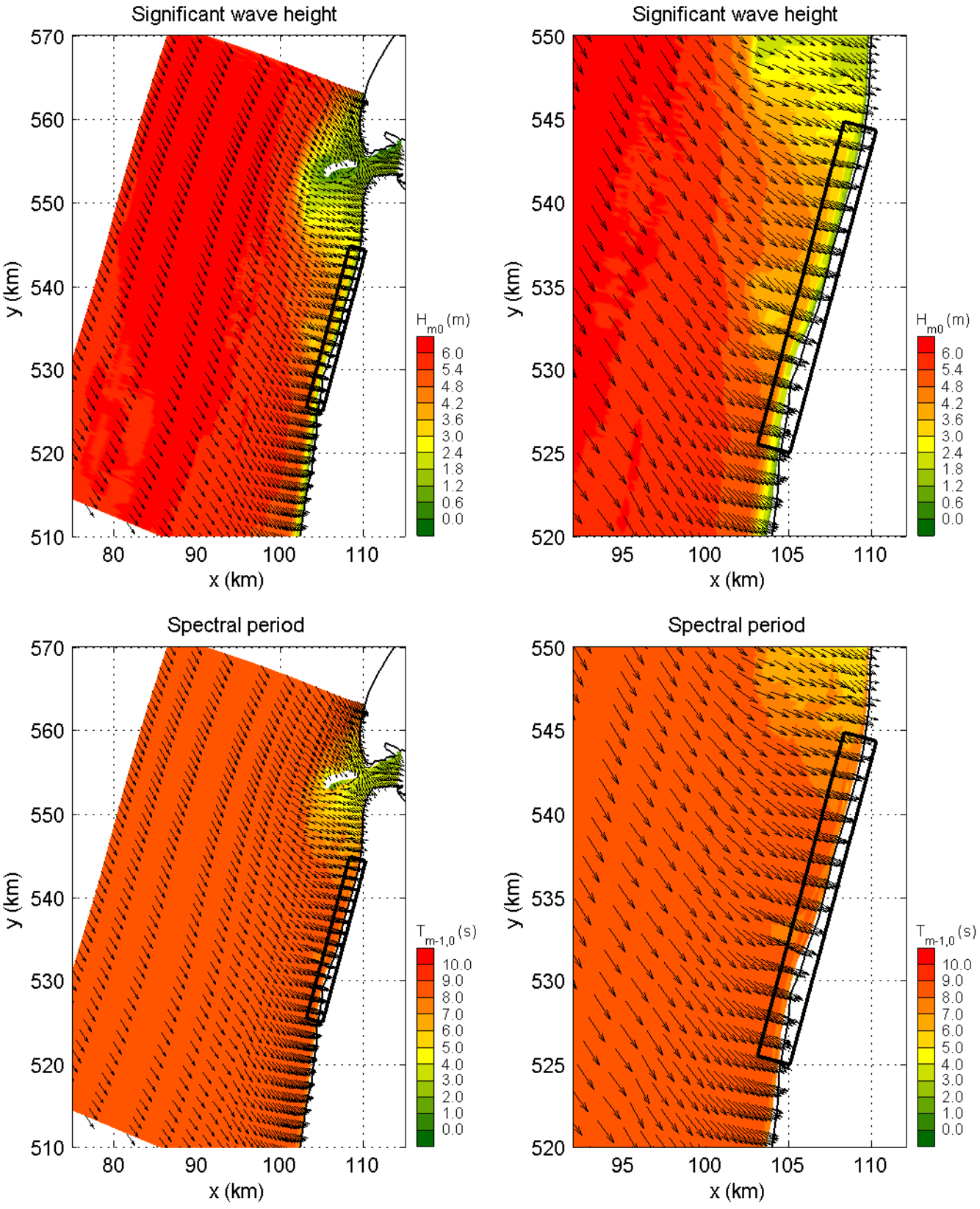

Variation of significant wave height H_{m0} and spectral period $T_{m-1,0}$ near Petten, Case: PETTEN 1995/1/1 10:00		SWAN 40.51A
		Numerical efficiency SWAN
DELTARES & ALKYON	H5107.46/A2214	Fig. 3.19

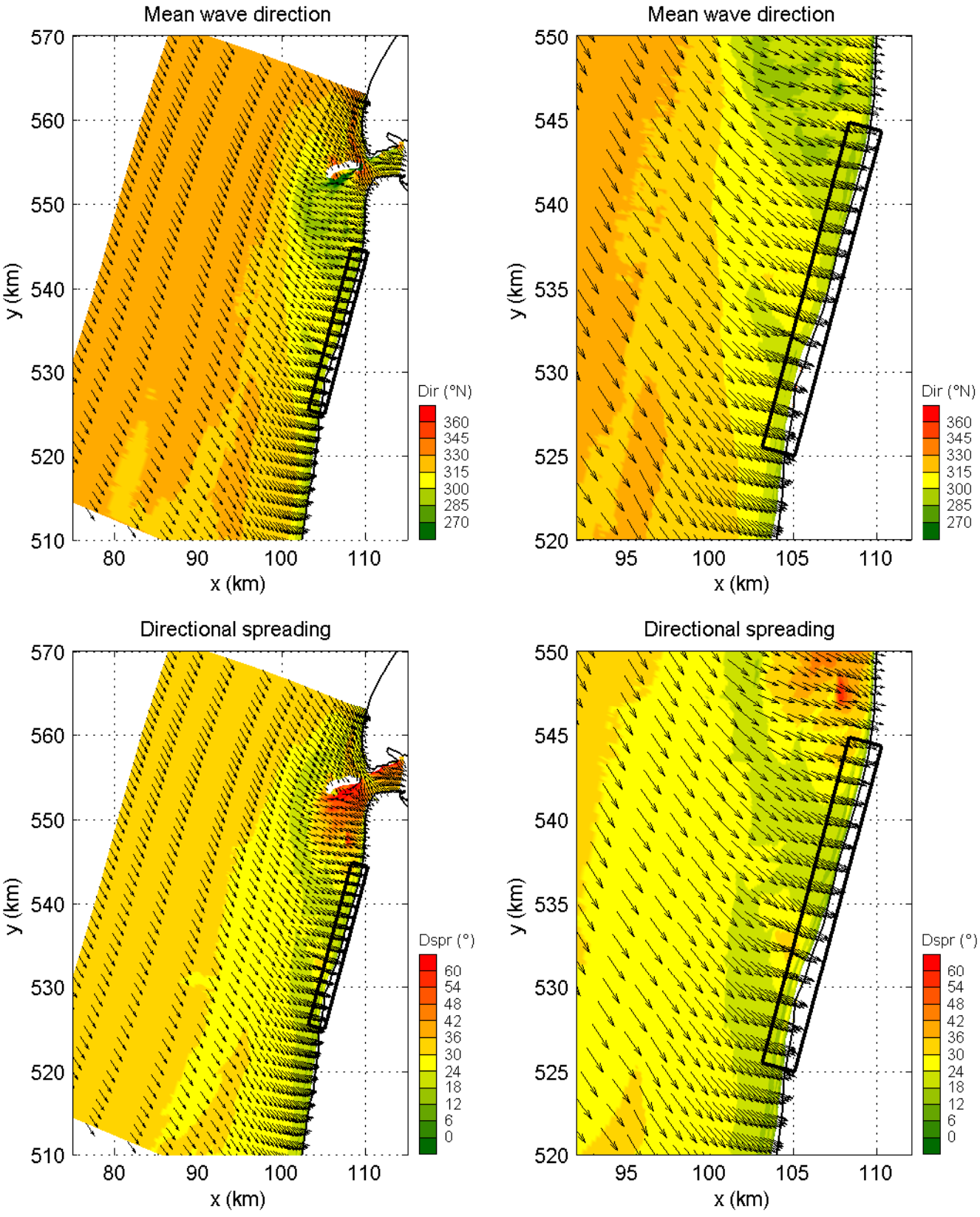

Variation of mean wave direction Dir and directional spreading Dspr near Petten, Case: PETTEN 1995/1/1 10:00		SWAN 40.51A
	Numerical efficiency SWAN	
DELTARES & ALKYON	H5107.46/A2214	Fig. 3.20

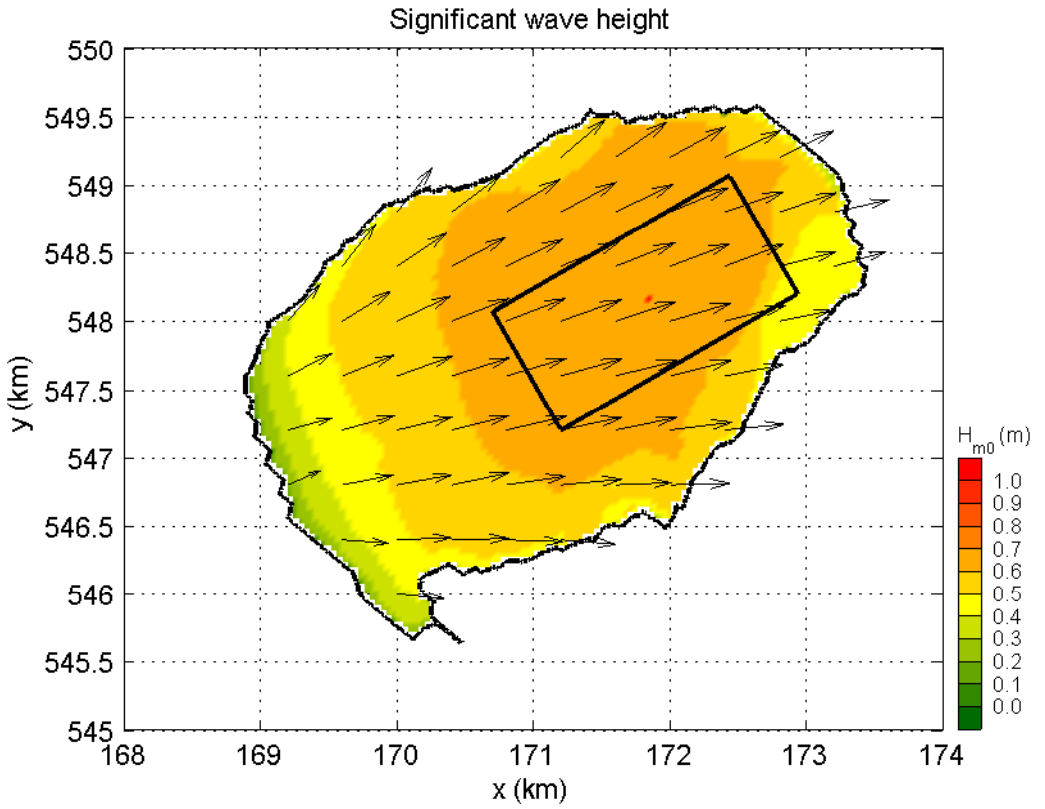

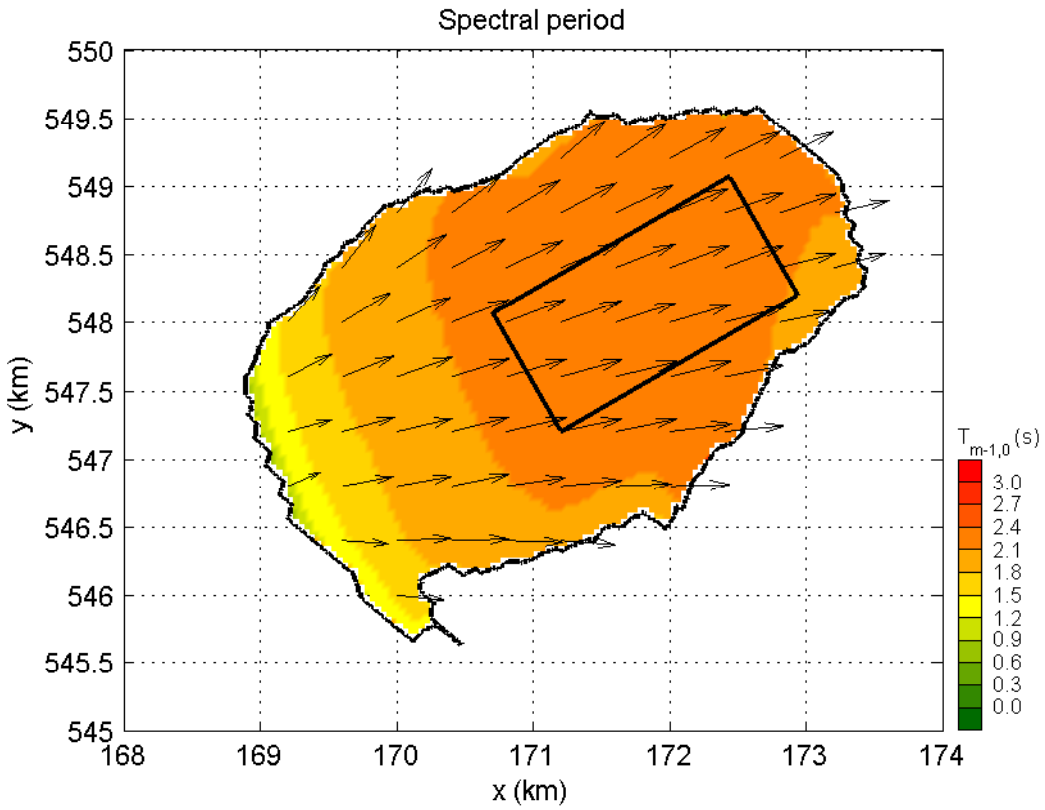

Variation of significant wave height H_{m0} and spectral period $T_{m-1,0}$ in Lake Sloten, Case: SLE 2002/10/27 15:00		SWAN 40.51A
	Numerical efficiency SWAN	
DELTARES & ALKYON	H5107.46/A2214	Fig. 3.21

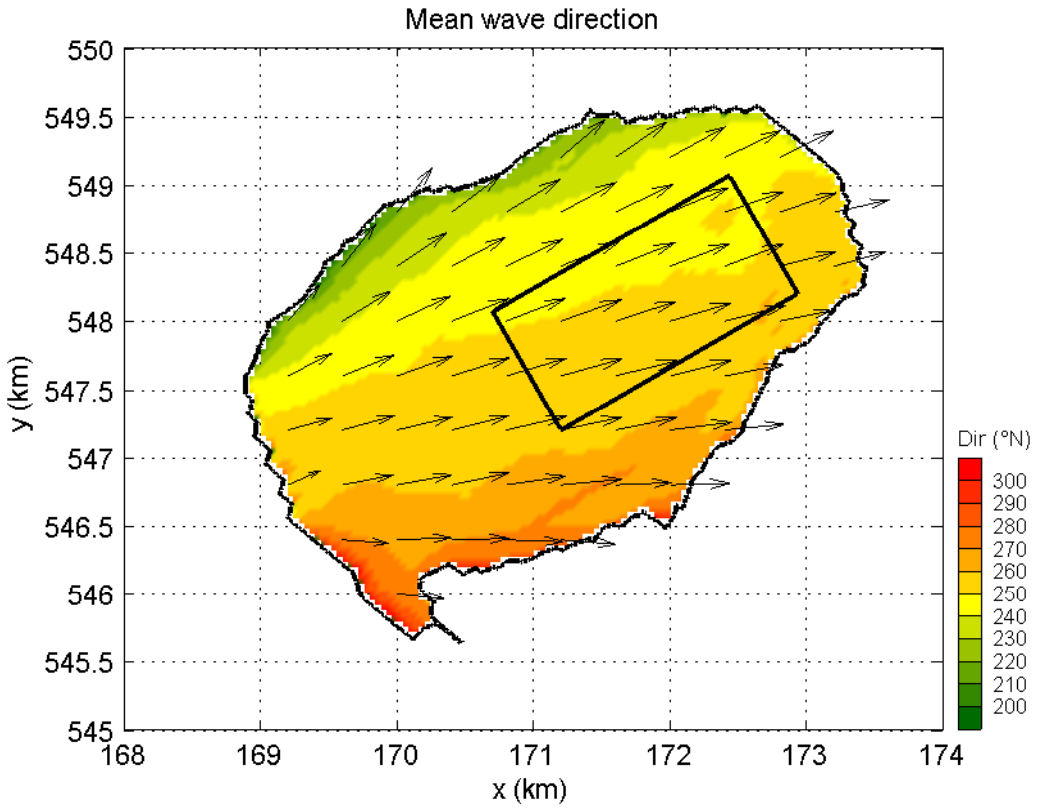

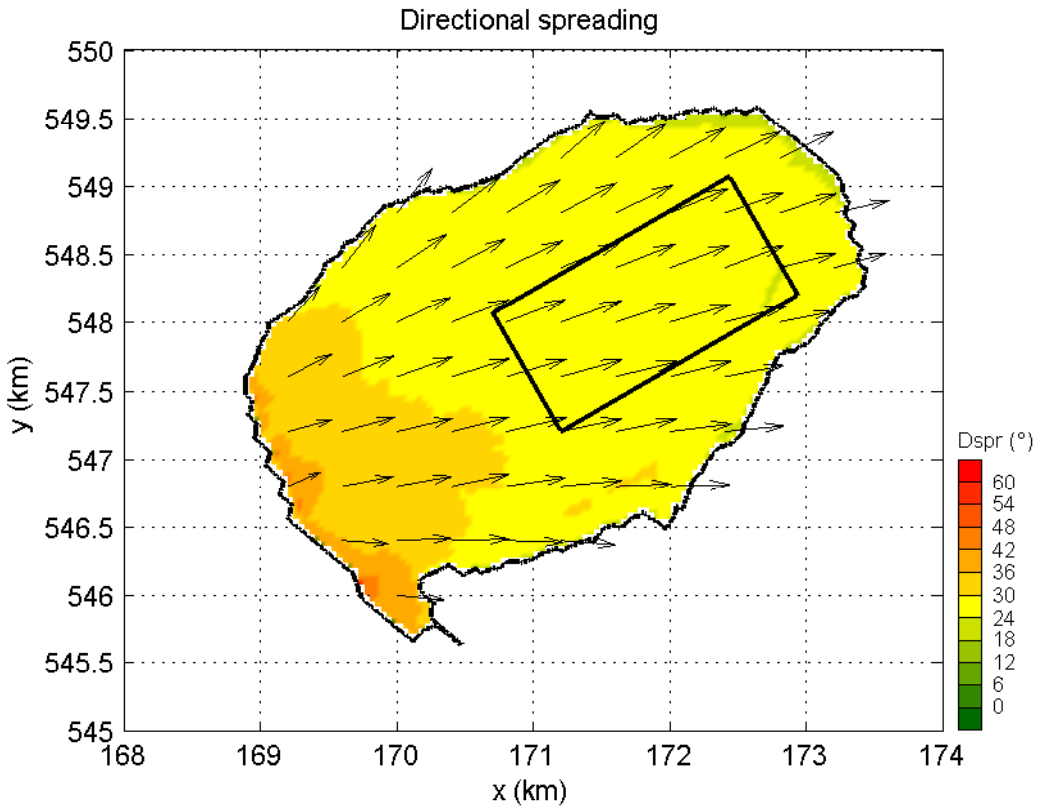

Variation of mean wave direction Dir and directional spreading Dspr in Lake Sloten, Case: SLE 2002/10/27 15:00		SWAN 40.51A
	Numerical efficiency SWAN	
DELTARES & ALKYON	H5107.46/A2214	Fig. 3.22

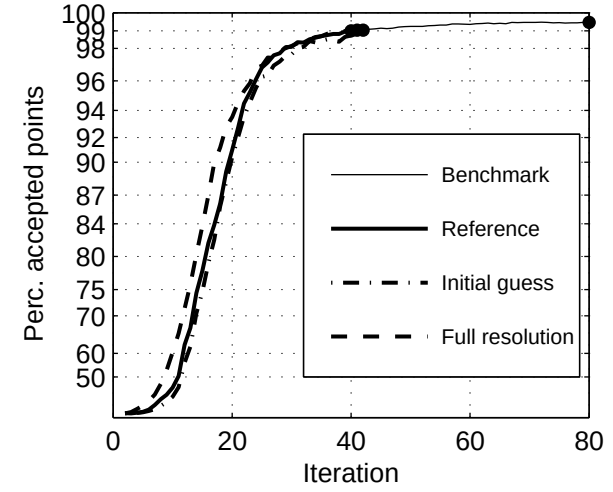

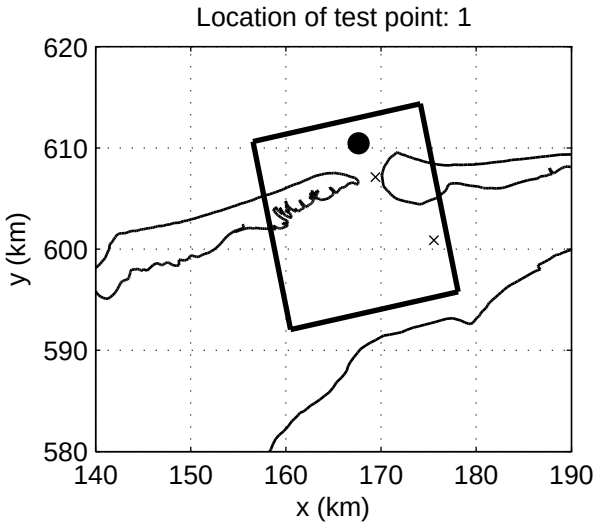

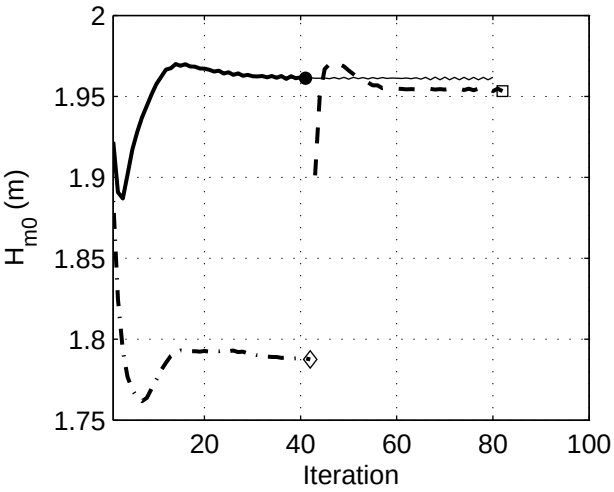

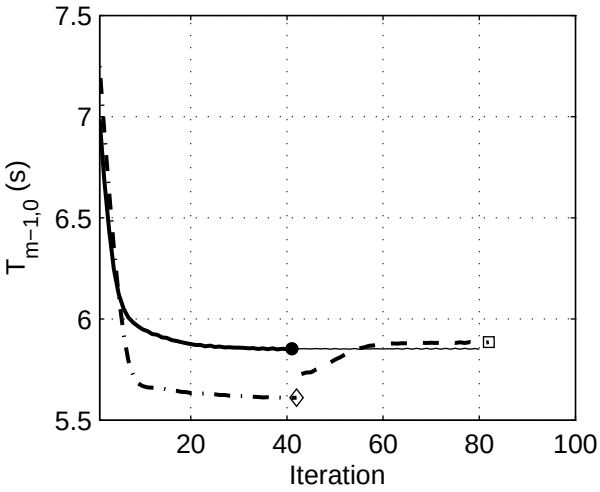

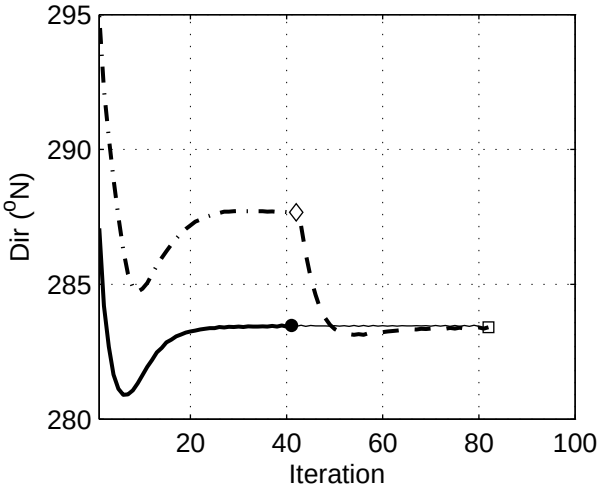

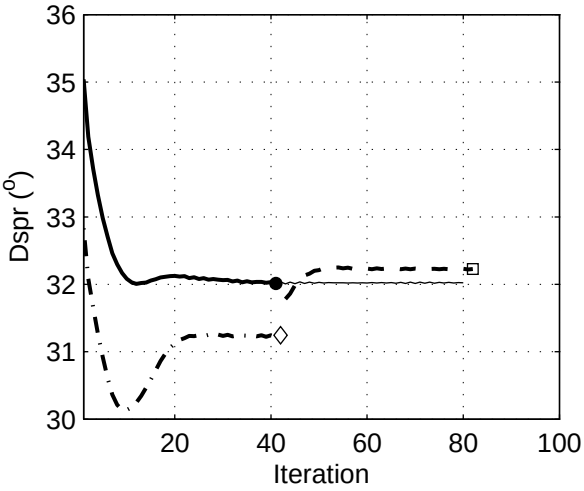

Convergence behaviour of integral wave parameters in the Amelander Zeegat Multigrid settings: Rx=2, Ry=2, Rθ=1, Rσ=1 (x2y2d1s1). Test point:1 Case: AZG3A 2005/1/2 10:00		SWAN 40.51A
		Numerical efficiency SWAN
DELTARES & ALKYON	H5107.46/A2114	Fig. 4.1

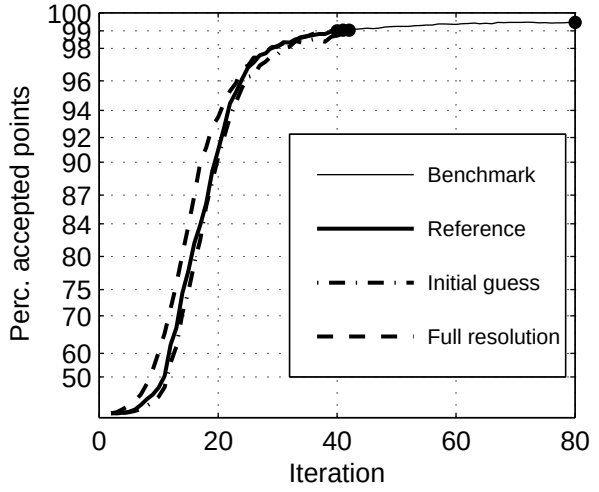

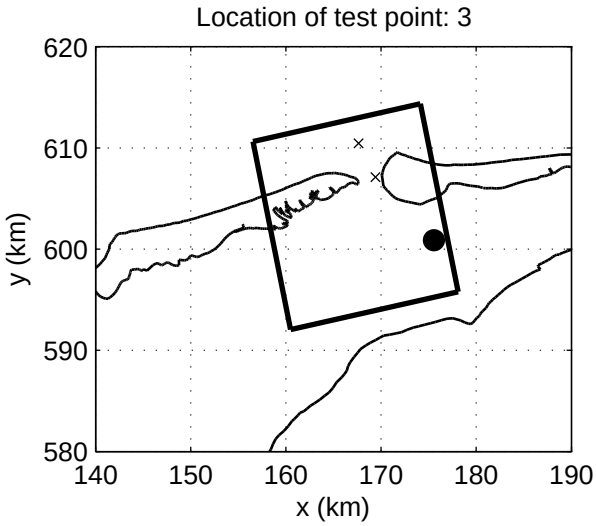

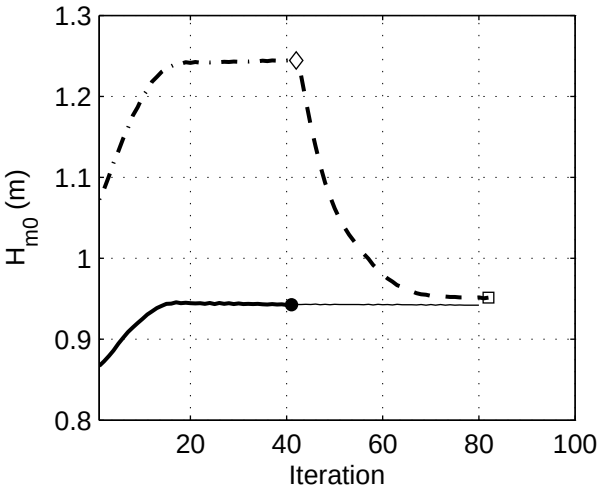

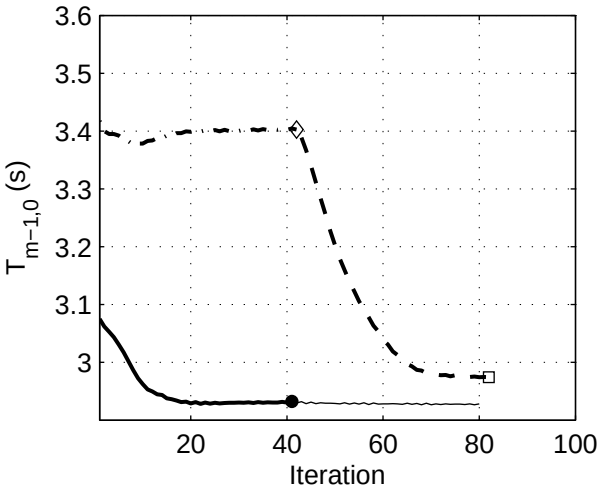

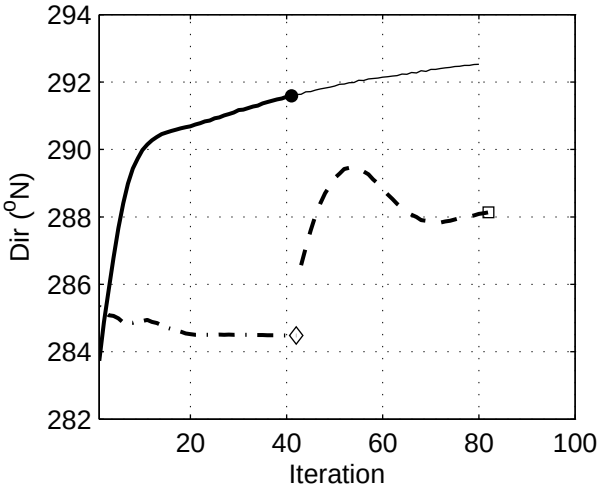

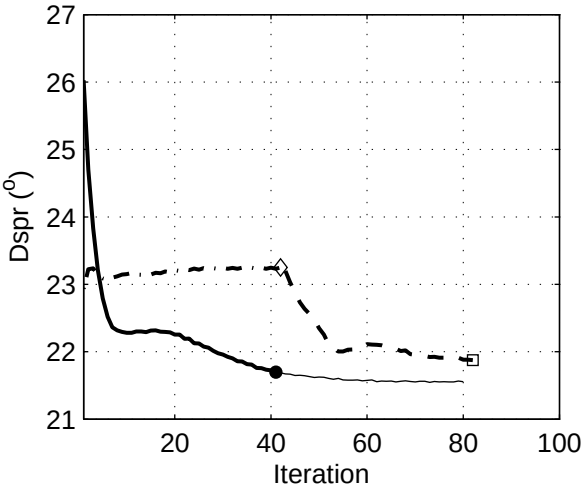

Convergence behaviour of integral wave parameters in the Amelander Zeegat Multigrid settings: Rx=2, Ry=2, Rθ=1, Rσ=1 (x2y2d1s1). Test point:3 Case: AZG3A 2005/1/2 10:00		SWAN 40.51A
		Numerical efficiency SWAN
DELTARES & ALKYON	H5107.46/A2114	Fig. 4.2

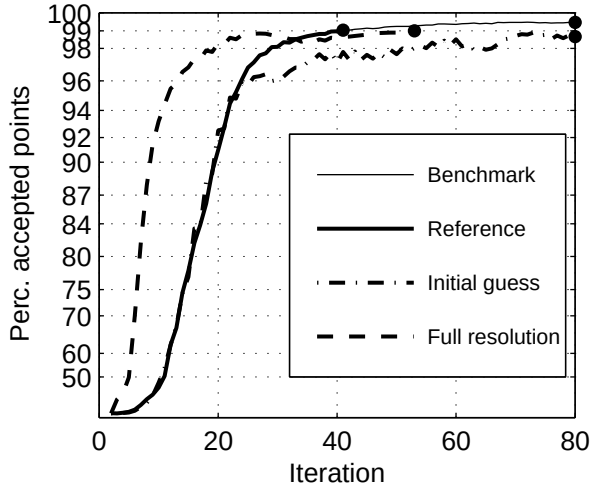

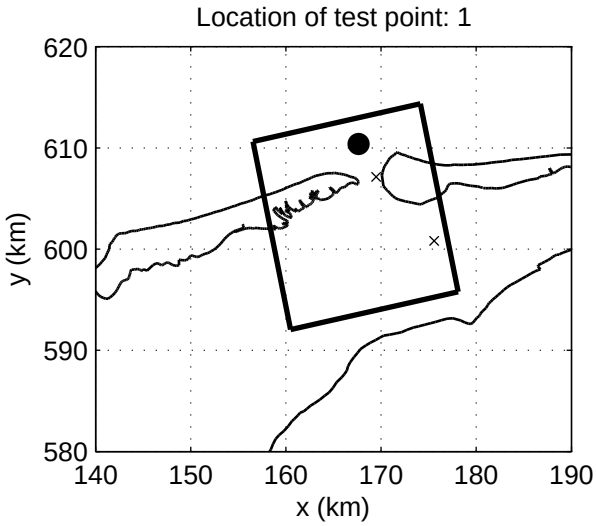

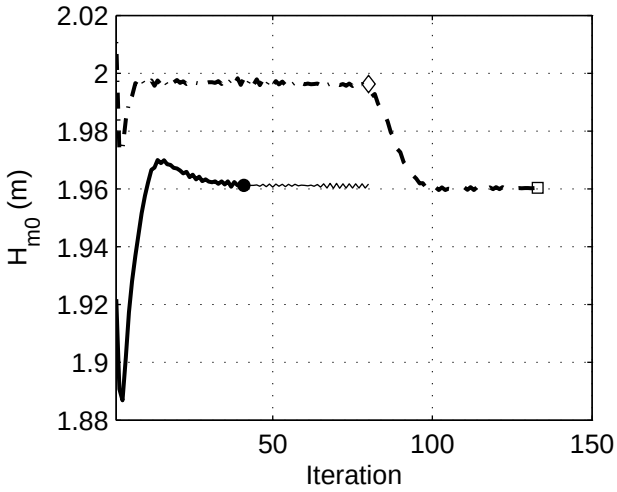

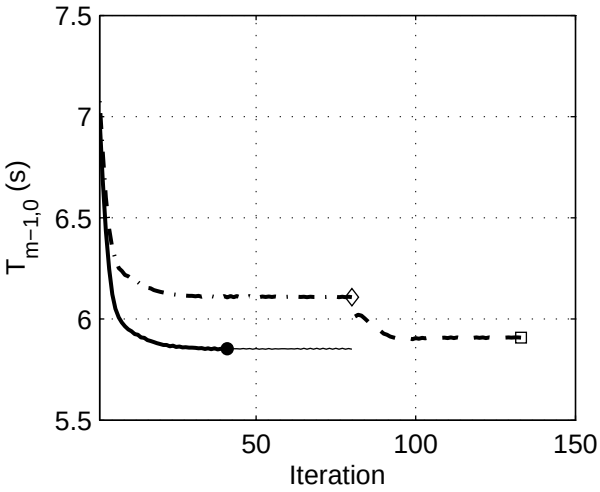

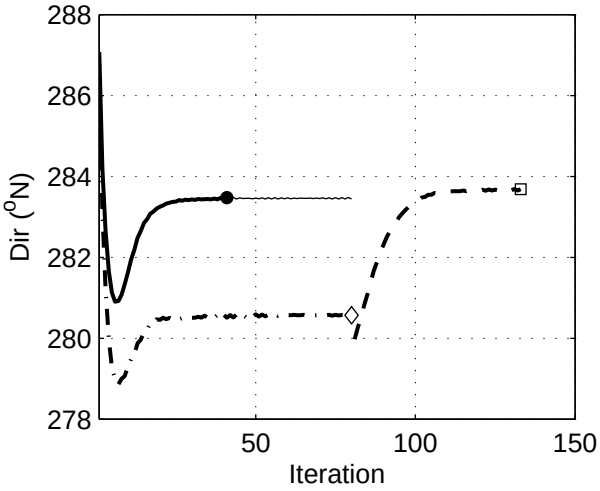

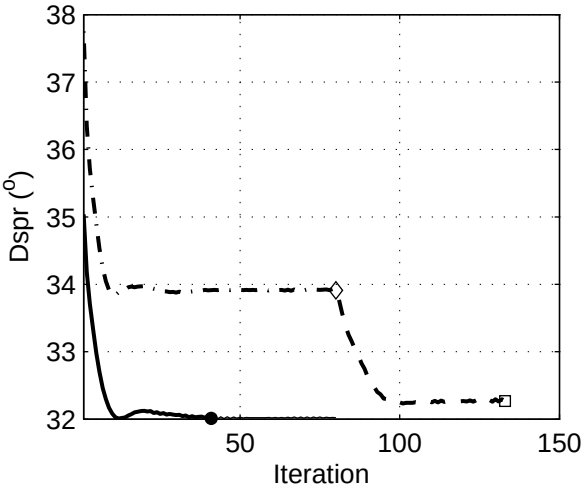

Convergence behaviour of integral wave parameters in the Amelander Zeegat Multigrid settings: Rx=1, Ry=1, Rθ=2, Rσ=2 (x1y1d2s2). Test point:1 Case: AZG3A 2005/1/2 10:00		SWAN 40.51A
		Numerical efficiency SWAN
DELTARES & ALKYON	H5107.46/A2114	Fig. 4.3

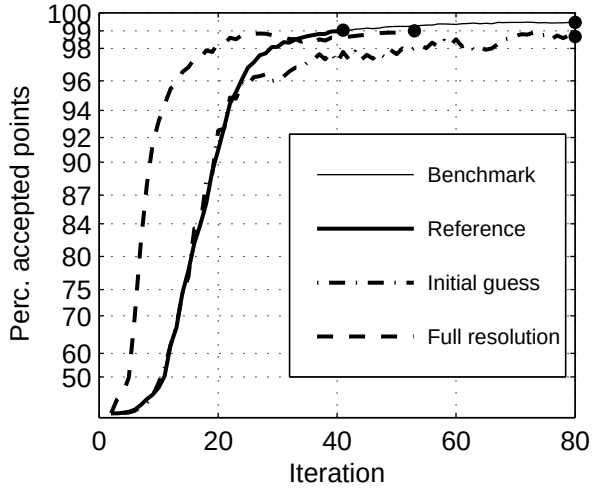

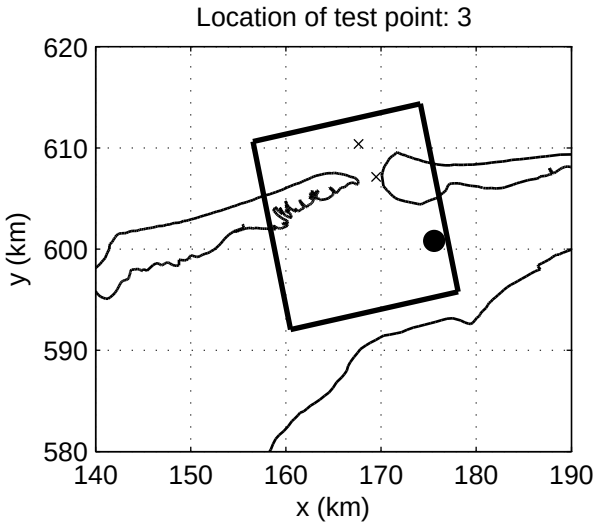

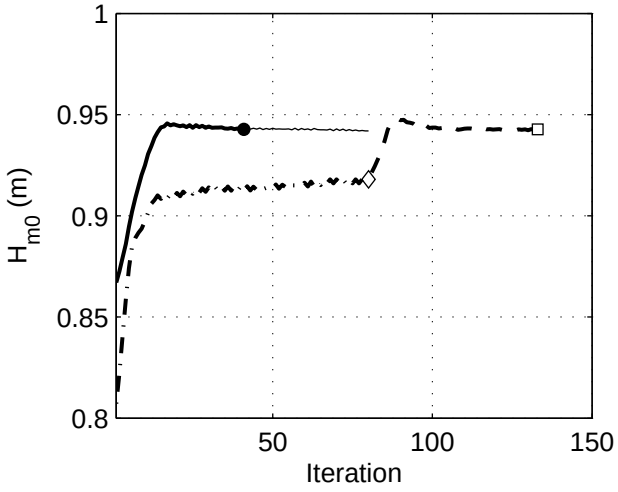

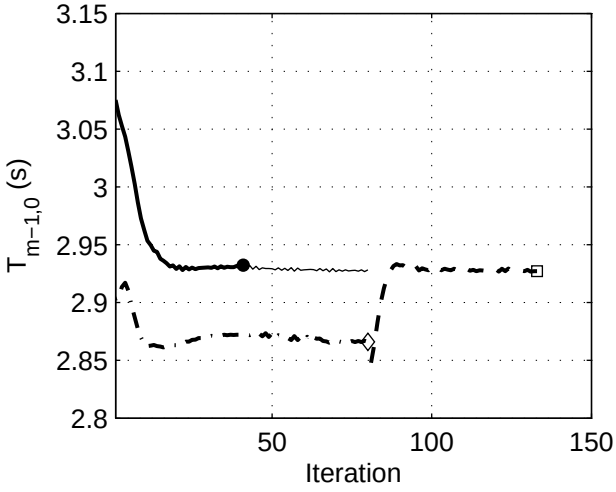

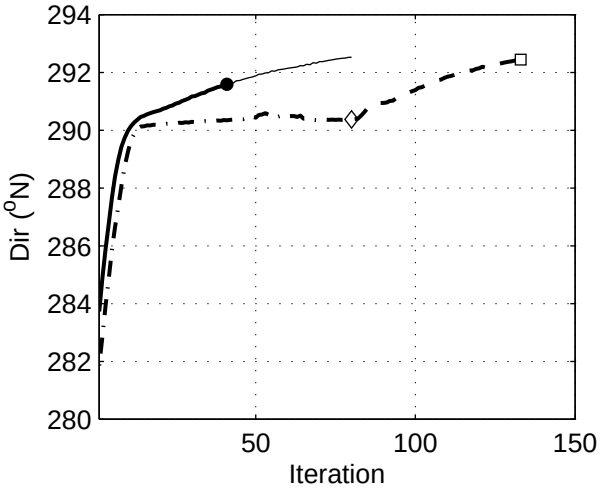

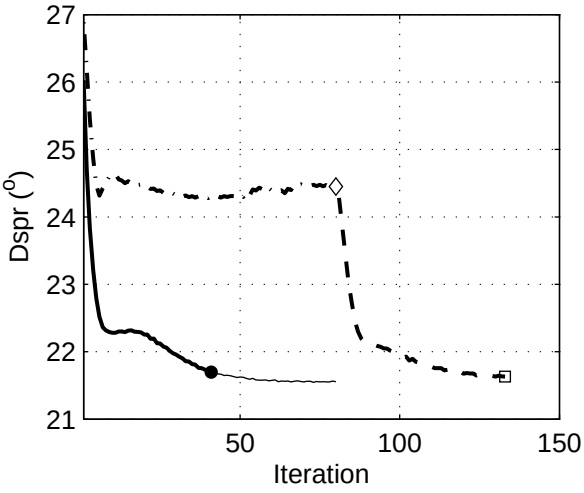

Convergence behaviour of integral wave parameters in the Amelander Zeegat Multigrid settings: Rx=1, Ry=1, Rθ=2, Rσ=2 (x1y1d2s2). Test point:3 Case: AZG3A 2005/1/2 10:00		SWAN 40.51A
		Numerical efficiency SWAN
DELTARES & ALKYON	H5107.46/A2114	Fig. 4.4

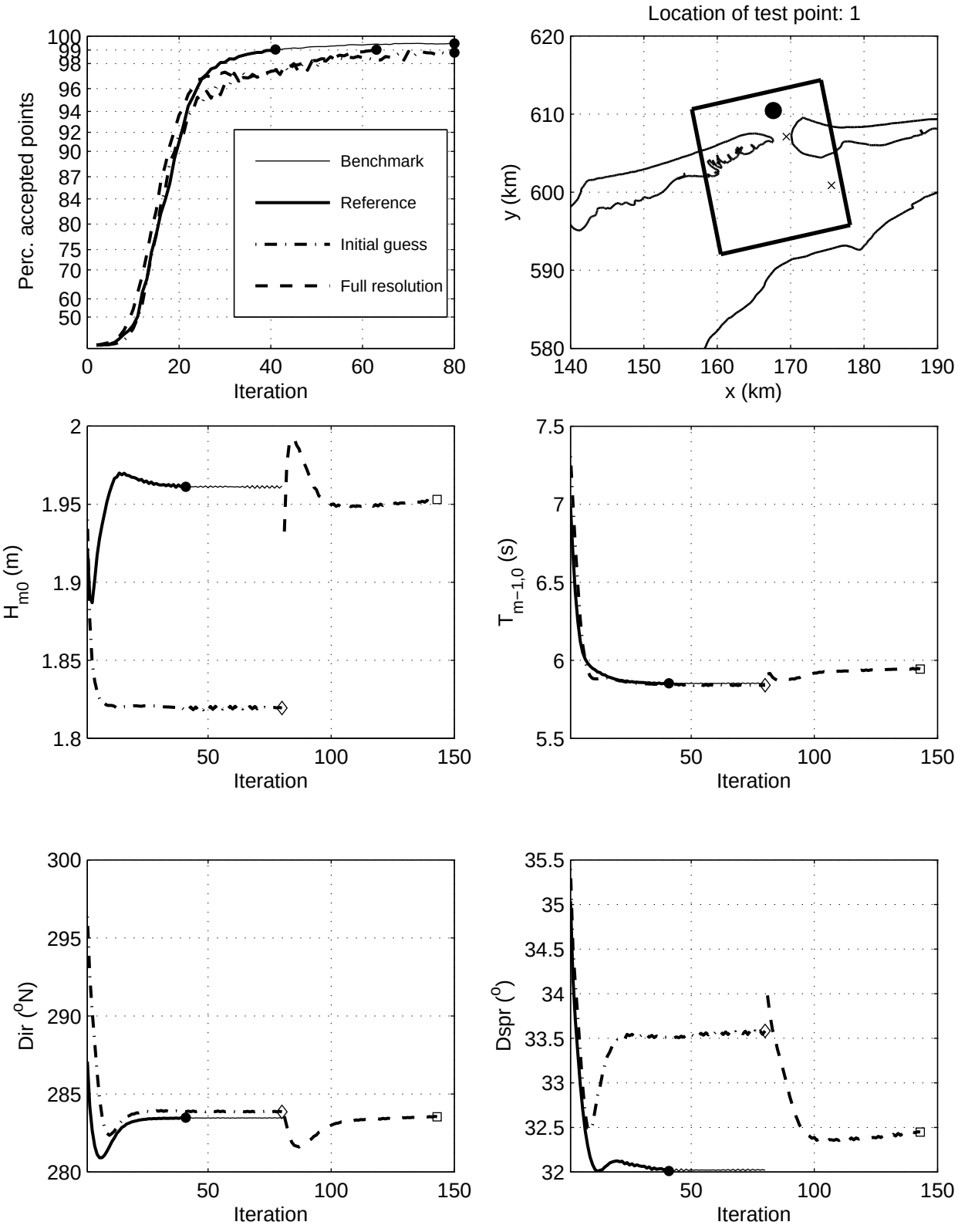

Convergence behaviour of integral wave parameters in the Amelander Zeegat Multigrid settings: Rx=2, Ry=2, Rθ=2, Rσ=2 (x2y2d2s2). Test point:1 Case: AZG3A 2005/1/2 10:00		SWAN 40.51A
		Numerical efficiency SWAN
DELTARES & ALKYON	H5107.46/A2114	Fig. 4.5

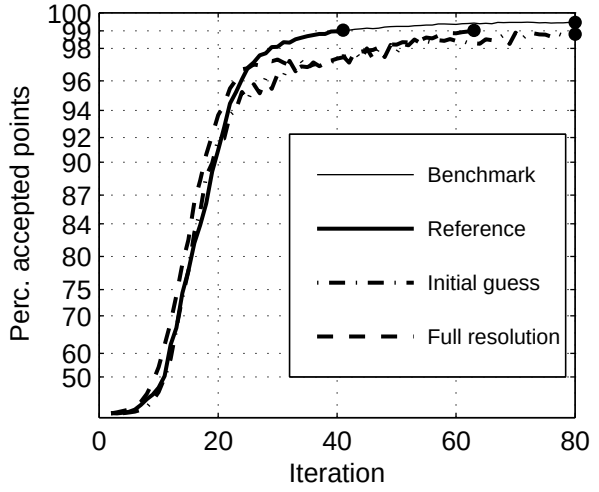

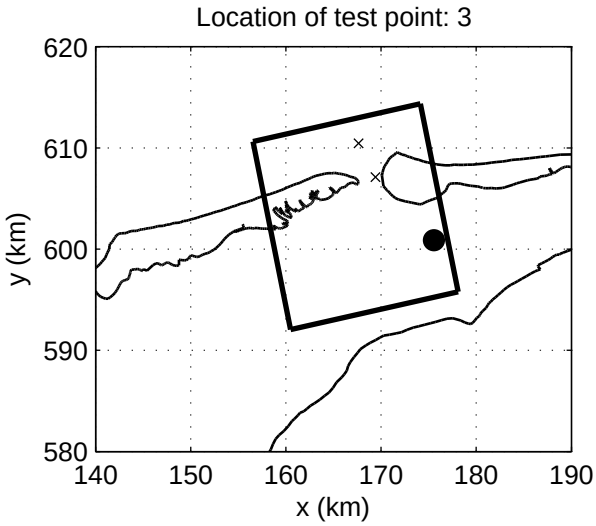

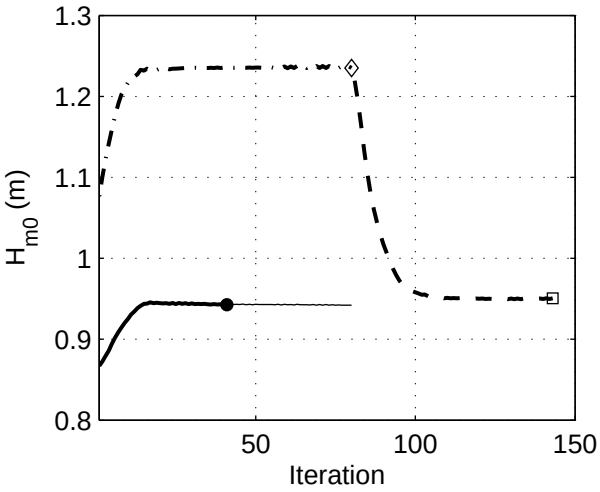

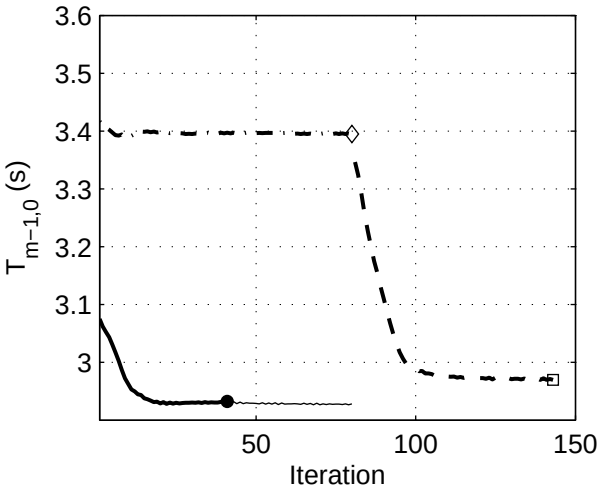

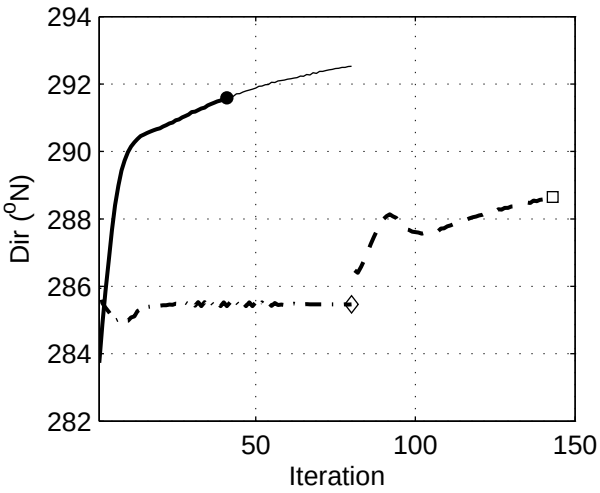

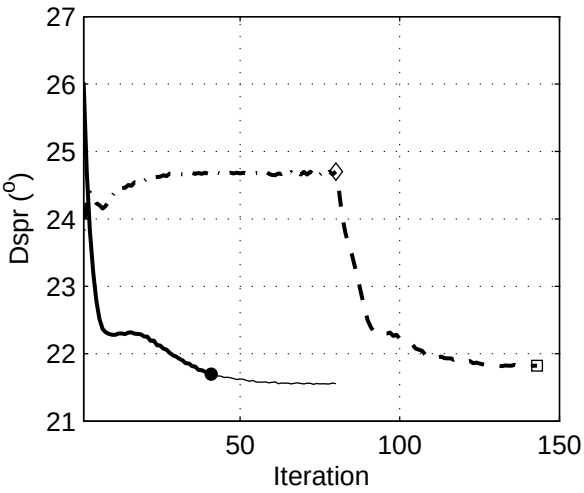

Convergence behaviour of integral wave parameters in the Amelander Zeegat Multigrid settings: Rx=2, Ry=2, Rθ=2, Rσ=2 (x2y2d2s2). Test point:3 Case: AZG3A 2005/1/2 10:00		SWAN 40.51A
		Numerical efficiency SWAN
DELTARES & ALKYON	H5107.46/A2114	Fig. 4.6

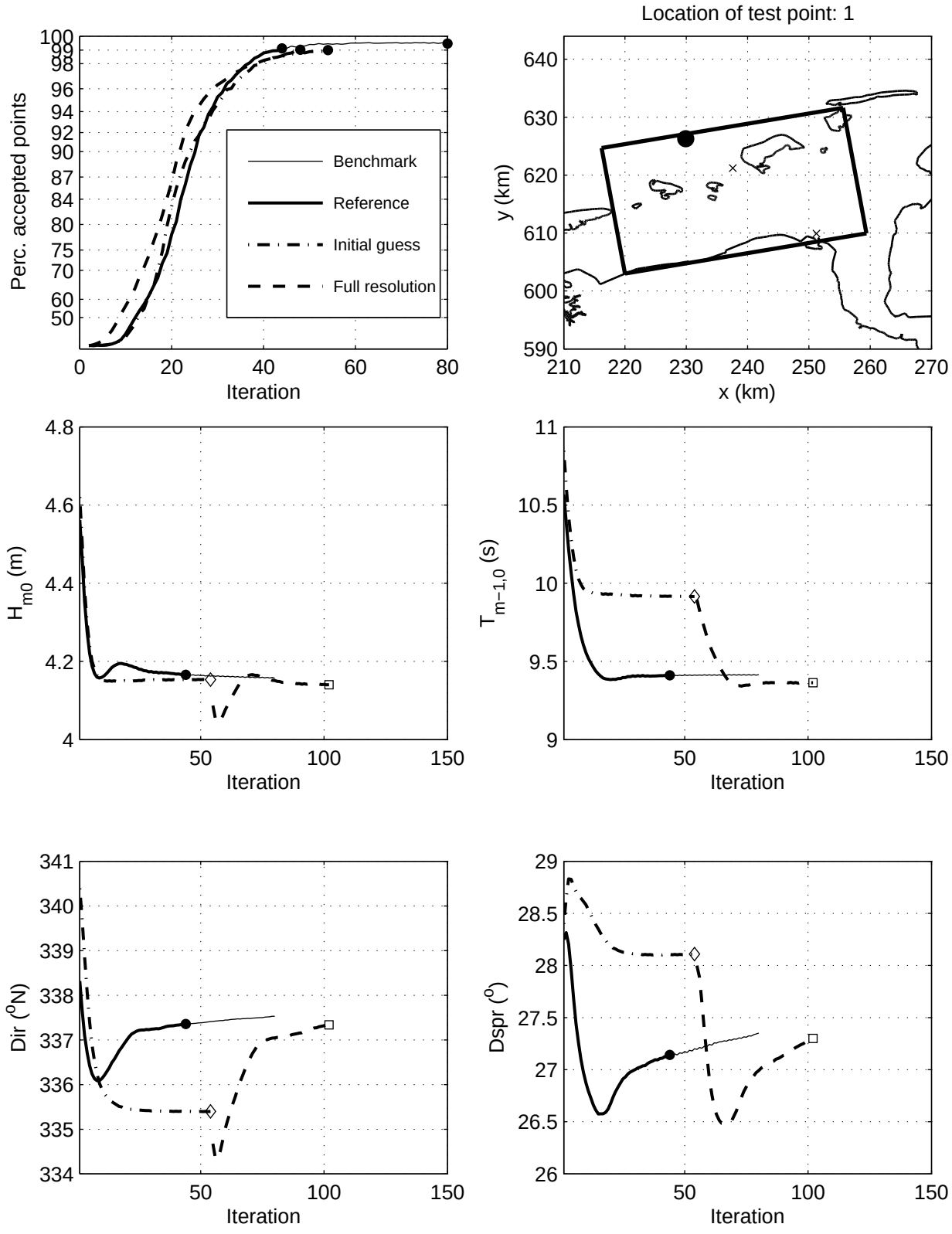

Convergence behaviour of integral wave parameters in the Eems−Dollard Multigrid settings: Rx=2, Ry=2, Rθ=1, Rσ=1 (x2y2d1s1). Test point:1 Case: EEMS3A 2006/11/1 06:30		SWAN 40.51A
		Numerical efficiency SWAN
DELTARES & ALKYON	H5107.46/A2114	Fig. 4.7

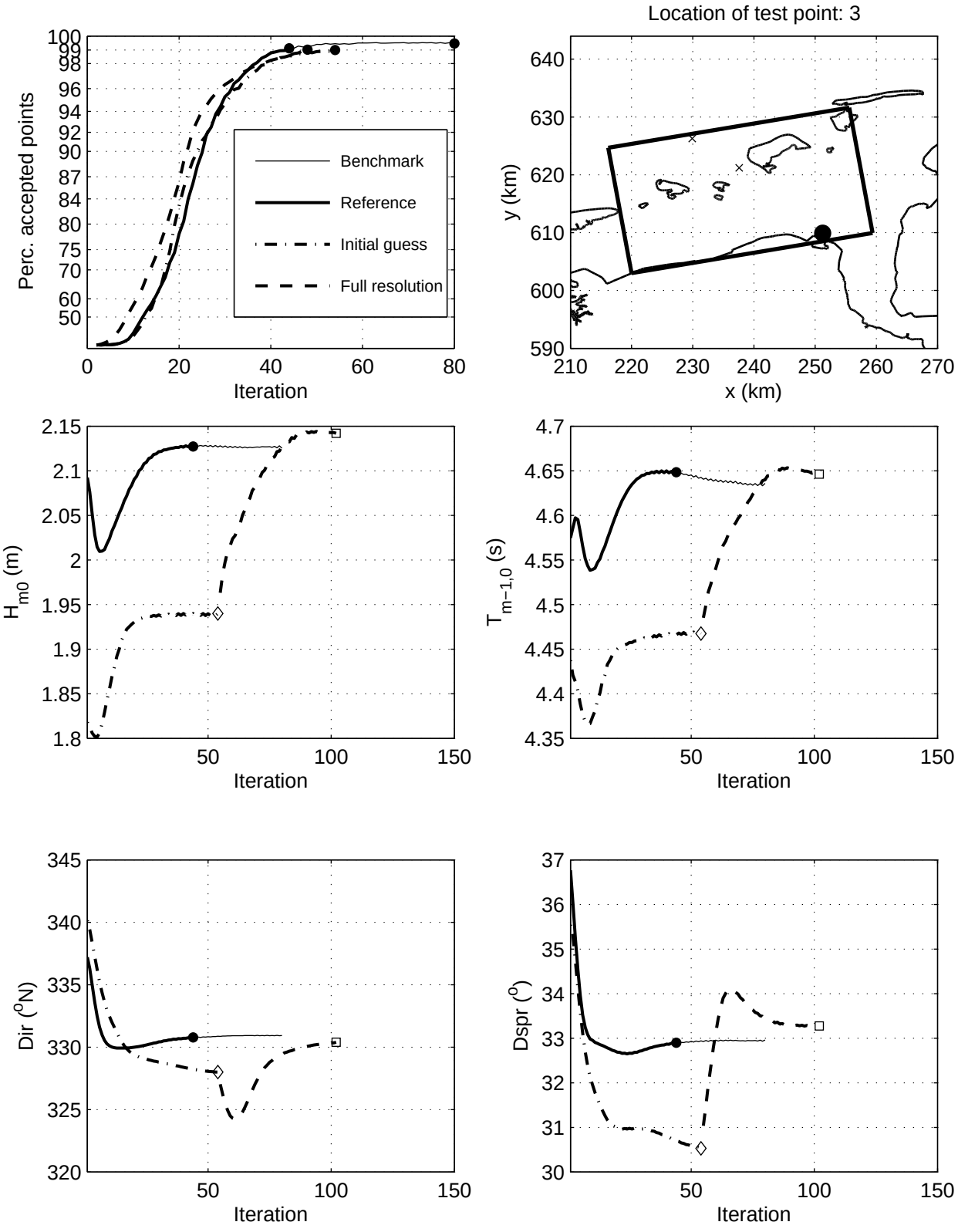

Convergence behaviour of integral wave parameters in the Eems−Dollard Multigrid settings: Rx=2, Ry=2, Rθ=1, Rσ=1 (x2y2d1s1). Test point:3 Case: EEMS3A 2006/11/1 06:30		SWAN 40.51A
		Numerical efficiency SWAN
DELTARES & ALKYON	H5107.46/A2114	Fig. 4.8

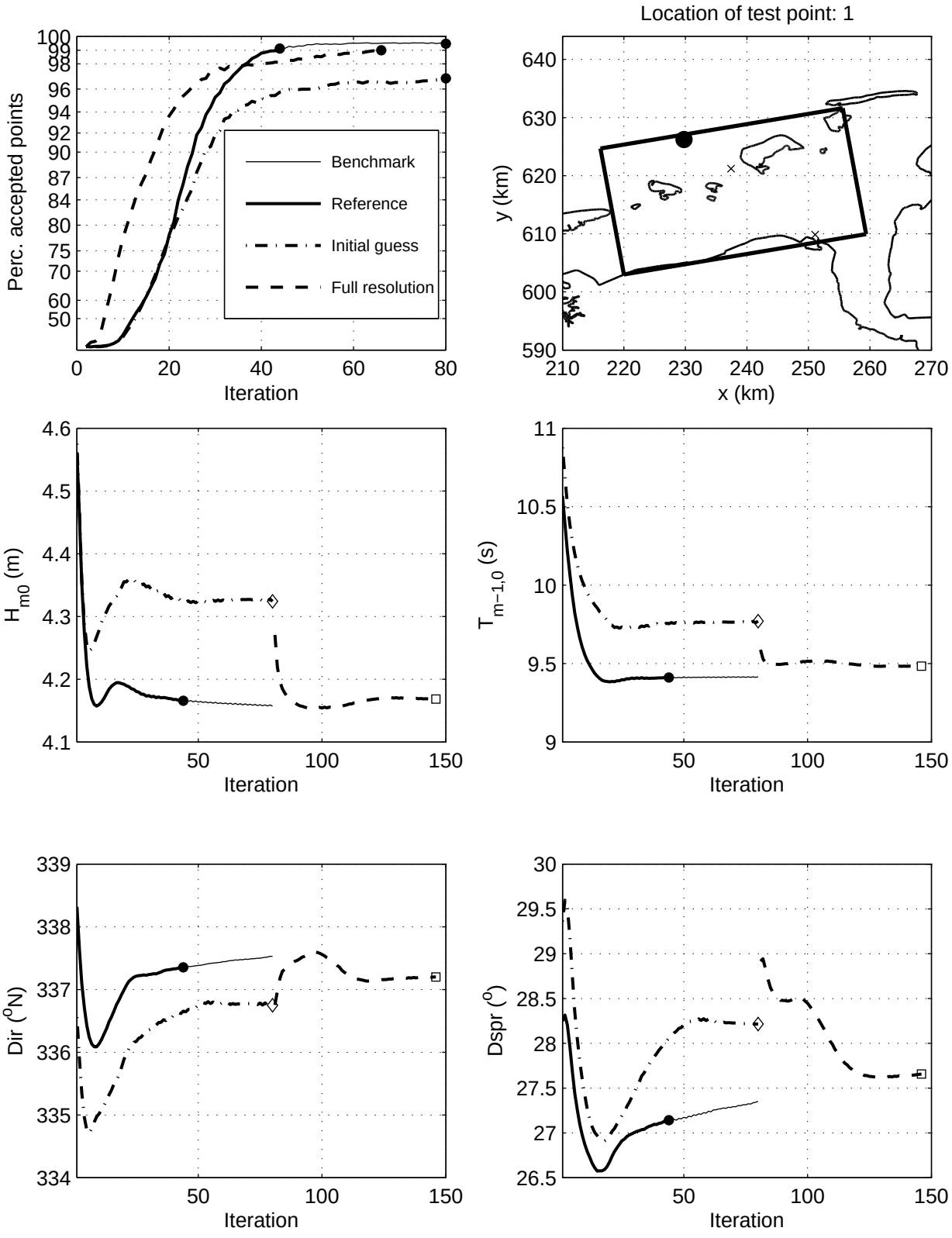

Convergence behaviour of integral wave parameters in the Eems−Dollard Multigrid settings: Rx=1, Ry=1, Rθ=2, Rσ=2 (x1y1d2s2). Test point:1 Case: EEMS3A 2006/11/1 06:30		SWAN 40.51A
		Numerical efficiency SWAN
DELTARES & ALKYON	H5107.46/A2114	Fig. 4.9

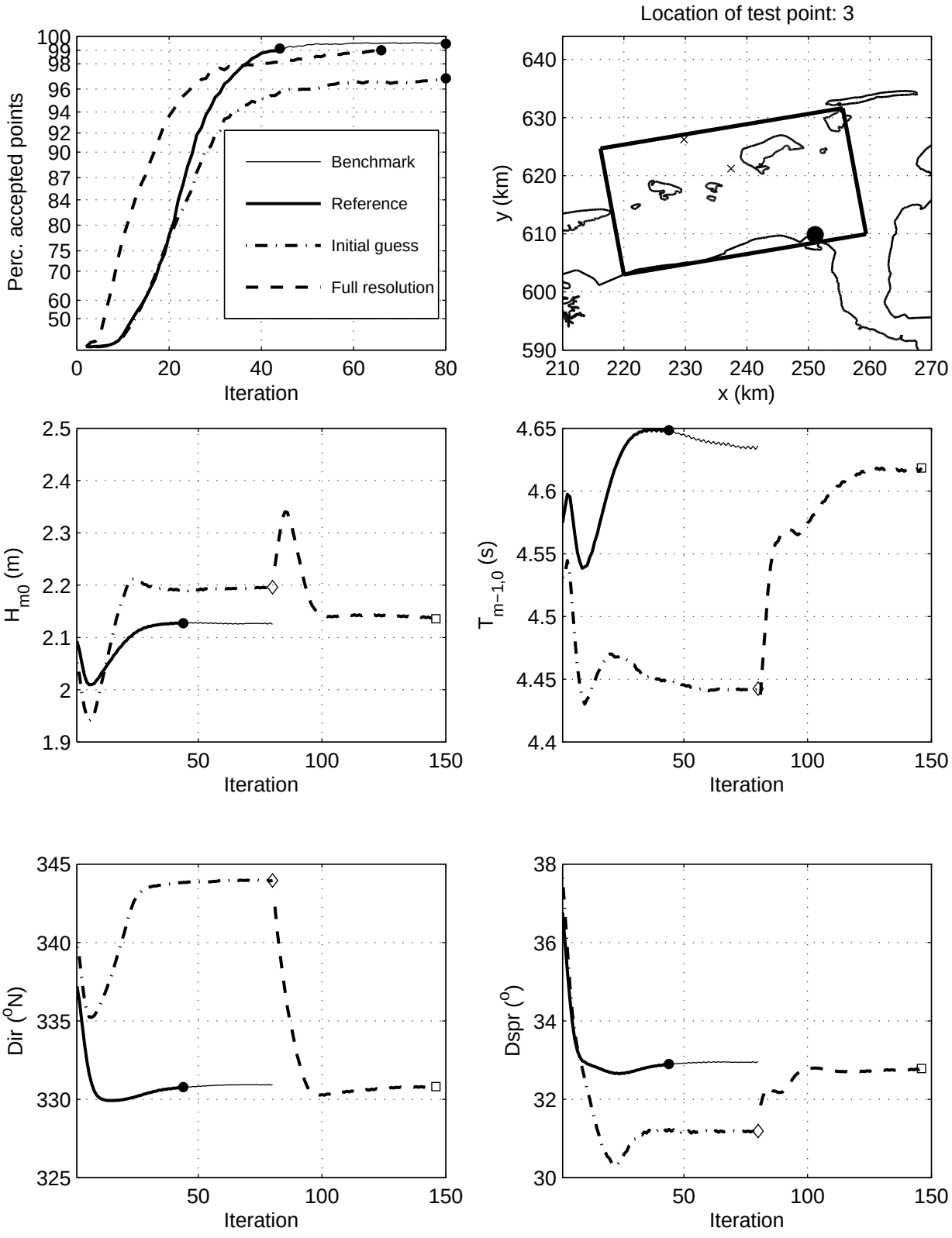

Convergence behaviour of integral wave parameters in the Eems−Dollard Multigrid settings: Rx=1, Ry=1, Rθ=2, Rσ=2 (x1y1d2s2). Test point:3 Case: EEMS3A 2006/11/1 06:30		SWAN 40.51A
		Numerical efficiency SWAN
DELTARES & ALKYON	H5107.46/A2114	Fig. 4.10

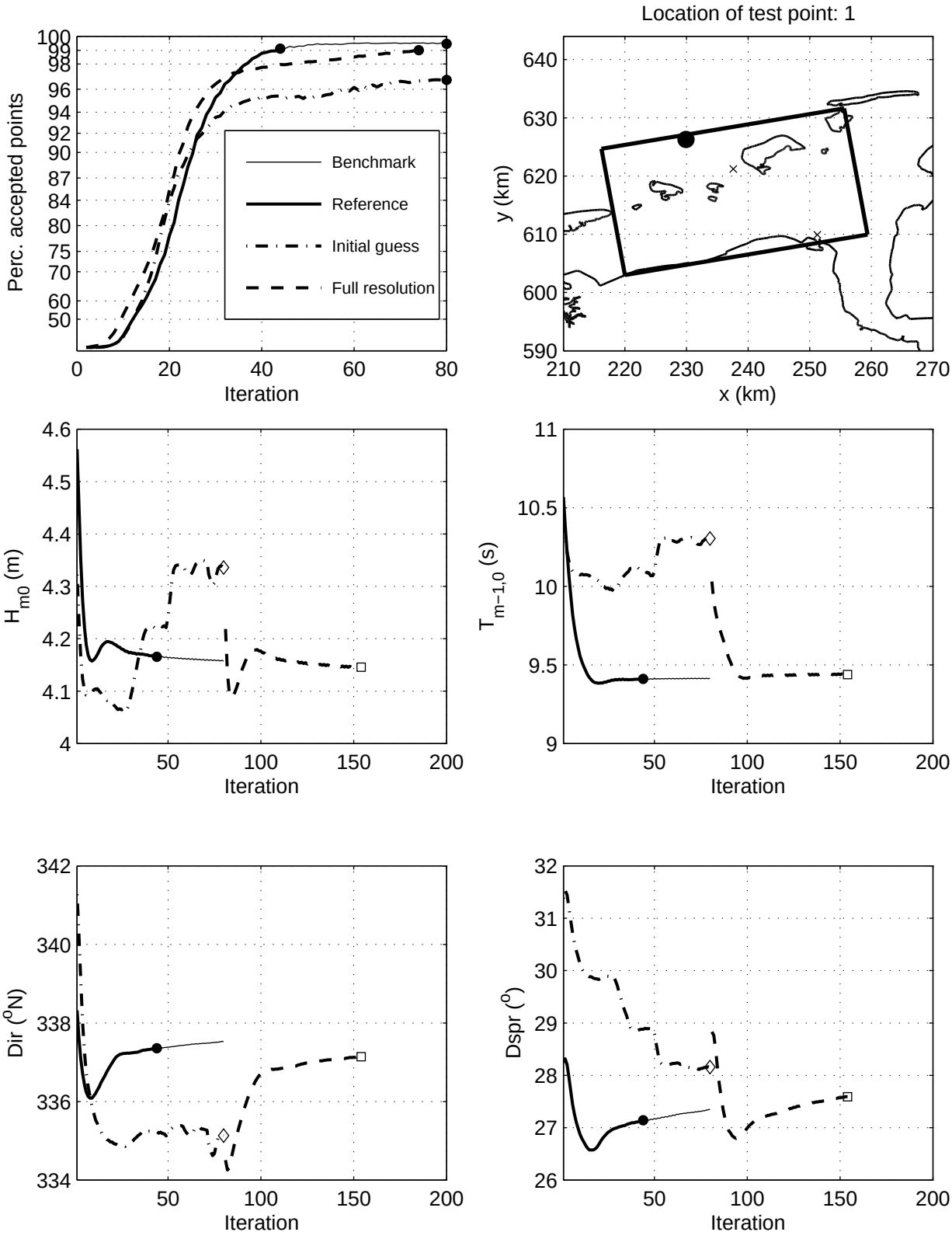

Convergence behaviour of integral wave parameters in the Eems−Dollard Multigrid settings: Rx=2, Ry=2, Rθ=2, Rσ=2 (x2y2d2s2). Test point:1 Case: EEMS3A 2006/11/1 06:30		SWAN 40.51A
		Numerical efficiency SWAN
DELTARES & ALKYON	H5107.46/A2114	Fig. 4.11

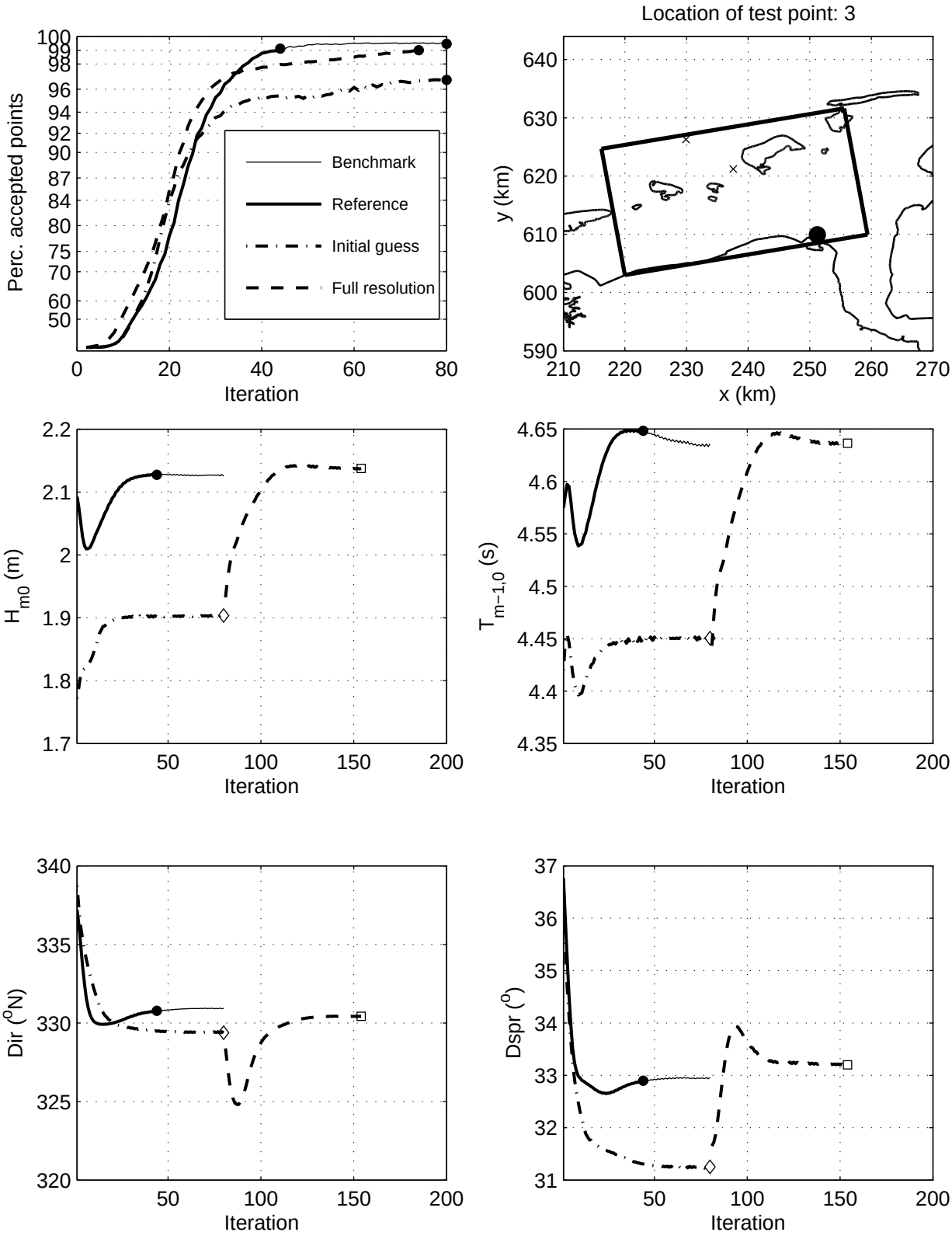

Convergence behaviour of integral wave parameters in the Eems−Dollard Multigrid settings: Rx=2, Ry=2, Rθ=2, Rσ=2 (x2y2d2s2). Test point:3 Case: EEMS3A 2006/11/1 06:30		SWAN 40.51A
		Numerical efficiency SWAN
DELTARES & ALKYON	H5107.46/A2114	Fig. 4.12

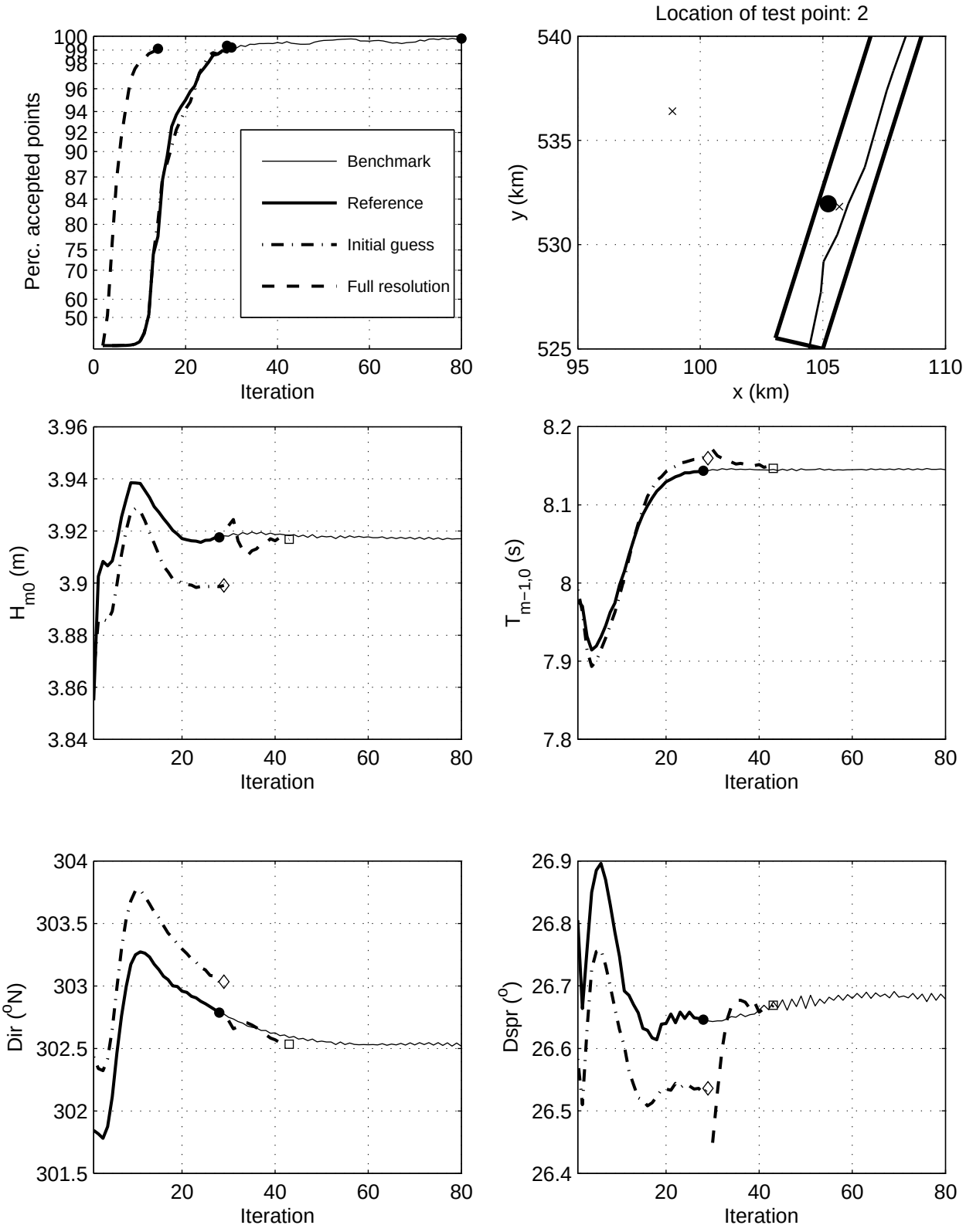

Convergence behaviour of integral wave parameters near Petten Multigrid settings: Rx=2, Ry=2, Rθ=1, Rσ=1 (x2y2d1s1). Test point:2 Case: PETTEN 1995/1/1 10:00		SWAN 40.51A
		Numerical efficiency SWAN
DELTARES & ALKYON	H5107.46/A2114	Fig. 4.13

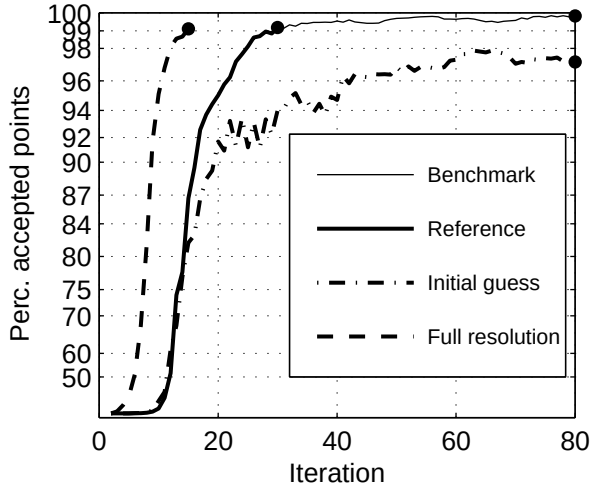

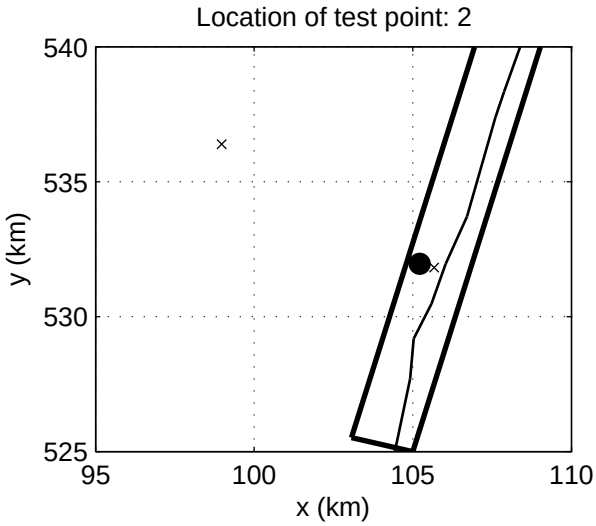

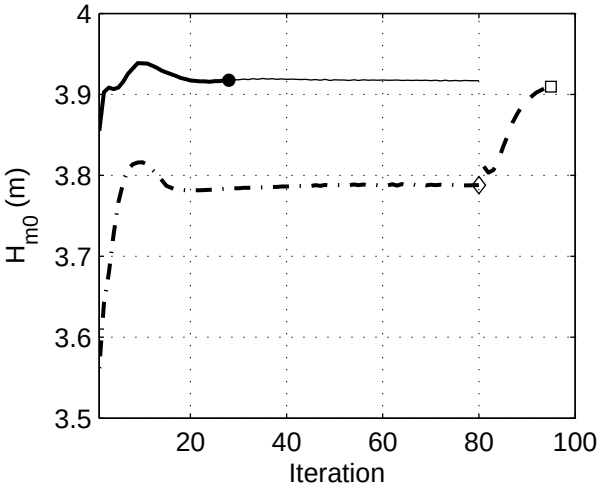

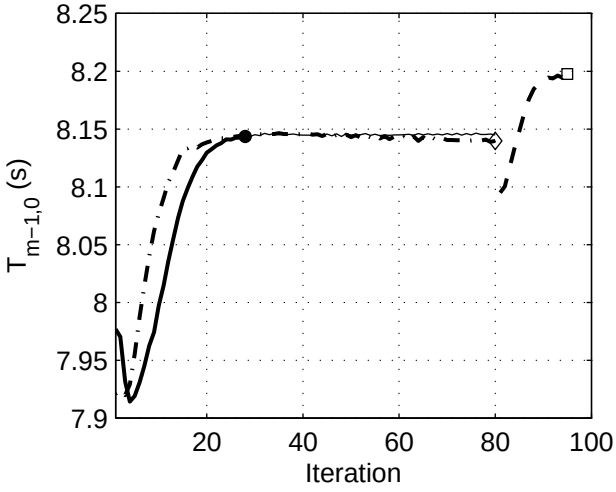

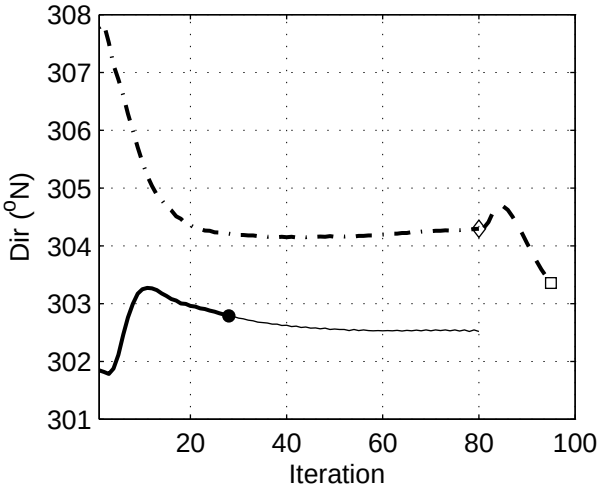

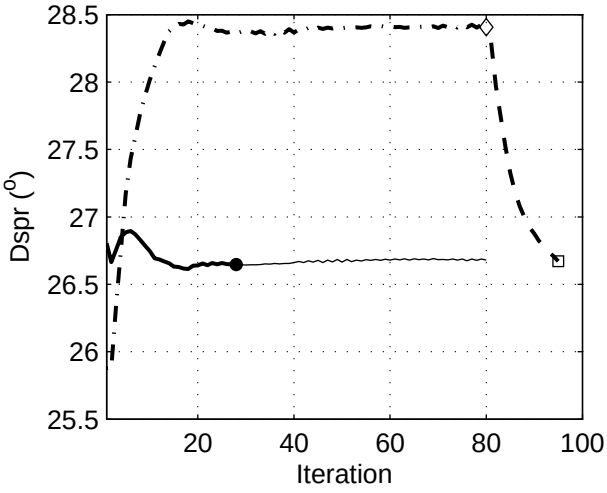

Convergence behaviour of integral wave parameters near Petten Multigrid settings: Rx=1, Ry=1, Rθ=2, Rσ=2 (x1y1d2s2). Test point:2 Case: PETTEN 1995/1/1 10:00		SWAN 40.51A
		Numerical efficiency SWAN
DELTARES & ALKYON	H5107.46/A2114	Fig. 4.14

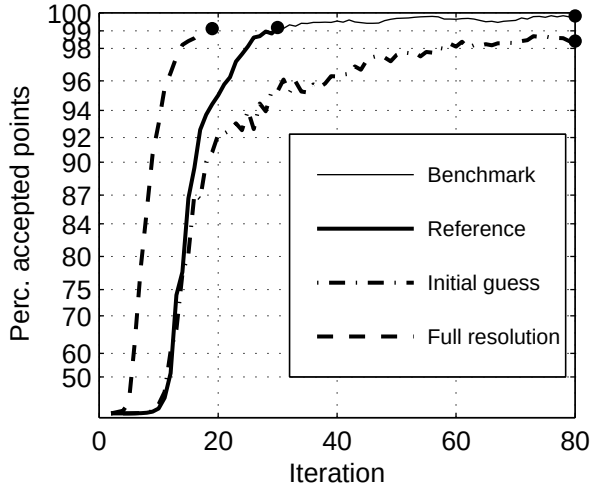

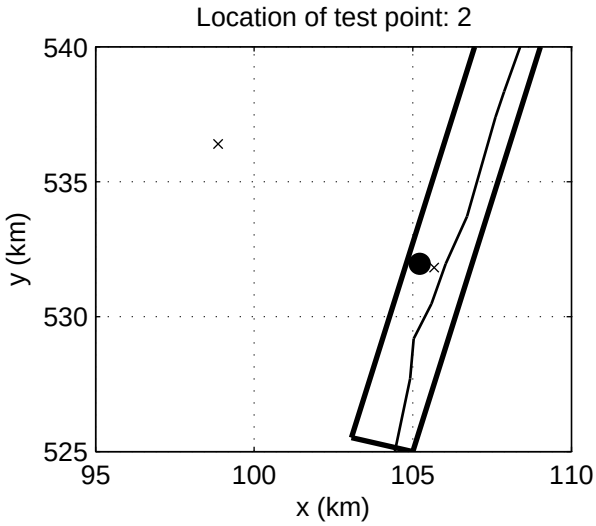

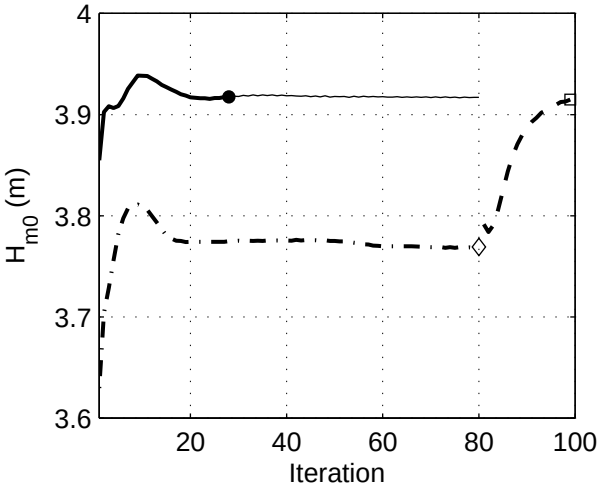

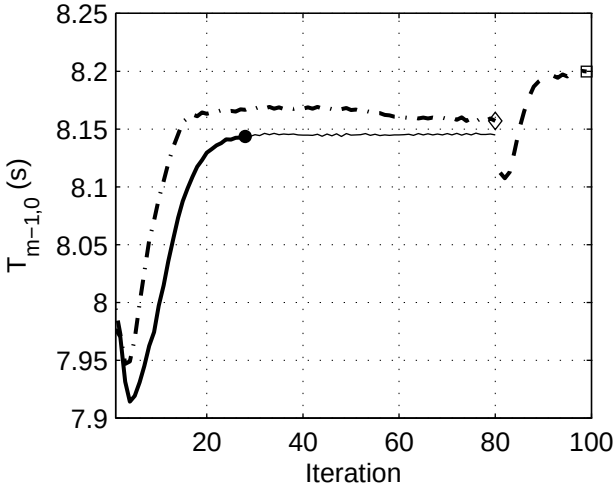

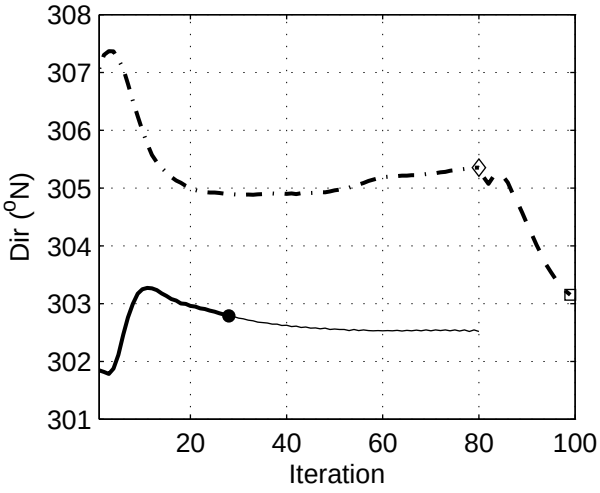

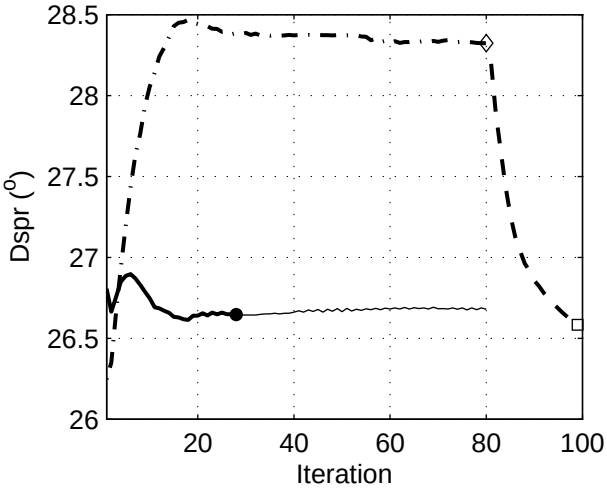

Convergence behaviour of integral wave parameters near Petten Multigrid settings: Rx=2, Ry=2, Rθ=2, Rσ=2 (x2y2d2s2). Test point:2 Case: PETTEN 1995/1/1 10:00		SWAN 40.51A
		Numerical efficiency SWAN
DELTARES & ALKYON	H5107.46/A2114	Fig. 4.15

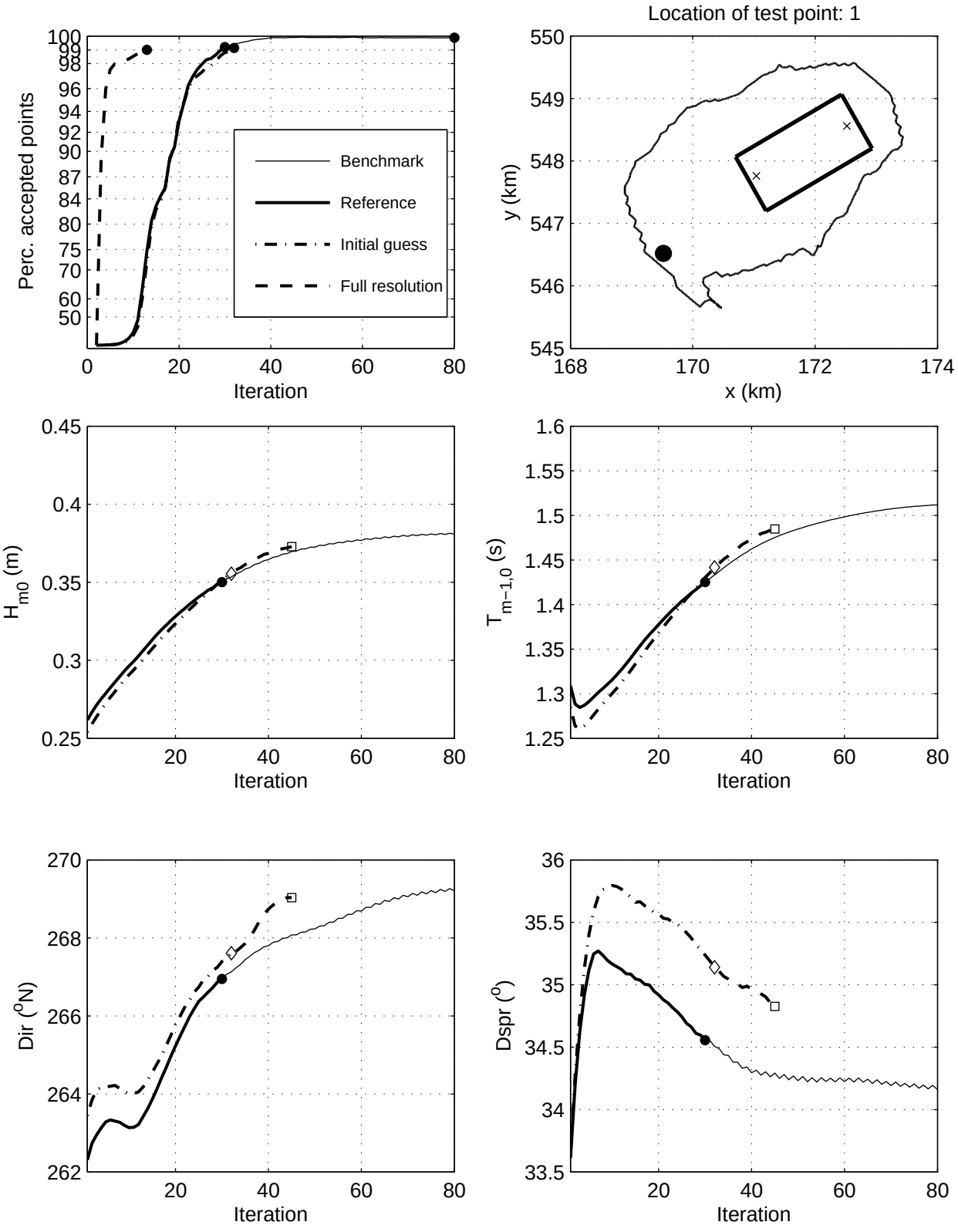

Convergence behaviour of integral wave parameters in Lake Sloten Multigrid settings: Rx=2, Ry=2, Rθ=1, Rσ=1 (x2y2d1s1). Test point:1 Case: SLE 2002/10/27 15:00		SWAN 40.51A
		Numerical efficiency SWAN
DELTARES & ALKYON	H5107.46/A2114	Fig. 4.16

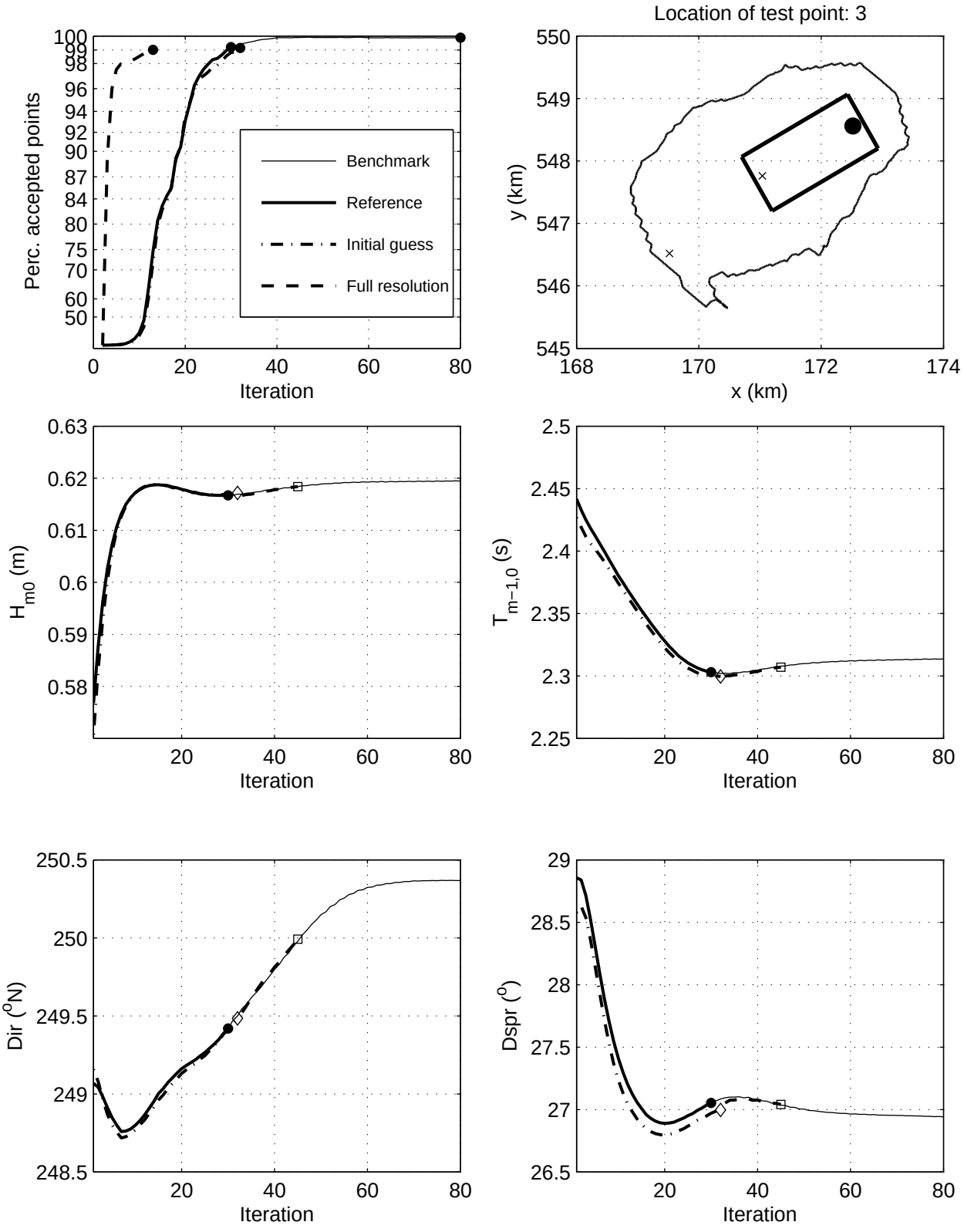

Convergence behaviour of integral wave parameters in Lake Sloten Multigrid settings: Rx=2, Ry=2, Rθ=1, Rσ=1 (x2y2d1s1). Test point:3 Case: SLE 2002/10/27 15:00		SWAN 40.51A
		Numerical efficiency SWAN
DELTARES & ALKYON	H5107.46/A2114	Fig. 4.17

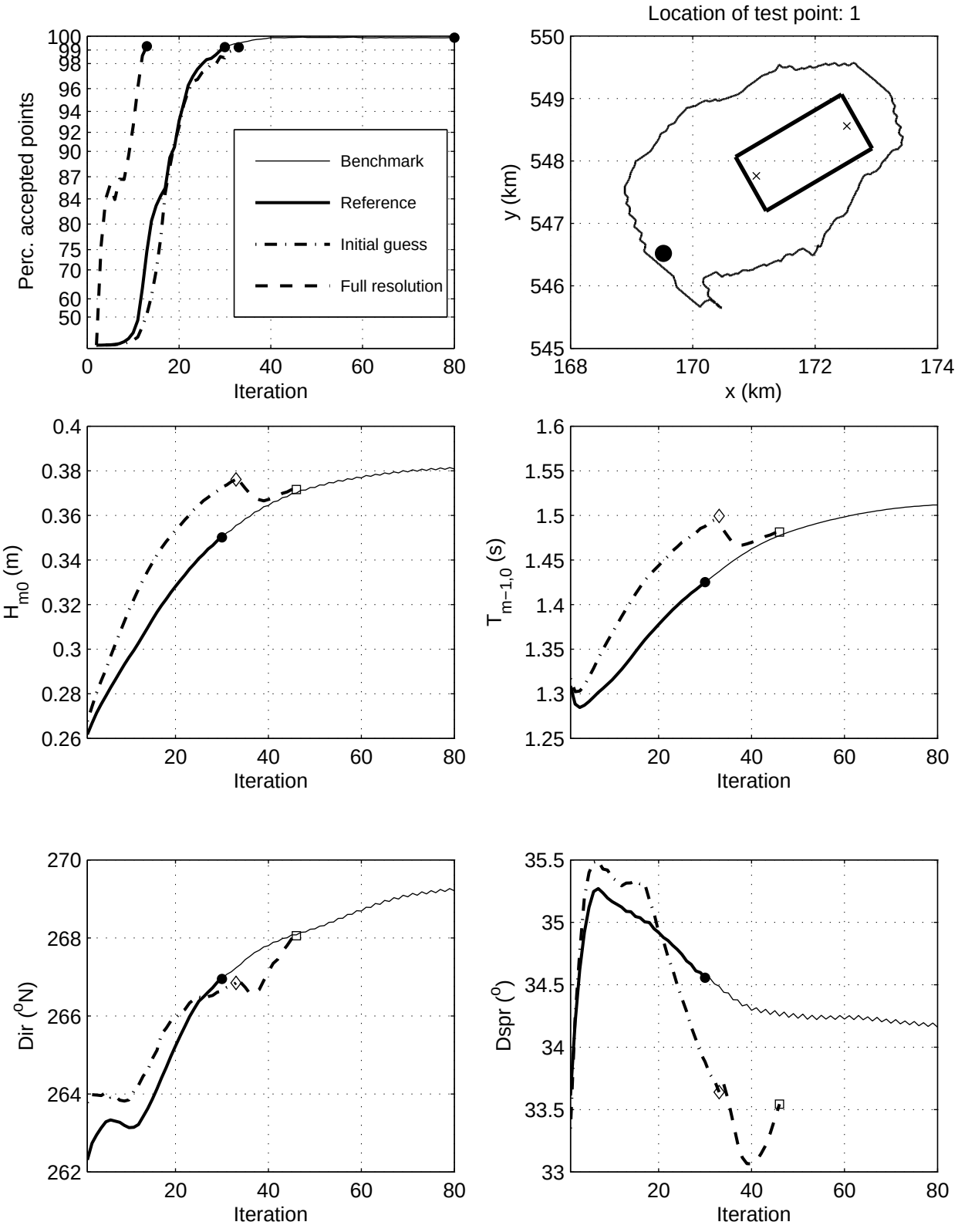

Convergence behaviour of integral wave parameters in Lake Sloten Multigrid settings: Rx=1, Ry=1, Rθ=2, Rσ=2 (x1y1d2s2). Test point:1 Case: SLE 2002/10/27 15:00		SWAN 40.51A
		Numerical efficiency SWAN
DELTARES & ALKYON	H5107.46/A2114	Fig. 4.18

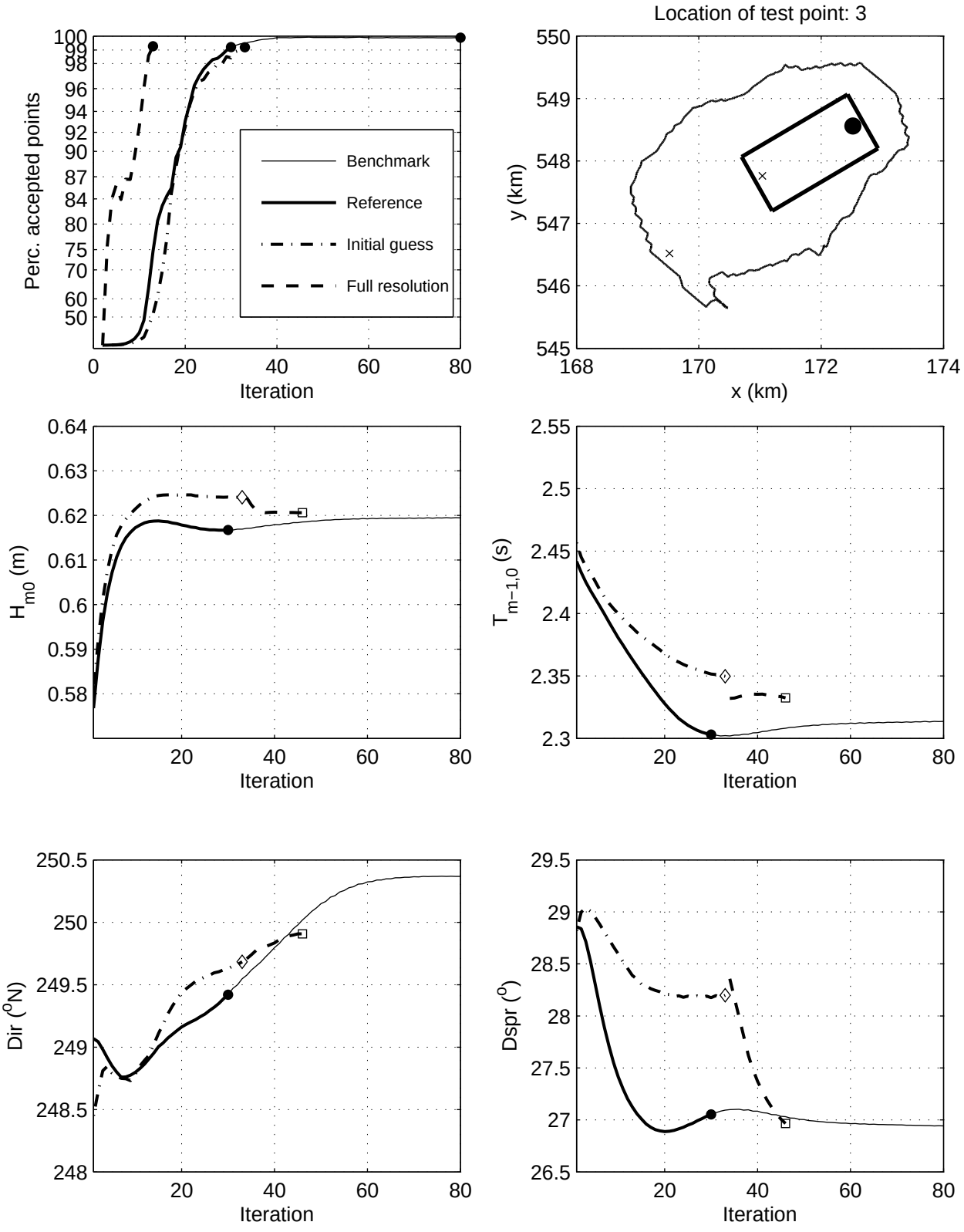

Convergence behaviour of integral wave parameters in Lake Sloten Multigrid settings: Rx=1, Ry=1, Rθ=2, Rσ=2 (x1y1d2s2). Test point:3 Case: SLE 2002/10/27 15:00		SWAN 40.51A
		Numerical efficiency SWAN
DELTARES & ALKYON	H5107.46/A2114	Fig. 4.19

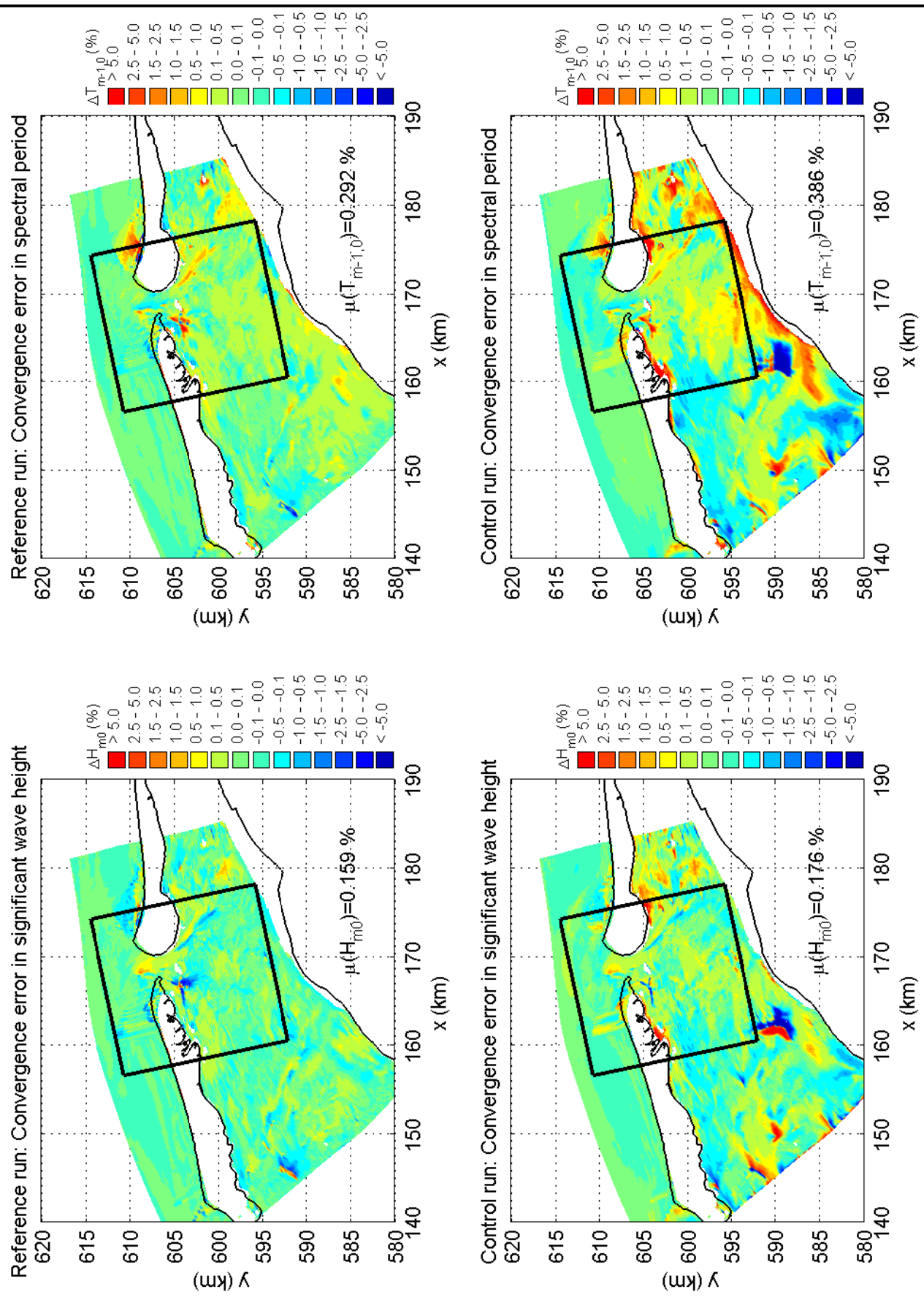

Convergence errors of reference and control run in the Amelander Zeegat for wave height and wave period. Case: AZG3A 2005/1/2 10:00 Multi grid settings: Rx=2, Ry=2, Rθ=1, Rσ=1 (x2y2d1s1)		SWAN 40.51A
		Numerical efficiency SWAN
DELTARES & ALKYON	H5107.46/A2114	Fig. 4.20

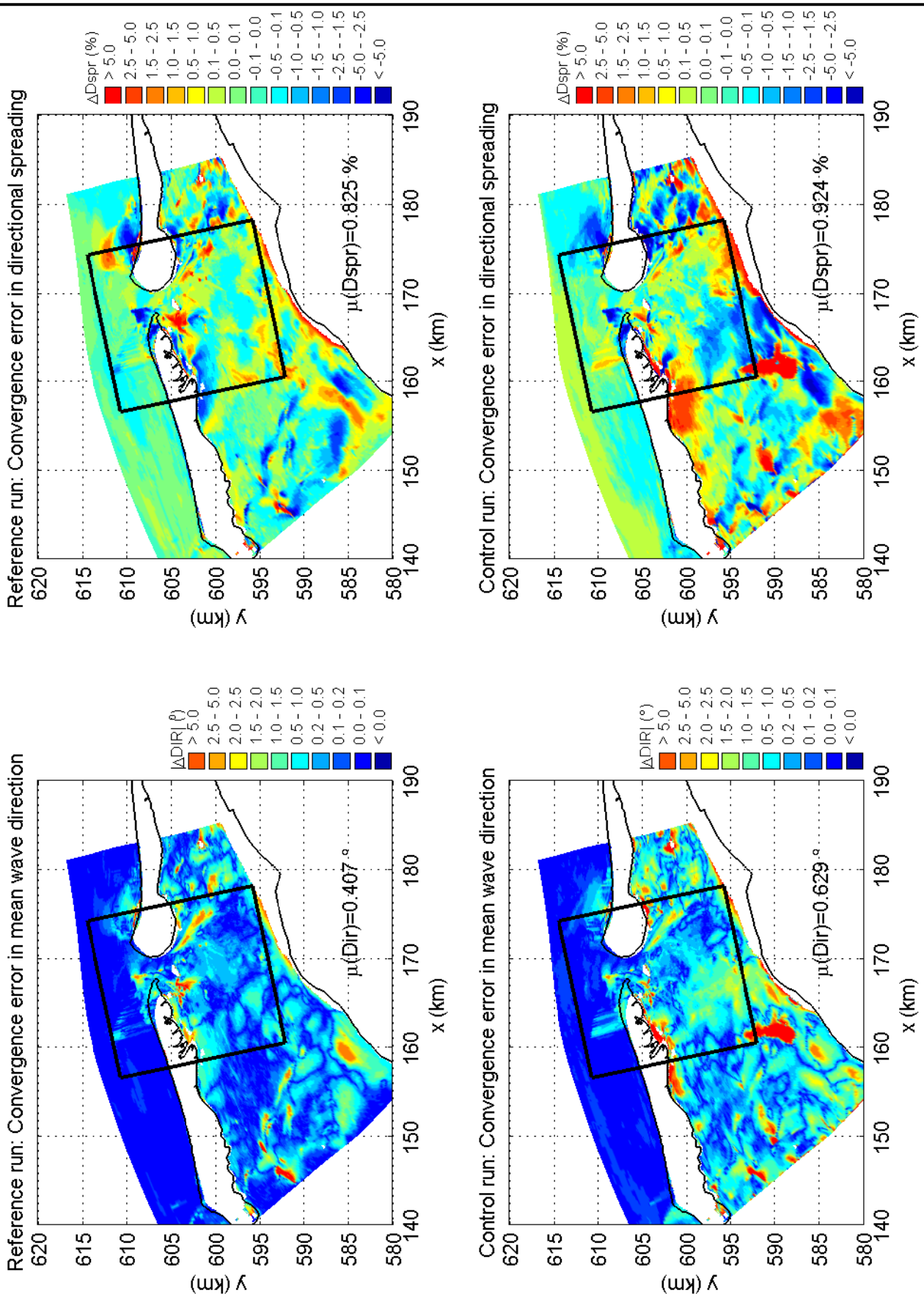

Convergence errors of reference and controle run in the Amelander Zeegat for mean direction and spreading. Case: AZG3A 2005/1/2 10:00 Multi grid settings: Rx=2, Ry=2, Rθ=1, Rσ=1 (x2y2d1s1)		SWAN 40.51A
	Numerical efficiency SWAN	
DELTARES & ALKYON	H5107.46/A2114	Fig. 4.21

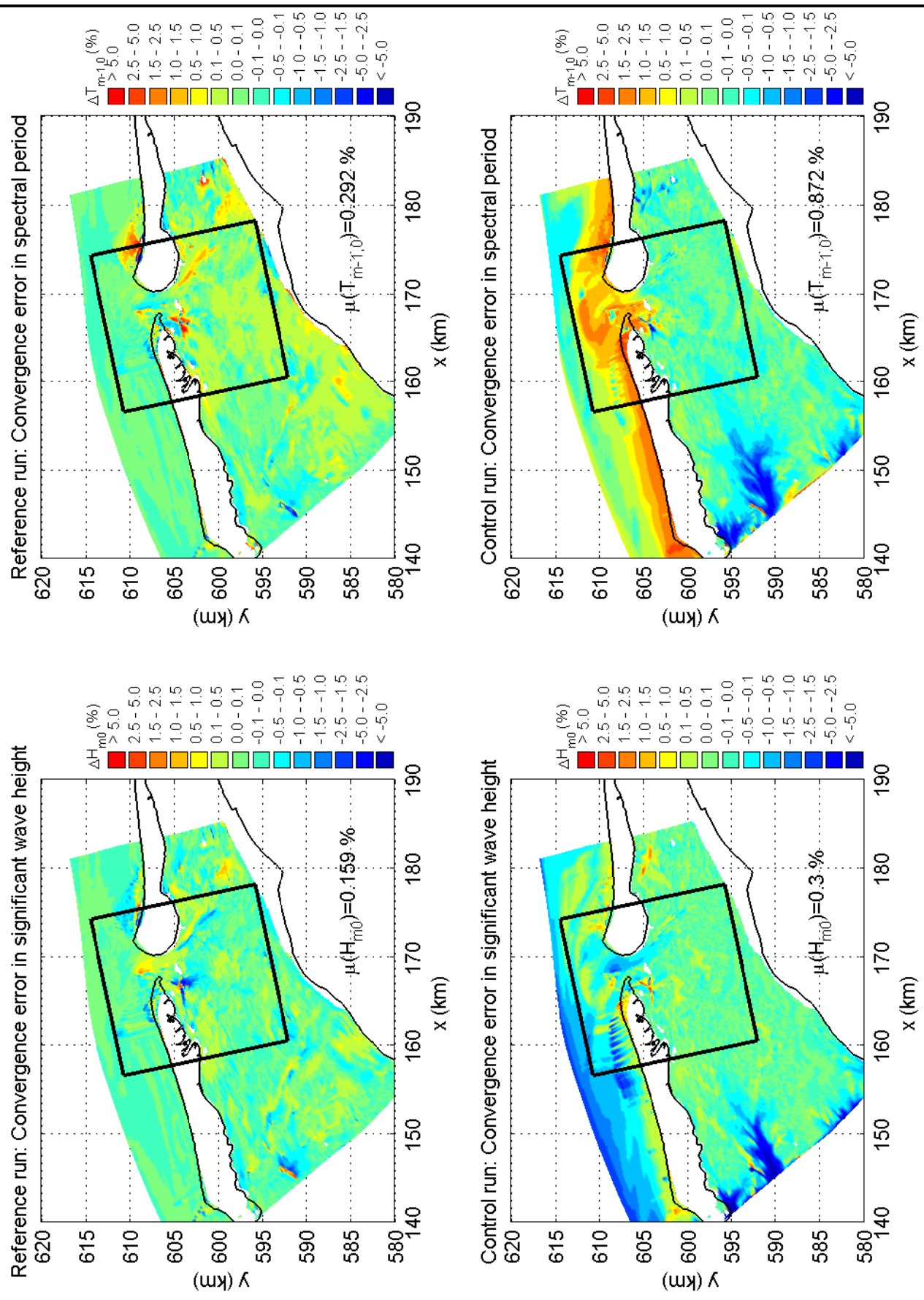

Convergence errors of reference and control run in the Amelander Zeegat for wave height and wave period. Case: AZG3A 2005/1/2 10:00 Multi grid settings: Rx=1, Ry=1, Rθ=2, Rσ=2 (x1y1d2s2)		SWAN 40.51A
		Numerical efficiency SWAN
DELTARES & ALKYON	H5107.46/A2114	Fig. 4.22

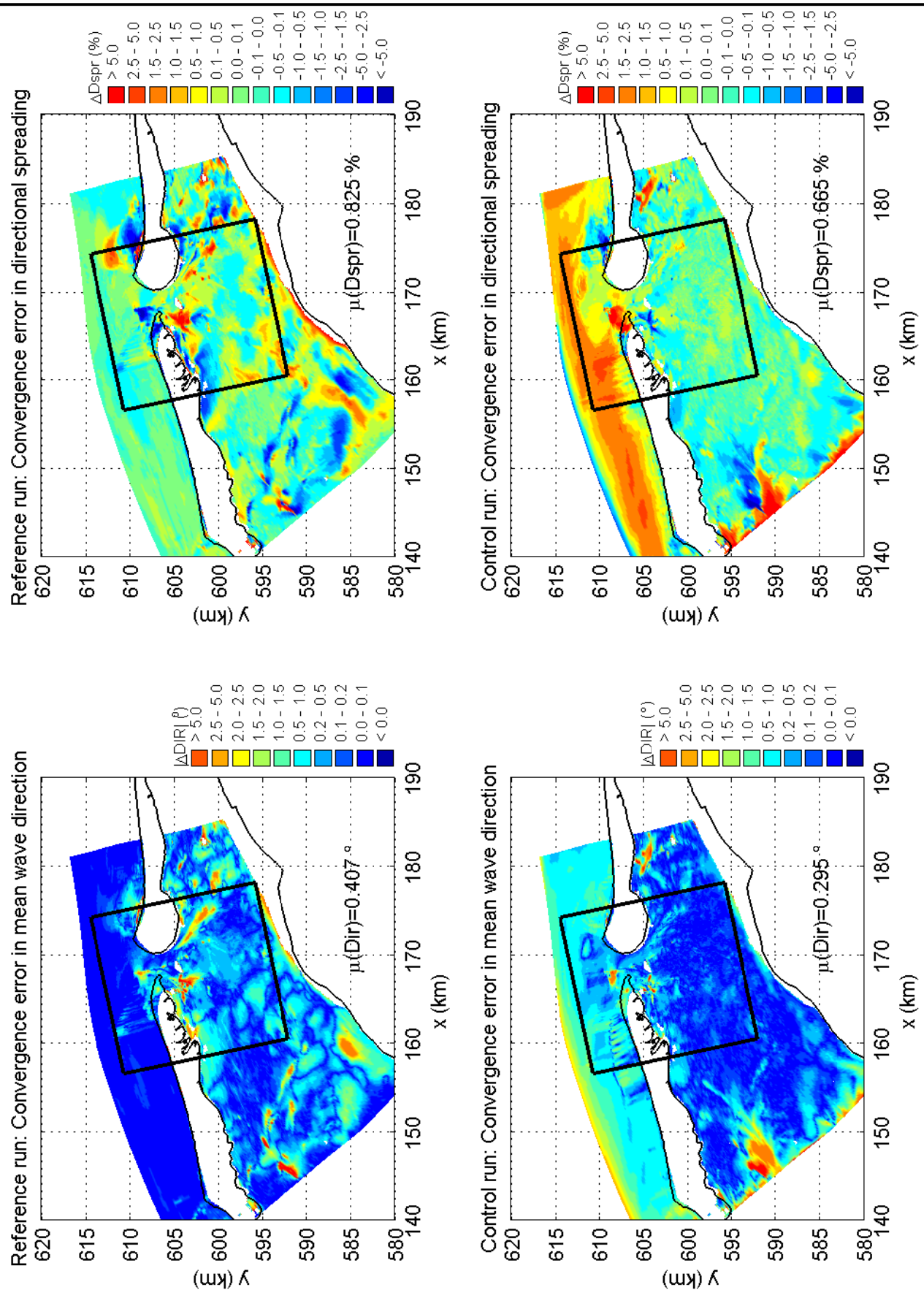

Convergence errors of reference and controle run in the Amelander Zeegat for mean direction and spreading. Case: AZG3A 2005/1/2 10:00 Multi grid settings: Rx=1, Ry=1, Rθ=2, Rσ=2 (x1y1d2s2)		SWAN 40.51A
		Numerical efficiency SWAN
DELTARES & ALKYON	H5107.46/A2114	Fig. 4.23

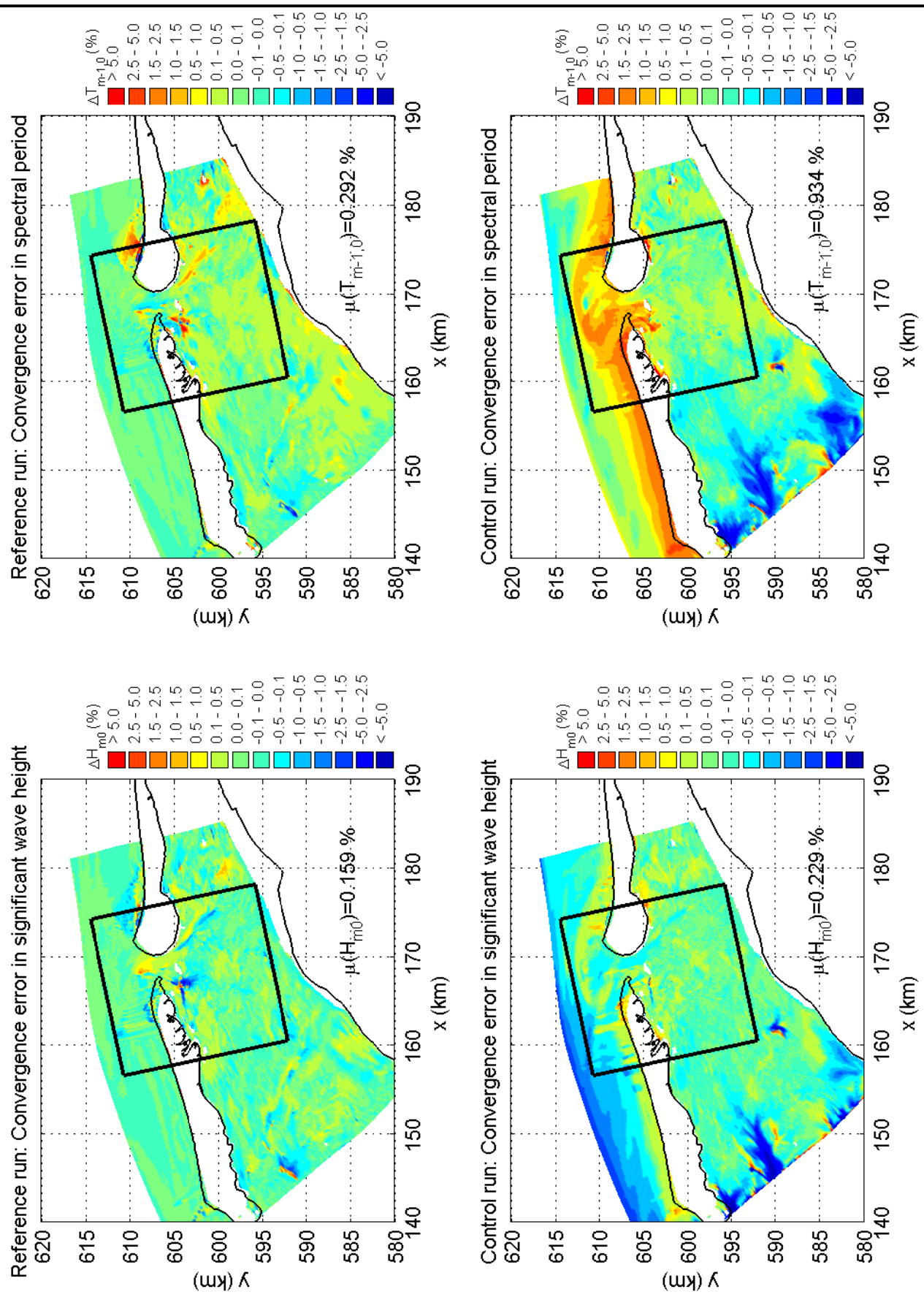

Convergence errors of reference and control run in the Amelander Zeegat for wave height and wave period. Case: AZG3A 2005/1/2 10:00 Multi grid settings: Rx=2, Ry=2, Rθ=2, Rσ=2 (x2y2d2s2)		SWAN 40.51A
		Numerical efficiency SWAN
DELTARES & ALKYON	H5107.46/A2114	Fig. 4.24

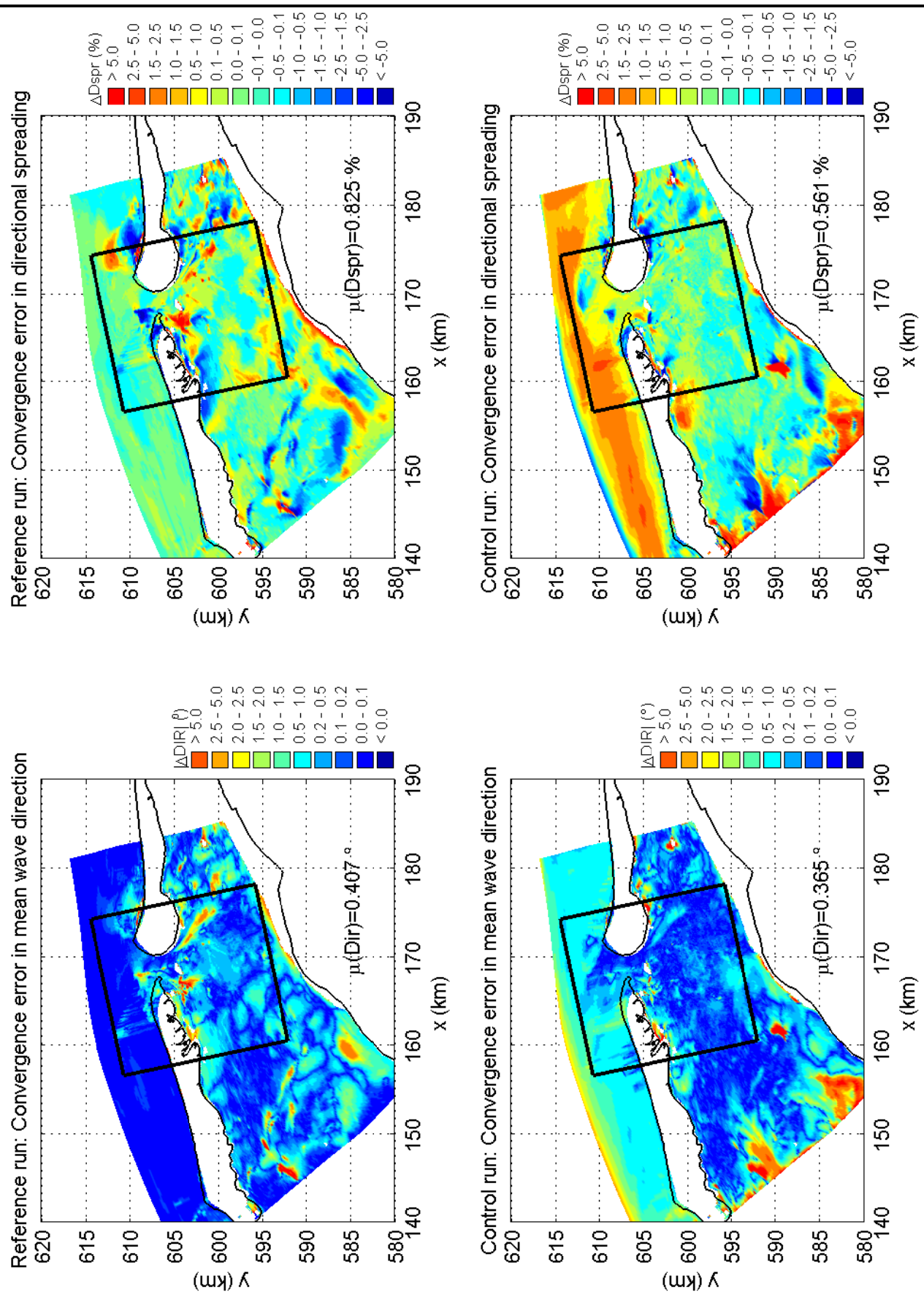

Convergence errors of reference and controle run in the Amelander Zeegat for mean direction and spreading. Case: AZG3A 2005/1/2 10:00 Multi grid settings: Rx=2, Ry=2, Rθ=2, Rσ=2 (x2y2d2s2)		SWAN 40.51A
	Numerical efficiency SWAN	
DELTARES & ALKYON	H5107.46/A2114	Fig. 4.25

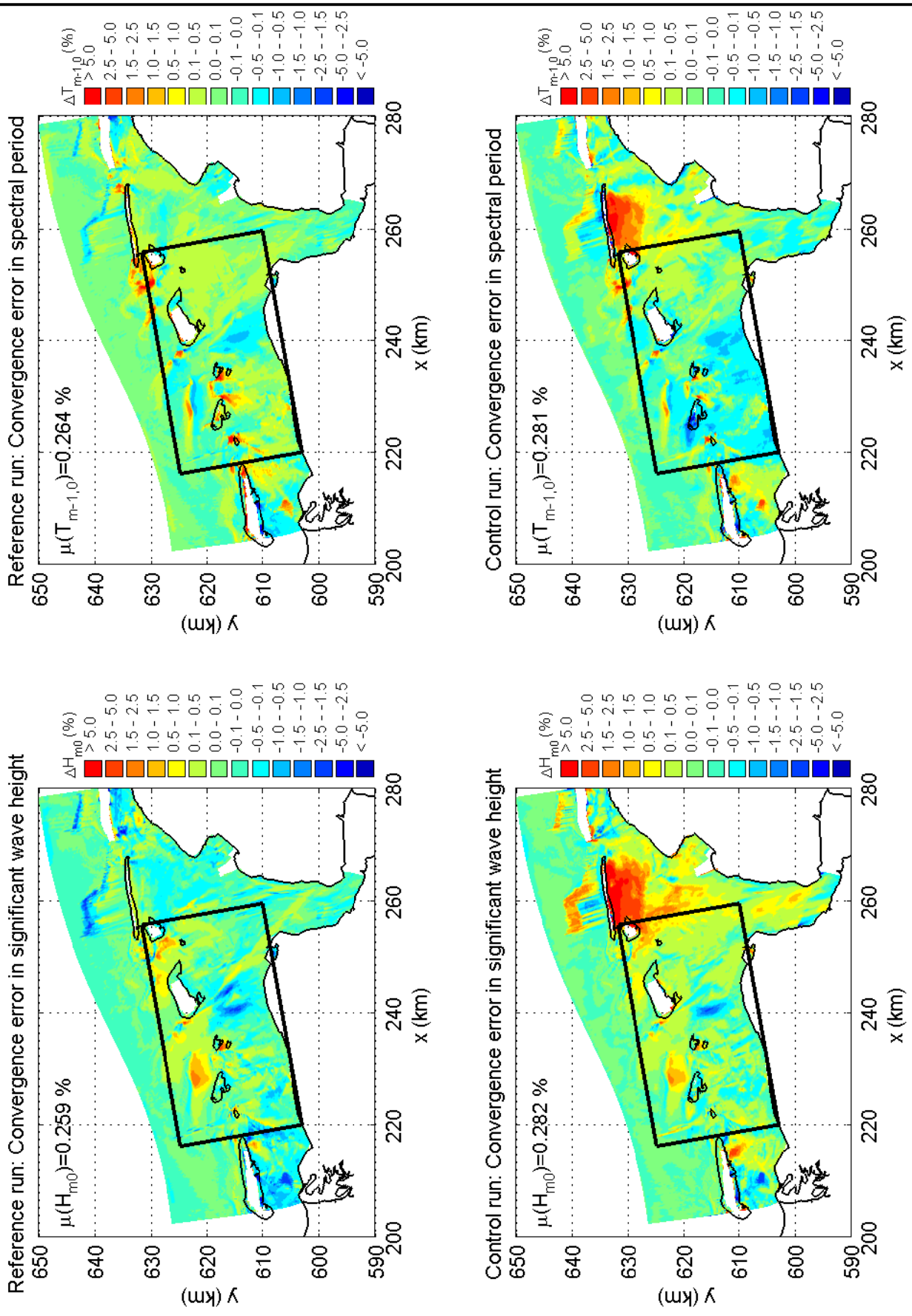

Convergence errors of reference and control run in the Eems-Dollard for wave height and wave period. Case: EEMS3A 2006/11/1 06:30 Multi grid settings: Rx=2, Ry=2, Rθ=1, Rσ=1 (x2y2d1s1)		SWAN 40.51A
		Numerical efficiency SWAN
DELTARES & ALKYON	H5107.46/A2114	Fig. 4.26

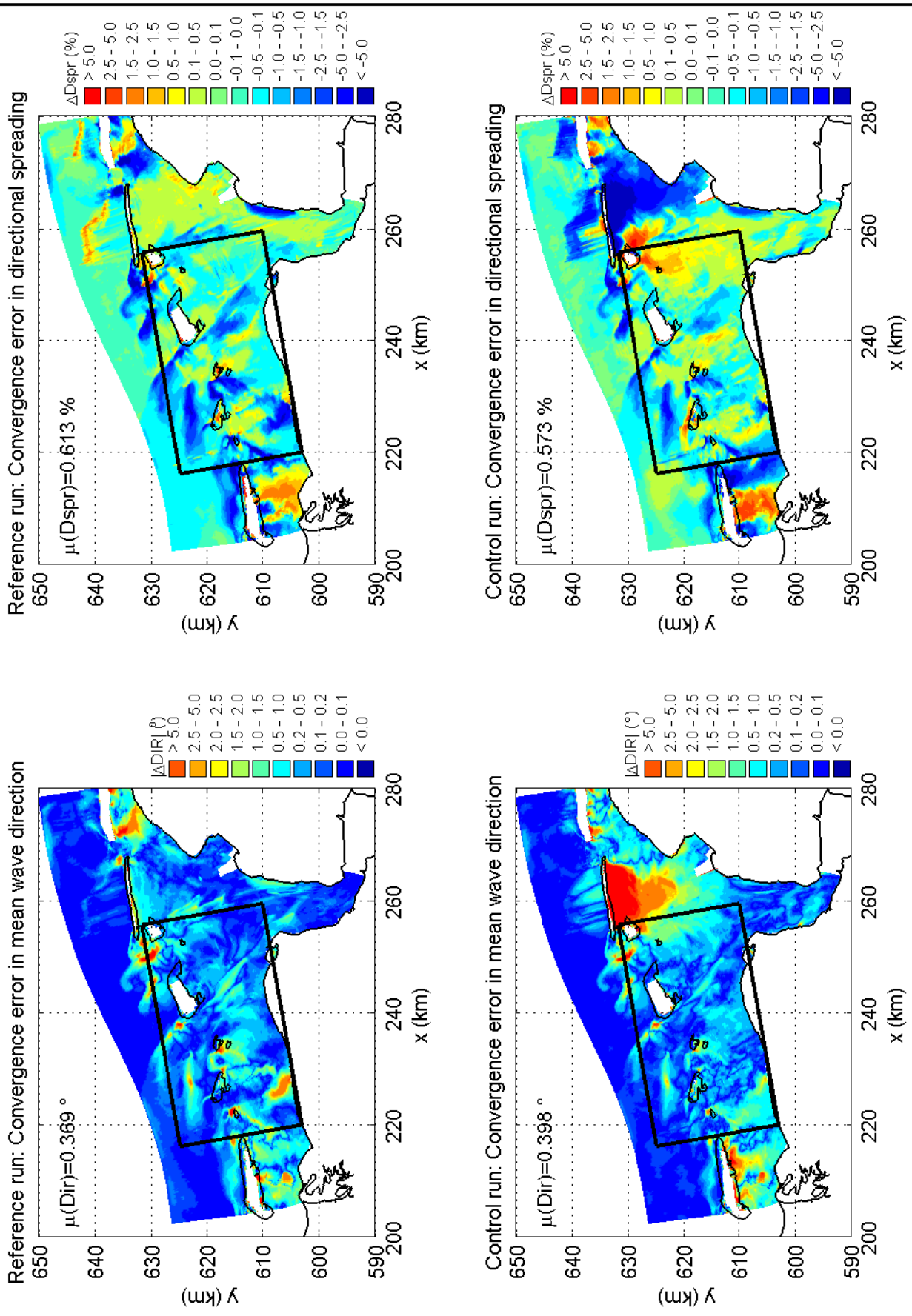

Convergence errors of reference and controle run in the Eems-Dollard for mean direction and spreading. Case: EEMS3A 2006/11/1 06:30 Multi grid settings: Rx=2, Ry=2, Rθ=1, Rσ=1 (x2y2d1s1)		SWAN 40.51A
	Numerical efficiency SWAN	
DELTARES & ALKYON	H5107.46/A2114	Fig. 4.27

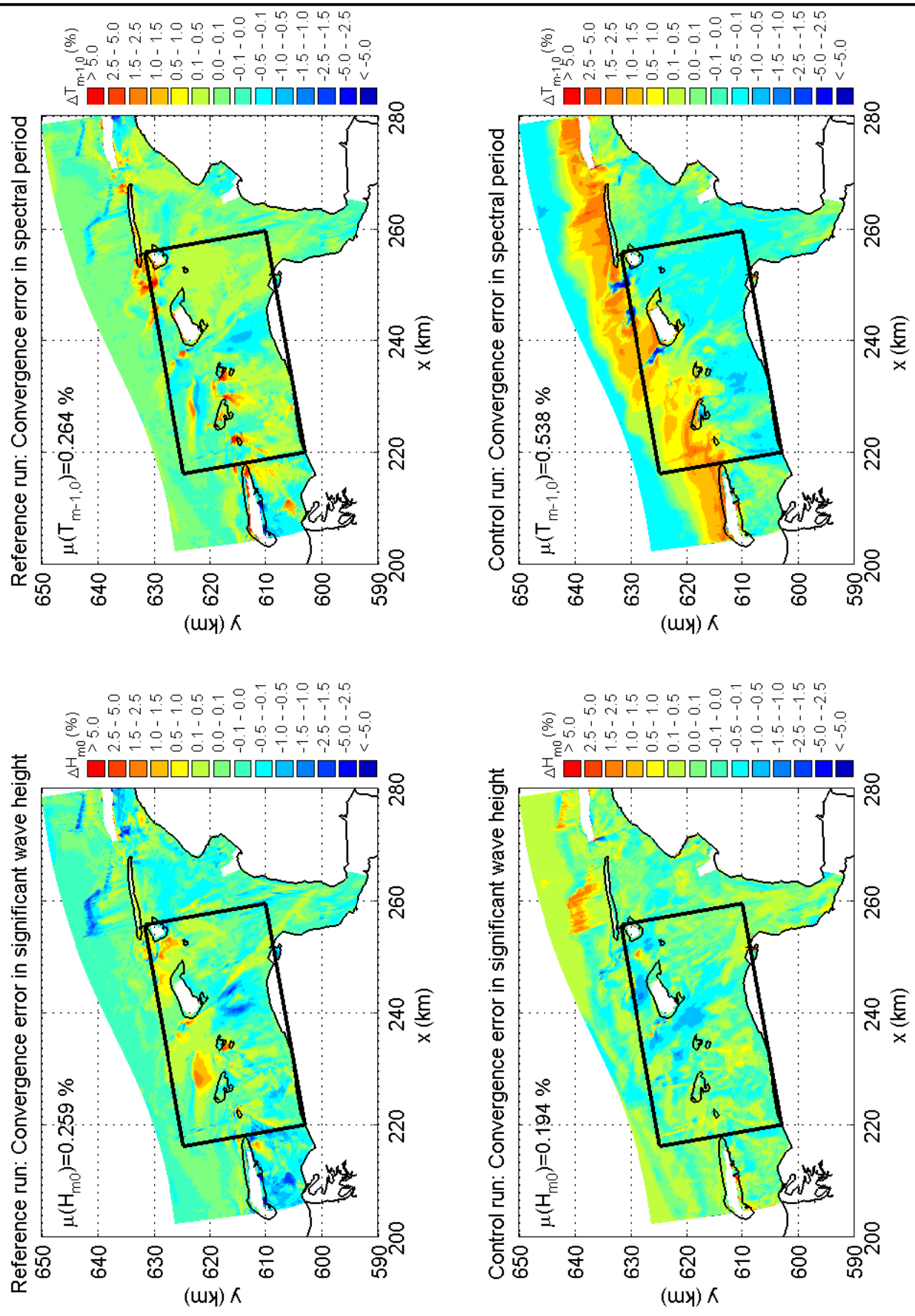

Convergence errors of reference and control run in the Eems-Dollard for wave height and wave period. Case: EEMS3A 2006/11/1 06:30 Multi grid settings: Rx=1, Ry=1, Rθ=2, Rσ=2 (x1y1d2s2)		SWAN 40.51A
		Numerical efficiency SWAN
DELTARES & ALKYON	H5107.46/A2114	Fig. 4.28

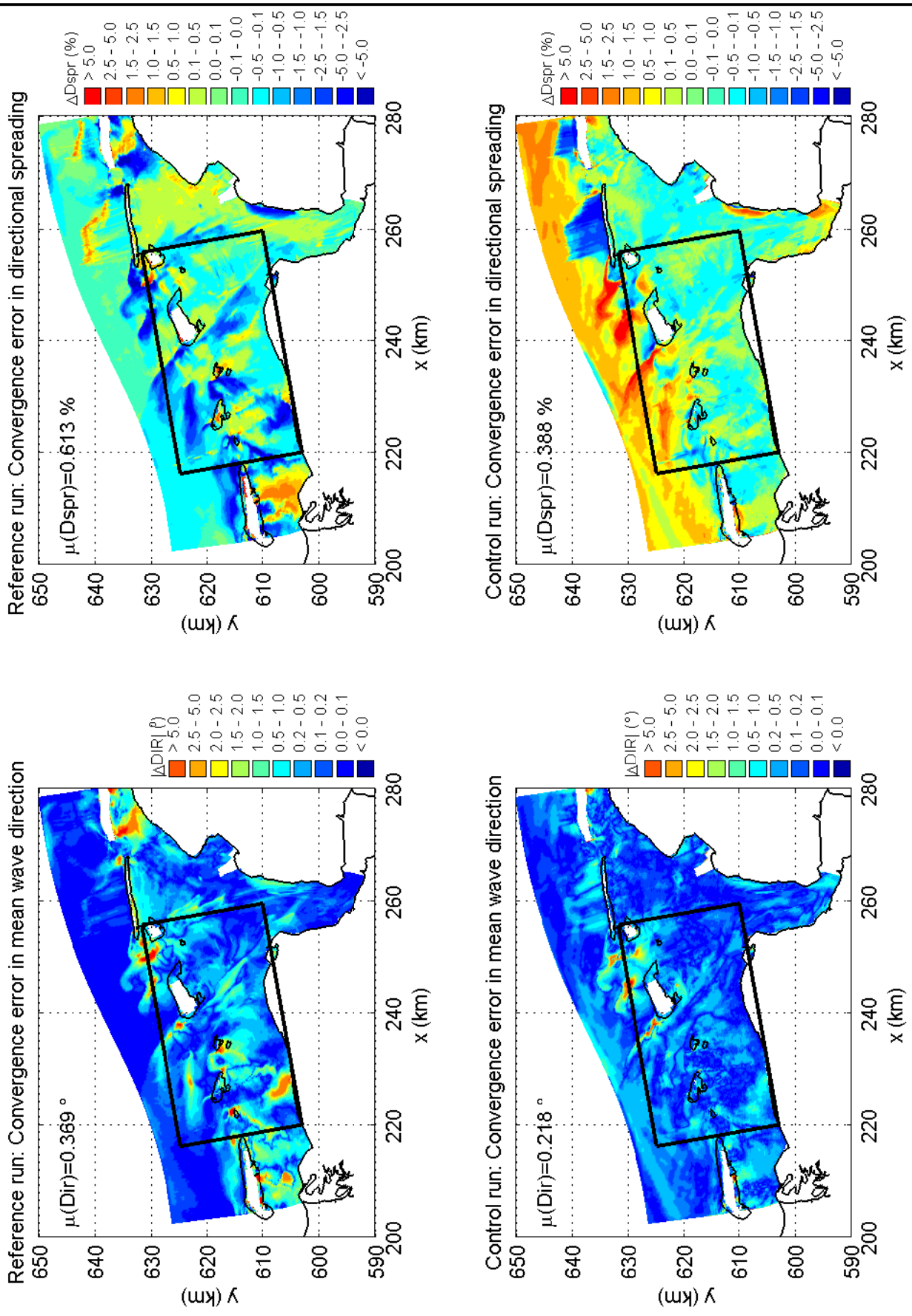

Convergence errors of reference and controle run in the Eems-Dollard for mean direction and spreading. Case: EEMS3A 2006/11/1 06:30 Multi grid settings: Rx=1, Ry=1, Rθ=2, Rσ=2 (x1y1d2s2)		SWAN 40.51A
	Numerical efficiency SWAN	
DELTARES & ALKYON	H5107.46/A2114	Fig. 4.29

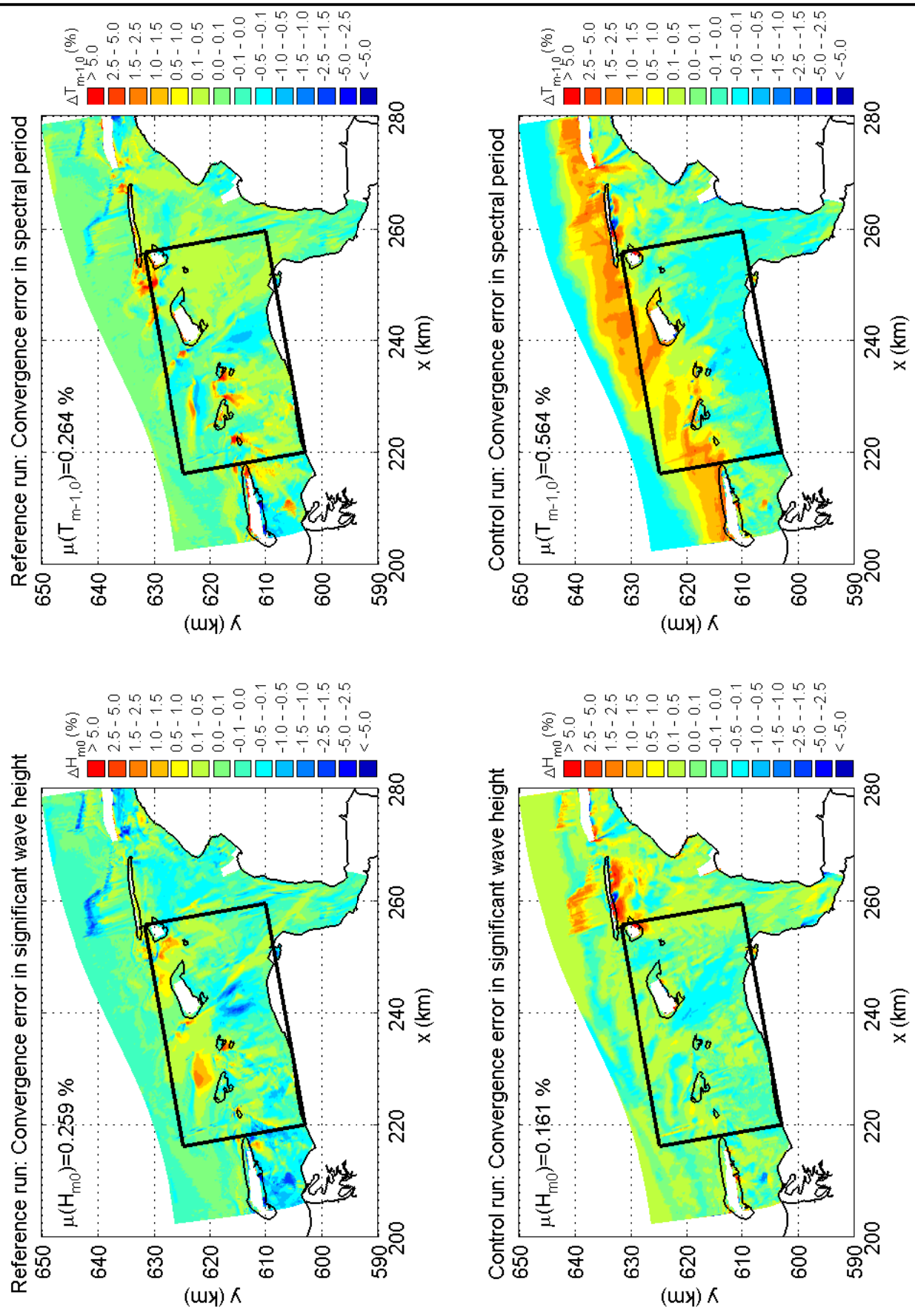

Convergence errors of reference and control run in the Eems-Dollard for wave height and wave period. Case: EEMS3A 2006/11/1 06:30 Multi grid settings: Rx=2, Ry=2, Rθ=2, Rσ=2 (x2y2d2s2)		SWAN 40.51A
		Numerical efficiency SWAN
DELTARES & ALKYON	H5107.46/A2114	Fig. 4.30

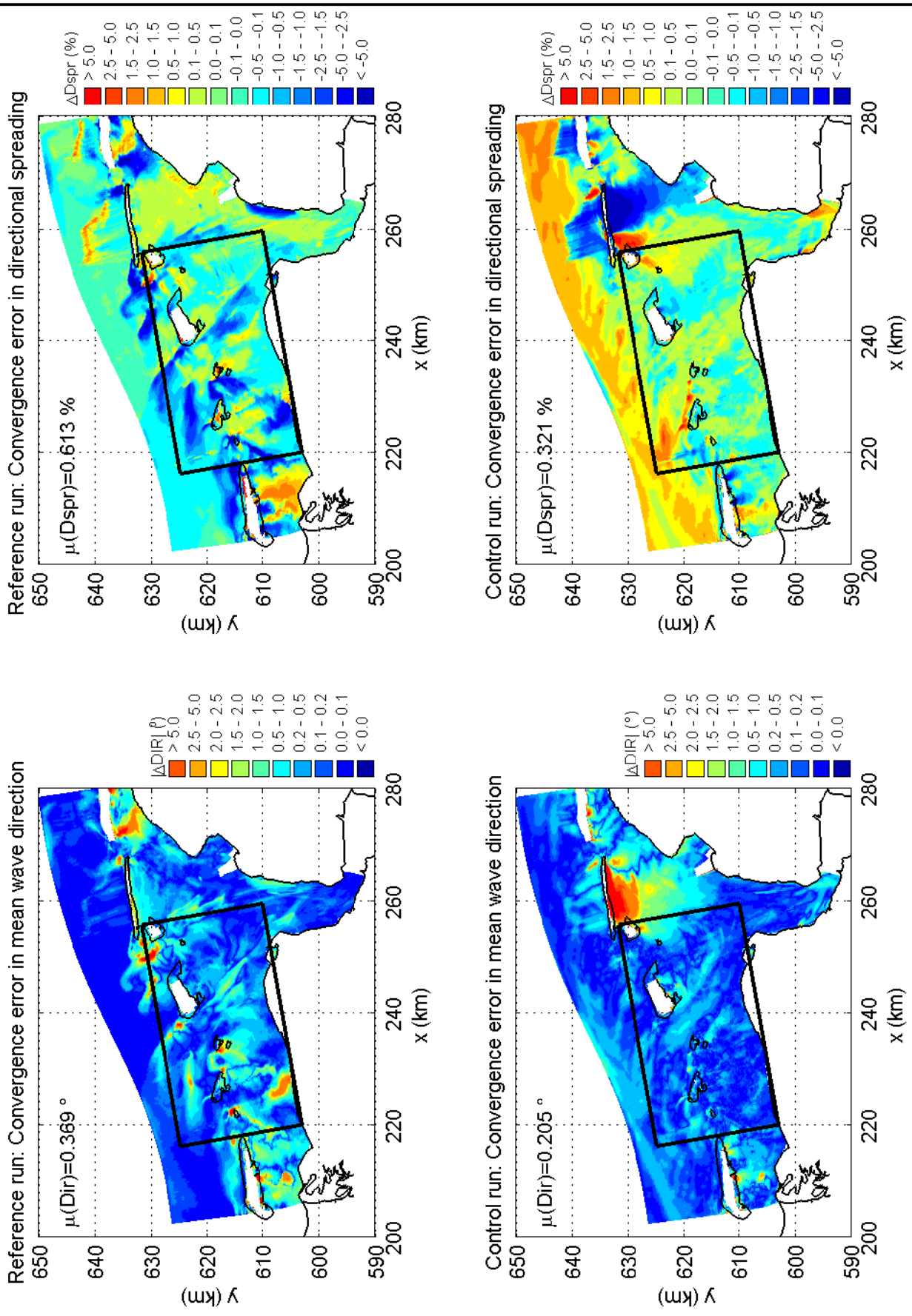

Convergence errors of reference and controle run in the Eems-Dollard for mean direction and spreading. Case: EEMS3A 2006/11/1 06:30 Multi grid settings: Rx=2, Ry=2, Rθ=2, Rσ=2 (x2y2d2s2)		SWAN 40.51A
	Numerical efficiency SWAN	
DELTARES & ALKYON	H5107.46/A2114	Fig. 4.31

Reference run: Convergence error in significant wave height

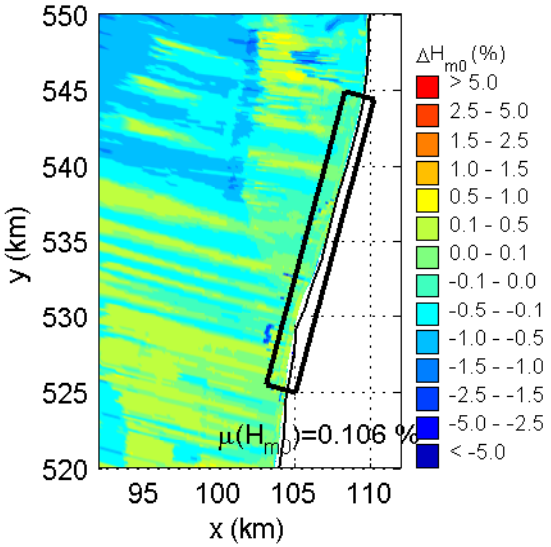

Reference run: Convergence error in spectral period

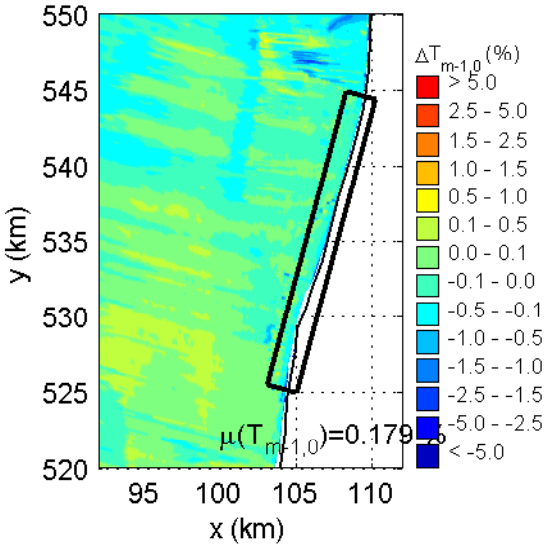

Control run: Convergence error in significant wave height

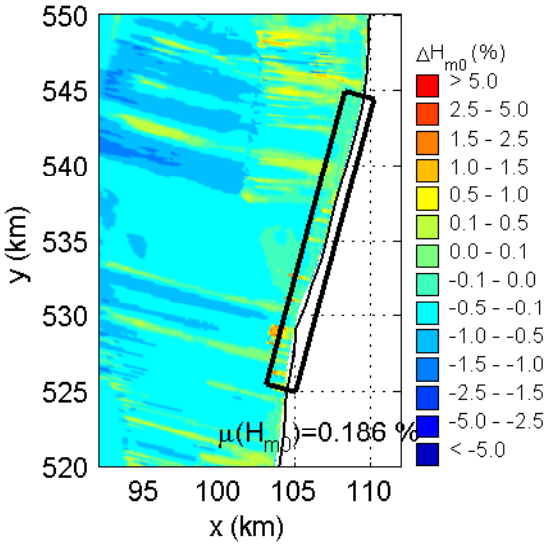

Control run: Convergence error in spectral period

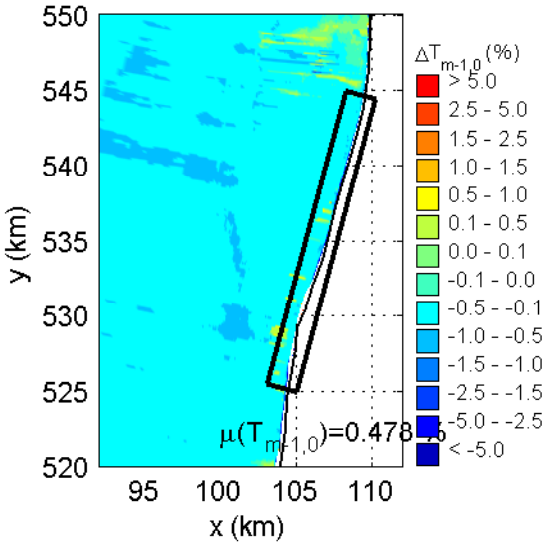

Convergence errors of reference and control run near Petten for wave height and wave period. Case: PETTEN 1995/1/1 10:00 Multi grid settings: Rx=2, Ry=2, Rθ=1, Rσ=1 (x2y2d1s1)

DELTARES & ALKYON

SWAN 40.51A

Numerical efficiency SWAN

H5107.46/A2114

Fig. 4.32

Reference run: Convergence error in mean wave direction

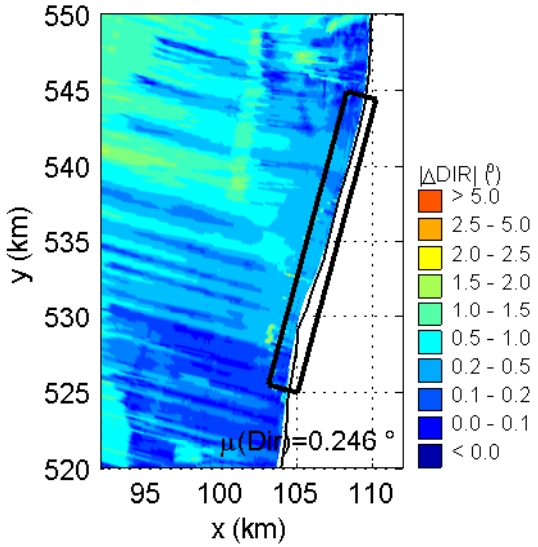

Reference run: Convergence error in directional spreading

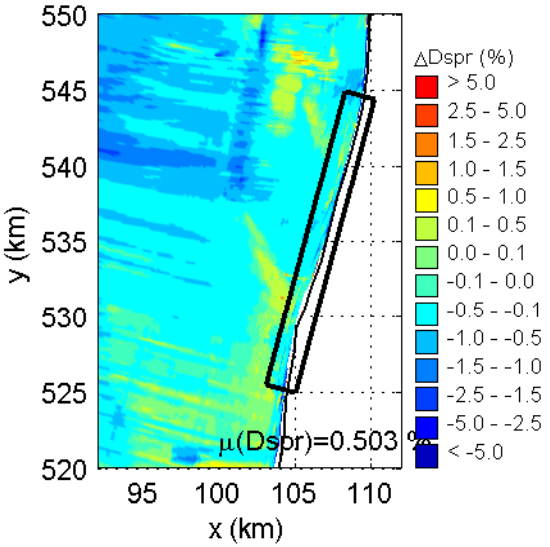

Control run: Convergence error in mean wave direction

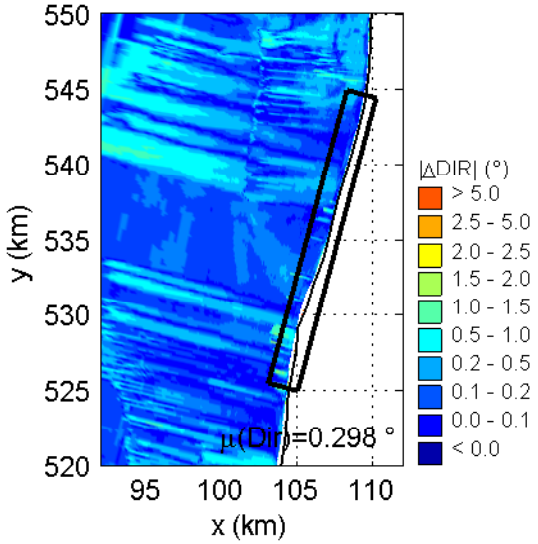

Control run: Convergence error in directional spreading

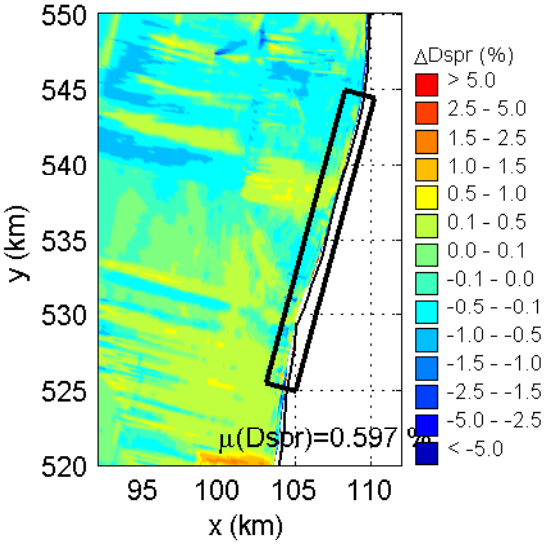

Convergence errors of reference and controle run near Petten for mean direction and spreading. Case: PETTEN 1995/1/1 10:00
Multi grid settings: Rx=2, Ry=2, Rθ=1, Rσ=1 (x2y2d1s1)

DELTARES & ALKYON

SWAN 40.51A

Numerical efficiency SWAN

H5107.46/A2114

Fig. 4.33

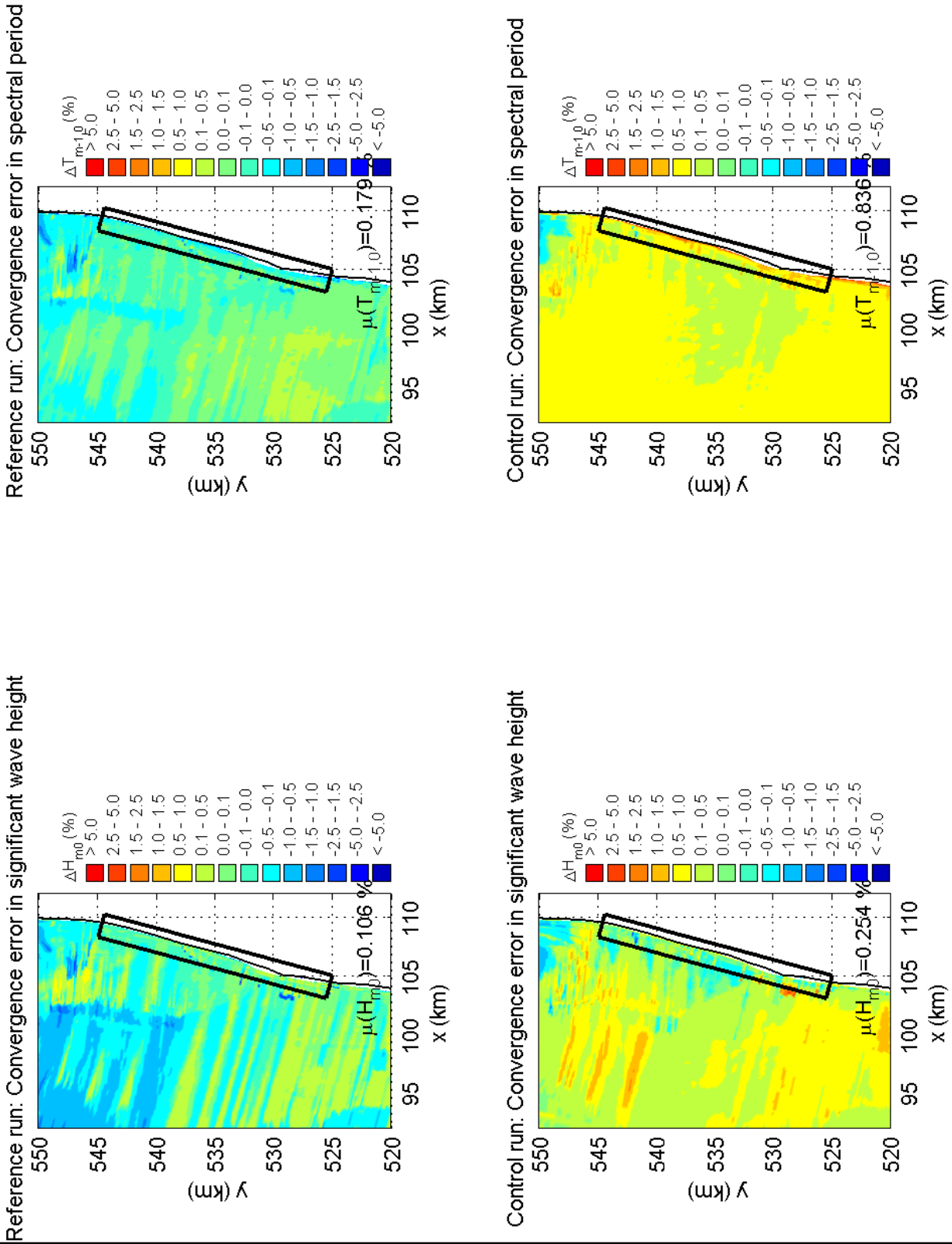

Convergence errors of reference and control run near Petten for wave height and wave period. Case: PETTEN 1995/1/1 10:00 Multi grid settings: Rx=1, Ry=1, Rθ=2, Rσ=2 (x1y1d2s2)		SWAN 40.51A
		Numerical efficiency SWAN
DELTARES & ALKYON	H5107.46/A2114	Fig. 4.34

Reference run: Convergence error in mean wave direction

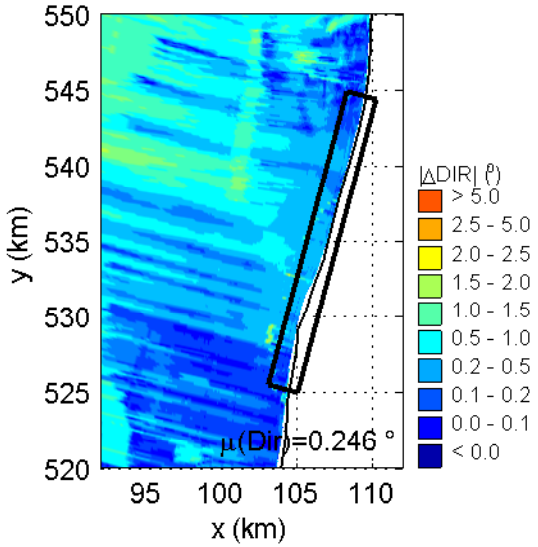

Reference run: Convergence error in directional spreading

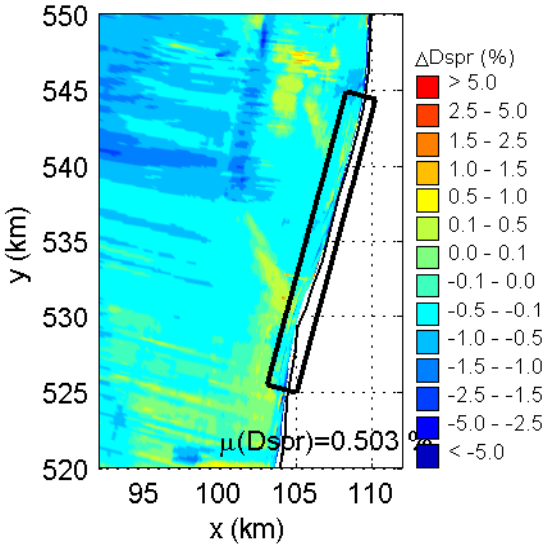

Control run: Convergence error in mean wave direction

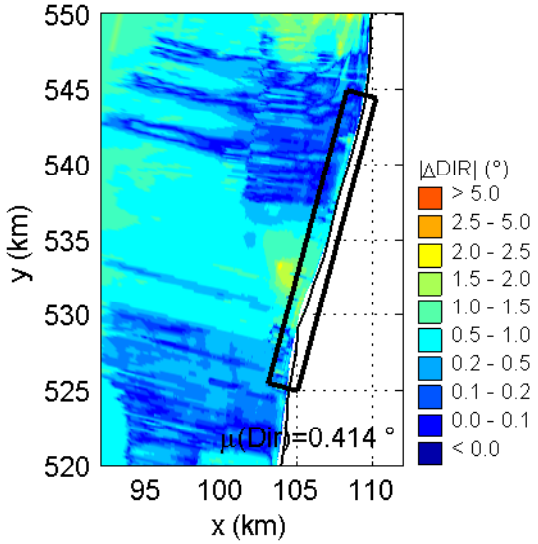

Control run: Convergence error in directional spreading

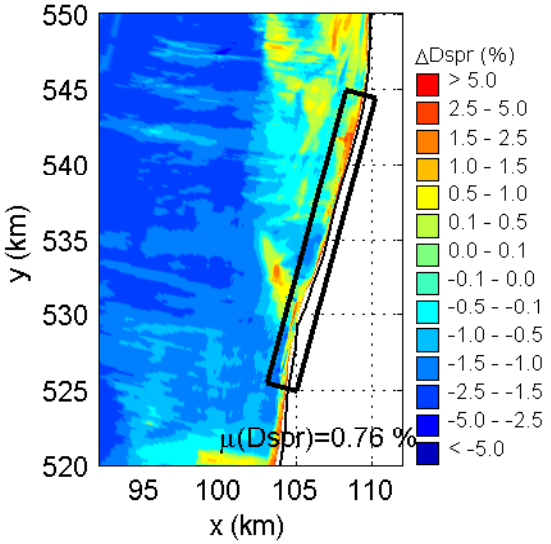

Convergence errors of reference and controle run near Petten for mean direction and spreading. Case: PETTEN 1995/1/1 10:00
Multi grid settings: Rx=1, Ry=1, Rθ=2, Rσ=2 (x1y1d2s2)

DELTARES & ALKYON

H5107.46/A2114

Numerical efficiency SWAN

SWAN 40.51A

Fig. 4.35

Reference run: Convergence error in significant wave height

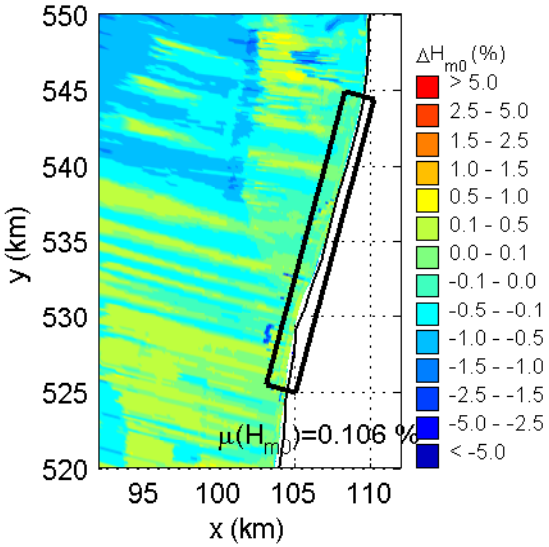

Reference run: Convergence error in spectral period

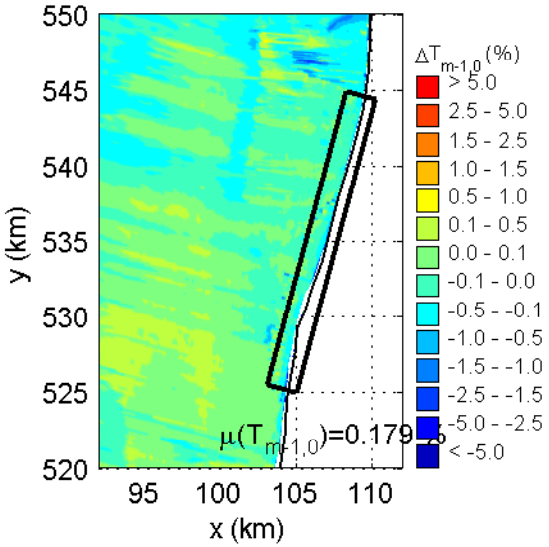

Control run: Convergence error in significant wave height

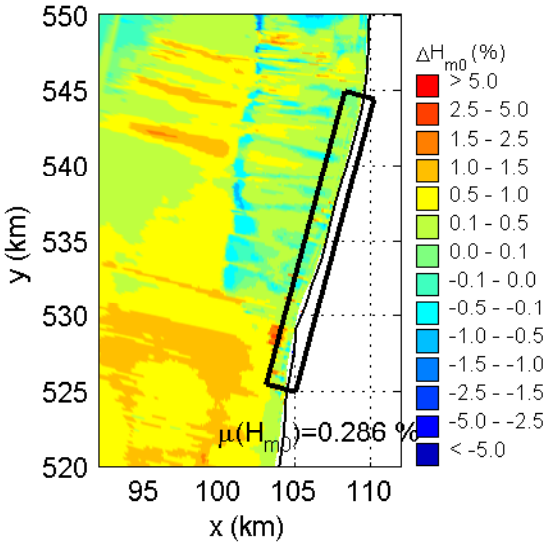

Control run: Convergence error in spectral period

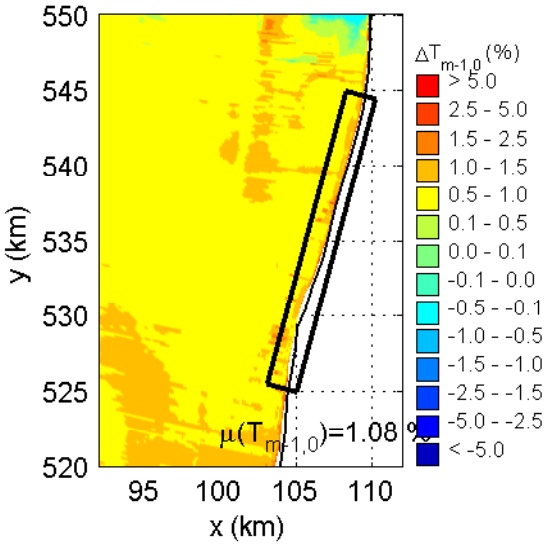

Convergence errors of reference and control run near Petten for wave height and wave period. Case: PETTEN 1995/1/1 10:00 Multi grid settings: Rx=2, Ry=2, Rθ=2, Rσ=2 (x2y2d2s2)

DELTARES & ALKYON

Numerical efficiency SWAN

SWAN 40.51A

H5107.46/A2114

Fig. 4.36

Convergence errors of reference and controle run near Petten for mean direction and spreading. Case: PETTEN 1995/1/1 10:00 Multi grid settings: Rx=2, Ry=2, Rθ=2, Rσ=2 (x2y2d2s2)		SWAN 40.51A
		Numerical efficiency SWAN
DELTARES & ALKYON	H5107.46/A2114	Fig. 4.37

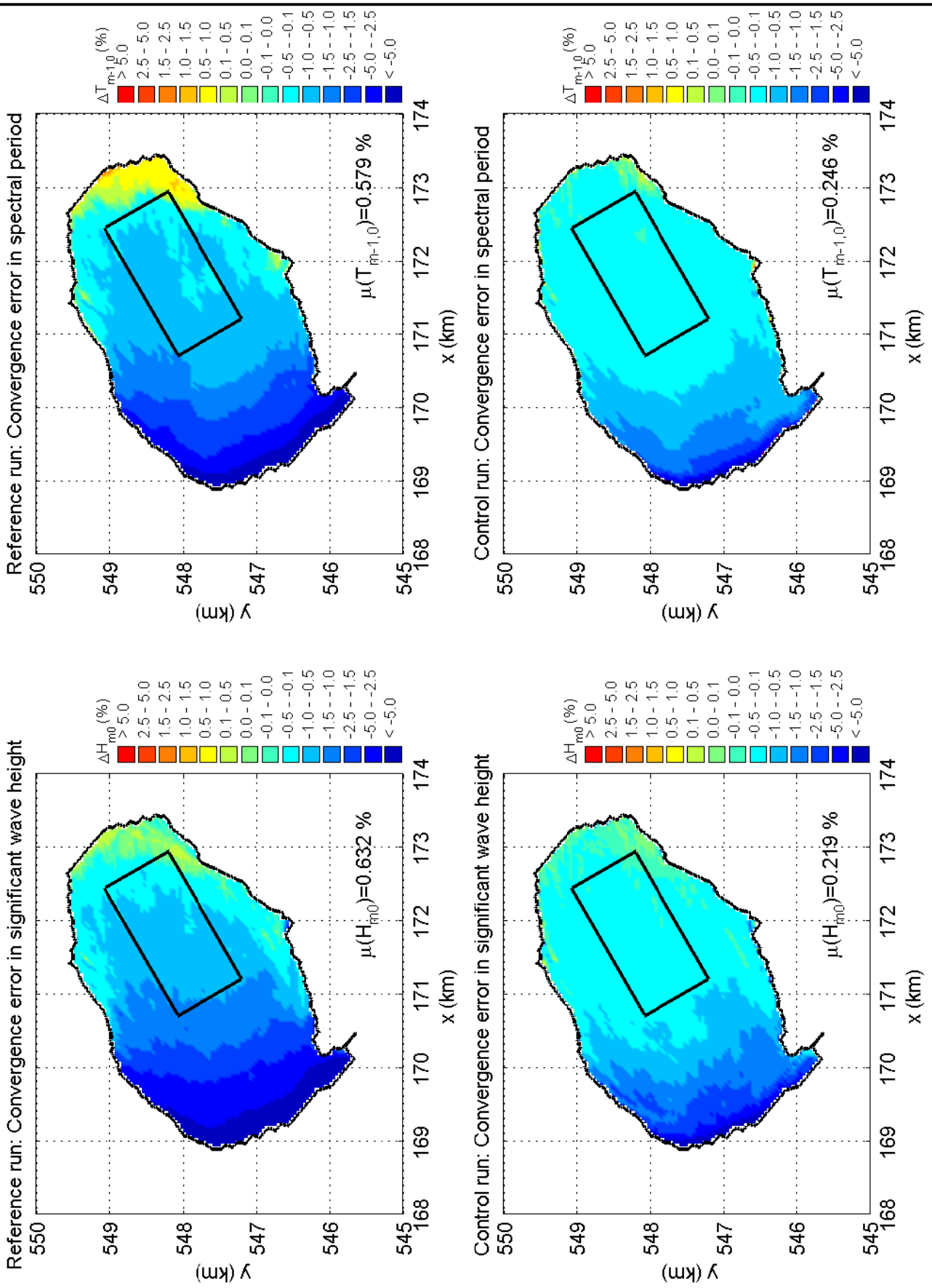

Convergence errors of reference and control run in Lake Sloten for wave height and wave period. Case: SLE 2002/10/27 15:00 Multi grid settings: Rx=2, Ry=2, Rθ=1, Rσ=1 (x2y2d1s1)		SWAN 40.51A
		Numerical efficiency SWAN
DELTARES & ALKYON	H5107.46/A2114	Fig. 4.38

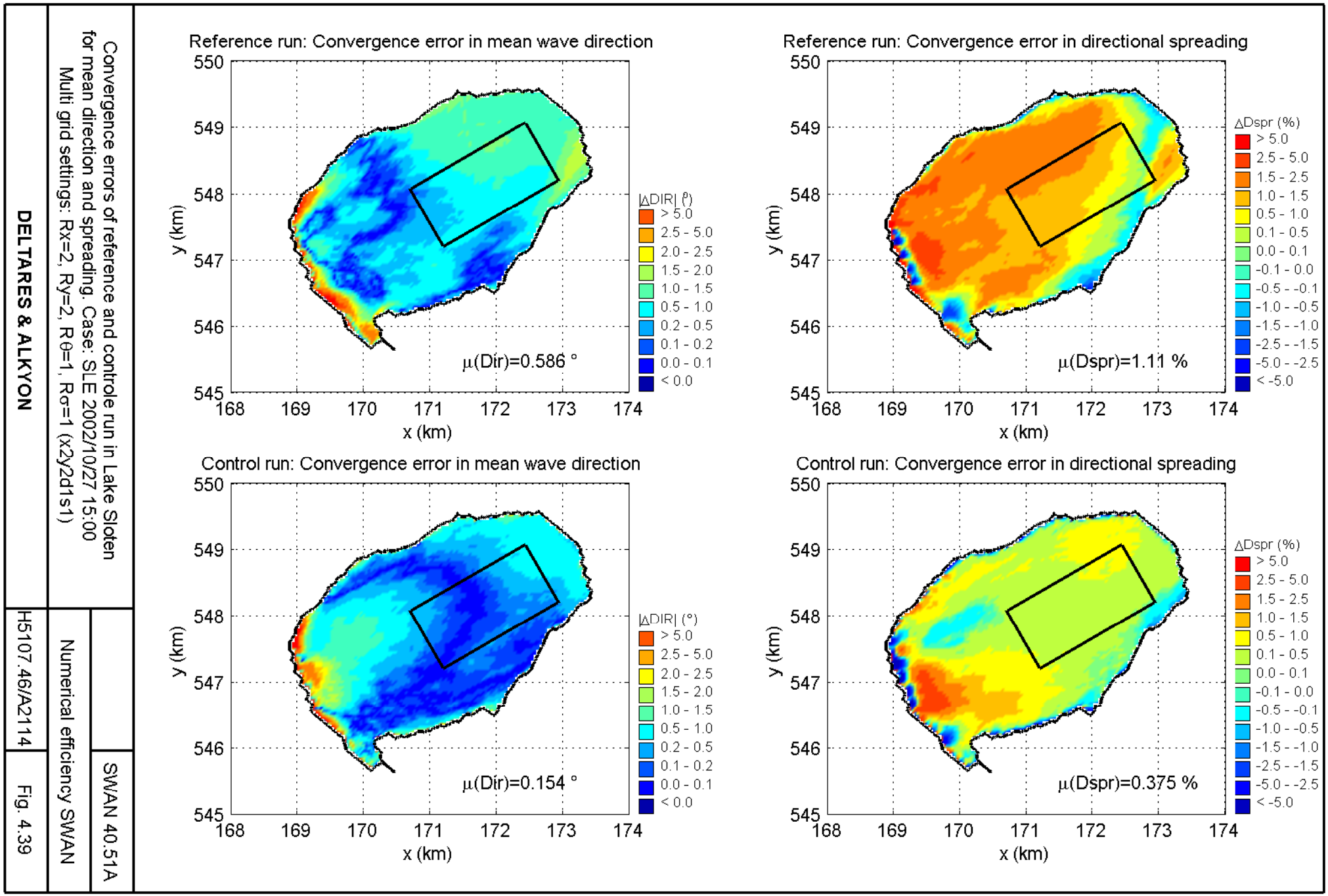

Convergence errors of reference and controle run in Lake Sloten for mean direction and spreading. Case: SLE 2002/10/27 15:00
Multi grid settings: Rx=2, Ry=2, Rθ=1, Rσ=1 (x2y2d1s1)

DELTARES & ALKYON

H5107.46/A2114

Numerical efficiency SWAN

SWAN 40.51A

Fig. 4.39

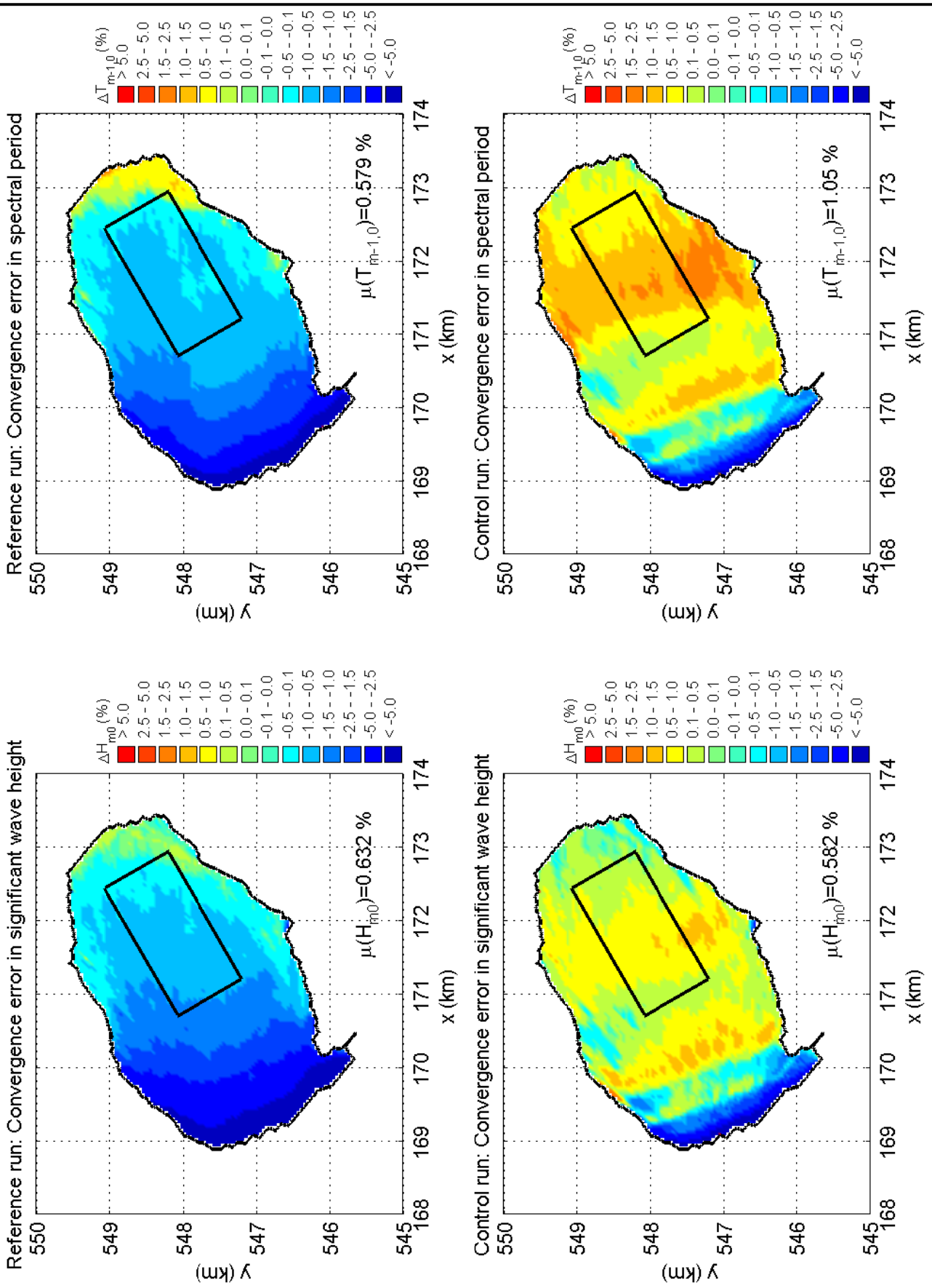

Convergence errors of reference and control run in Lake Sloten for wave height and wave period. Case: SLE 2002/10/27 15:00 Multi grid settings: Rx=1, Ry=1, Rθ=2, Rσ=2 (x1y1d2s2)		SWAN 40.51A
		Numerical efficiency SWAN
DELTARES & ALKYON	H5107.46/A2114	Fig. 4.40

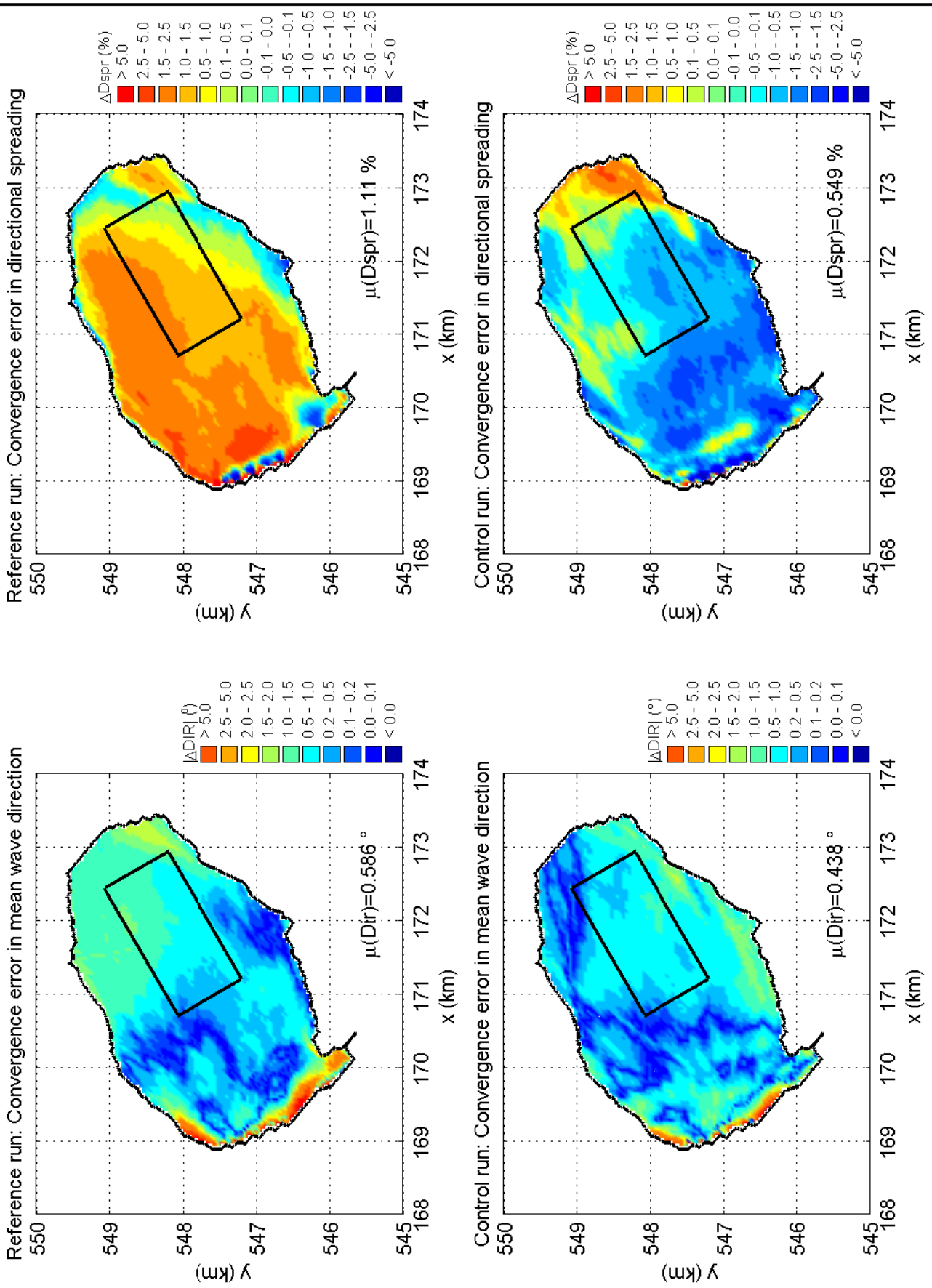

Convergence errors of reference and controle run in Lake Sloten for mean direction and spreading. Case: SLE 2002/10/27 15:00 Multi grid settings: Rx=1, Ry=1, Rθ=2, Rσ=2 (x1y1d2s2)		SWAN 40.51A
		Numerical efficiency SWAN
DELTARES & ALKYON	H5107.46/A2114	Fig. 4.41

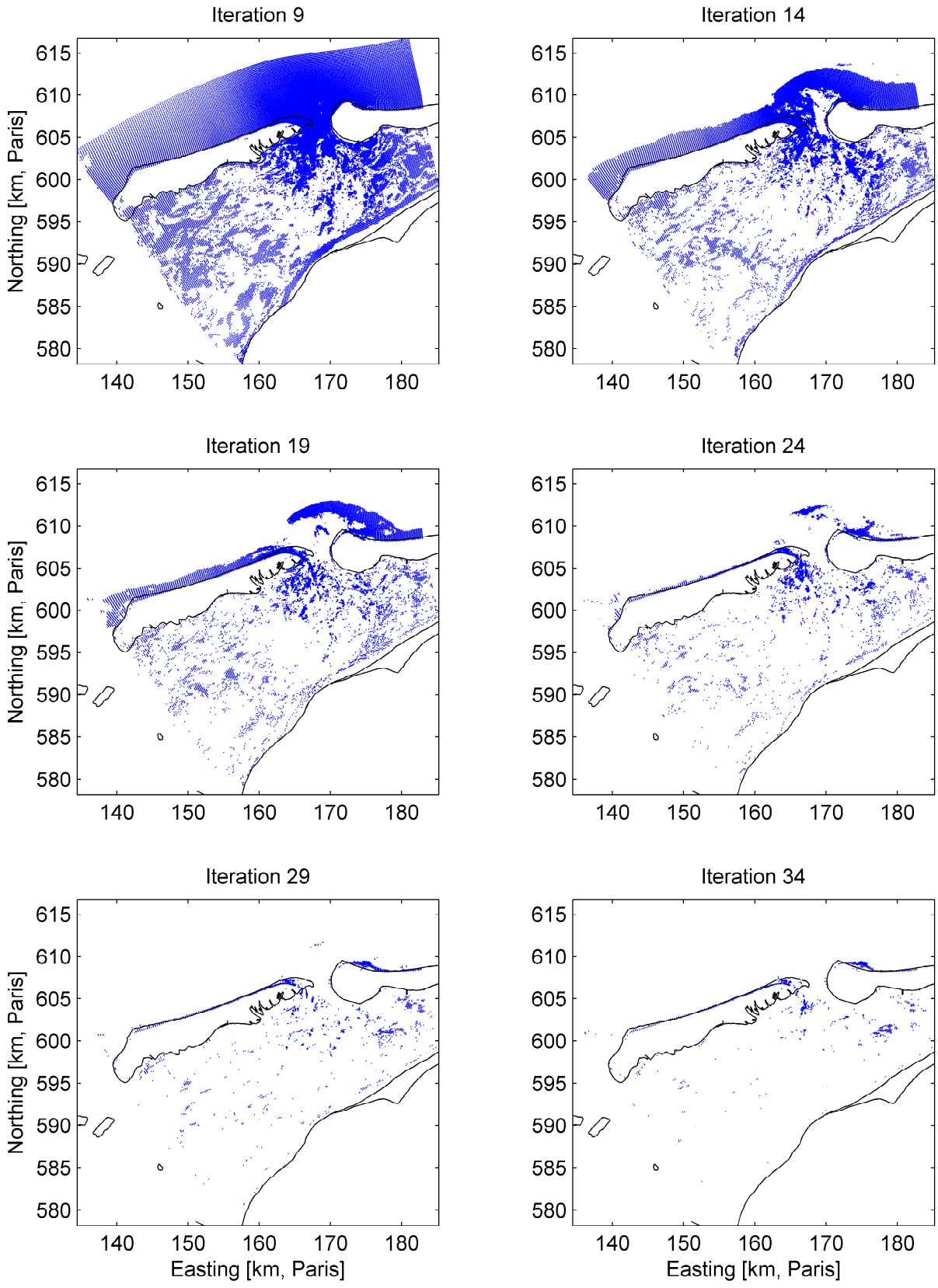

Amelander Zeegat storm of 2005/01/02 at 10:00 Calculation masks at various iteration levels, C_r05_d01		SWAN 40.51A
		Numerical efficiency SWAN
DELTARES & ALKYON	H5107.46/A2114	Fig. 5.1

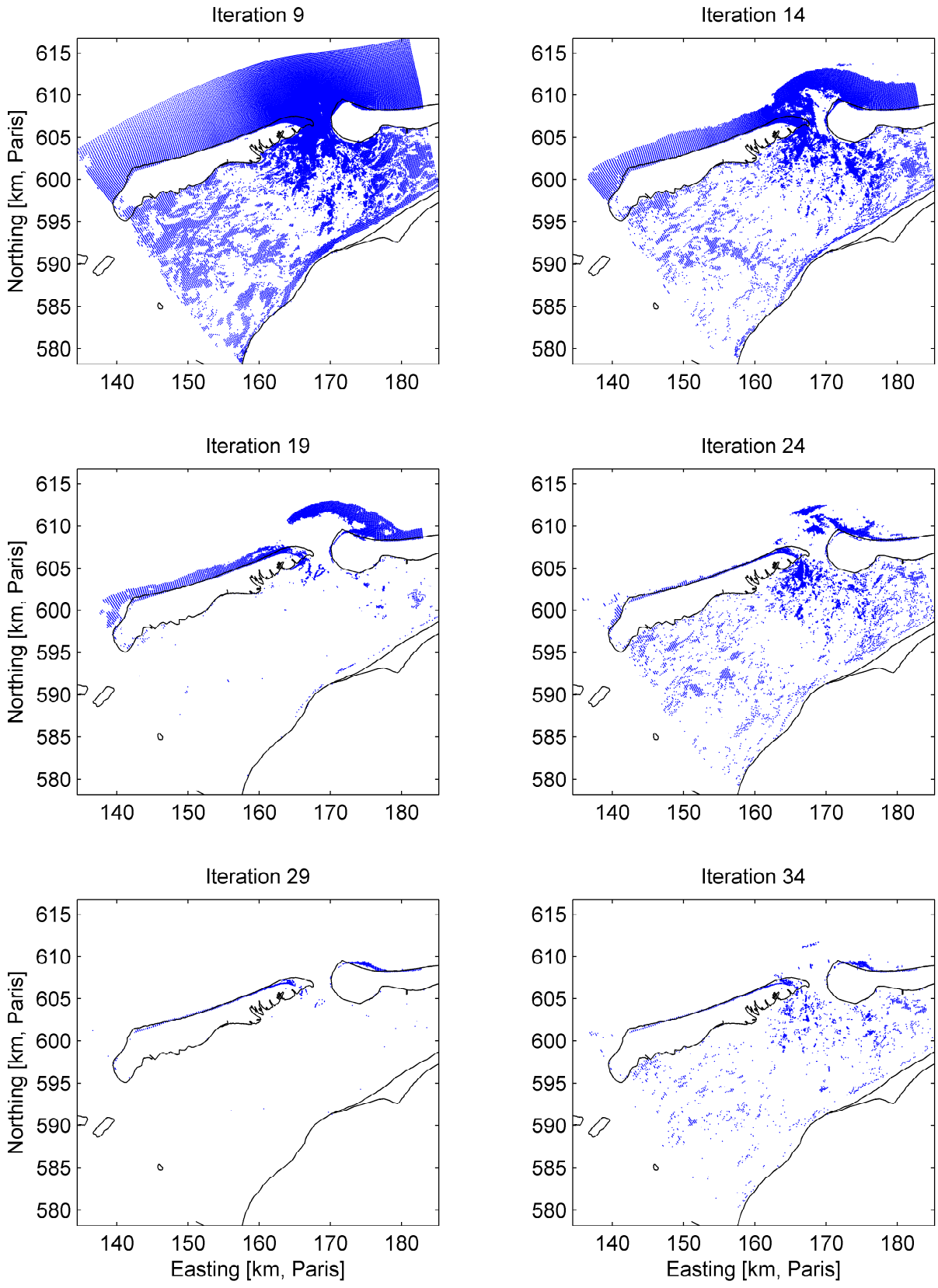

Amelander Zeegat storm of 2005/01/02 at 10:00 Calculation masks at various iteration levels, C_r10_d01		SWAN 40.51A
		Numerical efficiency SWAN
DELTARES & ALKYON	H5107.46/A2114	Fig. 5.2

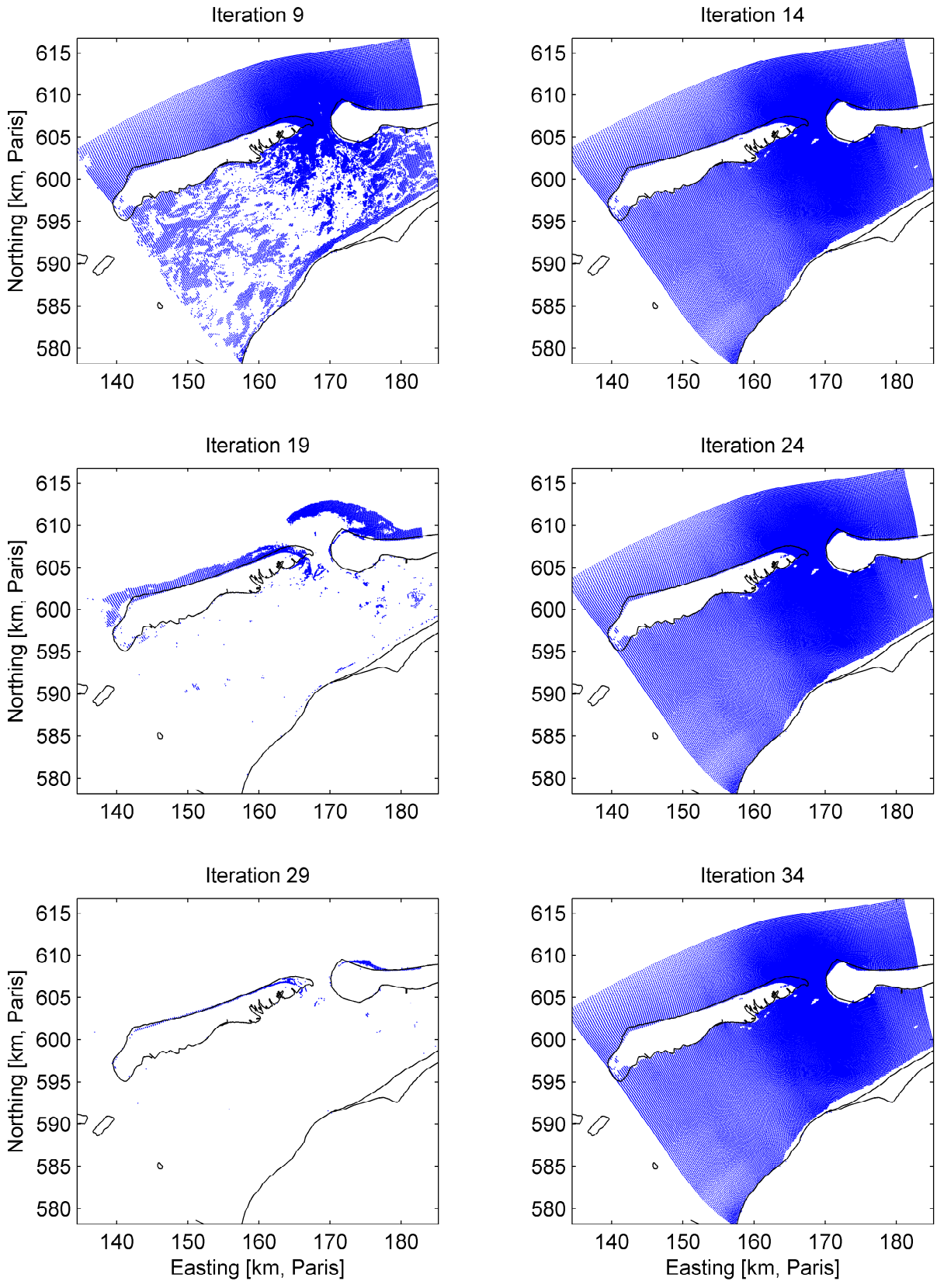

Amelander Zeegat storm of 2005/01/02 at 10:00 Calculation masks at various iteration levels, C_r10_d05		SWAN 40.51A
		Numerical efficiency SWAN
DELTARES & ALKYON	H5107.46/A2114	Fig. 5.3

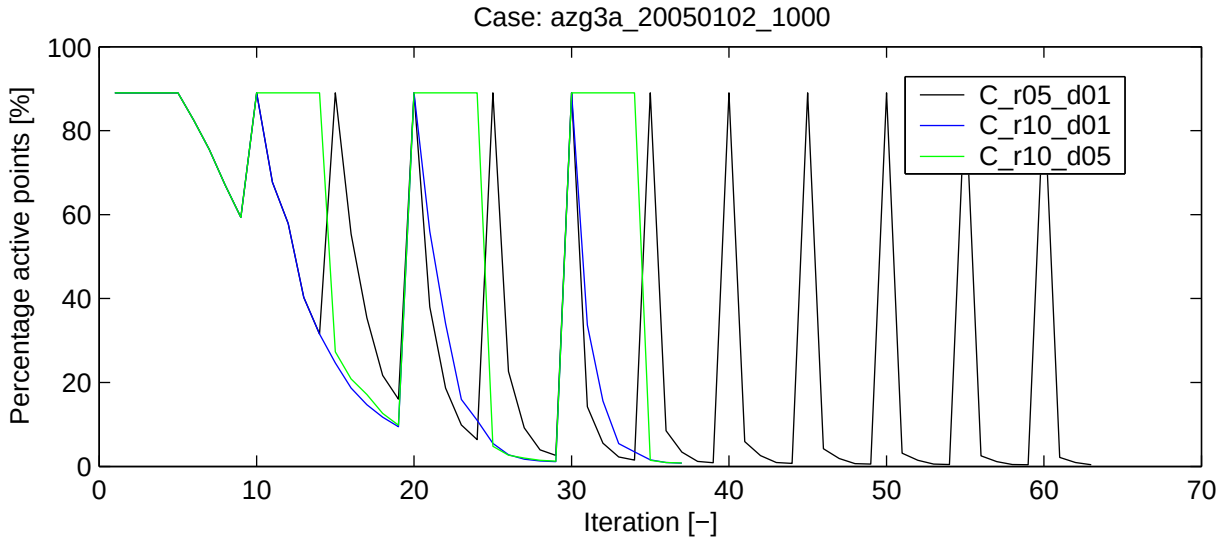

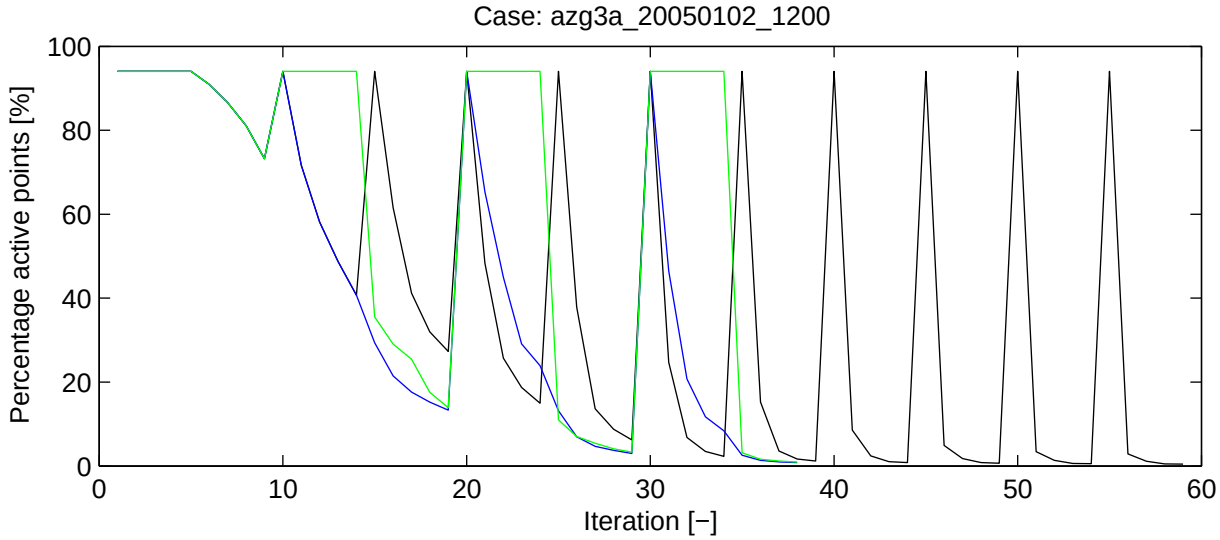

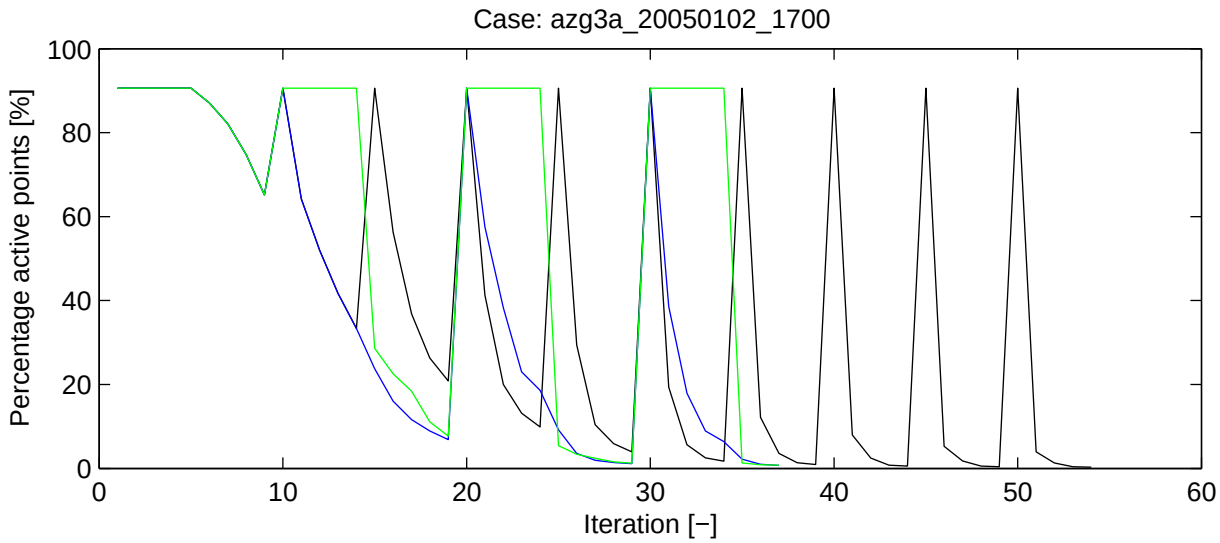

Amelander Zeegat storm of 2005/01/02 (flood, slack and ebb) Percentage of active grid points during the simulation		SWAN 40.51A
		Numerical efficiency SWAN
DELTARES & ALKYON	H5107.46/A2114	Fig. 5.4

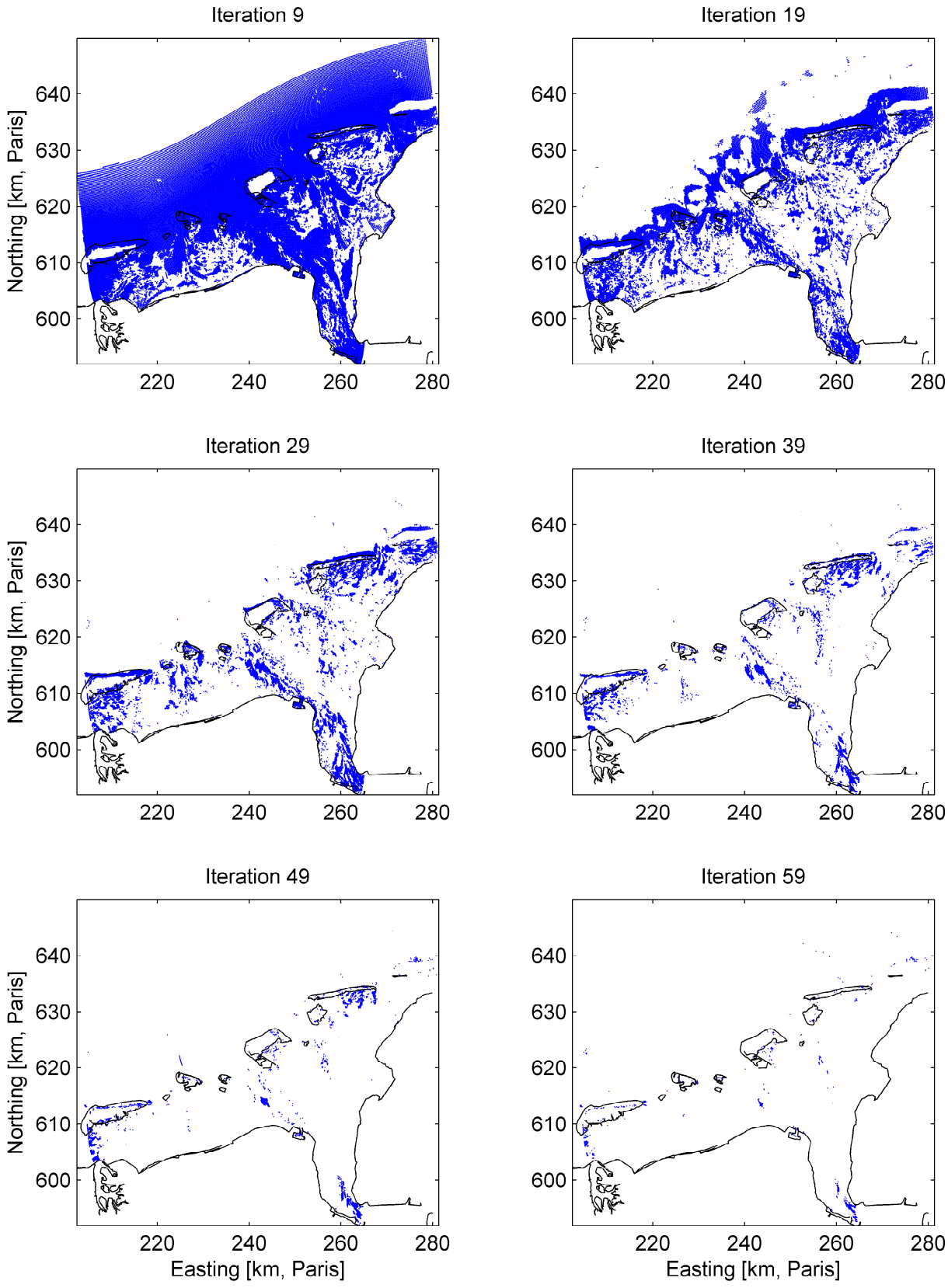

Eems-Dollard storm of 2006/11/01 at 03:00 Calculation masks at various iteration levels, C_r05_d01		SWAN 40.51A
		Numerical efficiency SWAN
DELTARES & ALKYON	H5107.46/A2114	Fig. 5.5

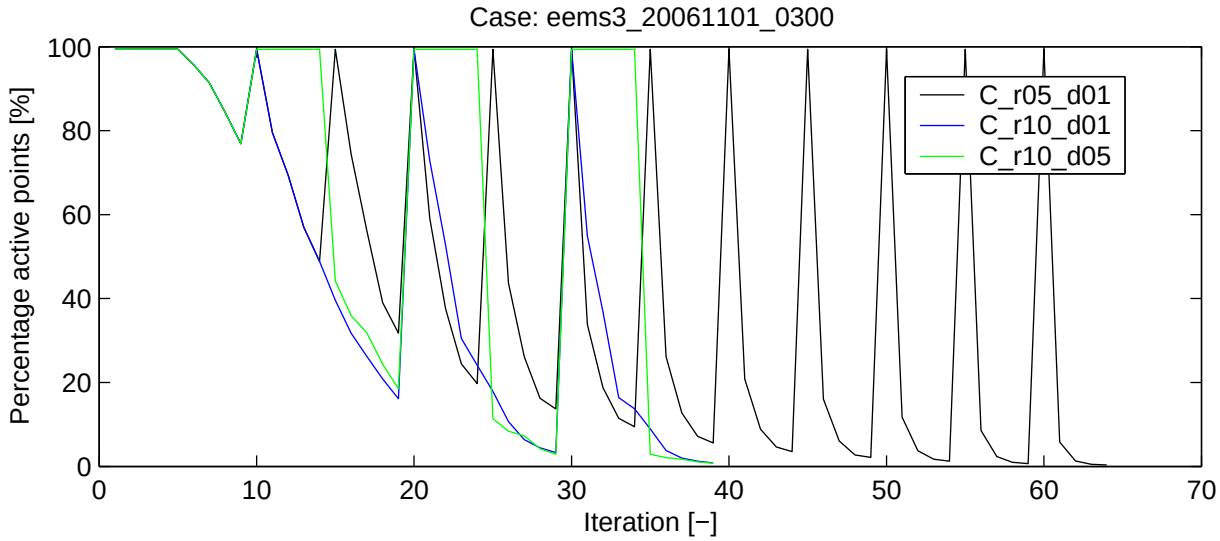

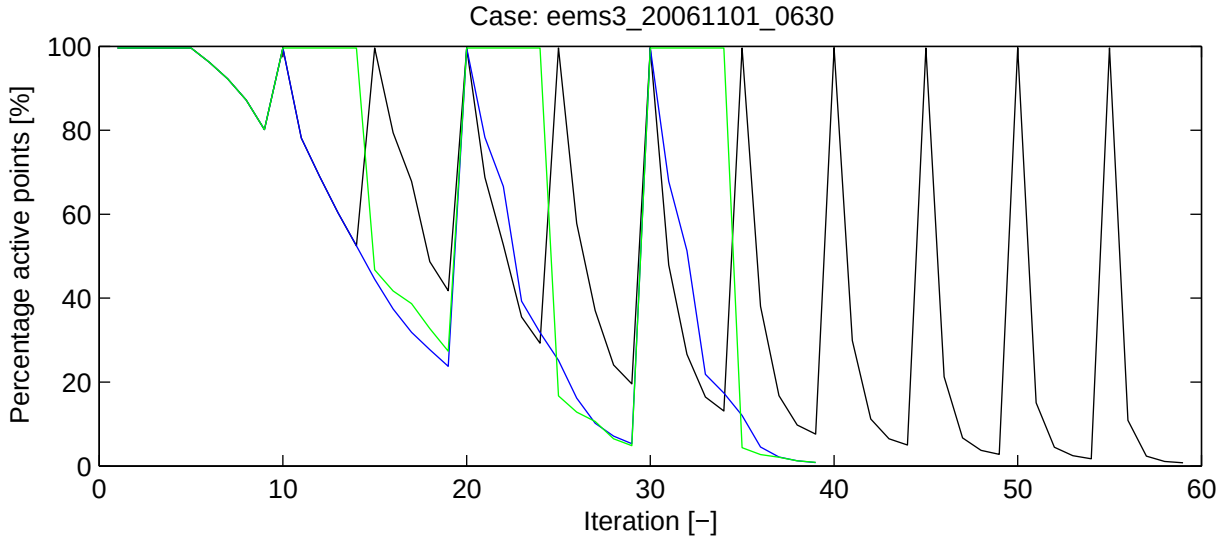

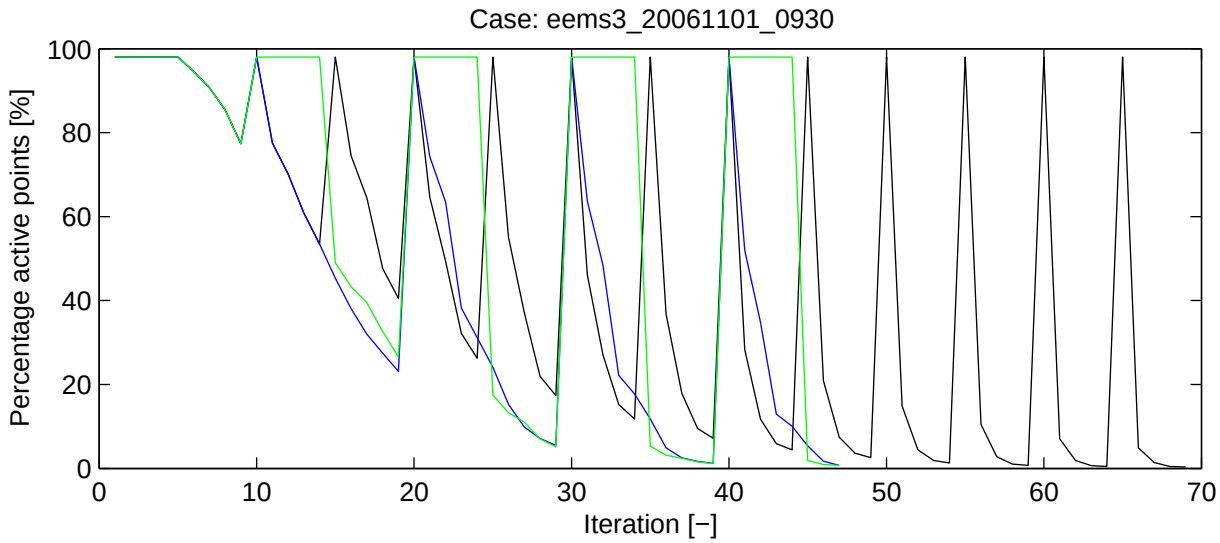

Eems−Dollard storm of 2006/11/01 (flood, slack and ebb) Percentage of active grid points during the simulation		SWAN 40.51A
		Numerical efficiency SWAN
DELTARES & ALKYON	H5107.46/A2114	Fig. 5.6

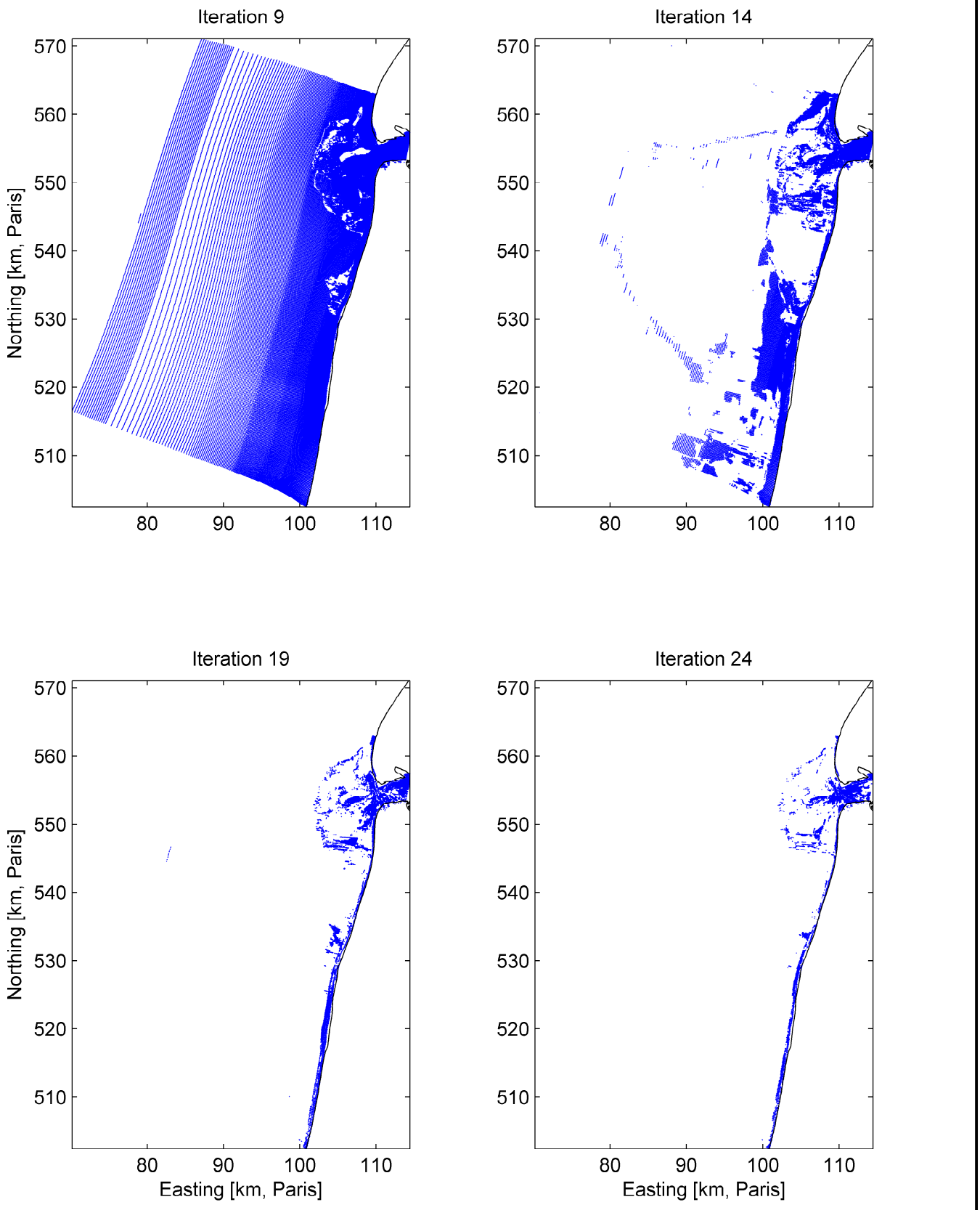

Petten storm of 1995/01/01 at 10:00 Calculation masks at various iteration levels, C_r05_d01		SWAN 40.51A
		Numerical efficiency SWAN
DELTARES & ALKYON	H5107.46/A2114	Fig. 5.7

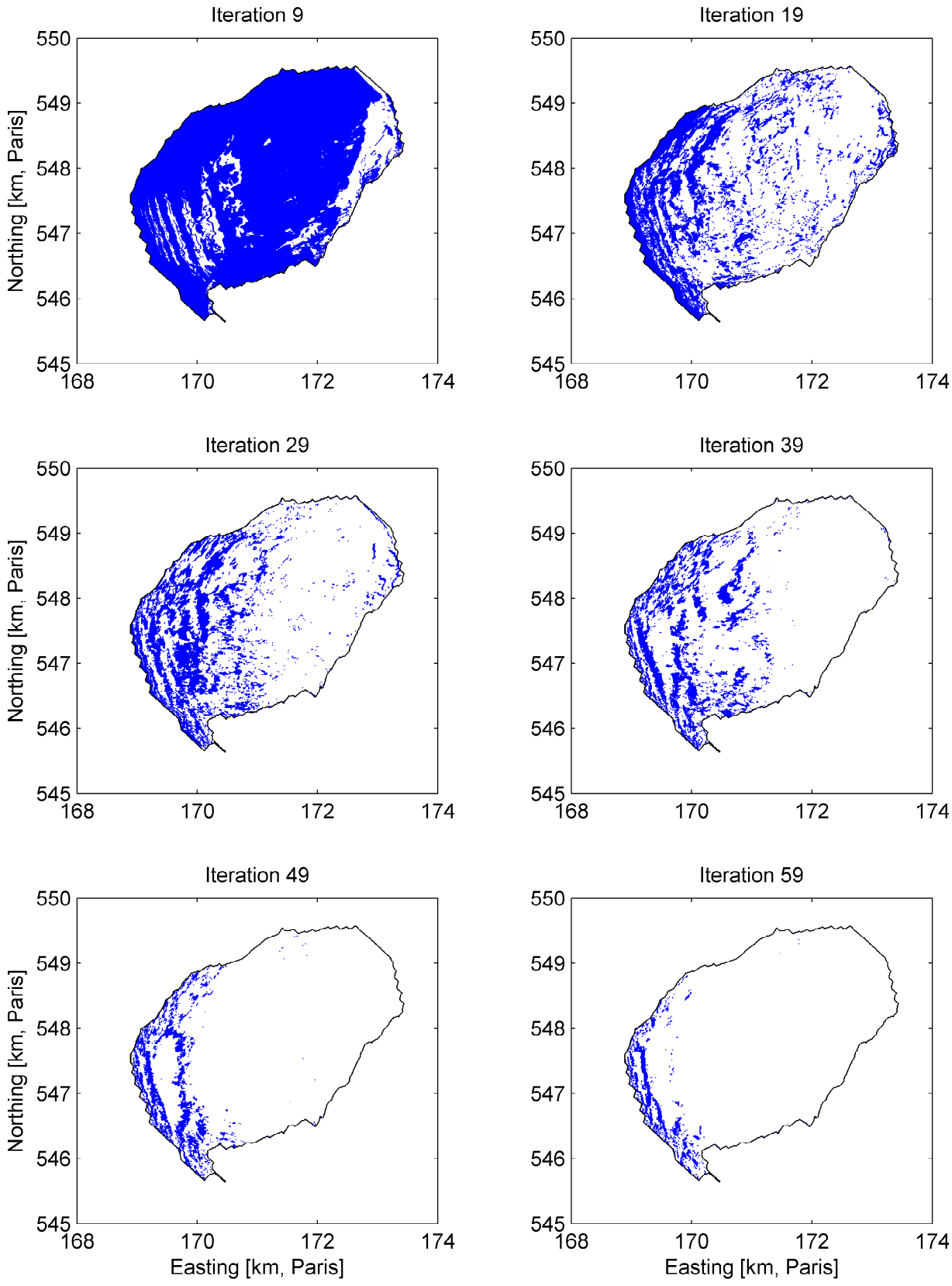

Lake Sloten storm of 2002/10/27 at 15:00 Calculation masks at various iteration levels, C_r05_d01		SWAN 40.51A
		Numerical efficiency SWAN
DELTARES & ALKYON	H5107.46/A2114	Fig. 5.8

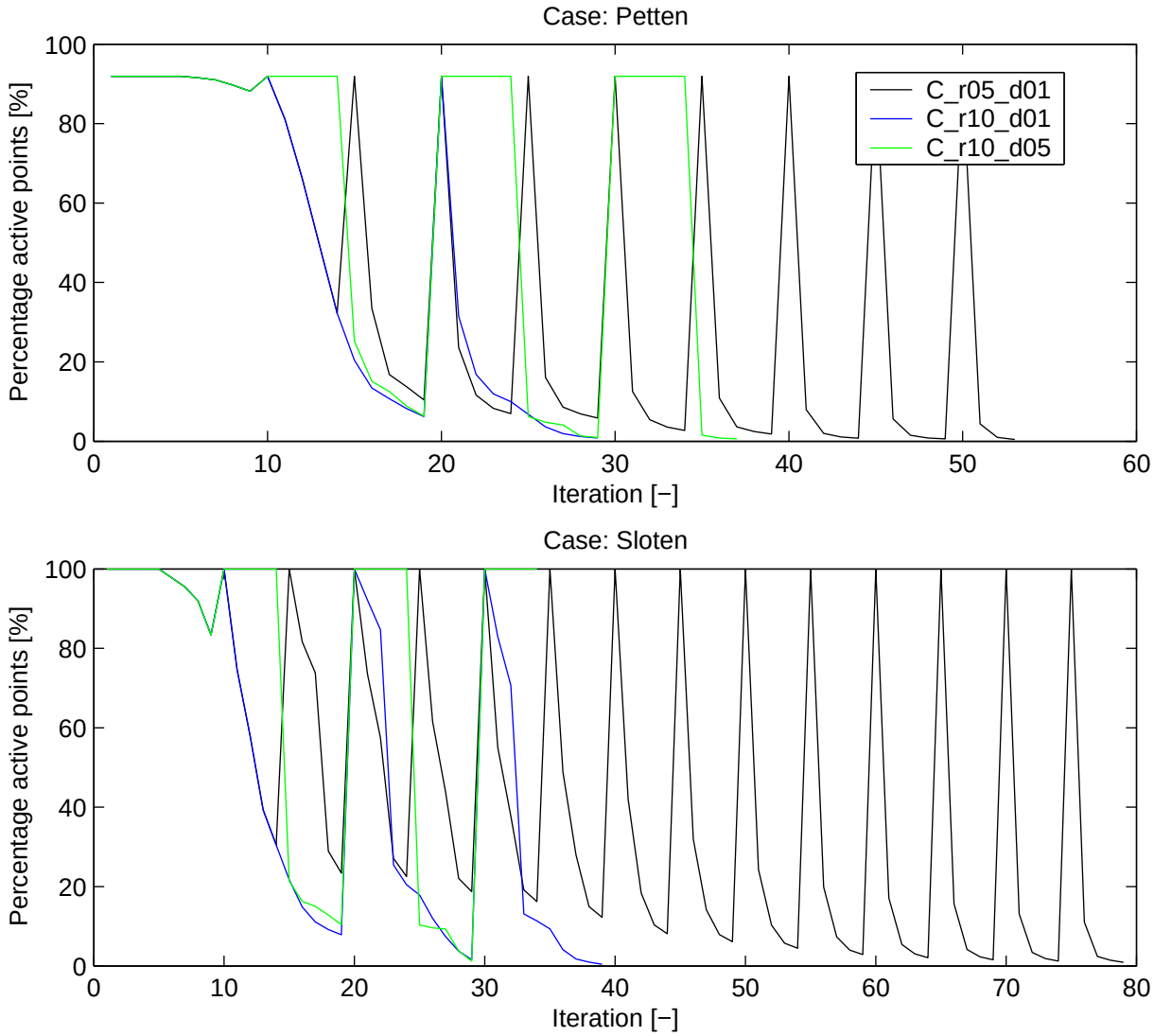

Petten storm of 1995/01/01 10:00 and Lake Sloten storm of 2002/10/27 15:00 Percentage of active grid points during the simulation		SWAN 40.51A
		Numerical efficiency SWAN
DELTARES & ALKYON	H5107.46/A2114	Fig. 5.9

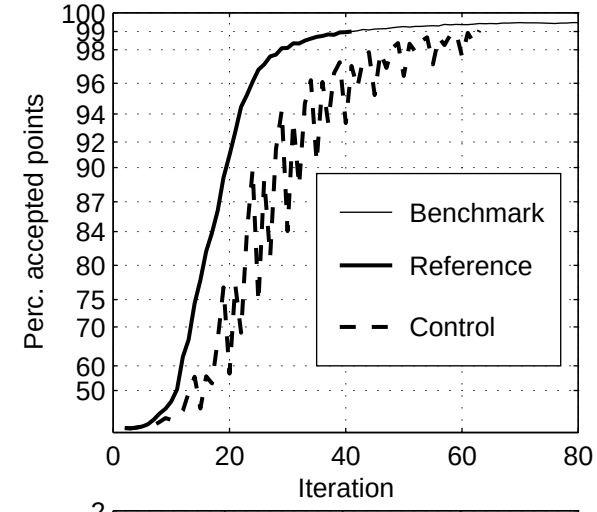

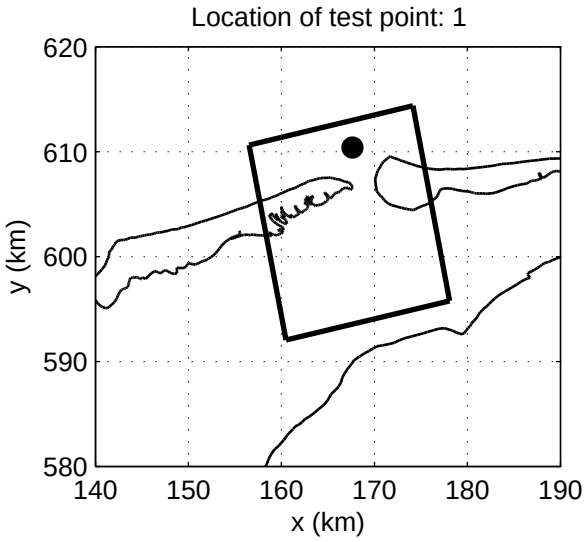

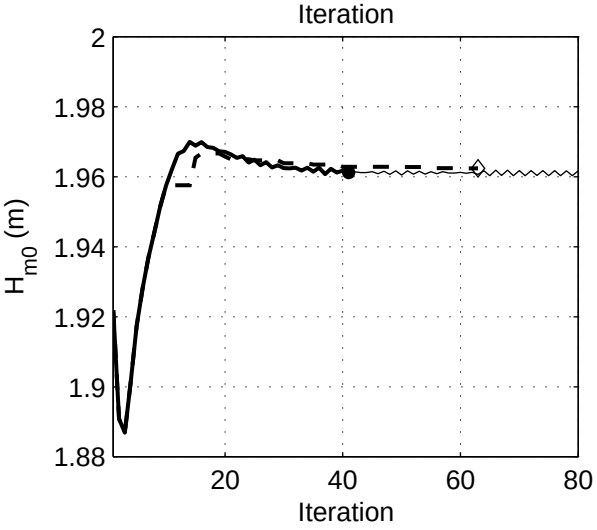

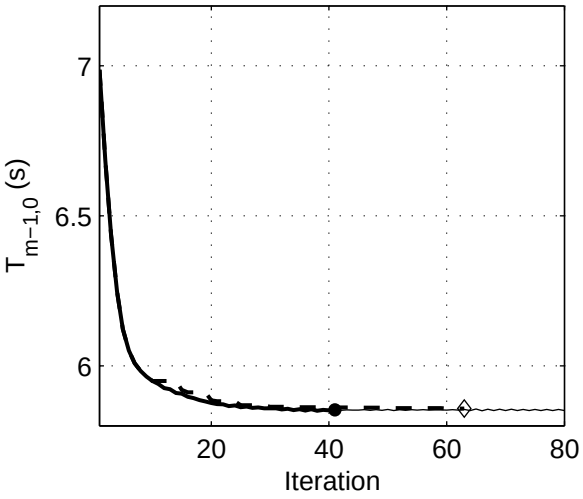

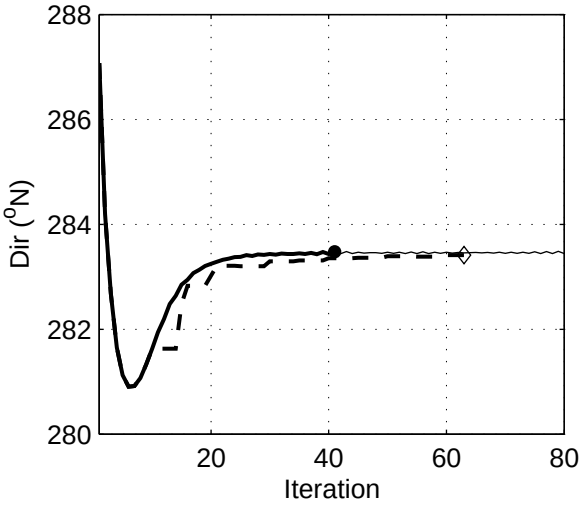

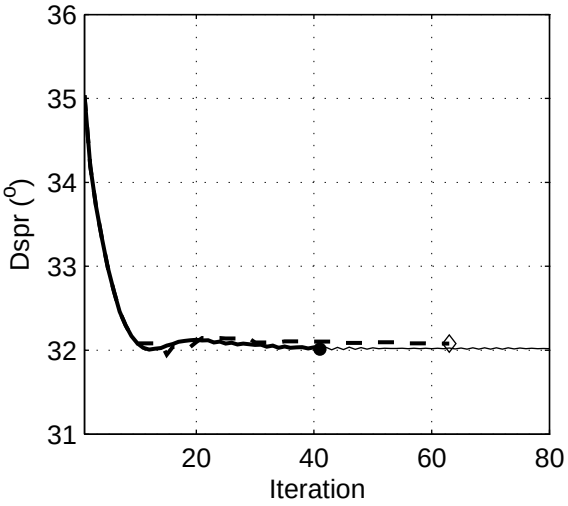

Convergence behaviour of the DDM simulation in the Amelander Zeegat, Case: AZG3A 2005/01/02 10:00, at point 1 Refresh domain every 05 iterations, for 1 iterations (C_r05_d01)		SWAN 40.51A
		Numerical efficiency SWAN
DELTARES & ALKYON	H5107.46/A2114	Fig. 5.10

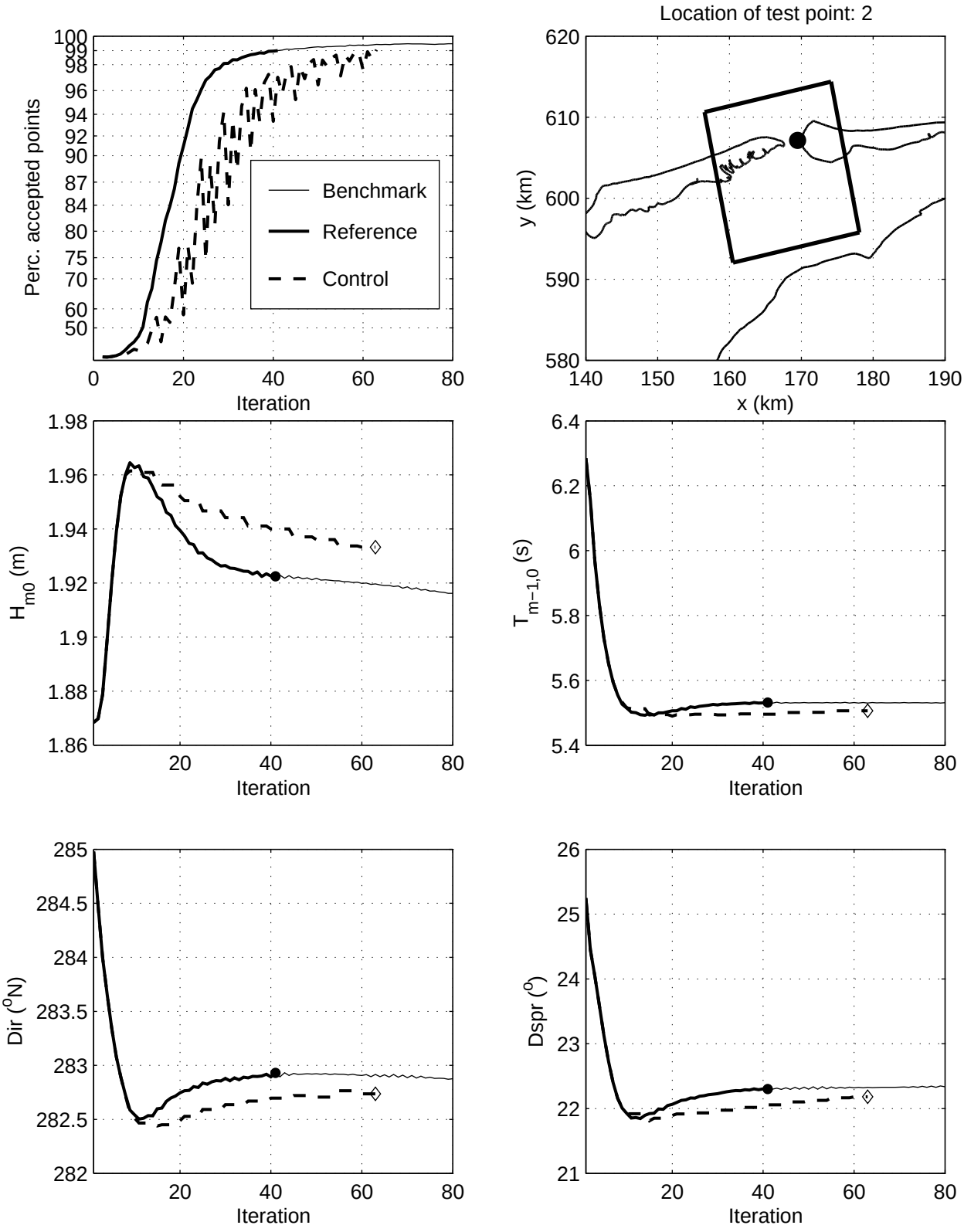

Convergence behaviour of the DDM simulation in the Amelander Zeegat, Case: AZG3A 2005/01/02 10:00, at point 2 Refresh domain every 05 iterations, for 1 iterations (C_r05_d01)		SWAN 40.51A
		Numerical efficiency SWAN
DELTARES & ALKYON	H5107.46/A2114	Fig. 5.11

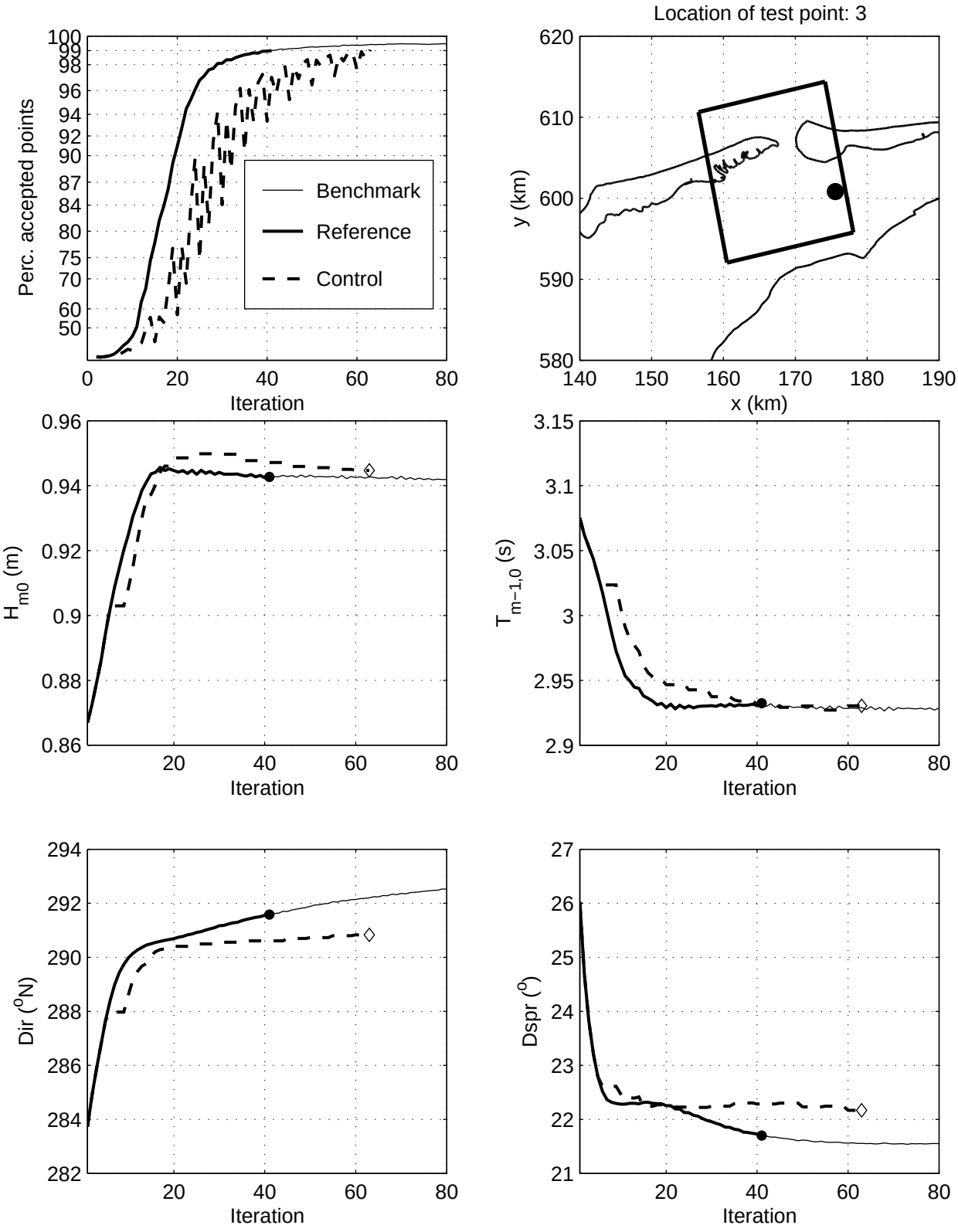

Convergence behaviour of the DDM simulation in the Amelander Zeegat, Case: AZG3A 2005/01/02 10:00, at point 3 Refresh domain every 05 iterations, for 1 iterations (C_r05_d01)		SWAN 40.51A
		Numerical efficiency SWAN
DELTARES & ALKYON	H5107.46/A2114	Fig. 5.12

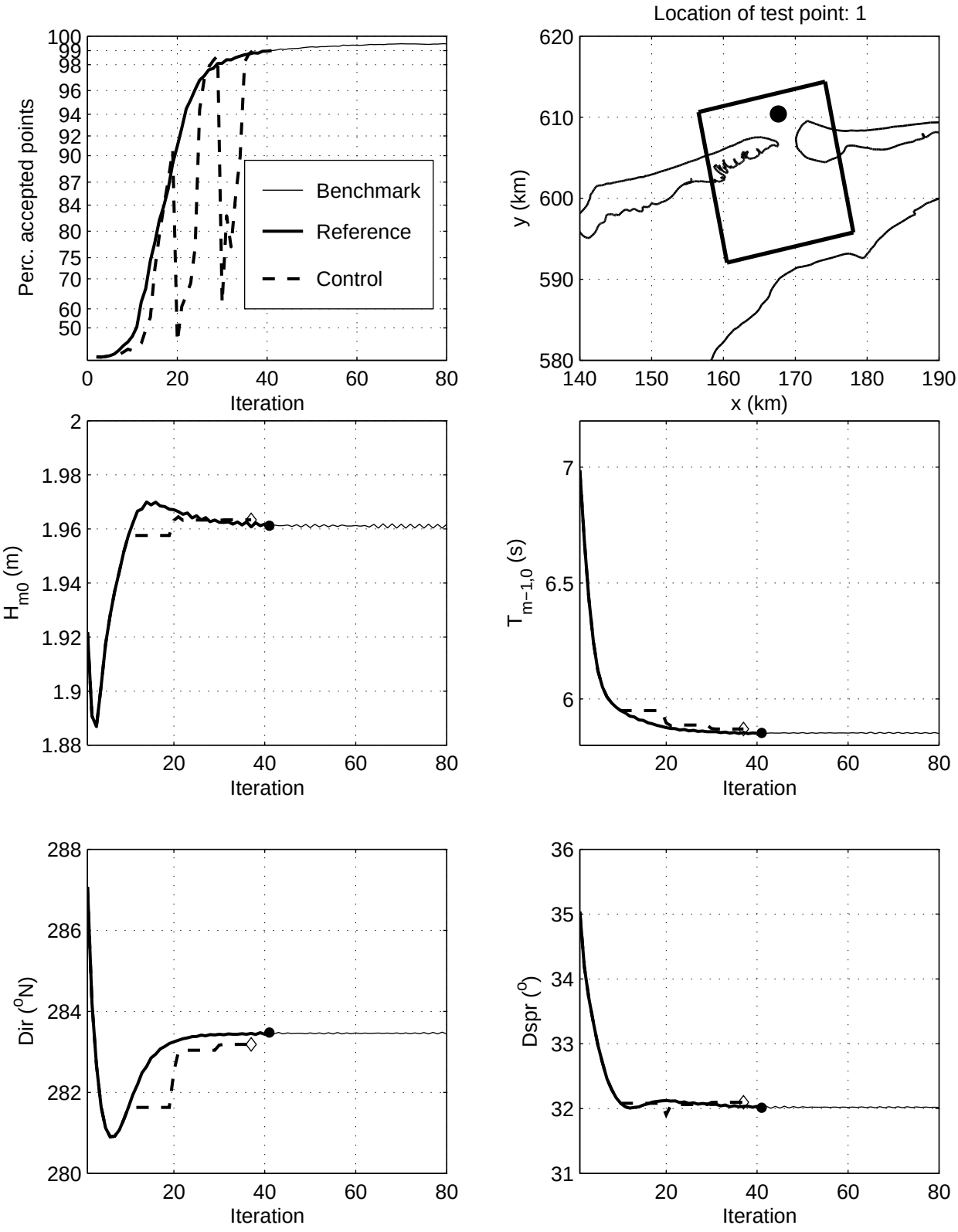

Convergence behaviour of the DDM simulation in the Amelander Zeegat, Case: AZG3A 2005/01/02 10:00, at point 1 Refresh domain every 10 iterations, for 1 iterations (C_r10_d01)		SWAN 40.51A
		Numerical efficiency SWAN
DELTARES & ALKYON	H5107.46/A2114	Fig. 5.13

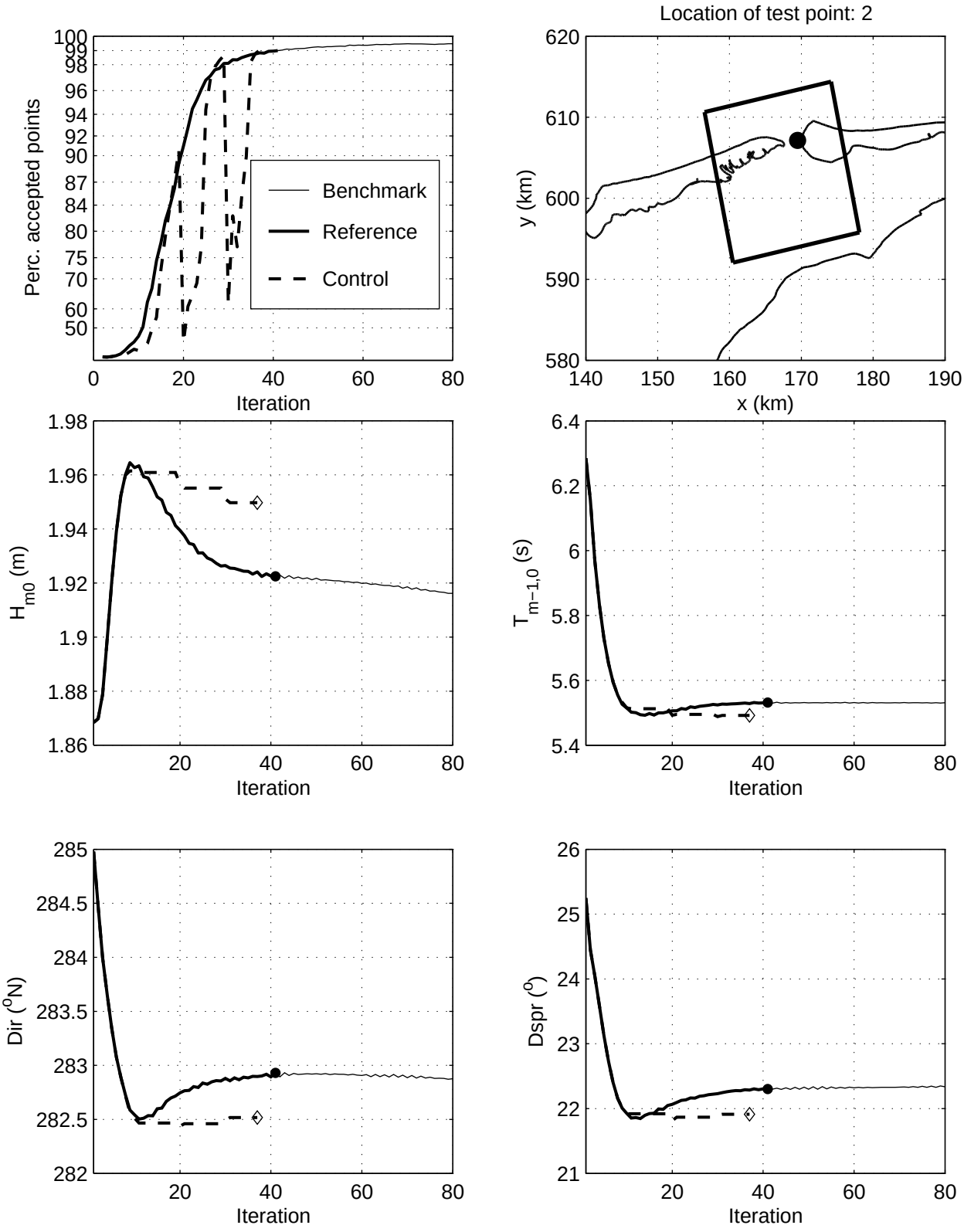

Convergence behaviour of the DDM simulation in the Amelander Zeegat, Case: AZG3A 2005/01/02 10:00, at point 2 Refresh domain every 10 iterations, for 1 iterations (C_r10_d01)		SWAN 40.51A
		Numerical efficiency SWAN
DELTARES & ALKYON	H5107.46/A2114	Fig. 5.14

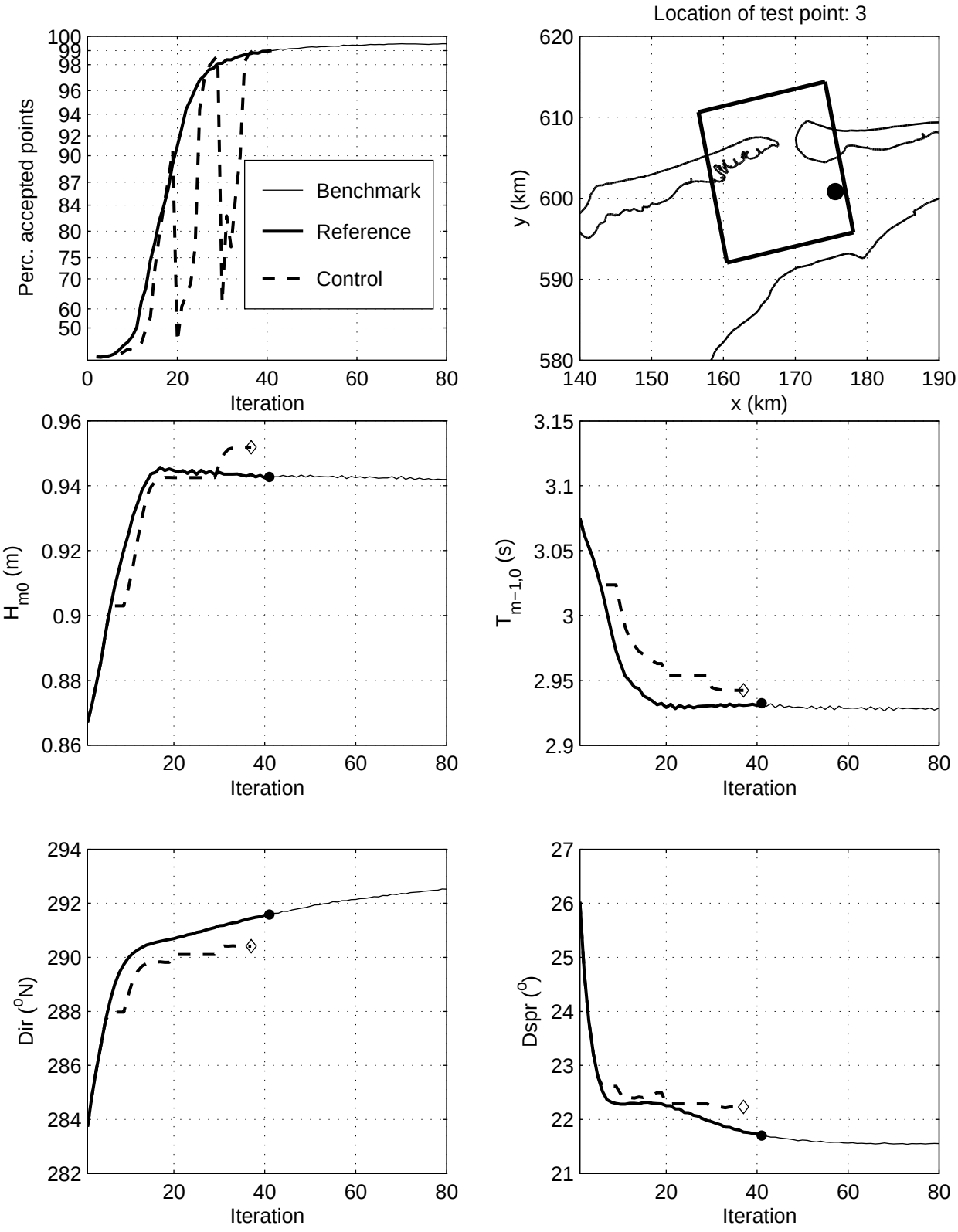

Convergence behaviour of the DDM simulation in the Amelander Zeegat, Case: AZG3A 2005/01/02 10:00, at point 3 Refresh domain every 10 iterations, for 1 iterations (C_r10_d01)		SWAN 40.51A
		Numerical efficiency SWAN
DELTARES & ALKYON	H5107.46/A2114	Fig. 5.15

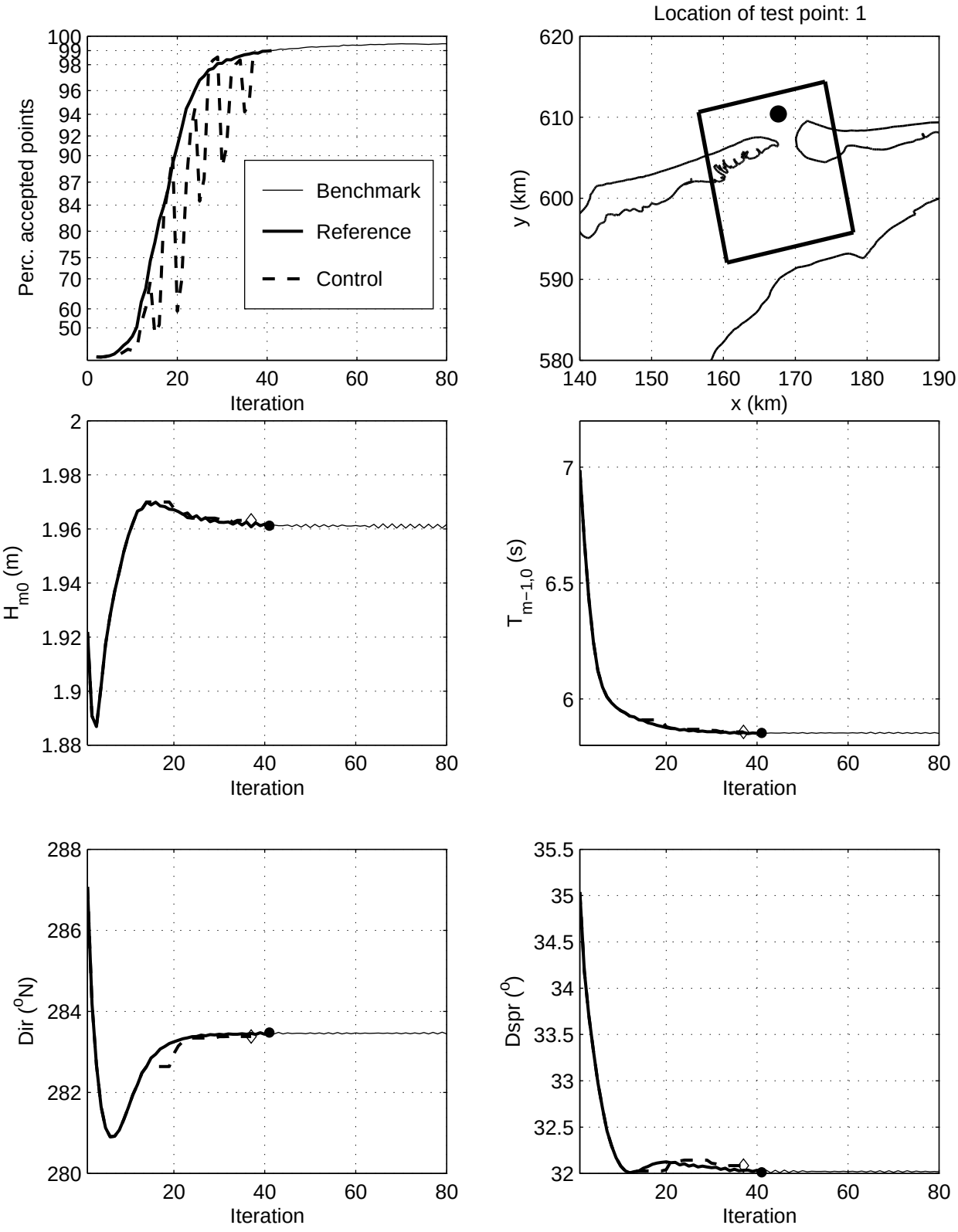

Convergence behaviour of the DDM simulation in the Amelander Zeegat, Case: AZG3A 2005/01/02 10:00, at point 1 Refresh domain every 10 iterations, for 5 iterations (C_r10_d05)		SWAN 40.51A
		Numerical efficiency SWAN
DELTARES & ALKYON	H5107.46/A2114	Fig. 5.16

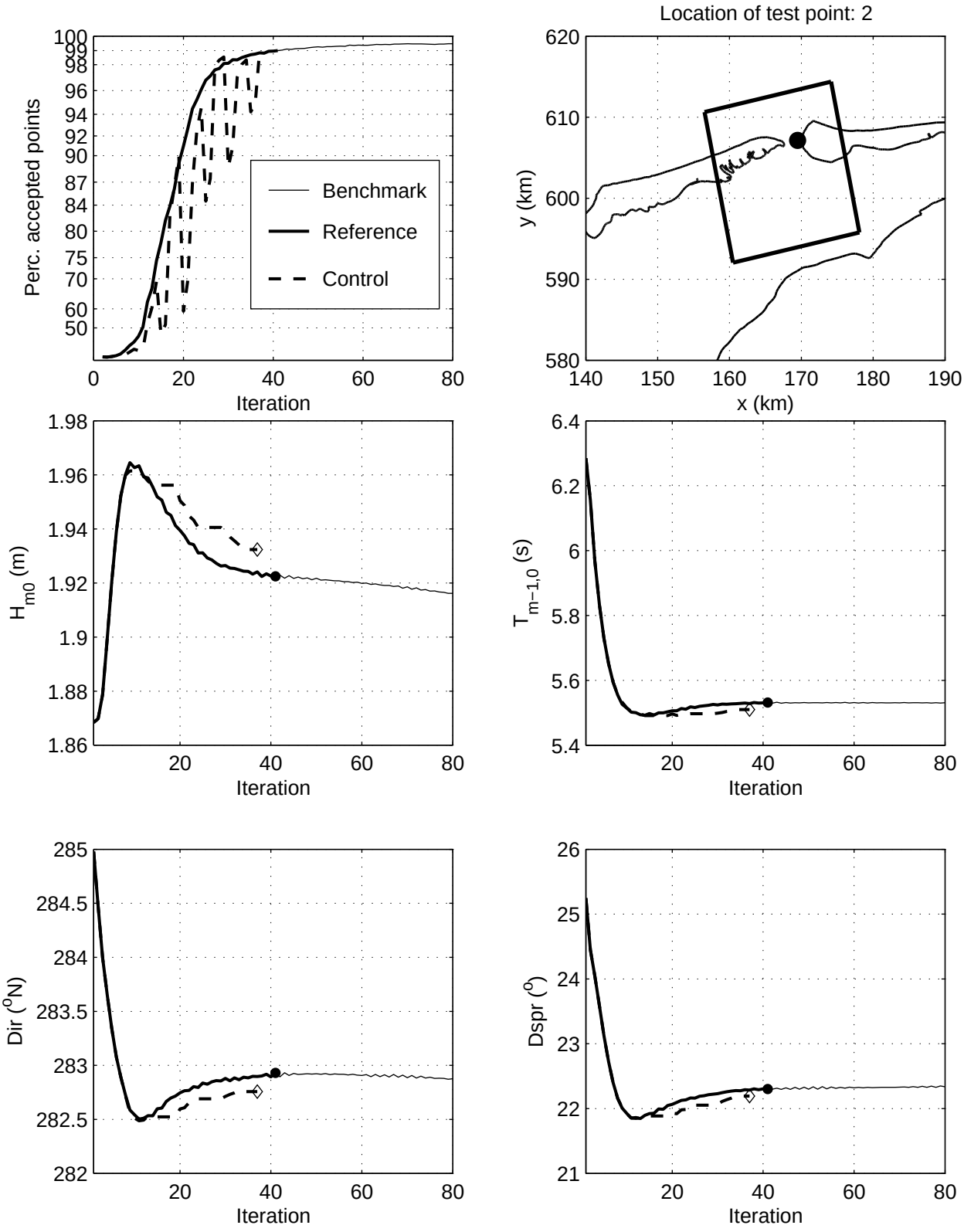

Convergence behaviour of the DDM simulation in the Amelander Zeegat, Case: AZG3A 2005/01/02 10:00, at point 2 Refresh domain every 10 iterations, for 5 iterations (C_r10_d05)		SWAN 40.51A
		Numerical efficiency SWAN
DELTARES & ALKYON	H5107.46/A2114	Fig. 5.17

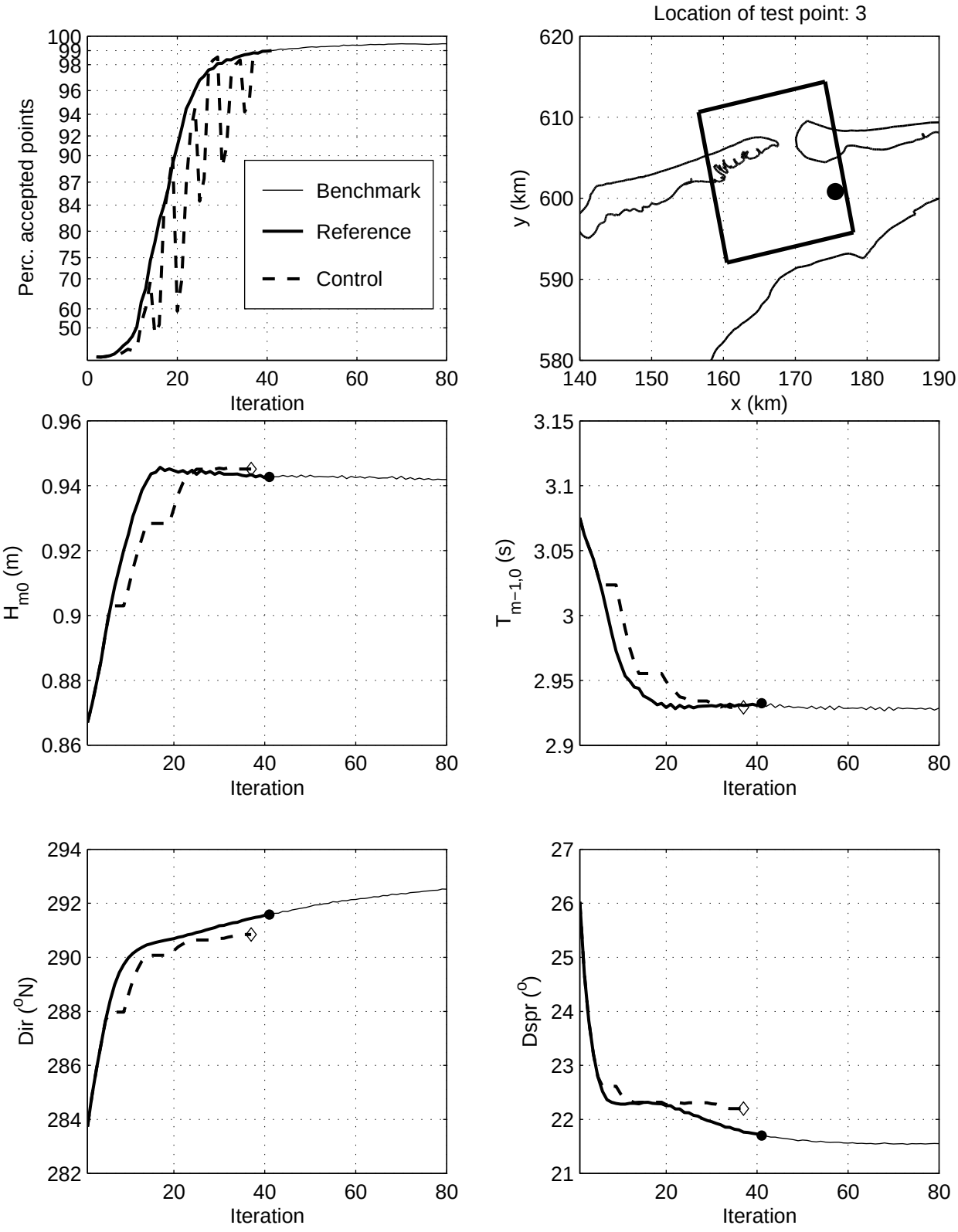

Convergence behaviour of the DDM simulation in the Amelander Zeegat, Case: AZG3A 2005/01/02 10:00, at point 3 Refresh domain every 10 iterations, for 5 iterations (C_r10_d05)		SWAN 40.51A
		Numerical efficiency SWAN
DELTARES & ALKYON	H5107.46/A2114	Fig. 5.18

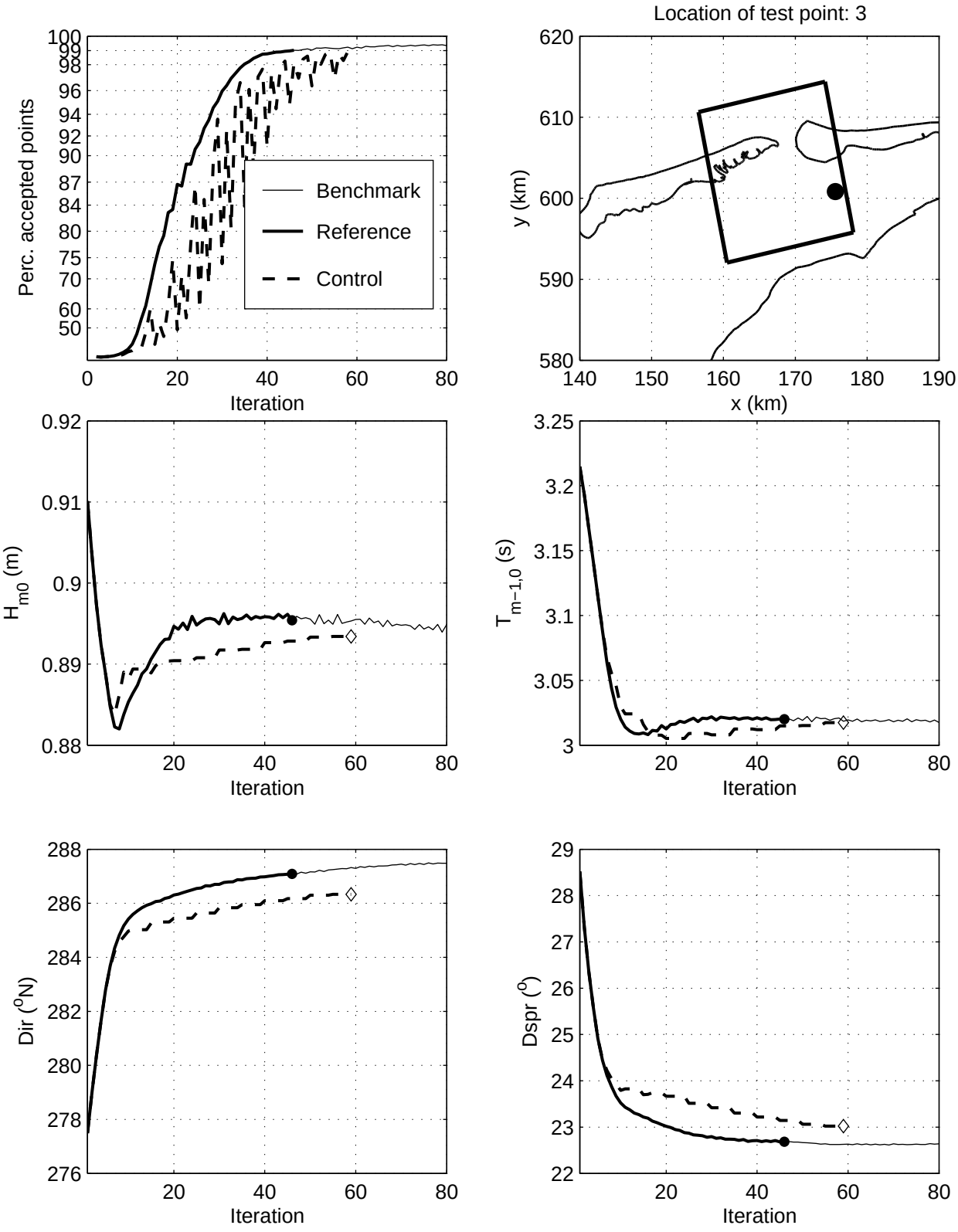

Convergence behaviour of the DDM simulation in the Amelander Zeegat, Case: AZG3A 2005/01/02 12:00, at point 3 Refresh domain every 05 iterations, for 1 iterations (C_r05_d01)		SWAN 40.51A
		Numerical efficiency SWAN
DELTARES & ALKYON	H5107.46/A2114	Fig. 5.19

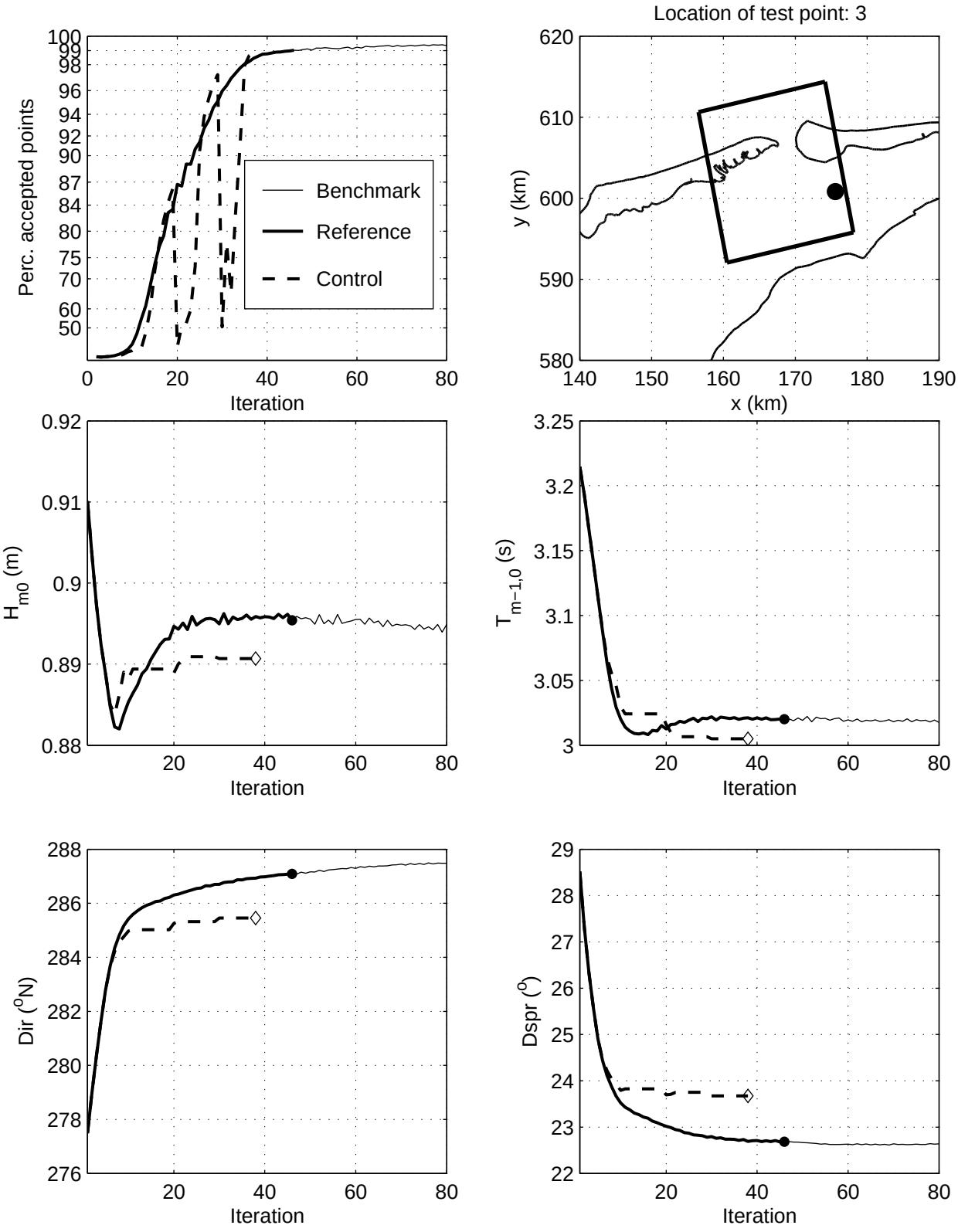

Convergence behaviour of the DDM simulation in the Amelander Zeegat, Case: AZG3A 2005/01/02 12:00, at point 3 Refresh domain every 10 iterations, for 1 iterations (C_r10_d01)		SWAN 40.51A
		Numerical efficiency SWAN
DELTARES & ALKYON	H5107.46/A2114	Fig. 5.20

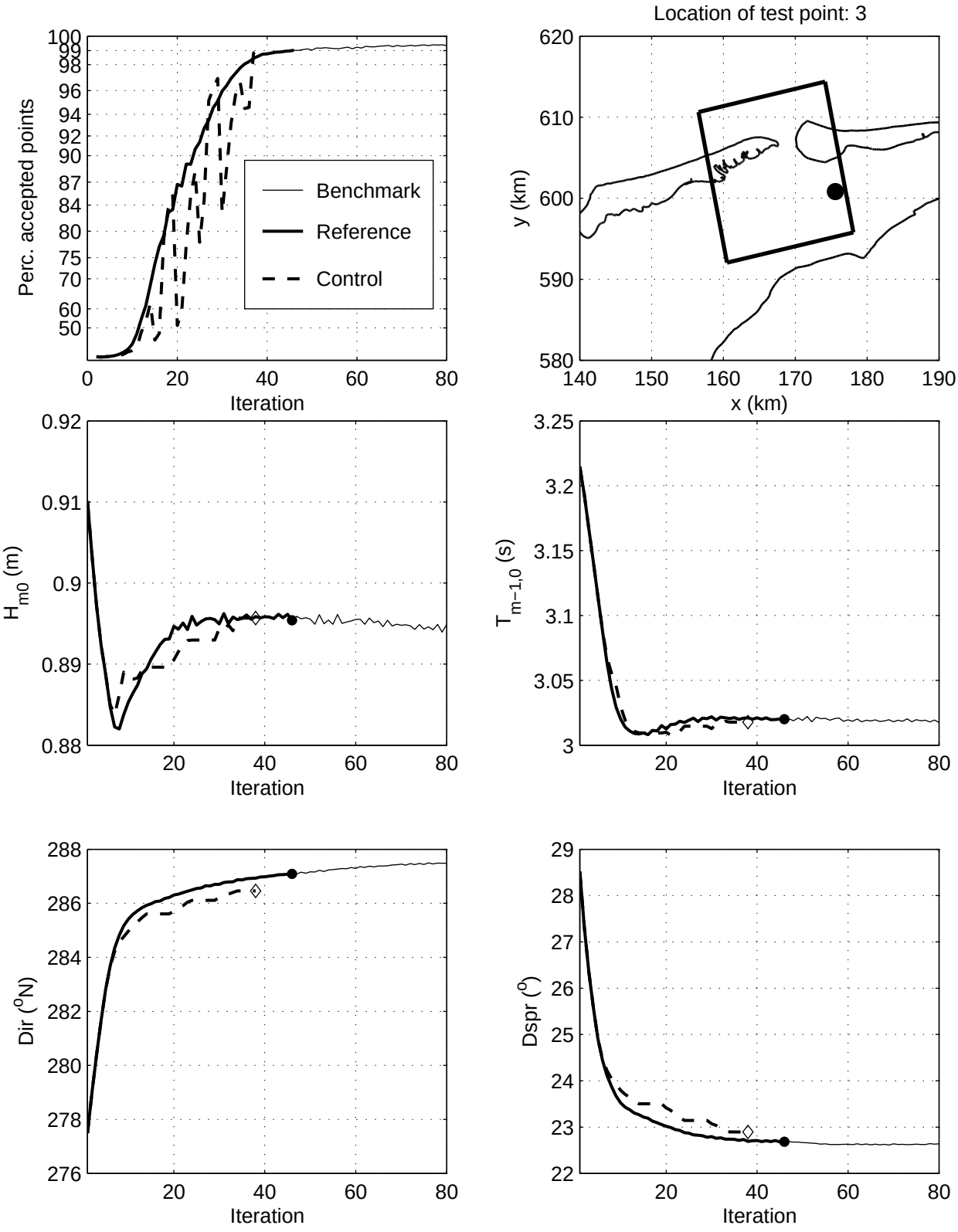

Convergence behaviour of the DDM simulation in the Amelander Zeegat, Case: AZG3A 2005/01/02 12:00, at point 3 Refresh domain every 10 iterations, for 5 iterations (C_r10_d05)		SWAN 40.51A
		Numerical efficiency SWAN
DELTARES & ALKYON	H5107.46/A2114	Fig. 5.21

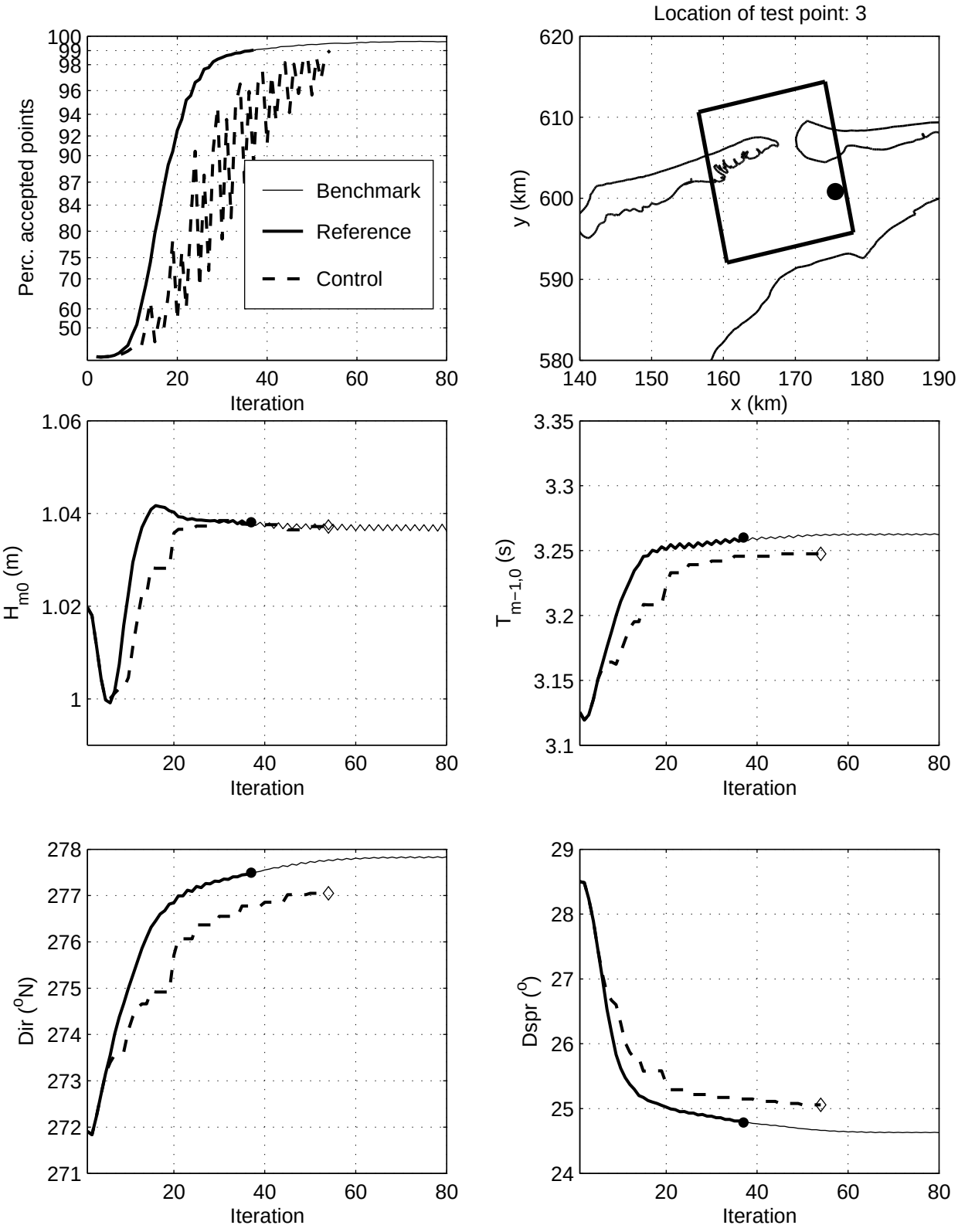

Convergence behaviour of the DDM simulation in the Amelander Zeegat, Case: AZG3A 2005/01/02 17:00, at point 3 Refresh domain every 05 iterations, for 1 iterations (C_r05_d01)		SWAN 40.51A
		Numerical efficiency SWAN
DELTARES & ALKYON	H5107.46/A2114	Fig. 5.22

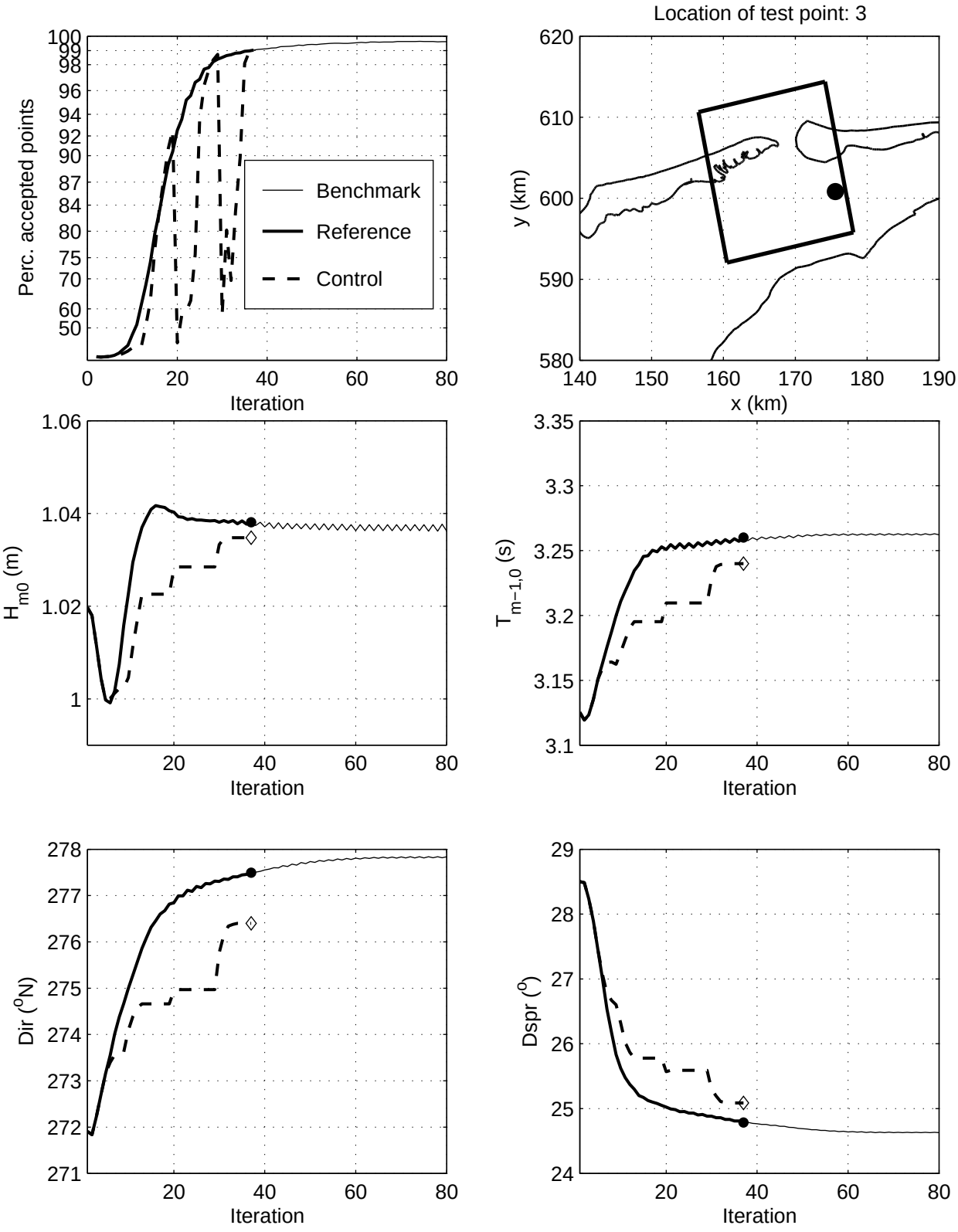

Convergence behaviour of the DDM simulation in the Amelander Zeegat, Case: AZG3A 2005/01/02 17:00, at point 3 Refresh domain every 10 iterations, for 1 iterations (C_r10_d01)		SWAN 40.51A
		Numerical efficiency SWAN
DELTARES & ALKYON	H5107.46/A2114	Fig. 5.23

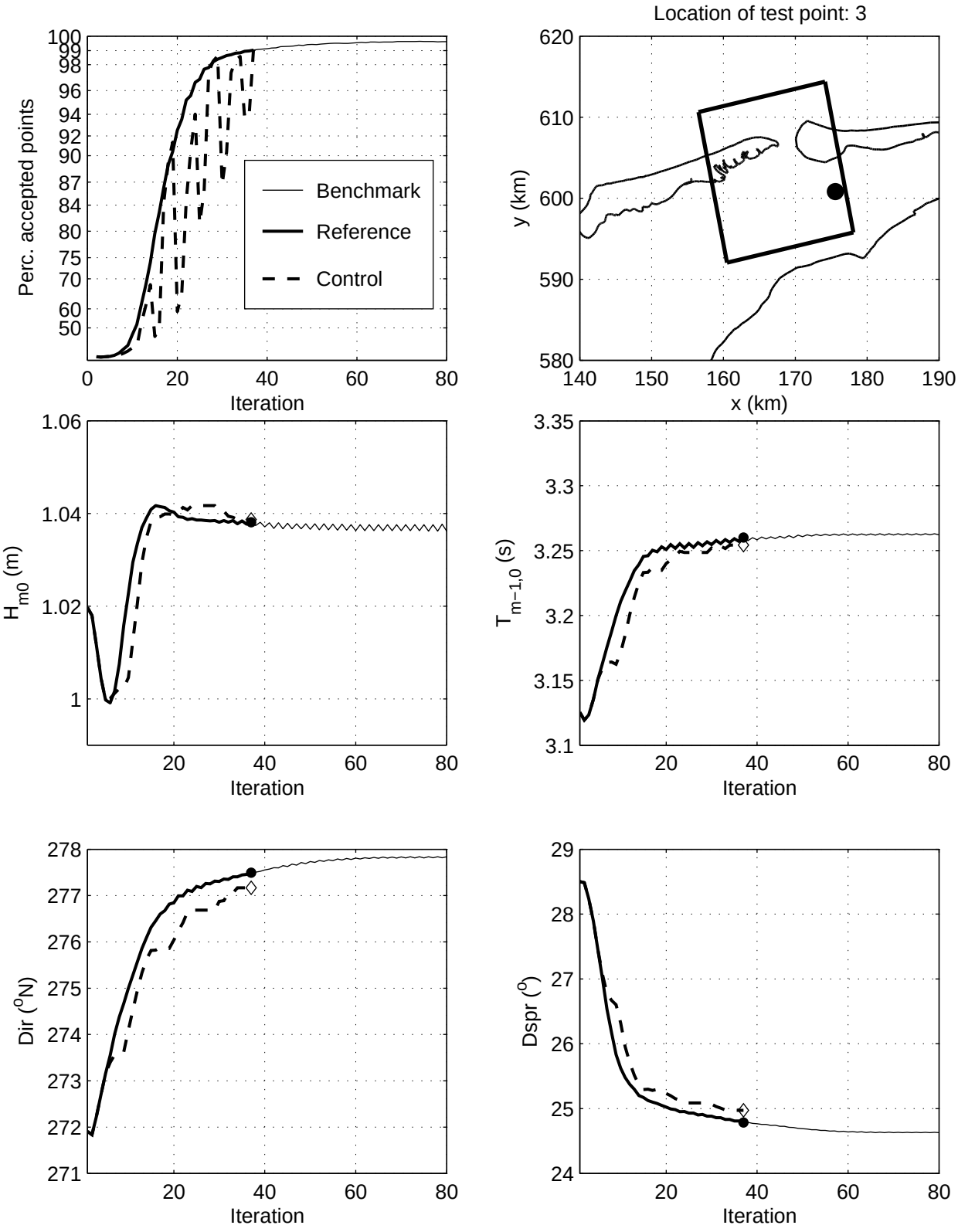

Convergence behaviour of the DDM simulation in the Amelander Zeegat, Case: AZG3A 2005/01/02 17:00, at point 3 Refresh domain every 10 iterations, for 5 iterations (C_r10_d05)		SWAN 40.51A
		Numerical efficiency SWAN
DELTARES & ALKYON	H5107.46/A2114	Fig. 5.24

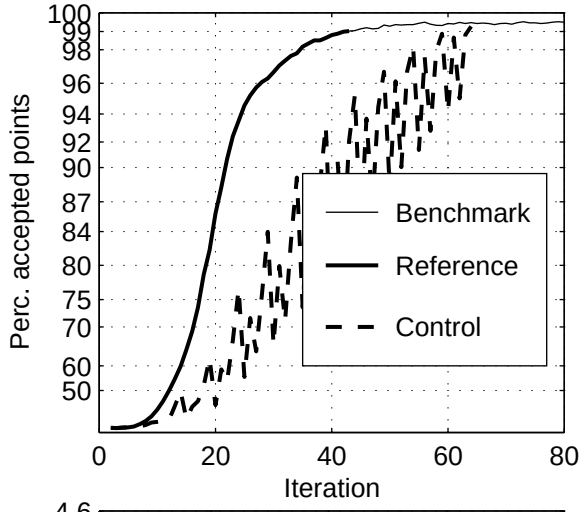

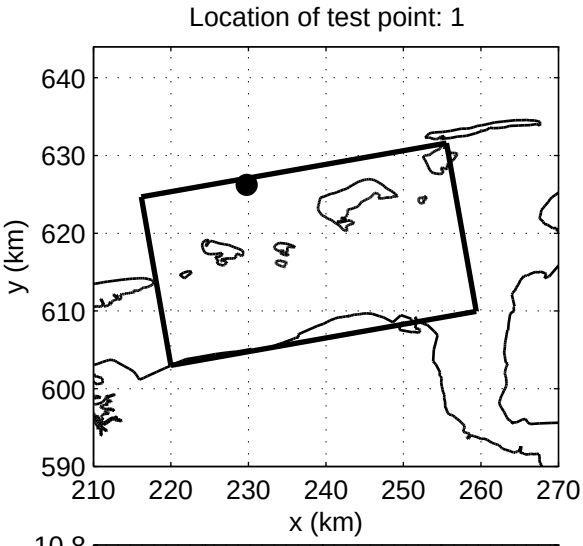

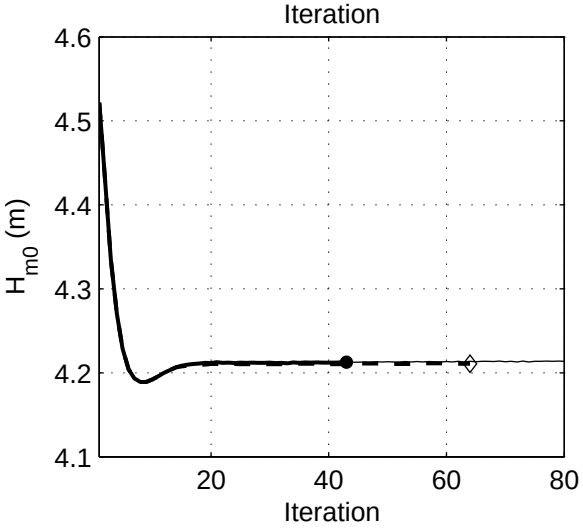

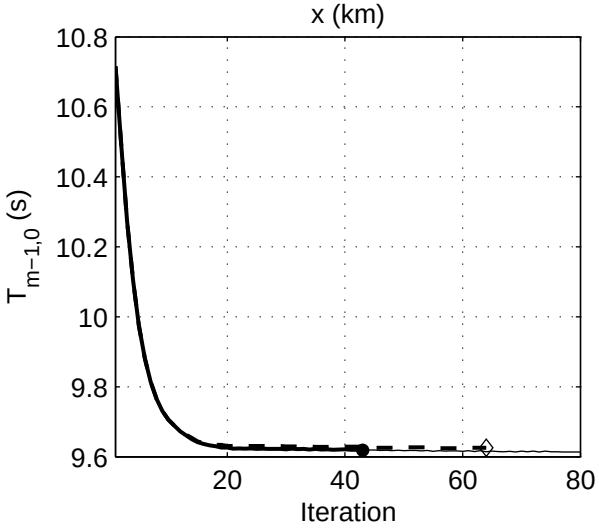

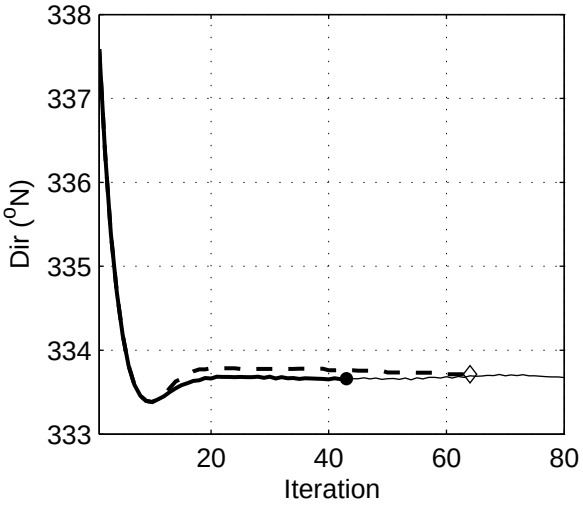

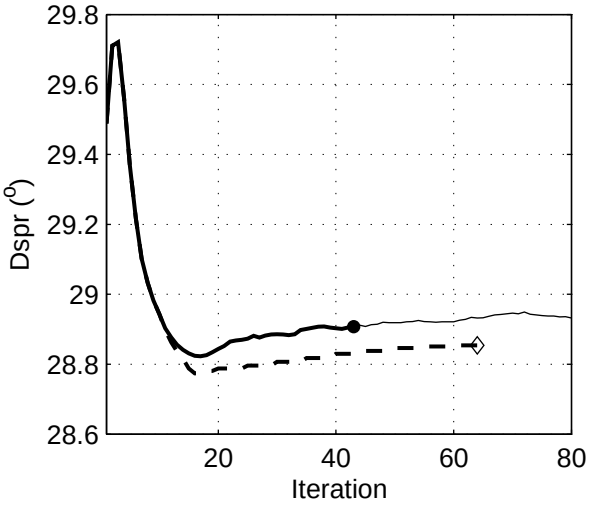

Convergence behaviour of the DDM simulation in the Eems−Dollard, Case: EEMS3A 2006/11/01 03:00, at point 1 Refresh domain every 05 iterations, for 1 iterations (C_r05_d01)		SWAN 40.51A
		Numerical efficiency SWAN
DELTARES & ALKYON	H5107.46/A2114	Fig. 5.25

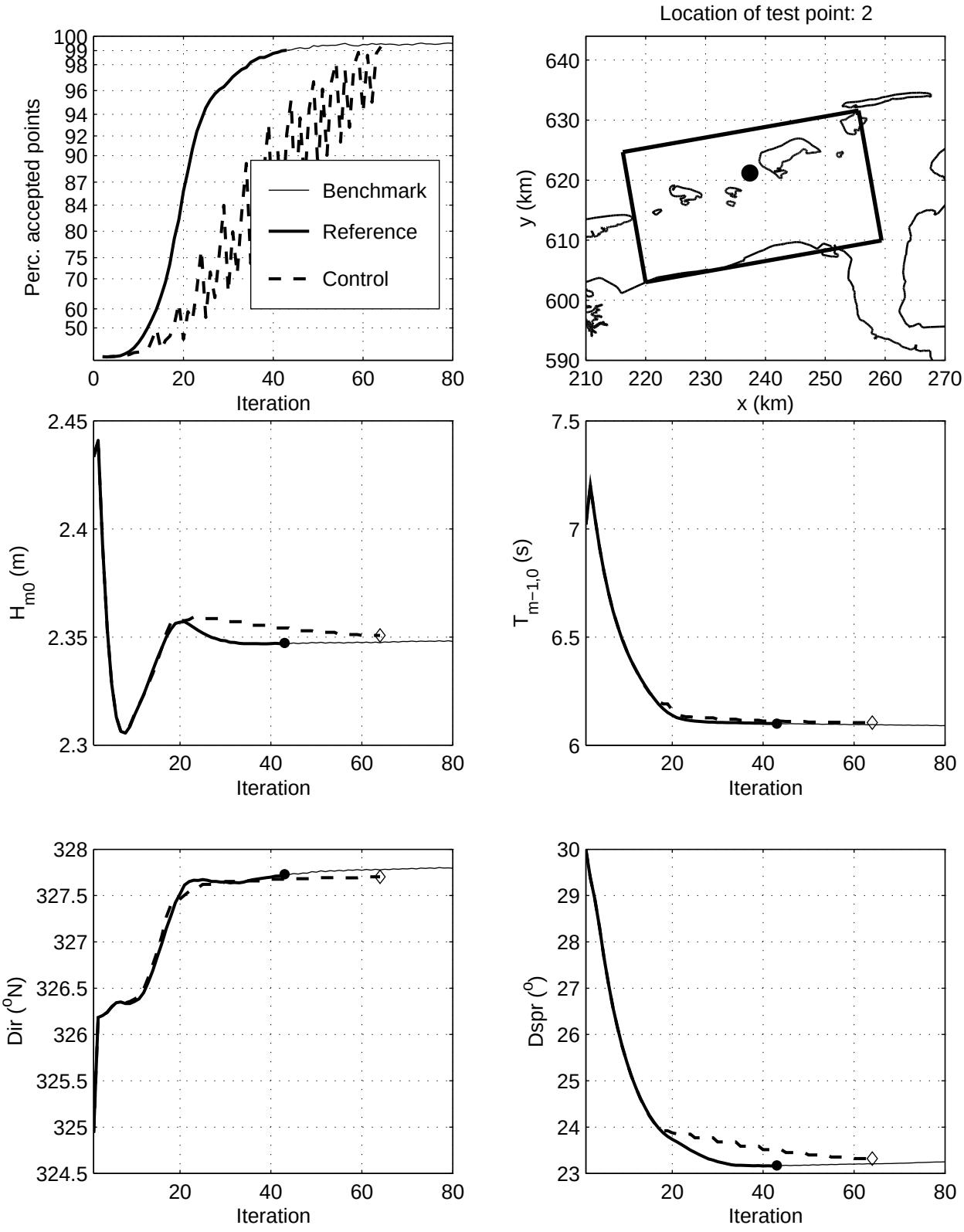

Convergence behaviour of the DDM simulation in the Eems−Dollard, Case: EEMS3A 2006/11/01 03:00, at point 2 Refresh domain every 05 iterations, for 1 iterations (C_r05_d01)		SWAN 40.51A
		Numerical efficiency SWAN
DELTARES & ALKYON	H5107.46/A2114	Fig. 5.26

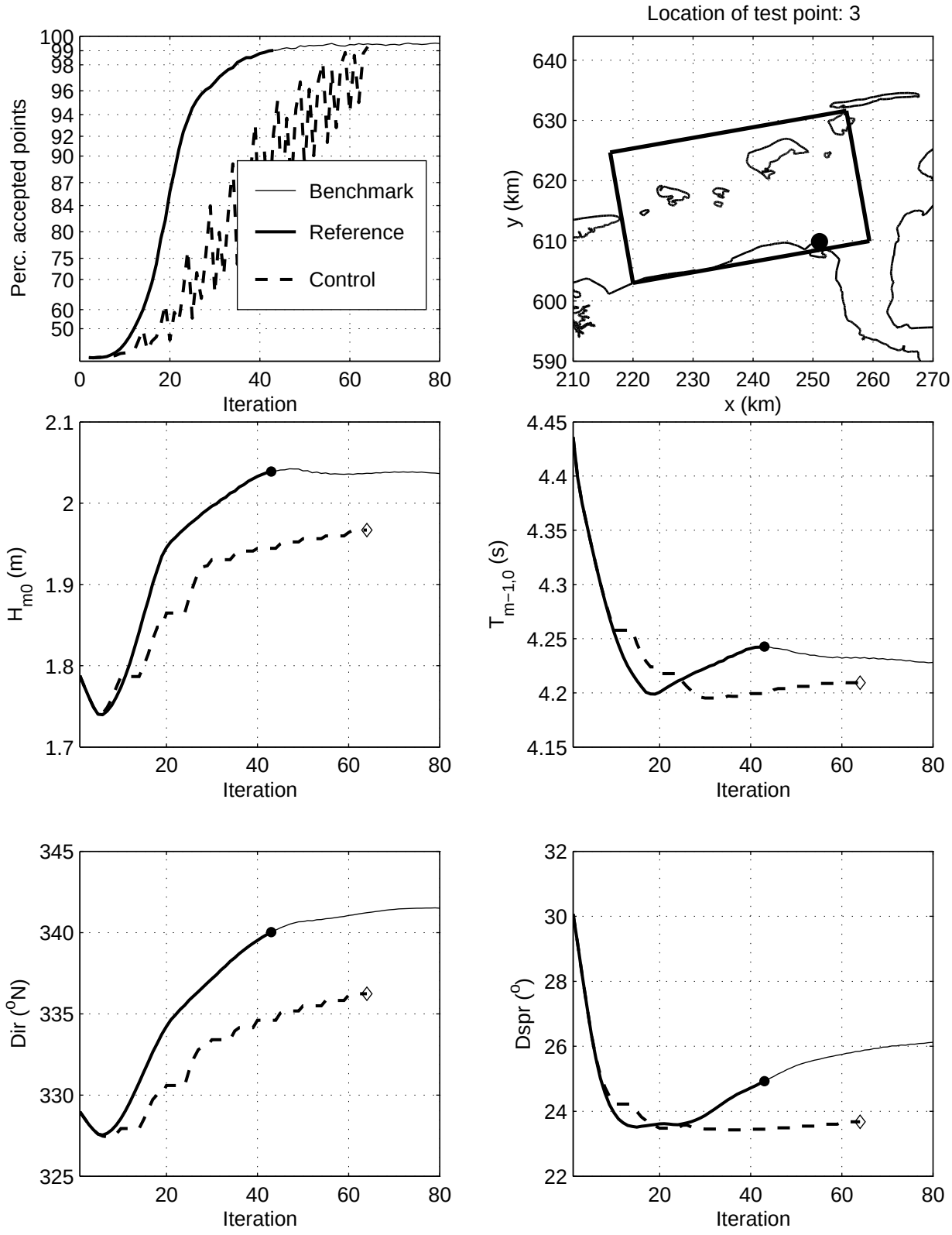

Convergence behaviour of the DDM simulation in the Eems−Dollard, Case: EEMS3A 2006/11/01 03:00, at point 3 Refresh domain every 05 iterations, for 1 iterations (C_r05_d01)		SWAN 40.51A
		Numerical efficiency SWAN
DELTARES & ALKYON	H5107.46/A2114	Fig. 5.27

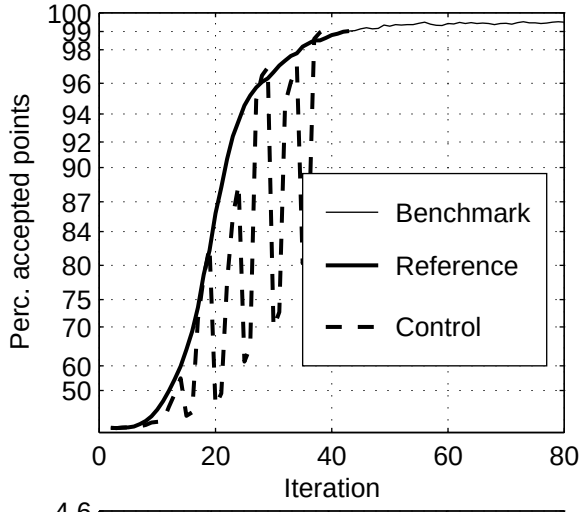

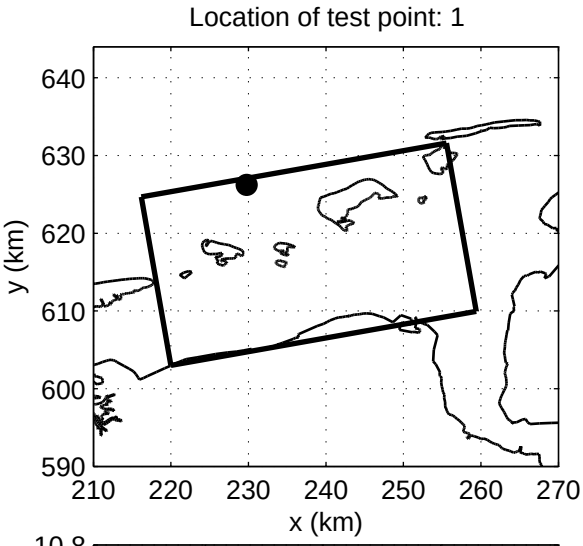

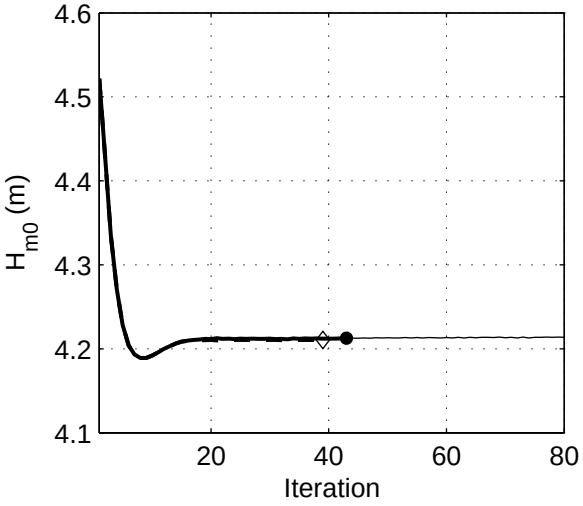

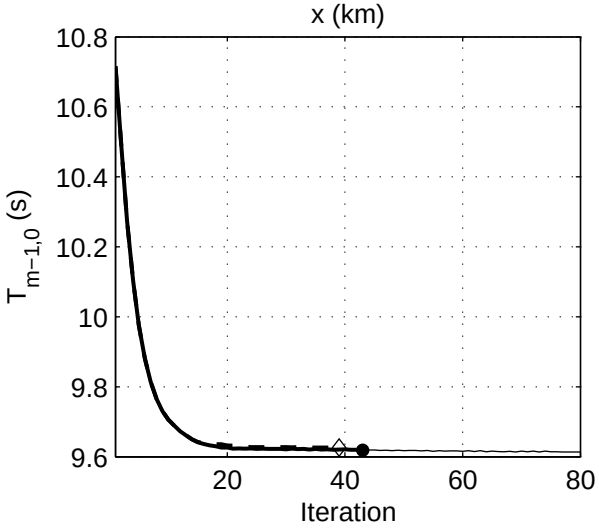

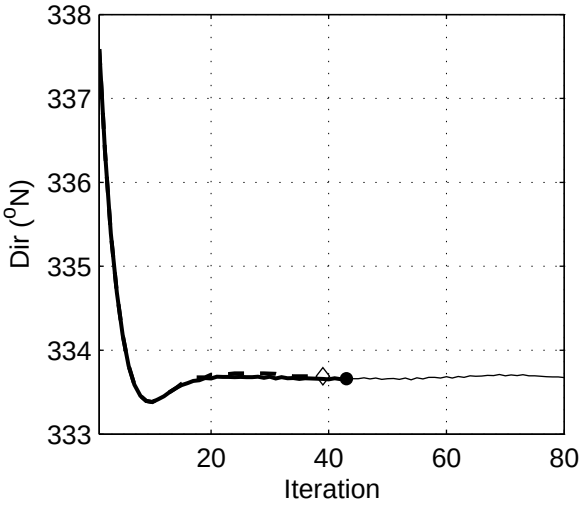

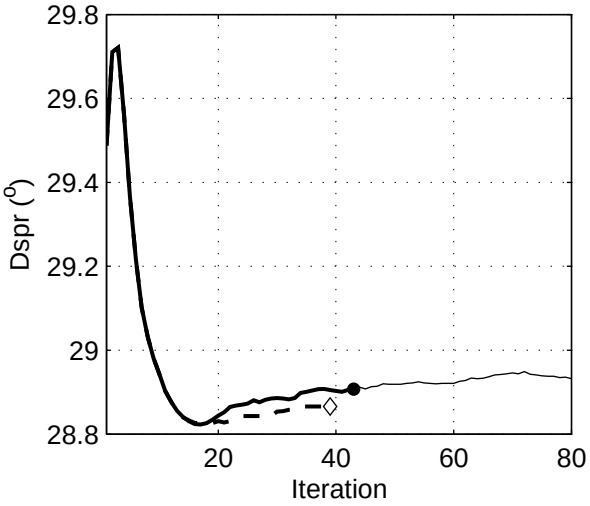

Convergence behaviour of the DDM simulation in the Eems−Dollard, Case: EEMS3A 2006/11/01 03:00, at point 1 Refresh domain every 10 iterations, for 5 iterations (C_r10_d05)		SWAN 40.51A
		Numerical efficiency SWAN
DELTARES & ALKYON	H5107.46/A2114	Fig. 5.28

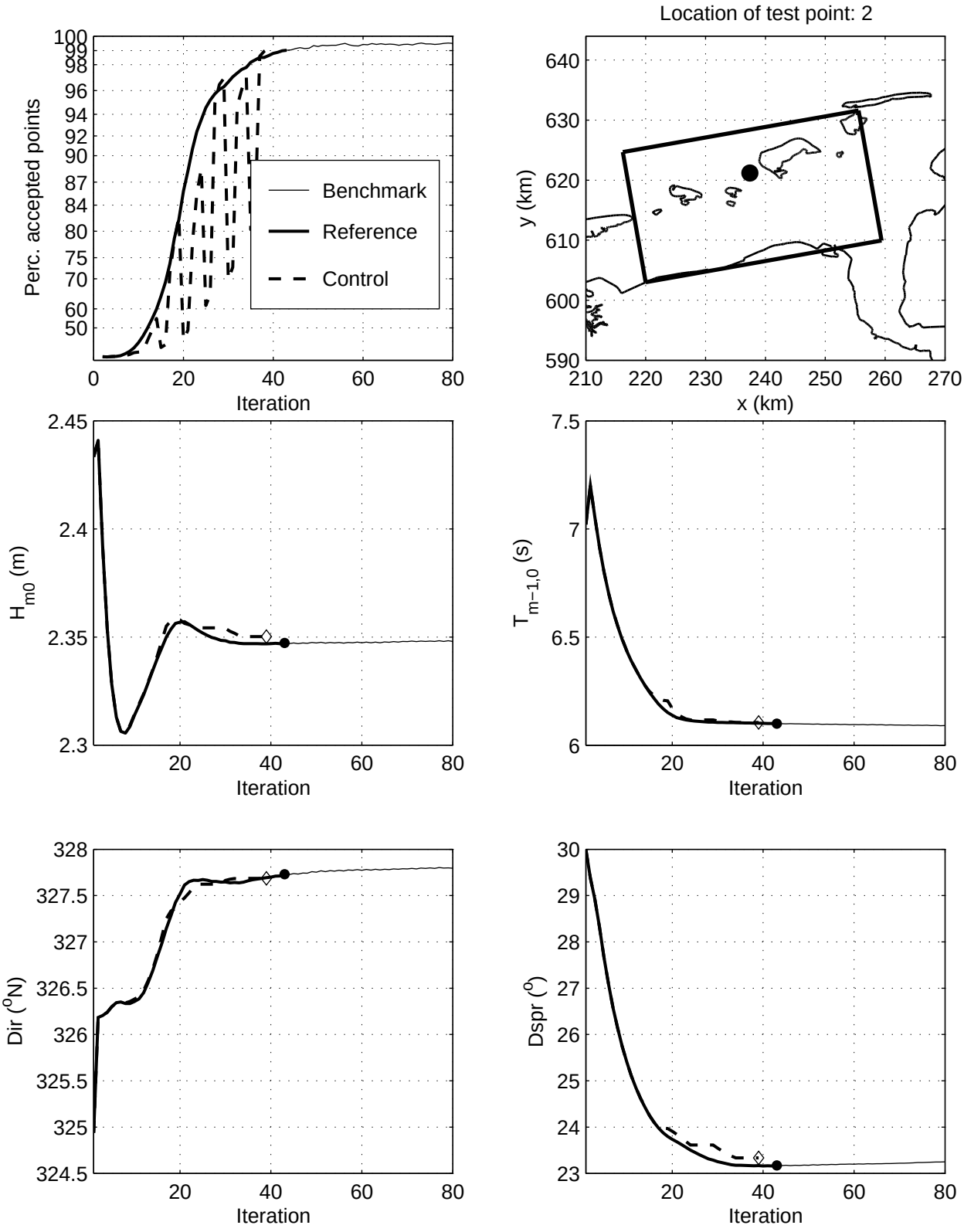

Convergence behaviour of the DDM simulation in the Eems−Dollard, Case: EEMS3A 2006/11/01 03:00, at point 2 Refresh domain every 10 iterations, for 5 iterations (C_r10_d05)		SWAN 40.51A
		Numerical efficiency SWAN
DELTARES & ALKYON	H5107.46/A2114	Fig. 5.29

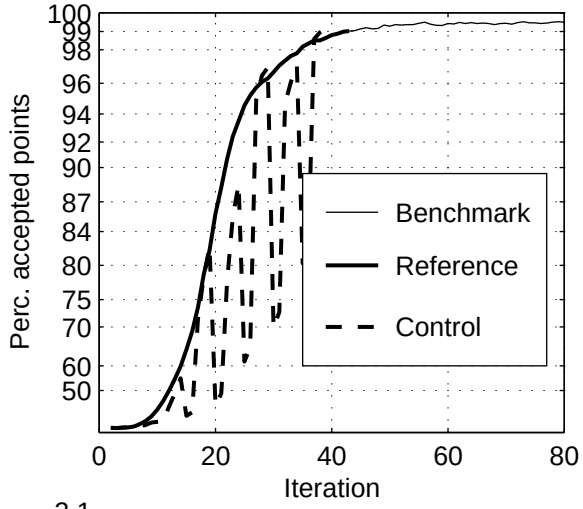

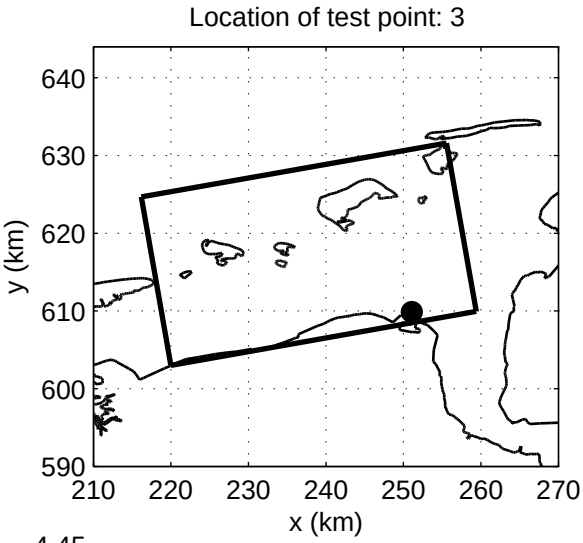

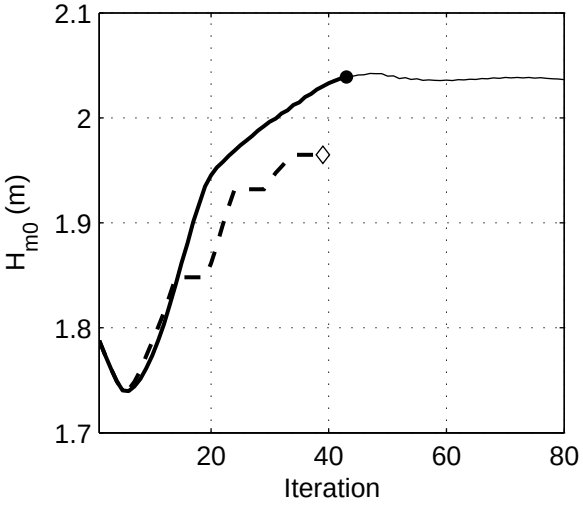

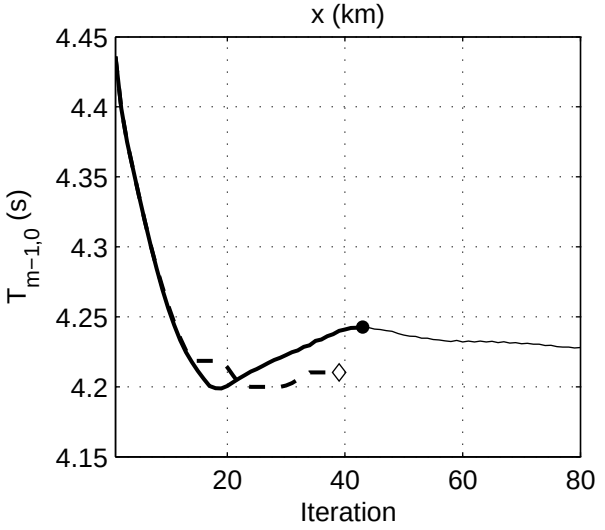

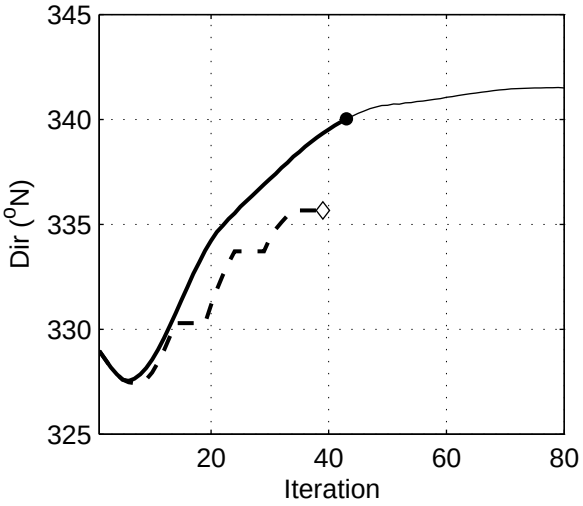

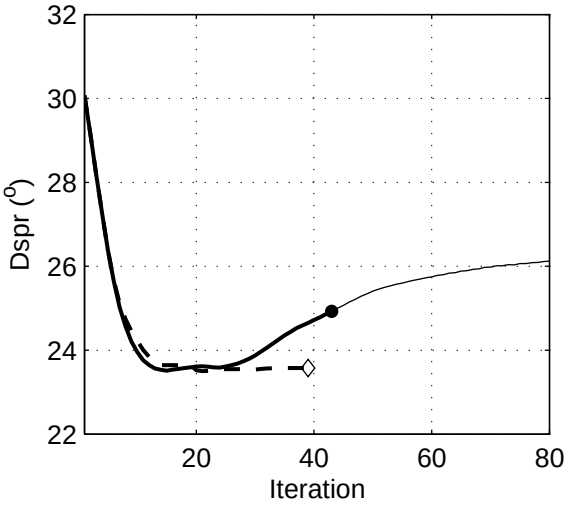

Convergence behaviour of the DDM simulation in the Eems−Dollard, Case: EEMS3A 2006/11/01 03:00, at point 3 Refresh domain every 10 iterations, for 5 iterations (C_r10_d05)		SWAN 40.51A
		Numerical efficiency SWAN
DELTARES & ALKYON	H5107.46/A2114	Fig. 5.30

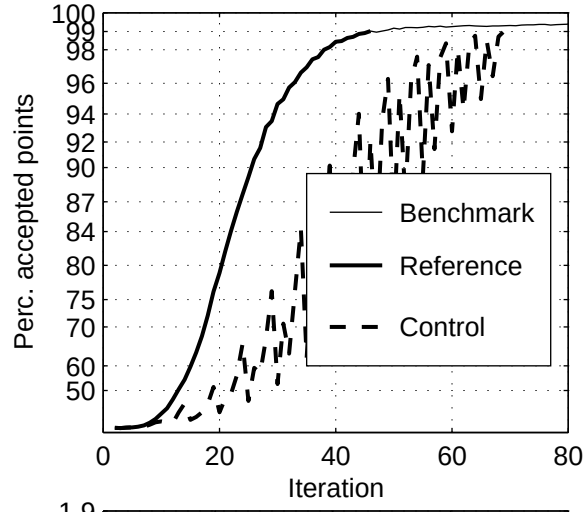

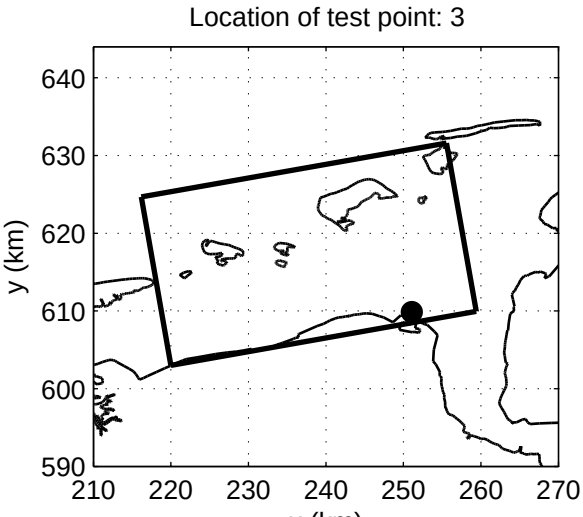

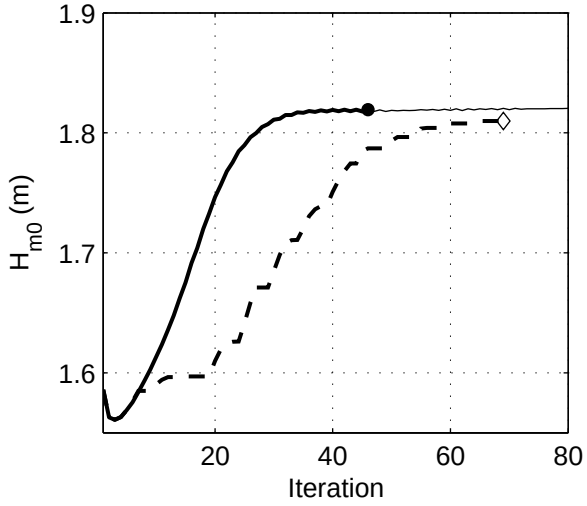

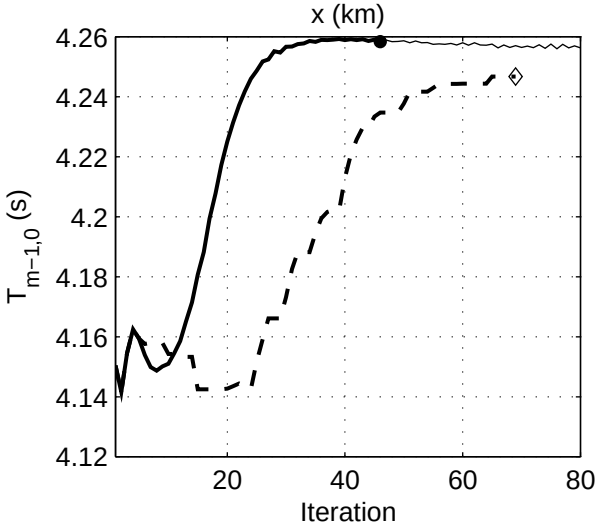

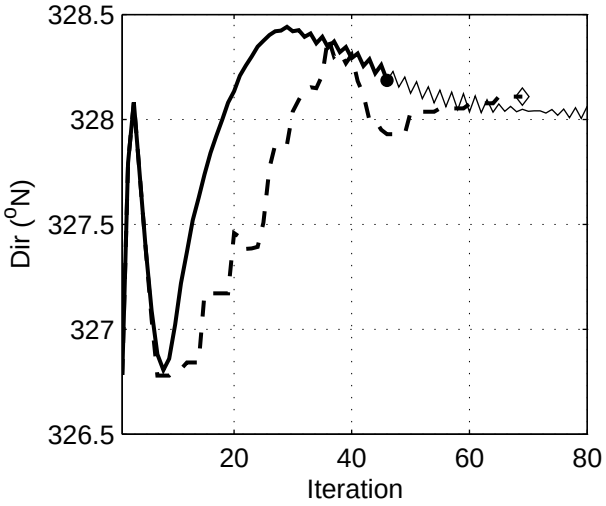

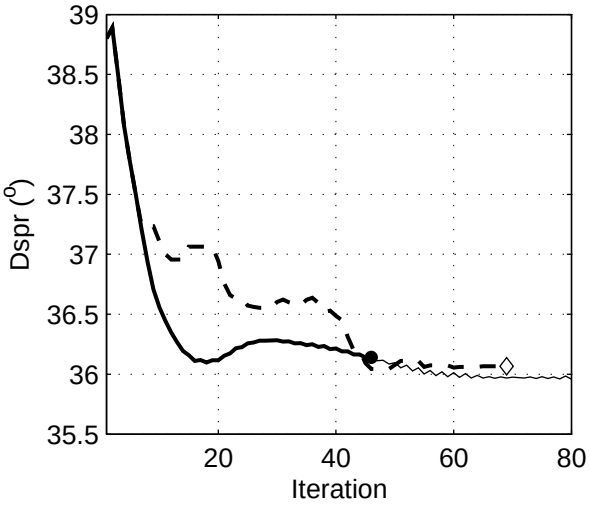

Convergence behaviour of the DDM simulation in the Eems−Dollard, Case: EEMS3A 2006/11/01 09:30, at point 3 Refresh domain every 05 iterations, for 1 iterations (C_r05_d01)		SWAN 40.51A
		Numerical efficiency SWAN
DELTARES & ALKYON	H5107.46/A2114	Fig. 5.31

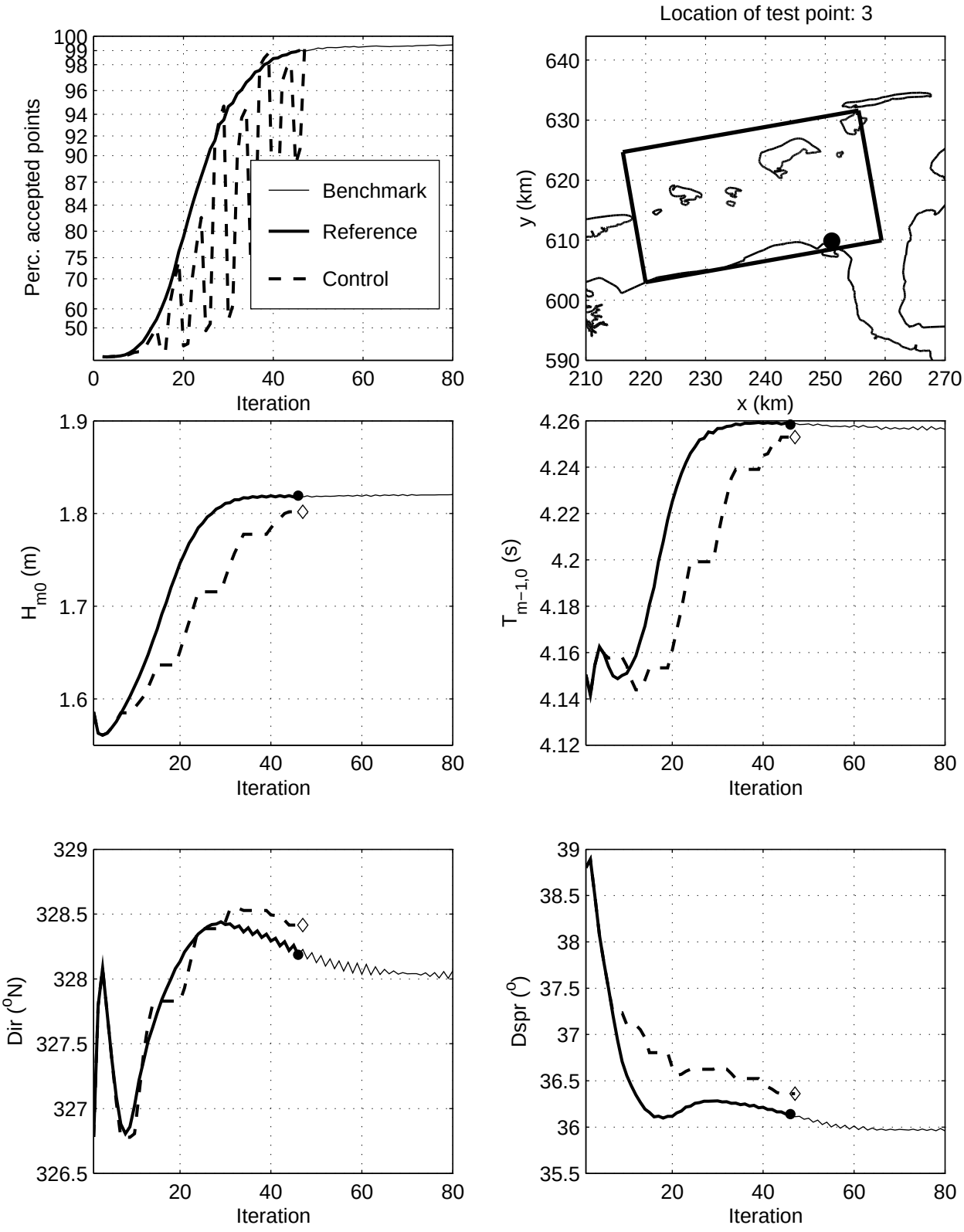

Convergence behaviour of the DDM simulation in the Eems−Dollard, Case: EEMS3A 2006/11/01 09:30, at point 3 Refresh domain every 10 iterations, for 5 iterations (C_r10_d05)		SWAN 40.51A
		Numerical efficiency SWAN
DELTARES & ALKYON	H5107.46/A2114	Fig. 5.32

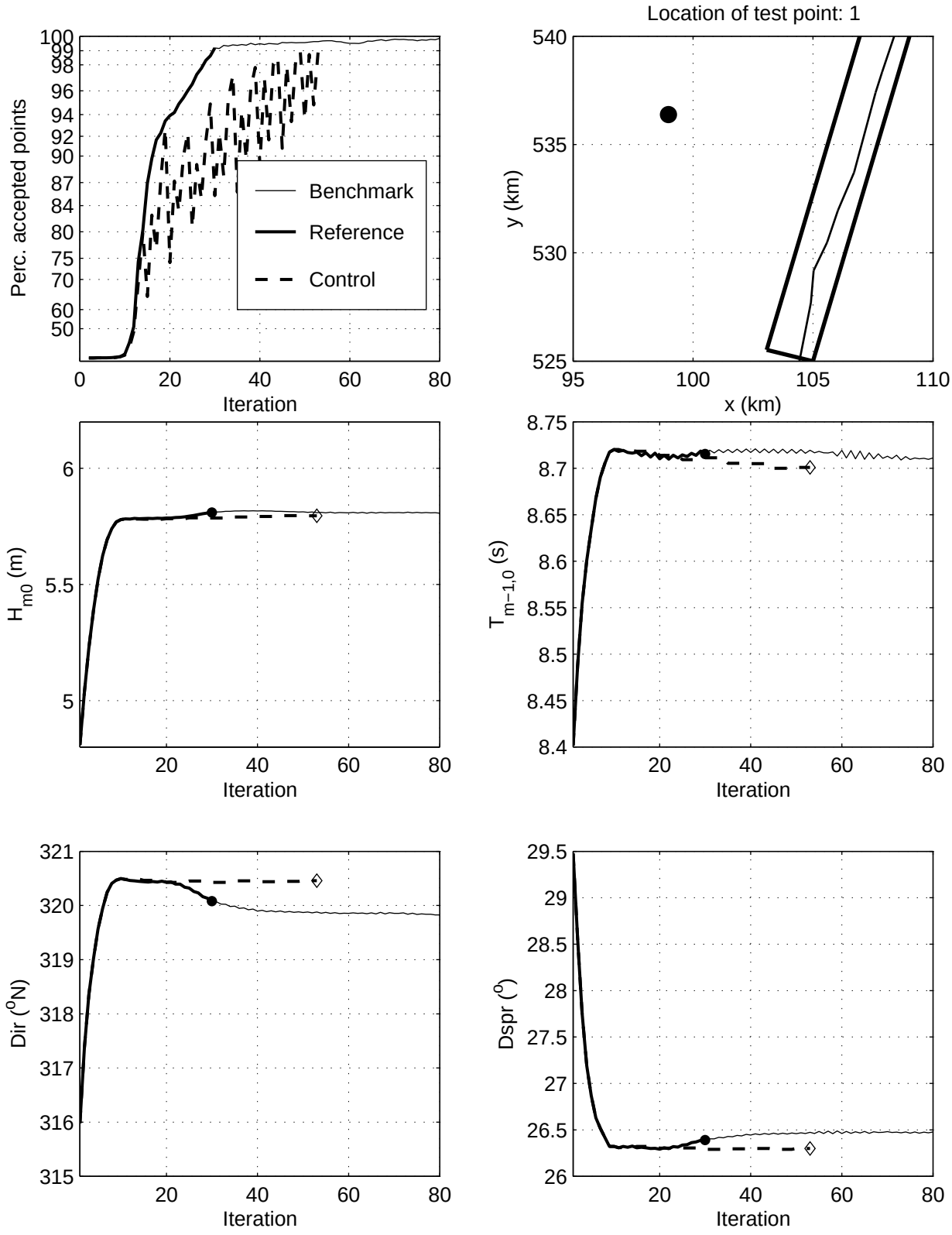

Convergence behaviour of the DDM simulation along the Dutch coast near Petten, Case: PETTEN 1995/01/01 10:00, at point 1 Refresh domain every 05 iterations, for 1 iterations (C_r05_d01)		SWAN 40.51A
		Numerical efficiency SWAN
DELTARES & ALKYON	H5107.46/A2114	Fig. 5.33

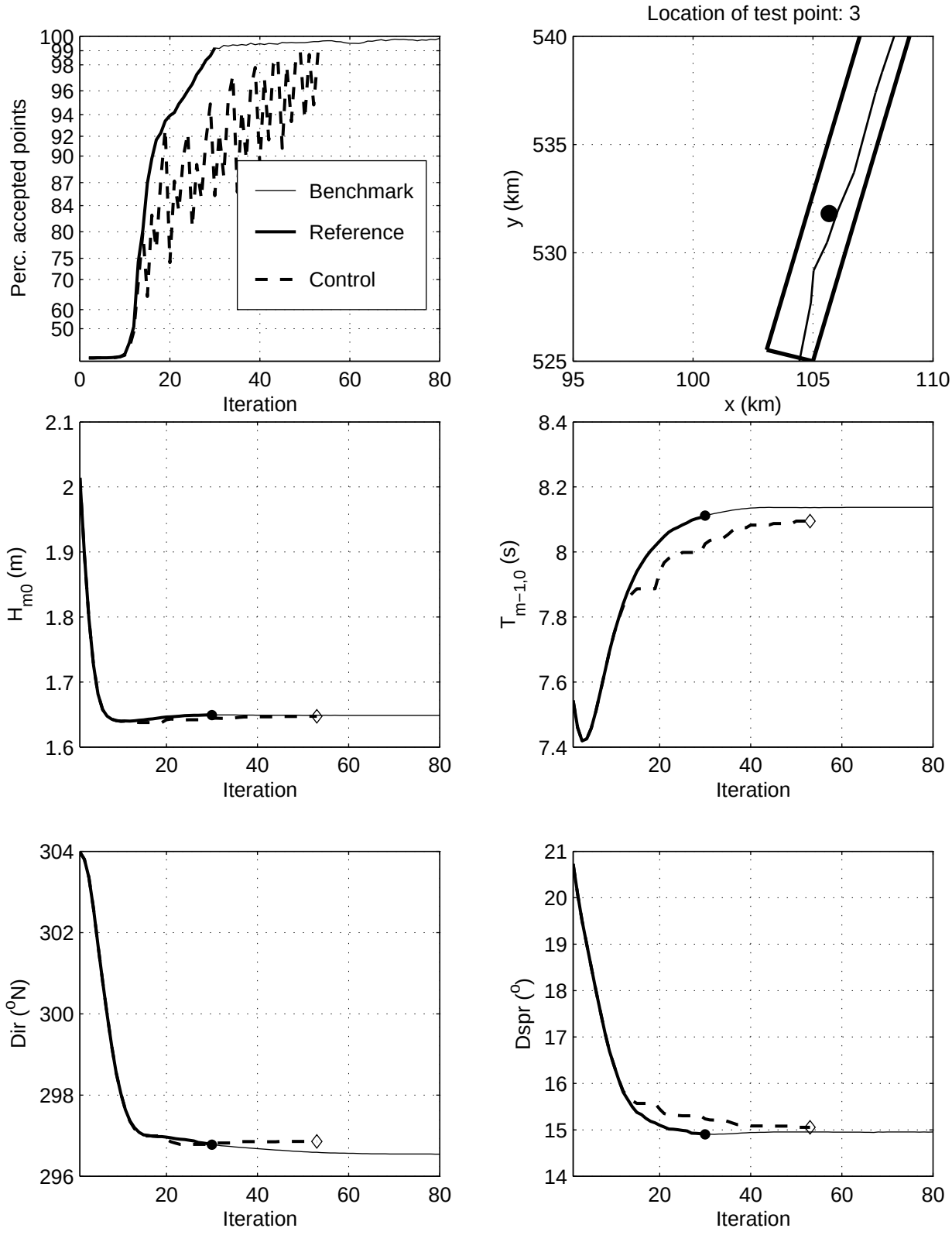

Convergence behaviour of the DDM simulation along the Dutch coast near Petten, Case: PETTEN 1995/01/01 10:00, at point 3 Refresh domain every 05 iterations, for 1 iterations (C_r05_d01)		SWAN 40.51A
		Numerical efficiency SWAN
DELTARES & ALKYON	H5107.46/A2114	Fig. 5.34

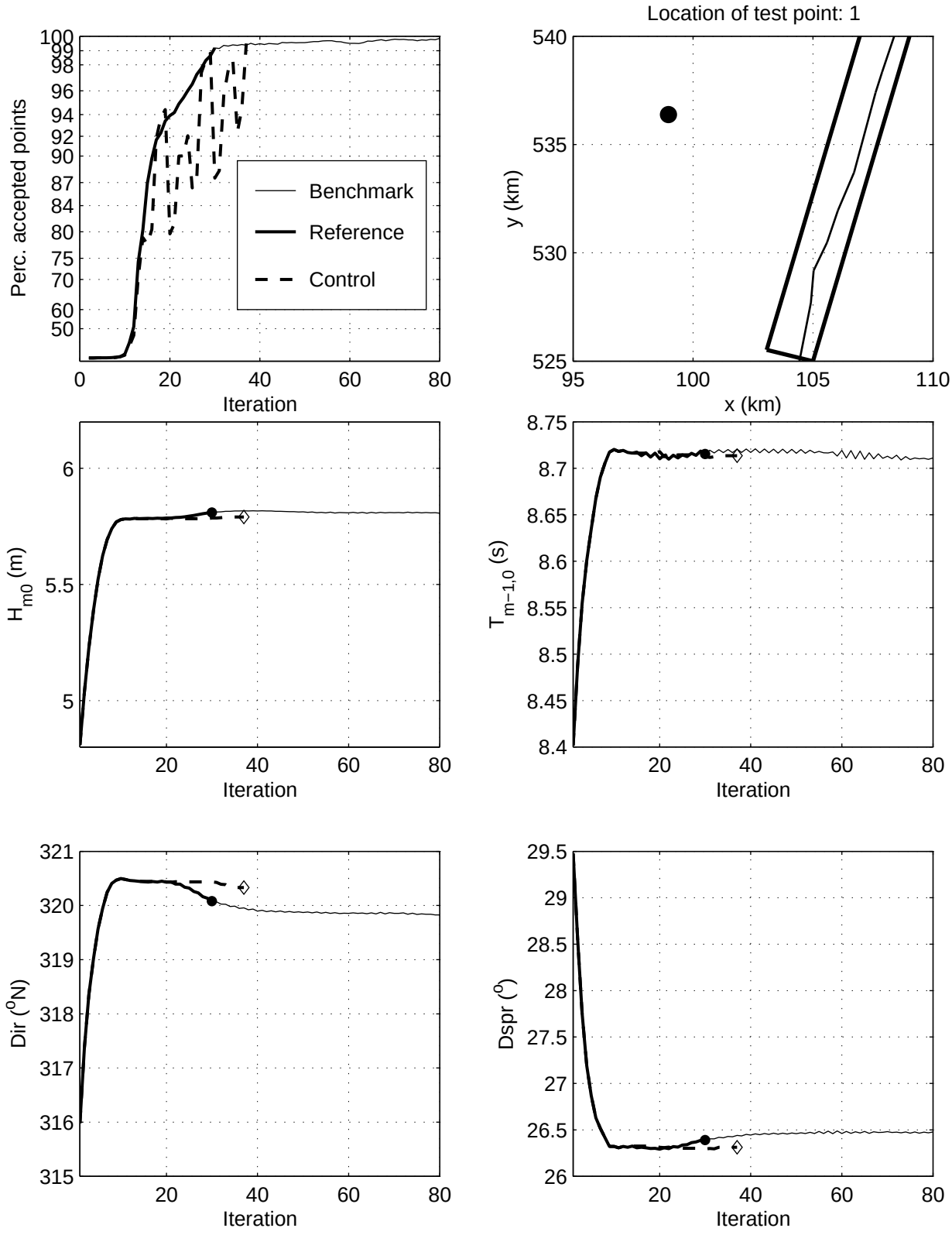

Convergence behaviour of the DDM simulation along the Dutch coast near Petten, Case: PETTEN 1995/01/01 10:00, at point 1 Refresh domain every 10 iterations, for 5 iterations (C_r10_d05)		SWAN 40.51A
		Numerical efficiency SWAN
DELTARES & ALKYON	H5107.46/A2114	Fig. 5.35

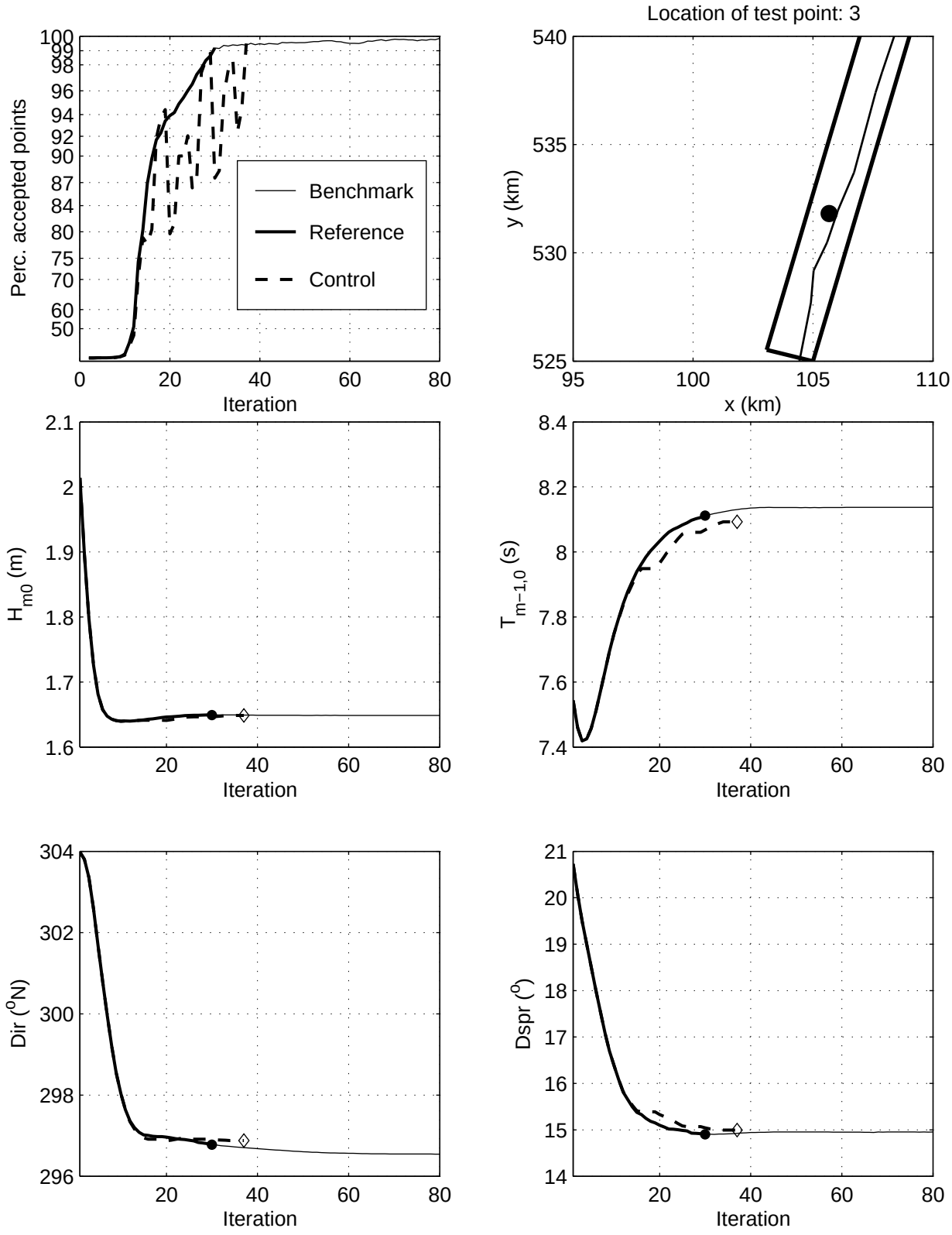

Convergence behaviour of the DDM simulation along the Dutch coast near Petten, Case: PETTEN 1995/01/01 10:00, at point 3 Refresh domain every 10 iterations, for 5 iterations (C_r10_d05)		SWAN 40.51A
		Numerical efficiency SWAN
DELTARES & ALKYON	H5107.46/A2114	Fig. 5.36

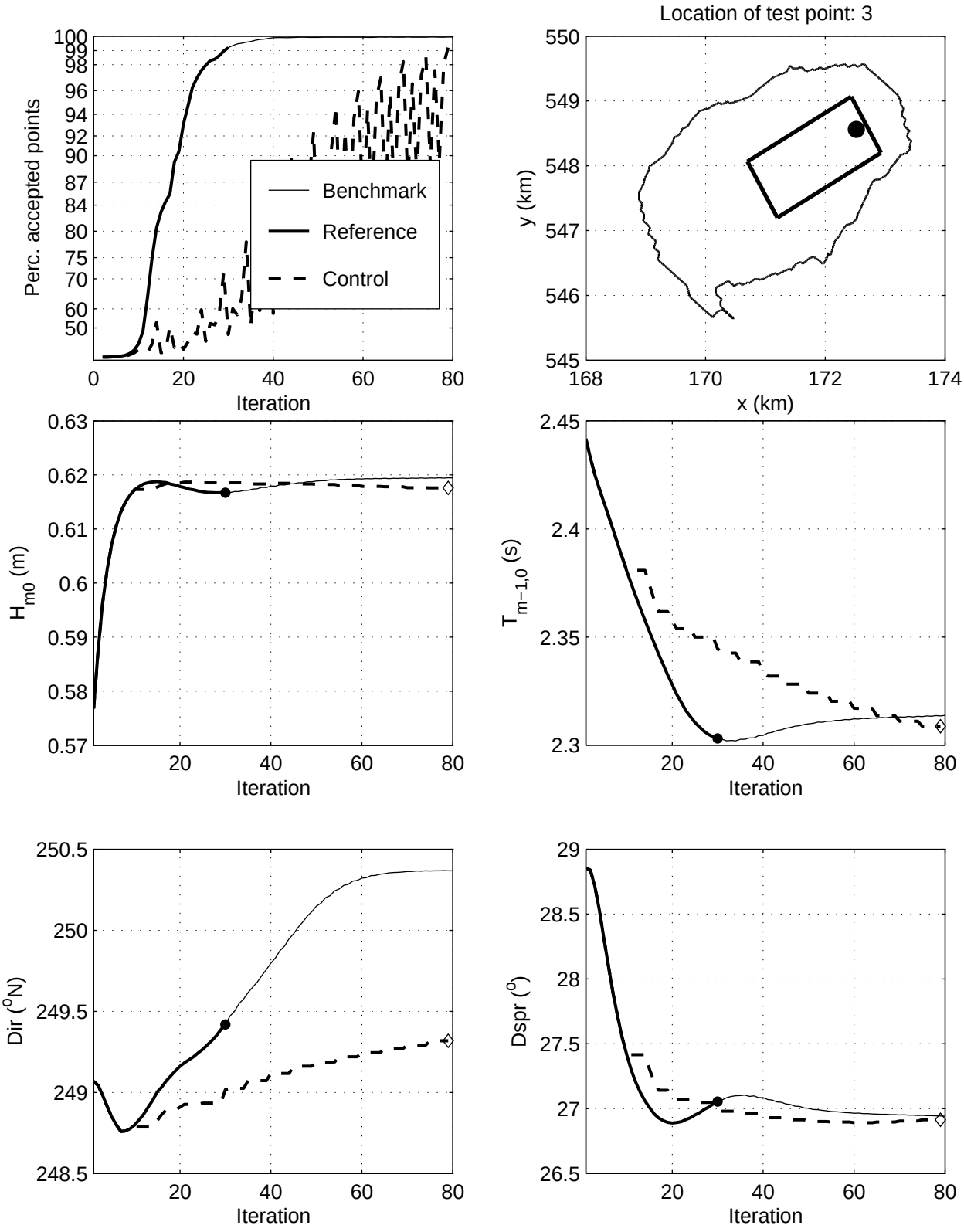

Convergence behaviour of the DDM simulation in Lake Sloten, Case: SLE 2002/10/27 15:00, at point 3 Refresh domain every 05 iterations, for 1 iterations (C_r05_d01)		SWAN 40.51A
		Numerical efficiency SWAN
DELTARES & ALKYON	H5107.46/A2114	Fig. 5.37

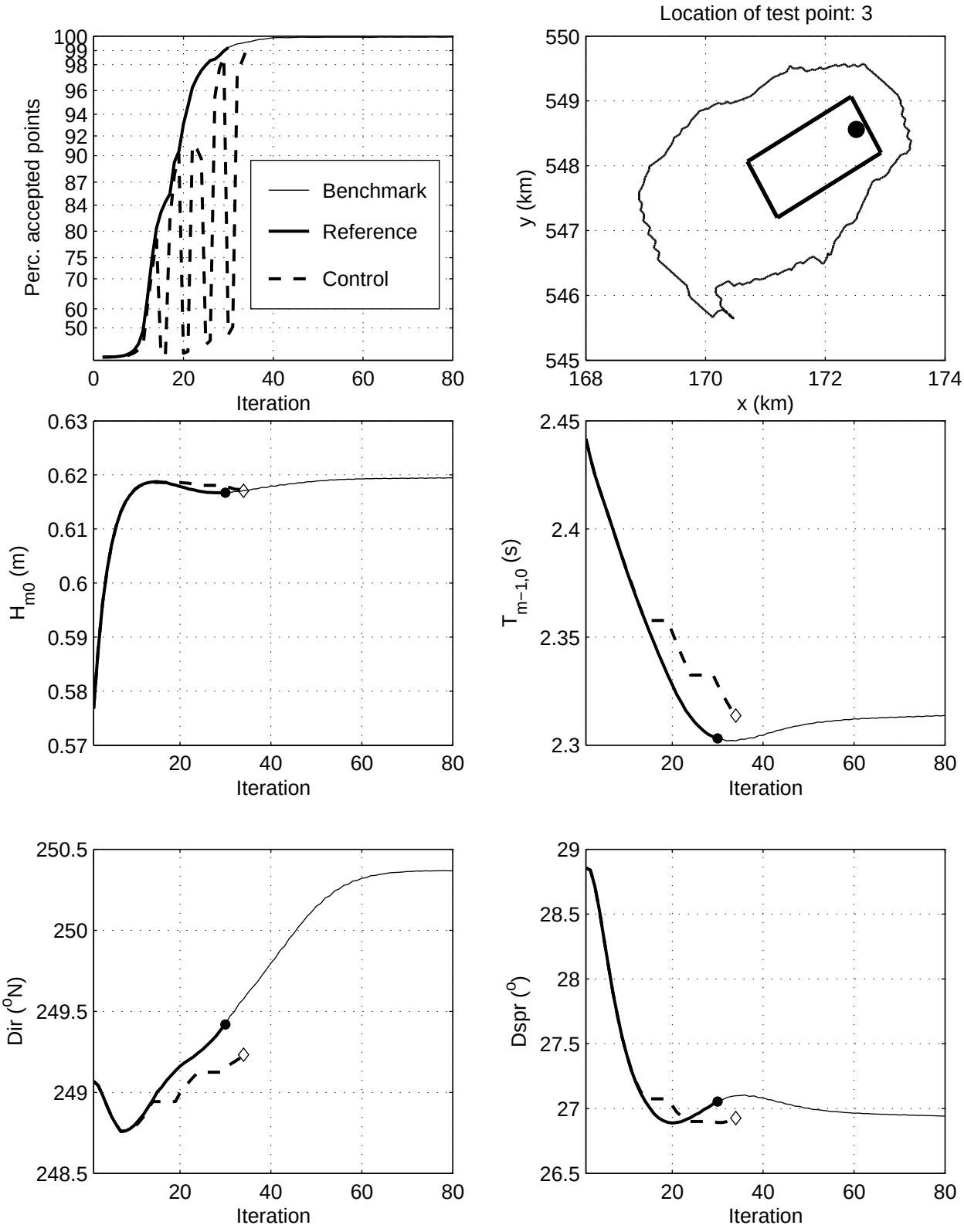

Convergence behaviour of the DDM simulation in Lake Sloten, Case: SLE 2002/10/27 15:00, at point 3 Refresh domain every 10 iterations, for 5 iterations (C_r10_d05)		SWAN 40.51A
		Numerical efficiency SWAN
DELTARES & ALKYON	H5107.46/A2114	Fig. 5.38

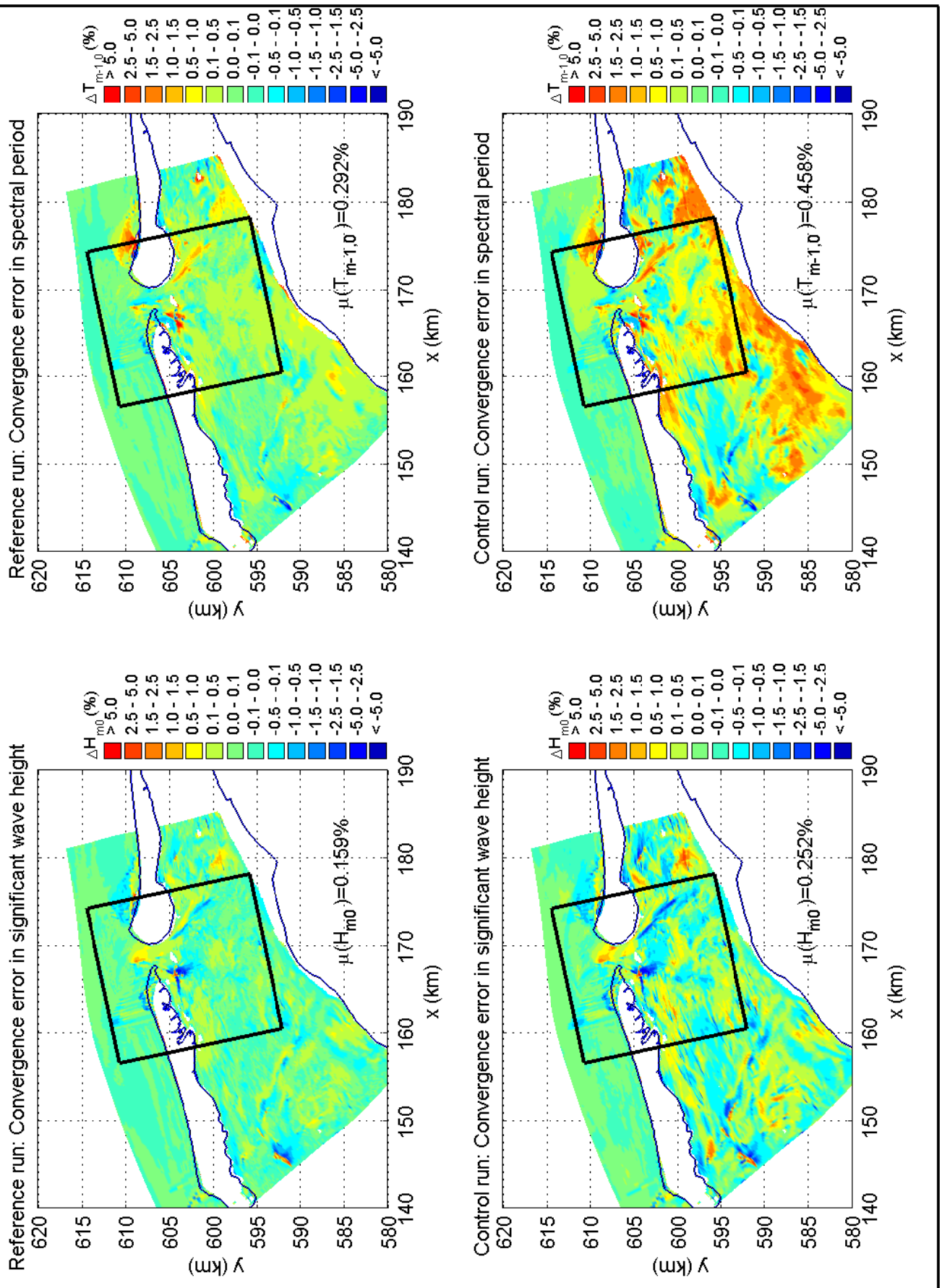

Convergence errors in H_{m0} and $T_{m-1,0}$ for the DDM simulation in the Amelander Zeegat, Case: AZG3A 2005/01/02 10:00 Refresh domain every 05 iterations, for 1 iterations (c_r05_d01)		SWAN 40.51A
		Numerical efficiency SWAN
DELTARES & ALKYON	H5107.46/A2114	Fig. 5.39

Convergence errors in Dir and Dspr for the DDM simulation in the Amelander Zeegat, Case: AZG3A 2005/01/02 10:00
Refresh domain every 05 iterations, for 1 iterations (c_r05_d01)

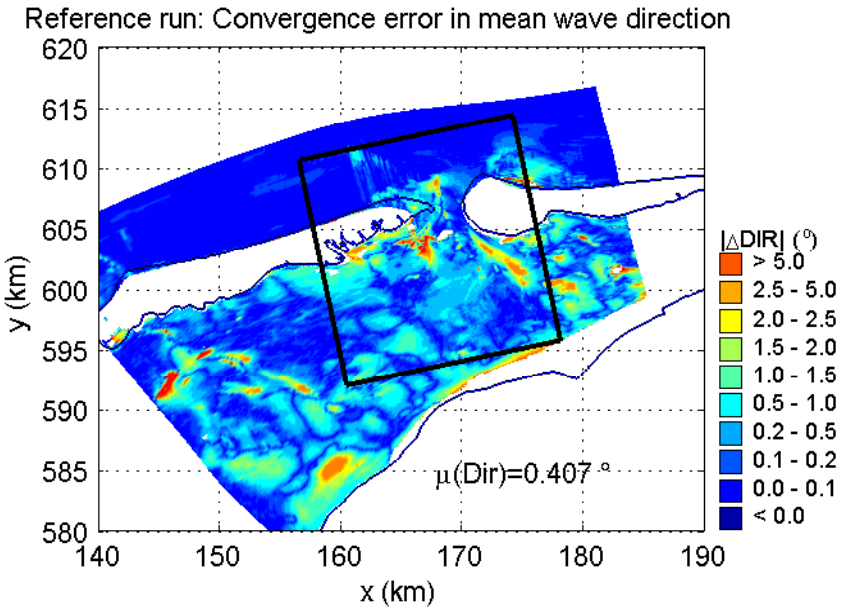

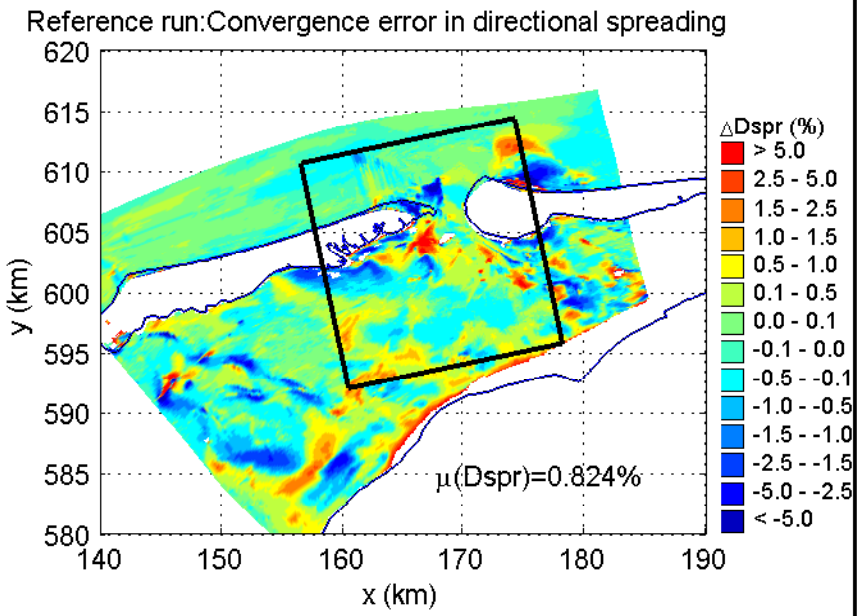

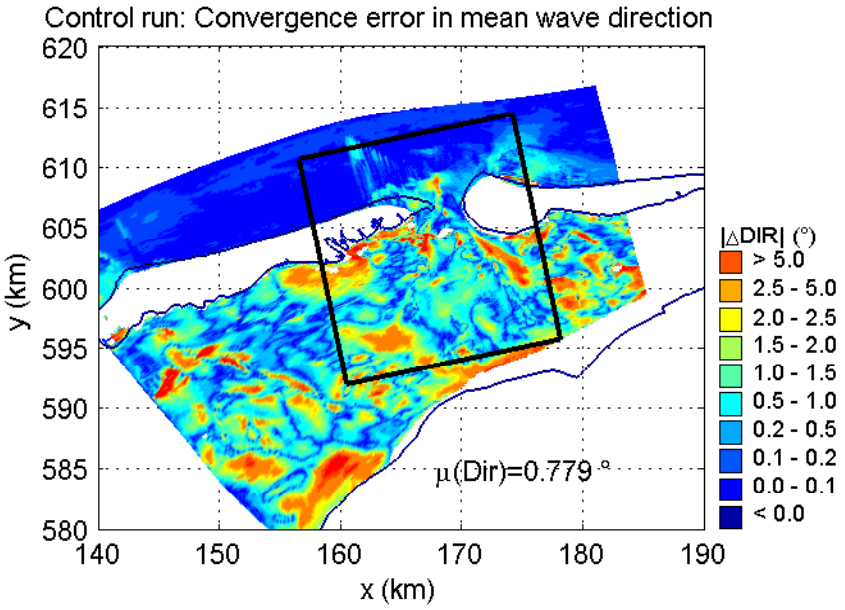

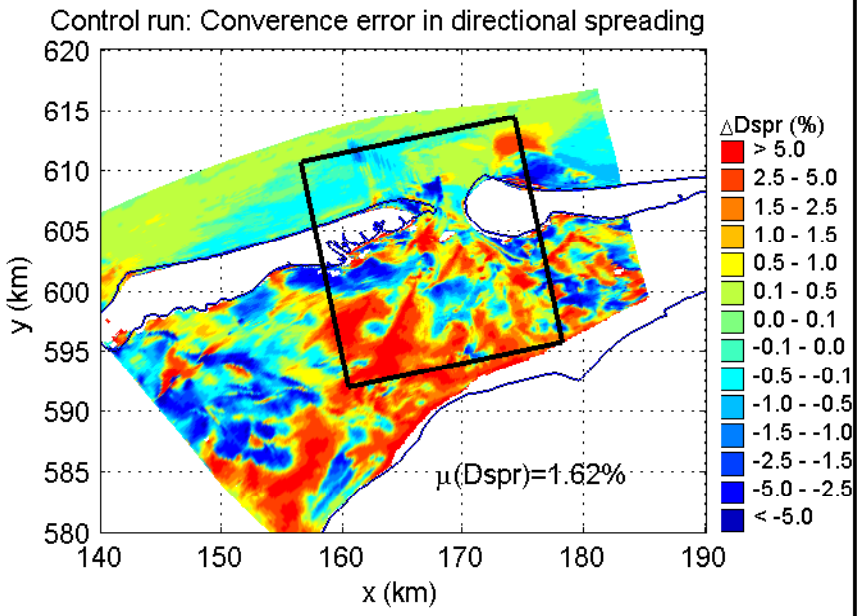

DELTARES & ALKYON

H5107.46/A2114

Numerical efficiency SWAN

SWAN 40.51A

Fig. 5.40

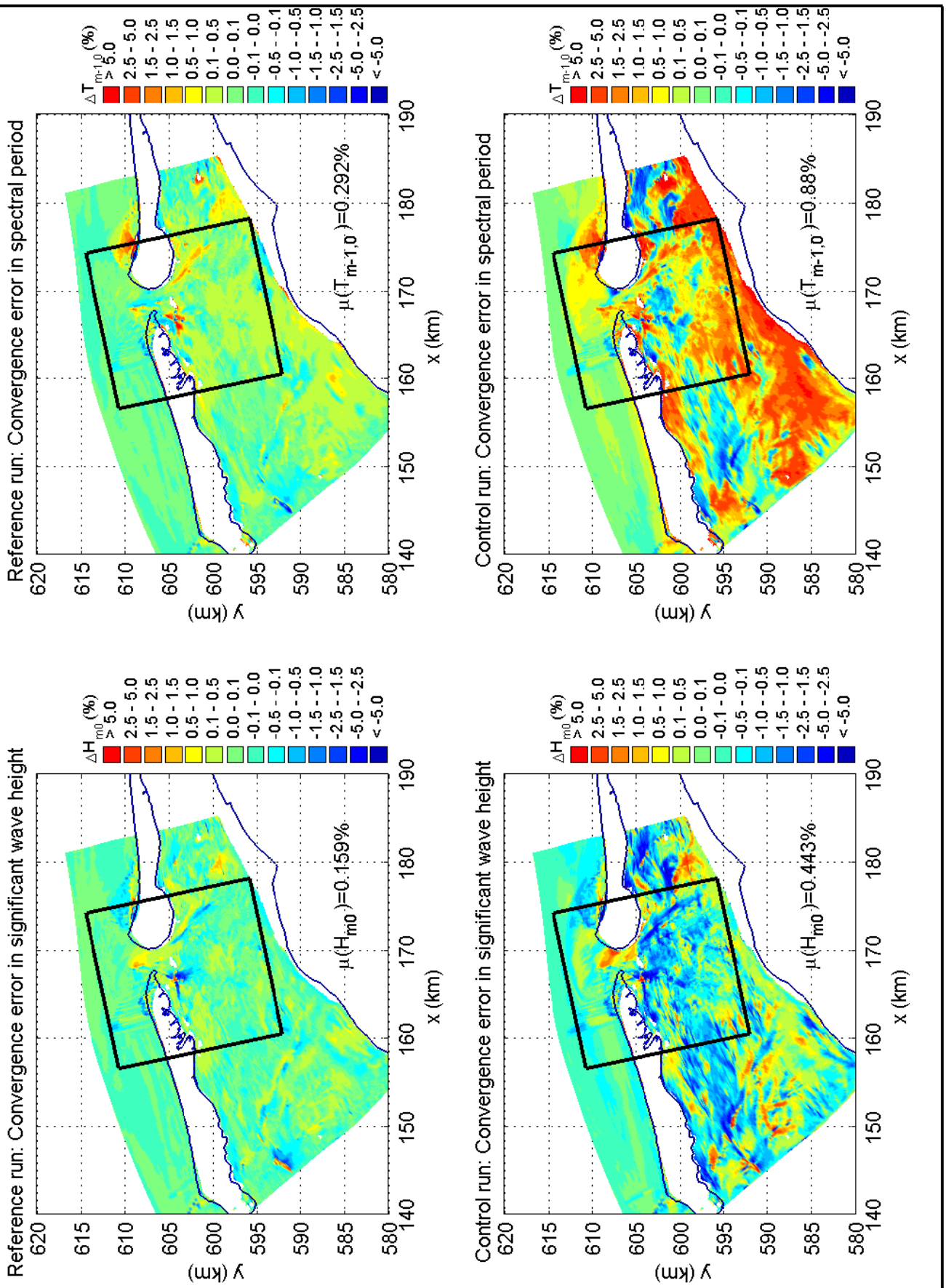

Convergence errors in H_{m0} and $T_{m-1,0}$ for the DDM simulation in the Amelander Zeegat, Case: AZG3A 2005/01/02 10:00 Refresh domain every 10 iterations, for 1 iterations (c_r10_d01)		SWAN 40.51A
	Numerical efficiency SWAN	
DELTARES & ALKYON	H5107.46/A2114	Fig. 5.41

DELTARES & ALKYON

Convergence errors in Dir and Dspr for the DDM simulation in the Amelander Zeegat, Case: AZG3A 2005/01/02 10:00
Refresh domain every 10 iterations, for 1 iterations (c_r10_d01)

H5107.46/A2114

Numerical efficiency SWAN

SWAN 40.51A

Fig. 5.42

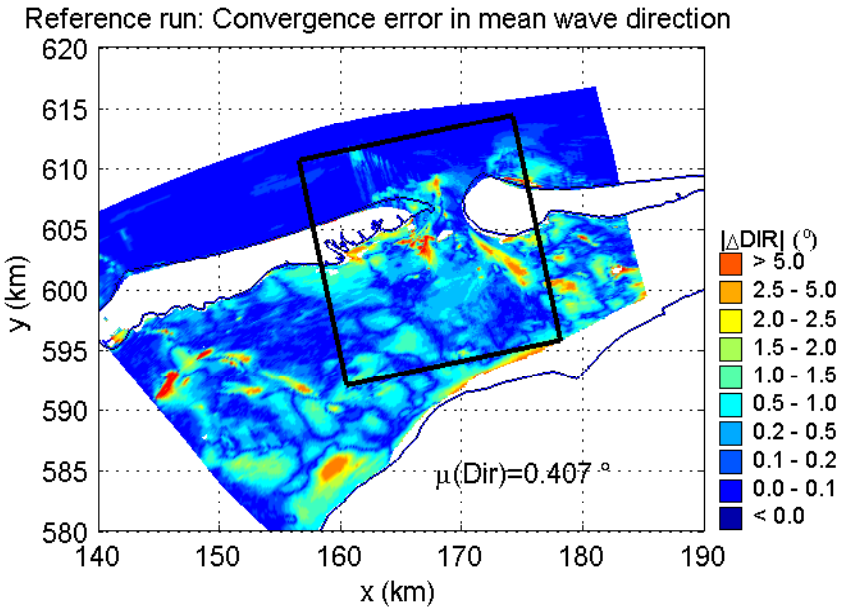

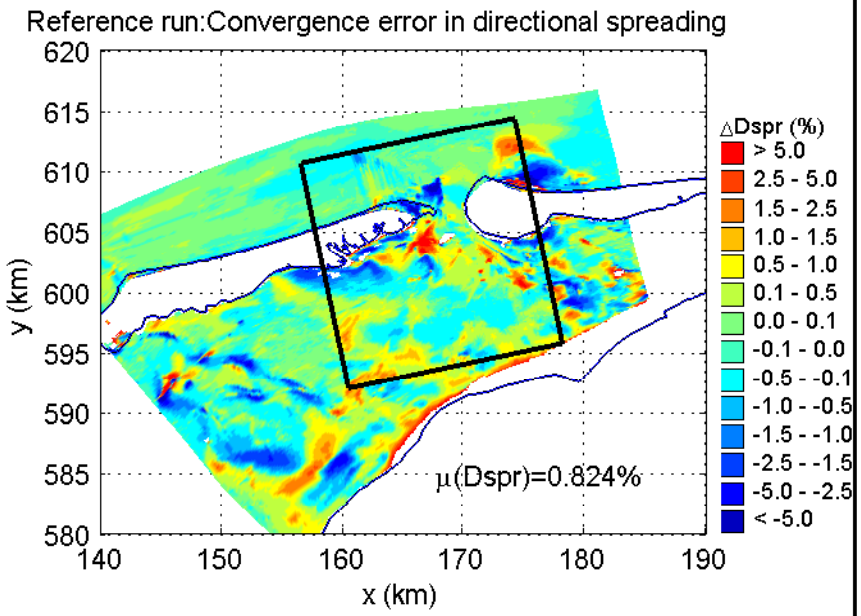

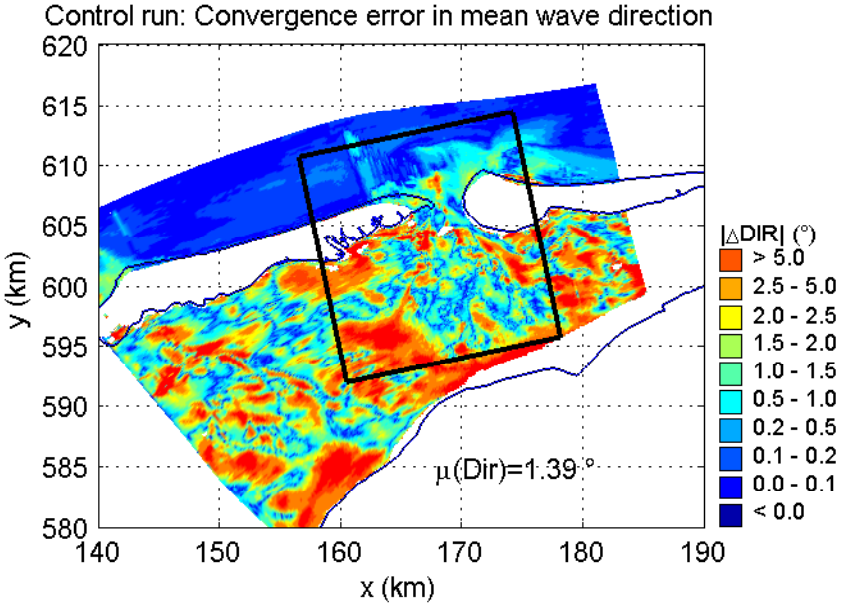

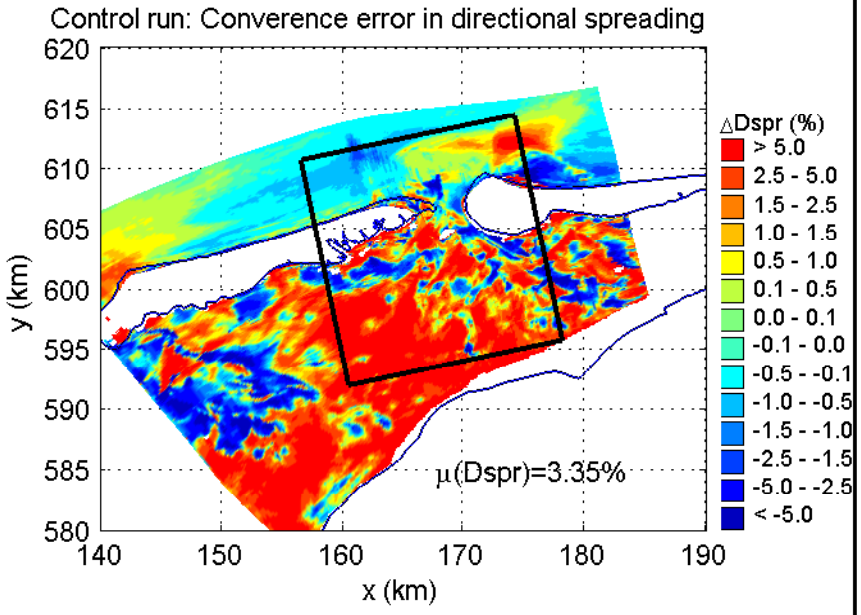

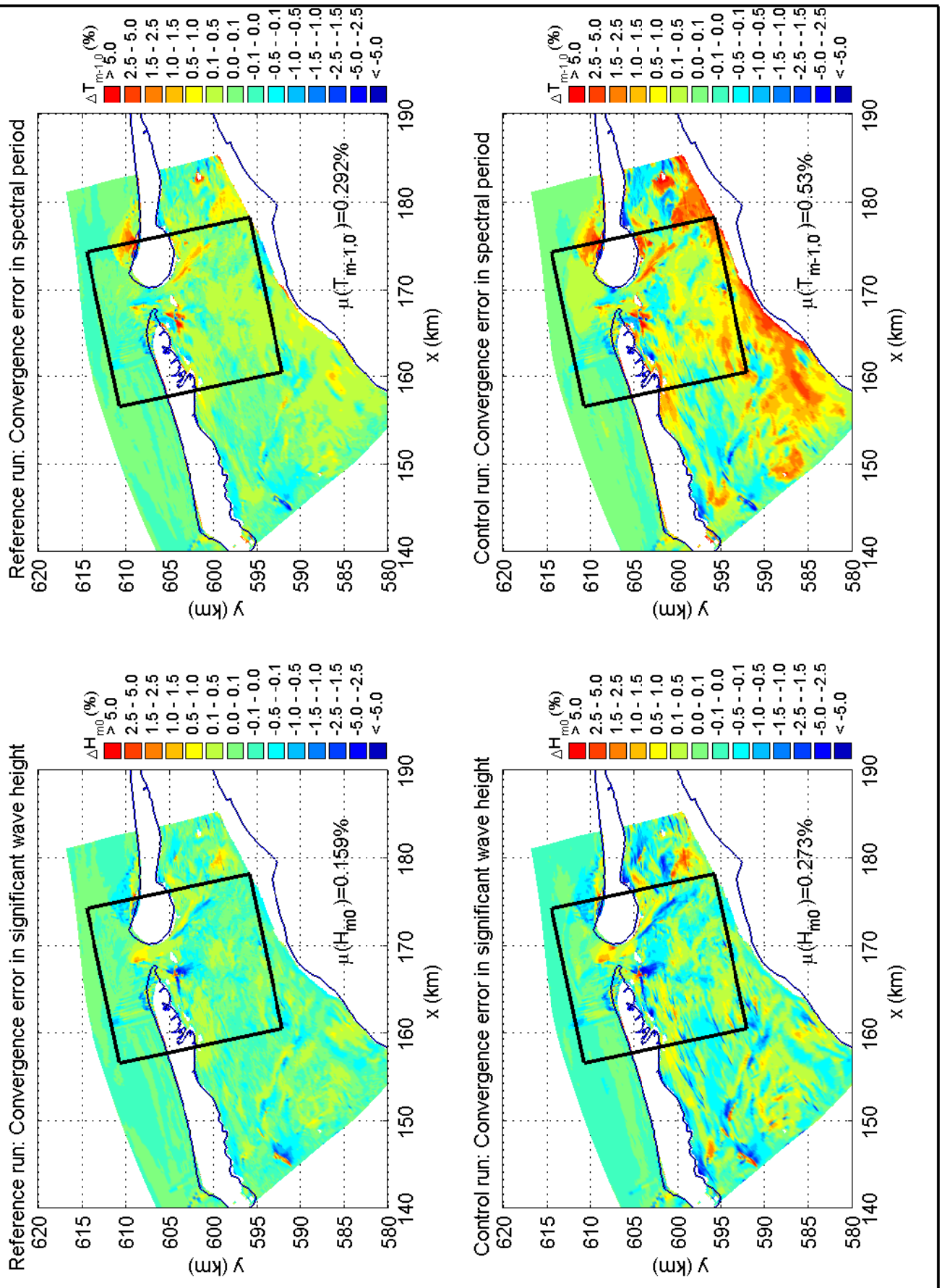

Convergence errors in H_{m0} and $T_{m-1,0}$ for the DDM simulation in the Amelander Zeegat, Case: AZG3A 2005/01/02 10:00 Refresh domain every 10 iterations, for 5 iterations (c_r10_d05)		SWAN 40.51A
		Numerical efficiency SWAN
DELTARES & ALKYON	H5107.46/A2114	Fig. 5.43

DELTARES & ALKYON

Convergence errors in Dir and Dspr for the DDM simulation in the Amelander Zeegat, Case: AZG3A 2005/01/02 10:00
Refresh domain every 10 iterations, for 5 iterations (c_r10_d05)

H5107.46/A2114

Numerical efficiency SWAN

SWAN 40.51A

Fig. 5.44

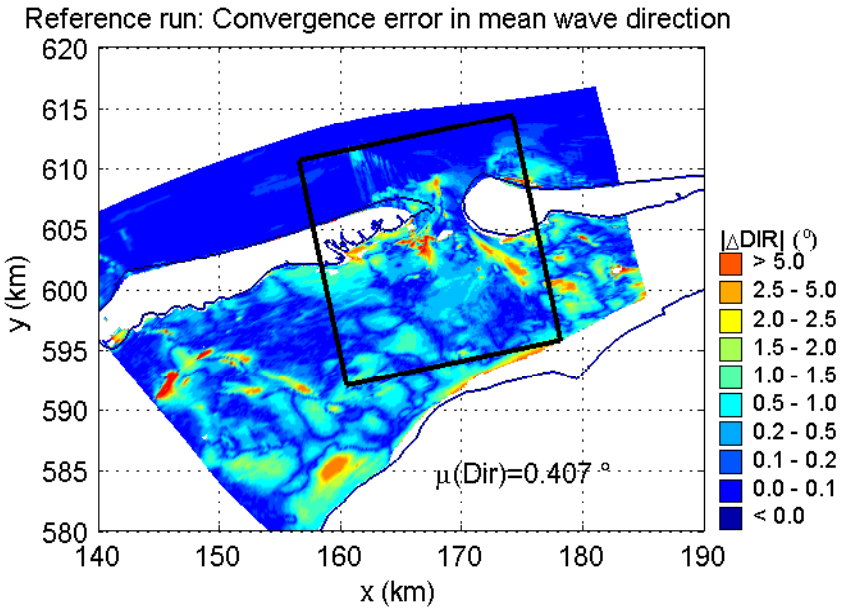

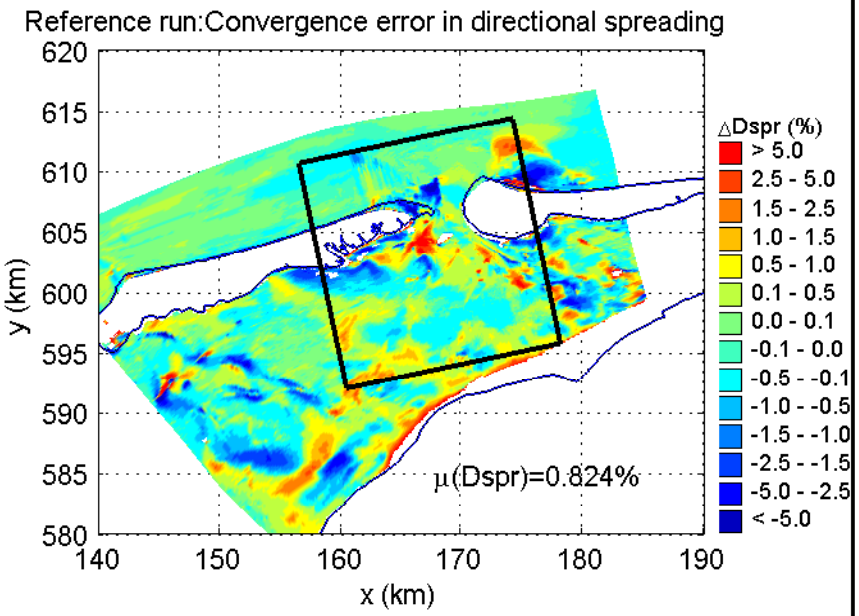

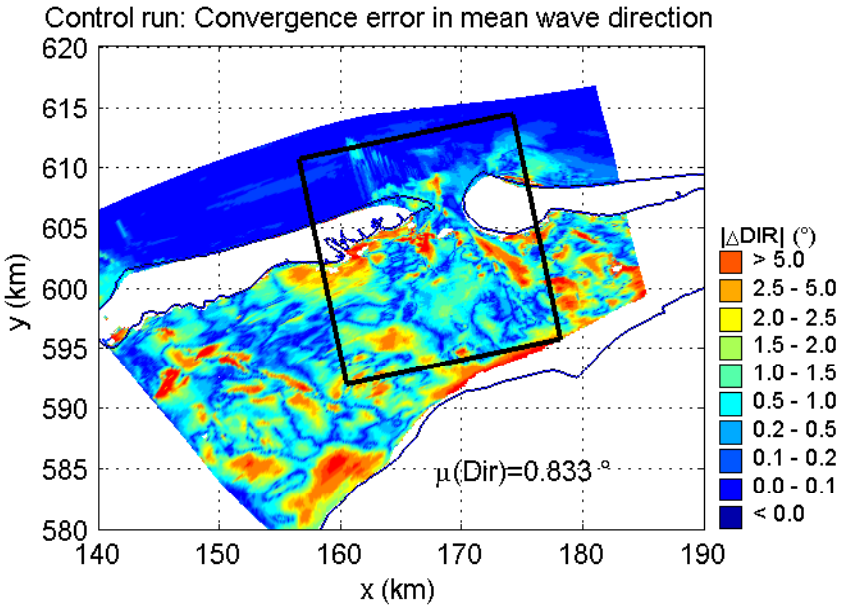

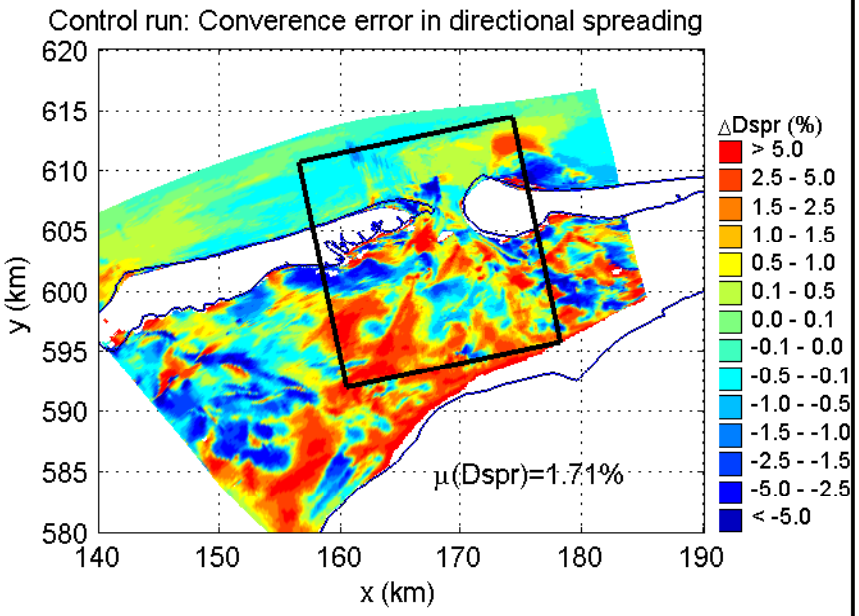

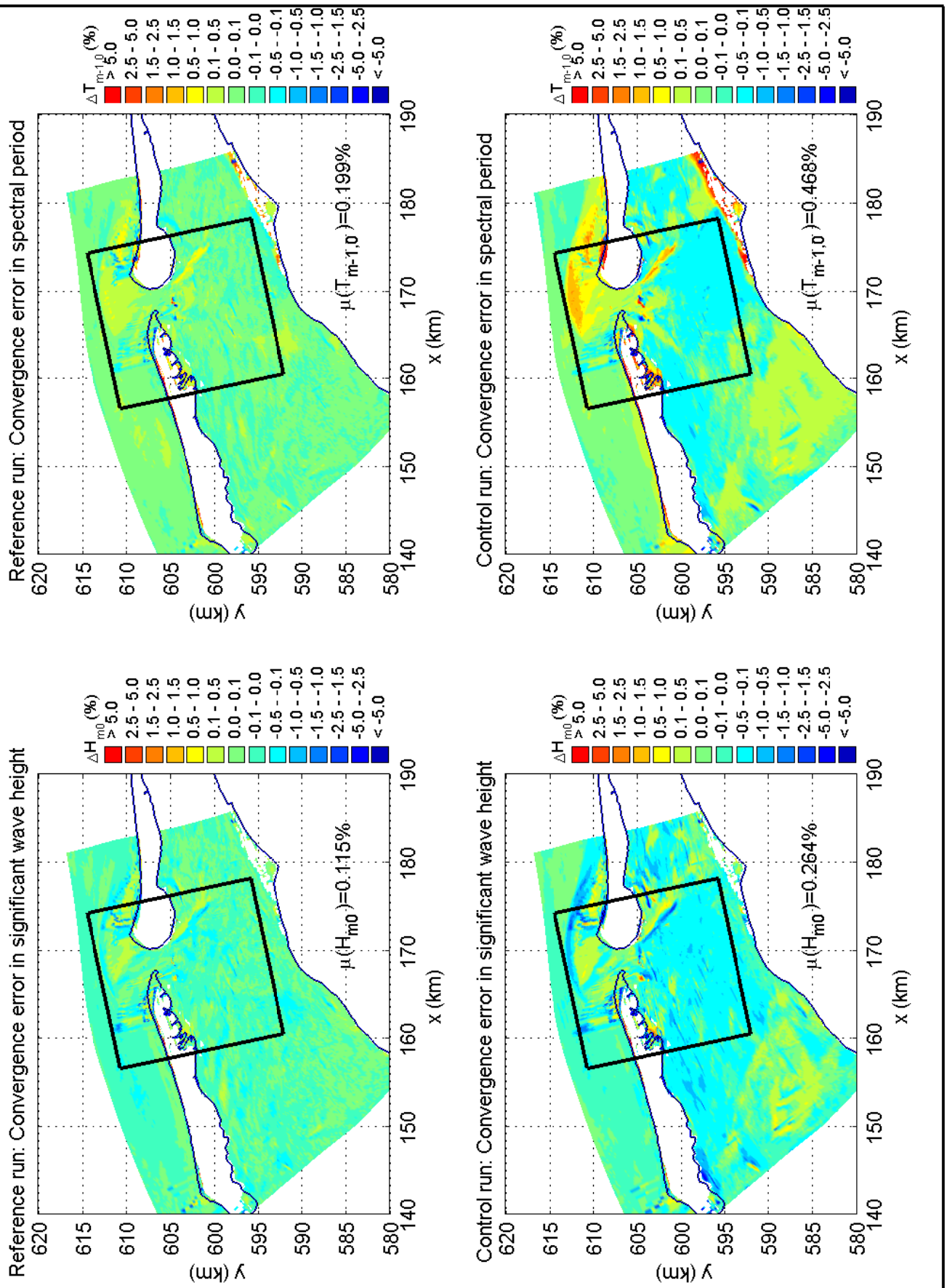

Convergence errors in H_{m0} and $T_{m-1,0}$ for the DDM simulation in the Amelander Zeegat, Case: AZG3A 2005/01/02 12:00 Refresh domain every 10 iterations, for 5 iterations (c_r10_d05)		SWAN 40.51A
		Numerical efficiency SWAN
DELTARES & ALKYON	H5107.46/A2114	Fig. 5.45

DELTARES & ALKYON

Convergence errors in Dir and Dspr for the DDM simulation in the Amelander Zeegat, Case: AZG3A 2005/01/02 12:00
Refresh domain every 10 iterations, for 5 iterations (c_r10_d05)

H5107.46/A2114

Numerical efficiency SWAN

SWAN 40.51A

Fig. 5.46

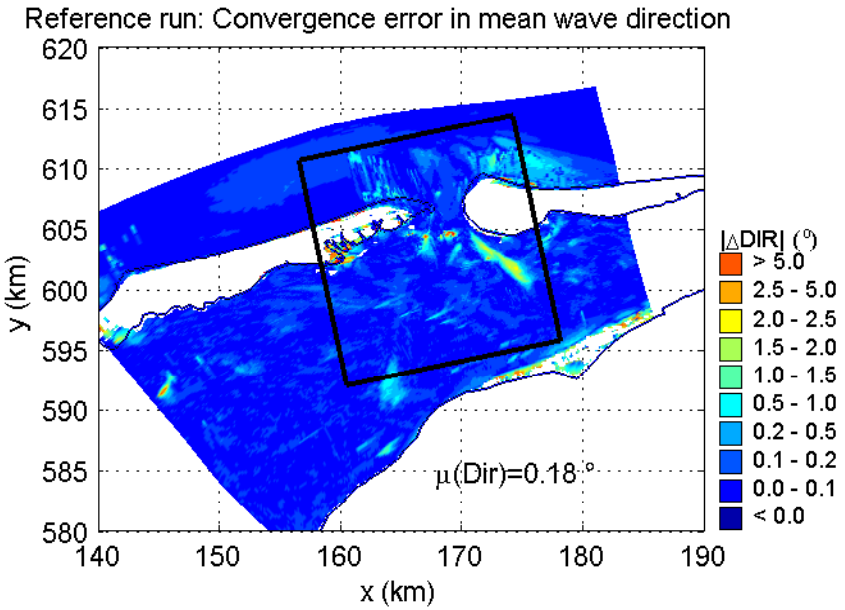

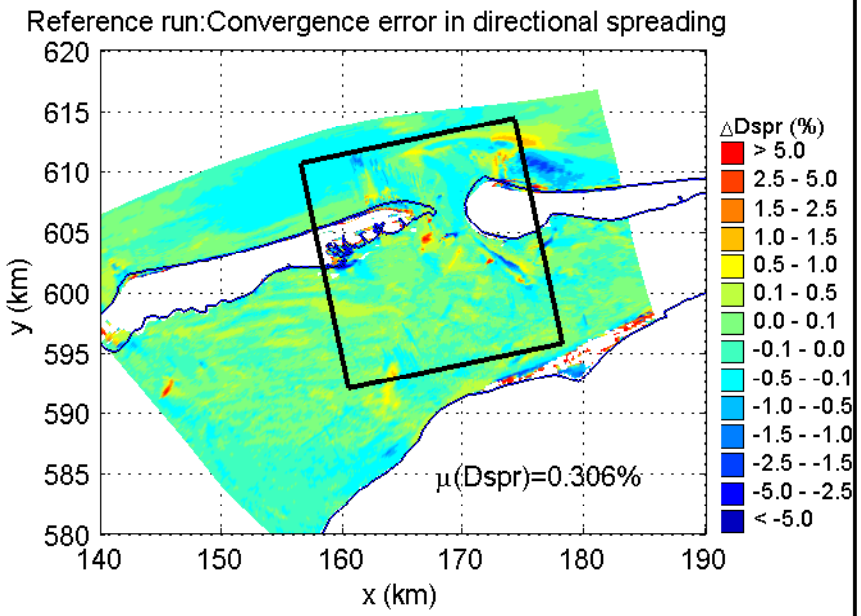

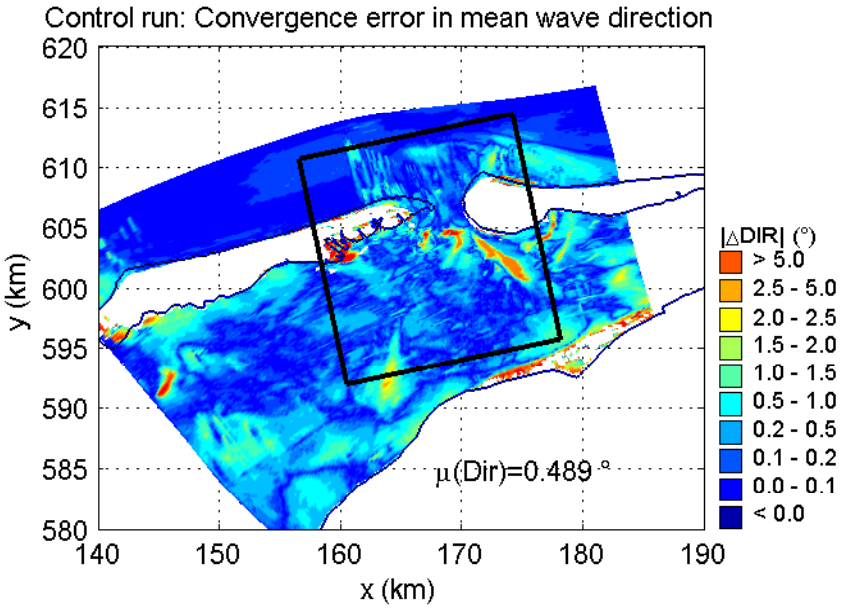

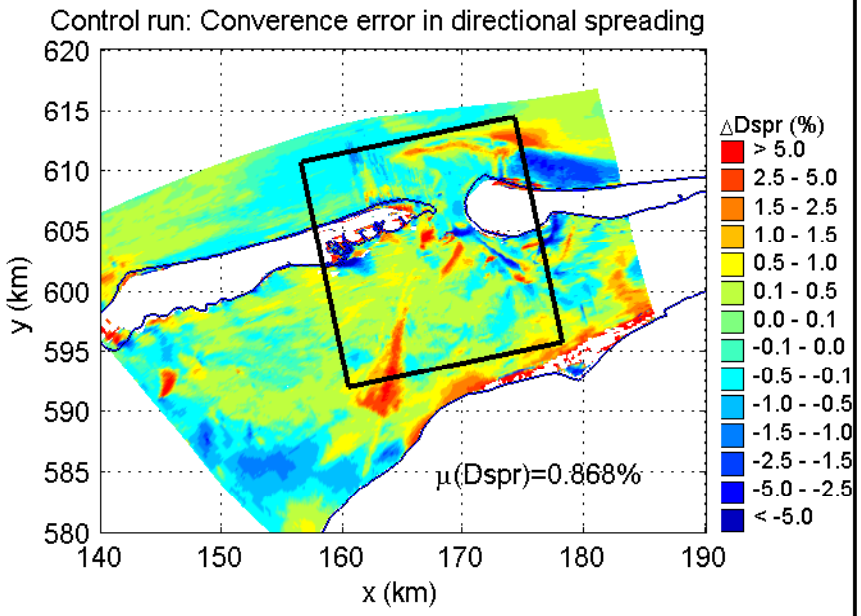

Reference run: Convergence error in significant wave height

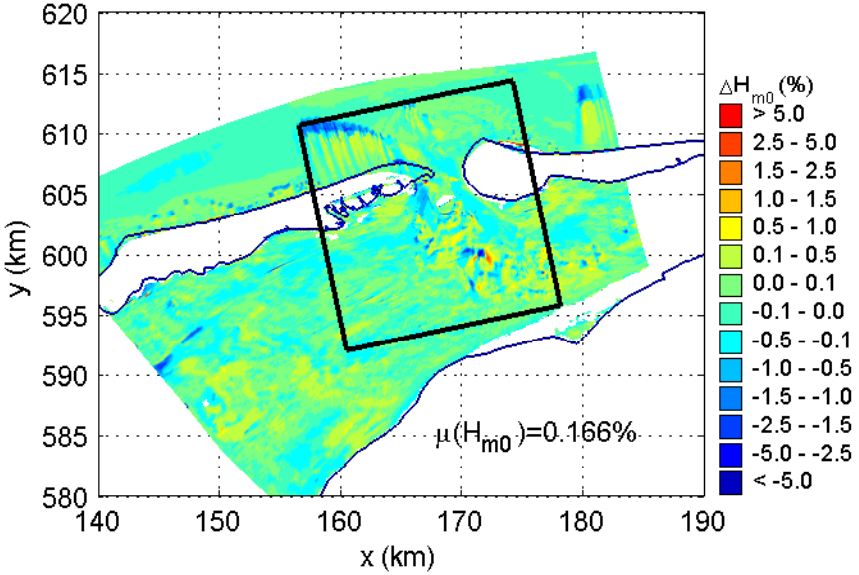

Reference run: Convergence error in spectral period

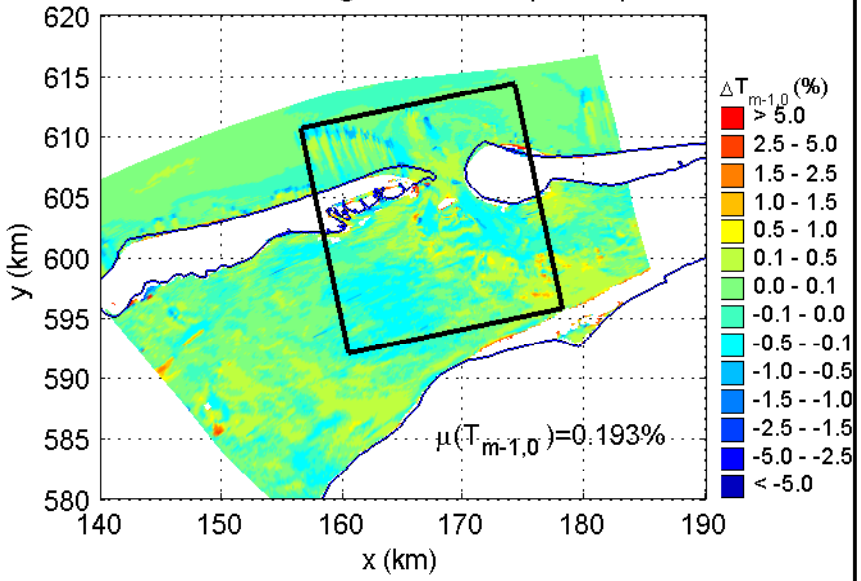

Control run: Convergence error in significant wave height

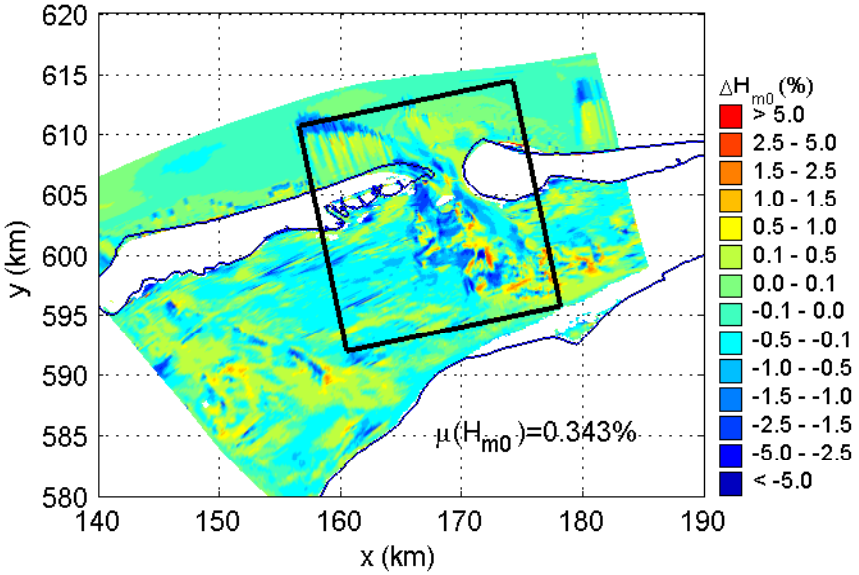

Control run: Convergence error in spectral period

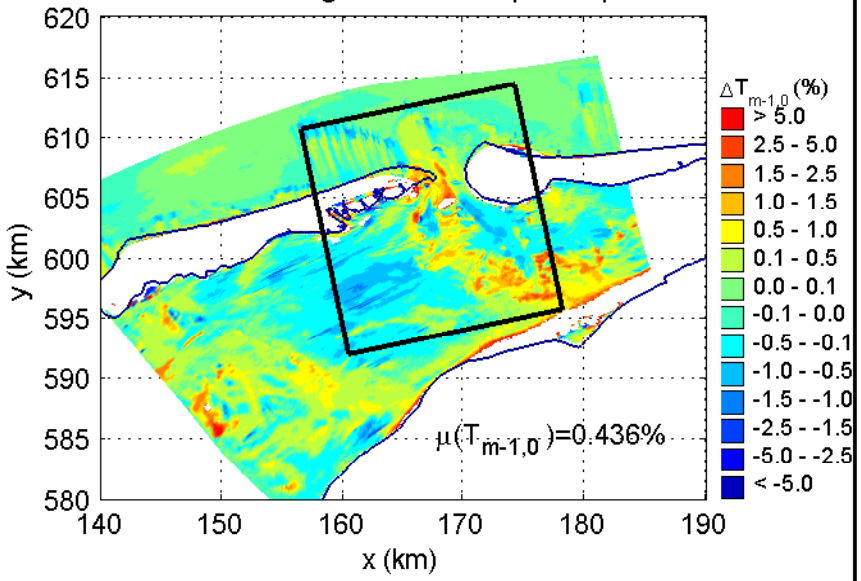

Convergence errors in H_{m0} and $T_{m-1,0}$ for the DDM simulation in the Amelander Zeegat, Case: AZG3A 2005/01/02 17:00
Refresh domain every 10 iterations, for 5 iterations (c_r10_d05)

DELTARES & ALKYON

H5107.46/A2114

Numerical efficiency SWAN

SWAN 40.51A

Fig. 5.47

DELTARES & ALKYON

Convergence errors in Dir and Dspr for the DDM simulation in the Amelander Zeegat, Case: AZG3A 2005/01/02 17:00
Refresh domain every 10 iterations, for 5 iterations (c_r10_d05)

H5107.46/A2114

Numerical efficiency SWAN

SWAN 40.51A

Fig. 5.48

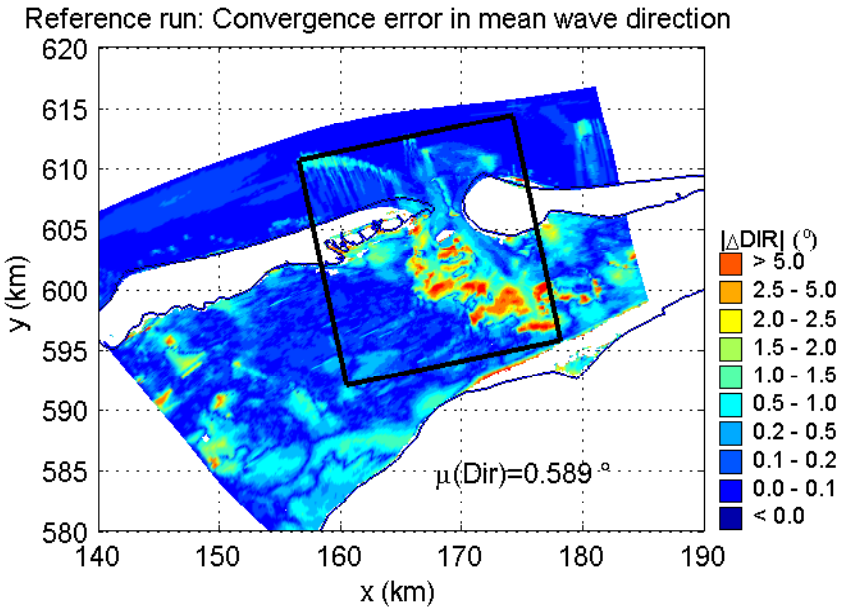

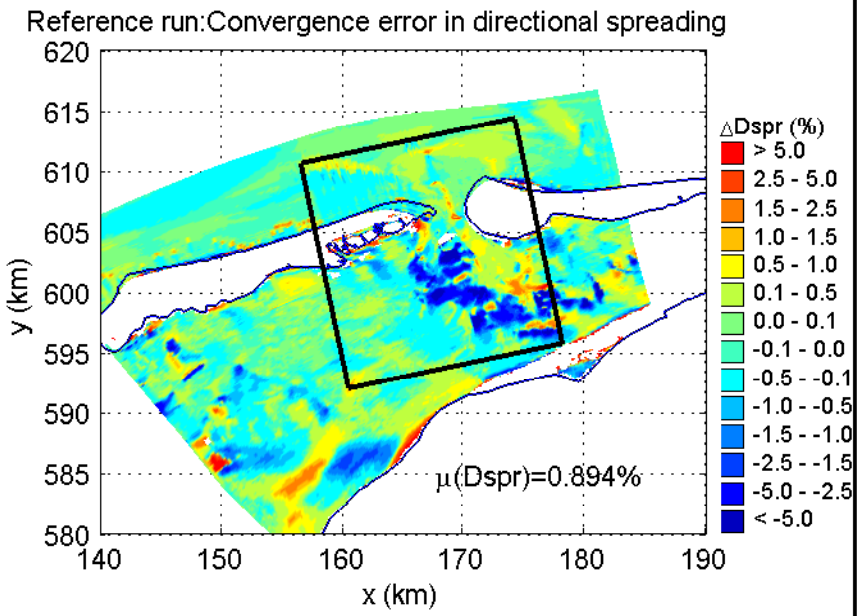

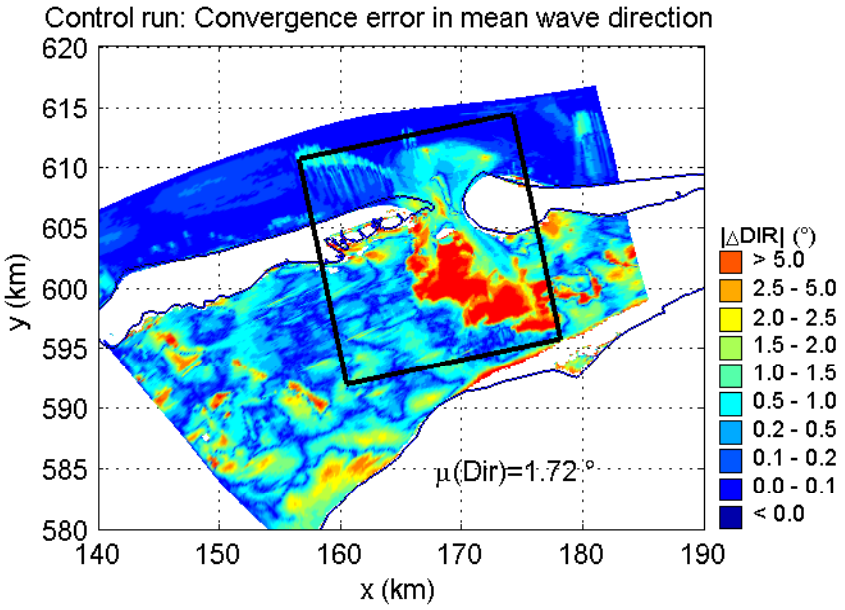

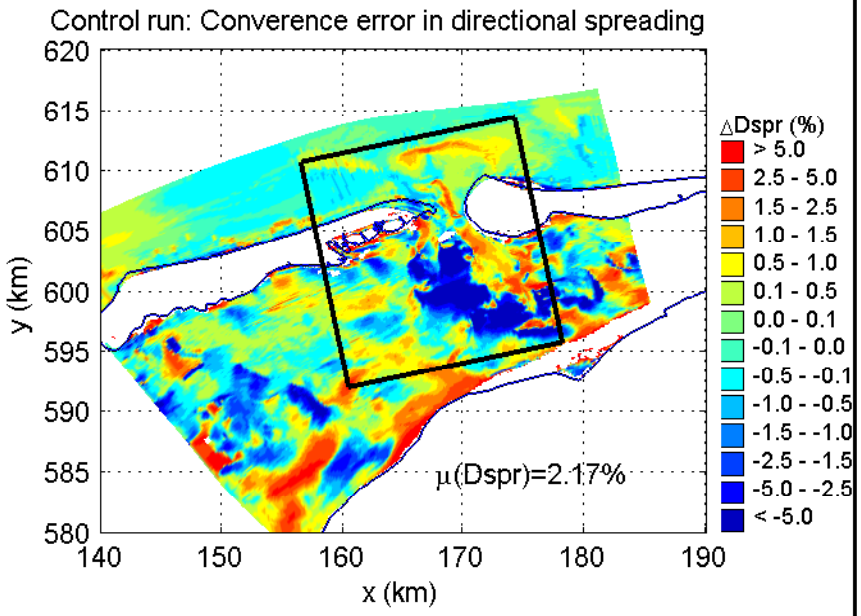

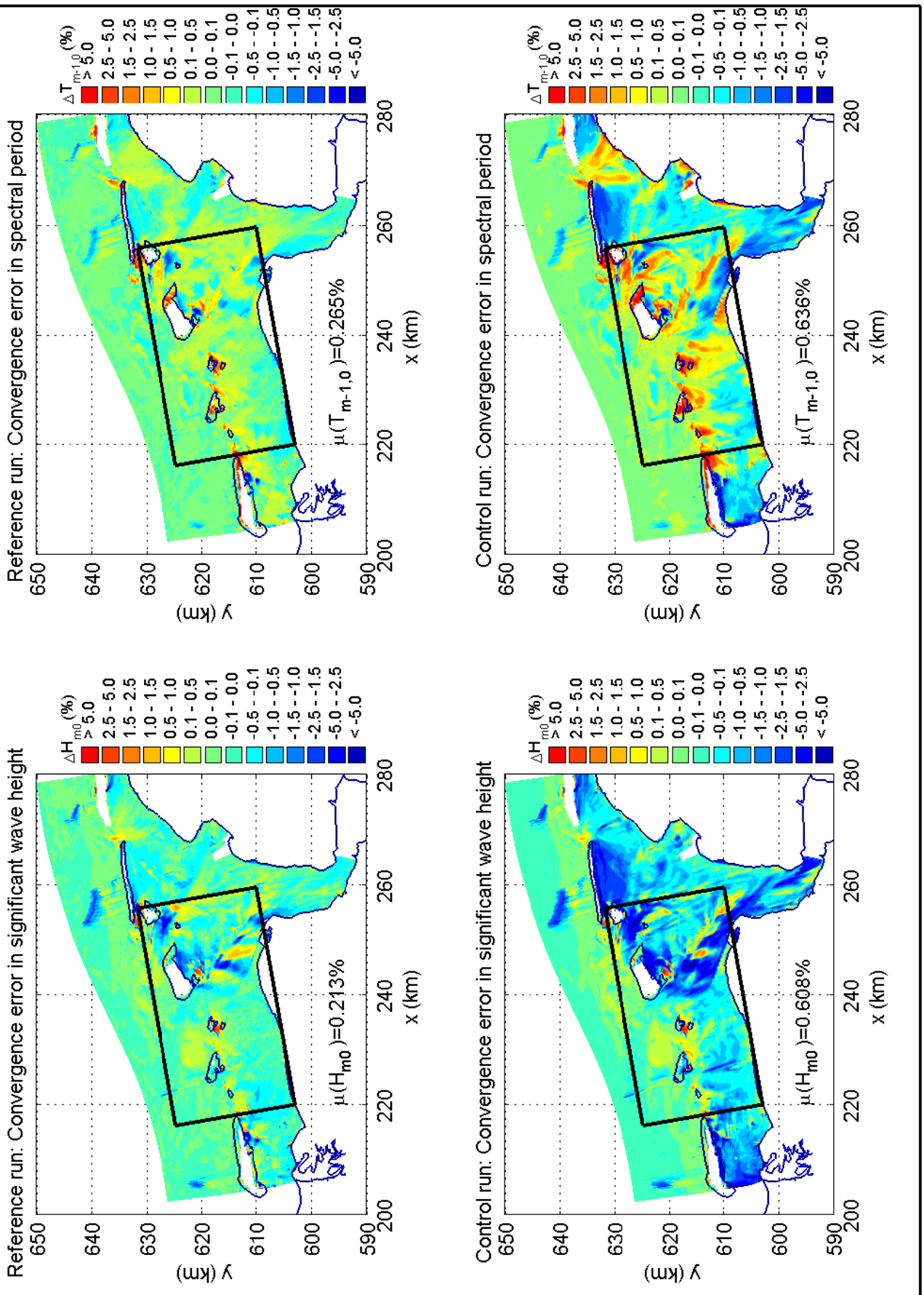

Convergence errors in H_{m0} and $T_{m-1,0}$ for the DDM simulation in the Eems-Dollard, Case: EEMS3A 2006/11/01 03:00 Refresh domain every 10 iterations, for 5 iterations (c_r10_d05)		SWAN 40.51A
		Numerical efficiency SWAN
DELTARES & ALKYON	H5107.46/A2114	Fig. 5.49

DELTARES & ALKYON

Convergence errors in Dir and Dspr for the DDM simulation in the Eems-Dollard, Case: EEMS3A 2006/11/01 03:00
Refresh domain every 10 iterations, for 5 iterations (c_r10_d05)

H5107.46/A2114

Numerical efficiency SWAN

SWAN 40.51A

Fig. 5.50

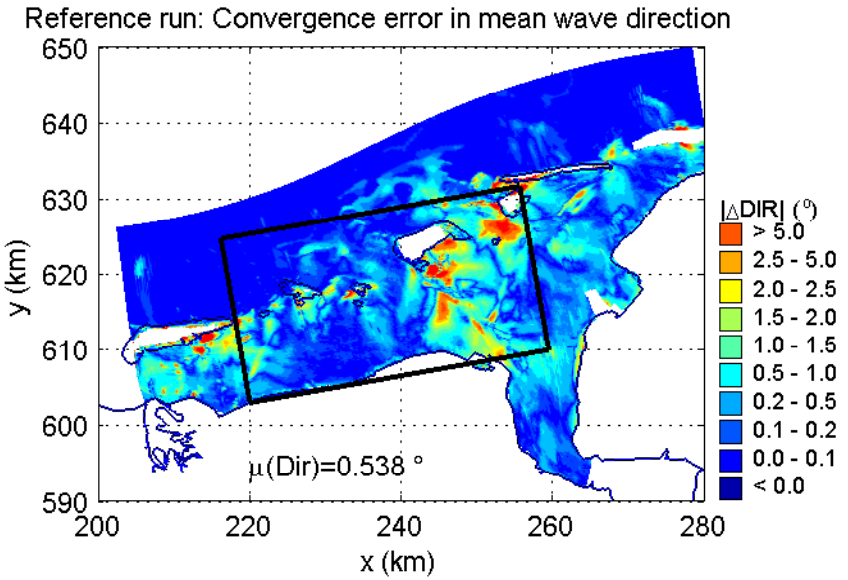

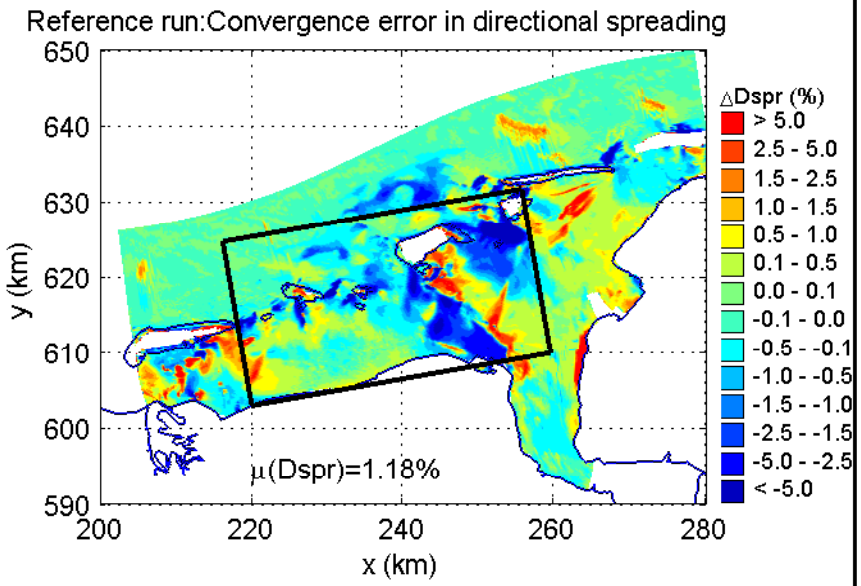

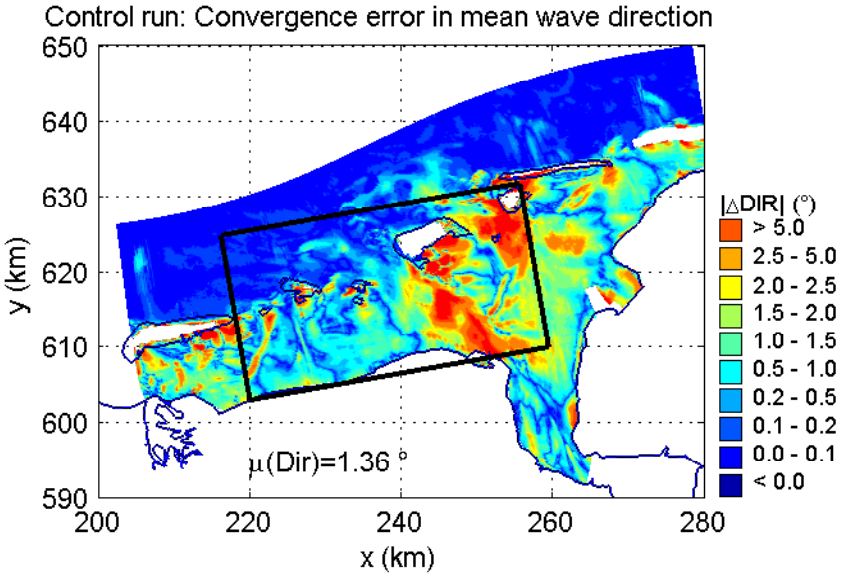

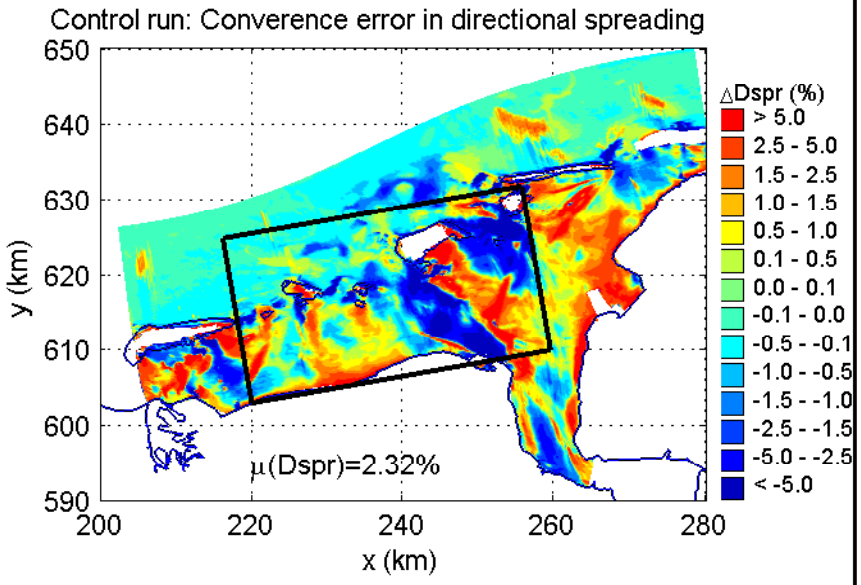

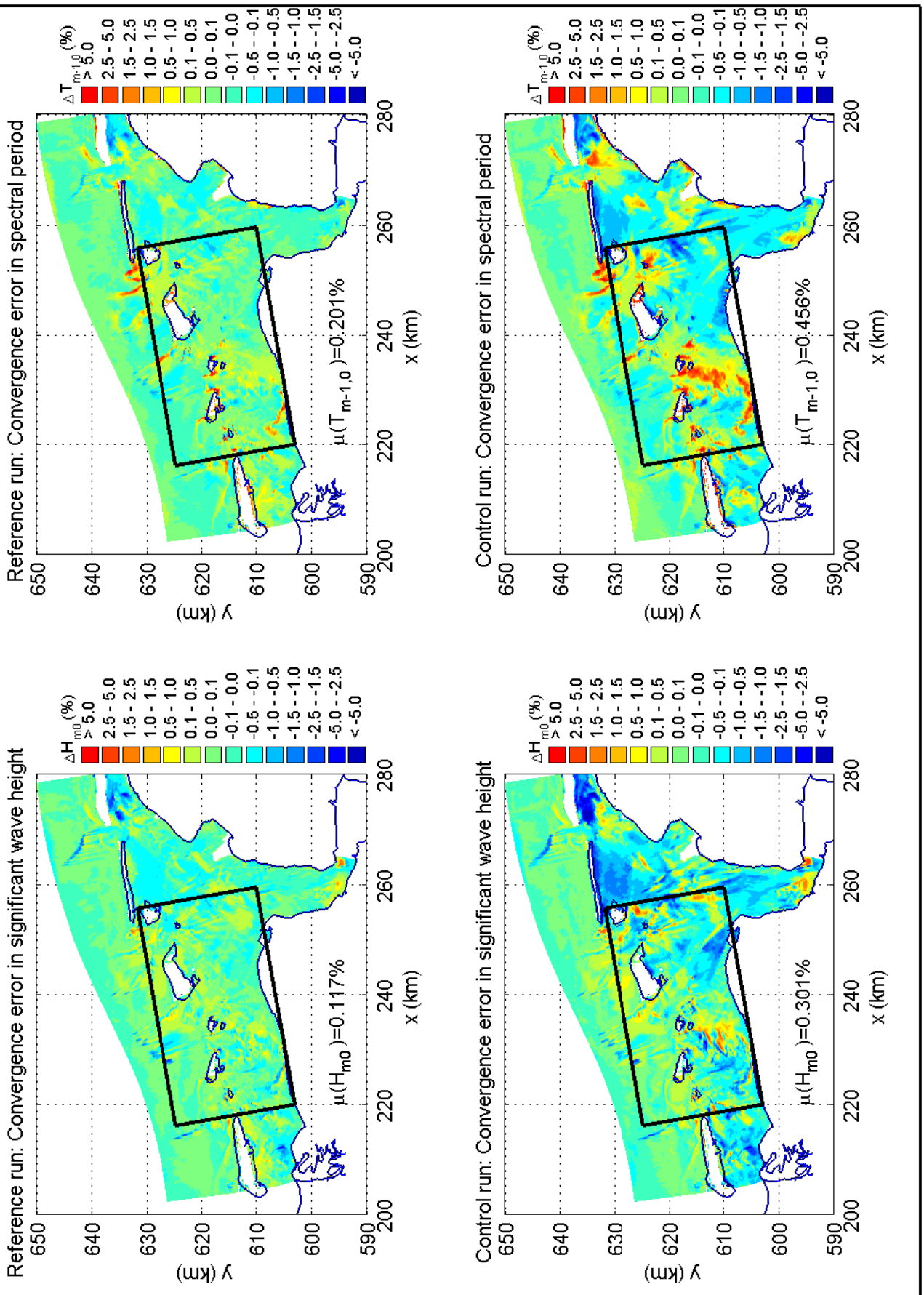

Convergence errors in H_{m0} and $T_{m-1,0}$ for the DDM simulation in the Eems-Dollard, Case: EEMS3A 2006/11/01 09:30 Refresh domain every 10 iterations, for 5 iterations (c_r10_d05)		SWAN 40.51A
		Numerical efficiency SWAN
DELTARES & ALKYON	H5107.46/A2114	Fig. 5.51

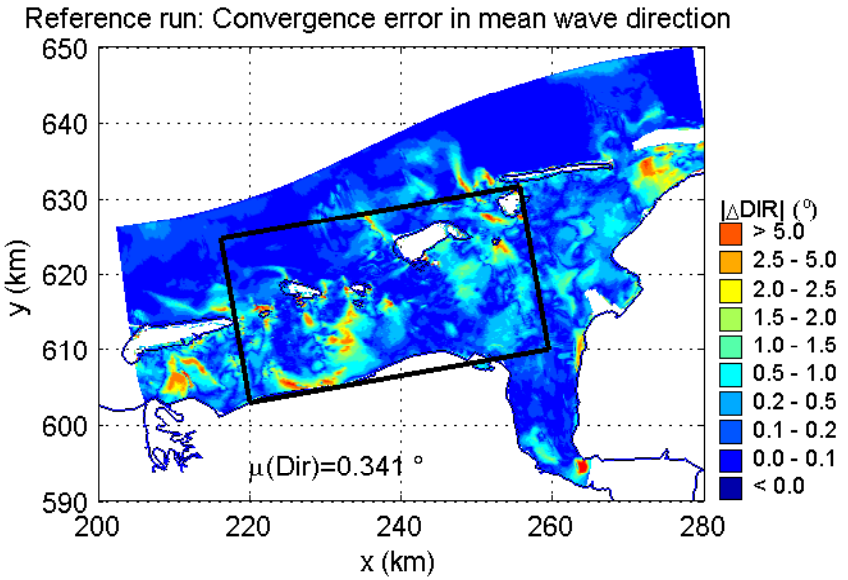

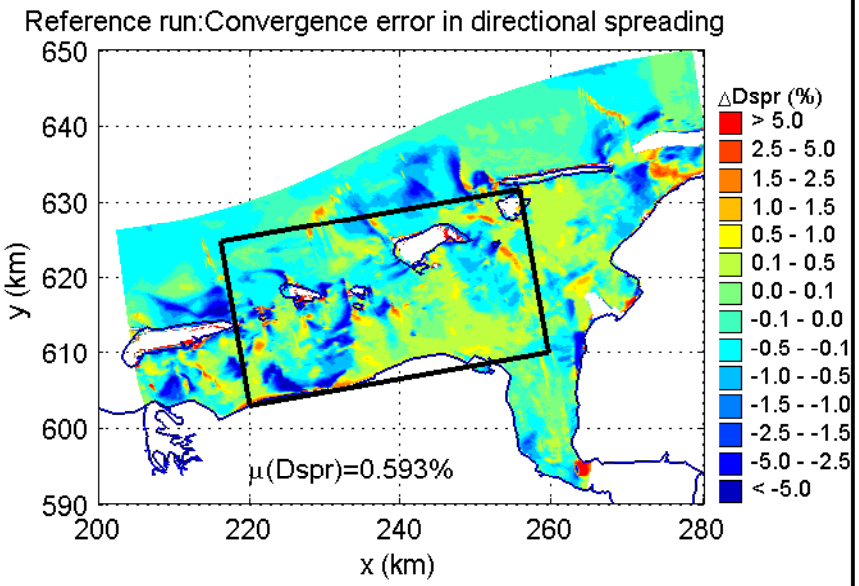

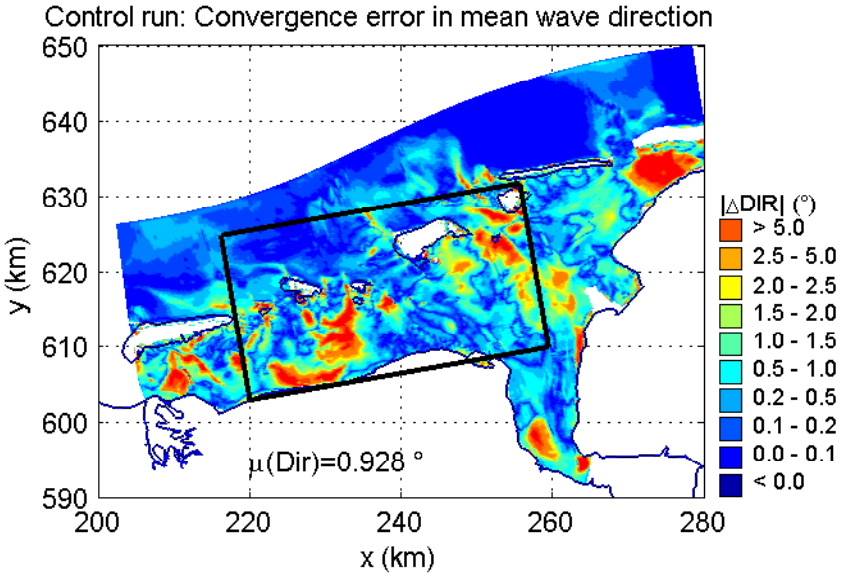

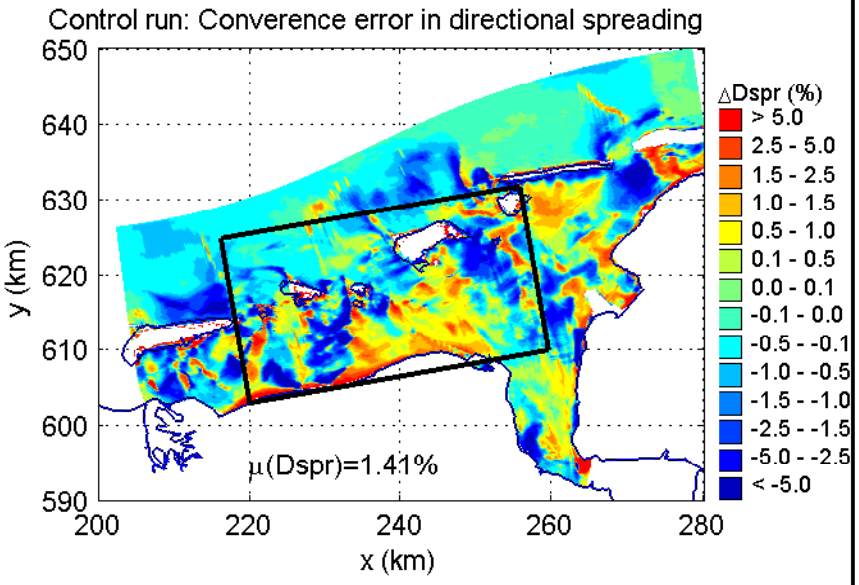

Convergence errors in Dir and Dspr for the DDM simulation in the Eems-Dollard, Case: EEMS3A 2006/11/01 09:30
Refresh domain every 10 iterations, for 5 iterations (c_r10_d05)

DELTARES & ALKYON

H5107.46/A2114

Numerical efficiency SWAN

SWAN 40.51A

Fig. 5.52

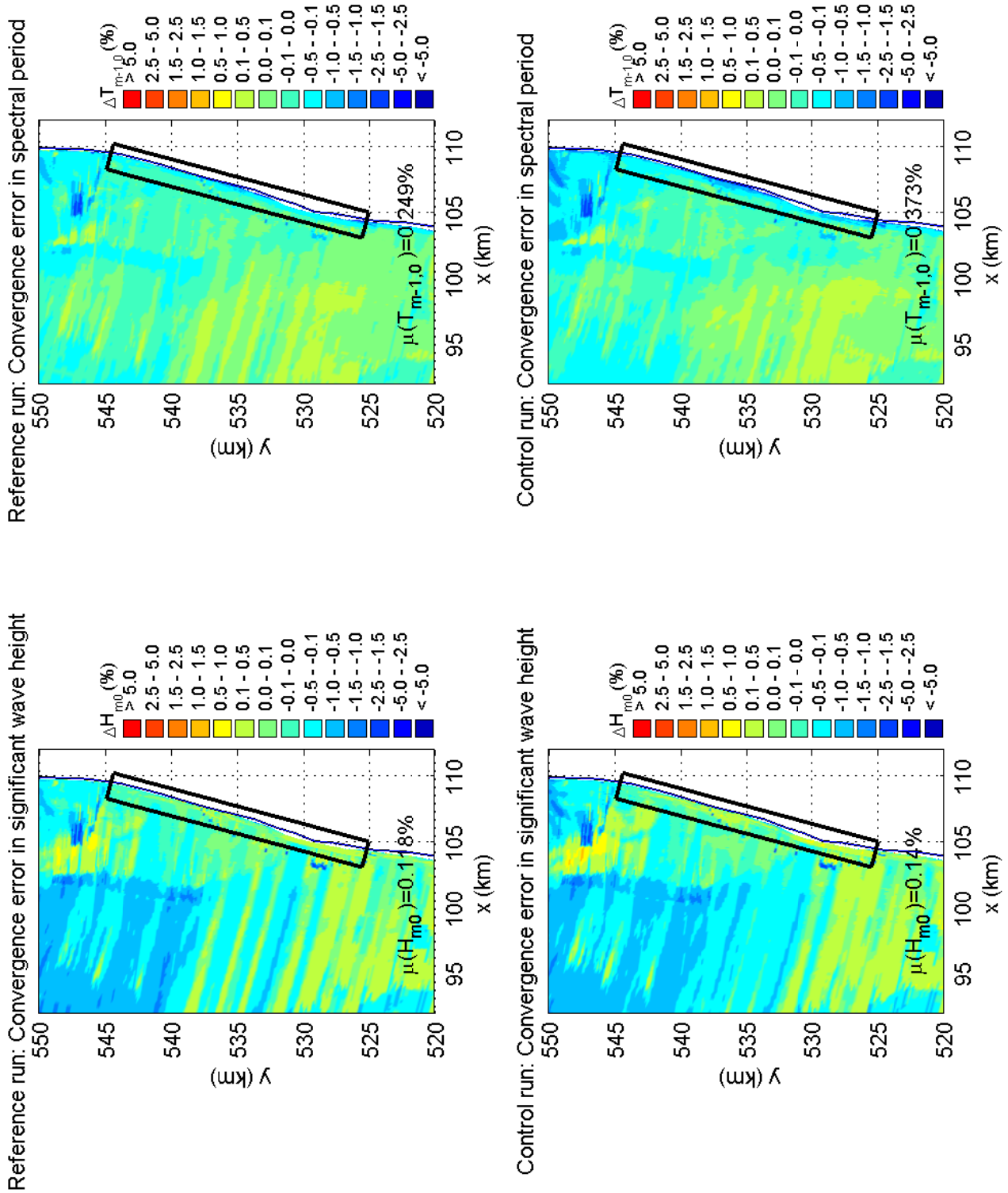

Convergence errors in H_{m0} and $T_{m-1,0}$ for the DDM simulation along the Dutch coast near Petten, Case: PETTEN 1995/01/01 10:00 Refresh domain every 10 iterations, for 5 iterations (c_r10_d05)		SWAN 40.51A
		Numerical efficiency SWAN
DELTARES & ALKYON	H5107.46/A2114	Fig. 5.53

DELTARES & ALKYON

Convergence errors in Dir and Dspr for the DDM simulation along the Dutch coast near Petten, Case: PETTEN 1995/01/01 10:00 Refresh domain every 10 iterations, for 5 iterations (c_r10_d05)

Reference run: Convergence error in mean wave direction

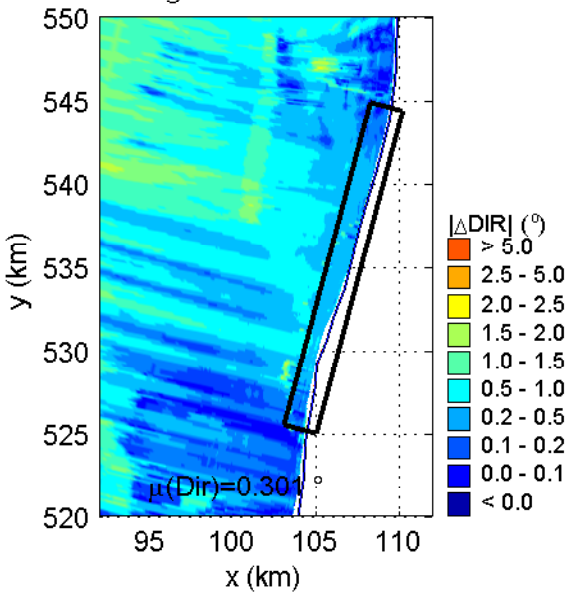

Reference run:Convergence error in directional spreading

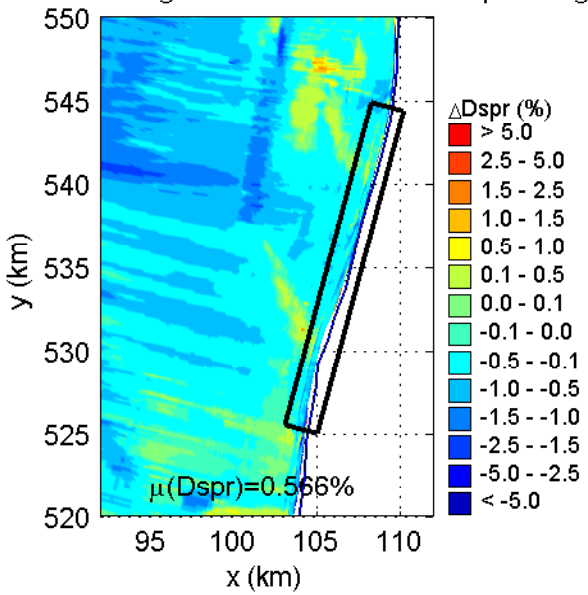

Control run: Convergence error in mean wave direction

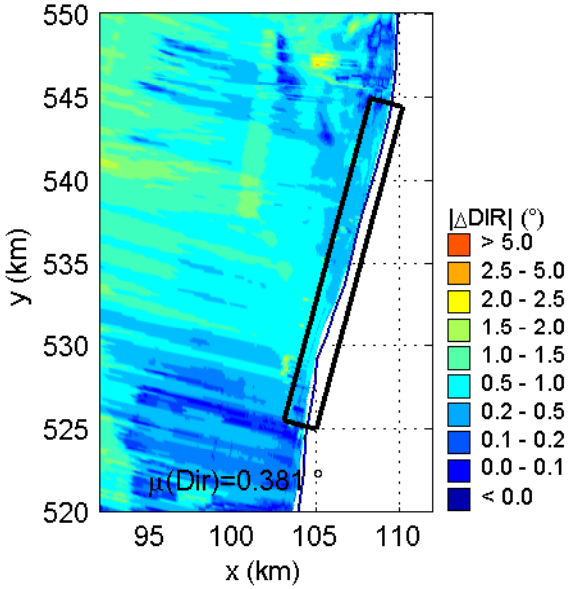

Control run: Converence error in directional spreading

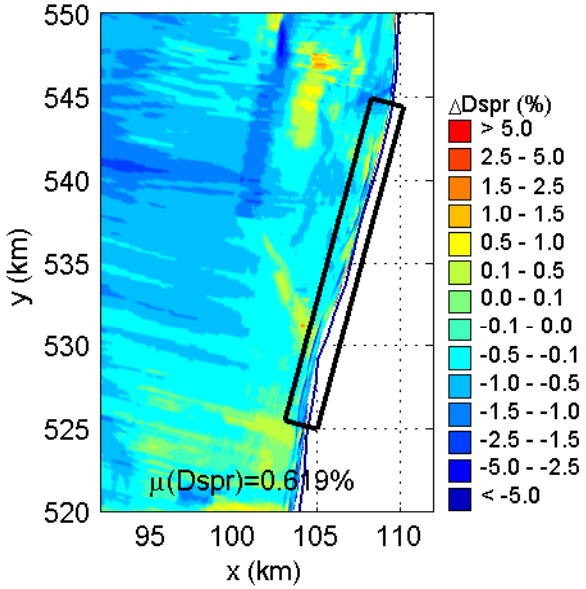

H5107.46/A2114

Numerical efficiency SWAN

SWAN 40.51A

Fig. 5.54

DELTARES & ALKYON

Convergence errors in H_{m0} and $T_{m-1,0}$ for the DDM simulation in Lake Sloten, Case: SLE 2002/10/27 15:00
Refresh domain every 10 iterations, for 5 iterations (c_r10_d05)

H5107.46/A2114

Numerical efficiency SWAN

SWAN 40.51A

Fig. 5.55

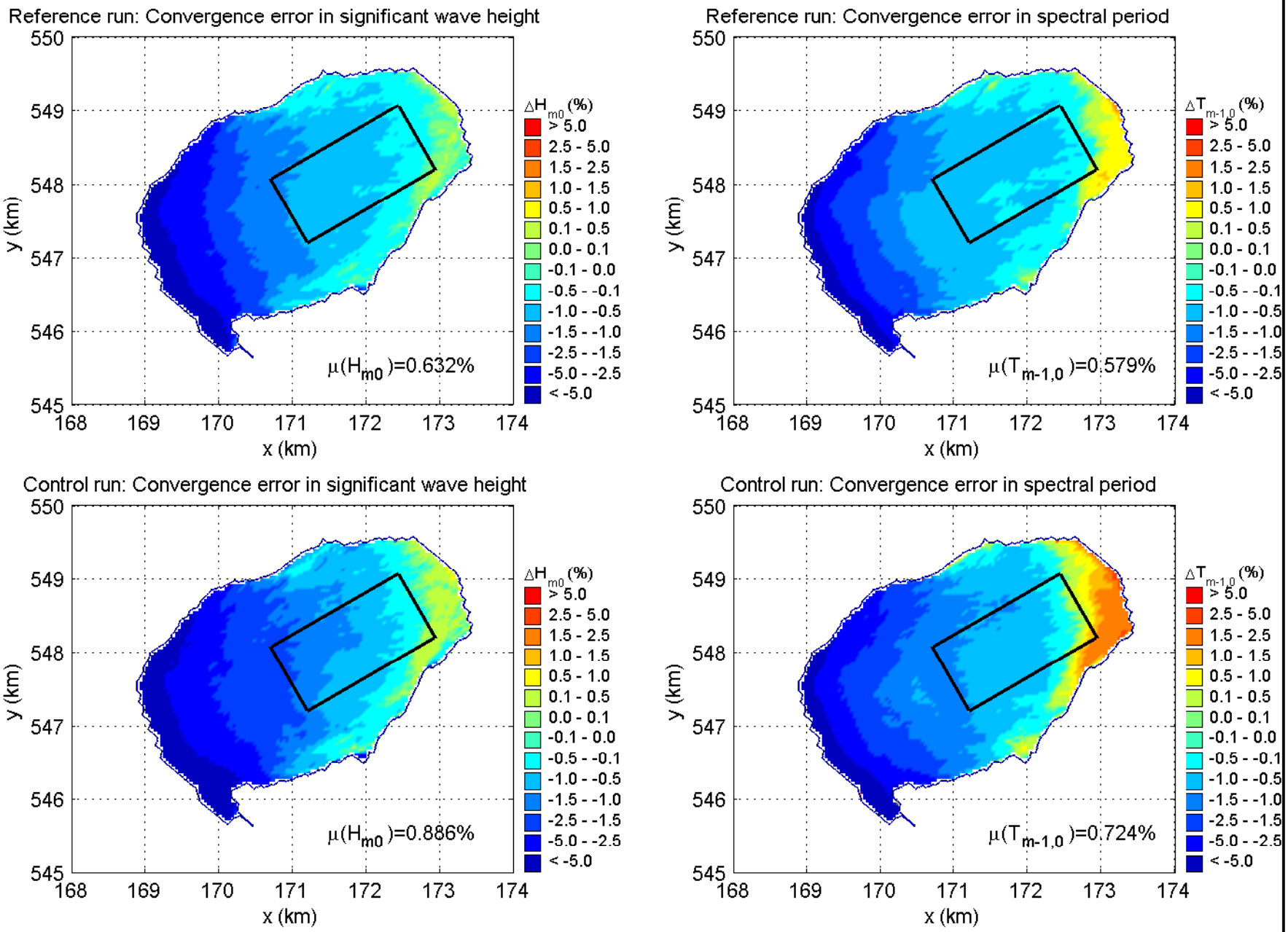

Convergence errors in Dir and Dspr for the DDM simulation
in Lake Sloten, Case: SLE 2002/10/27 15:00
Refresh domain every 10 iterations, for 5 iterations (c_r10_d05)

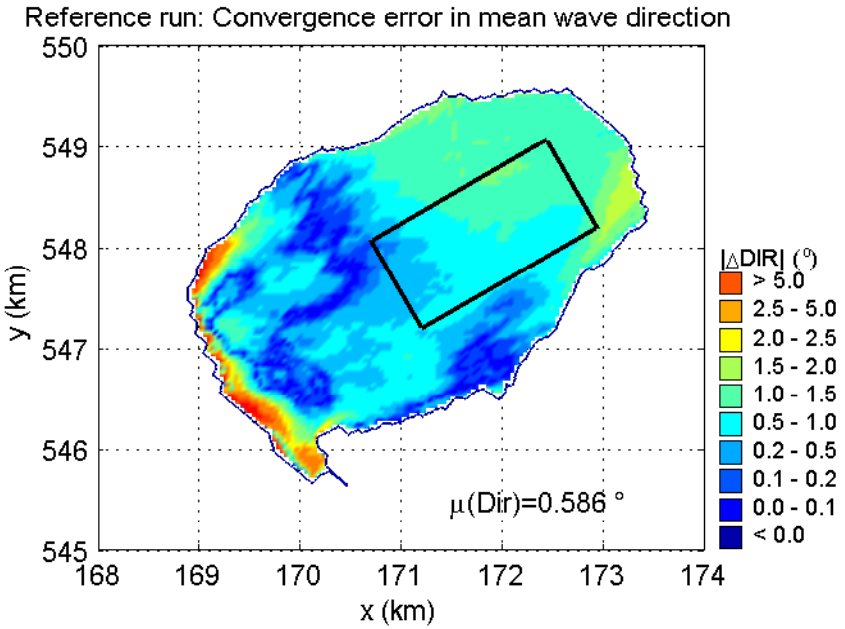

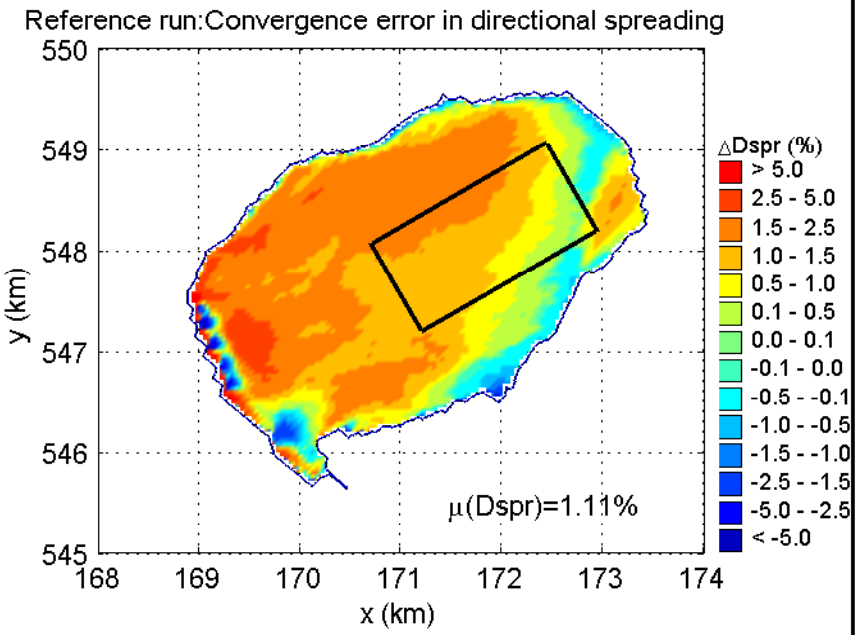

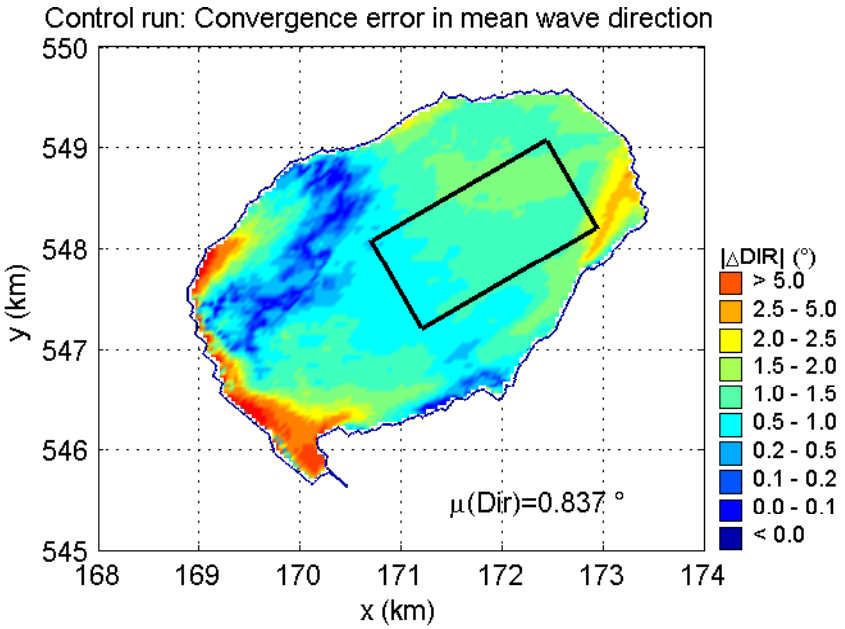

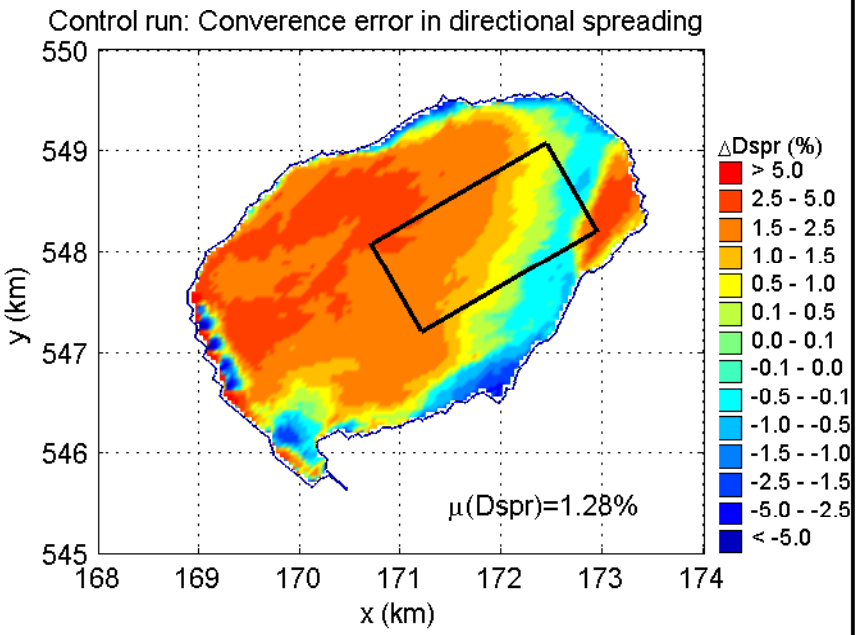

DELTARES & ALKYON

H5107.46/A2114

Numerical efficiency SWAN

SWAN 40.51A

Fig. 5.56

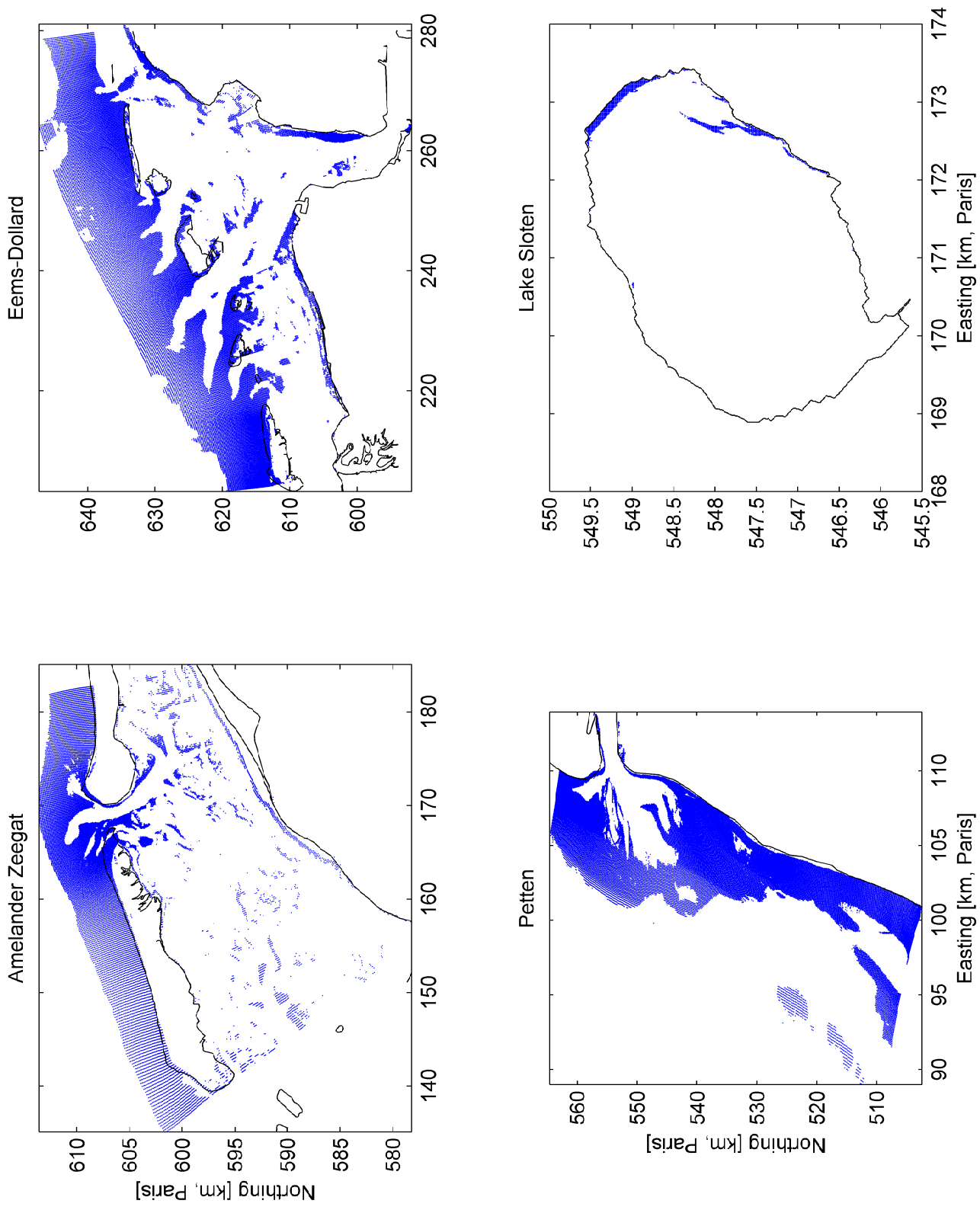

Regions over which action limiter and quadruplet interactions are deactivated when using a limit of Ursell = 0.10 (run C_urs_010, at final iteration)		SWAN 40.51A
		Numerical efficiency SWAN
DELTARES & ALKYON	H5107.46/A2114	Fig. 6.1

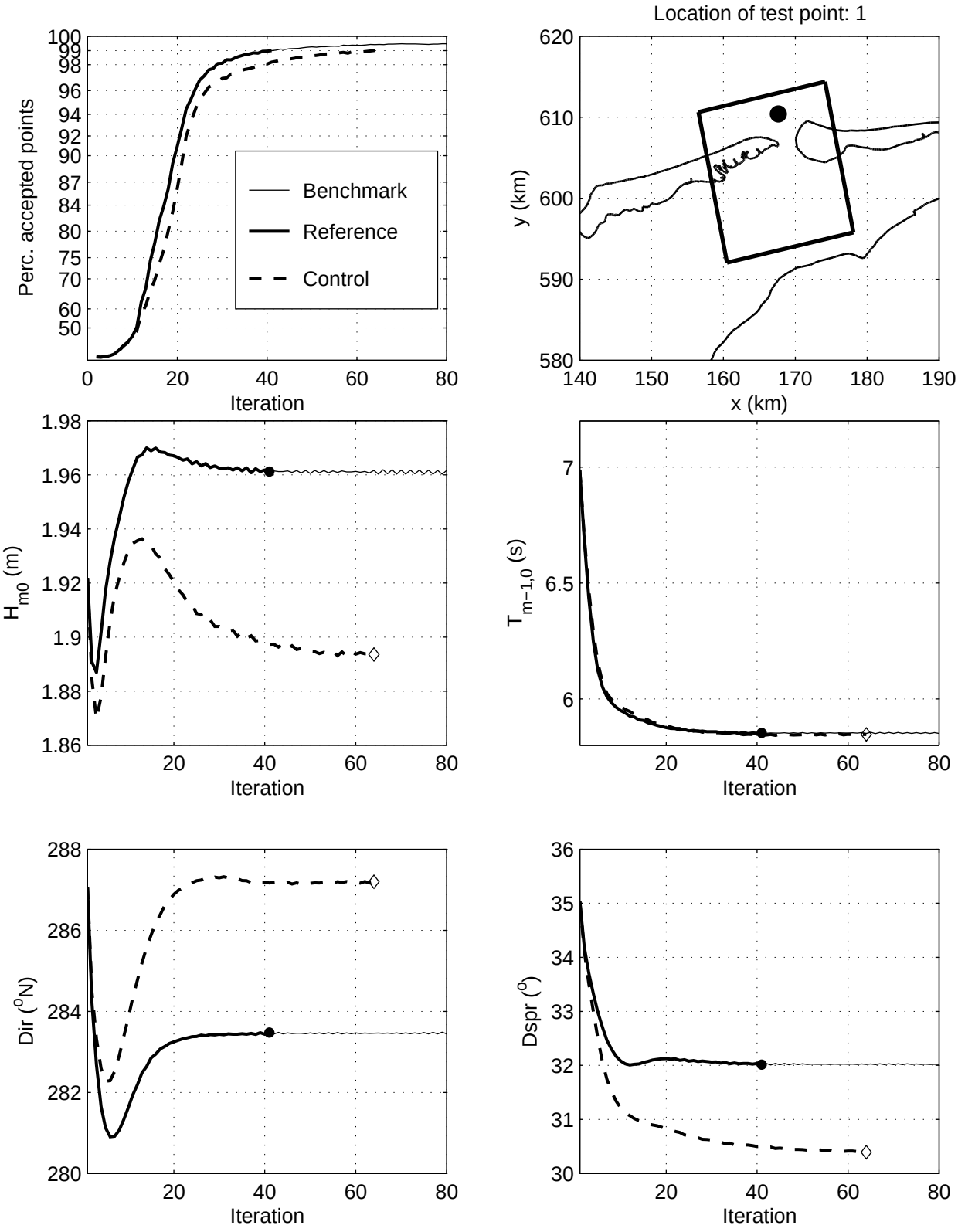

Convergence behaviour: deactivation of action limiter and S_{nl4} in the surf zone in the Amelander Zeegat, Case: AZG3A 2005/01/02 10:00, at point 1 Deactivation at Ursell = 0.10 (C_urs_010)		SWAN 40.51A
		Numerical efficiency SWAN
DELTARES & ALKYON	H5107.46/A2114	Fig. 6.2

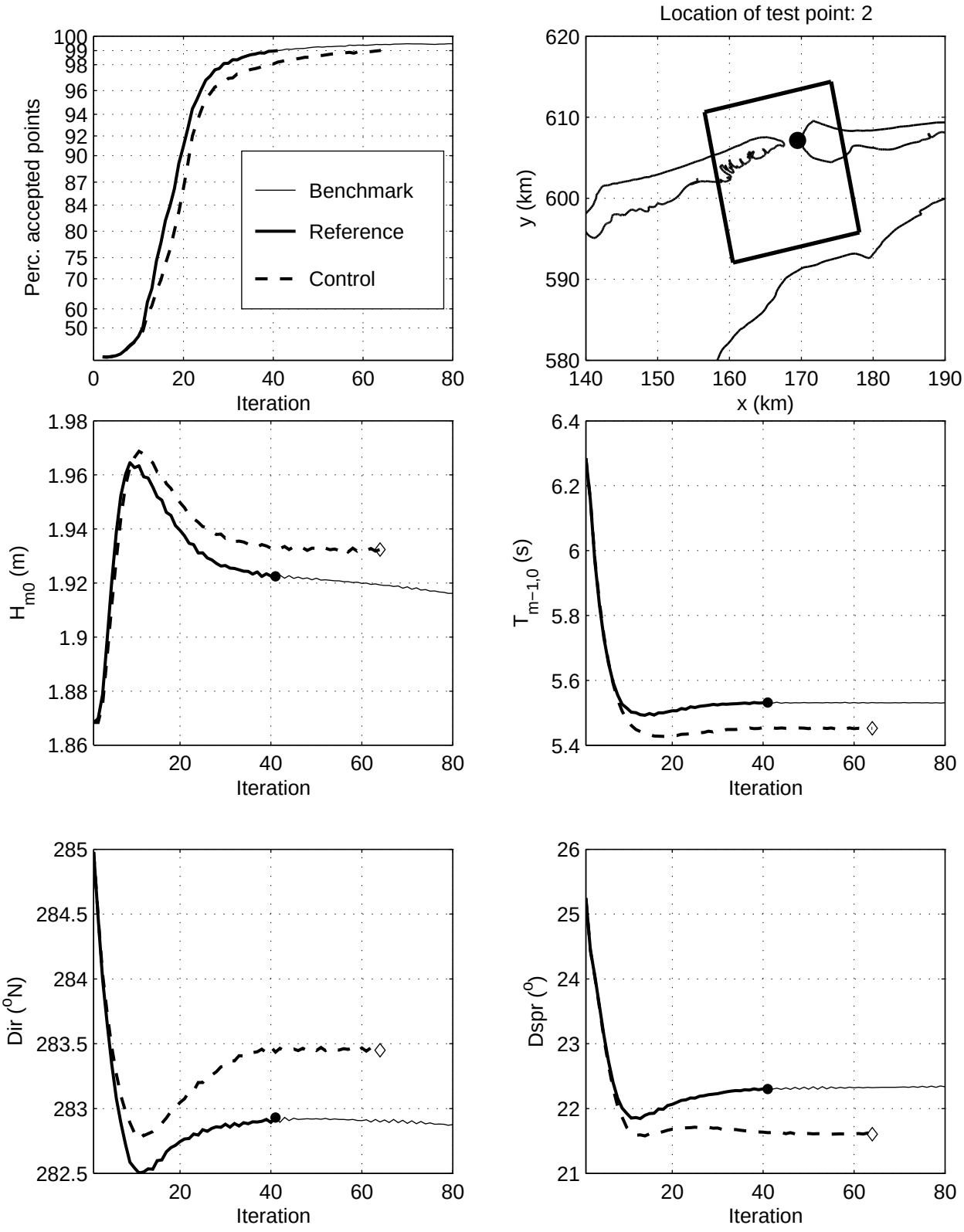

Convergence behaviour: deactivation of action limiter and S_{nl4} in the surf zone in the Amelander Zeegat, Case: AZG3A 2005/01/02 10:00, at point 2 Deactivation at Ursell = 0.10 (C_urs_010)		SWAN 40.51A
		Numerical efficiency SWAN
DELTARES & ALKYON	H5107.46/A2114	Fig. 6.3

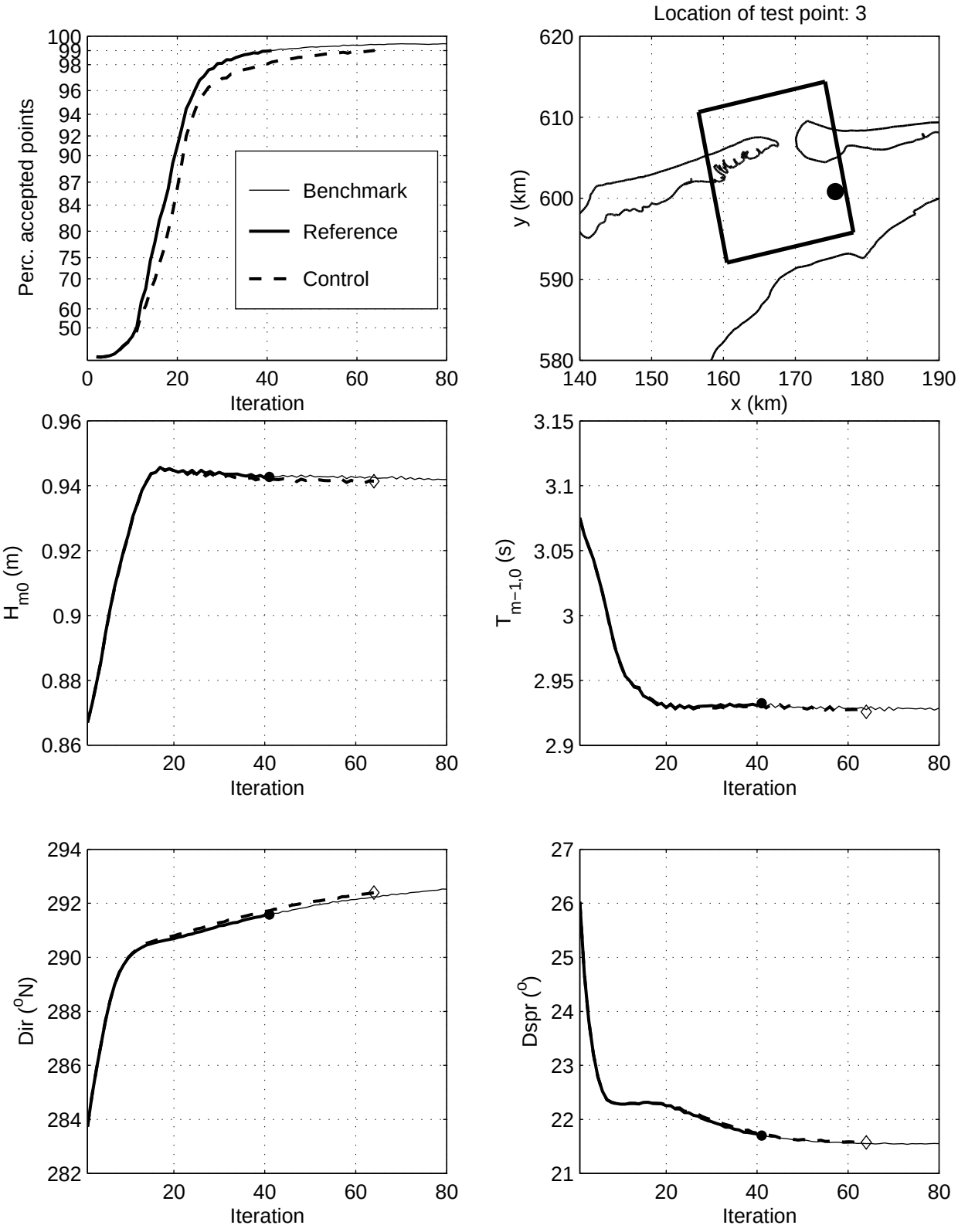

Convergence behaviour: deactivation of action limiter and S_{nl4} in the surf zone in the Amelander Zeegat, Case: AZG3A 2005/01/02 10:00, at point 3 Deactivation at Ursell = 0.10 (C_urs_010)		SWAN 40.51A
		Numerical efficiency SWAN
DELTARES & ALKYON	H5107.46/A2114	Fig. 6.4

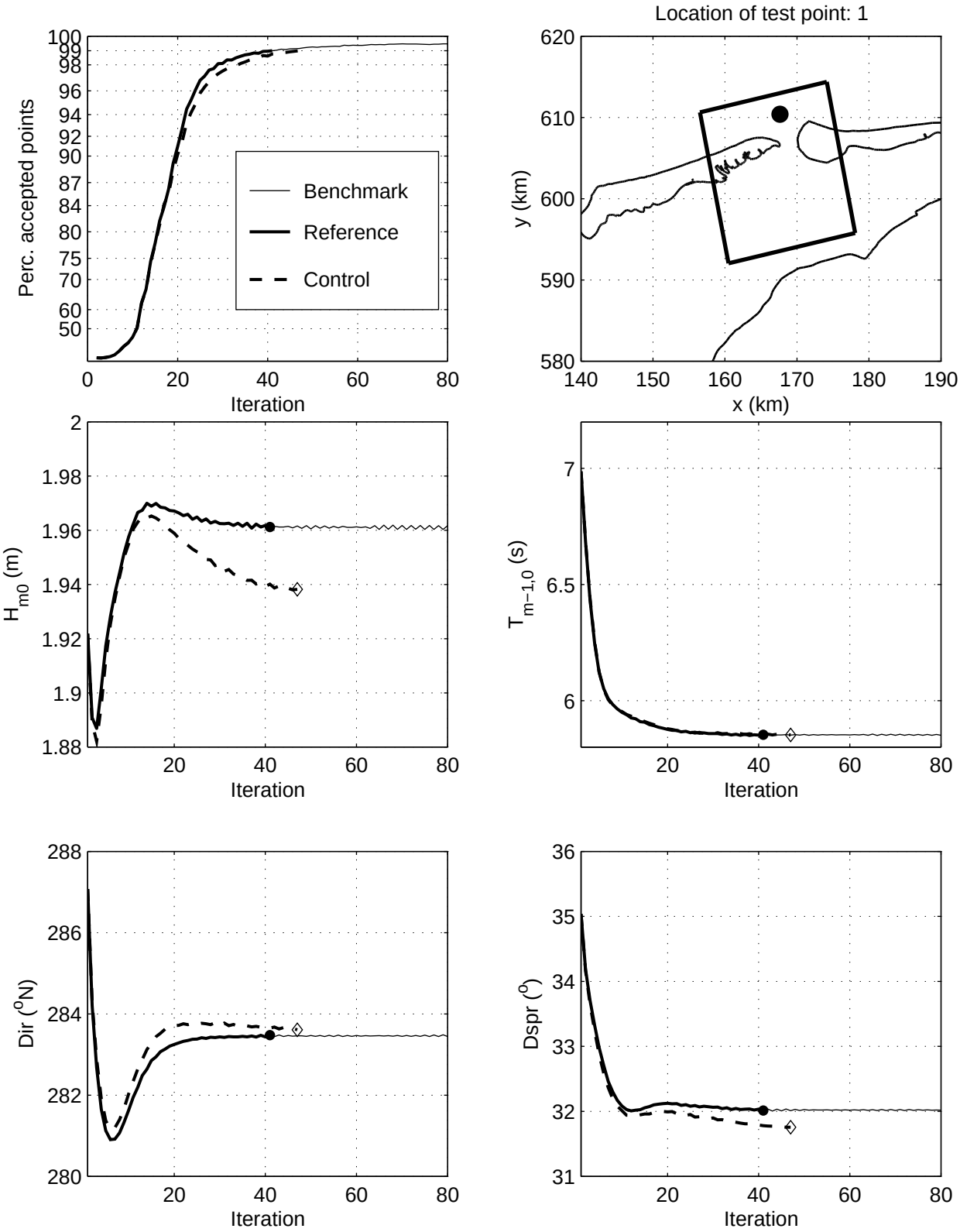

Convergence behaviour: deactivation of action limiter and S_{nl4} in the surf zone in the Amelander Zeegat, Case: AZG3A 2005/01/02 10:00, at point 1 Deactivation at Ursell = 0.20 (C_urs_020)		SWAN 40.51A
	Numerical efficiency SWAN	
DELTARES & ALKYON	H5107.46/A2114	Fig. 6.5

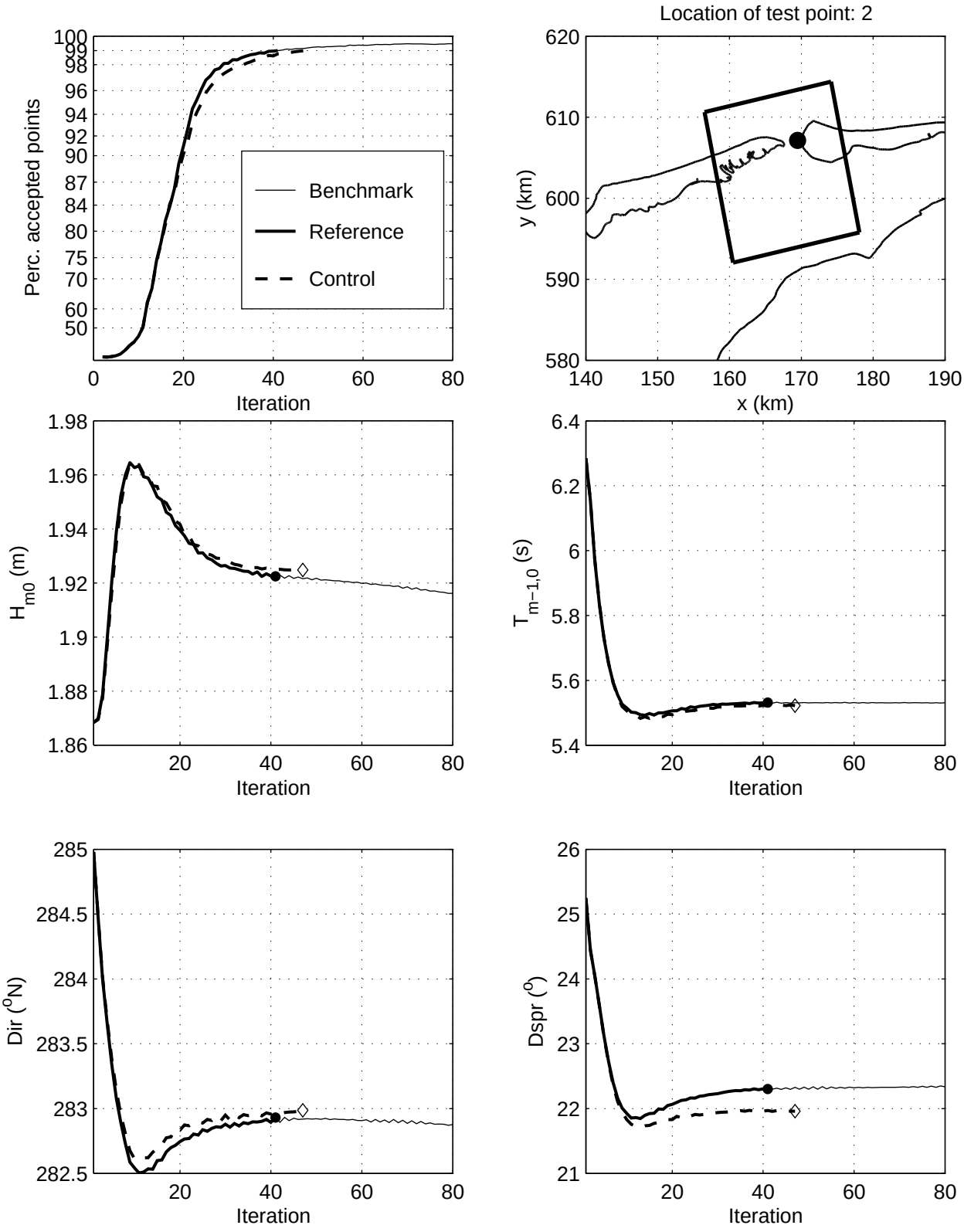

Convergence behaviour: deactivation of action limiter and S_{nl4} in the surf zone in the Amelander Zeegat, Case: AZG3A 2005/01/02 10:00, at point 2 Deactivation at Ursell = 0.20 (C_urs_020)		SWAN 40.51A
	Numerical efficiency SWAN	
DELTARES & ALKYON	H5107.46/A2114	Fig. 6.6

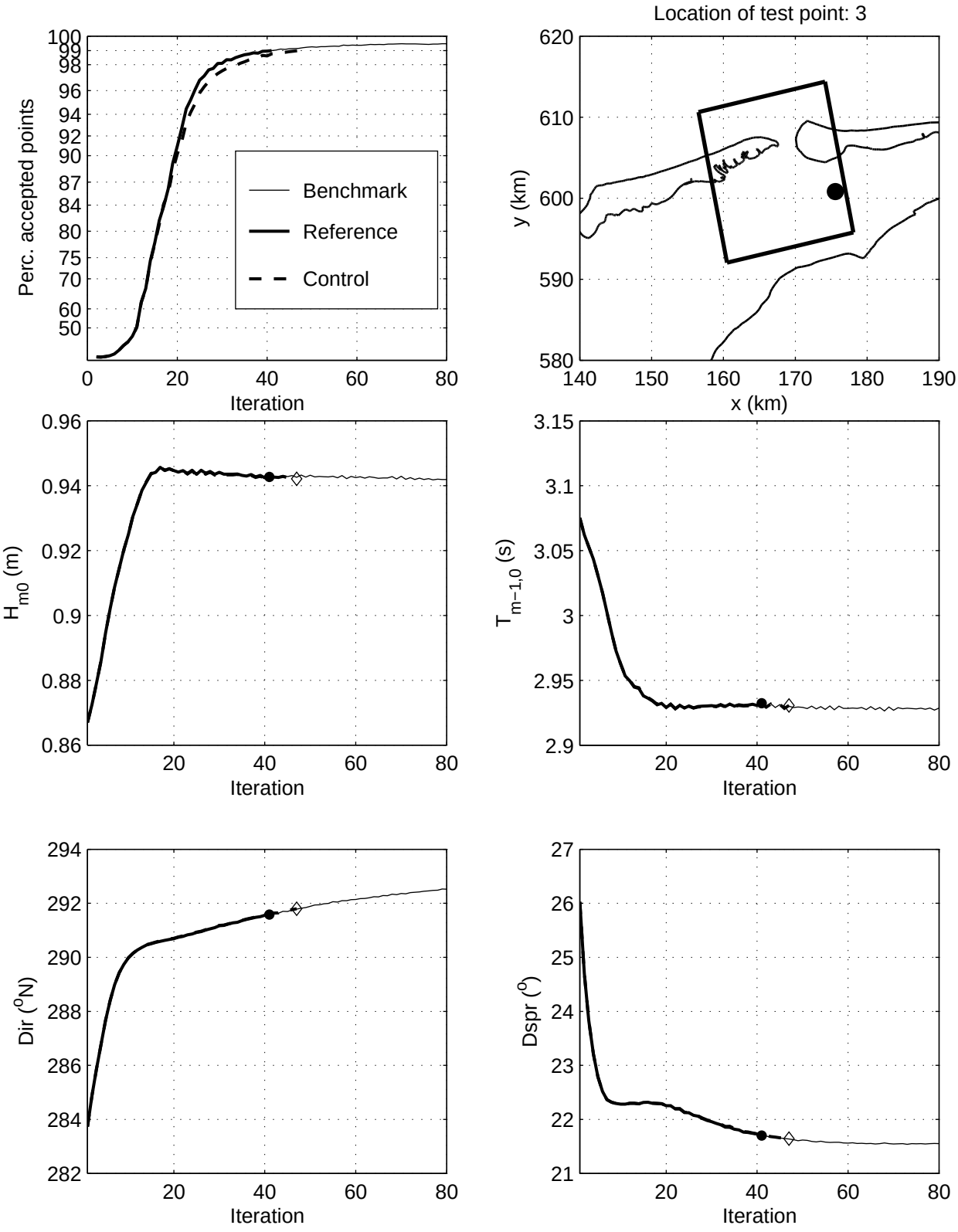

Convergence behaviour: deactivation of action limiter and S_{nl4} in the surf zone in the Amelander Zeegat, Case: AZG3A 2005/01/02 10:00, at point 3 Deactivation at Ursell = 0.20 (C_urs_020)		SWAN 40.51A
	Numerical efficiency SWAN	
DELTARES & ALKYON	H5107.46/A2114	Fig. 6.7

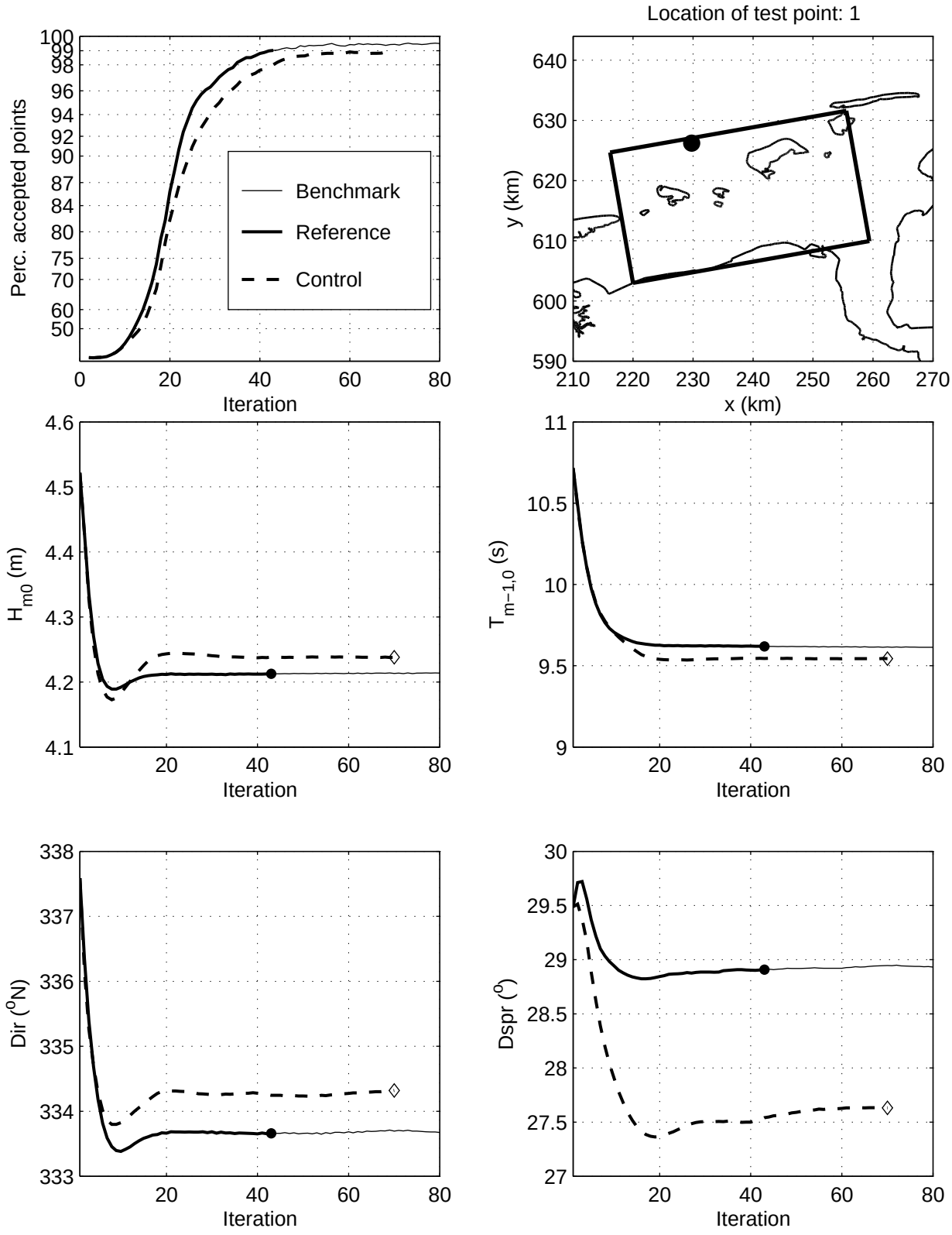

Convergence behaviour: deactivation of action limiter and S_{nl4} in the surf zone in the Eems−Dollard, Case: EEMS3A 2006/11/01 03:00, at point 1 Deactivation at Ursell = 0.10 (C_urs_010)		SWAN 40.51A
		Numerical efficiency SWAN
DELTARES & ALKYON	H5107.46/A2114	Fig. 6.8

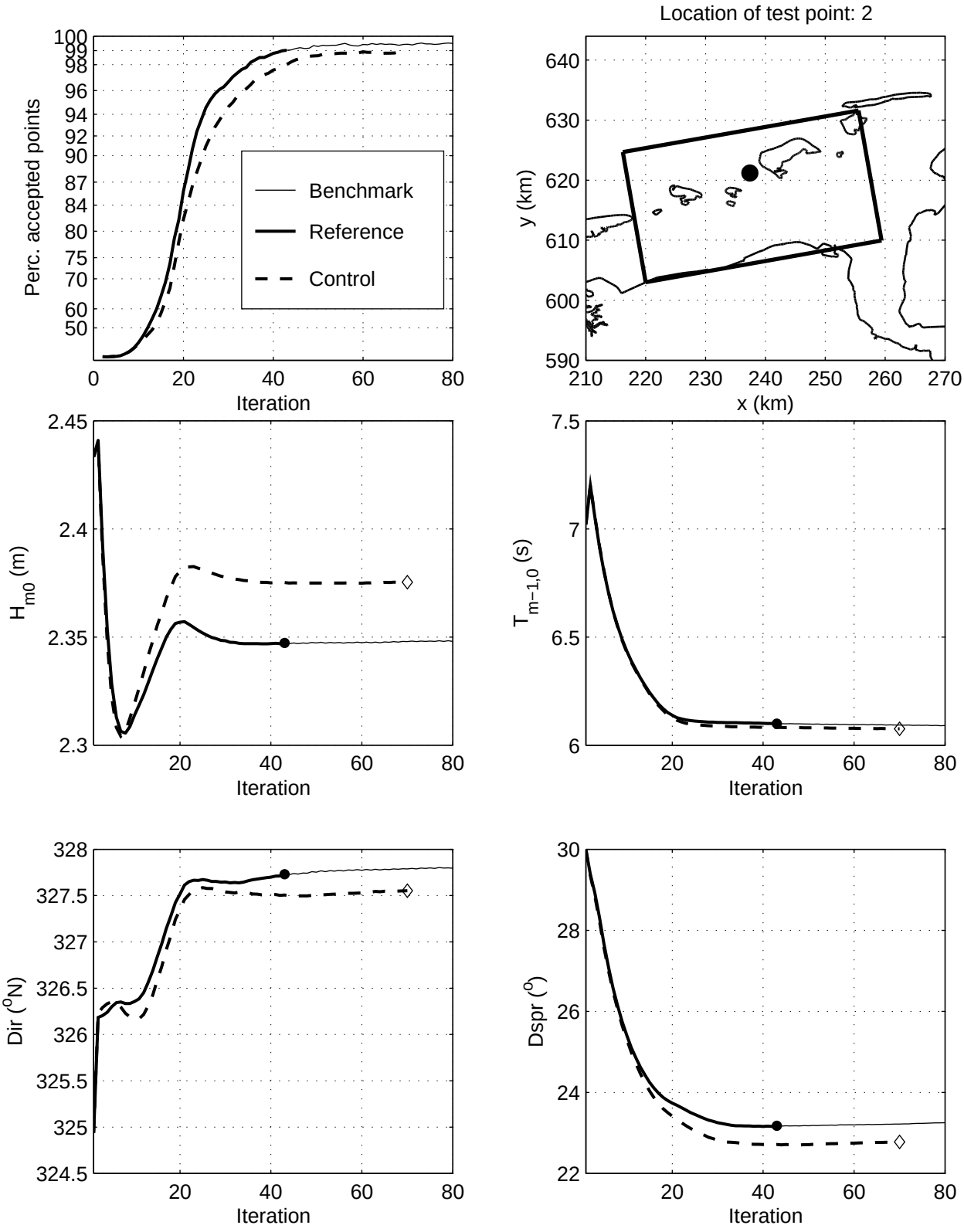

Convergence behaviour: deactivation of action limiter and S_{nl4} in the surf zone in the Eems−Dollard, Case: EEMS3A 2006/11/01 03:00, at point 2 Deactivation at Ursell = 0.10 (C_urs_010)		SWAN 40.51A
		Numerical efficiency SWAN
DELTARES & ALKYON	H5107.46/A2114	Fig. 6.9

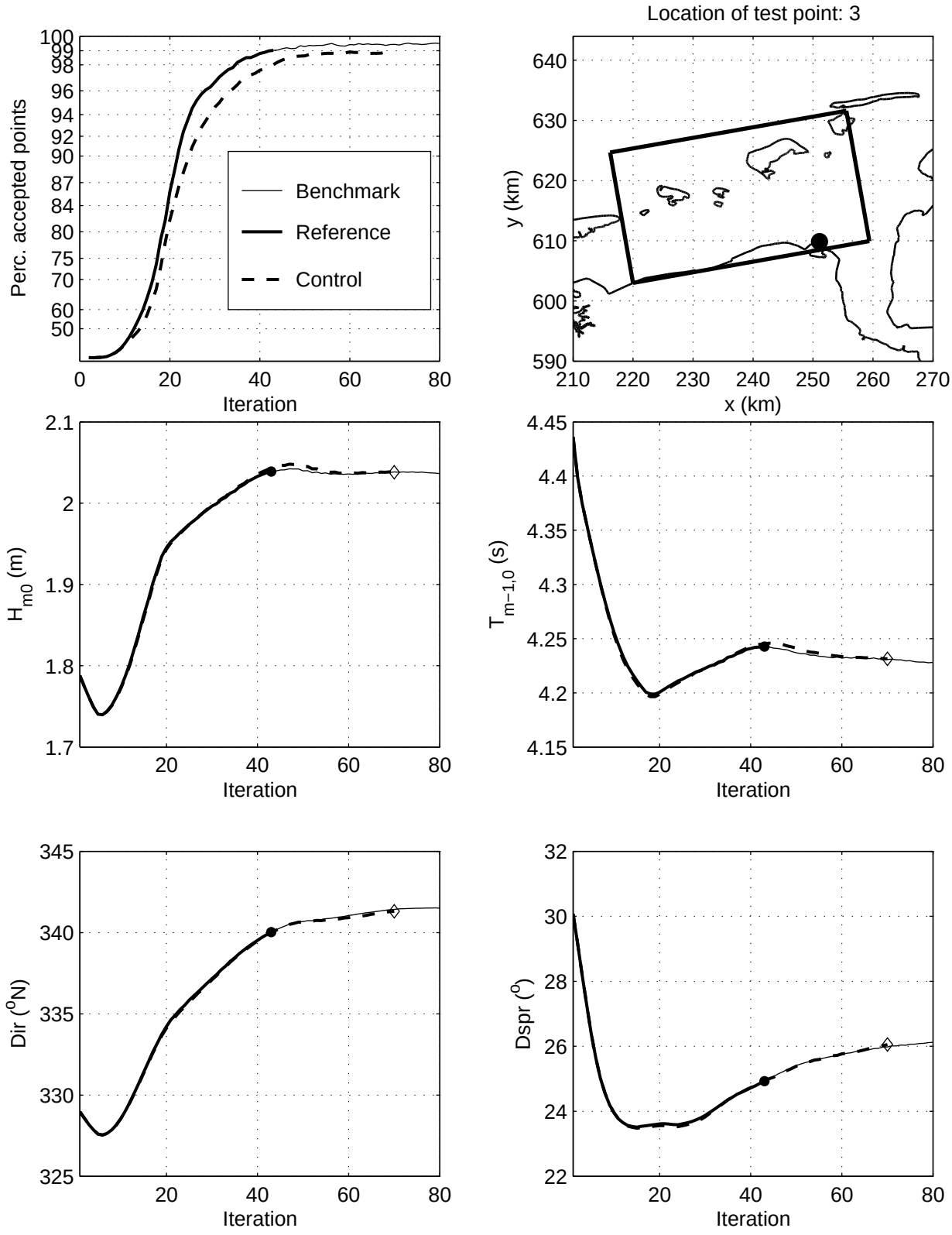

Convergence behaviour: deactivation of action limiter and S_{nl4} in the surf zone in the Eems−Dollard, Case: EEMS3A 2006/11/01 03:00, at point 3 Deactivation at Ursell = 0.10 (C_urs_010)		SWAN 40.51A
	Numerical efficiency SWAN	
DELTARES & ALKYON	H5107.46/A2114	Fig. 6.10

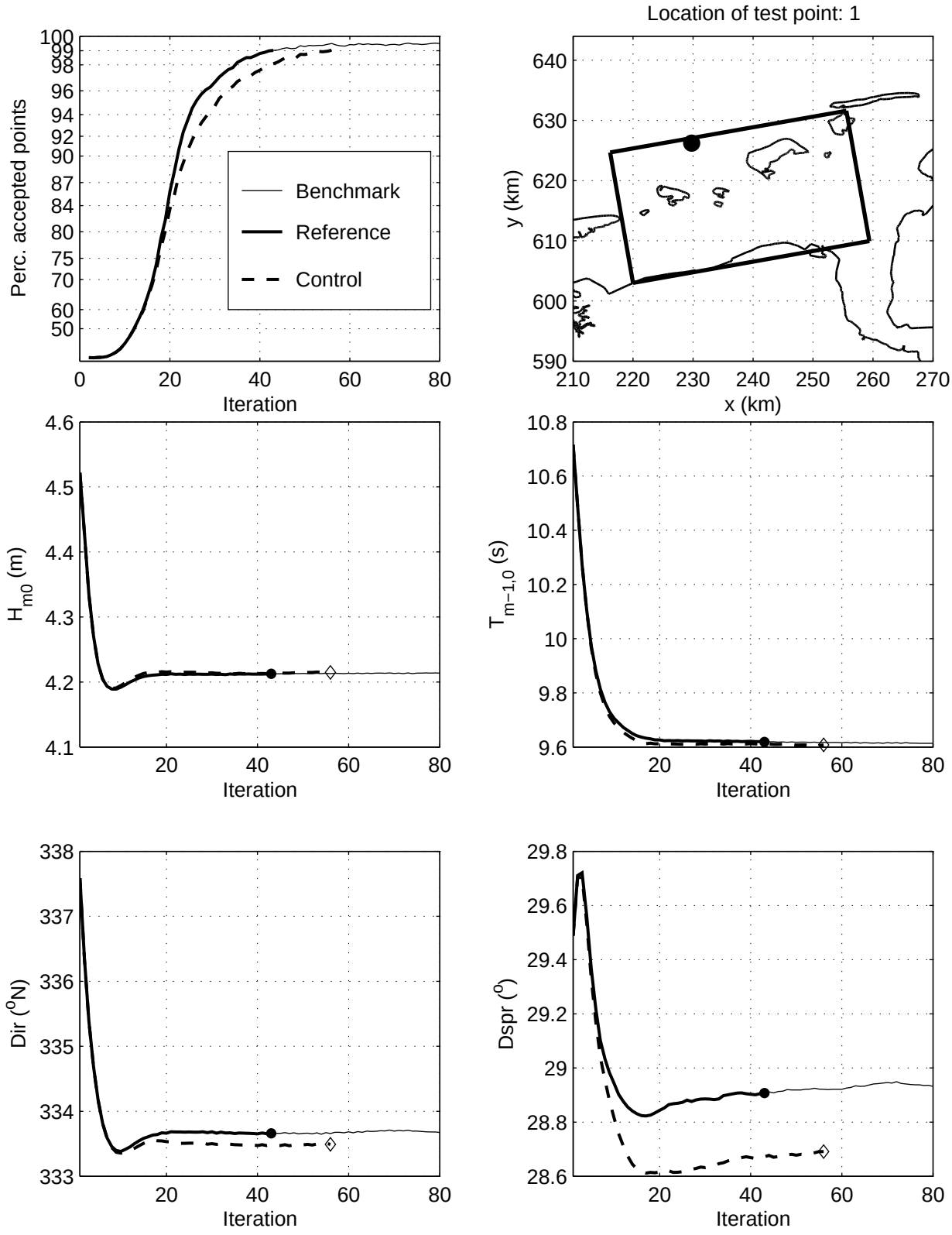

Convergence behaviour: deactivation of action limiter and S_{nl4} in the surf zone in the Eems−Dollard, Case: EEMS3A 2006/11/01 03:00, at point 1 Deactivation at Ursell = 0.20 (C_urs_020)		SWAN 40.51A
	Numerical efficiency SWAN	
DELTARES & ALKYON	H5107.46/A2114	Fig. 6.11

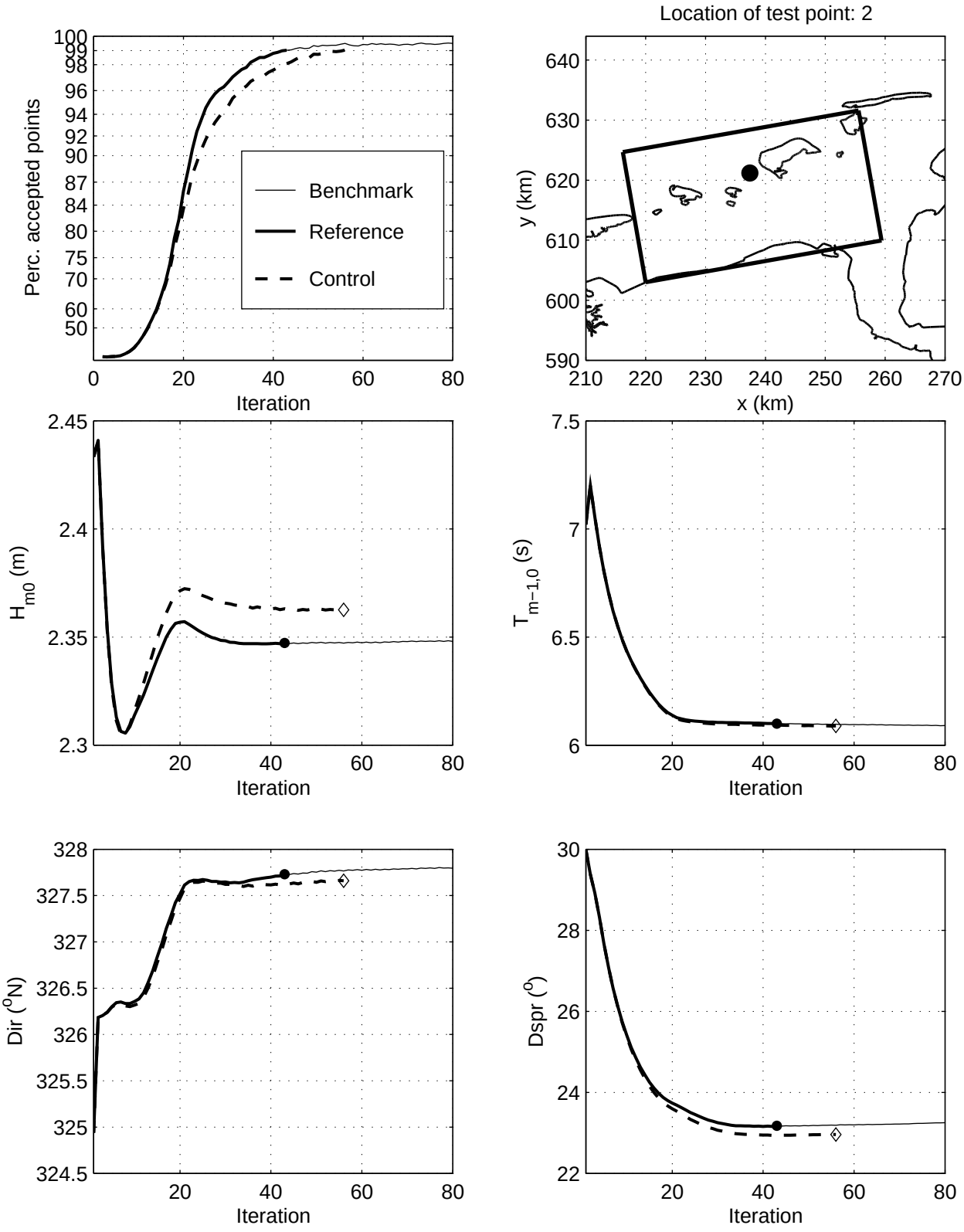

Convergence behaviour: deactivation of action limiter and S_{nl4} in the surf zone in the Eems−Dollard, Case: EEMS3A 2006/11/01 03:00, at point 2 Deactivation at Ursell = 0.20 (C_urs_020)		SWAN 40.51A
	Numerical efficiency SWAN	
DELTARES & ALKYON	H5107.46/A2114	Fig. 6.12

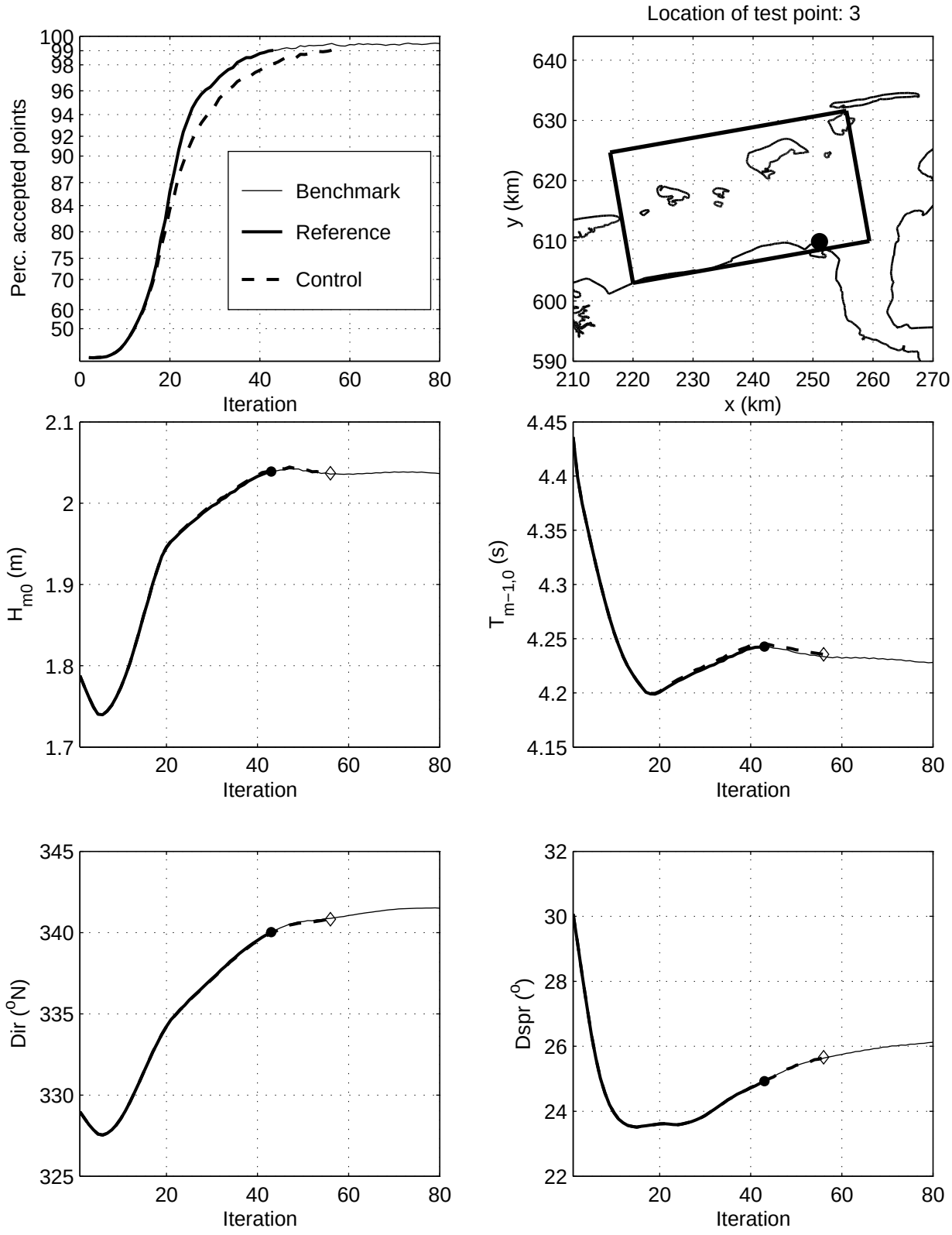

Convergence behaviour: deactivation of action limiter and S_{nl4} in the surf zone in the Eems−Dollard, Case: EEMS3A 2006/11/01 03:00, at point 3 Deactivation at Ursell = 0.20 (C_urs_020)		SWAN 40.51A
	Numerical efficiency SWAN	
DELTARES & ALKYON	H5107.46/A2114	Fig. 6.13

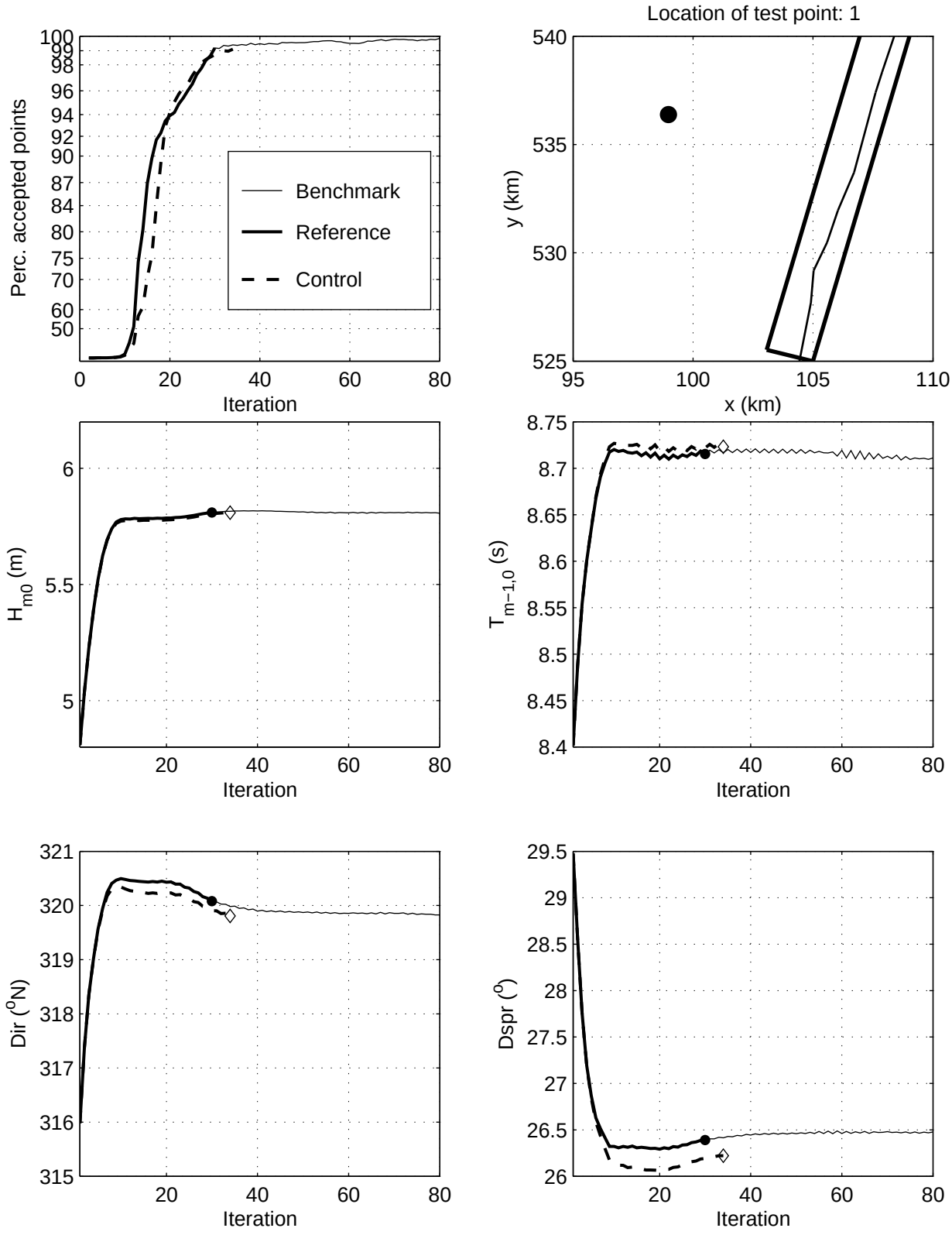

Convergence behaviour: deactivation of action limiter and S_{nl4} in the surf zone along the Dutch coast near Petten, Case: PETTEN 1995/01/01 10:00, at point 1 Deactivation at Ursell = 0.10 (C_urs_010)		SWAN 40.51A
	Numerical efficiency SWAN	
DELTARES & ALKYON	H5107.46/A2114	Fig. 6.14

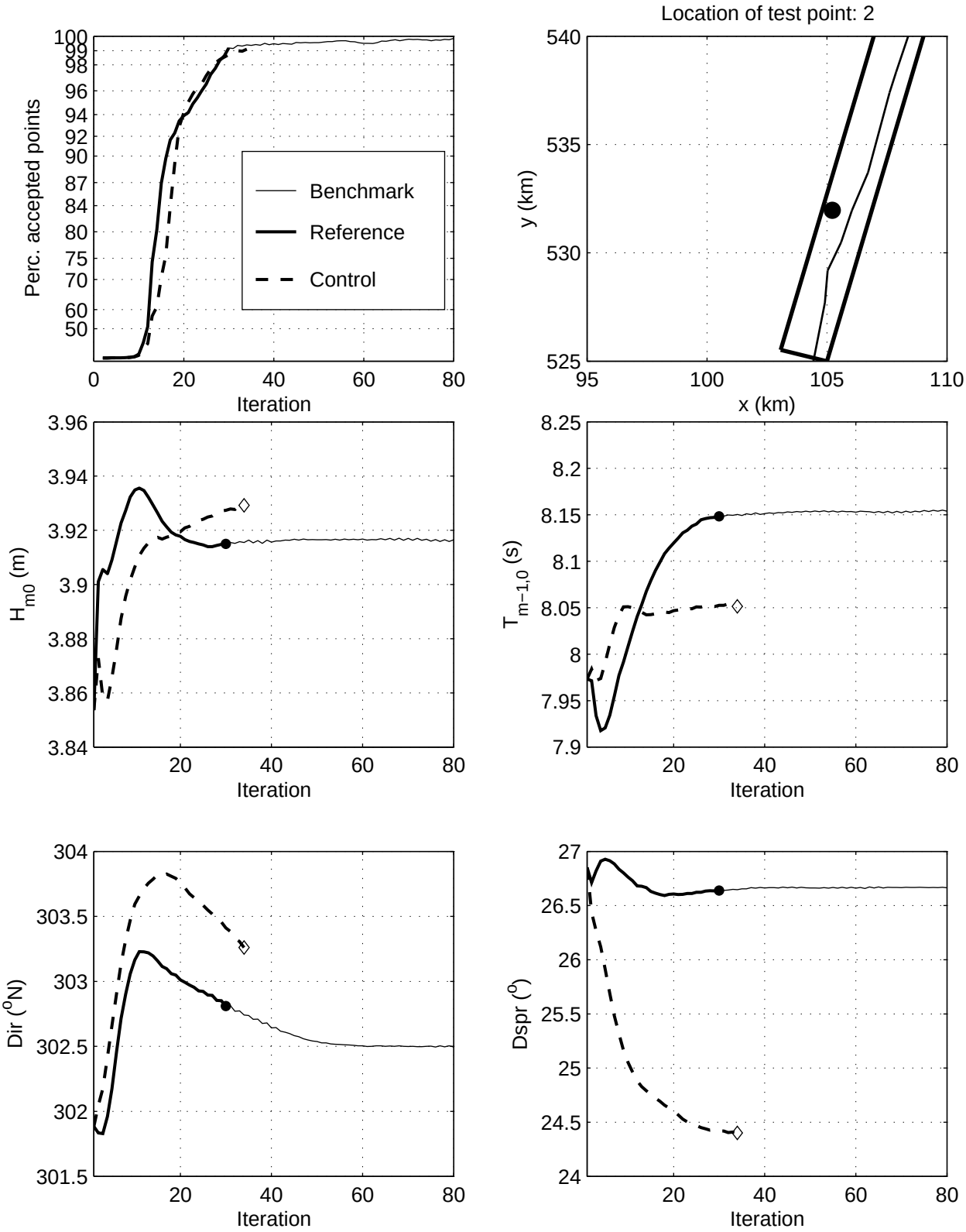

Convergence behaviour: deactivation of action limiter and S_{nl4} in the surf zone along the Dutch coast near Petten, Case: PETTEN 1995/01/01 10:00, at point 2 Deactivation at Ursell = 0.10 (C_urs_010)		SWAN 40.51A
	Numerical efficiency SWAN	
DELTARES & ALKYON	H5107.46/A2114	Fig. 6.15

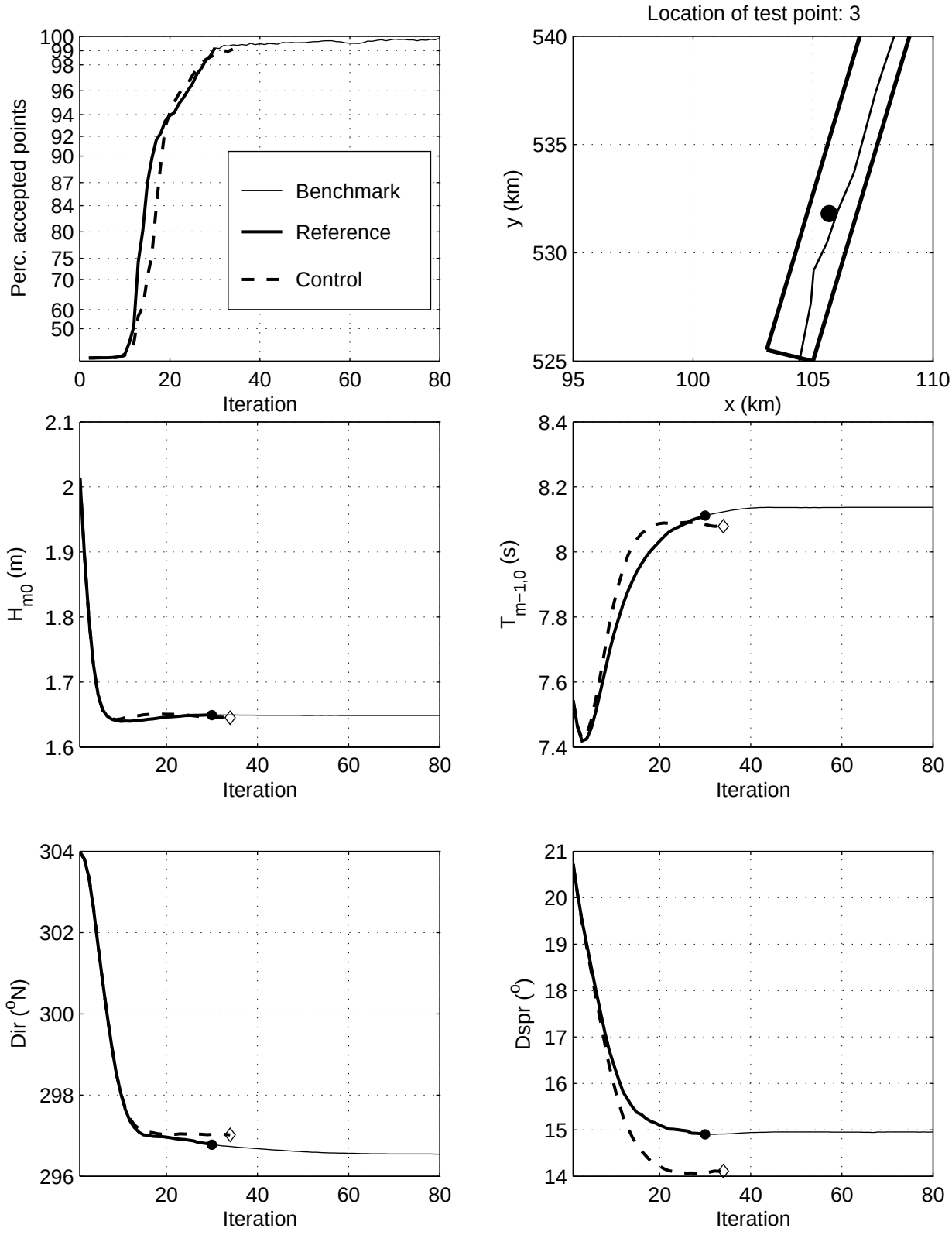

Convergence behaviour: deactivation of action limiter and S_{nl4} in the surf zone along the Dutch coast near Petten, Case: PETTEN 1995/01/01 10:00, at point 3 Deactivation at Ursell = 0.10 (C_urs_010)		SWAN 40.51A
	Numerical efficiency SWAN	
DELTARES & ALKYON	H5107.46/A2114	Fig. 6.16

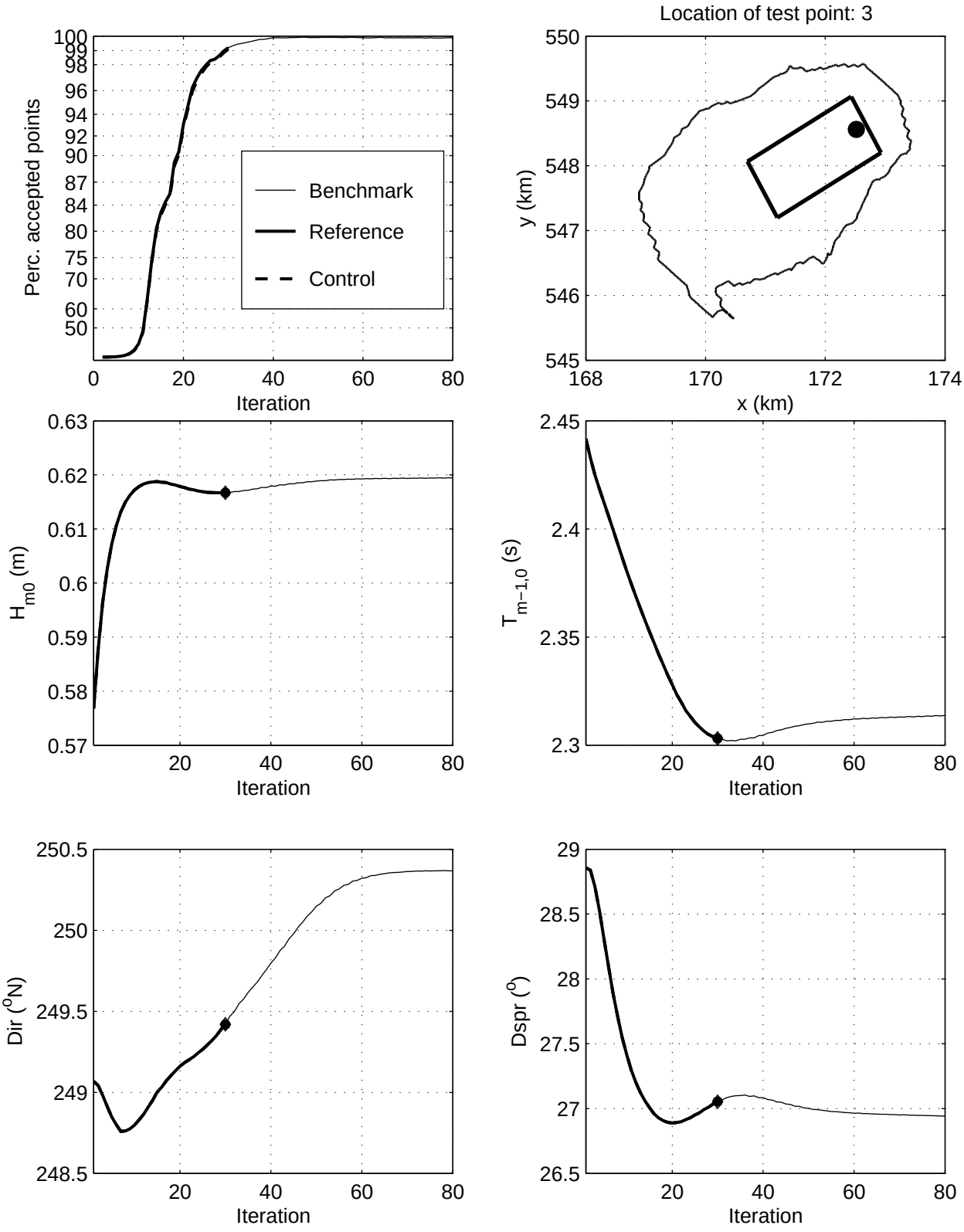

Convergence behaviour: deactivation of action limiter and S_{nl4} in the surf zone in Lake Sloten, Case: SLE 2002/10/27 15:00, at point 3 Deactivation at Ursell = 0.10 (C_urs_010)		SWAN 40.51A
	Numerical efficiency SWAN	
DELTARES & ALKYON	H5107.46/A2114	Fig. 6.17

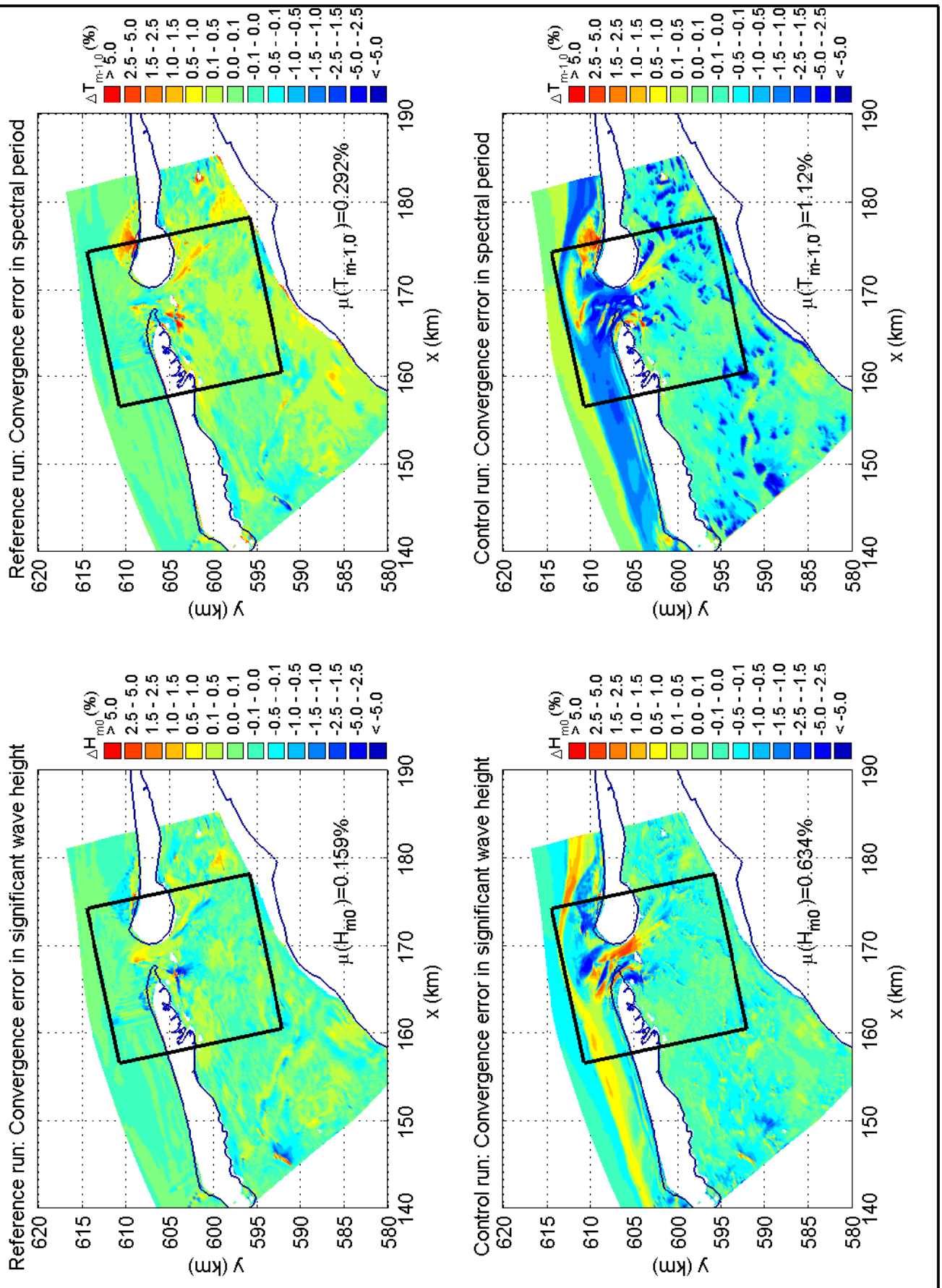

Convergence errors in H_{m0} and $T_{m-1,0}$ for action limiter deactivation in the Amelander Zeegat, Case: AZG3A 2005/01/02 10:00 Deactivation at Ursell = 0.10 (urs_010)		SWAN 40.51A
	Numerical efficiency SWAN	
DELTARES & ALKYON	H5107.46/A2114	Fig. 6.18

DELTARES & ALKYON

Convergence errors in Dir and Dspr for action limiter deactivation in the Amelander Zeegat, Case: AZG3A 2005/01/02 10:00
Deactivation at Ursell = 0.10 (urs_010)

H5107.46/A2114

Numerical efficiency SWAN

SWAN 40.51A

Fig. 6.19

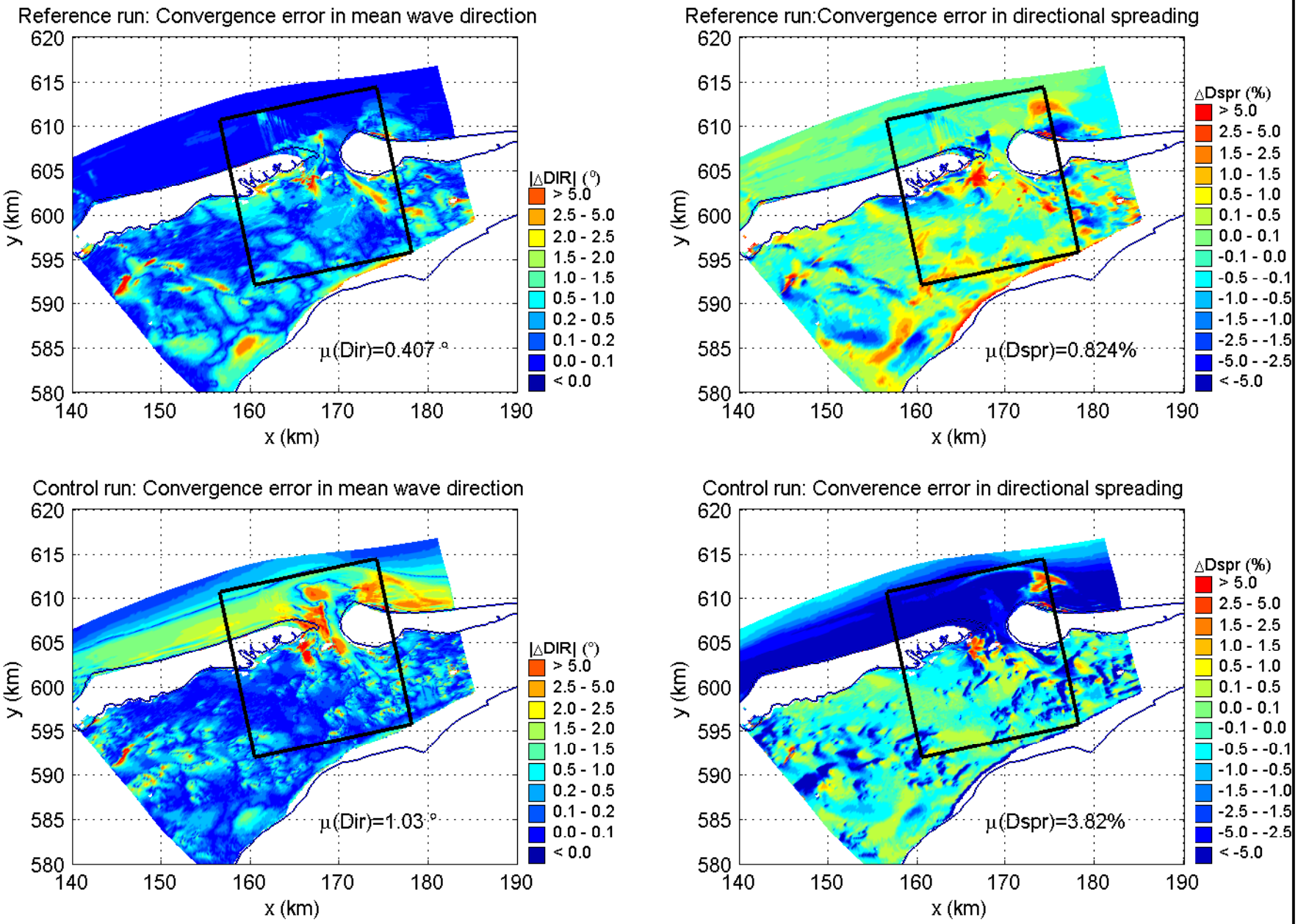

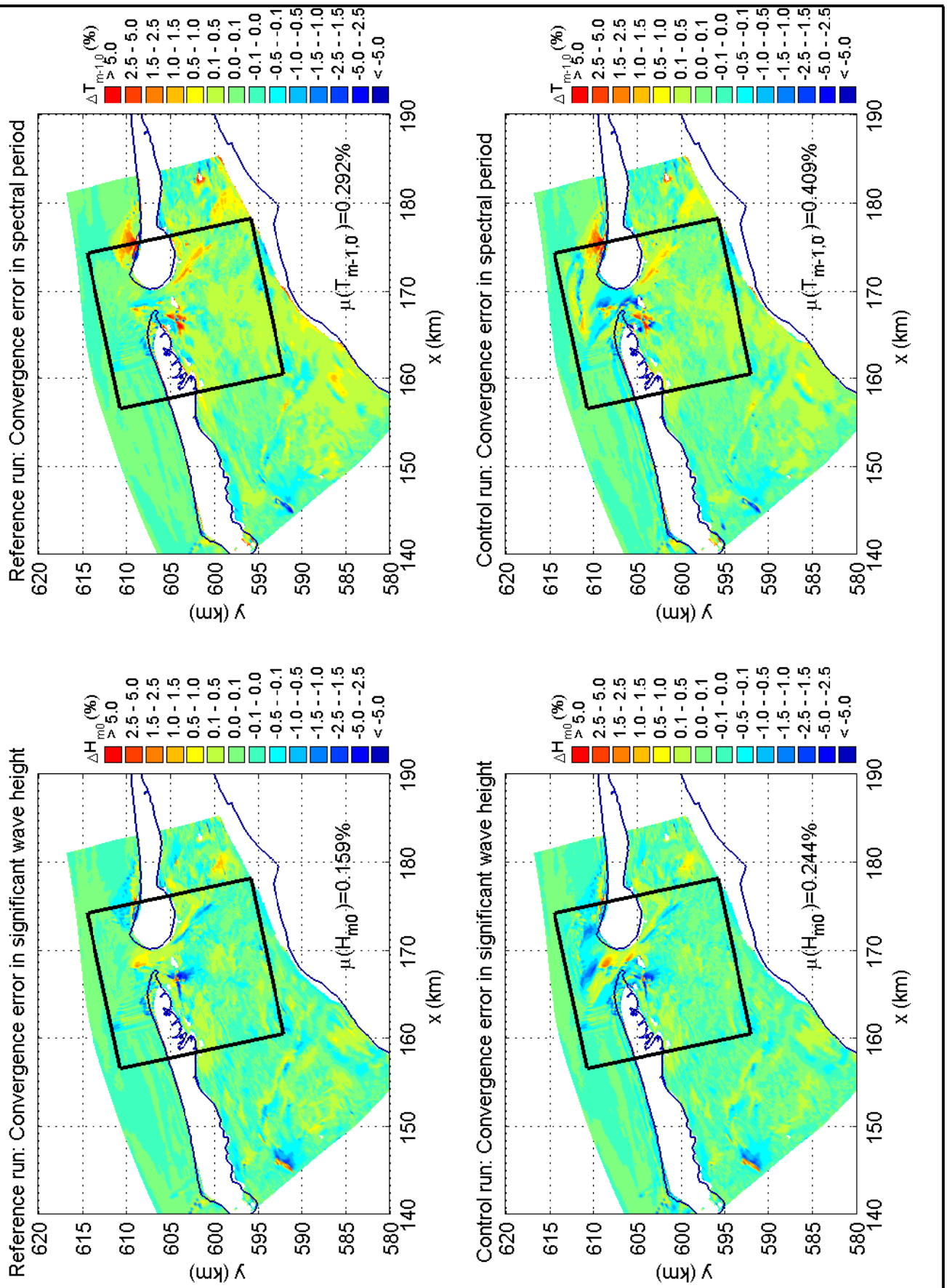

Convergence errors in H_{m0} and $T_{m-1,0}$ for action limiter deactivation in the Amelander Zeegat, Case: AZG3A 2005/01/02 10:00 Deactivation at Ursell = 0.20 (urs_020)		SWAN 40.51A
	Numerical efficiency SWAN	
DELTARES & ALKYON	H5107.46/A2114	Fig. 6.20

DELTARES & ALKYON

Convergence errors in Dir and Dspr for action limiter deactivation in the Amelander Zeegat, Case: AZG3A 2005/01/02 10:00
Deactivation at Ursell = 0.20 (urs_020)

H5107.46/A2114

Numerical efficiency SWAN

SWAN 40.51A

Fig. 6.21

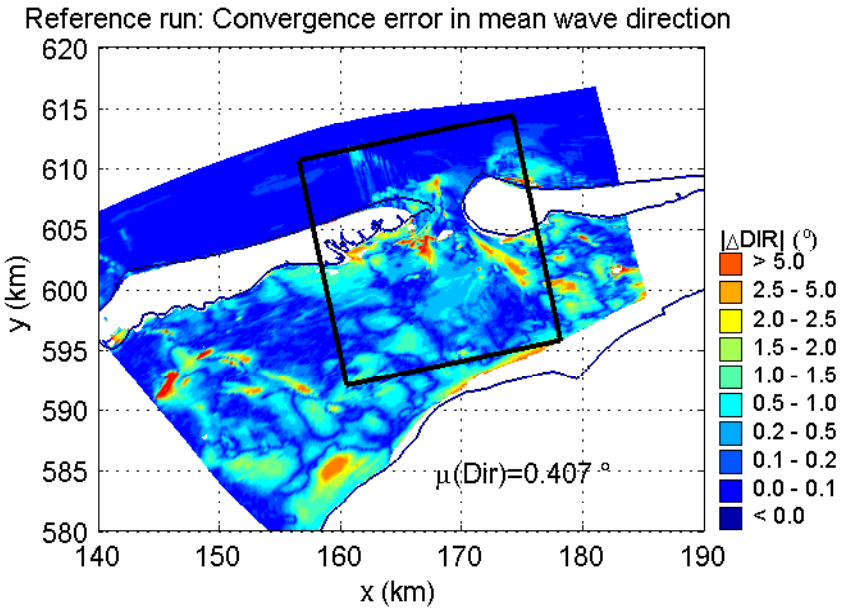

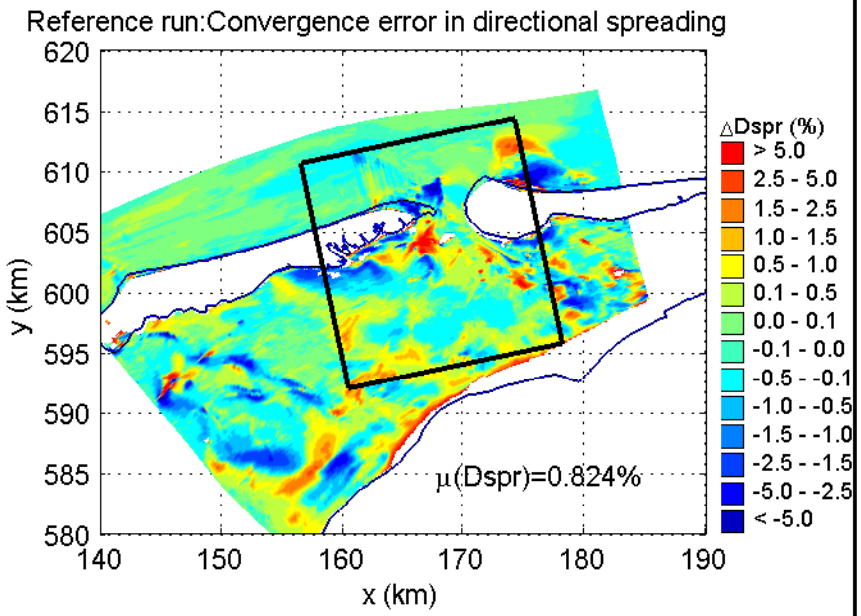

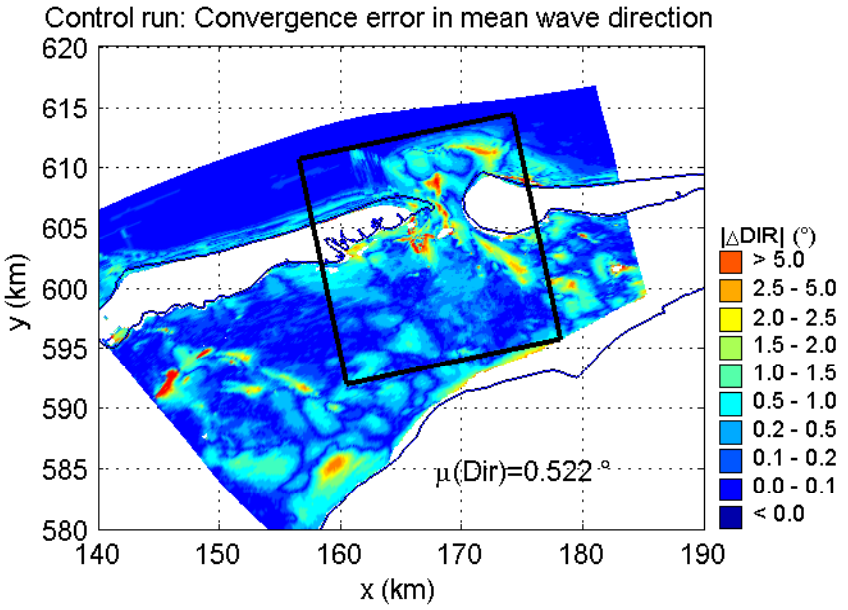

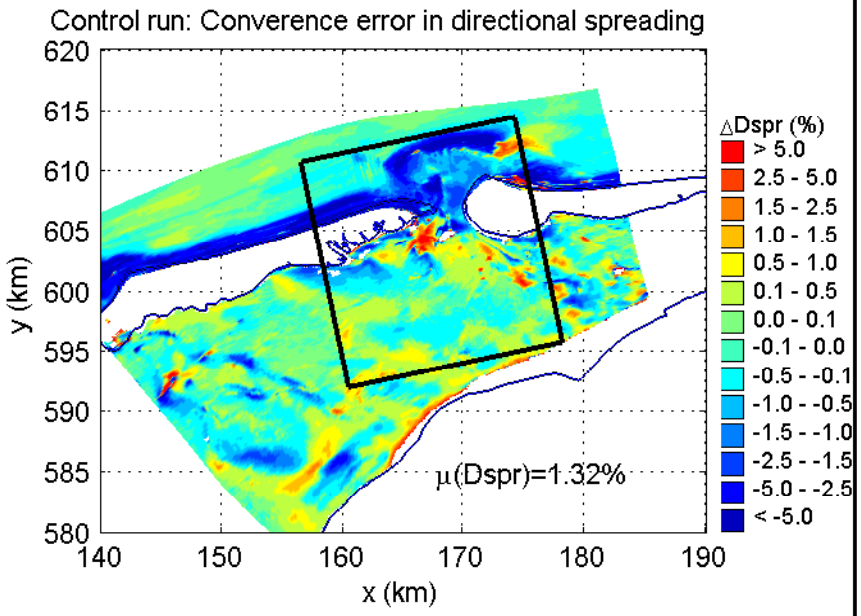

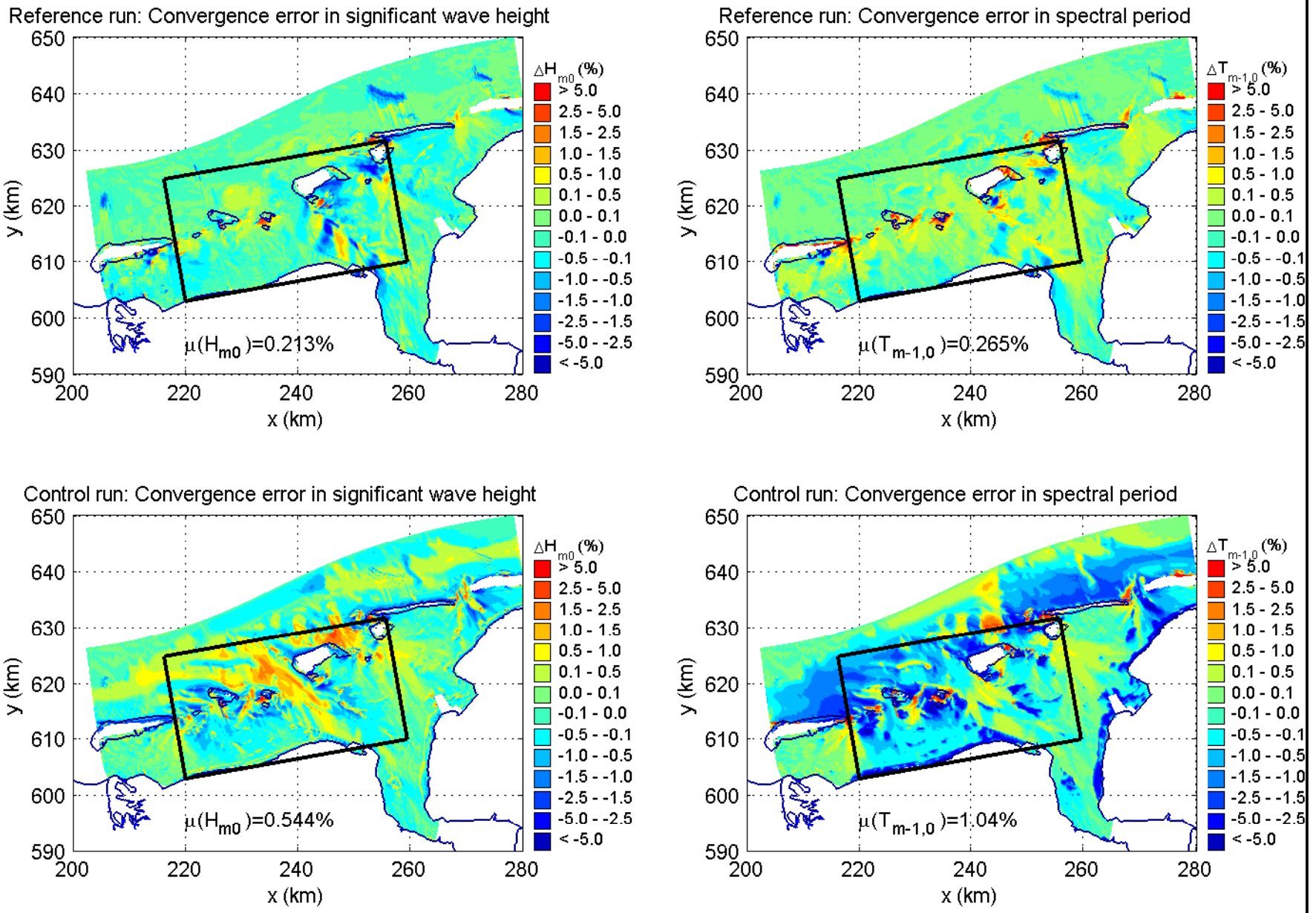

Convergence errors in H_{m0} and $T_{m-1,0}$ for action limiter deactivation in the Eems-Dollard, Case: EEMS3A 2006/11/01 03:00 Deactivation at Ursell = 0.10 (urs_010)

DELTARES & ALKYON		
H5107.46/A2114	Numerical efficiency SWAN	SWAN 40.51A
Fig. 6.22		

Convergence errors in Dir and Dspr for action limiter deactivation in the Eems-Dollard, Case: EEMS3A 2006/11/01 03:00 Deactivation at Ursell = 0.10 (urs_010)		SWAN 40.51A
		Numerical efficiency SWAN
DELTARES & ALKYON	H5107.46/A2114	Fig. 6.23

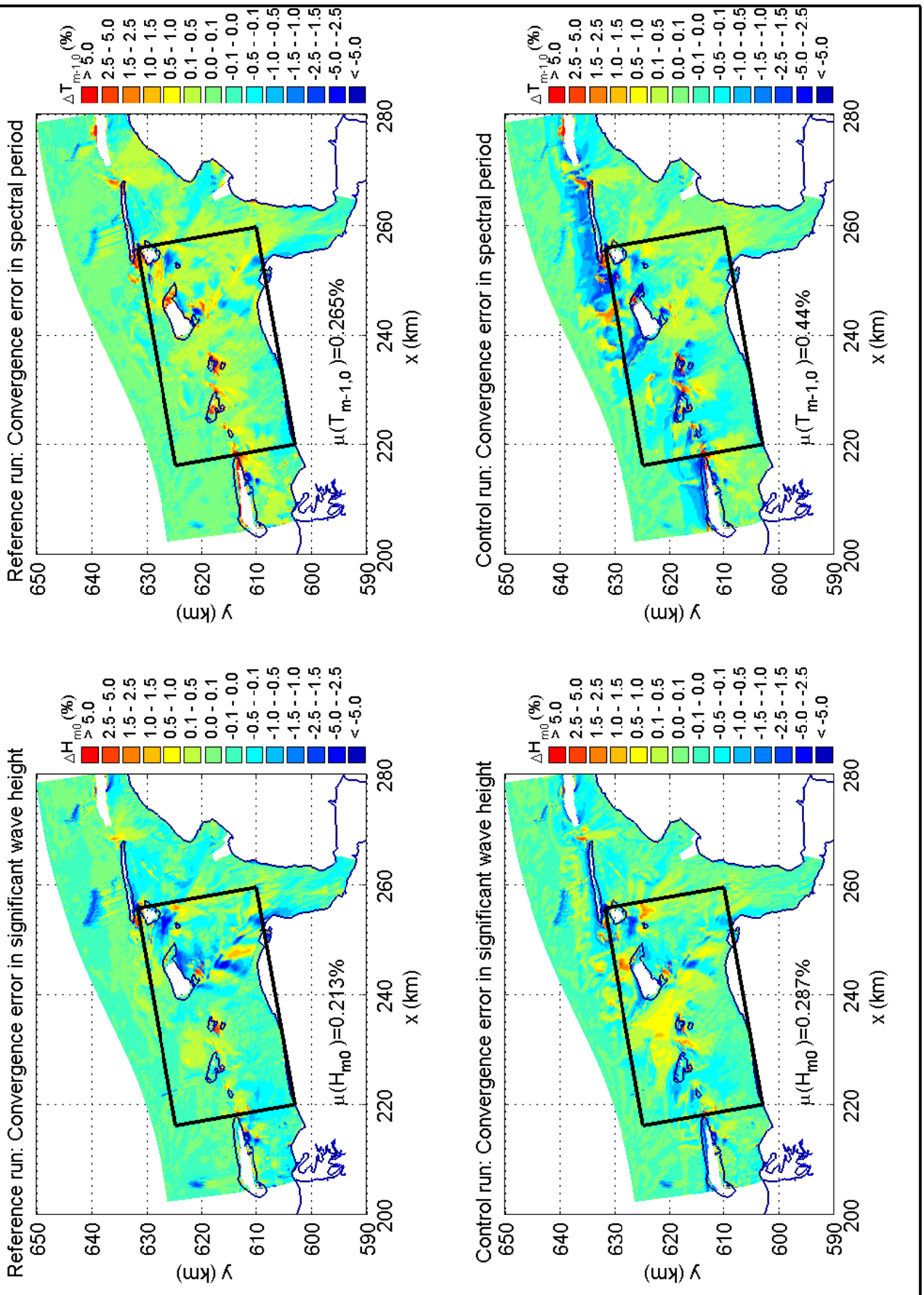

Convergence errors in H_{m0} and $T_{m-1,0}$ for action limiter deactivation in the Eems-Dollard, Case: EEMS3A 2006/11/01 03:00 Deactivation at Ursell = 0.20 (urs_020)		SWAN 40.51A
		Numerical efficiency SWAN
DELTARES & ALKYON	H5107.46/A2114	Fig. 6.24

Convergence errors in Dir and Dspr for action limiter deactivation in the Eems-Dollard, Case: EEMS3A 2006/11/01 03:00 Deactivation at Ursell = 0.20 (urs_020)		SWAN 40.51A
		Numerical efficiency SWAN
DELTARES & ALKYON	H5107.46/A2114	Fig. 6.25

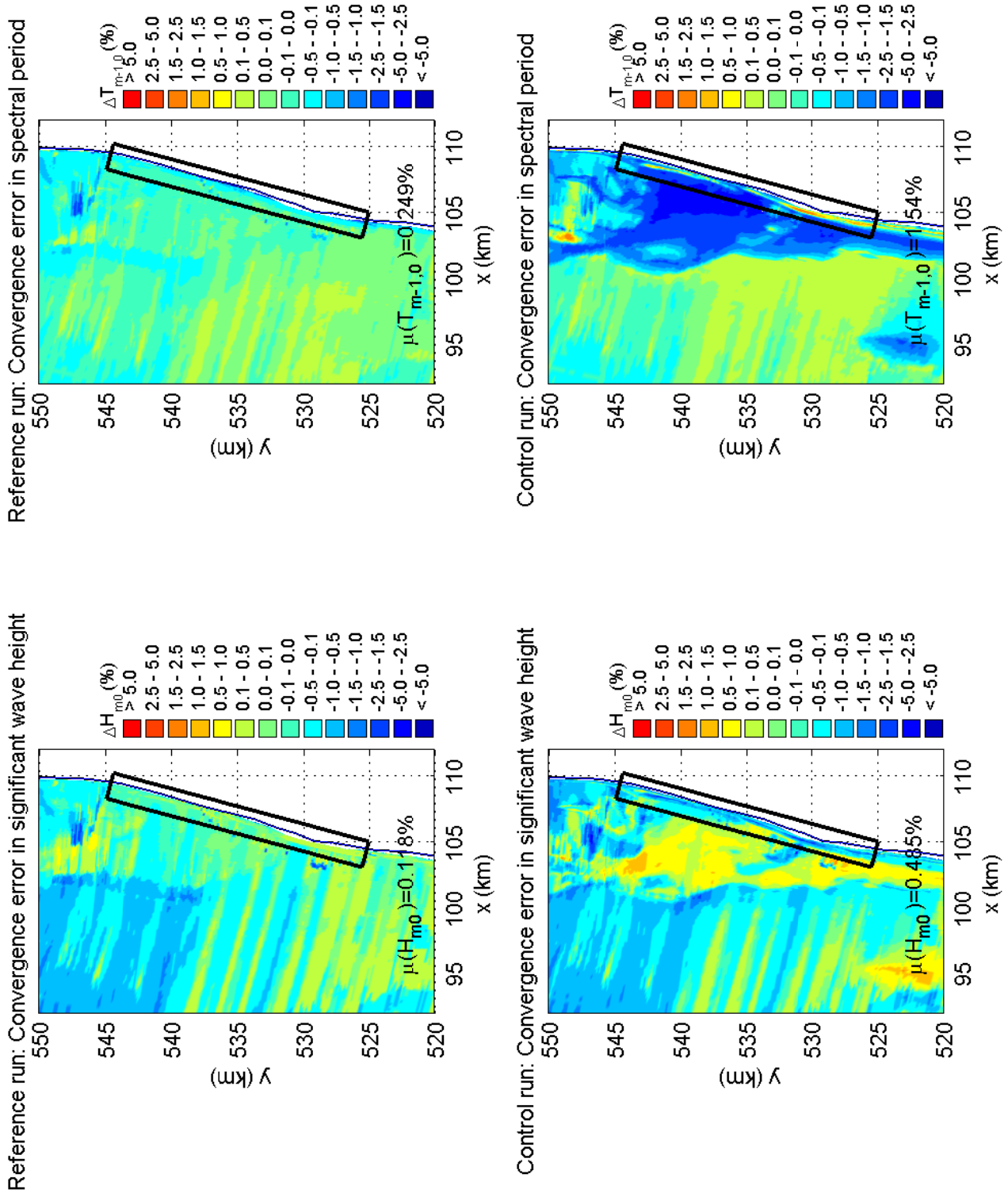

Convergence errors in H_{m0} and $T_{m-1,0}$ for action limiter deactivation along the Dutch coast near Petten, Case: PETTEN 1995/01/01 10:00 Deactivation at Ursell = 0.10 (urs_010)		SWAN 40.51A
		Numerical efficiency SWAN
DELTARES & ALKYON	H5107.46/A2114	Fig. 6.26

Reference run: Convergence error in mean wave direction

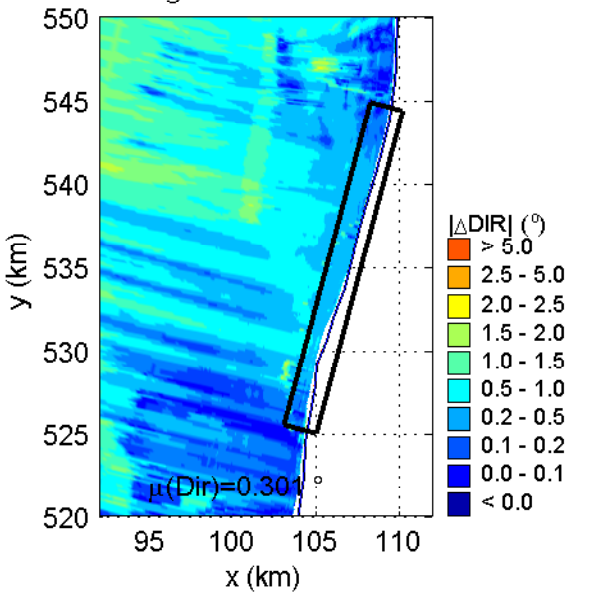

Reference run:Convergence error in directional spreading

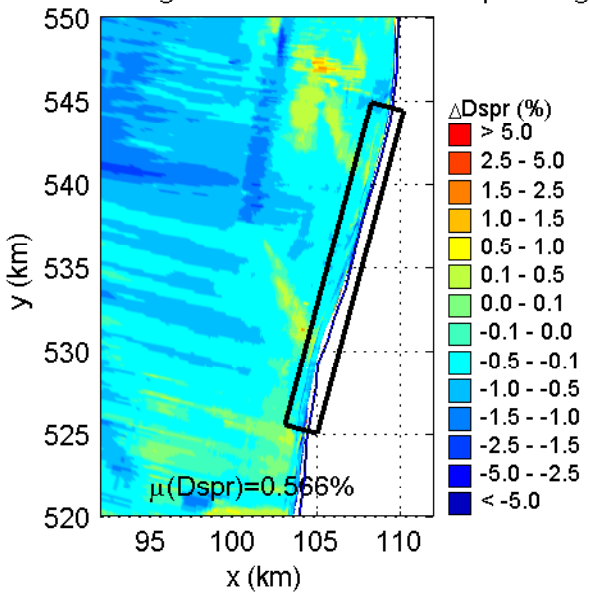

Control run: Convergence error in mean wave direction

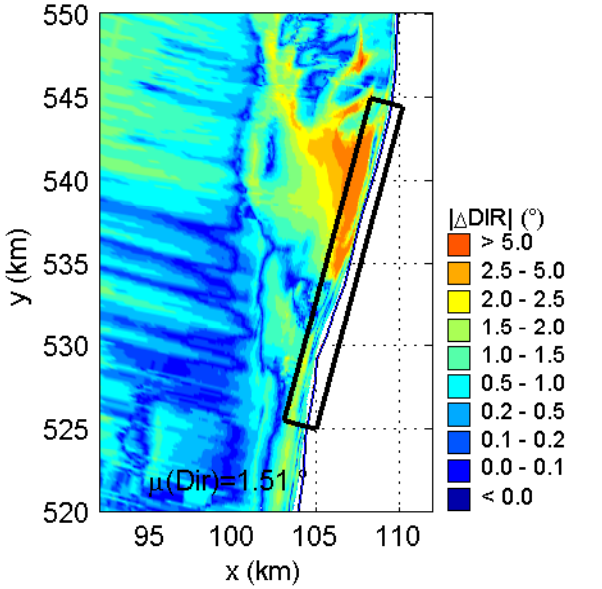

Control run: Converence error in directional spreading

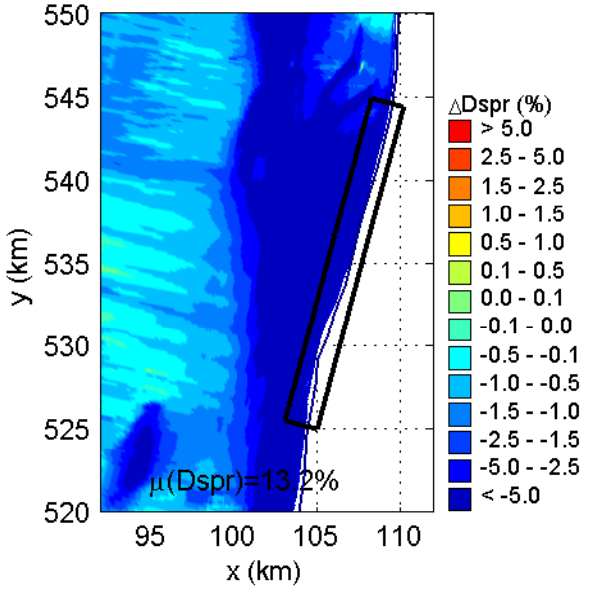

Convergence errors in Dir and Dspr for action limiter deactivation
along the Dutch coast near Petten, Case: PETTEN 1995/01/01 10:00
Deactivation at Ursell = 0.10 (urs_010)

Numerical efficiency SWAN

SWAN 40.51A

H5107.46/A2114

Fig. 6.27

DELTARES & ALKYON

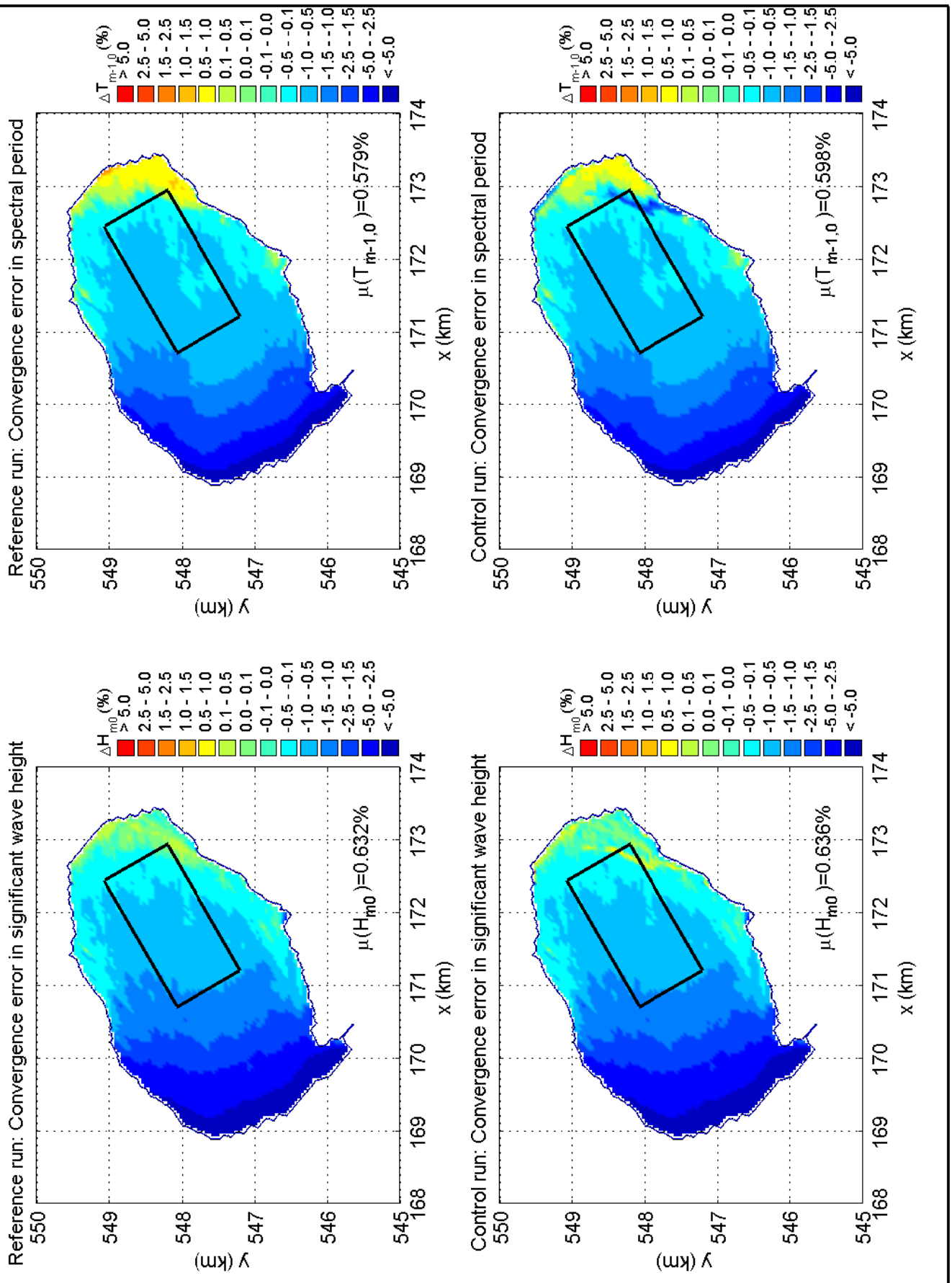

Convergence errors in H_{m0} and $T_{m-1,0}$ for action limiter deactivation in Lake Sloten, Case: SLE 2002/10/27 15:00 Deactivation at Ursell = 0.10 (urs_010)		SWAN 40.51A
		Numerical efficiency SWAN
DELTARES & ALKYON	H5107.46/A2114	Fig. 6.28

Convergence errors in Dir and Dspr for action limiter deactivation
in Lake Sloten, Case: SLE 2002/10/27 15:00
Deactivation at Ursell = 0.10 (urs_010)

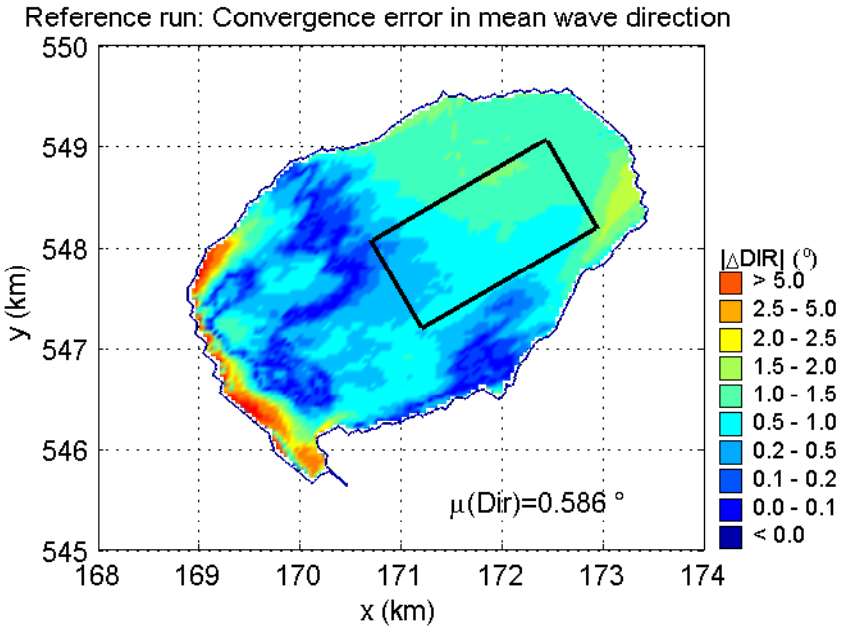

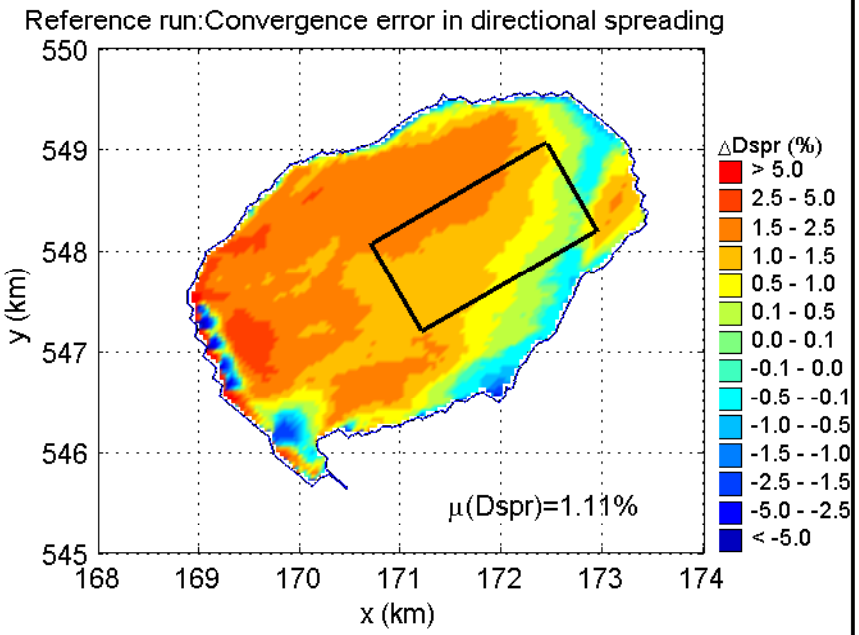

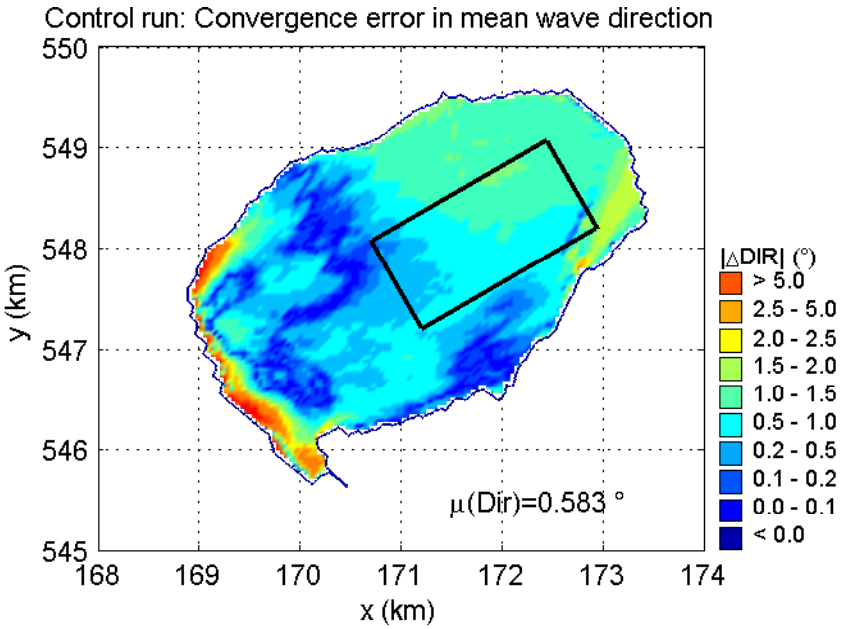

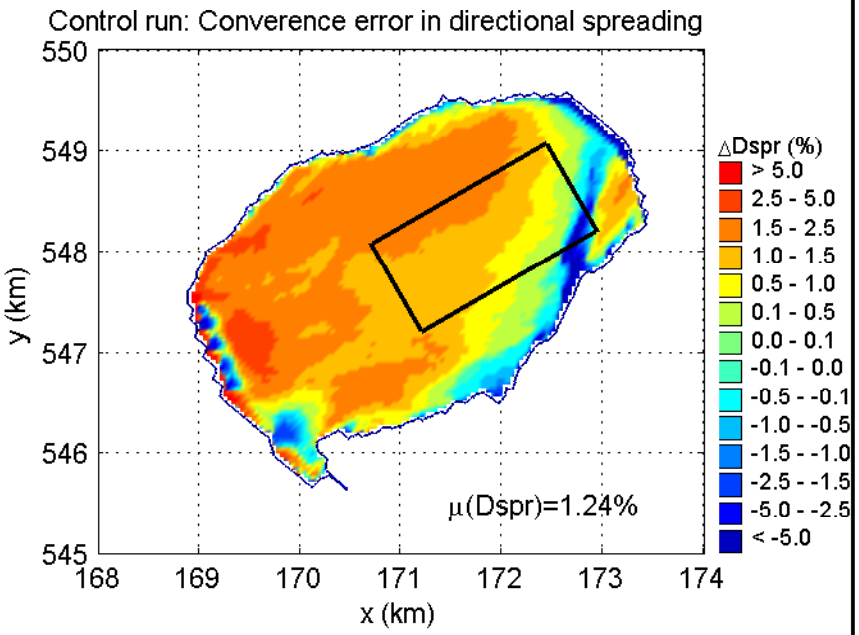

DELTARES & ALKYON

H5107.46/A2114

Numerical efficiency SWAN

SWAN 40.51A

Fig. 6.29

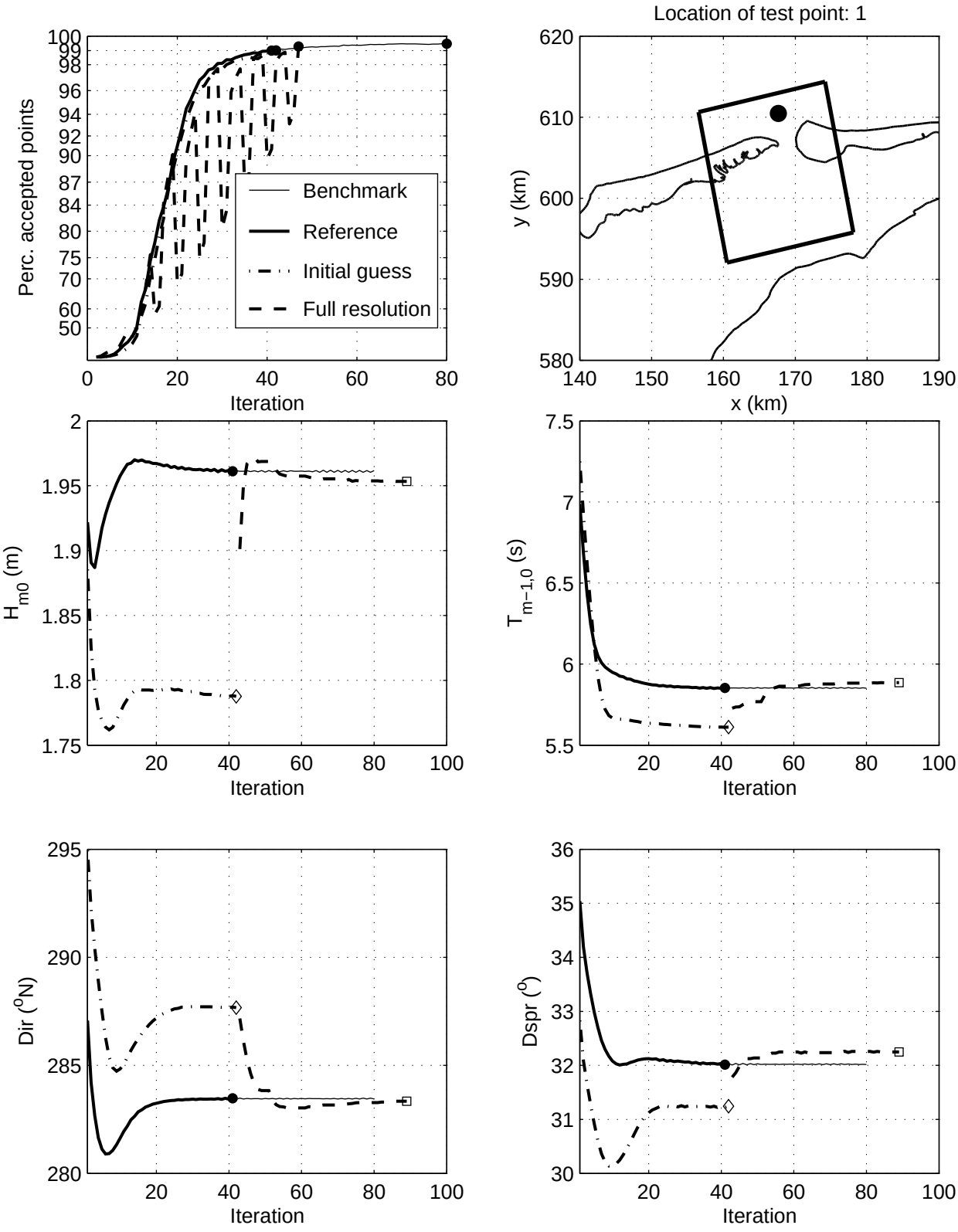

Convergence behaviour of the combined MG and DDM simulation in the Amelander Zeegat, Case: AZG3A 2005/01/02 10:00, at point 1 MG option: x2y2d1s1, DDM option: r10_d05 (C2211_105)		SWAN 40.51A
		Numerical efficiency SWAN
DELTARES & ALKYON	H5107.46/A2114	Fig. 7.1

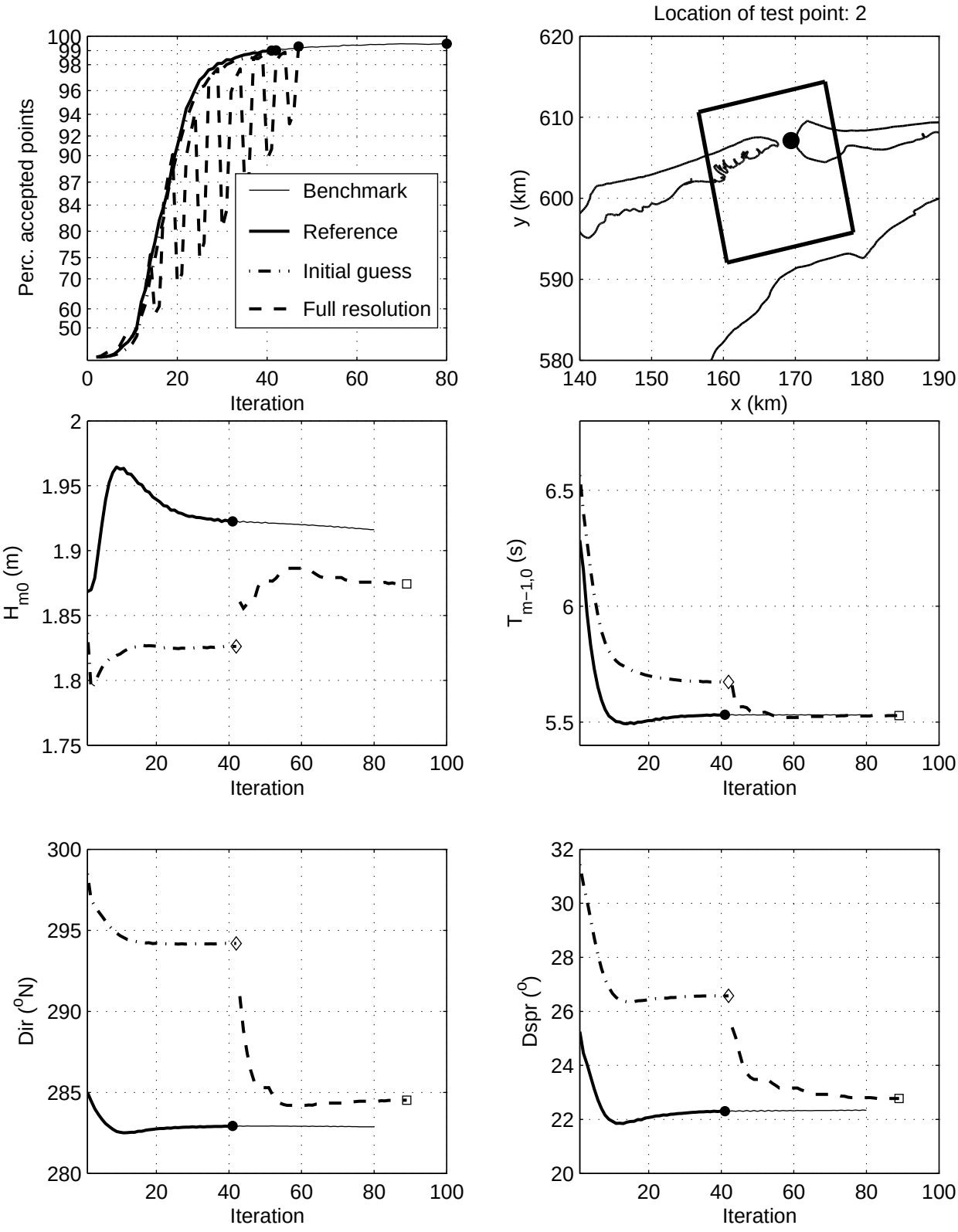

Convergence behaviour of the combined MG and DDM simulation in the Amelander Zeegat, Case: AZG3A 2005/01/02 10:00, at point 2 MG option: x2y2d1s1, DDM option: r10_d05 (C2211_105)		SWAN 40.51A
		Numerical efficiency SWAN
DELTARES & ALKYON	H5107.46/A2114	Fig. 7.2

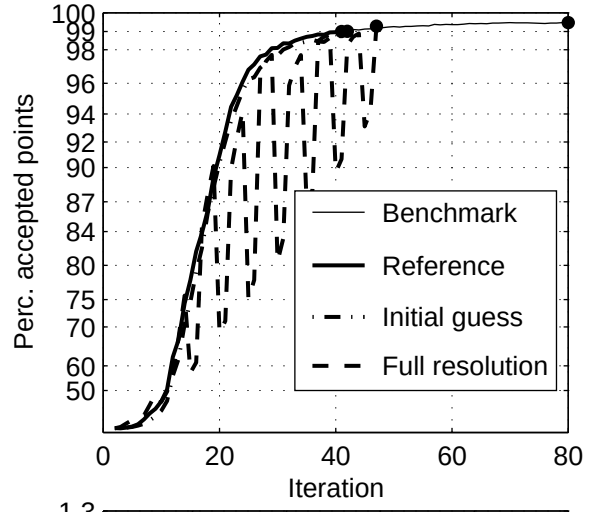

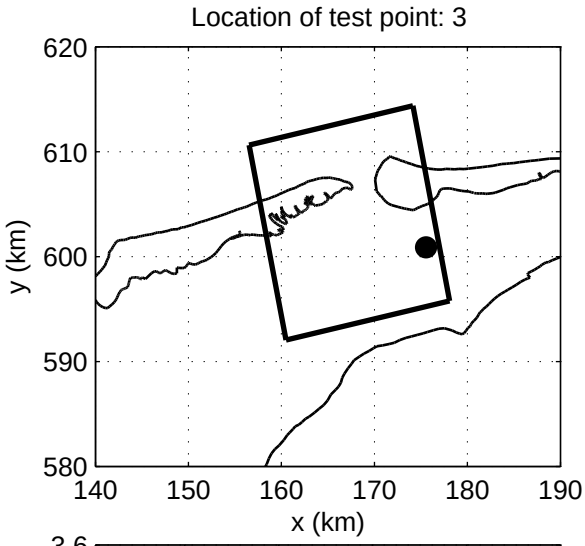

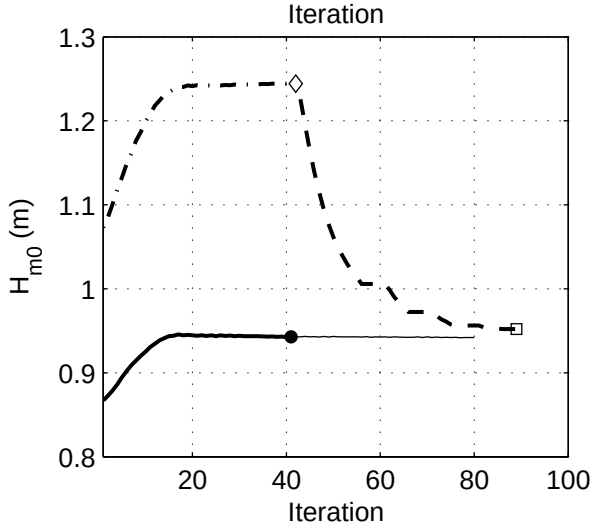

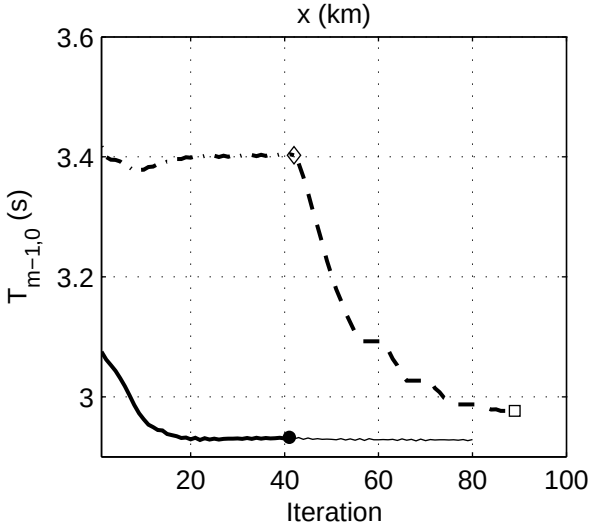

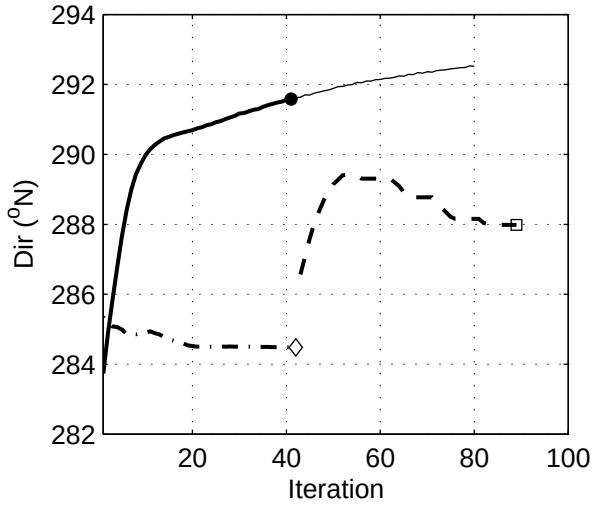

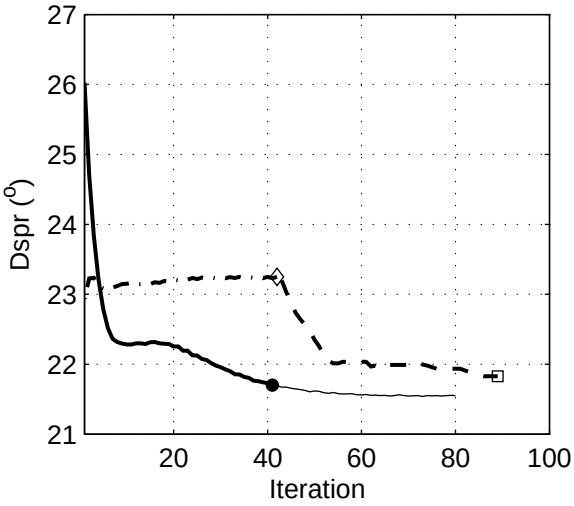

Convergence behaviour of the combined MG and DDM simulation in the Amelander Zeegat, Case: AZG3A 2005/01/02 10:00, at point 3 MG option: x2y2d1s1, DDM option: r10_d05 (C2211_105)		SWAN 40.51A
		Numerical efficiency SWAN
DELTARES & ALKYON	H5107.46/A2114	Fig. 7.3

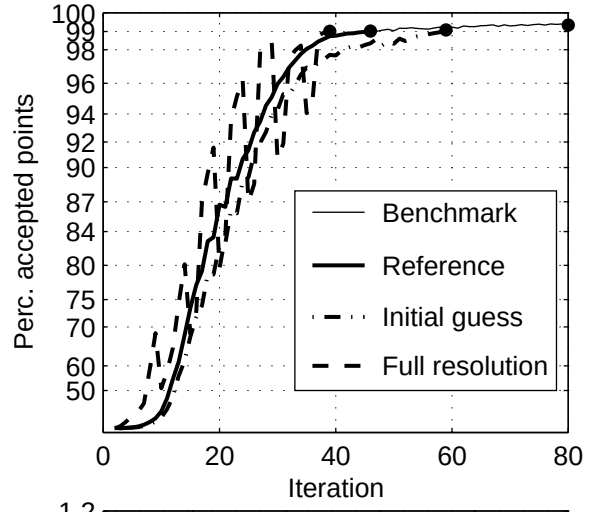

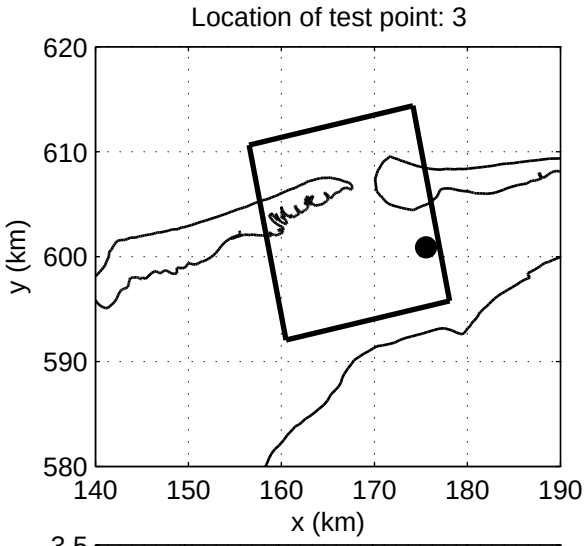

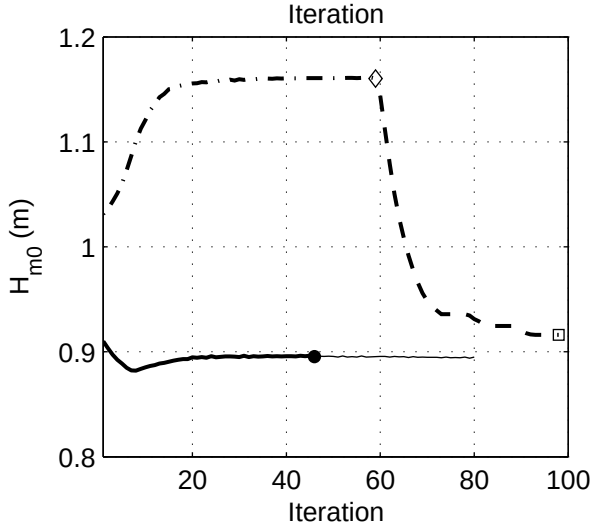

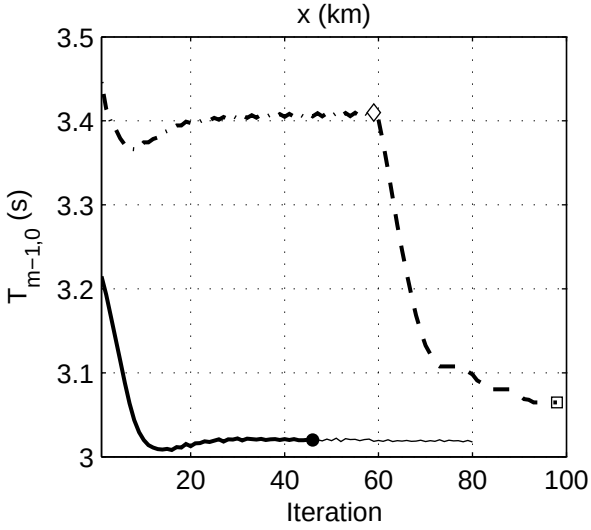

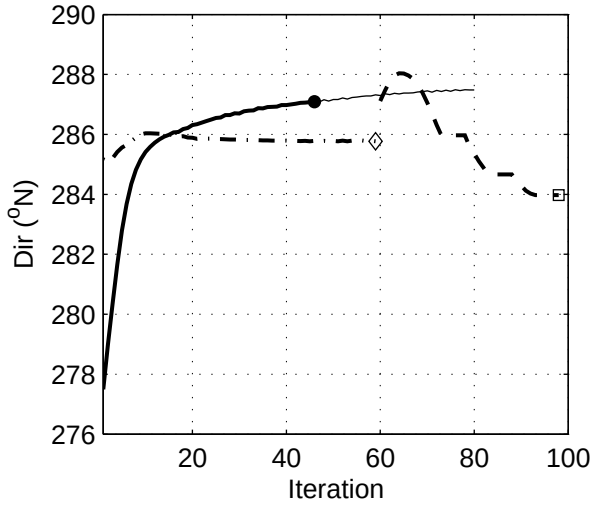

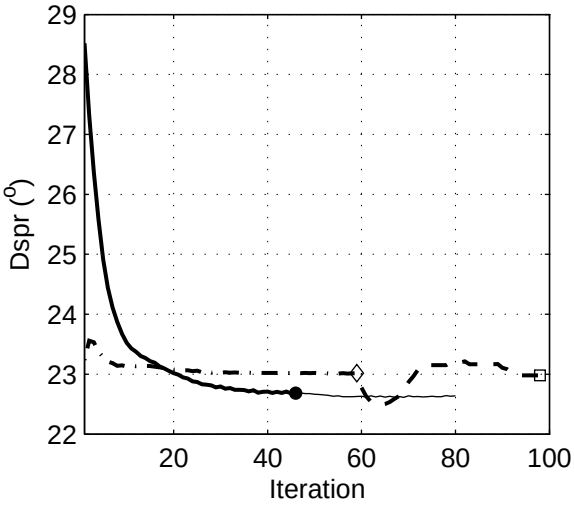

Convergence behaviour of the combined MG and DDM simulation in the Amelander Zeegat, Case: AZG3A 2005/01/02 12:00, at point 3 MG option: x2y2d1s1, DDM option: r10_d05 (C2211_105)		SWAN 40.51A
		Numerical efficiency SWAN
DELTARES & ALKYON	H5107.46/A2114	Fig. 7.4

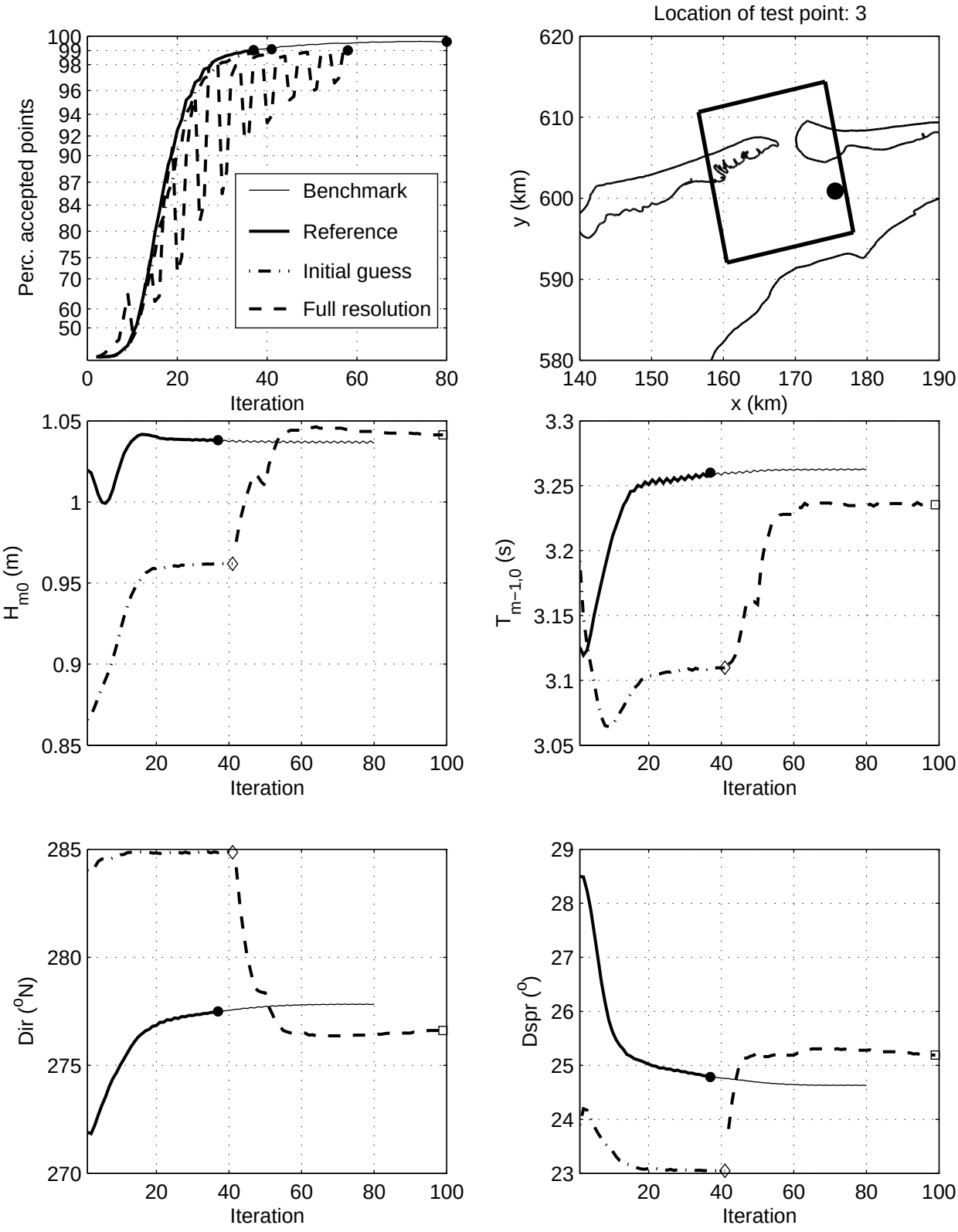

Convergence behaviour of the combined MG and DDM simulation in the Amelander Zeegat, Case: AZG3A 2005/01/02 17:00, at point 3 MG option: x2y2d1s1, DDM option: r10_d05 (C2211_105)		SWAN 40.51A
		Numerical efficiency SWAN
DELTARES & ALKYON	H5107.46/A2114	Fig. 7.5

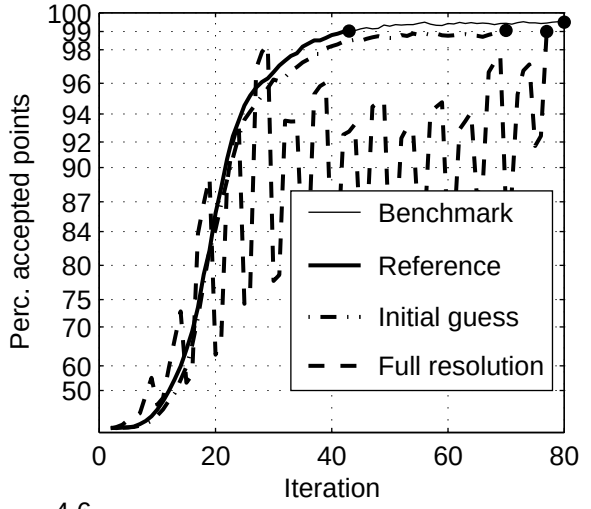

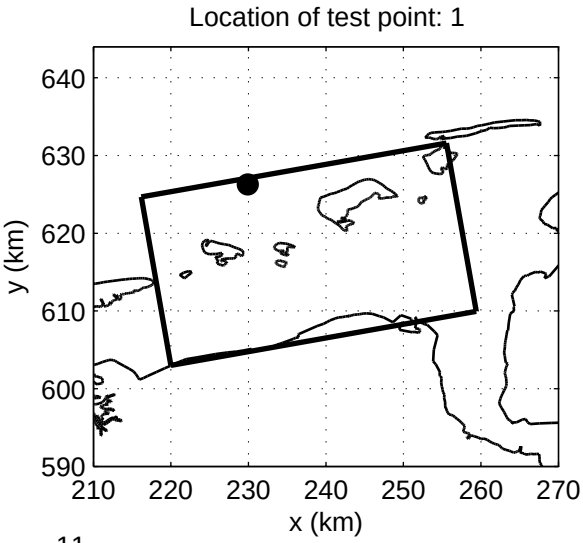

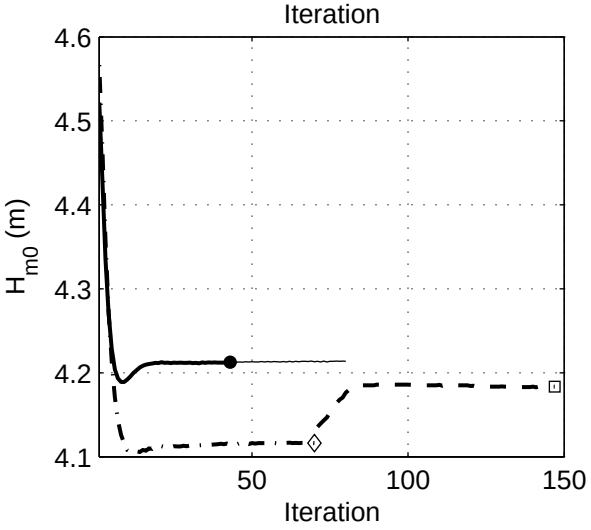

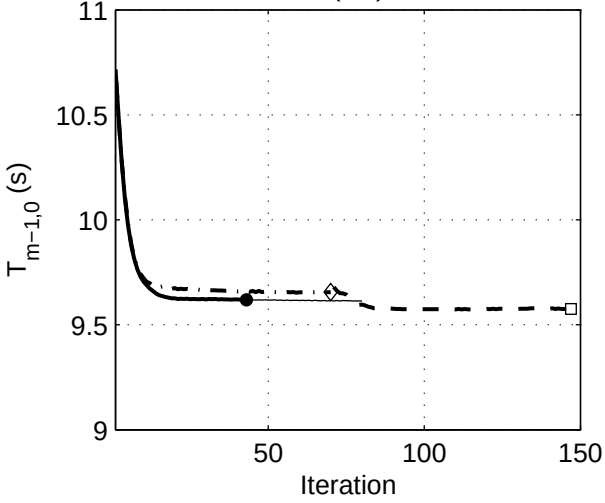

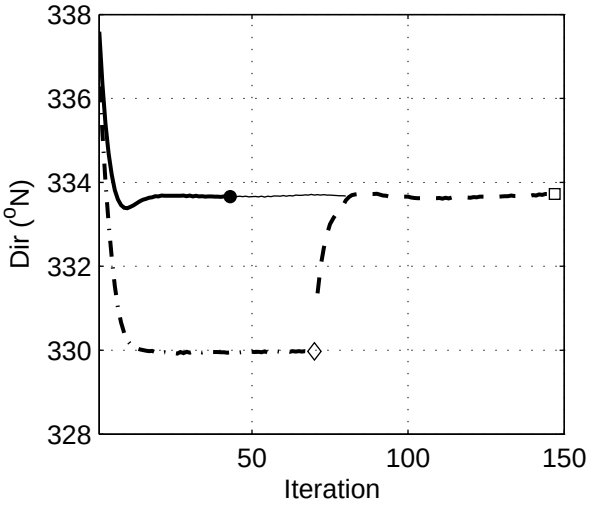

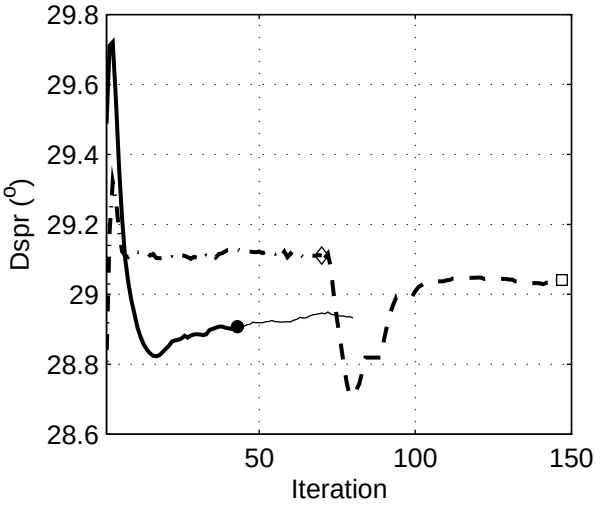

Convergence behaviour of the combined MG and DDM simulation in the Eems−Dollard, Case: EEMS3A 2006/11/01 03:00, at point 1 MG option: x2y2d1s1, DDM option: r10_d05 (C2211_105)		SWAN 40.51A
		Numerical efficiency SWAN
DELTARES & ALKYON	H5107.46/A2114	Fig. 7.6

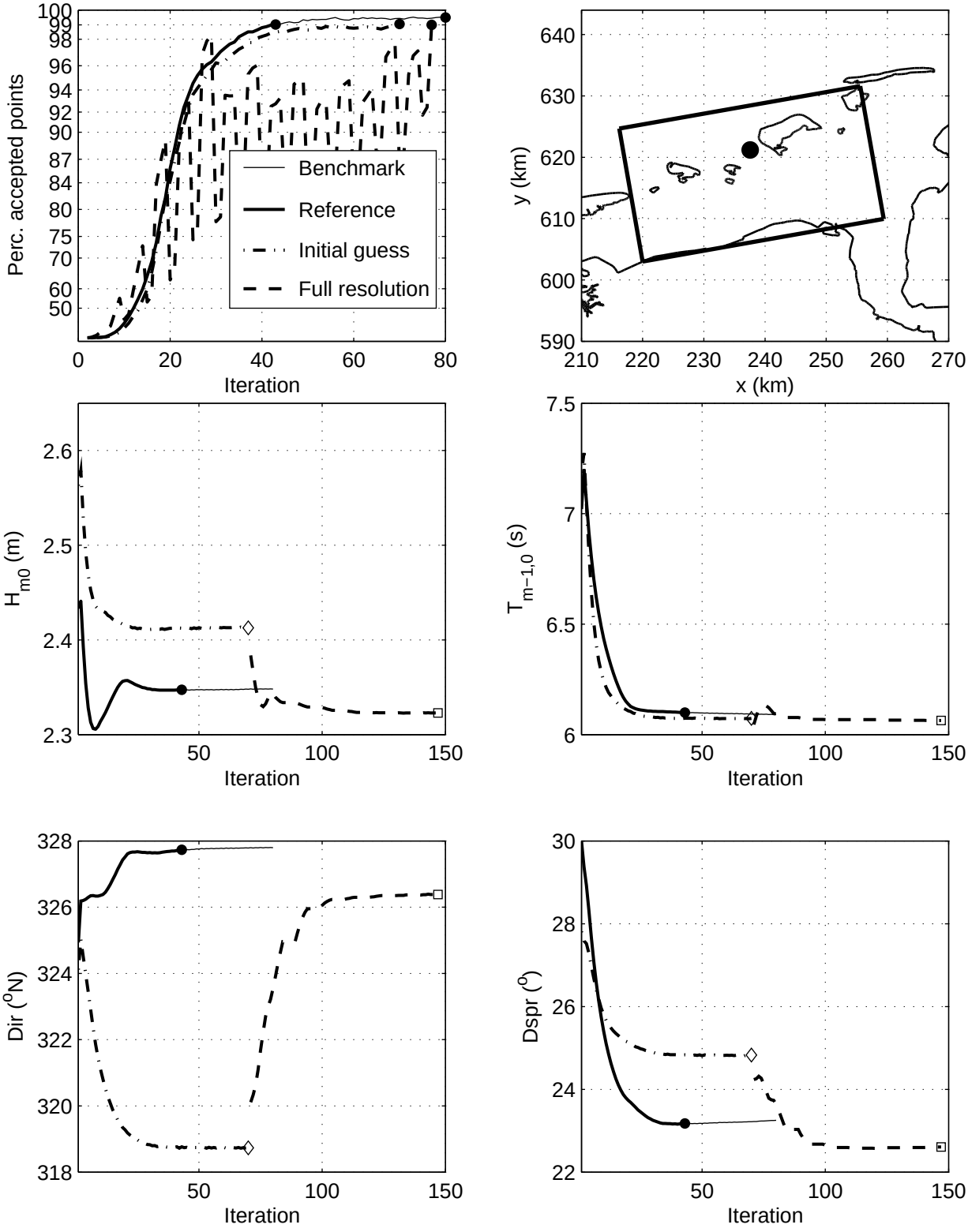

Convergence behaviour of the combined MG and DDM simulation in the Eems−Dollard, Case: EEMS3A 2006/11/01 03:00, at point 2 MG option: x2y2d1s1, DDM option: r10_d05 (C2211_105)		SWAN 40.51A
		Numerical efficiency SWAN
DELTARES & ALKYON	H5107.46/A2114	Fig. 7.7

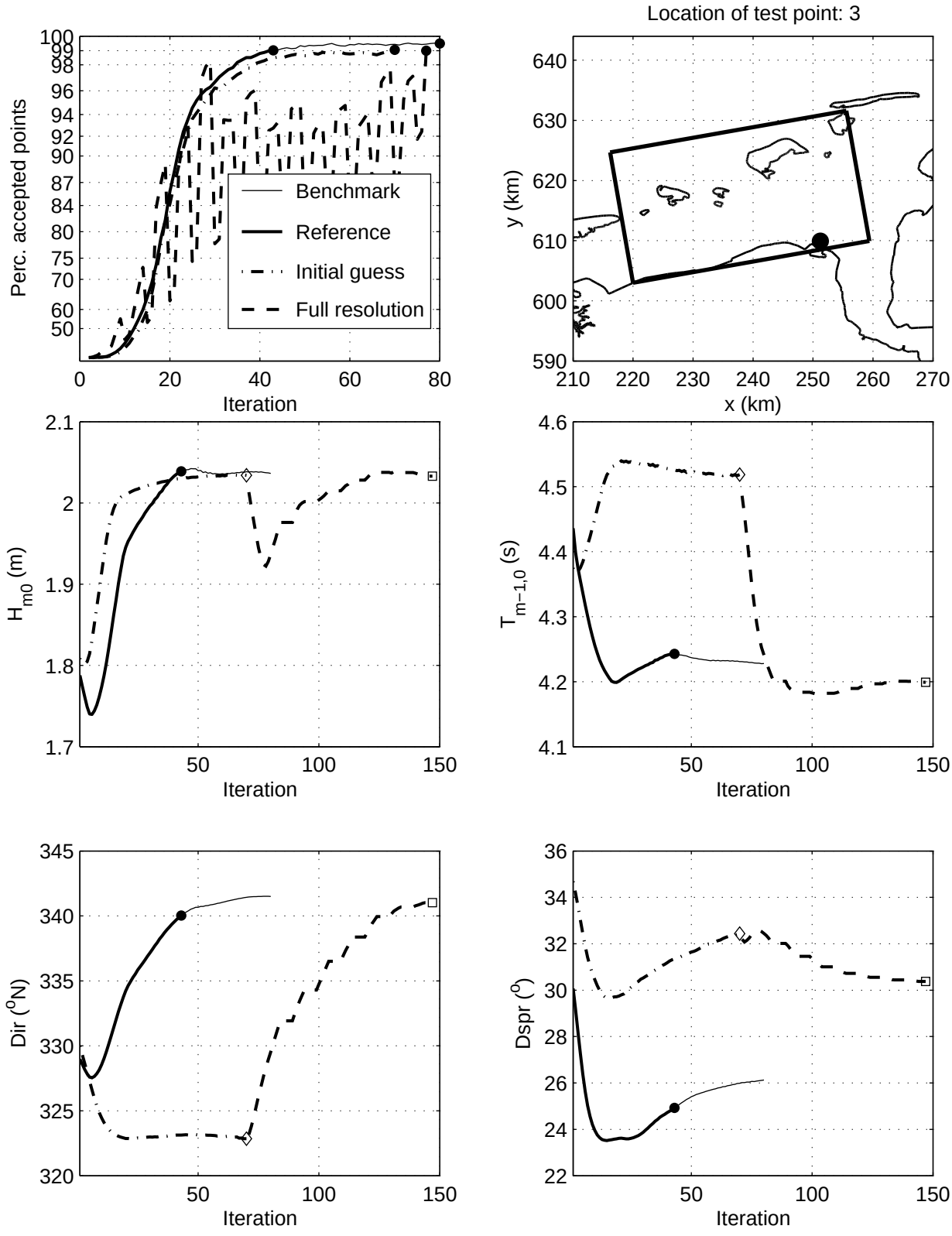

Convergence behaviour of the combined MG and DDM simulation in the Eems−Dollard, Case: EEMS3A 2006/11/01 03:00, at point 3 MG option: x2y2d1s1, DDM option: r10_d05 (C2211_105)		SWAN 40.51A
		Numerical efficiency SWAN
DELTARES & ALKYON	H5107.46/A2114	Fig. 7.8

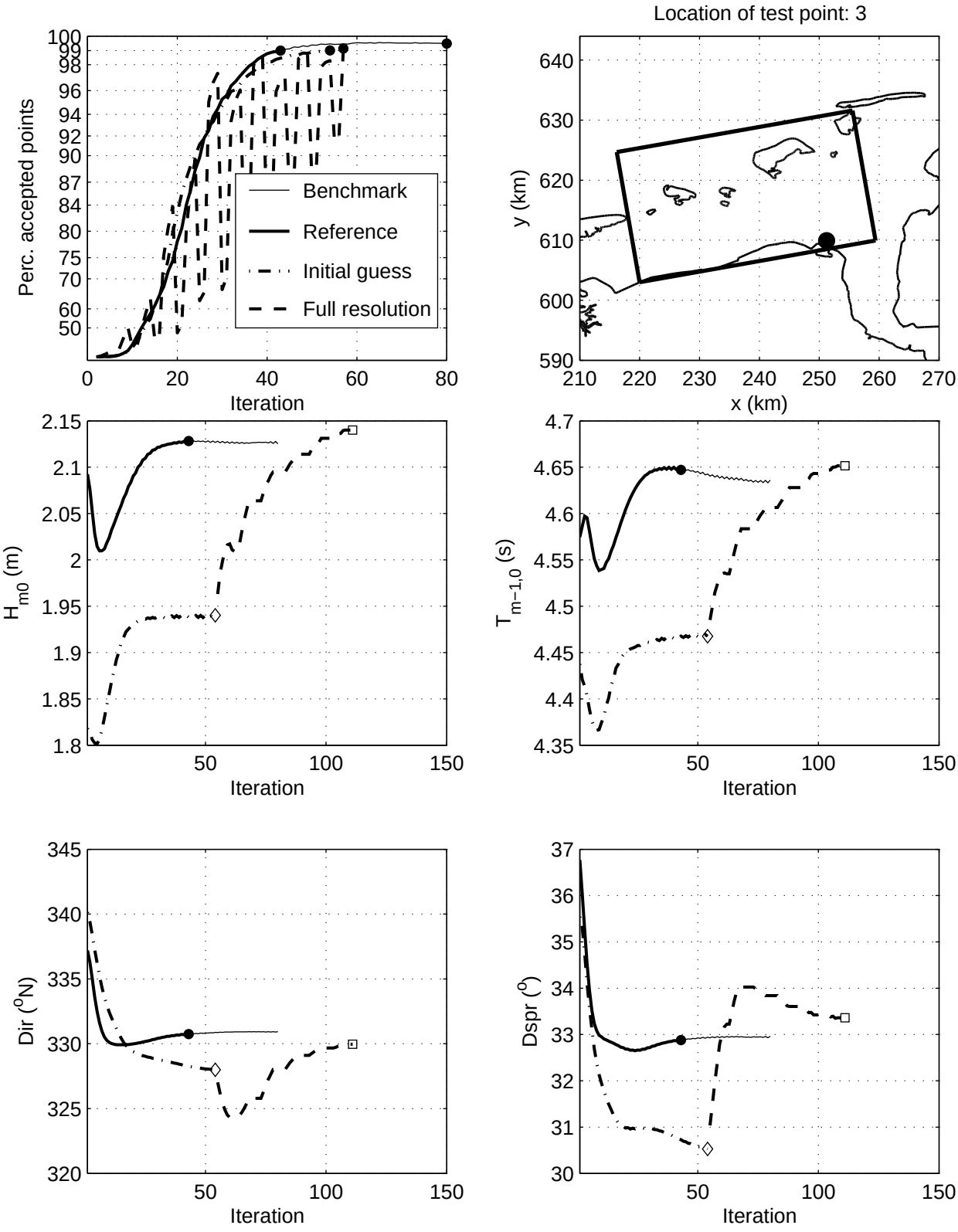

Convergence behaviour of the combined MG and DDM simulation in the Eems−Dollard, Case: EEMS3A 2006/11/01 06:30, at point 3 MG option: x2y2d1s1, DDM option: r10_d05 (C2211_105)		SWAN 40.51A
		Numerical efficiency SWAN
DELTARES & ALKYON	H5107.46/A2114	Fig. 7.9

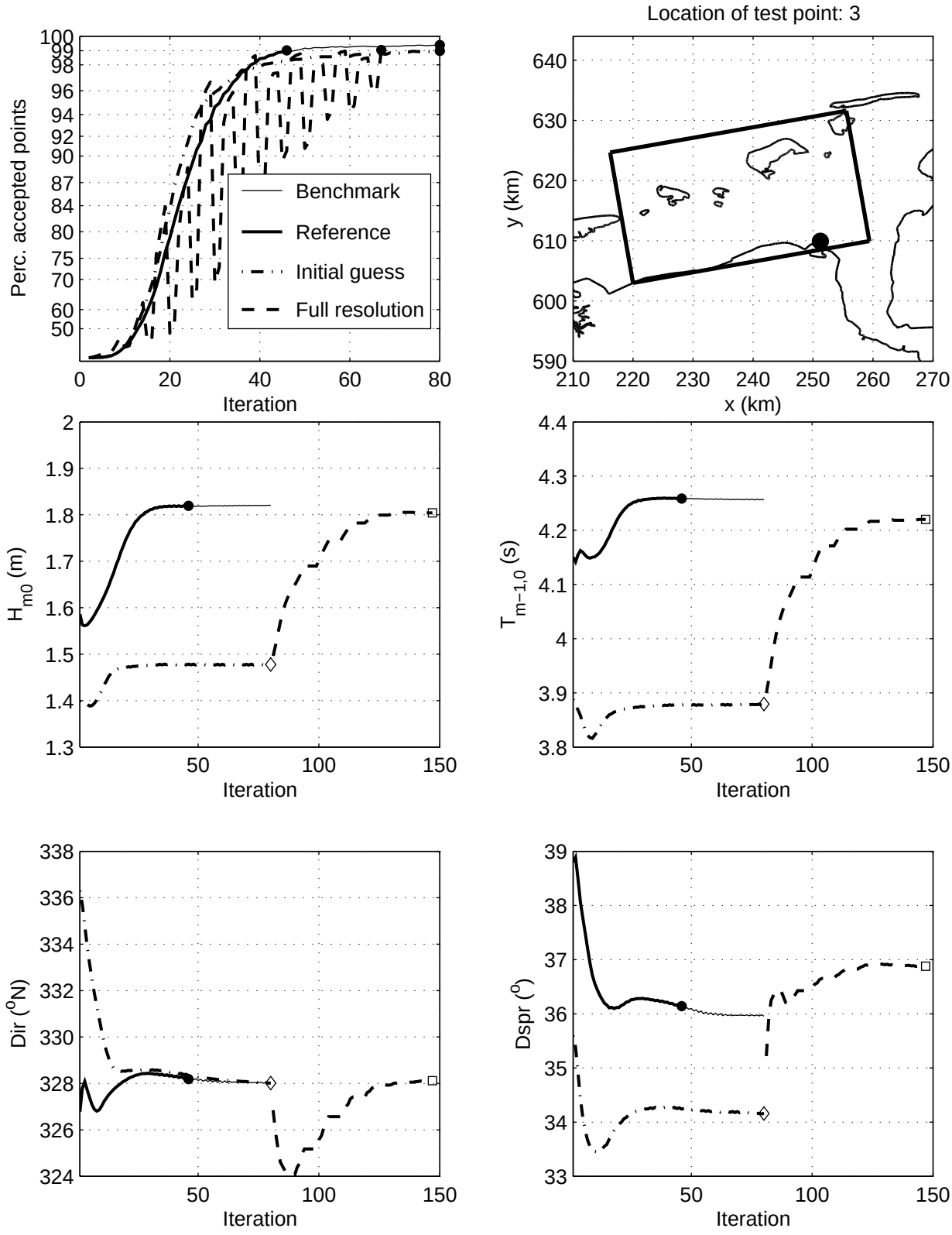

Convergence behaviour of the combined MG and DDM simulation in the Eems−Dollard, Case: EEMS3A 2006/11/01 09:30, at point 3 MG option: x2y2d1s1, DDM option: r10_d05 (C2211_105)		SWAN 40.51A
		Numerical efficiency SWAN
DELTARES & ALKYON	H5107.46/A2114	Fig. 7.10

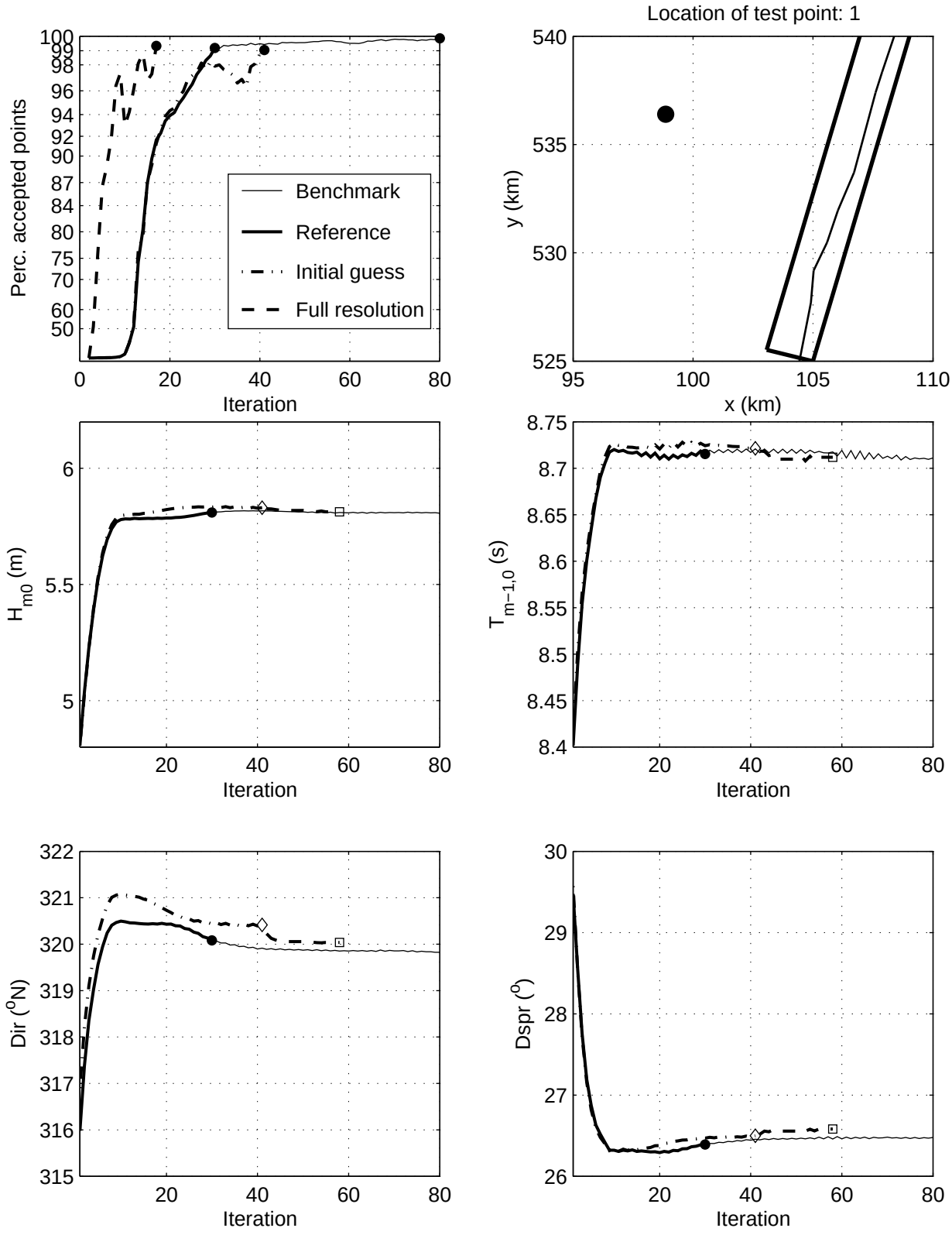

Convergence behaviour of the combined MG and DDM simulation along the Dutch coast near Petten, Case: PETTEN 1995/01/01 10:00, at point 1 MG option: x2y2d1s1, DDM option: r10_d05 (C2211_105)		SWAN 40.51A
		Numerical efficiency SWAN
DELTARES & ALKYON	H5107.46/A2114	Fig. 7.11

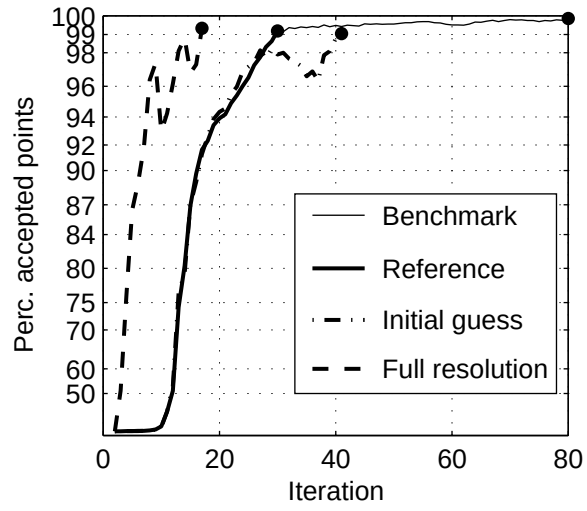

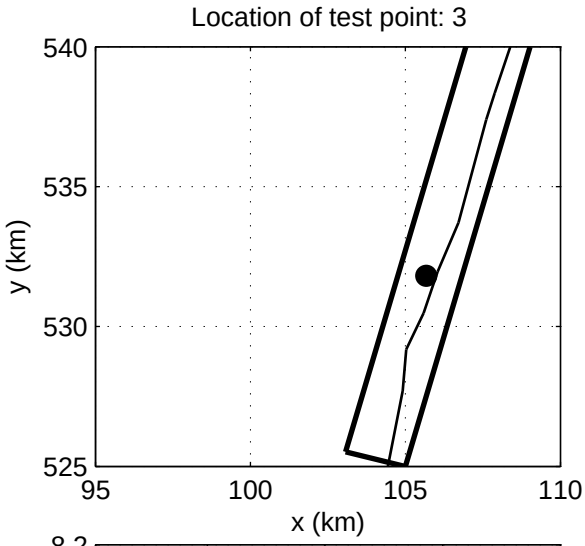

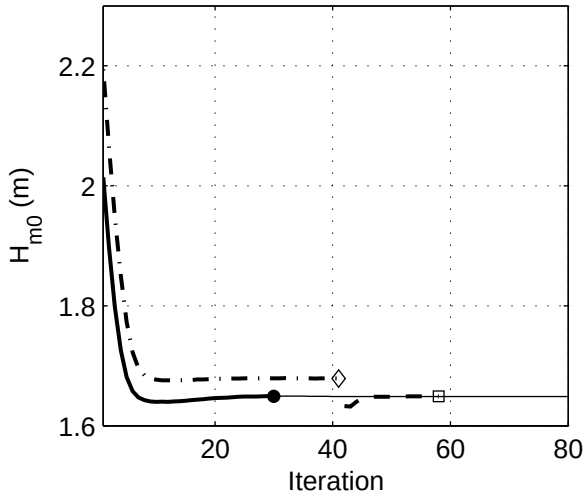

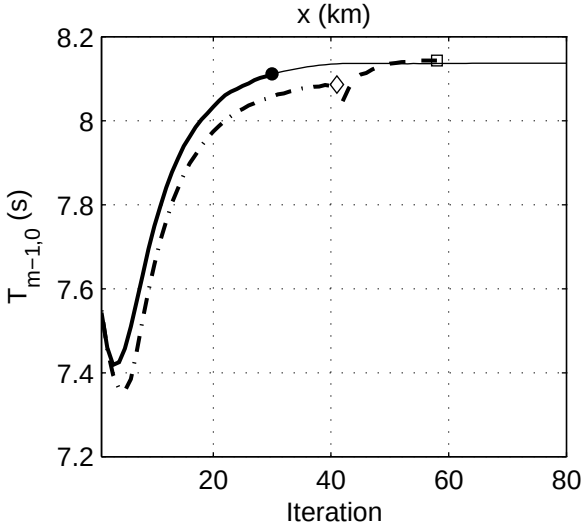

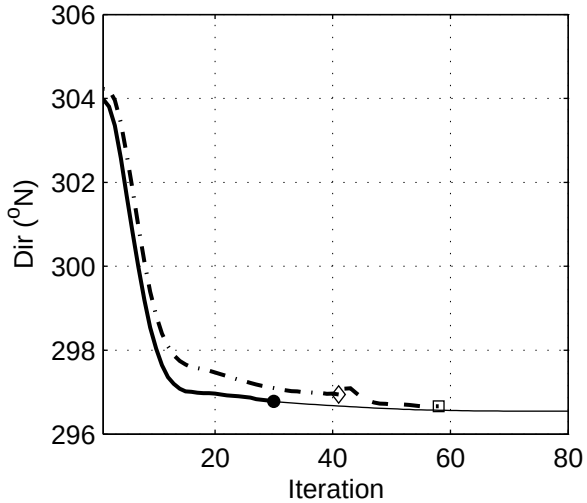

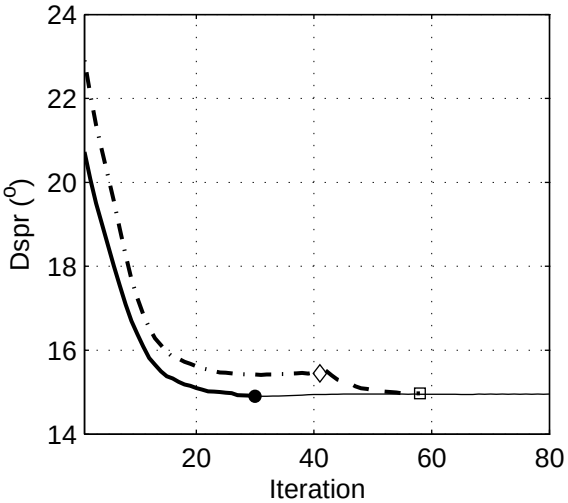

Convergence behaviour of the combined MG and DDM simulation along the Dutch coast near Petten, Case: PETTEN 1995/01/01 10:00, at point 3 MG option: x2y2d1s1, DDM option: r10_d05 (C2211_105)		SWAN 40.51A
	Numerical efficiency SWAN	
DELTARES & ALKYON	H5107.46/A2114	Fig. 7.12

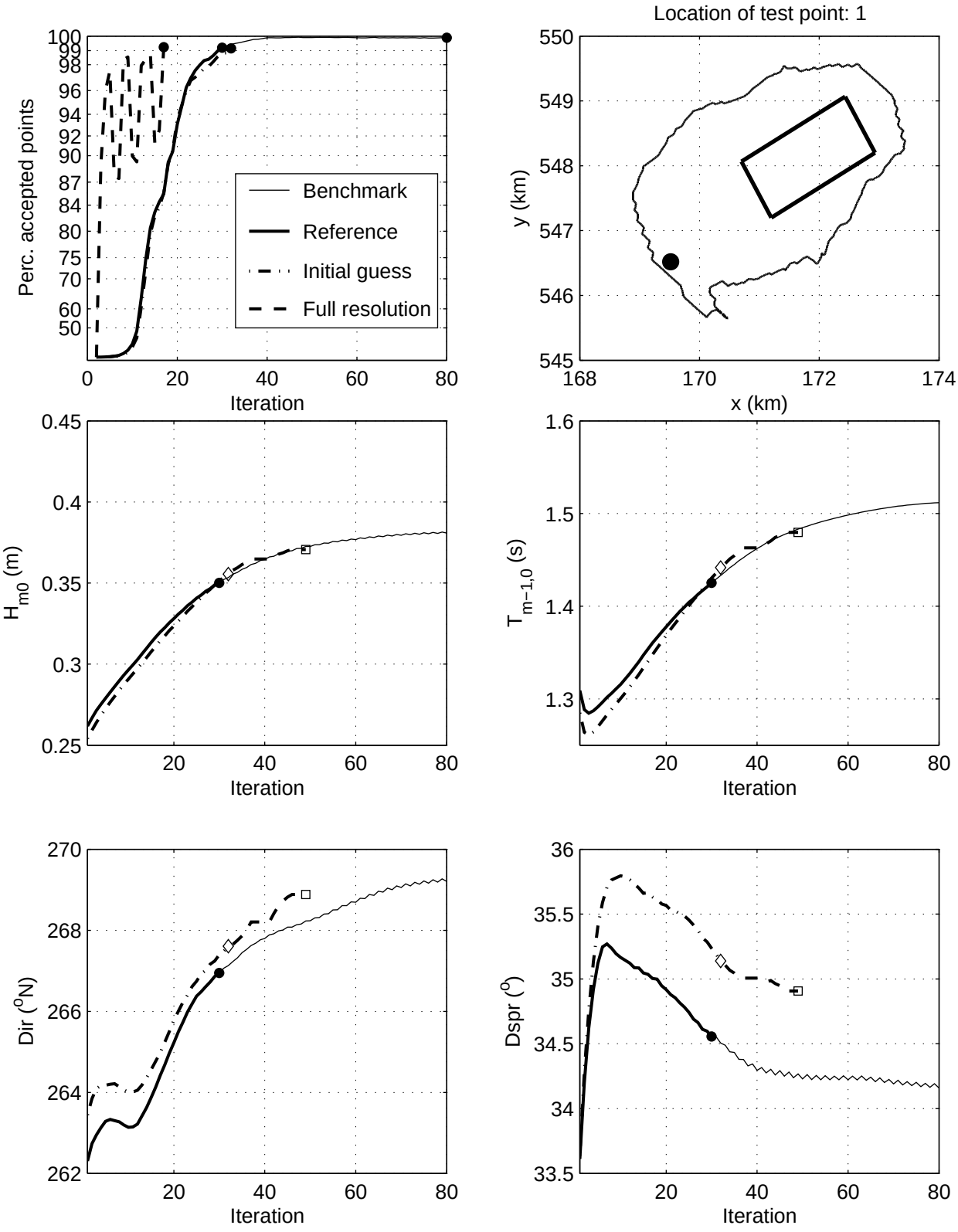

Convergence behaviour of the combined MG and DDM simulation in Lake Sloten, Case: SLE 2002/10/27 15:00, at point 1 MG option: x2y2d1s1, DDM option: r10_d05 (C2211_105)		SWAN 40.51A
		Numerical efficiency SWAN
DELTARES & ALKYON	H5107.46/A2114	Fig. 7.13

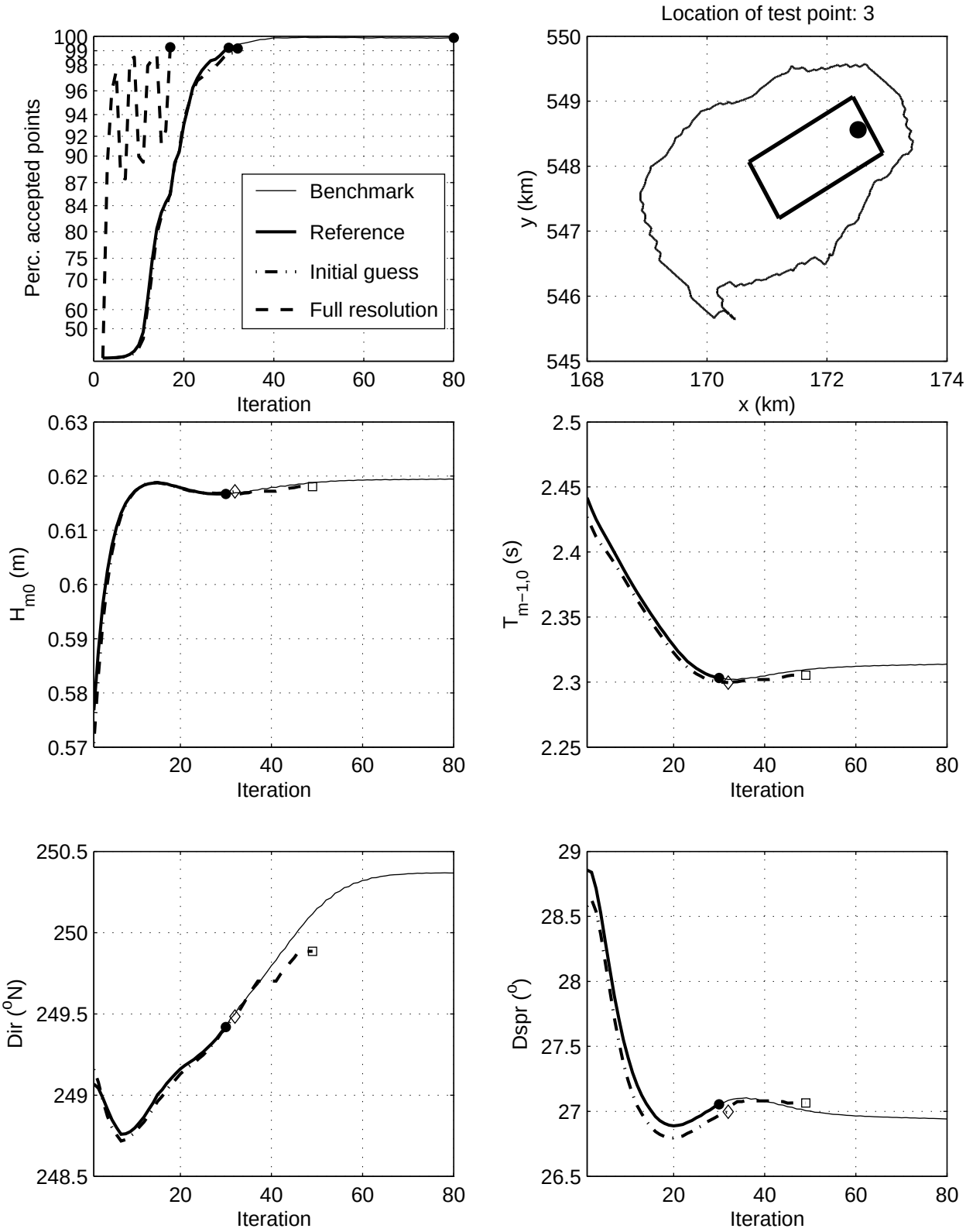

Convergence behaviour of the combined MG and DDM simulation in Lake Sloten, Case: SLE 2002/10/27 15:00, at point 3 MG option: x2y2d1s1, DDM option: r10_d05 (C2211_105)		SWAN 40.51A
		Numerical efficiency SWAN
DELTARES & ALKYON	H5107.46/A2114	Fig. 7.14

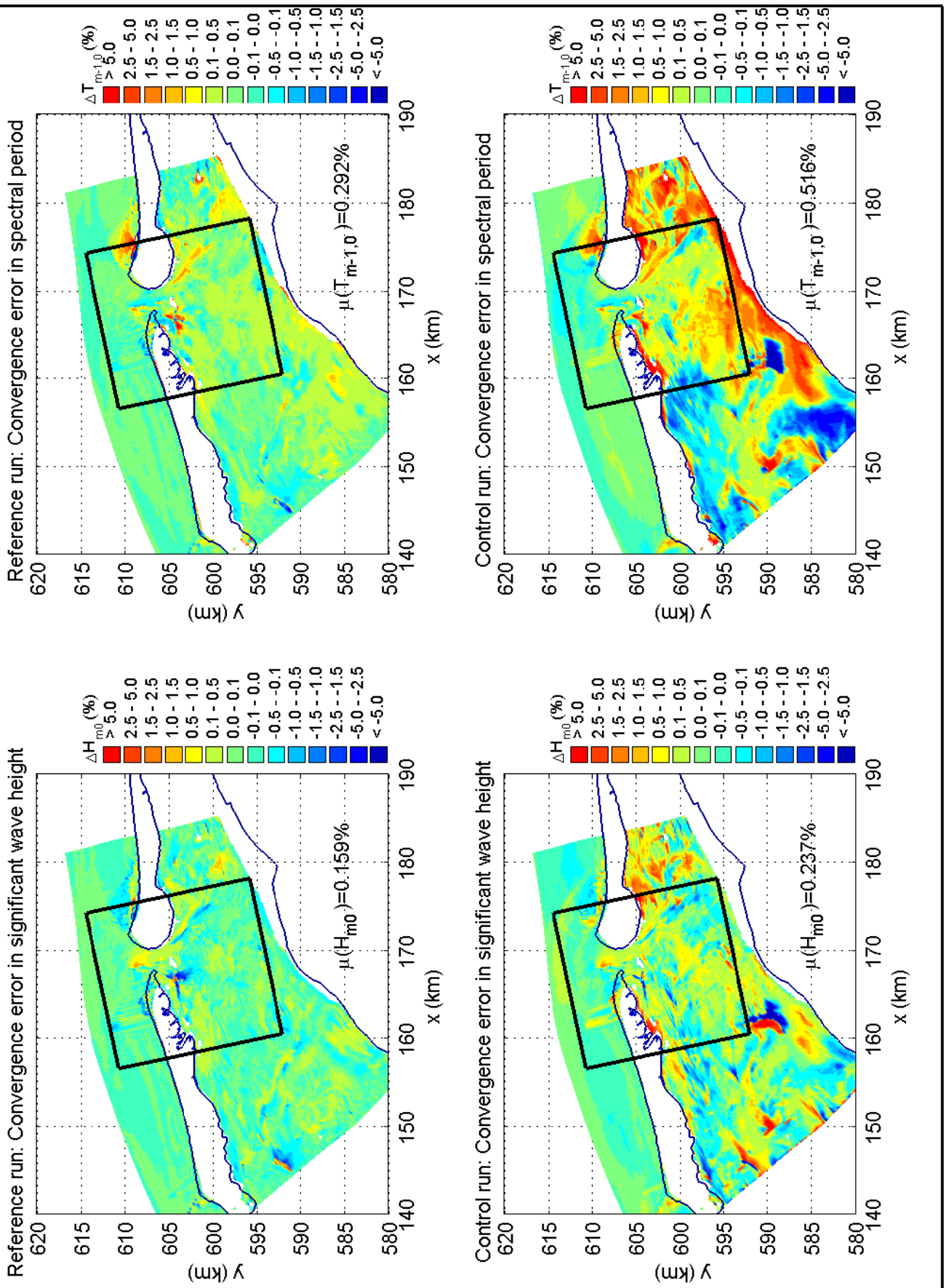

Convergence errors in H_{m0} and $T_{m-1,0}$ for the MG-DDM simulation in the Amelander Zeegat, Case: AZG3A 2005/01/02 10:00 MG option: x2y2d1s1, DDM option: r10_d05 (C2211_105)		SWAN 40.51A
	Numerical efficiency SWAN	
DELTARES & ALKYON	H5107.46/A2114	Fig. 7.15

Convergence errors in Dir and Dspr for the Multigrid simulation in the Amelander Zeegat, Case: AZG3A 2005/01/02 10:00
MG option: x2y2d1s1, DDM option: r10_d05 (C2211_105)

DELTARES & ALKYON

H5107.46/A2114

Numerical efficiency SWAN

SWAN 40.51A

Fig. 7.16

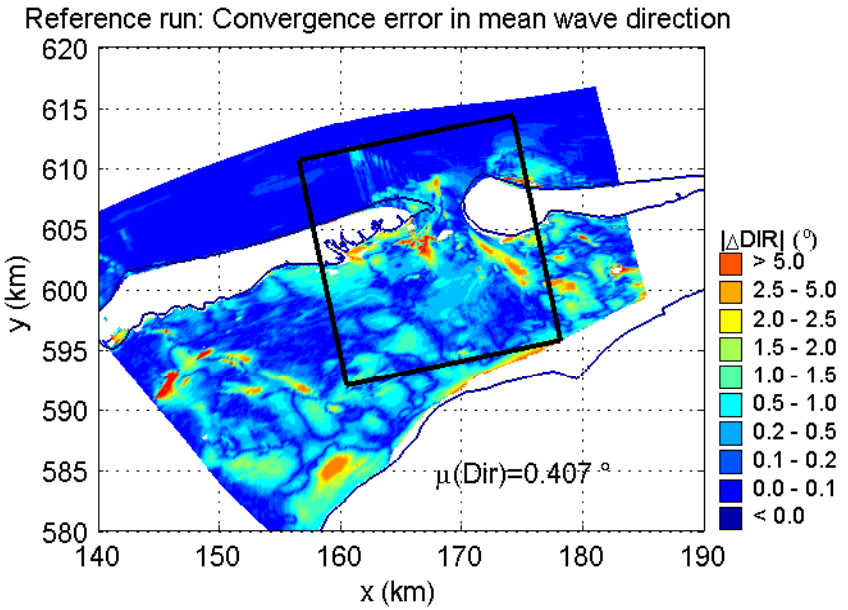

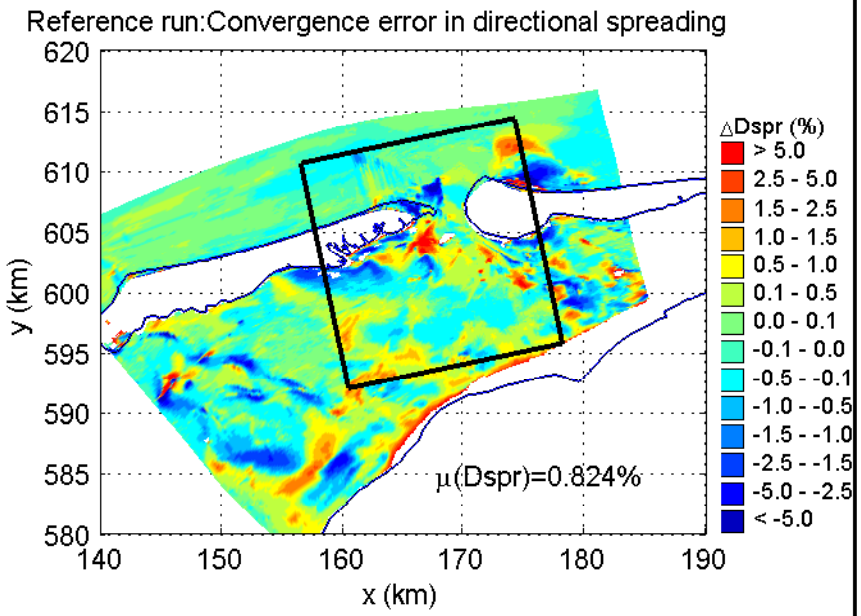

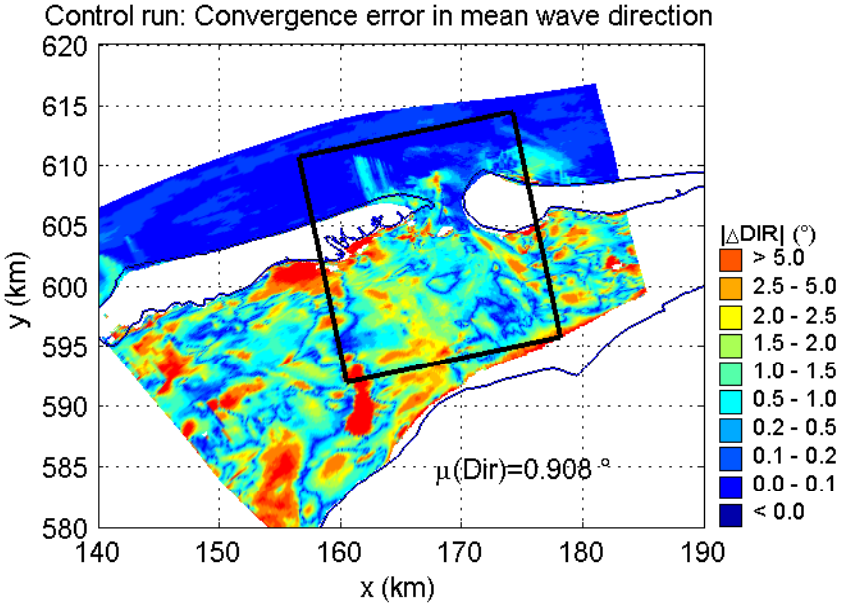

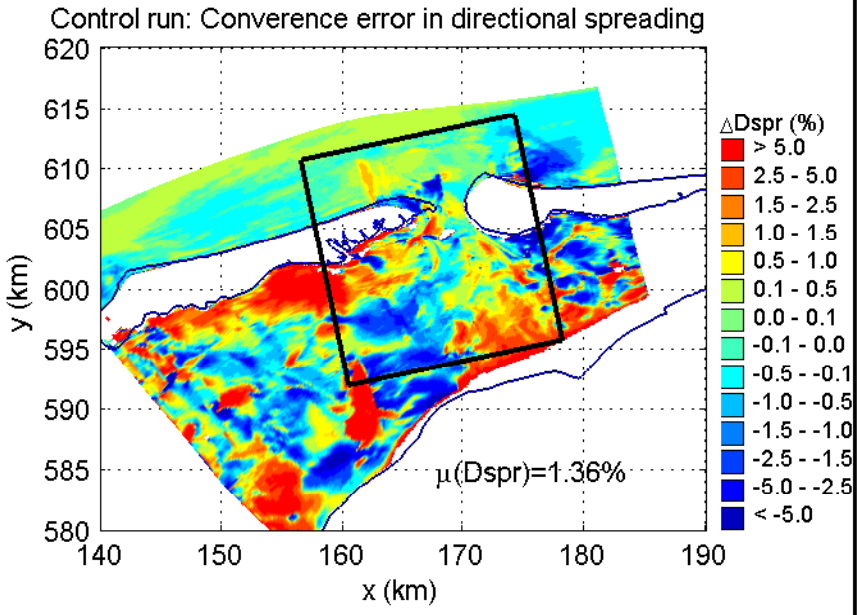

Convergence errors in H_{m0} and $T_{m-1,0}$ for the MG-DDM simulation in the Eems-Dollard, Case: EEMS3A 2006/11/01 03:00
MG option: x2y2d1s1, DDM option: r10_d05 (C2211_105)

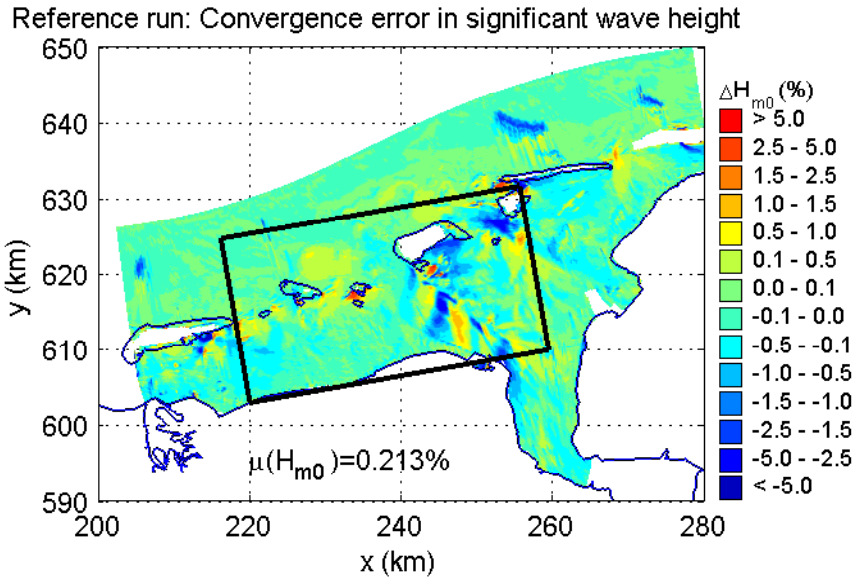

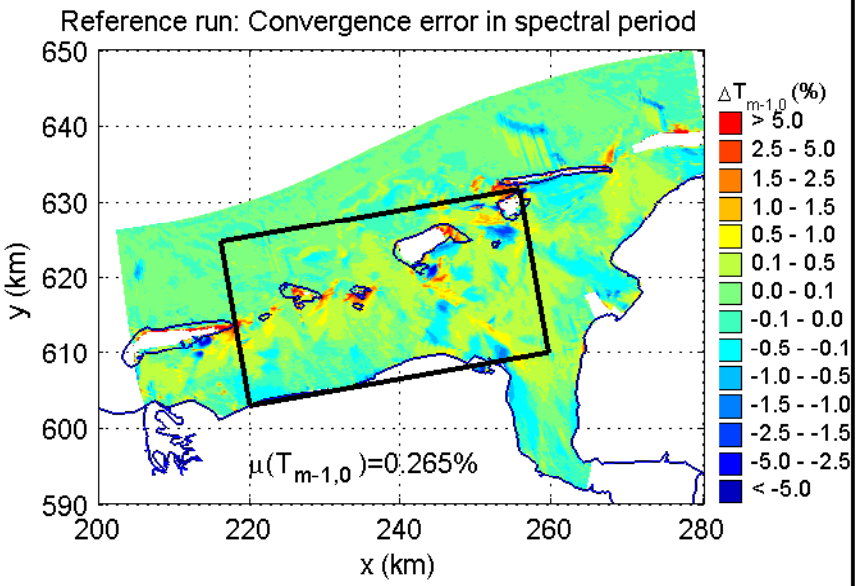

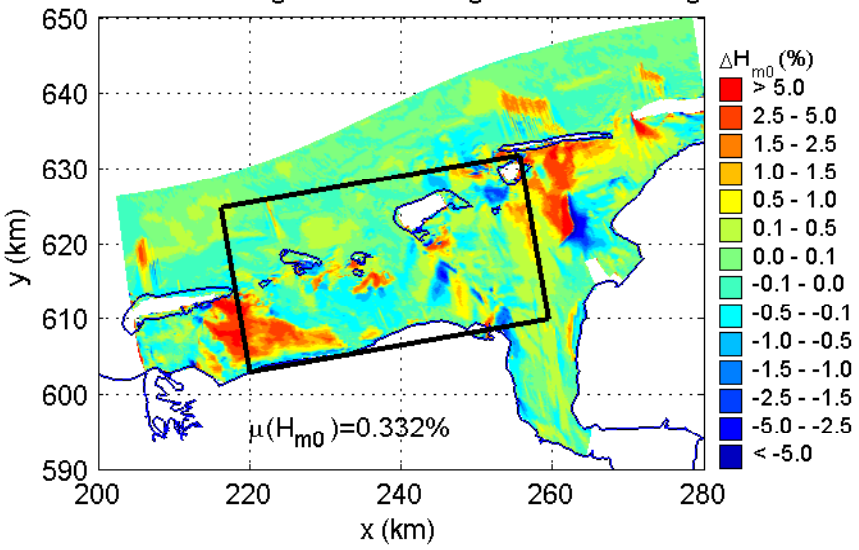

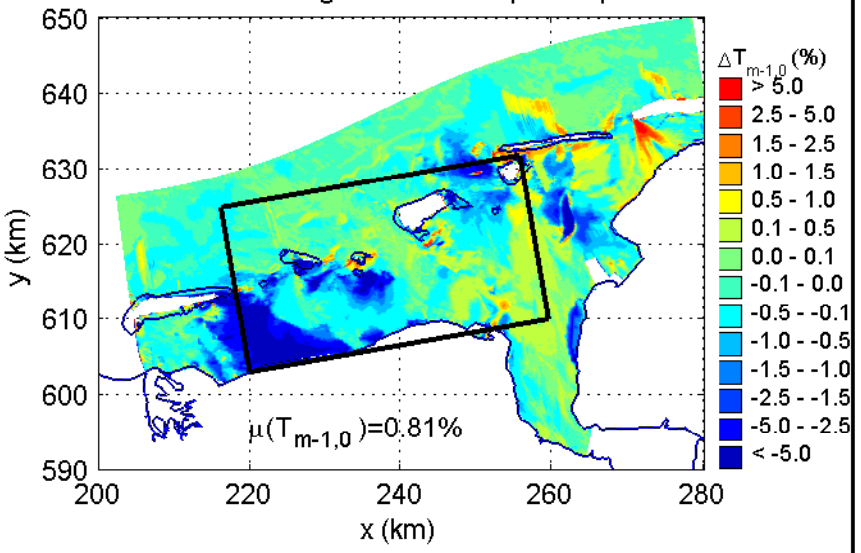

DELTARES & ALKYON		
H5107.46/A2114	Numerical efficiency SWAN	SWAN 40.51A
Fig. 7.17		

Convergence errors in Dir and Dspr for the Multigrid simulation in the Eems-Dollard, Case: EEMS3A 2006/11/01 03:00 MG option: x2y2d1s1, DDM option: r10_d05 (C2211_105)		SWAN 40.51A
	Numerical efficiency SWAN	
DELTARES & ALKYON	H5107.46/A2114	Fig. 7.18

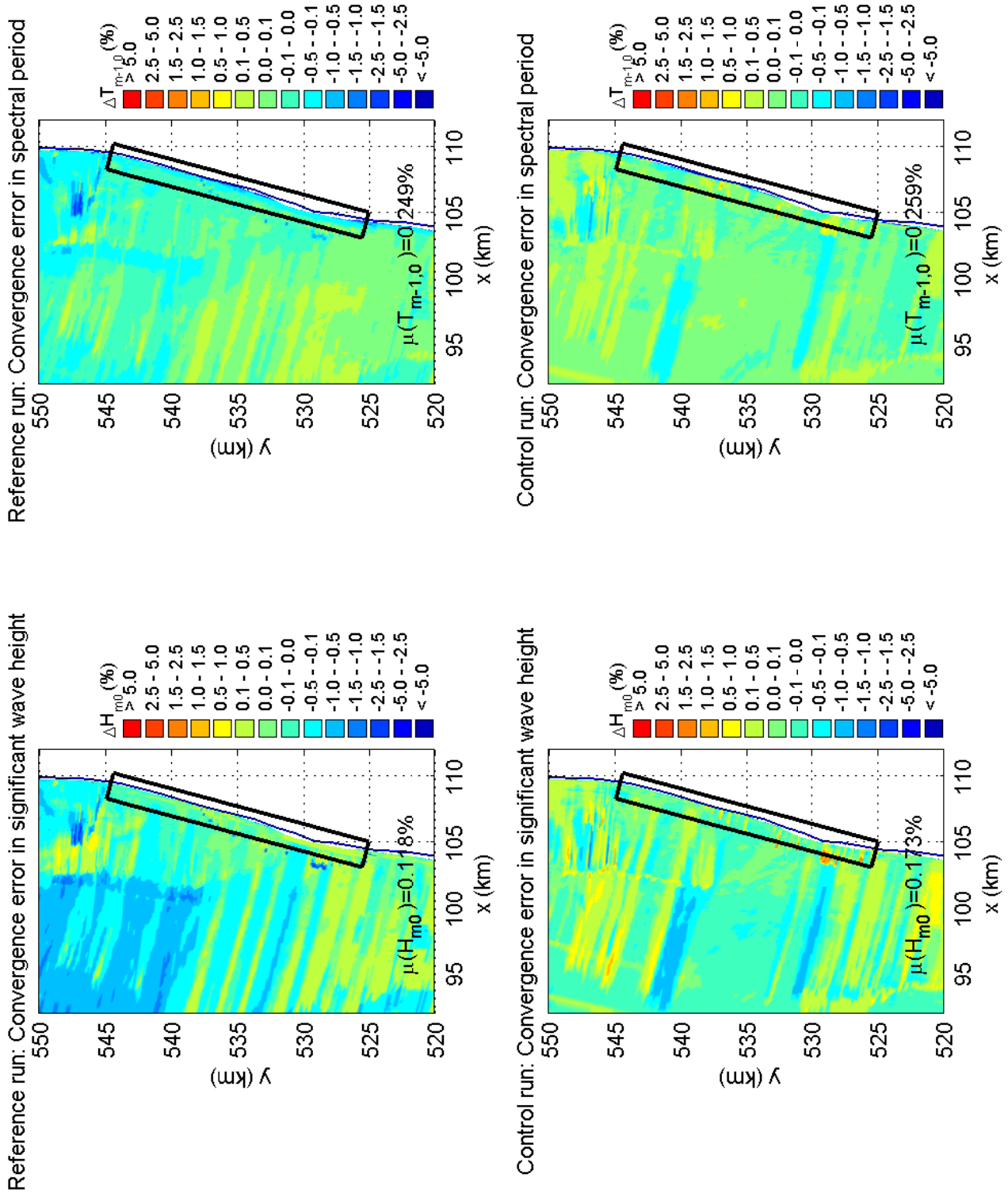

Convergence errors in H_{m0} and $T_{m-1,0}$ for the MG-DDM simulation along the Dutch coast near Petten, Case: PETTEN 1995/01/01 10:00 MG option: x2y2d1s1, DDM option: r10_d05 (C2211_105)		SWAN 40.51A
		Numerical efficiency SWAN
DELTARES & ALKYON	H5107.46/A2114	Fig. 7.19

Reference run: Convergence error in mean wave direction

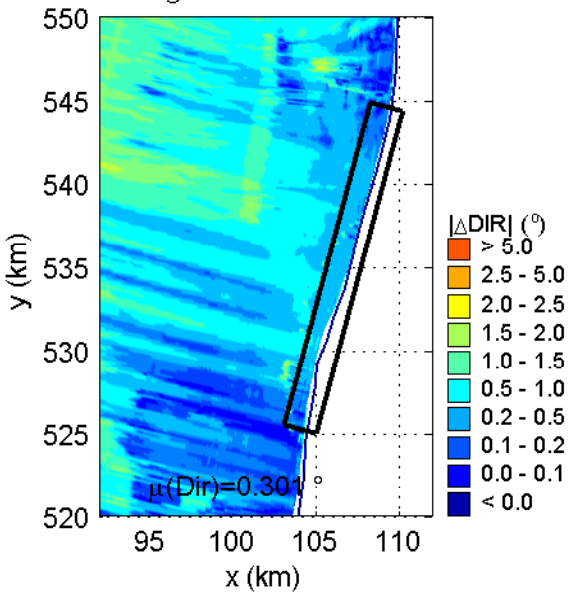

Reference run:Convergence error in directional spreading

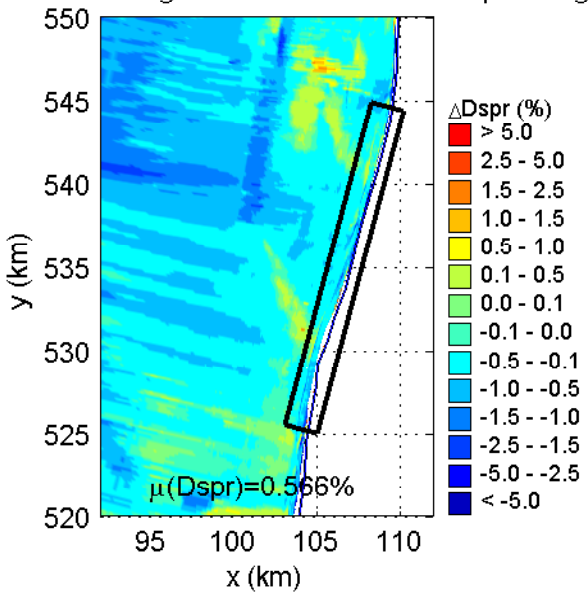

Control run: Convergence error in mean wave direction

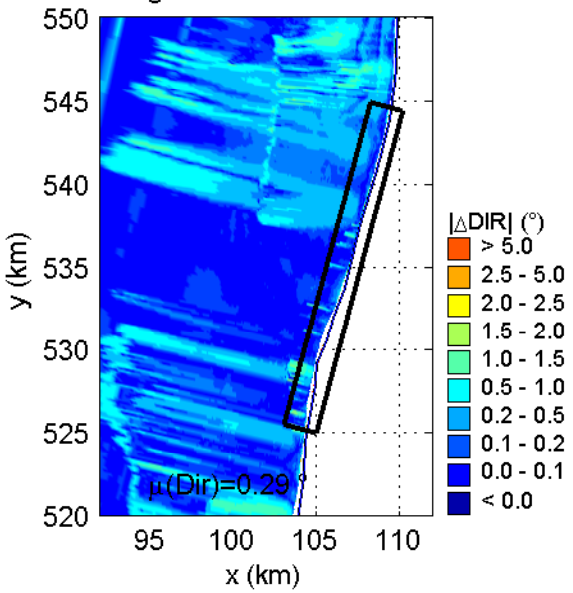

Control run: Converence error in directional spreading

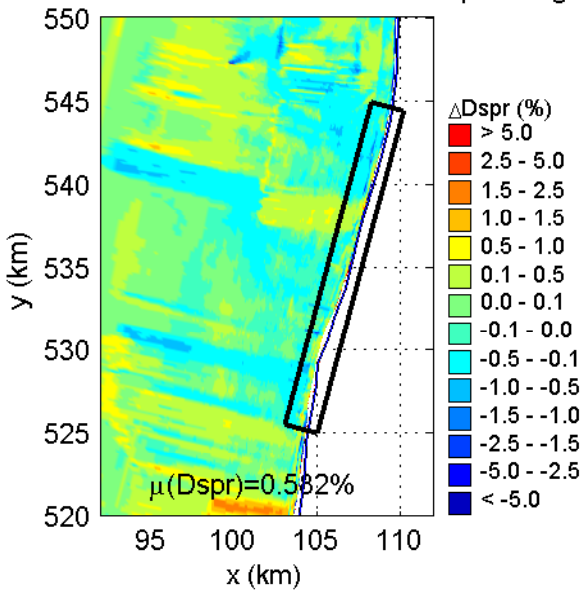

Convergence errors in Dir and Dspr for the Multigrid simulation along the Dutch coast near Petten, Case: PETTEN 1995/01/01 10:00 MG option: x2y2d1s1, DDM option: r10_d05 (C2211_105)

SWAN 40.51A

Numerical efficiency SWAN

H5107.46/A2114

Fig. 7.20

DELTARES & ALKYON

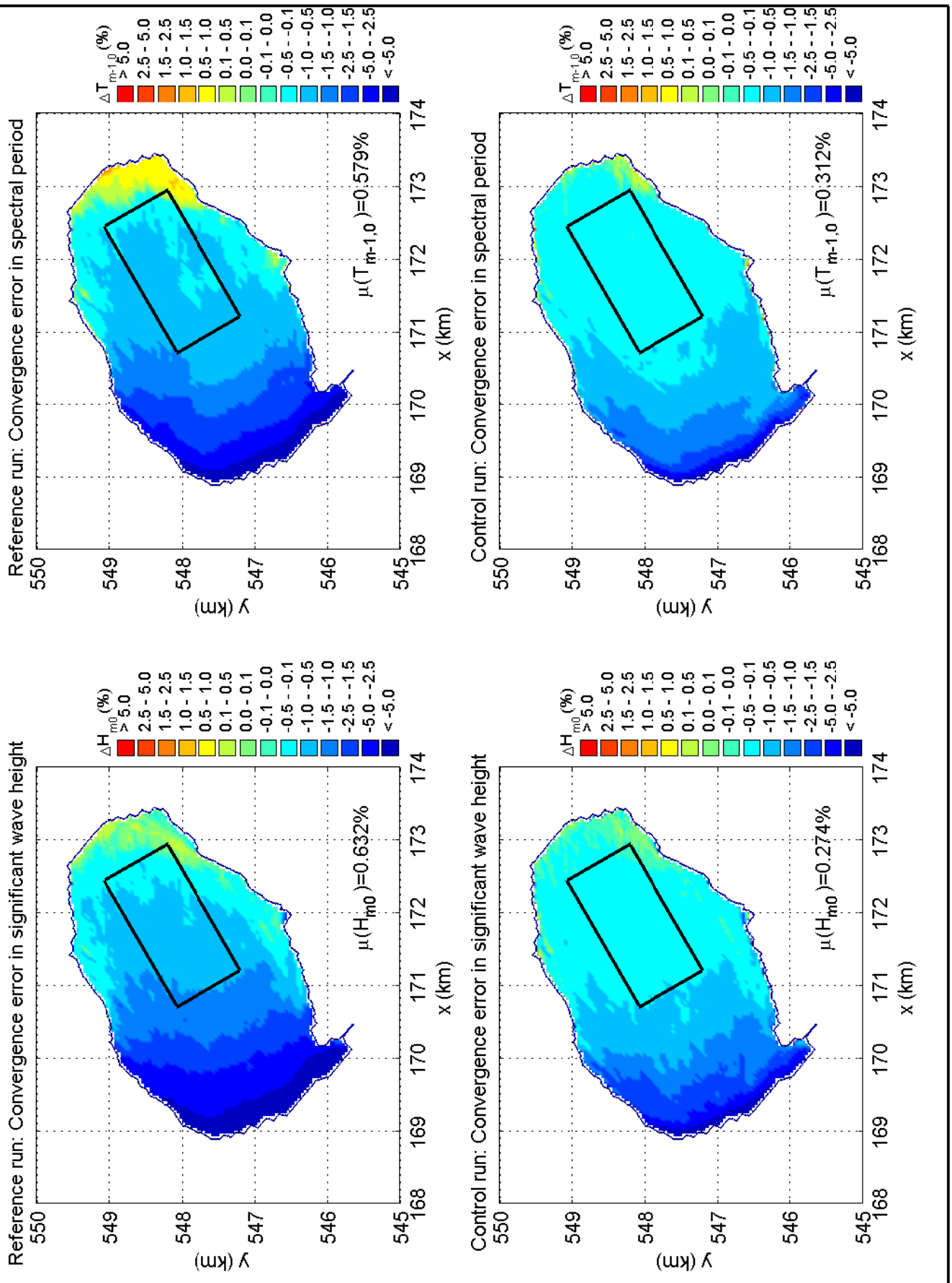

Convergence errors in H_{m0} and $T_{m-1,0}$ for the MG-DDM simulation in Lake Sloten, Case: SLE 2002/10/27 15:00 MG option: x2y2d1s1, DDM option: r10_d05 (C2211_105)		SWAN 40.51A
		Numerical efficiency SWAN
DELTARES & ALKYON	H5107.46/A2114	Fig. 7.21

Convergence errors in Dir and Dspr for the Multigrid simulation in Lake Sloten, Case: SLE 2002/10/27 15:00
MG option: x2y2d1s1, DDM option: r10_d05 (C2211_105)

DELTARES & ALKYON

H5107.46/A2114

Numerical efficiency SWAN

SWAN 40.51A

Fig. 7.22

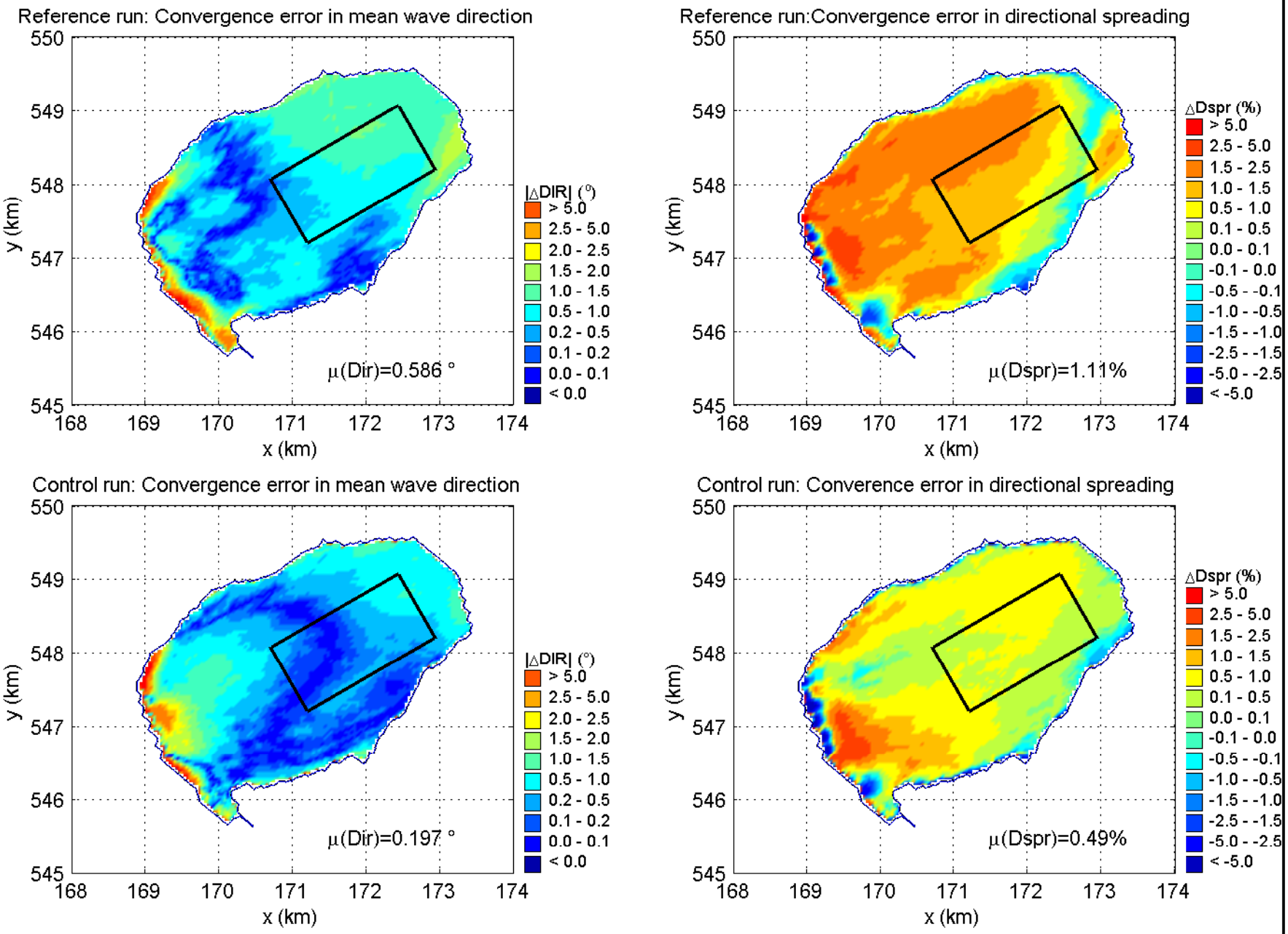

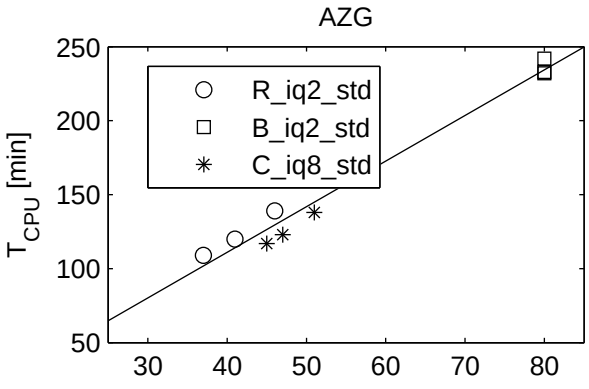

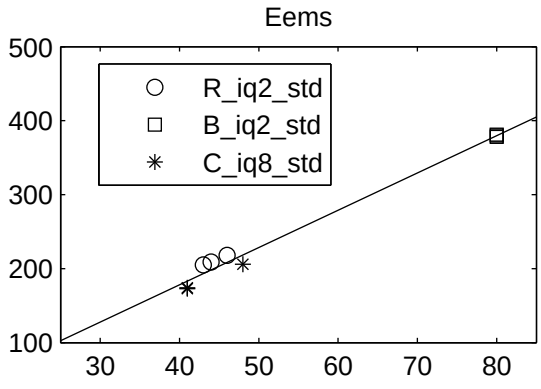

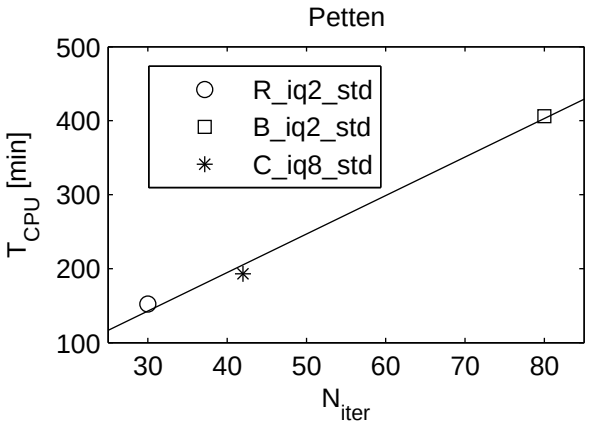

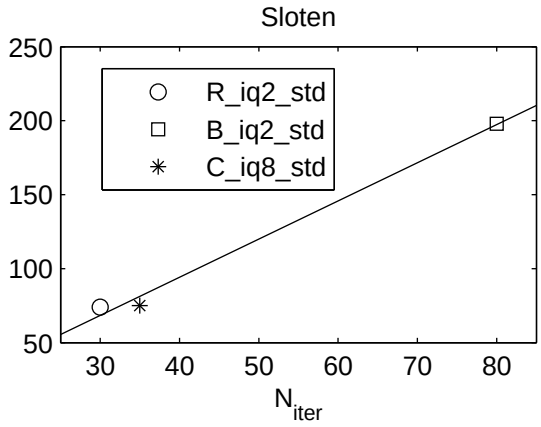

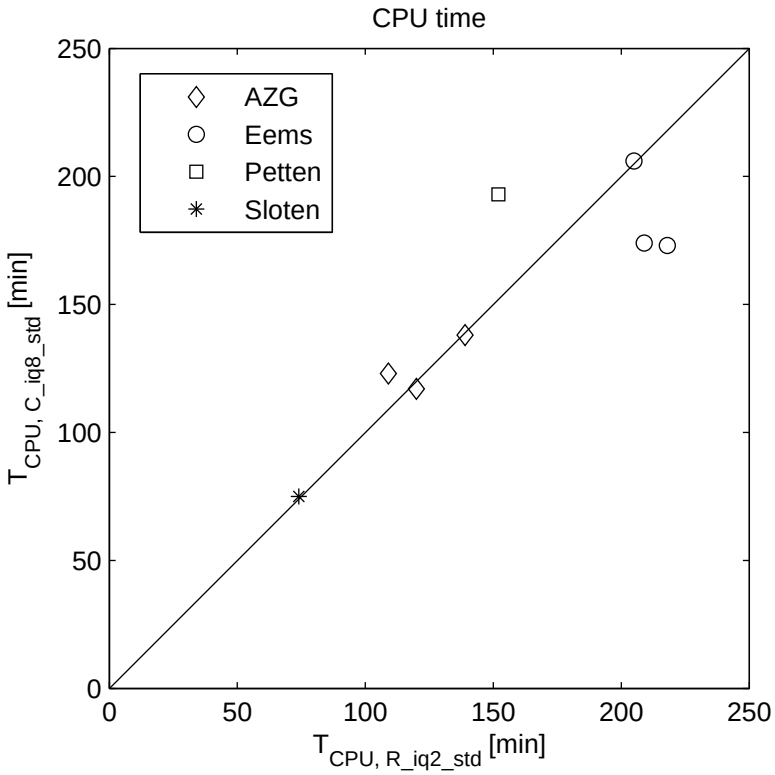

CPU time as function of number of iterations, displayed per field case and per DIA version (images above) CPU time of reference runs versus control runs (image below)	SWAN	40.51A
	Numerical efficiency SWAN	
DELTARES & ALKYON	H5107.46/A2114	8.1

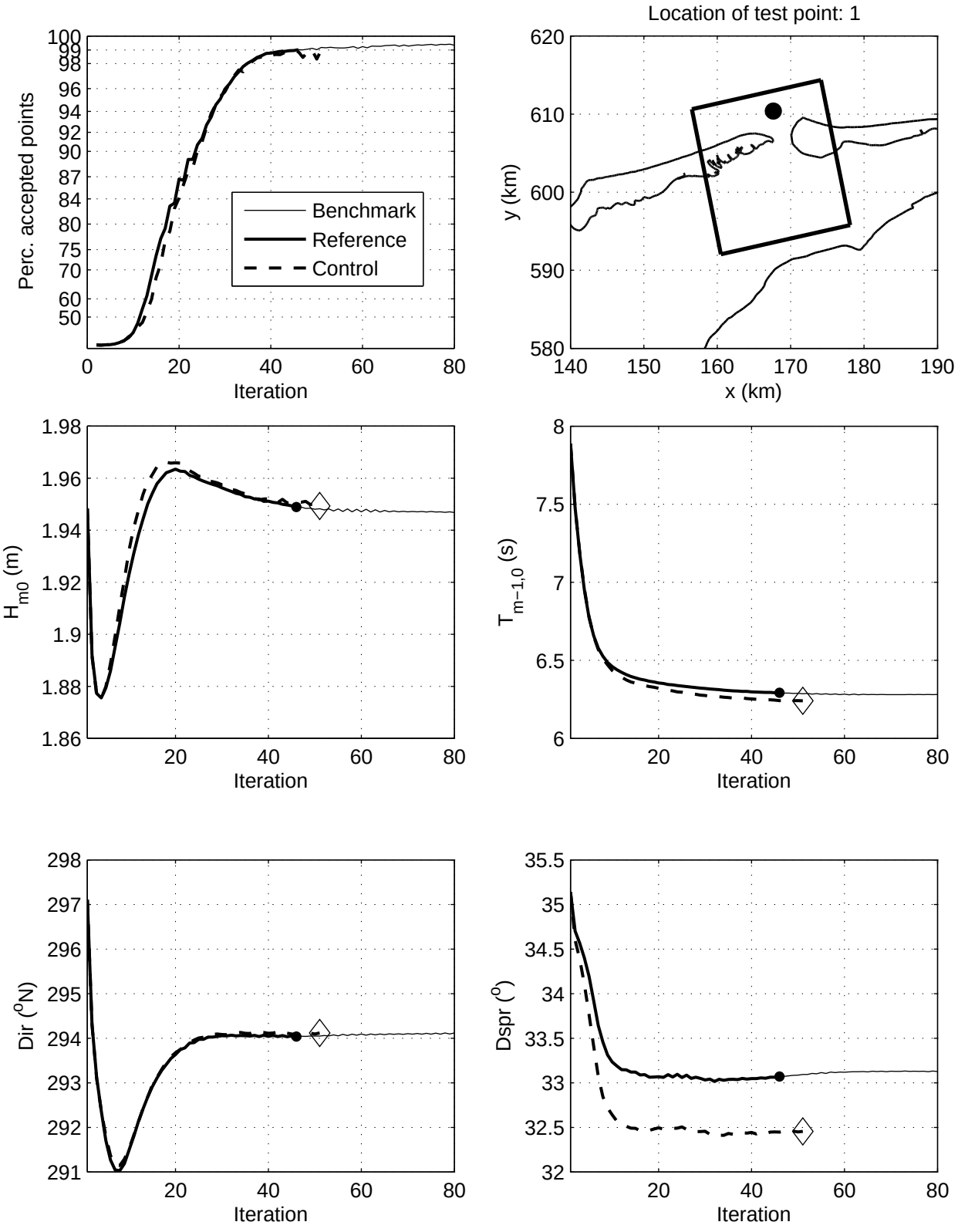

Convergence behaviour of simulations with various DIA options for the Amelander Zeegat, case AZG3A 20050102 1200 Runs B_iq2_std, R_iq2_std (IQUAD=2) and C_iq8_std (IQUAD=8)	SWAN	4051A
	Numerical efficiency SWAN	
DELTARES & ALKYON	H5107.46/A2114	Fig. 8.2

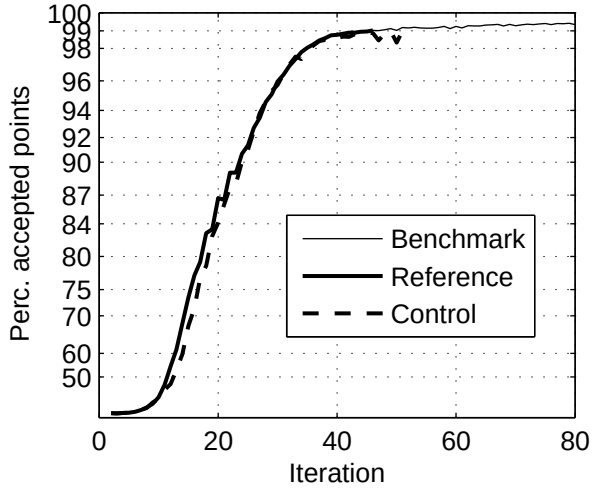

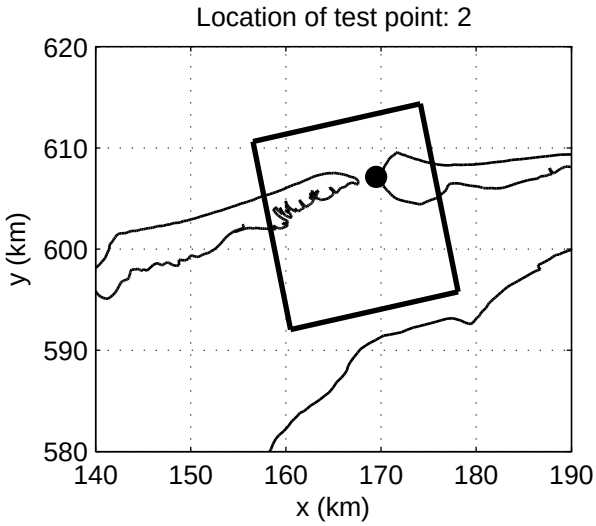

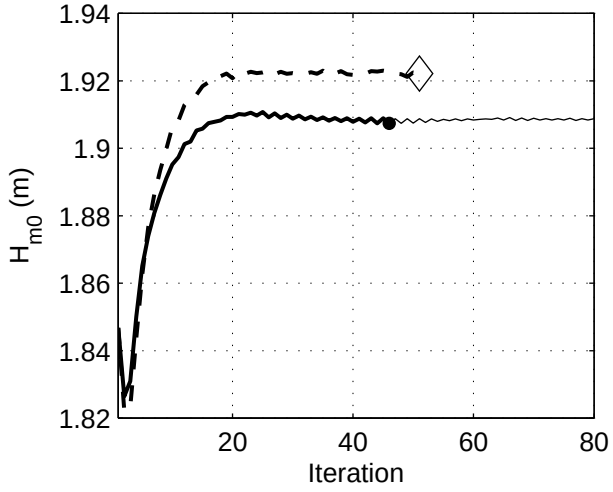

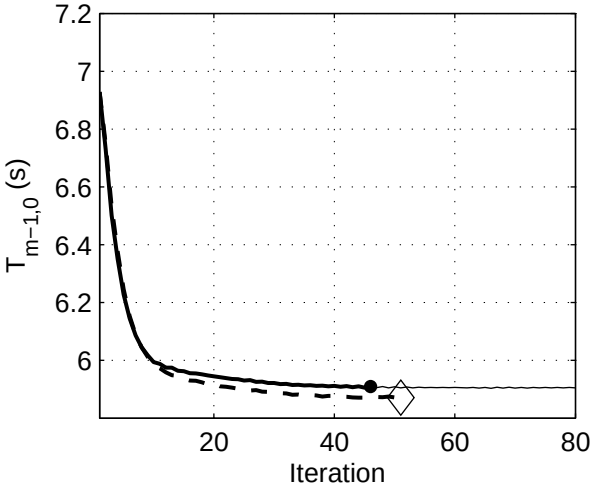

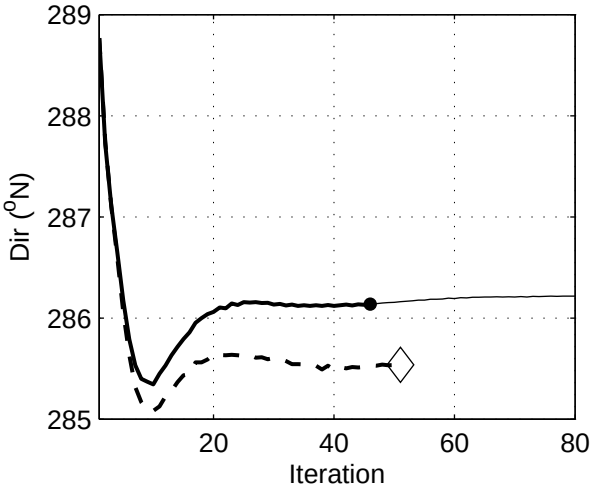

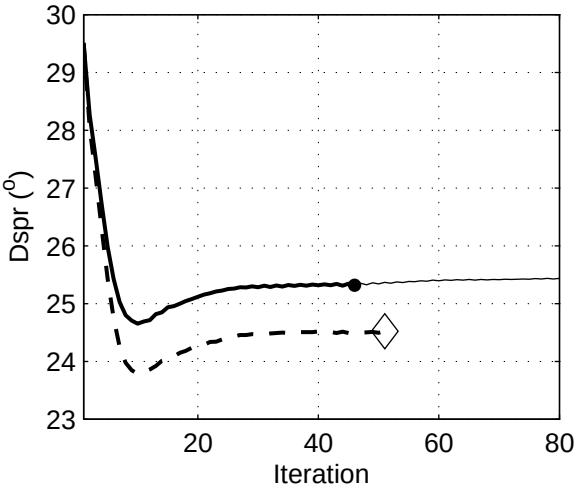

Convergence behaviour of simulations with various DIA options for the Amelander Zeegat, case AZG3A 20050102 1200 Runs B_iq2_std, R_iq2_std (IQUAD=2) and C_iq8_std (IQUAD=8)	SWAN	4051A
	Numerical efficiency SWAN	
DELTARES & ALKYON	H5107.46/A2114	Fig. 8.3

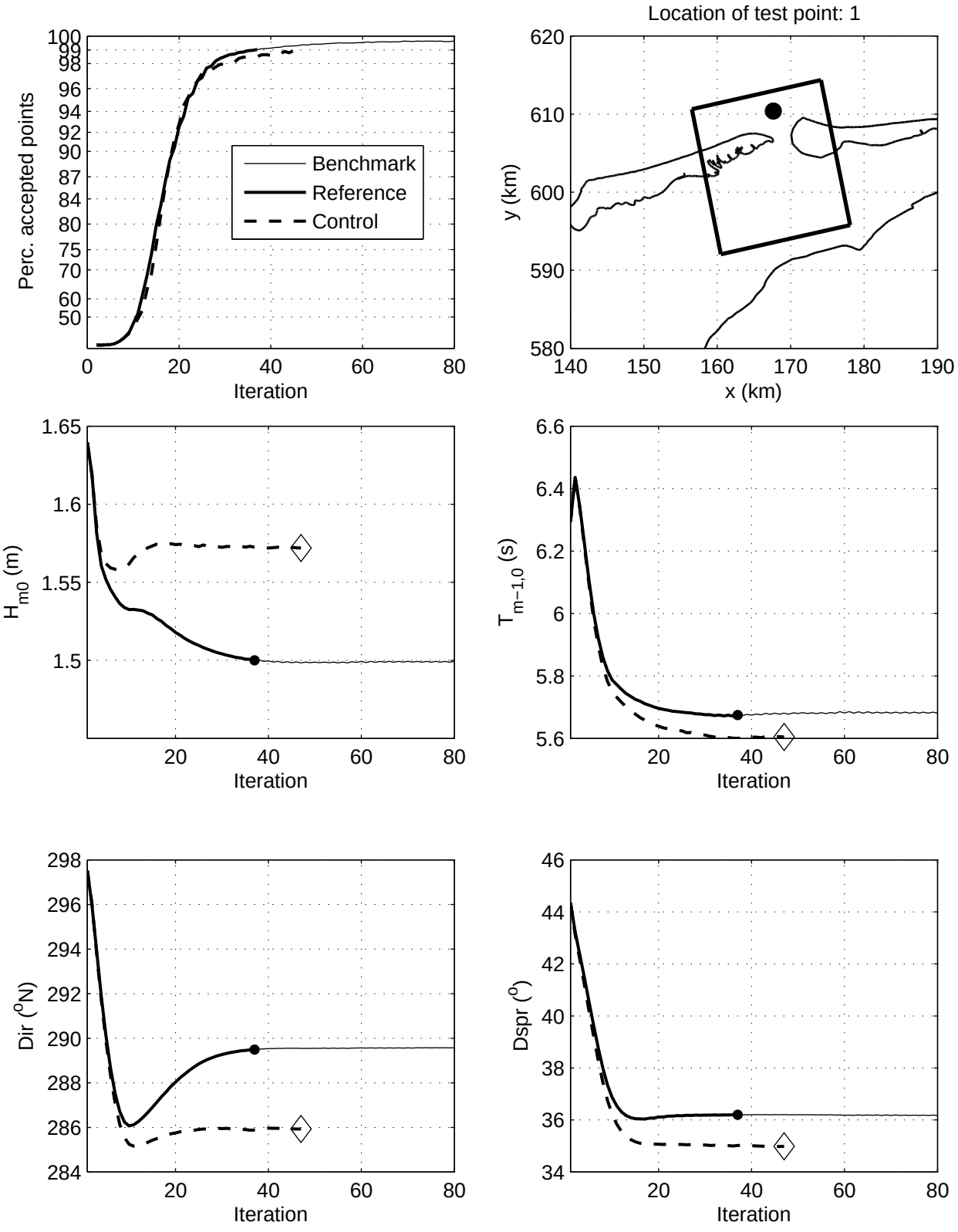

Convergence behaviour of simulations with various DIA options for the Amelander Zeegat, case AZG3A 20050102 1700 Runs B_iq2_std, R_iq2_std (IQUAD=2) and C_iq8_std (IQUAD=8)	SWAN	4051A
	Numerical efficiency SWAN	
DELTARES & ALKYON	H5107.46/A2114	Fig. 8.4

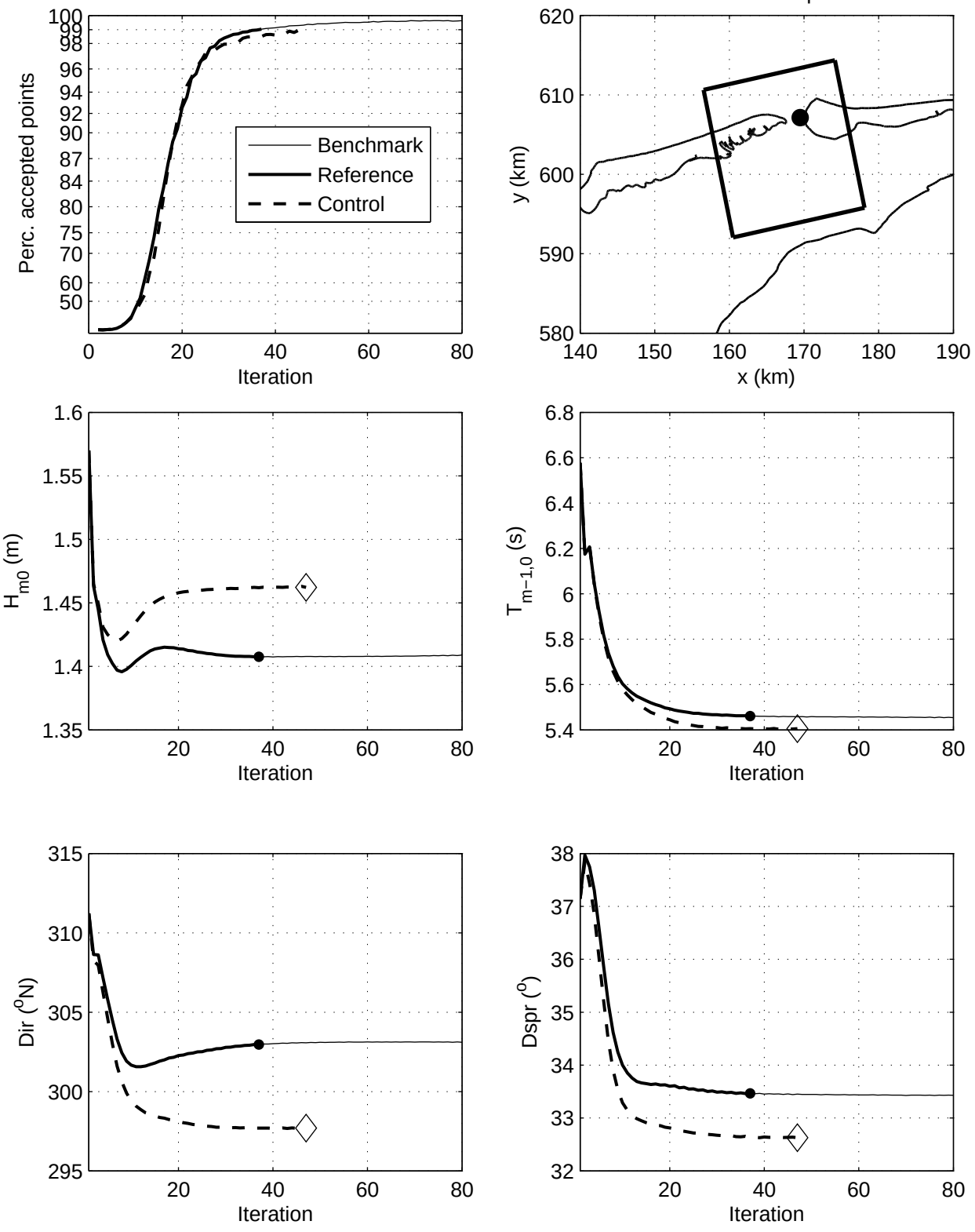

Convergence behaviour of simulations with various DIA options for the Amelander Zeegat, case AZG3A 20050102 1700 Runs B_iq2_std, R_iq2_std (IQUAD=2) and C_iq8_std (IQUAD=8)	SWAN	4051A
	Numerical efficiency SWAN	
DELTARES & ALKYON	H5107.46/A2114	Fig. 8.5

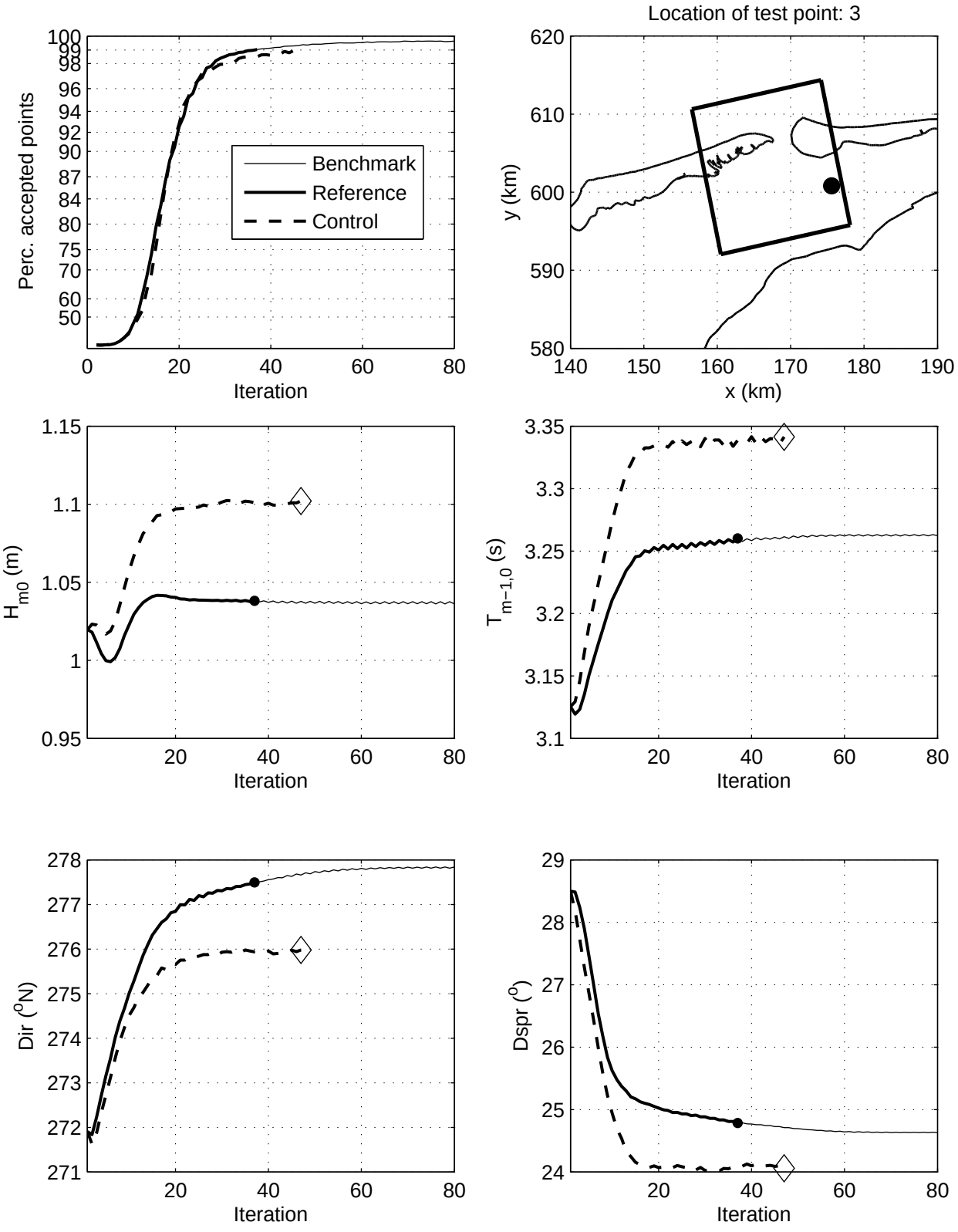

Convergence behaviour of simulations with various DIA options for the Amelander Zeegat, case AZG3A 20050102 1700 Runs B_iq2_std, R_iq2_std (IQUAD=2) and C_iq8_std (IQUAD=8)	SWAN	4051A
	Numerical efficiency SWAN	
DELTARES & ALKYON	H5107.46/A2114	Fig. 8.6

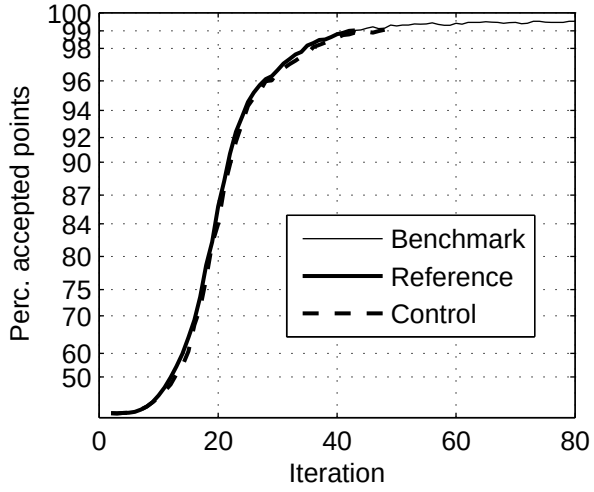

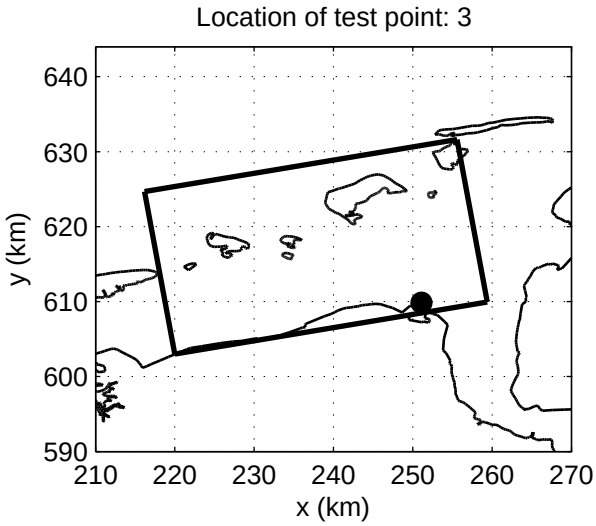

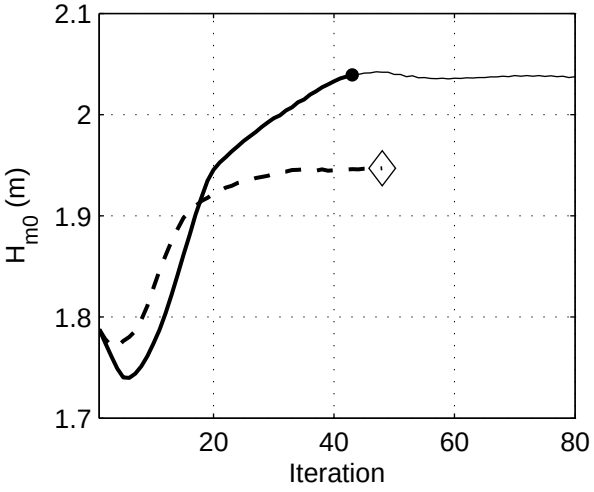

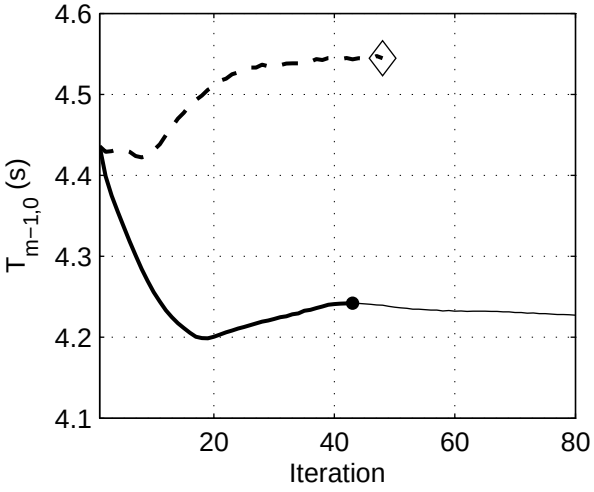

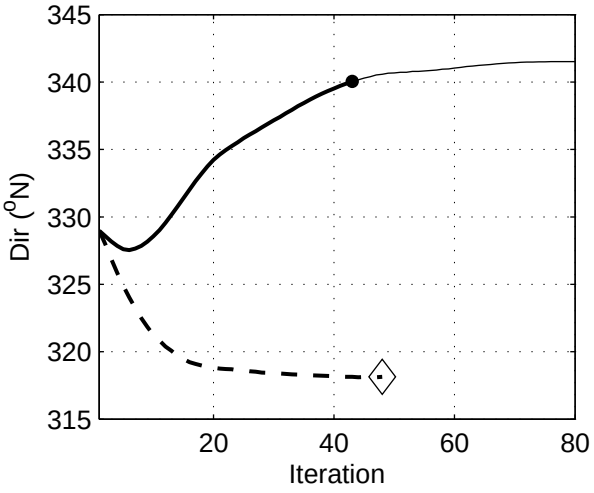

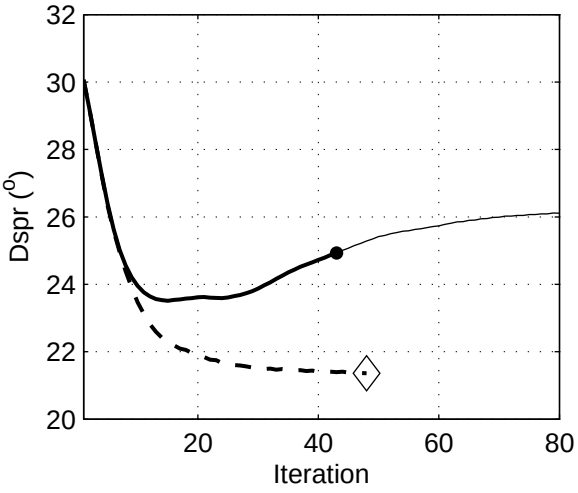

Convergence behaviour of simulations with various DIA options for Eems−Dollard, case EEMS3 20061101 0300 Runs B_iq2_std, R_iq2_std (IQUAD=2) and C_iq8_std (IQUAD=8)	SWAN	4051A
	Numerical efficiency SWAN	
DELTARES & ALKYON	H5107.46/A2114	Fig. 8.7

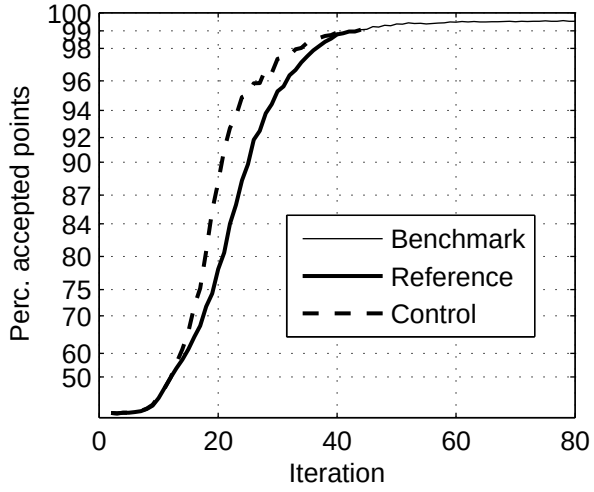

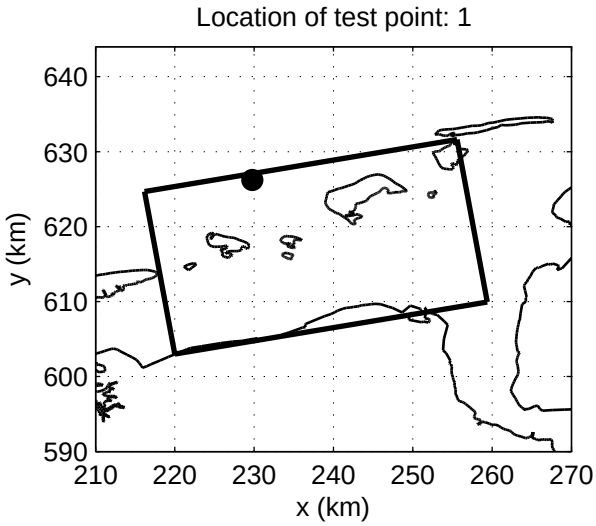

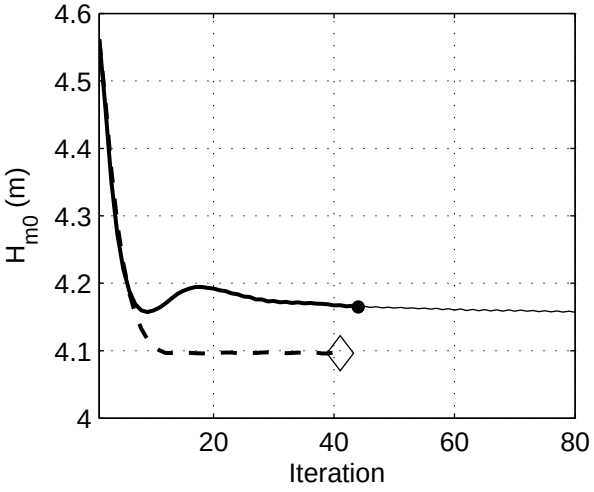

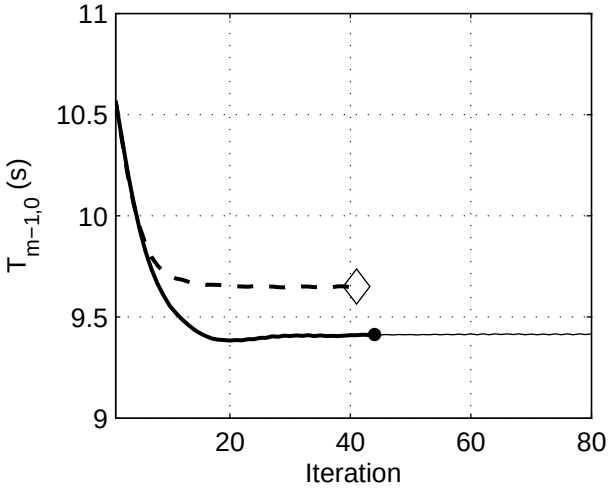

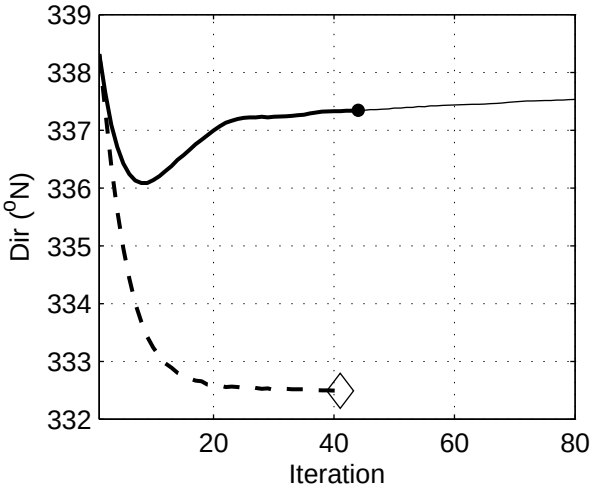

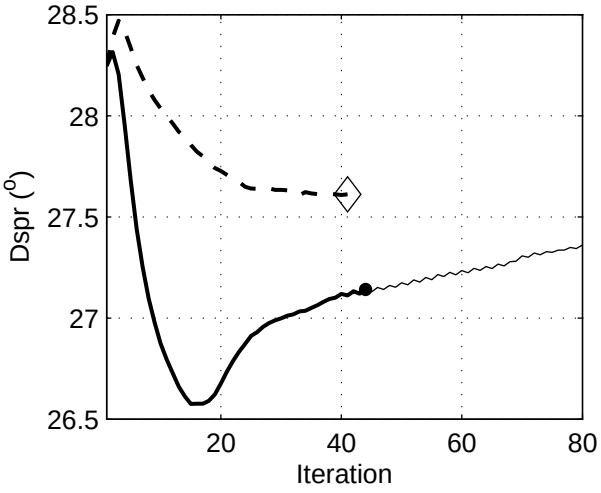

Convergence behaviour of simulations with various DIA options for Eems−Dollard, case EEMS3 20061101 0630 Runs B_iq2_std, R_iq2_std (IQUAD=2) and C_iq8_std (IQUAD=8)	SWAN	4051A
	Numerical efficiency SWAN	
DELTARES & ALKYON	H5107.46/A2114	Fig. 8.8

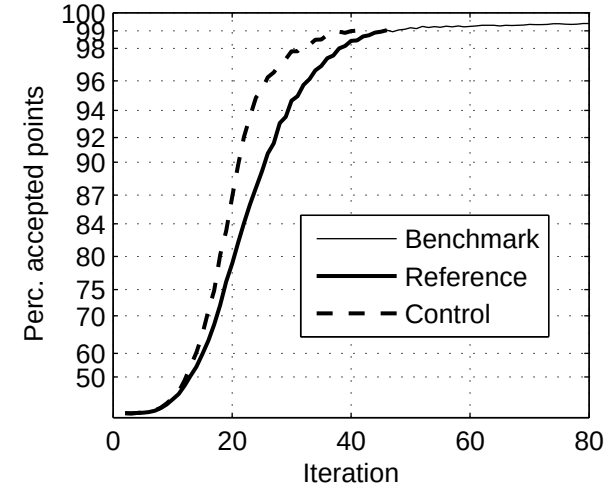

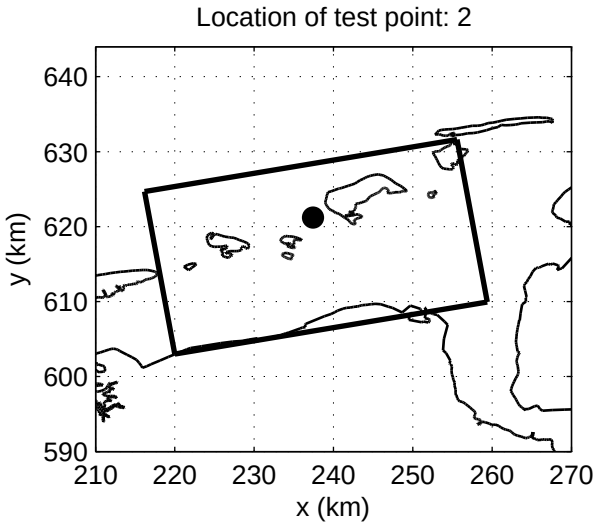

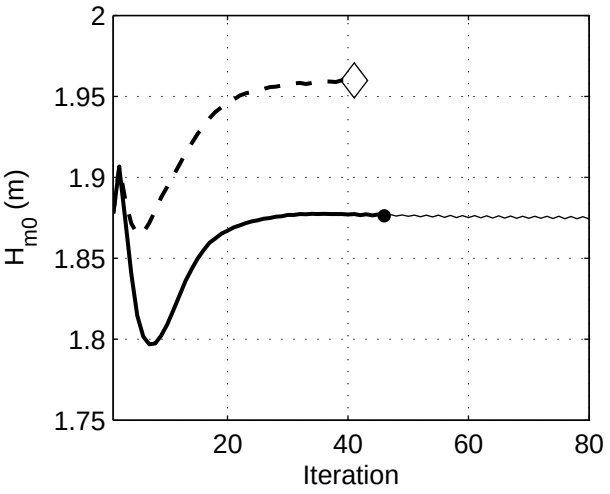

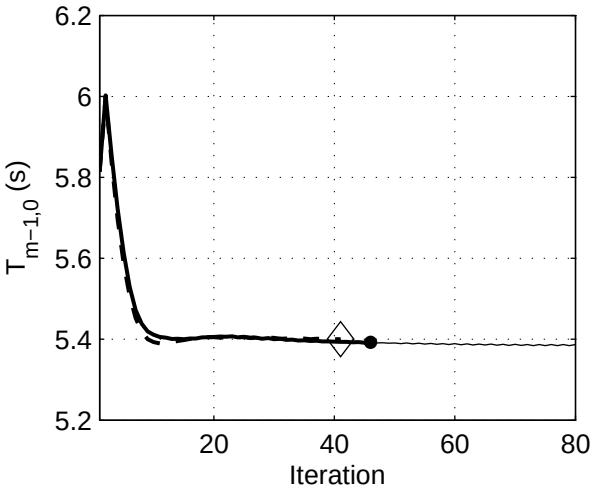

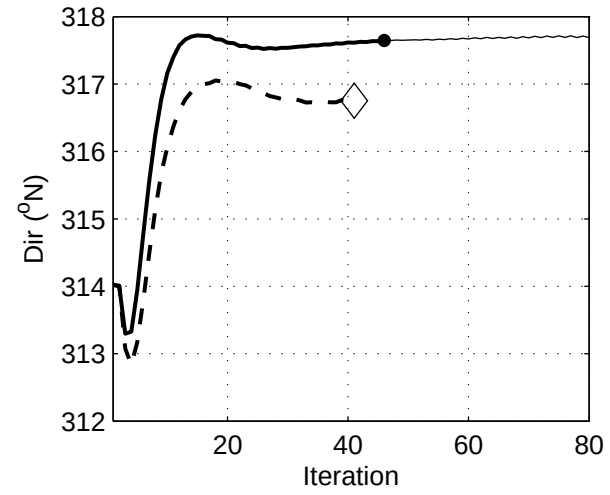

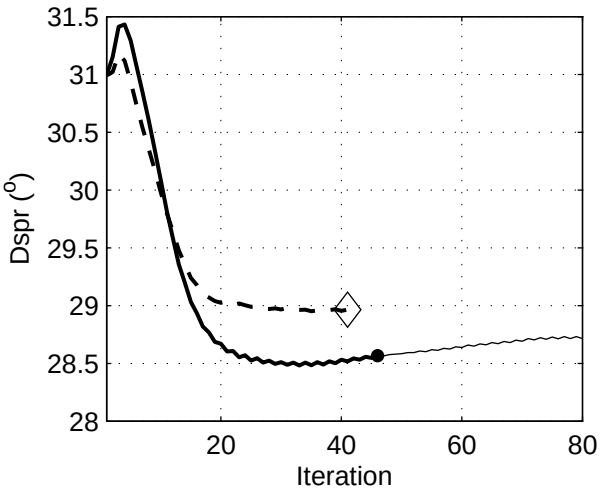

Convergence behaviour of simulations with various DIA options for Eems−Dollard, case EEMS3 20061101 0930 Runs B_iq2_std, R_iq2_std (IQUAD=2) and C_iq8_std (IQUAD=8)	SWAN	4051A
	Numerical efficiency SWAN	
DELTARES & ALKYON	H5107.46/A2114	Fig. 8.9

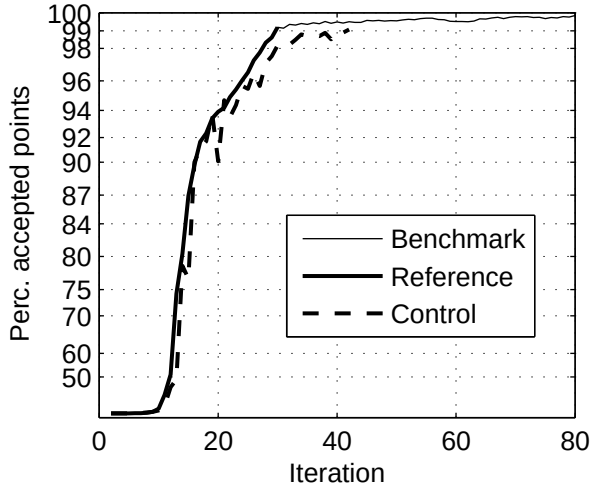

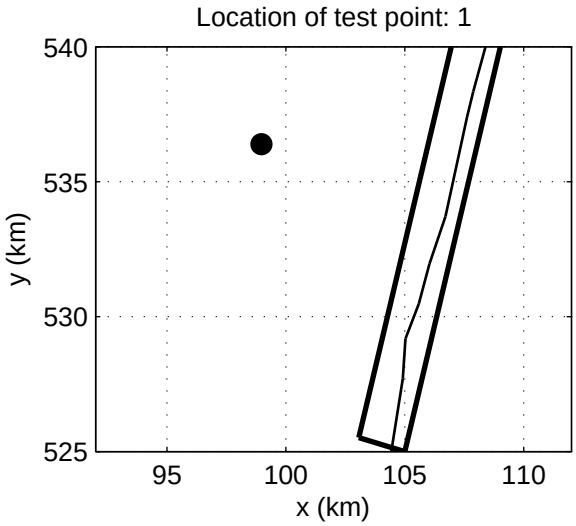

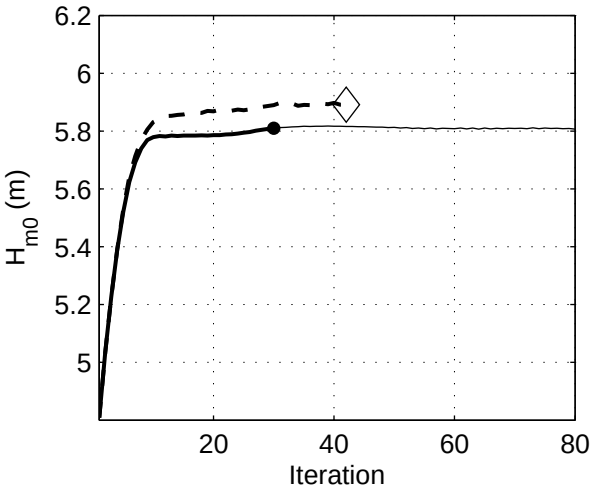

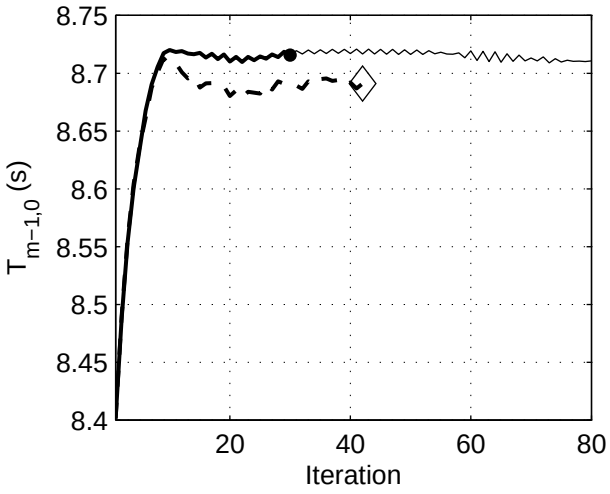

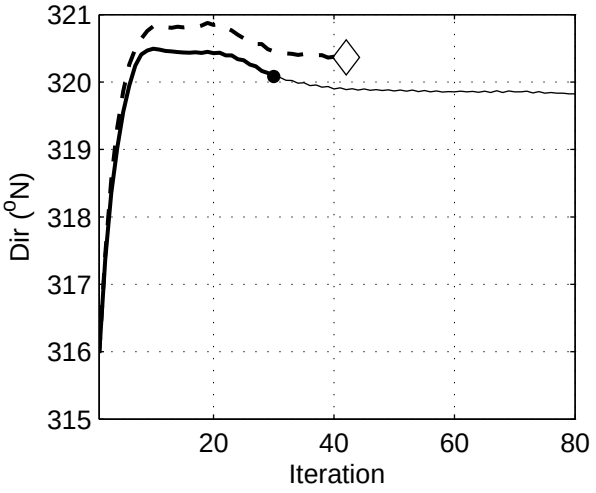

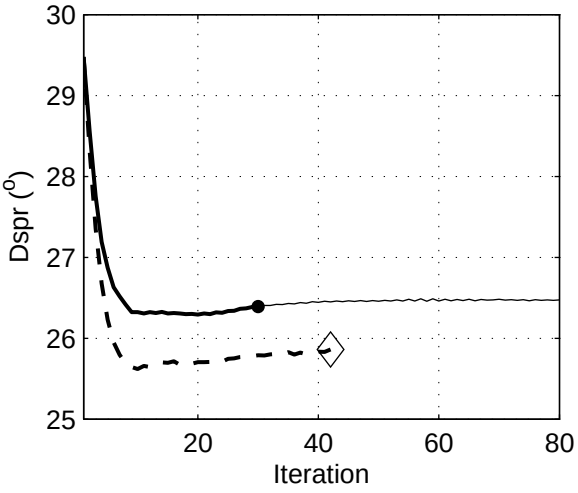

Convergence behaviour of simulations with various DIA options along Dutch coast near Petten, case PETTEN 19950101 1000 Runs B_iq2_std, R_iq2_std (IQUAD=2) and C_iq8_std (IQUAD=8)	SWAN	4051A
	Numerical efficiency SWAN	
DELTARES & ALKYON	H5107.46/A2114	Fig. 8.10

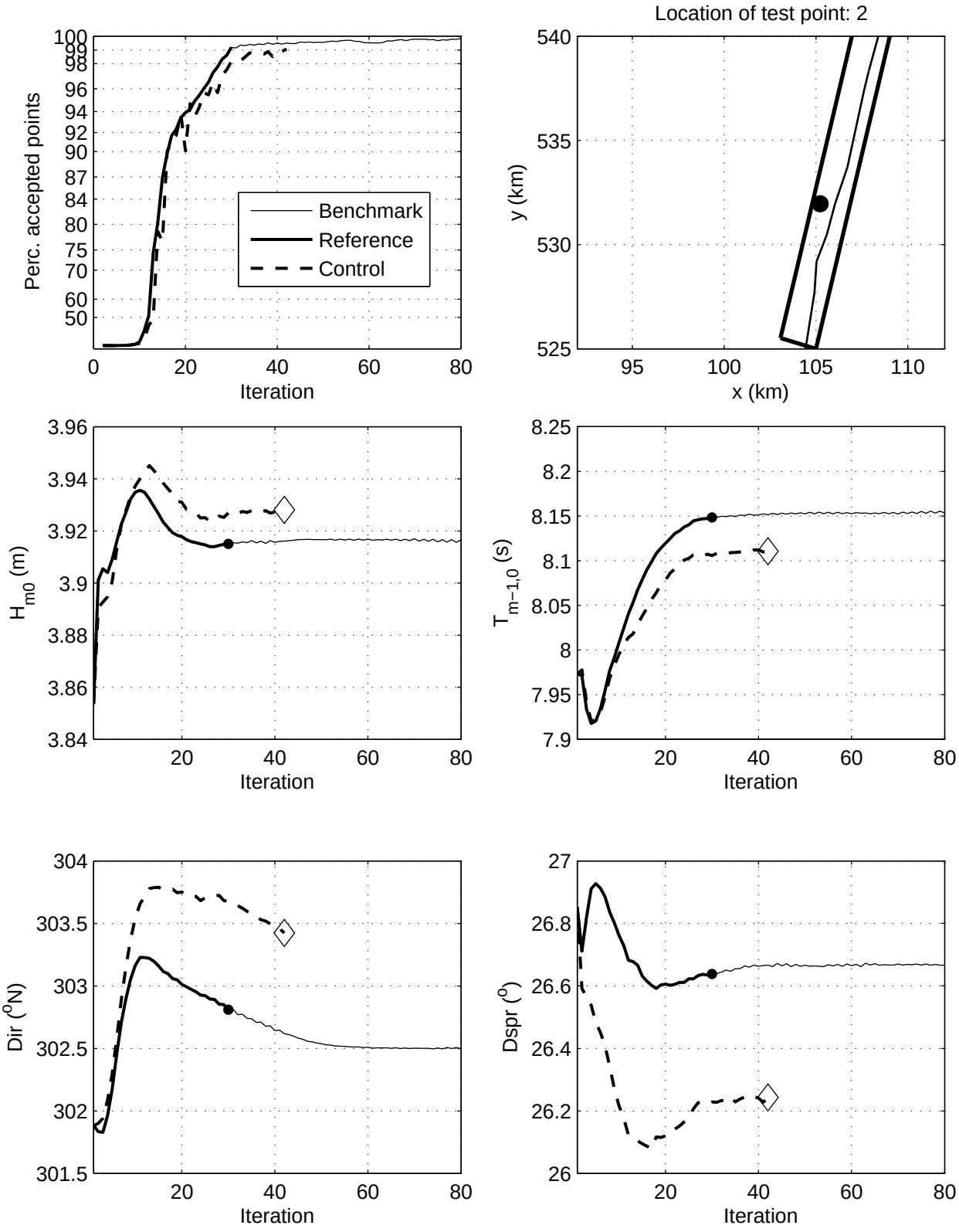

Convergence behaviour of simulations with various DIA options along Dutch coast near Petten, case PETTEN 19950101 1000 Runs B_iq2_std, R_iq2_std (IQUAD=2) and C_iq8_std (IQUAD=8)	SWAN	4051A
	Numerical efficiency SWAN	
DELTARES & ALKYON	H5107.46/A2114	Fig. 8.11

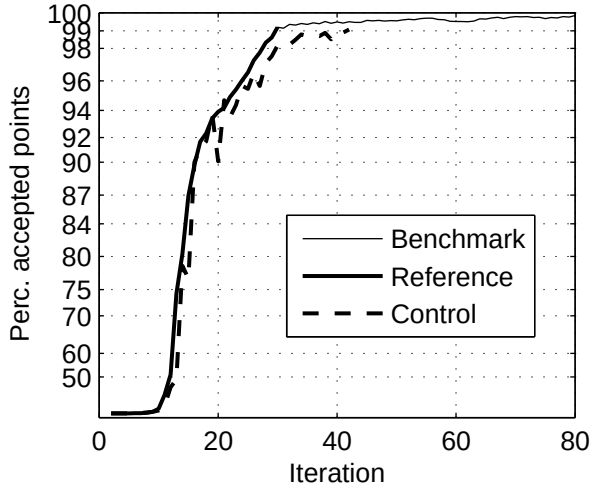

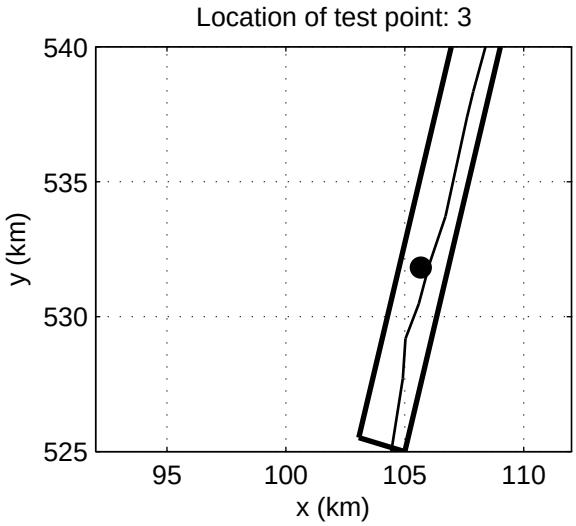

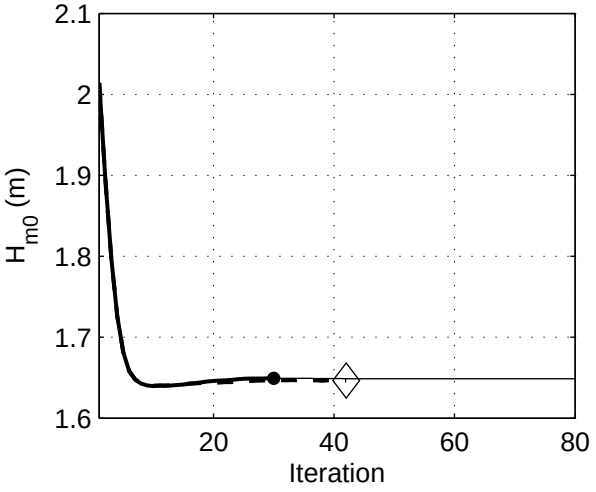

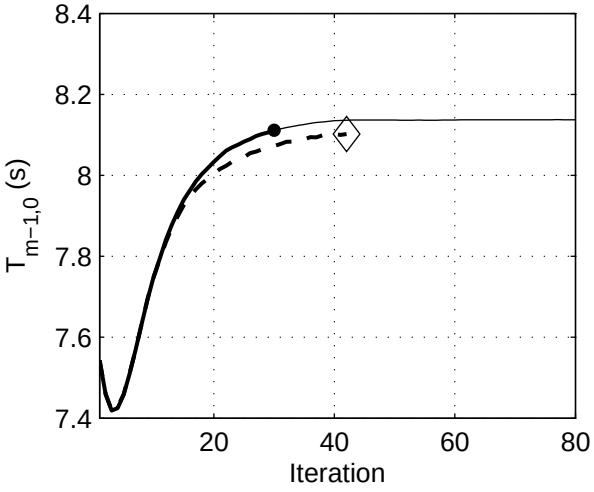

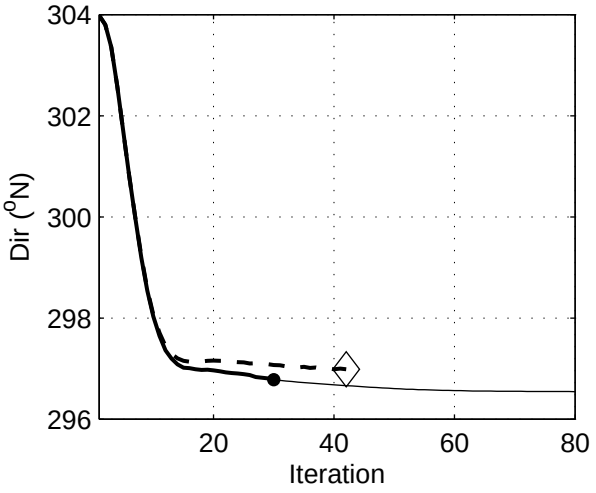

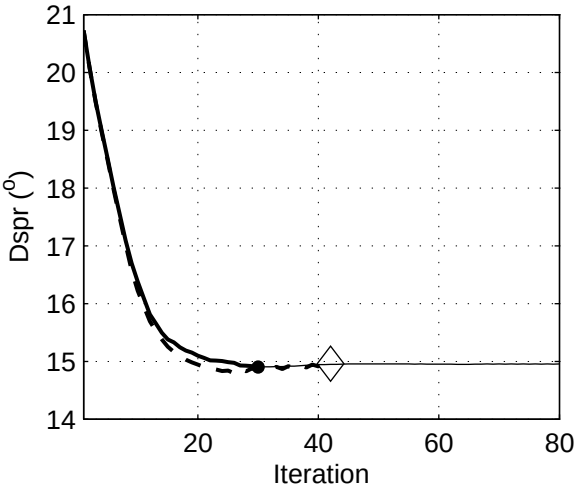

Convergence behaviour of simulations with various DIA options along Dutch coast near Petten, case PETTEN 19950101 1000 Runs B_iq2_std, R_iq2_std (IQUAD=2) and C_iq8_std (IQUAD=8)	SWAN	4051A
	Numerical efficiency SWAN	
DELTARES & ALKYON	H5107.46/A2114	Fig. 8.12

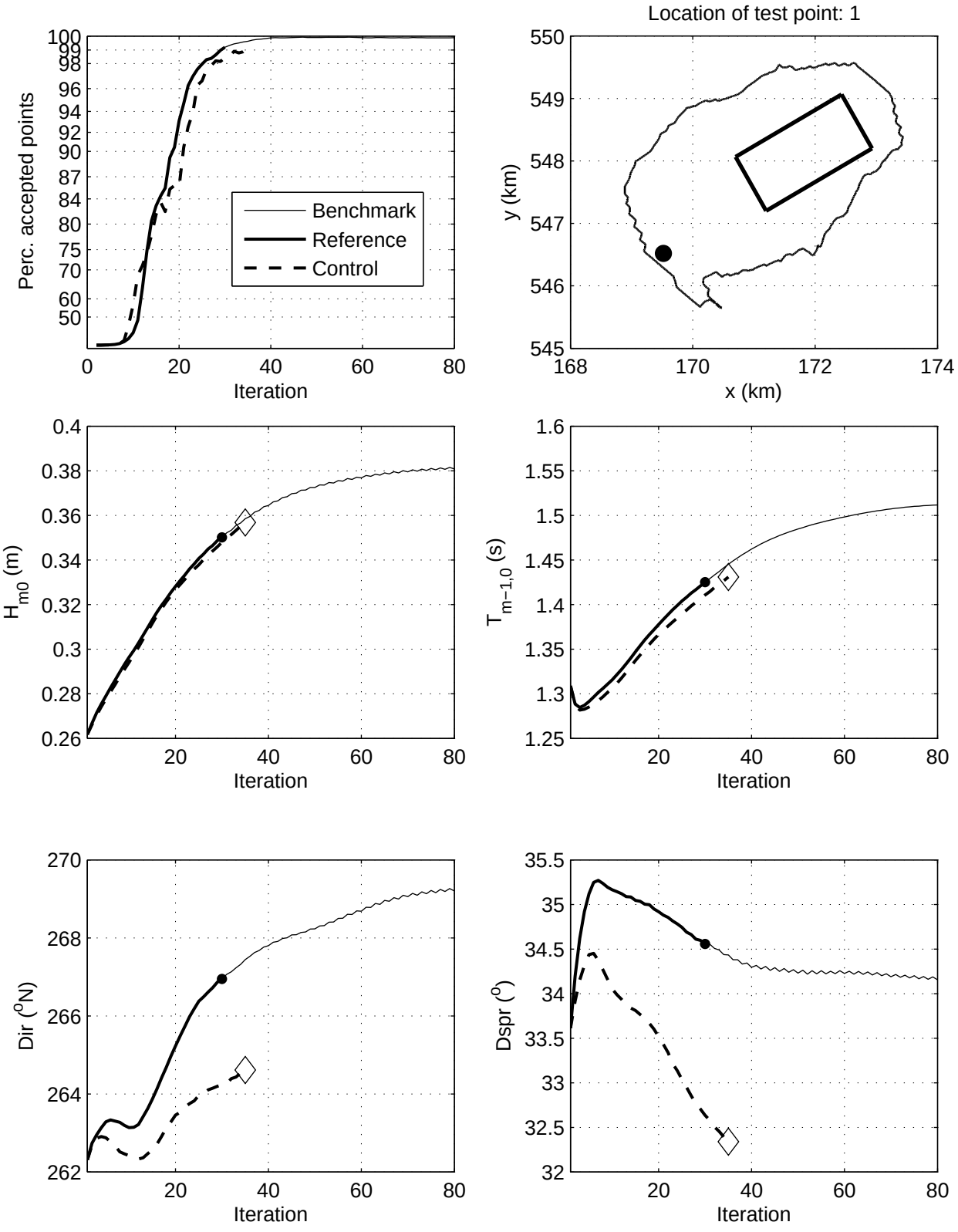

Convergence behaviour of simulations with various DIA options for Lake Sloten, case SLE 20021027 1500 Runs B_iq2_std, R_iq2_std (IQUAD=2) and C_iq8_std (IQUAD=8)	SWAN	4051A
	Numerical efficiency SWAN	
DELTARES & ALKYON	H5107.46/A2114	Fig. 8.13

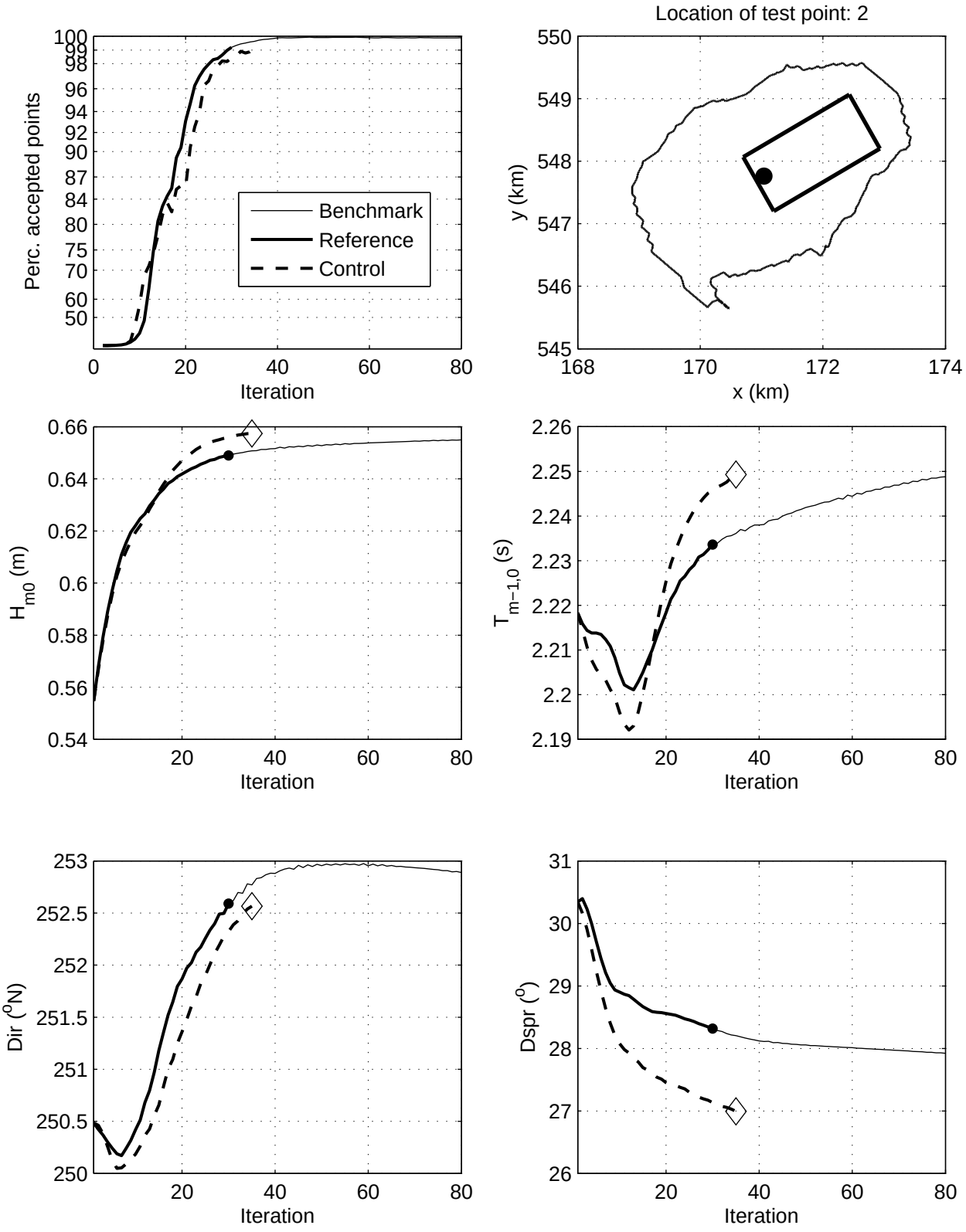

Convergence behaviour of simulations with various DIA options for Lake Sloten, case SLE 20021027 1500 Runs B_iq2_std, R_iq2_std (IQUAD=2) and C_iq8_std (IQUAD=8)	SWAN	4051A
	Numerical efficiency SWAN	
DELTARES & ALKYON	H5107.46/A2114	Fig. 8.14

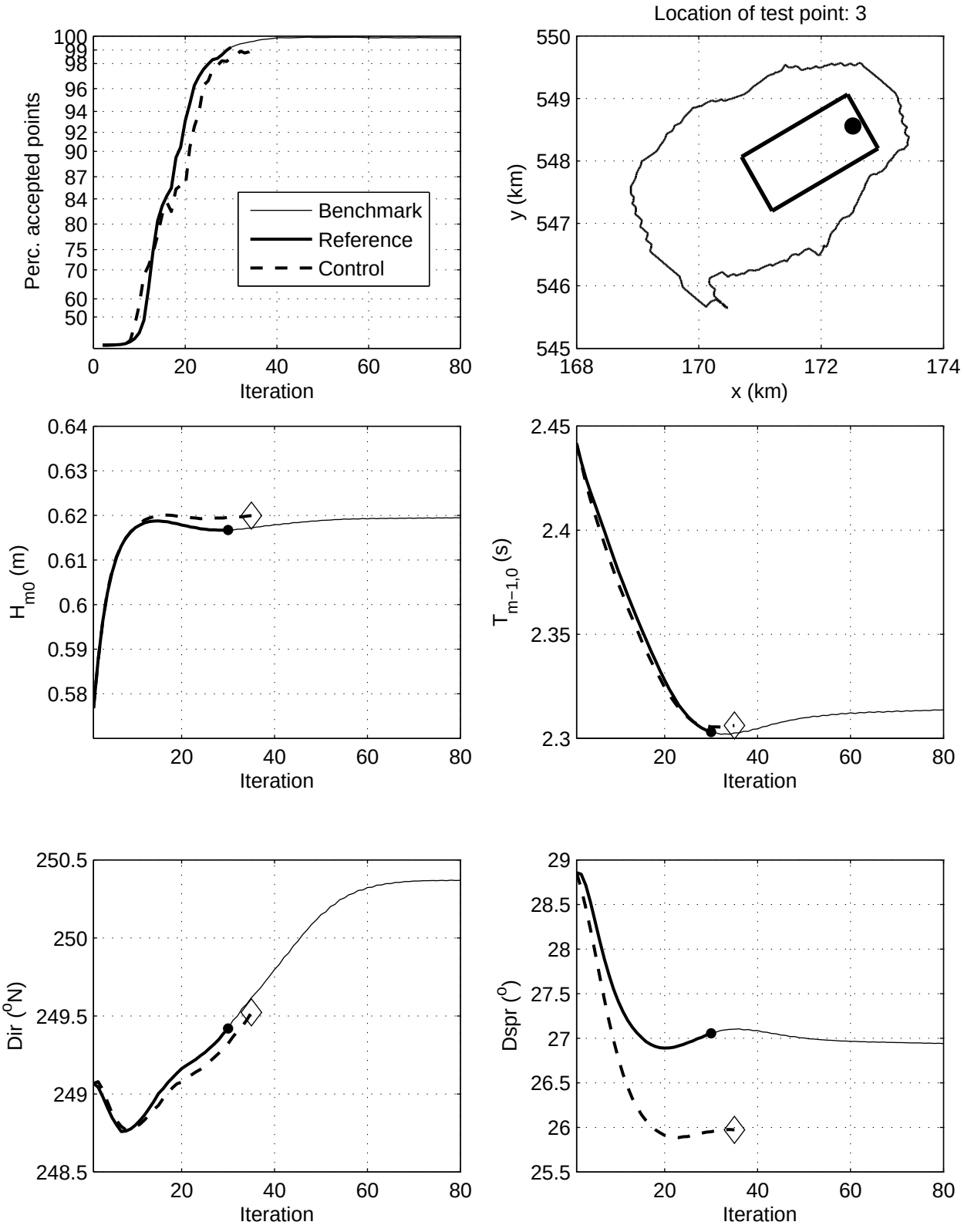

Convergence behaviour of simulations with various DIA options for Lake Sloten, case SLE 20021027 1500 Runs B_iq2_std, R_iq2_std (IQUAD=2) and C_iq8_std (IQUAD=8)	SWAN	4051A
	Numerical efficiency SWAN	
DELTARES & ALKYON	H5107.46/A2114	Fig. 8.15

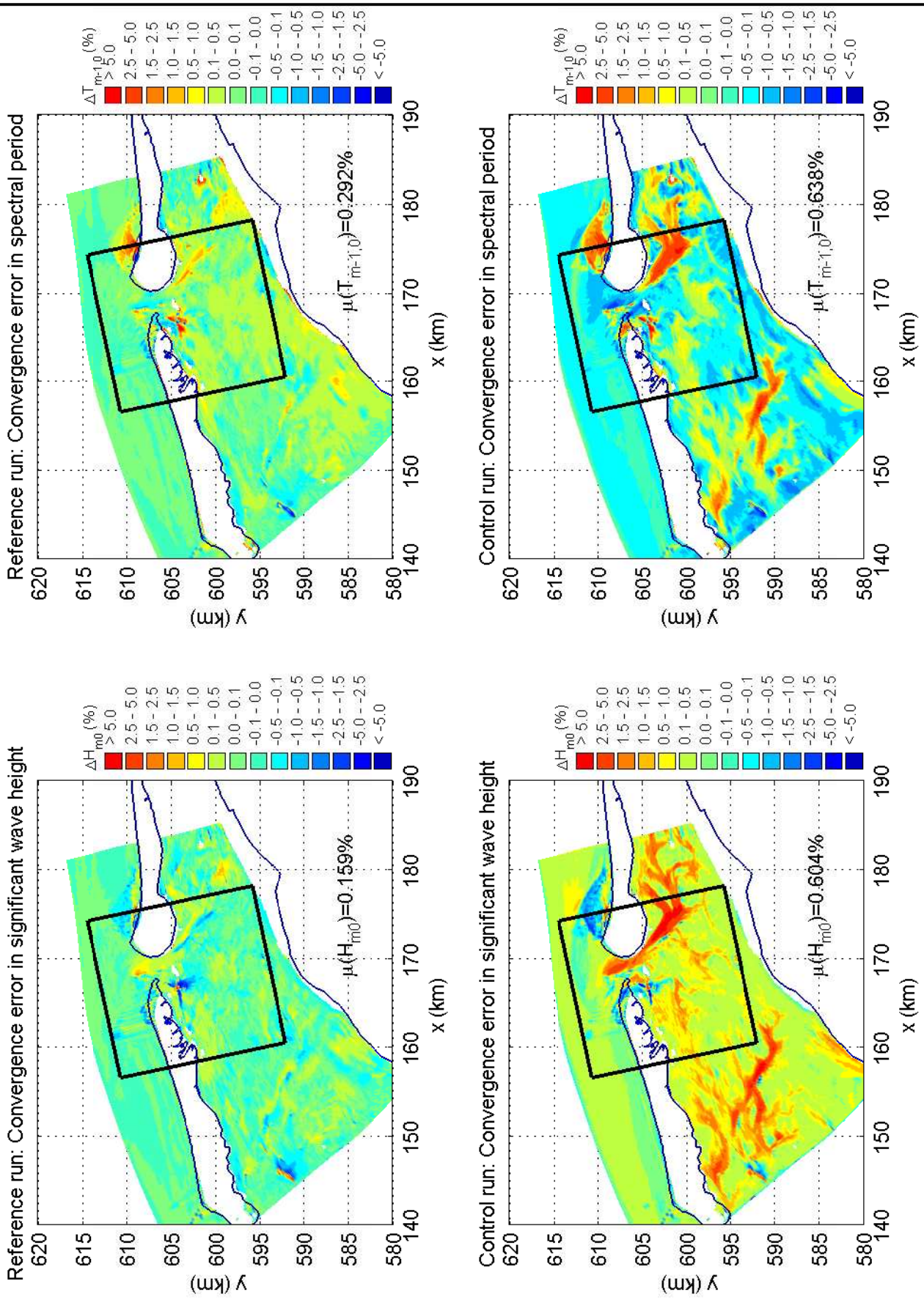

Convergence error in H_{m0} and $T_{m-1,0}$ for DIA IQUAD=8 for the Amelander Zeegat, case AZG3A 20050102 1000 Reference run (R_iq2_std) and control run (C_iq8_std)	SWAN	4051A
	Numerical efficiency SWAN	
DELTARES & ALKYON	H5107.46/A2114	Fig. 8.16

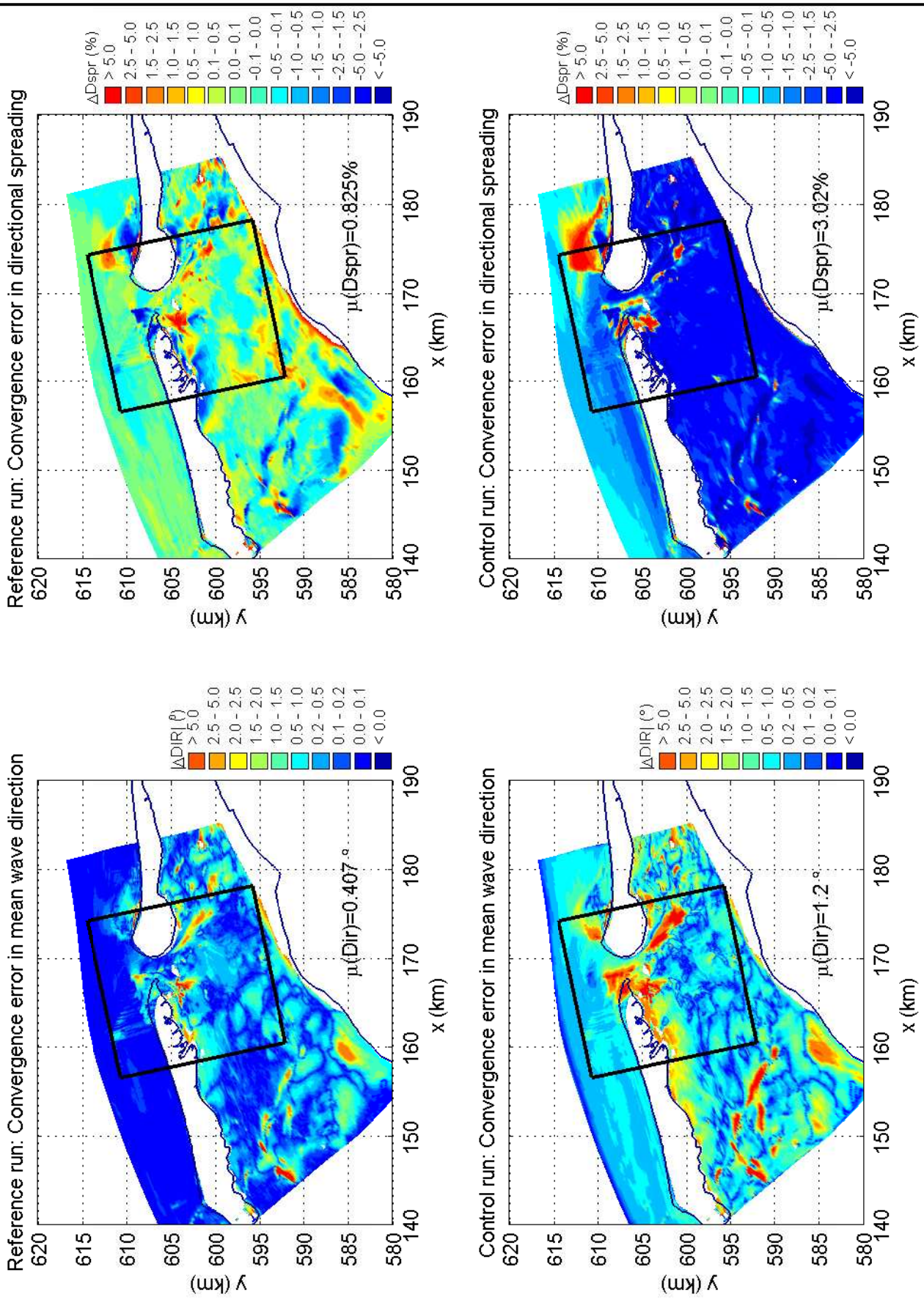

Convergence error in Dir and Dspr for DIA IQUAD=8 for the Amelander Zeegat, case AZG3A 20050102 1000 Reference run (R_iq2_std) and control run (C_iq8_std)	SWAN	4051A
	Numerical efficiency SWAN	
DELTARES & ALKYON	H5107.46/A2114	Fig. 8.17

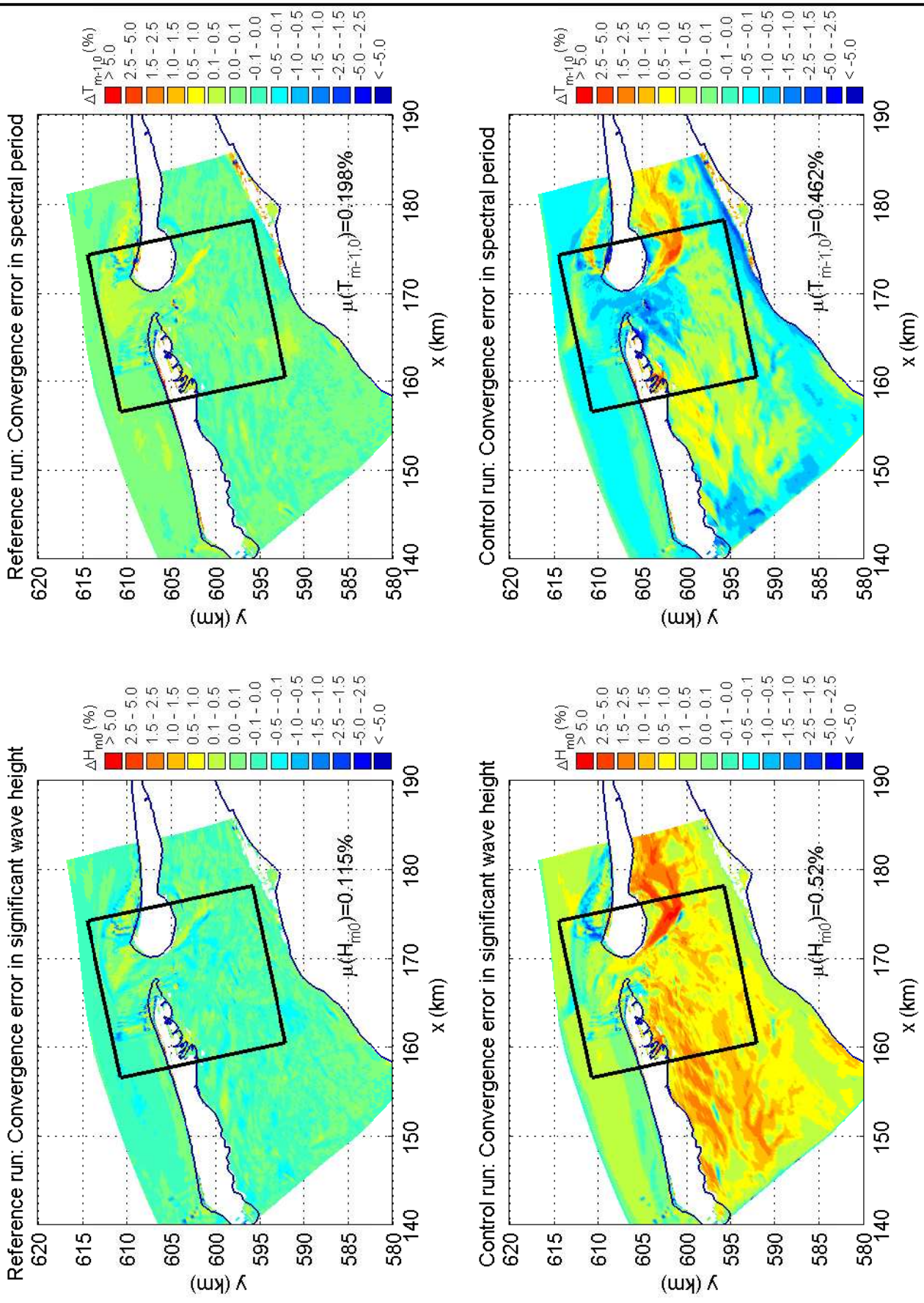

Convergence error in H_{m0} and $T_{m-1,0}$ for DIA IQUAD=8 for the Amelander Zeegat, case AZG3A 20050102 1200 Reference run (R_iq2_std) and control run (C_iq8_std)	SWAN	4051A
	Numerical efficiency SWAN	
DELTARES & ALKYON	H5107.46/A2114	Fig. 8.18

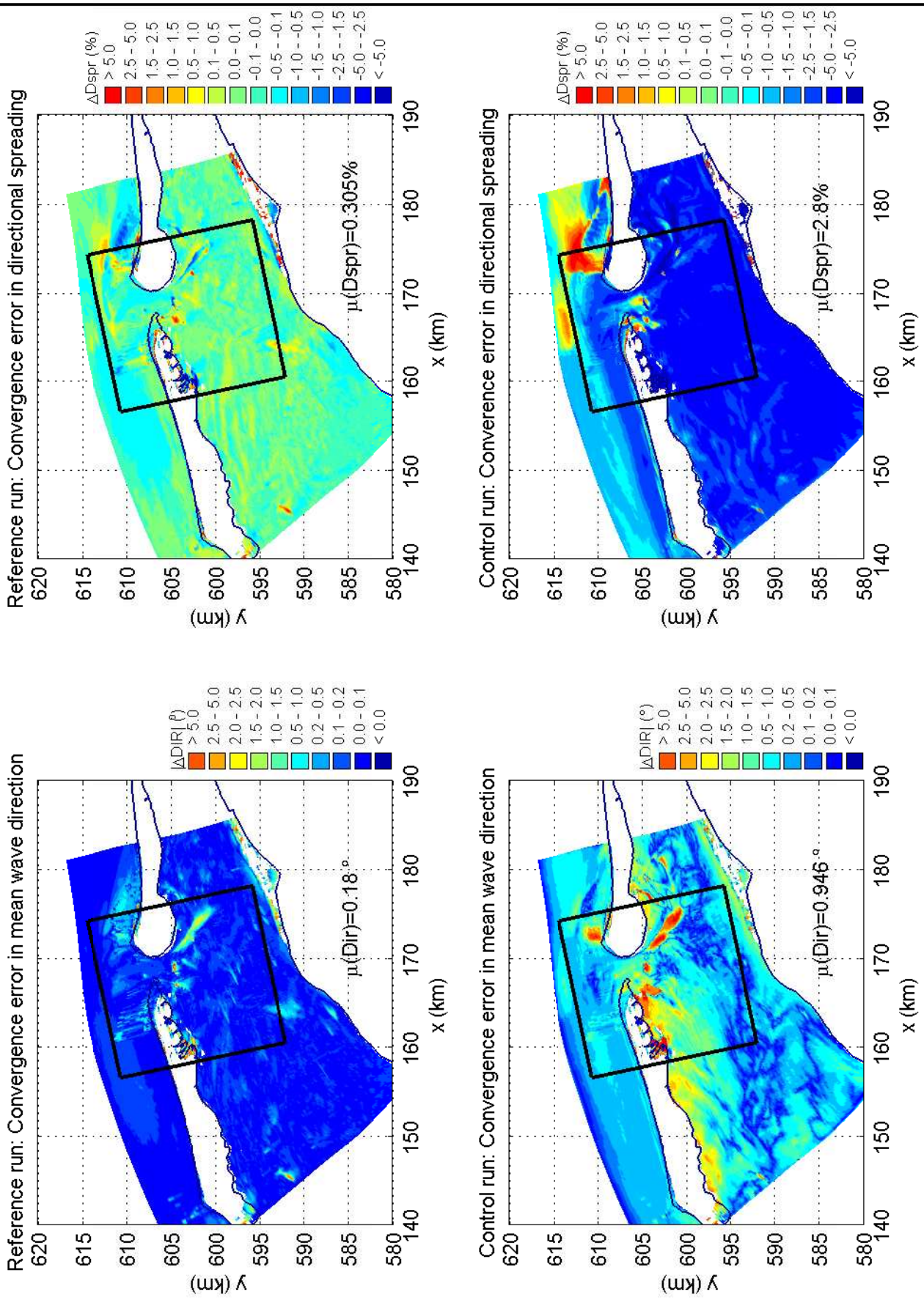

Convergence error in Dir and Dspr for DIA IQUAD=8 for the Amelander Zeegat, case AZG3A 20050102 1200 Reference run (R_iq2_std) and control run (C_iq8_std)	SWAN	4051A
	Numerical efficiency SWAN	
DELTARES & ALKYON	H5107.46/A2114	Fig. 8.19

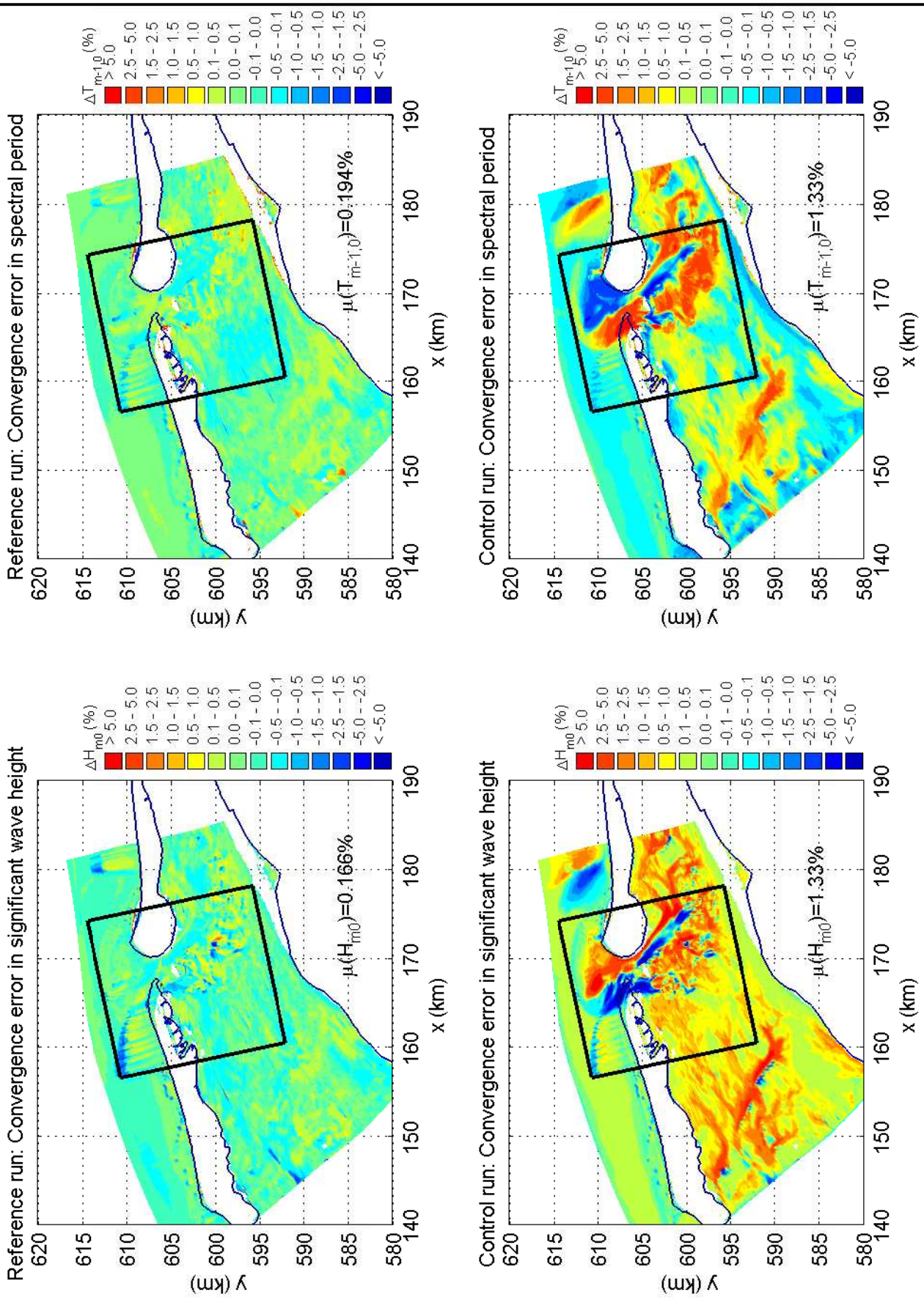

Convergence error in H_{m0} and $T_{m-1,0}$ for DIA IQUAD=8 for the Amelander Zeegat, case AZG3A 20050102 1700 Reference run (R_iq2_std) and control run (C_iq8_std)	SWAN	4051A
	Numerical efficiency SWAN	
DELTARES & ALKYON	H5107.46/A2114	Fig. 8.20

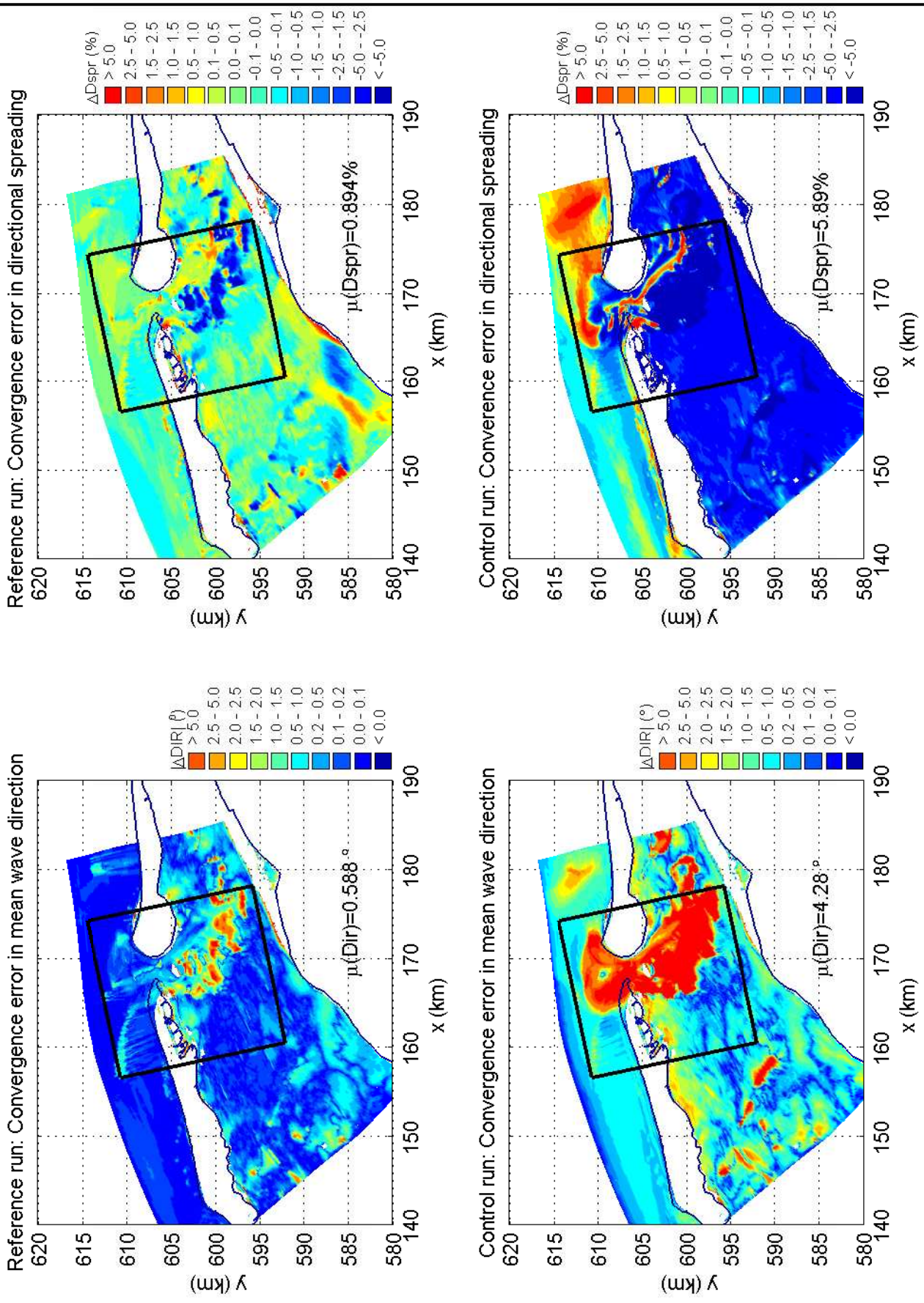

Convergence error in Dir and Dspr for DIA IQUAD=8 for the Amelander Zeegat, case AZG3A 20050102 1700 Reference run (R_iq2_std) and control run (C_iq8_std)	SWAN	4051A
	Numerical efficiency SWAN	
DELTARES & ALKYON	H5107.46/A2114	Fig. 8.21

DELTARES & ALKYON

Convergence error in H_{m0} and $T_{m-1,0}$ for triplet method
for the Amelander Zeegat,case AZG3A 20050102 1200
Control runs C_iq2_tri (IQUAD=2) and C_iq8_tri (IQUAD=8)

SWAN

Numerical efficiency SWAN

H5107.46/A2114

4051A

Fig. 8.22

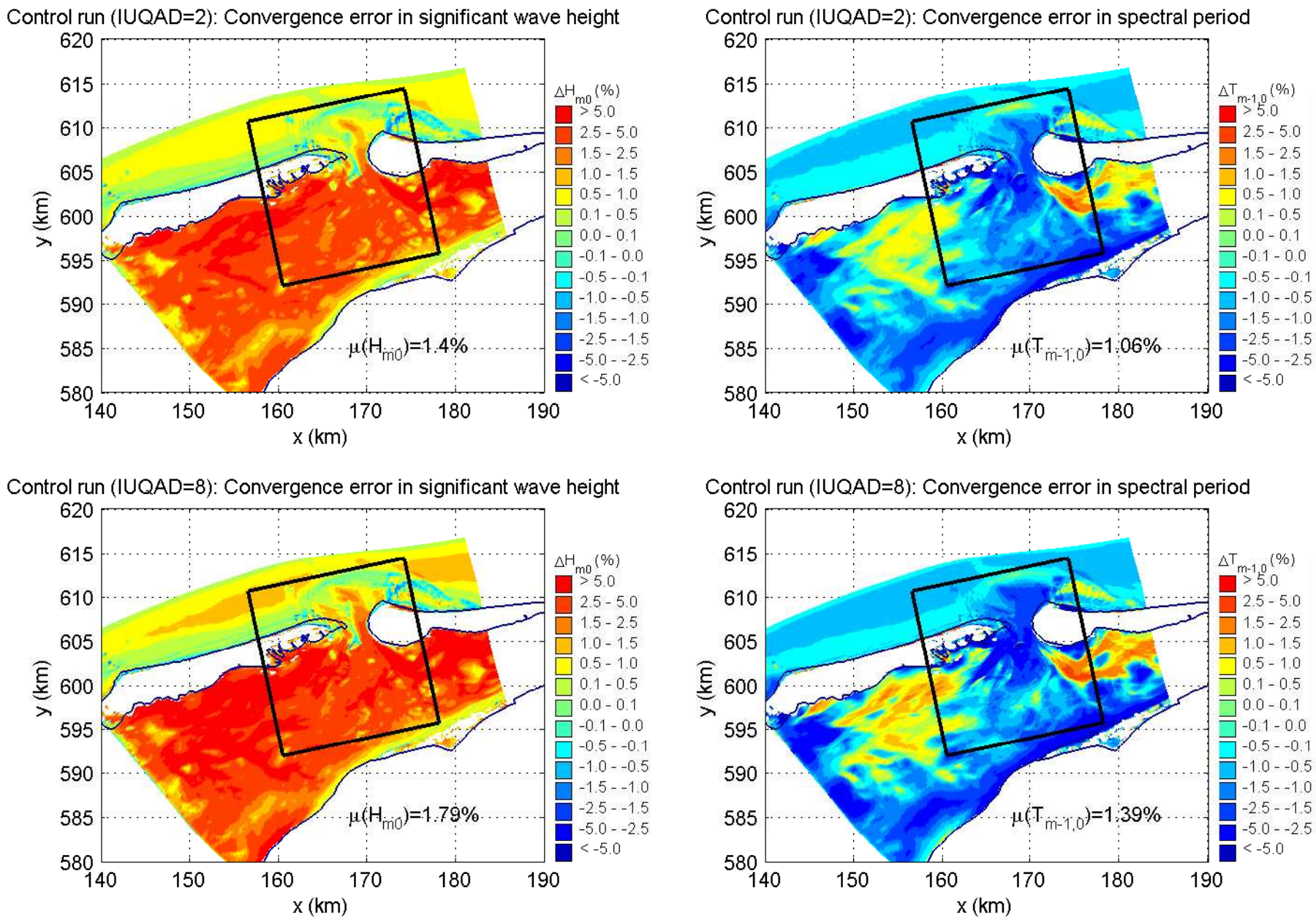

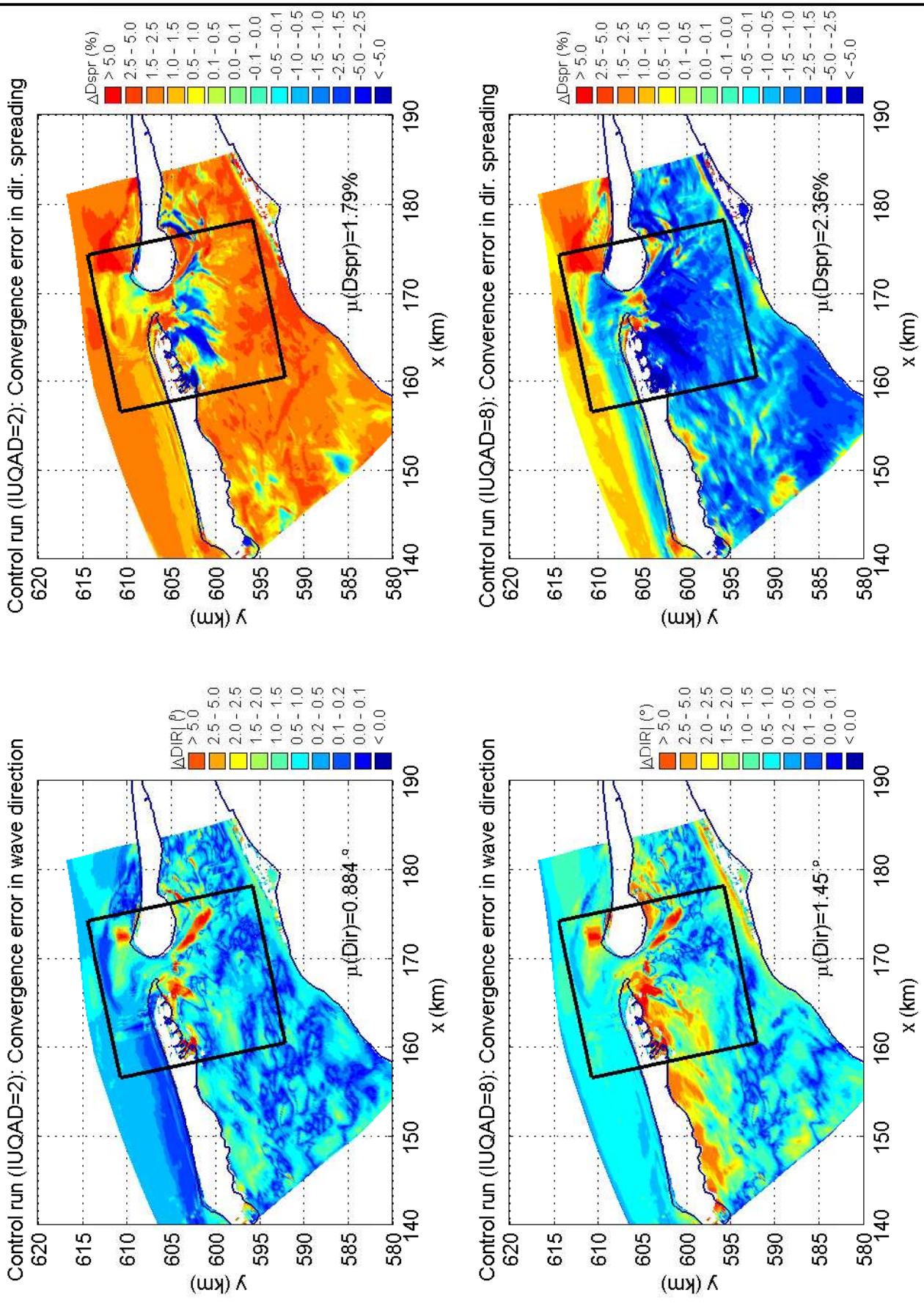

Convergence errors in Dir and Dspr for triplet method for the Amelander Zeegat, case AZG3A 20050102 1200 Control runs C_iq2_tri (IQUAD=2) and C_iq8_tri (IQUAD=8)	SWAN	4051A
	Numerical efficiency SWAN	
DELTARES & ALKYON	H5107.46/A2114	Fig. 8.23

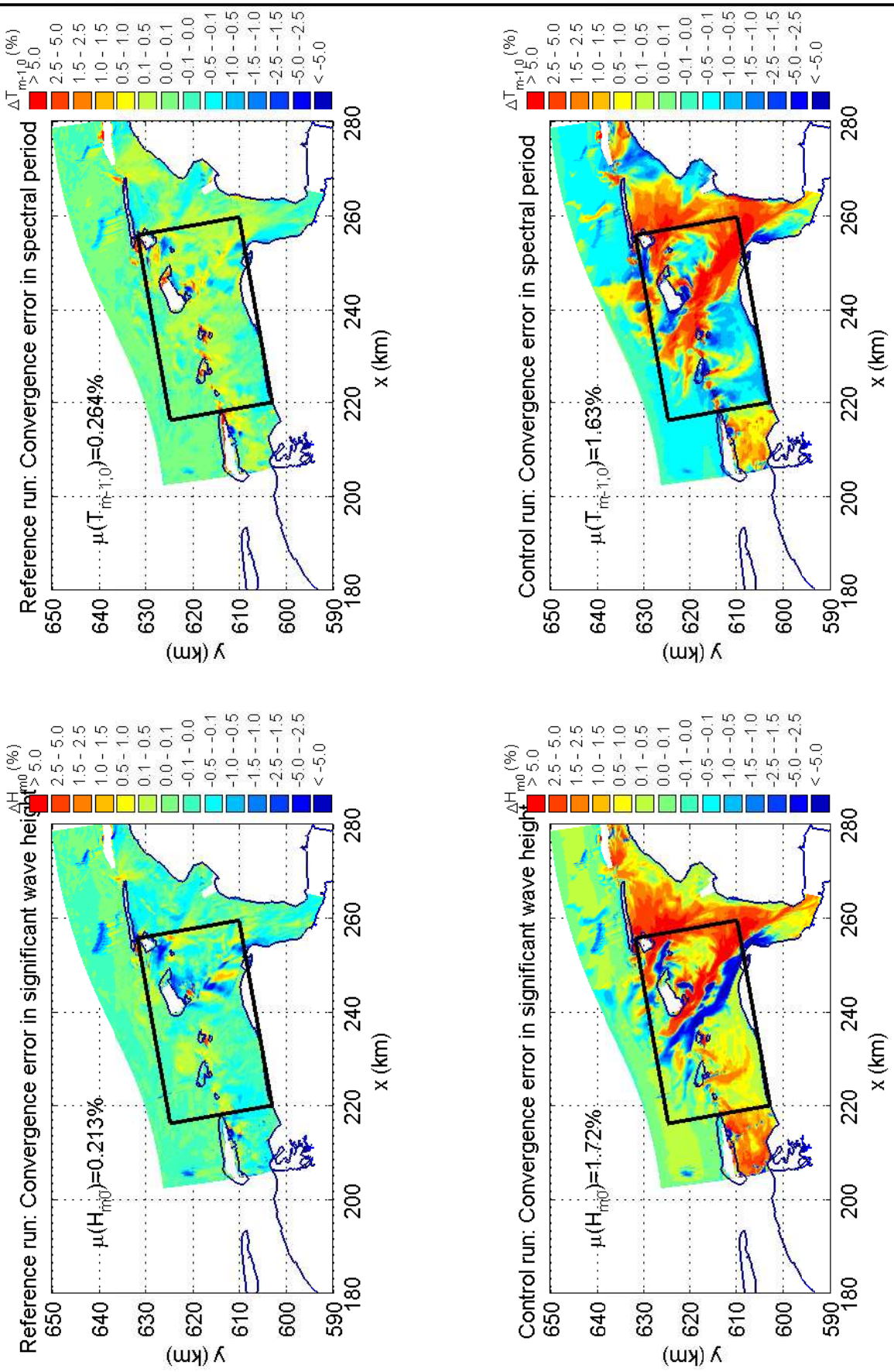

Convergence error in H_{m0} and $T_{m-1,0}$ for DIA IQUAD=8 for Eems-Dollard, case EEMS3 20061101 0300 Reference run (R_iq2_std) and control run (C_iq8_std)	SWAN	4051A
	Numerical efficiency SWAN	
DELTARES & ALKYON	H5107.46/A2114	Fig. 8.24

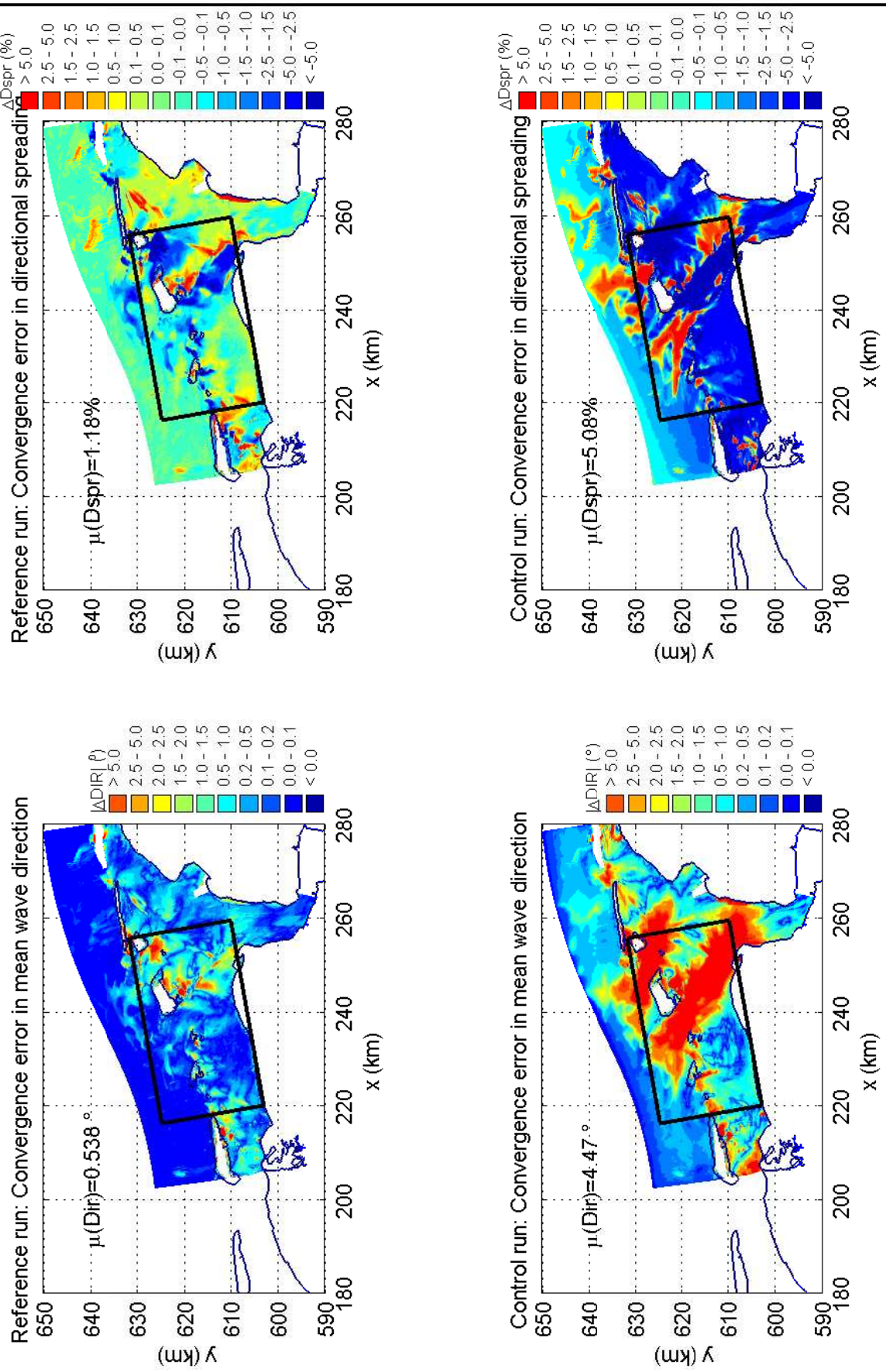

Convergence error in Dir and Dspr for DIA IQUAD=8 for Eems-Dollard, case EEMS3 20061101 0300 Reference run (R_iq2_std) and control run (C_iq8_std)	SWAN	4051A
	Numerical efficiency SWAN	
DELTARES & ALKYON	H5107.46/A2114	Fig. 8.25

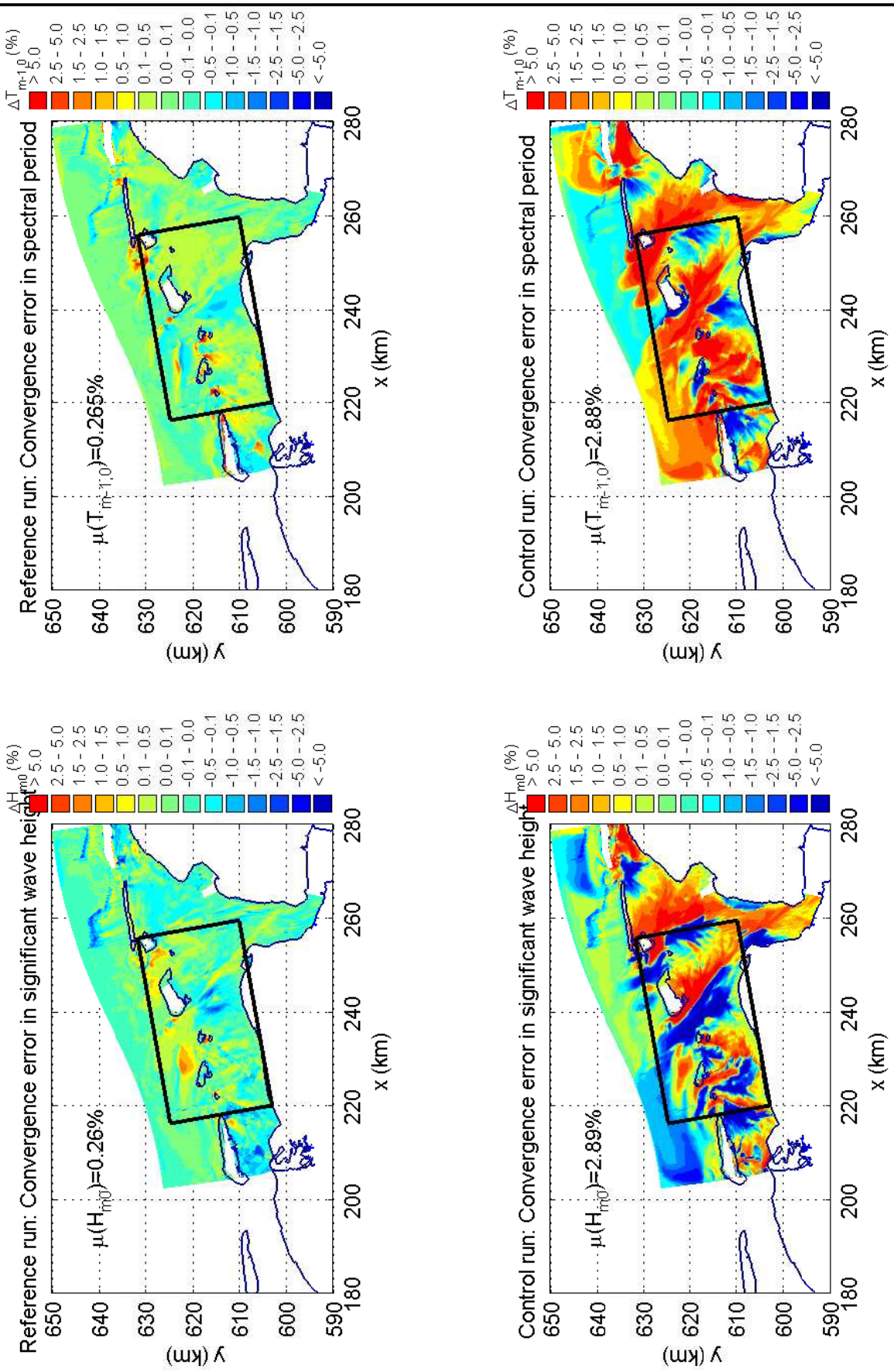

Convergence error in H_{m0} and $T_{m-1,0}$ for DIA IQUAD=8 for Eems-Dollard, case EEMS3 20061101 0630 Reference run (R_iq2_std) and control run (C_iq8_std)	SWAN	4051A
	Numerical efficiency SWAN	
DELTARES & ALKYON	H5107.46/A2114	Fig. 8.26

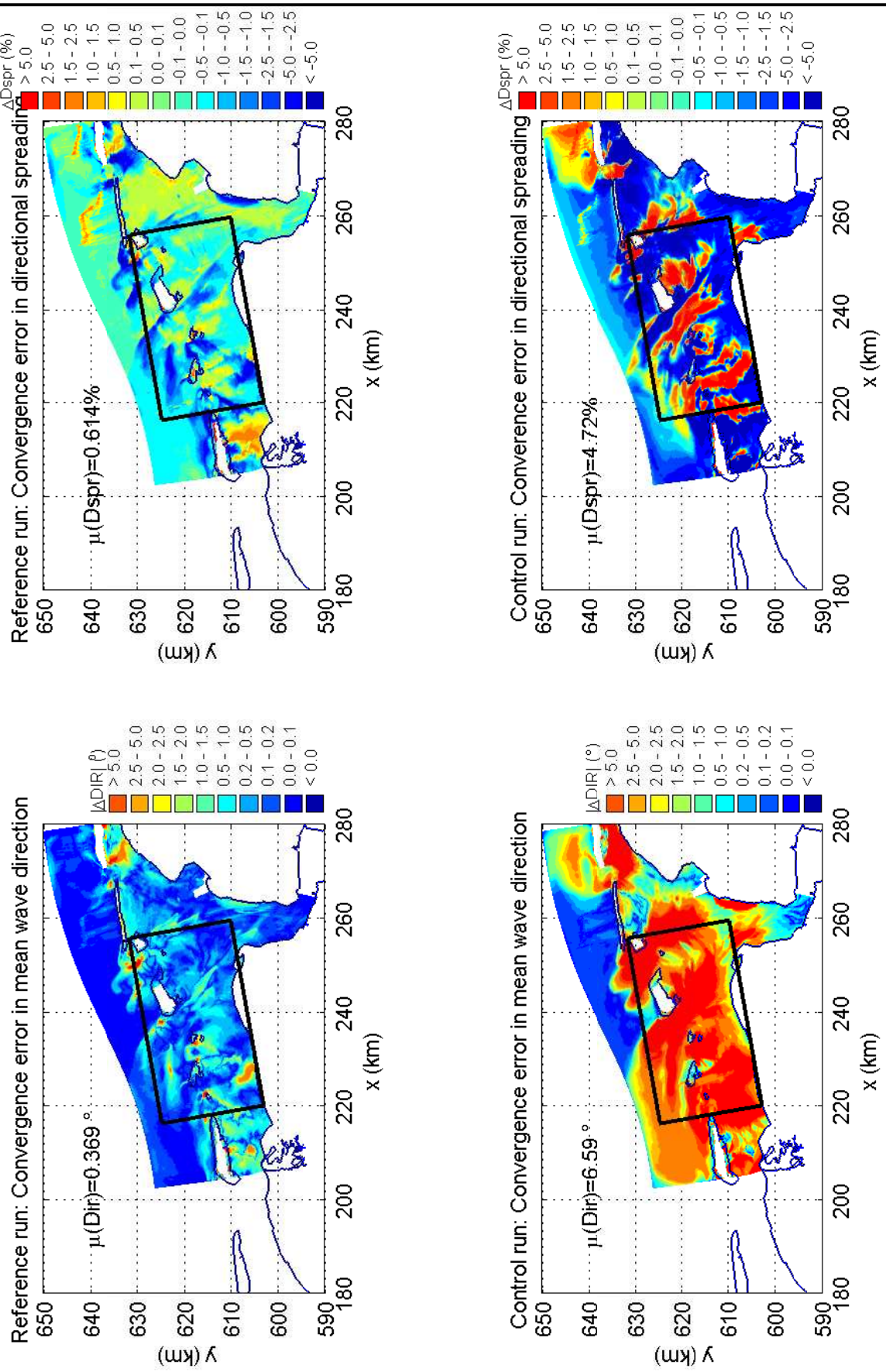

Convergence error in Dir and Dspr for DIA IQUAD=8 for Eems-Dollard, case EEMS3 20061101 0630 Reference run (R_iq2_std) and control run (C_iq8_std)	SWAN	4051A
	Numerical efficiency SWAN	
DELTARES & ALKYON	H5107.46/A2114	Fig. 8.27

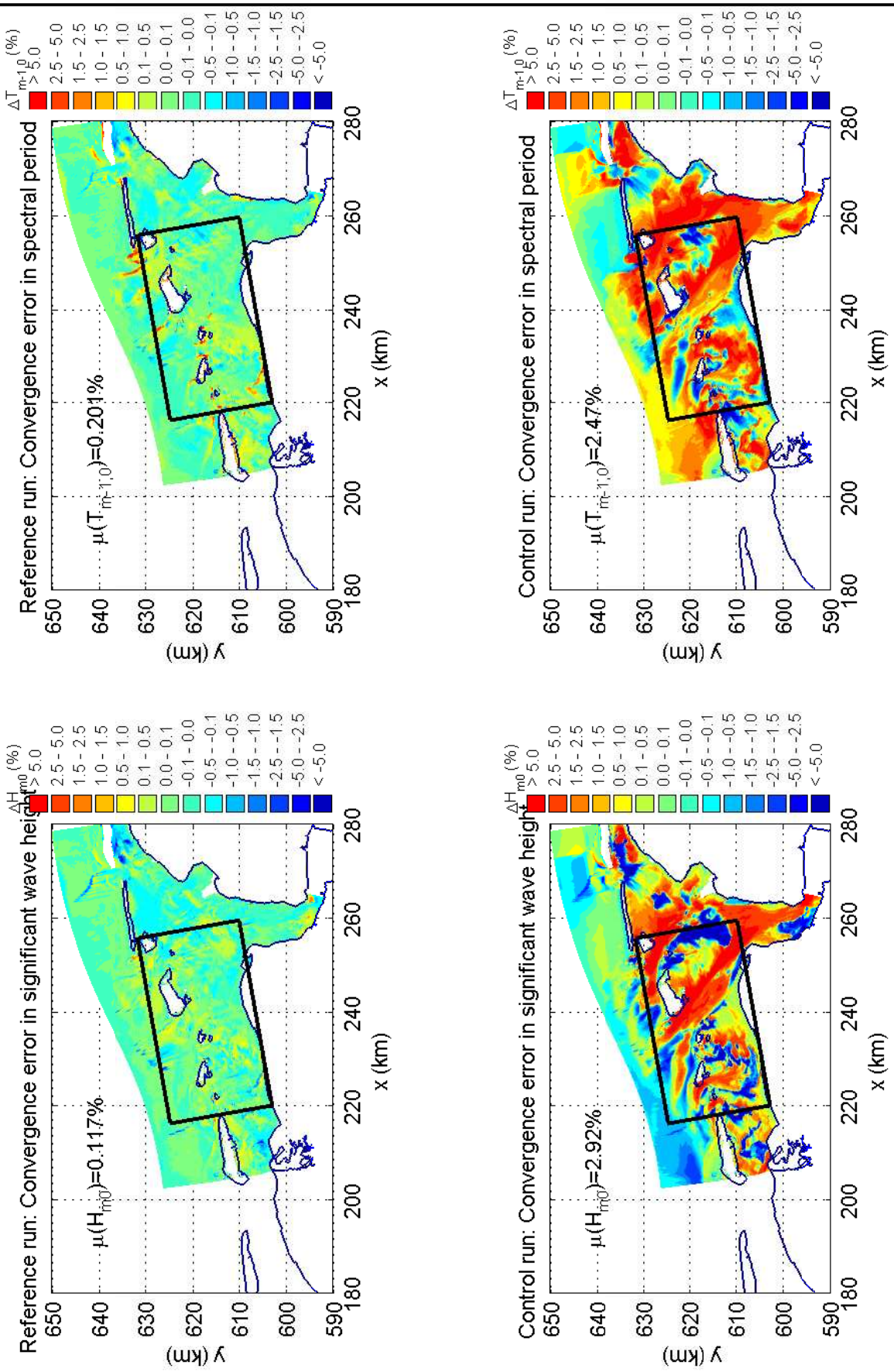

Convergence error in H_{m0} and $T_{m-1,0}$ for DIA IQUAD=8 for Eems-Dollard, case EEMS3 20061101 0930 Reference run (R_iq2_std) and control run (C_iq8_std)	SWAN	4051A
	Numerical efficiency SWAN	
DELTARES & ALKYON	H5107.46/A2114	Fig. 8.28

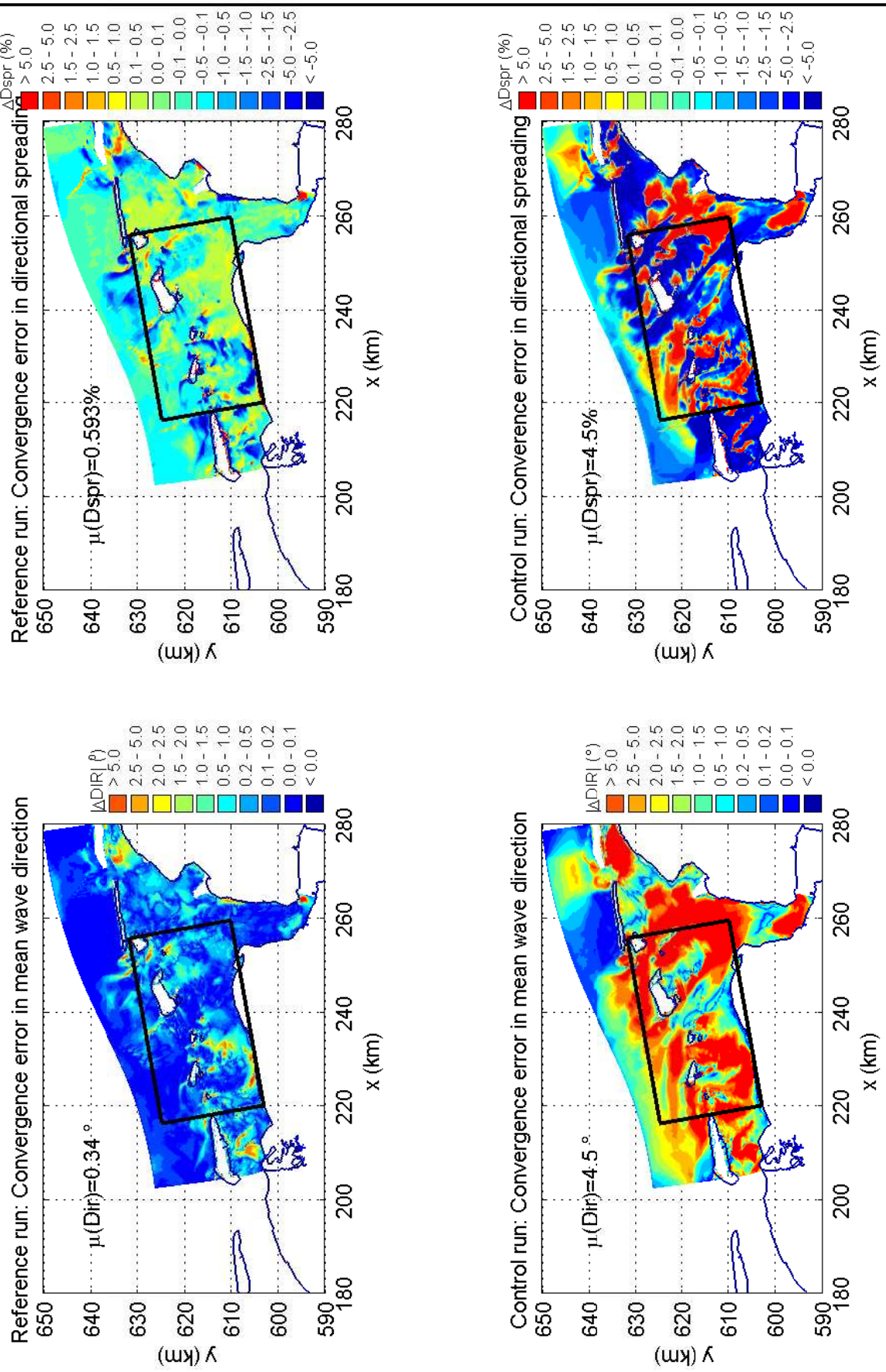

Convergence error in Dir and Dspr for DIA IQUAD=8 for Eems-Dollard, case EEMS3 20061101 0930 Reference run (R_iq2_std) and control run (C_iq8_std)	SWAN	4051A
	Numerical efficiency SWAN	
DELTARES & ALKYON	H5107.46/A2114	Fig. 8.29

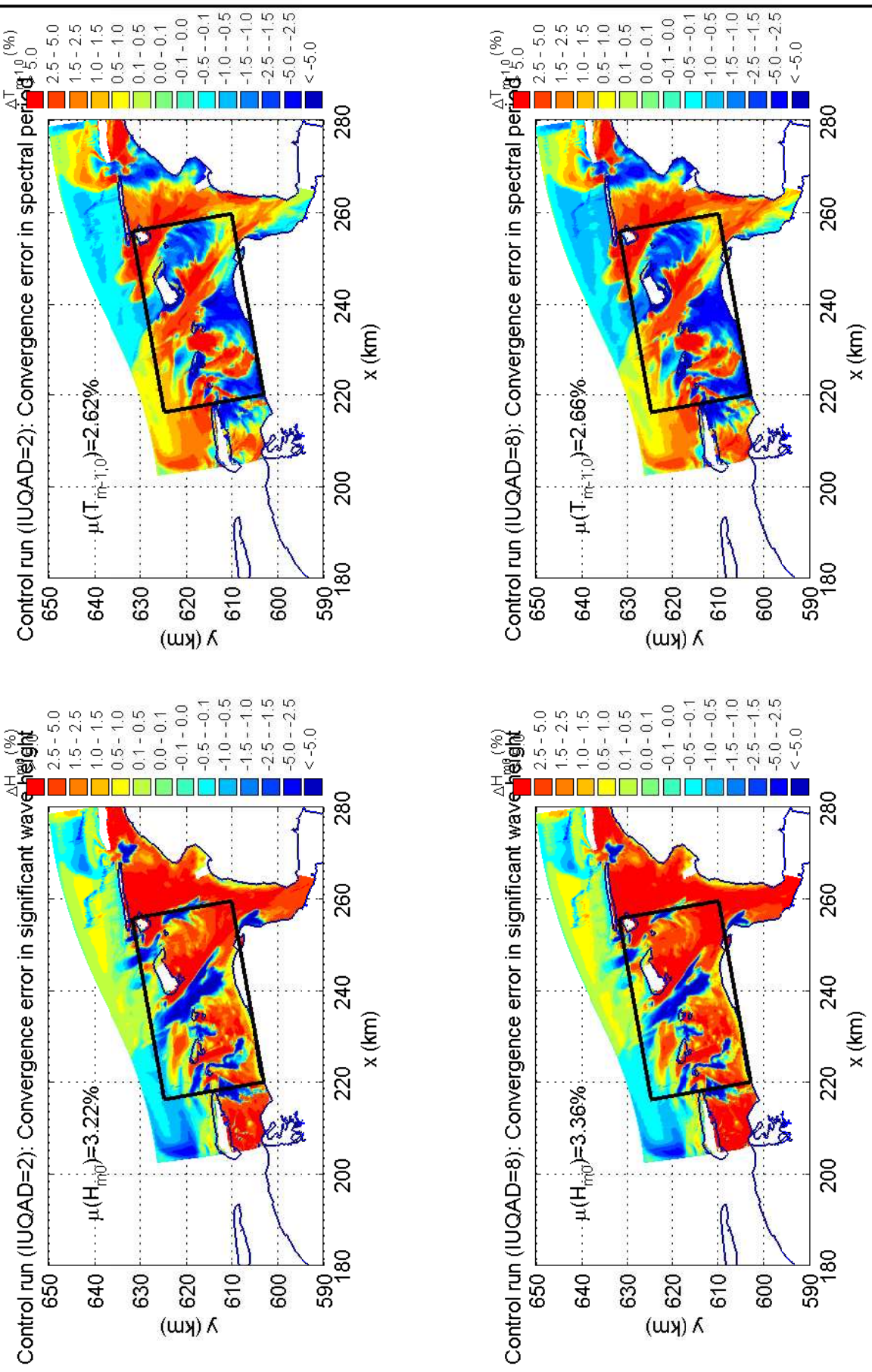

Convergence error in H_{m0} and $T_{m-1,0}$ for triplet method for Eems-Dollard,case EEMS3 20061101 0630 Control runs C_iq2_tri (IQUAD=2) and C_iq8_tri (IQUAD=8)	SWAN	4051A
	Numerical efficiency SWAN	
DELTARES & ALKYON	H5107.46/A2114	Fig. 8.30

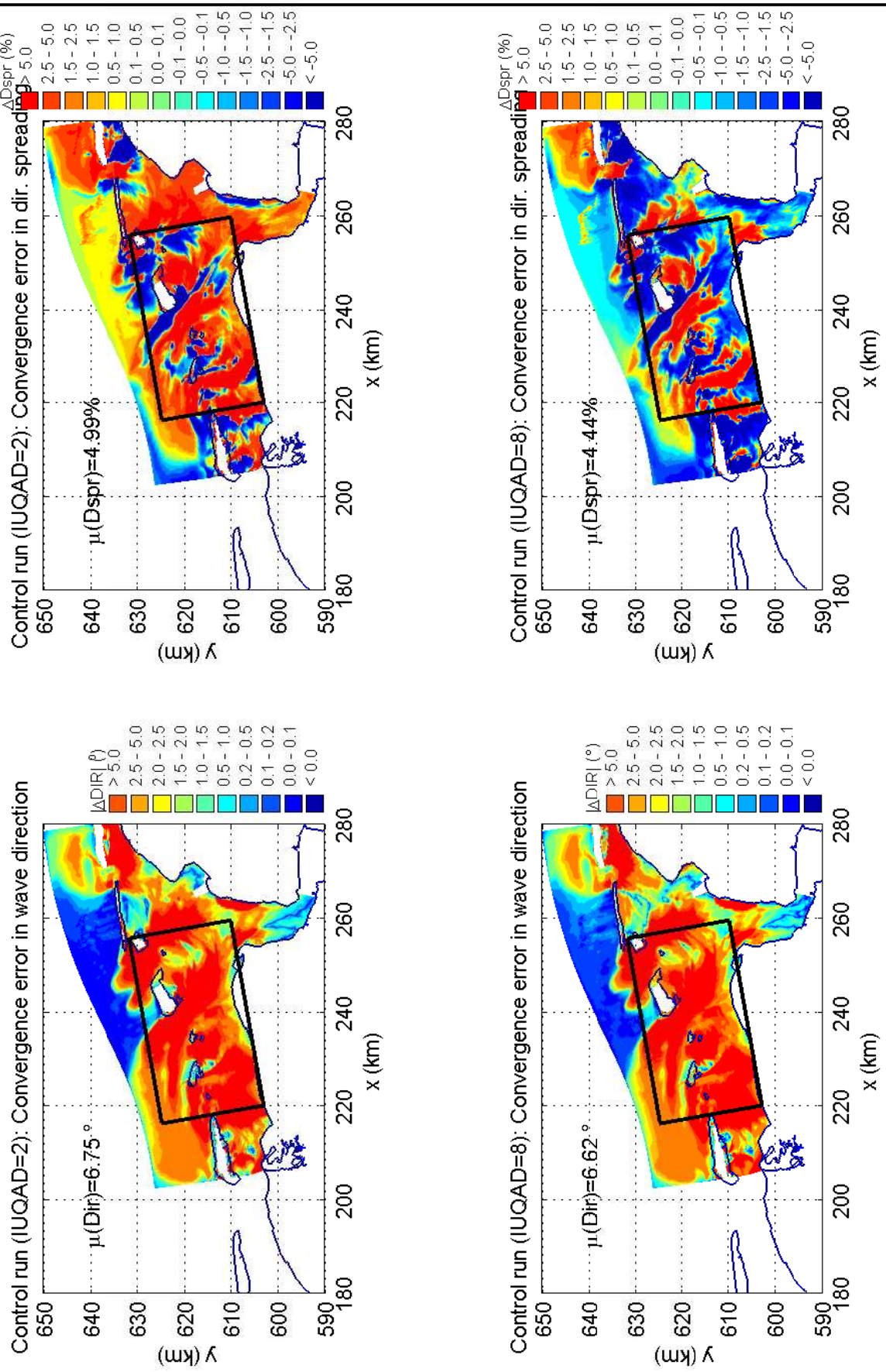

Convergence errors in Dir and Dspr for triplet method for Eems-Dollard, case EEMS3 20061101 0630 Control runs C_iq2_tri (IQUAD=2) and C_iq8_tri (IQUAD=8)	SWAN	4051A
	Numerical efficiency SWAN	
DELTARES & ALKYON	H5107.46/A2114	Fig. 8.31

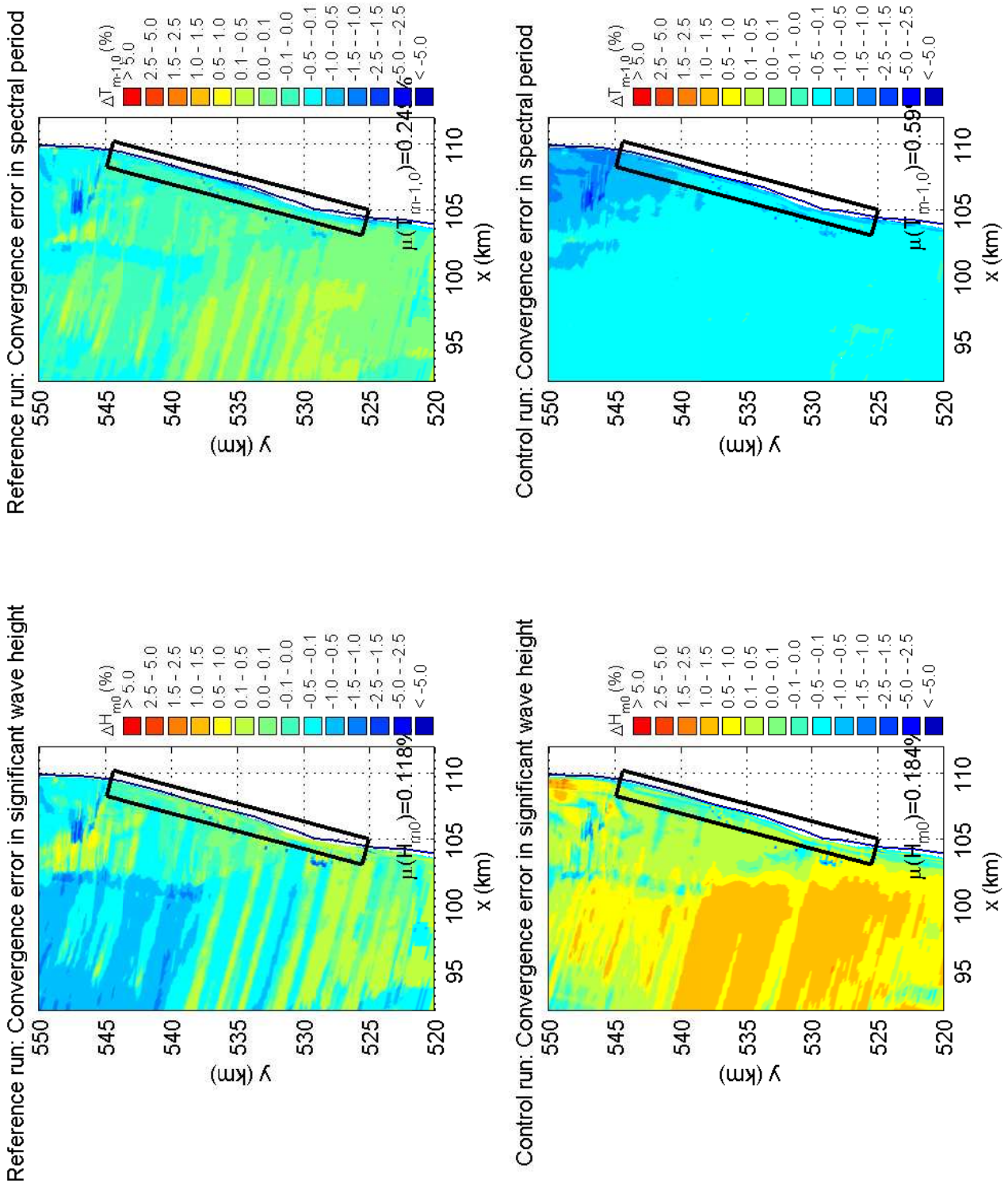

Convergence error in H_{m0} and $T_{m-1,0}$ for DIA IQUAD=8 along Dutch coast near Petten, case PETTEN 19950101 1000 Reference run (R_iq2_std) and control run (C_iq8_std)	SWAN	4051A
	Numerical efficiency SWAN	
DELTARES & ALKYON	H5107.46/A2114	Fig. 8.32

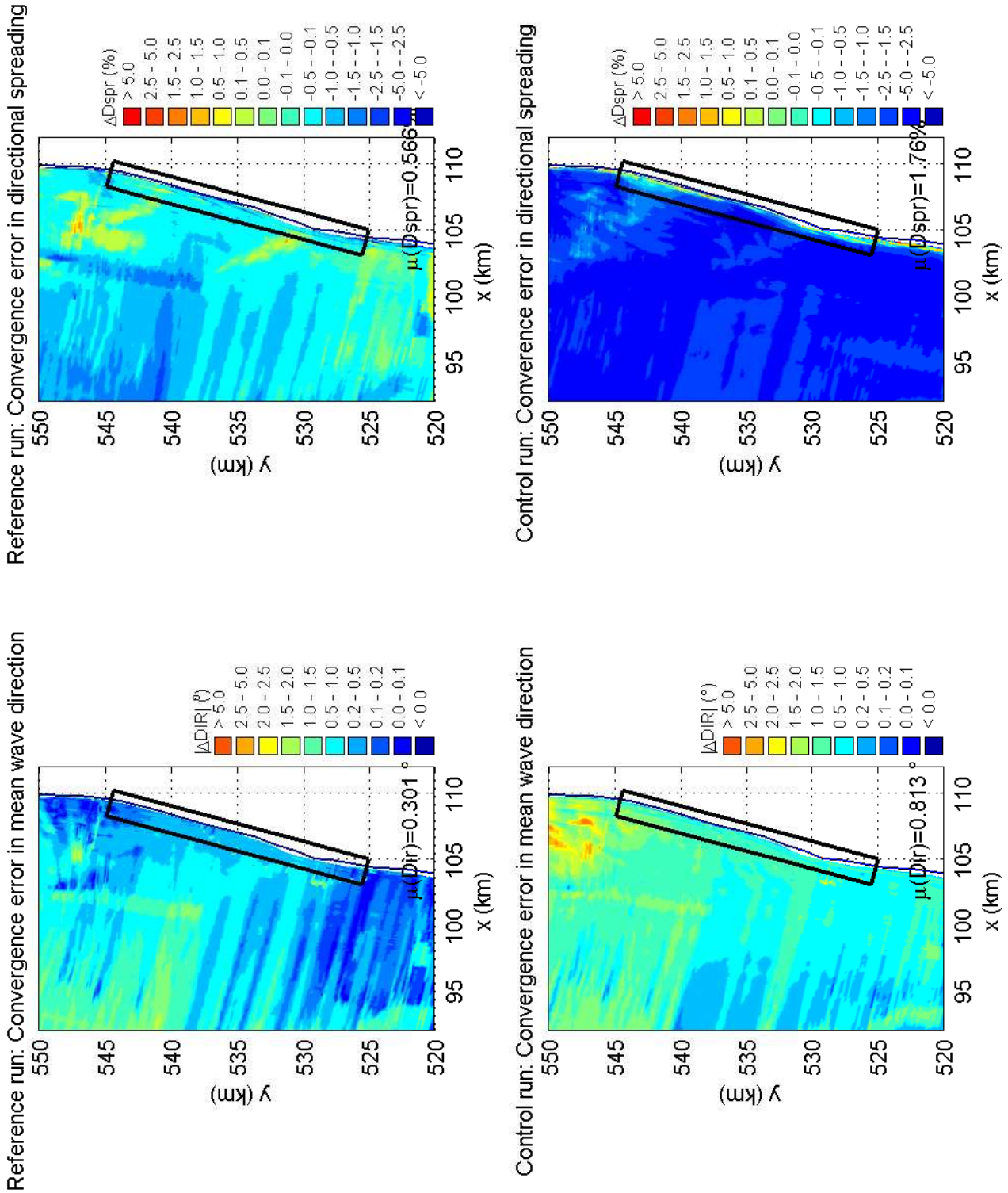

Convergence error in Dir and Dspr for DIA IQUAD=8 along Dutch coast near Petten, case PETTEN 19950101 1000 Reference run (R_iq2_std) and control run (C_iq8_std)	SWAN	4051A
	Numerical efficiency SWAN	
DELTARES & ALKYON	H5107.46/A2114	Fig. 8.33

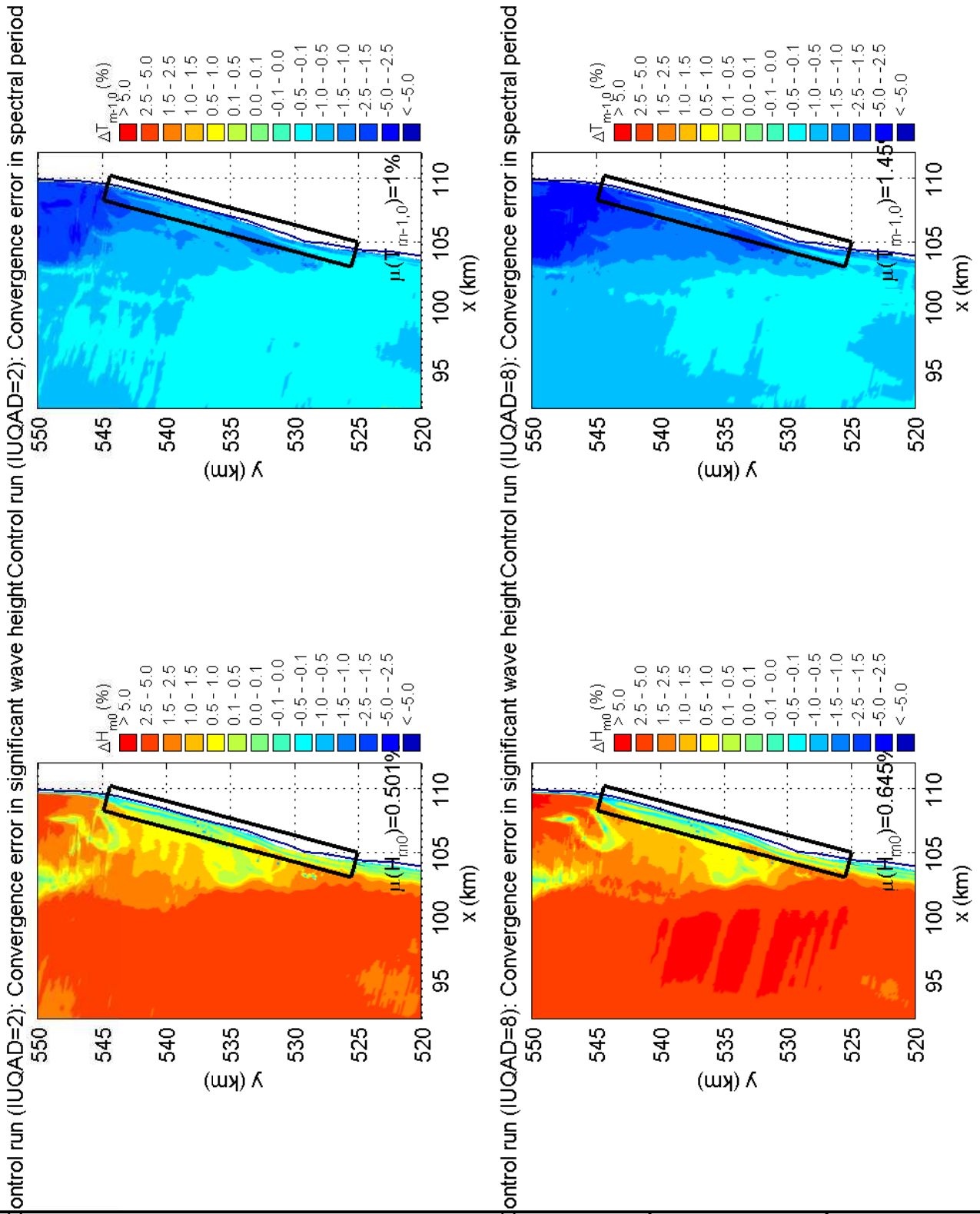

Convergence error in H_{m0} and $T_{m-1,0}$ for triplet method along Dutch coast near Petten,case PETTEN 19950101 1000 Control runs C_iq2_tri (IQUAD=2) and C_iq8_tri (IQUAD=8)	SWAN	4051A
	Numerical efficiency SWAN	
DELTARES & ALKYON	H5107.46/A2114	Fig. 8.34

Convergence errors in Dir and Dspr for triplet method along Dutch coast near Petten, case PETTEN 19950101 1000 Control runs C_iq2_tri (IQUAD=2) and C_iq8_tri (IQUAD=8)	SWAN	4051A
	Numerical efficiency SWAN	
DELTARES & ALKYON	H5107.46/A2114	Fig. 8.35

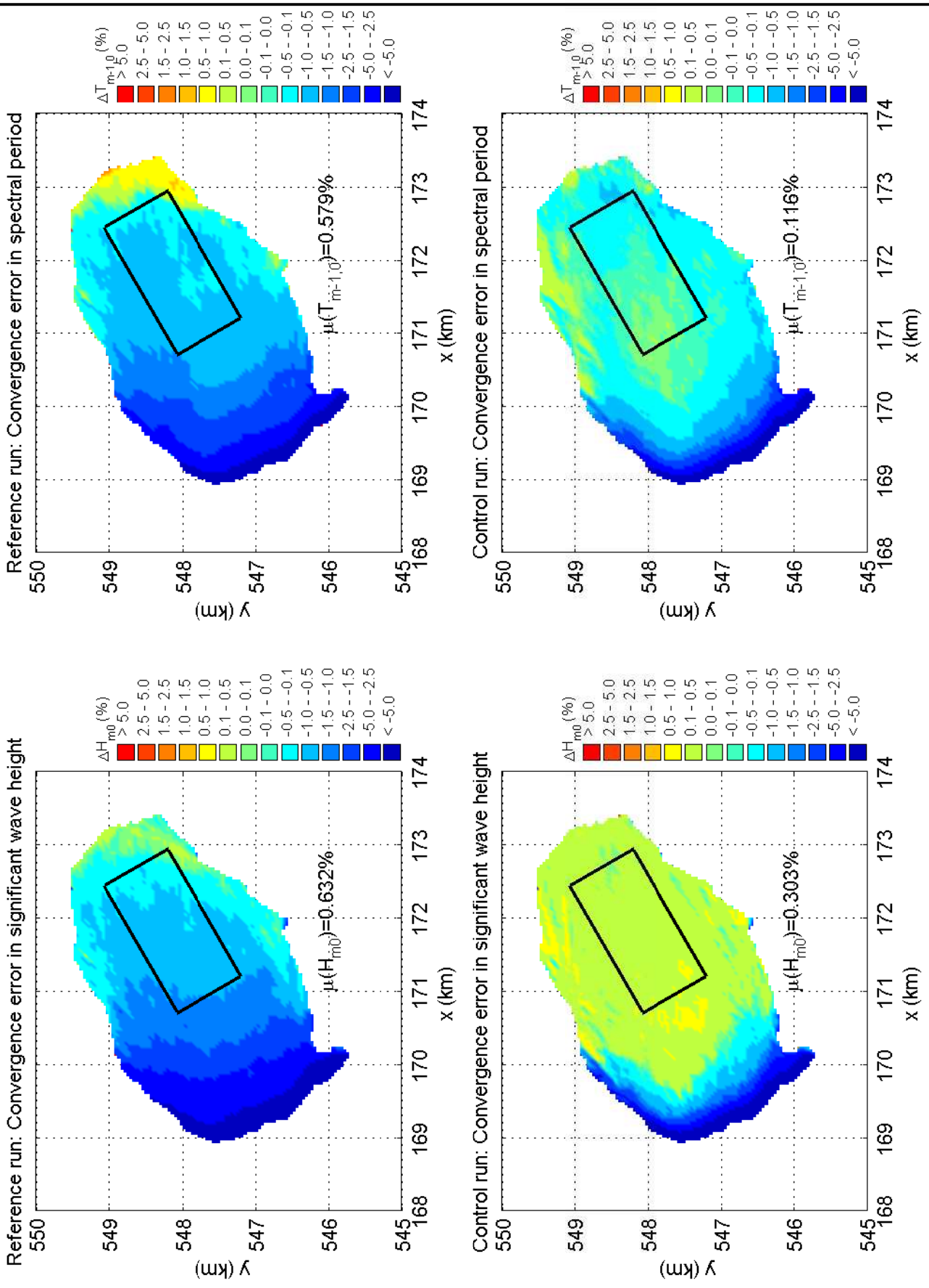

Convergence error in H_{m0} and $T_{m-1,0}$ for DIA IQUAD=8 for Lake Sloten, case SLE 20021027 1500 Reference run (R_iq2_std) and control run (C_iq8_std)	SWAN	4051A
	Numerical efficiency SWAN	
DELTARES & ALKYON	H5107.46/A2114	Fig. 8.36

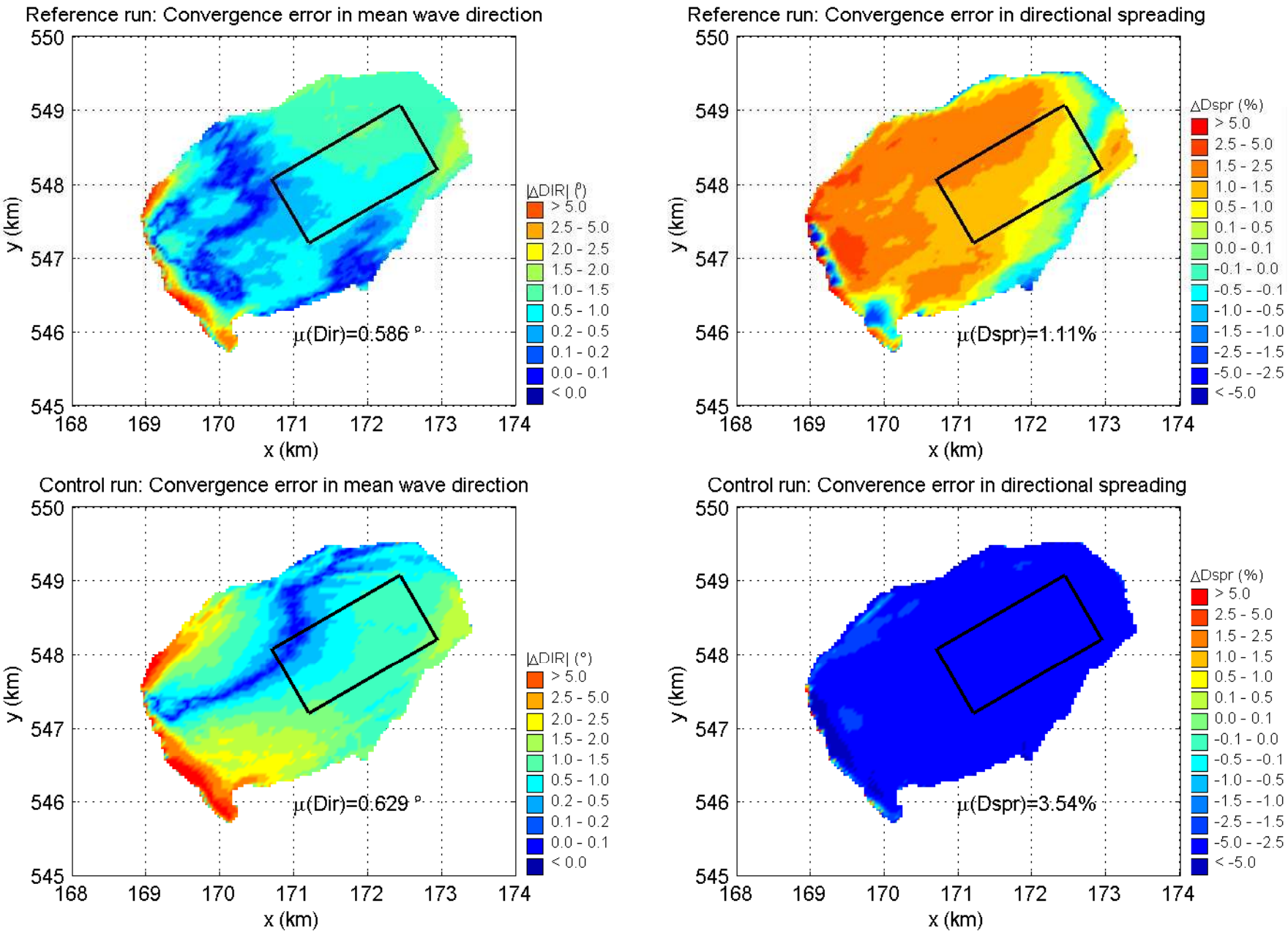

Convergence error in Dir and Dspr for DIA IQUAD=8
for Lake Sloten, case SLE 20021027 1500
Reference run (R_iq2_std) and control run (C_iq8_std)

DELTARES & ALKYON

SWAN	4051A
Numerical efficiency SWAN	Fig. 8.37
H5107.46/A2114	

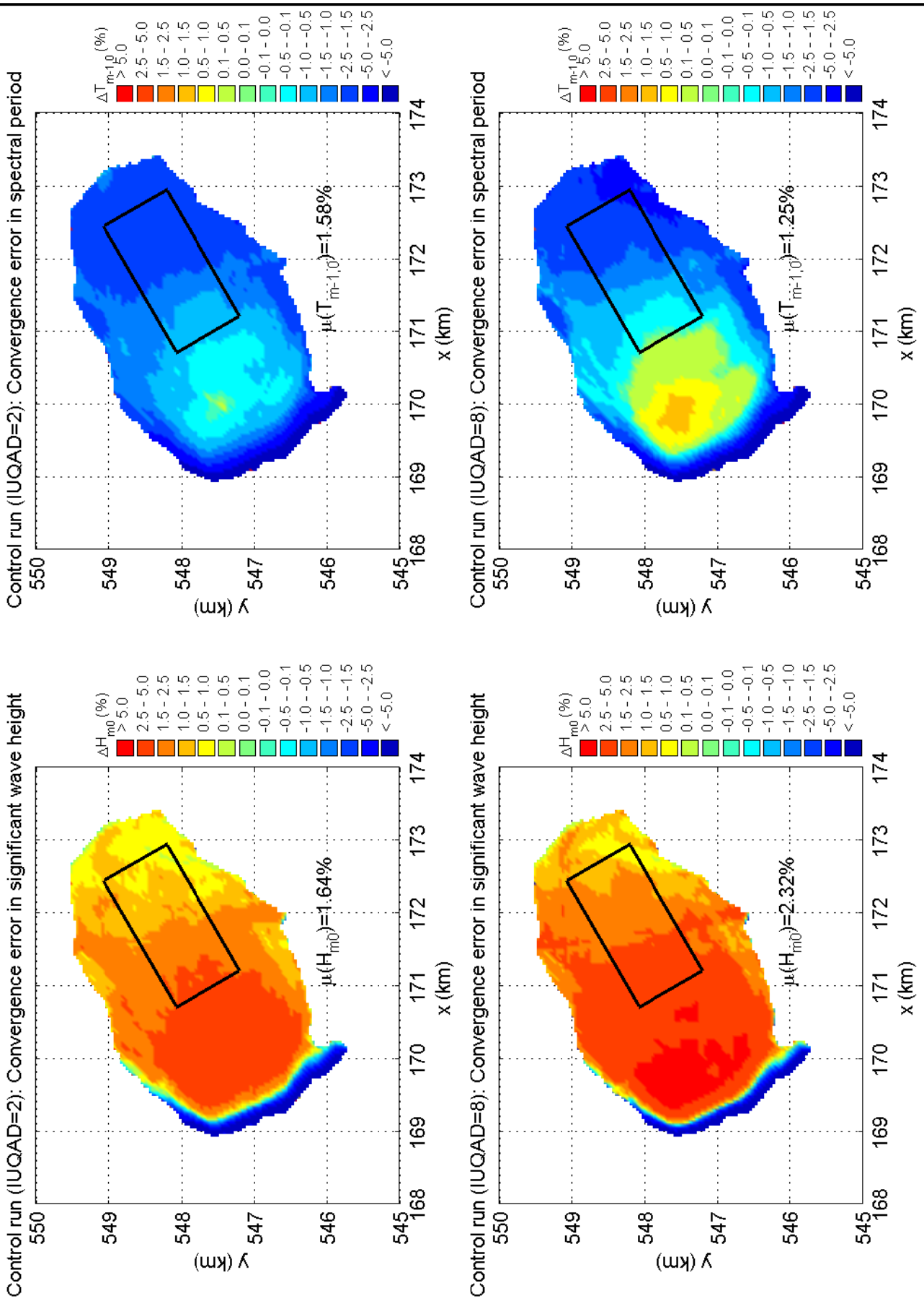

Convergence error in H_{m0} and $T_{m-1,0}$ for triplet method for Lake Sloten,case SLE 20021027 1500 Control runs C_iq2_tri (IQUAD=2) and C_iq8_tri (IQUAD=8)	SWAN	4051A
	Numerical efficiency SWAN	
DELTARES & ALKYON	H5107.46/A2114	Fig. 8.38

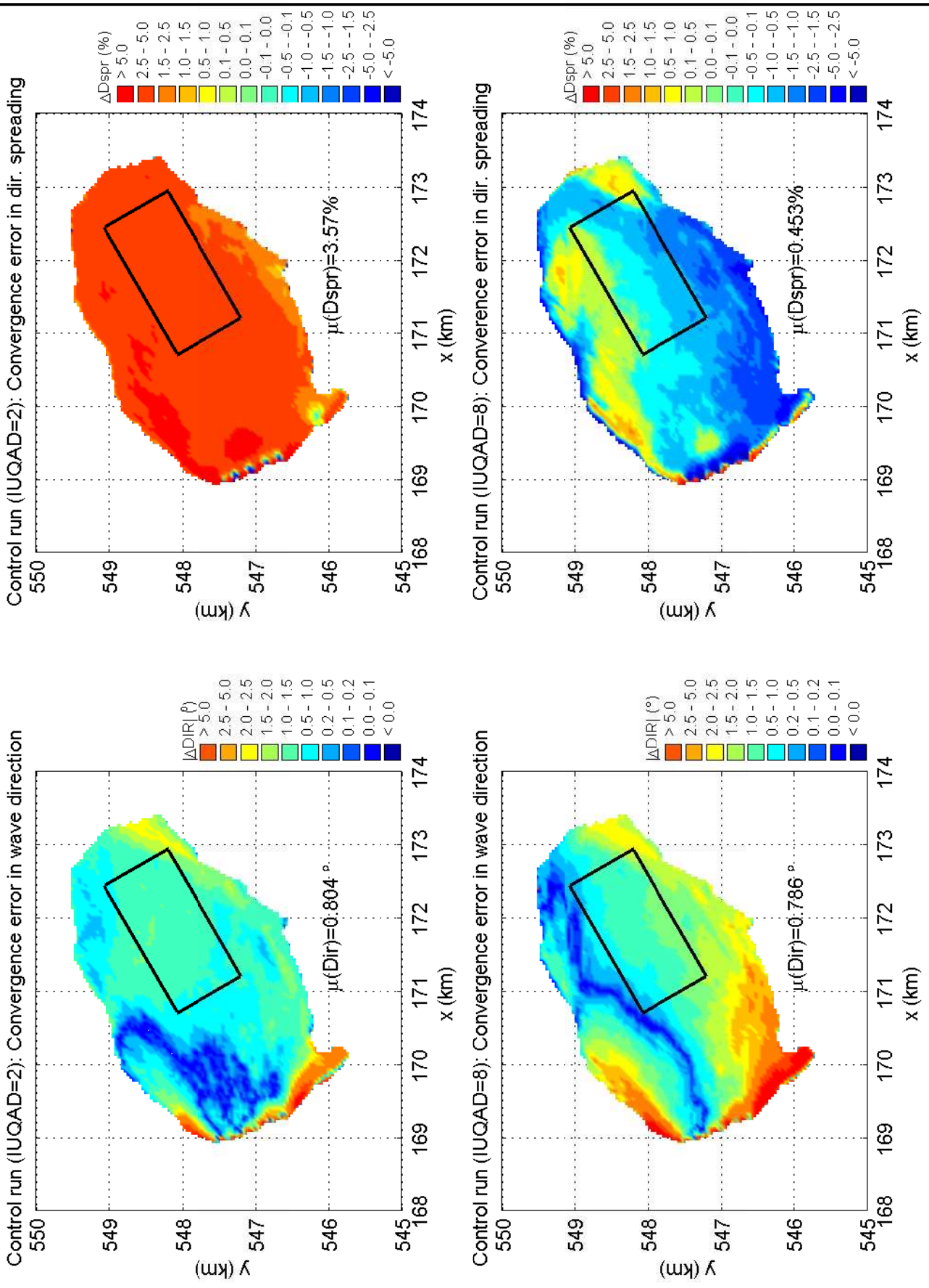

Convergence errors in Dir and Dspr for triplet method for Lake Sloten, case SLE 20021027 1500 Control runs C_iq2_tri (IQUAD=2) and C_iq8_tri (IQUAD=8)	SWAN	4051A
	Numerical efficiency SWAN	
DELTARES & ALKYON	H5107.46/A2114	Fig. 8.39

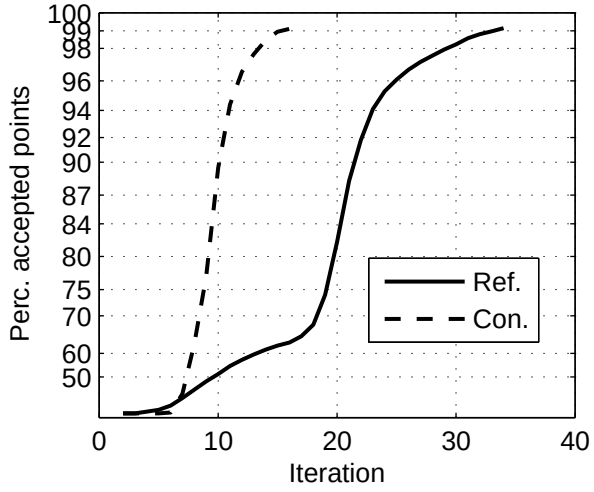

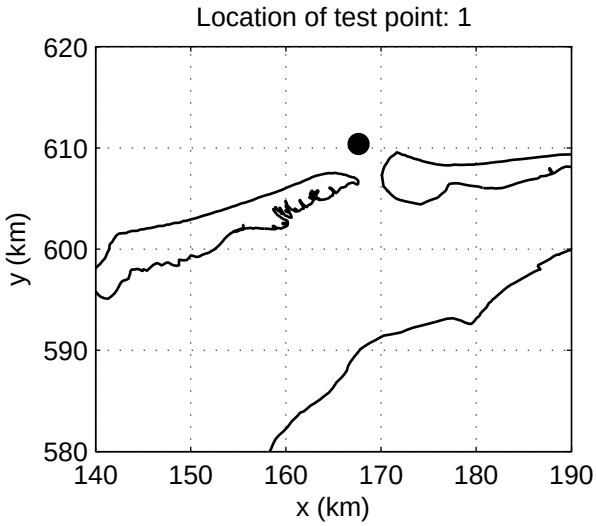

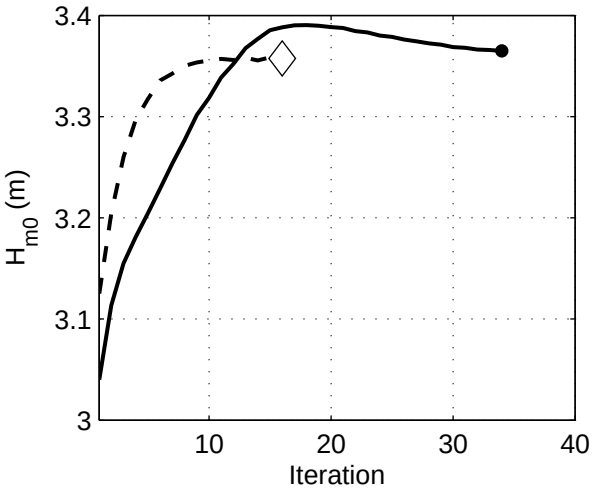

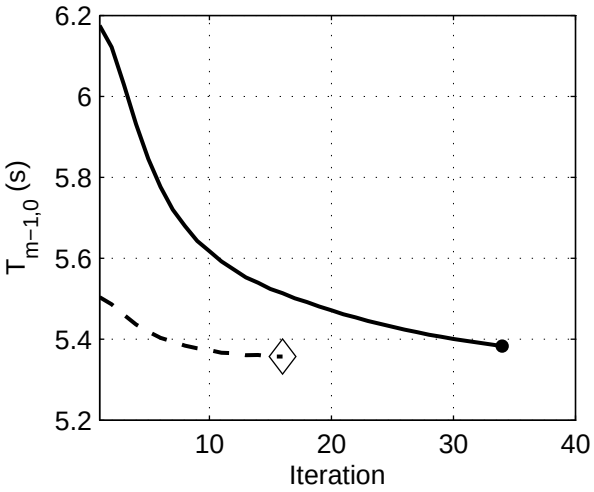

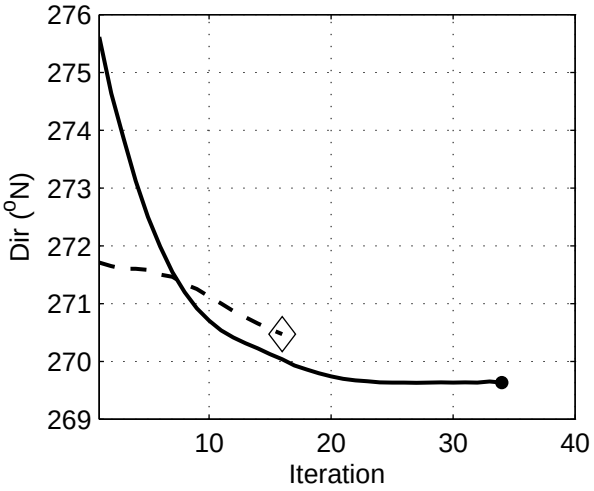

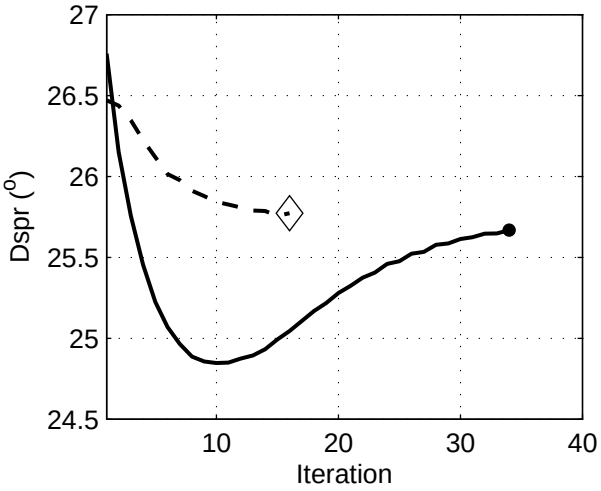

Convergence behaviour of batch file simulation with hotfile for the Amelander Zeegat, case AZG3A 20050102 1200 Wind speed increment runs R_k40_270 and C_k40_270	SWAN	4051A
	Numerical efficiency SWAN	
DELTARES & ALKYON	H5107.46/A2114	Fig. 9.1

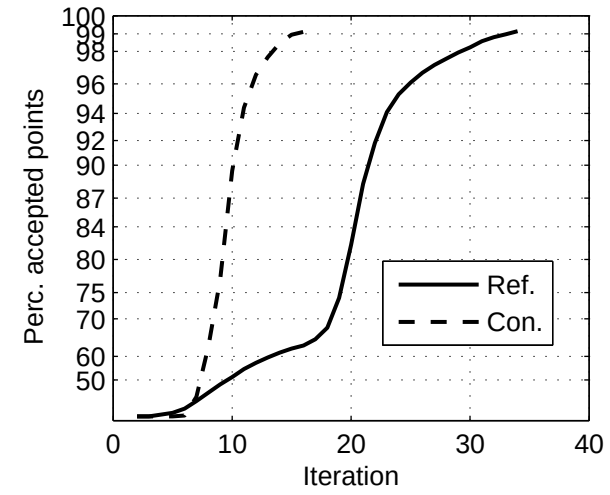

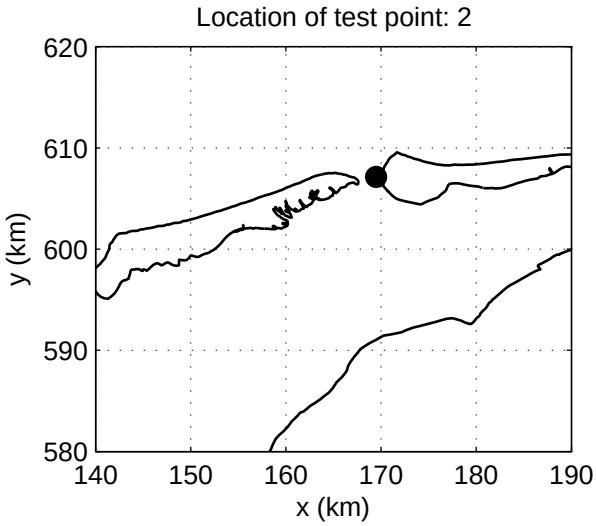

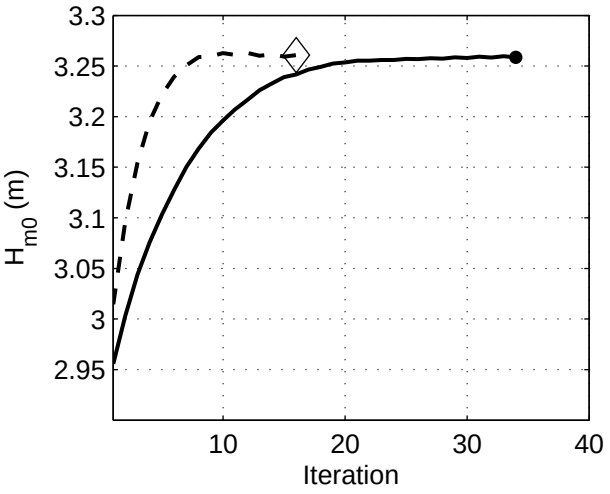

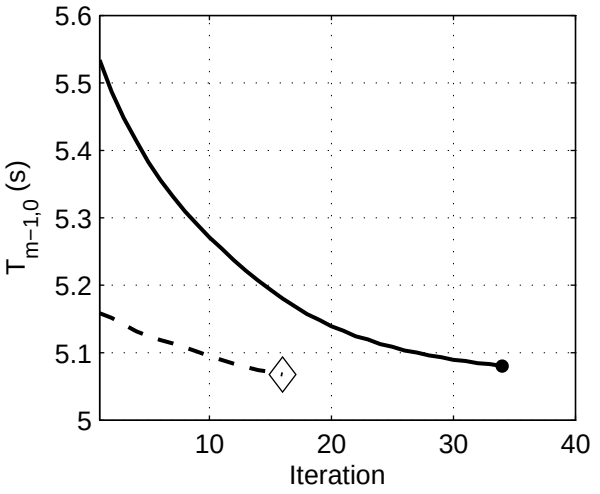

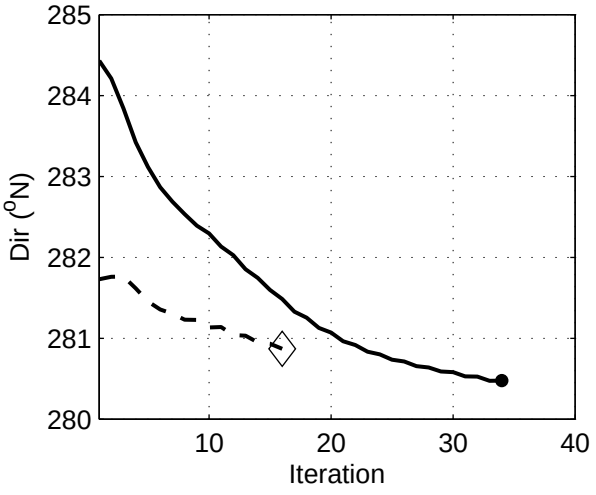

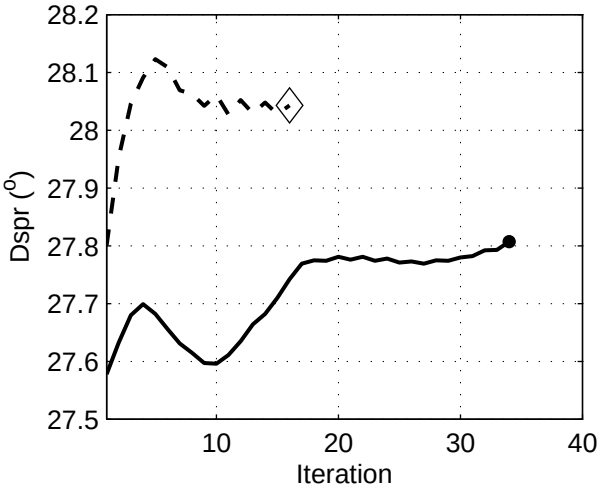

Convergence behaviour of batch file simulation with hotfile for the Amelander Zeegat, case AZG3A 20050102 1200 Wind speed increment runs R_k40_270 and C_k40_270	SWAN	4051A
	Numerical efficiency SWAN	
DELTARES & ALKYON	H5107.46/A2114	Fig. 9.2

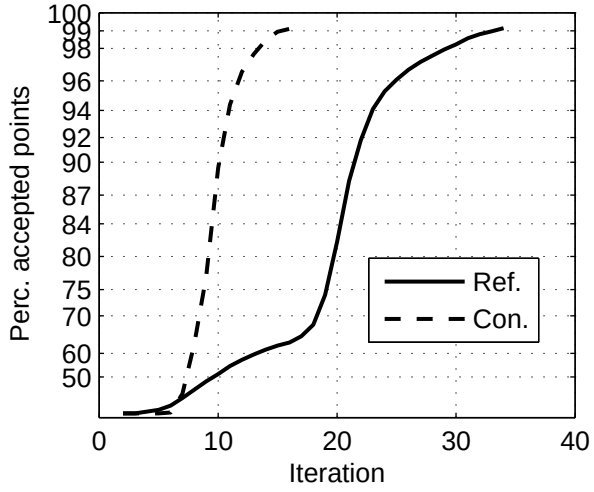

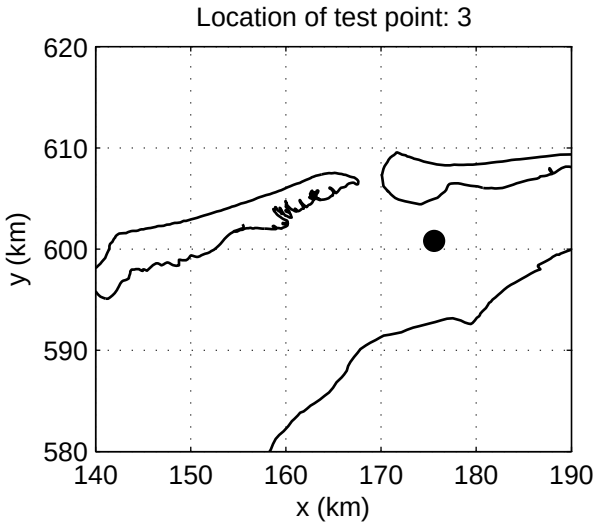

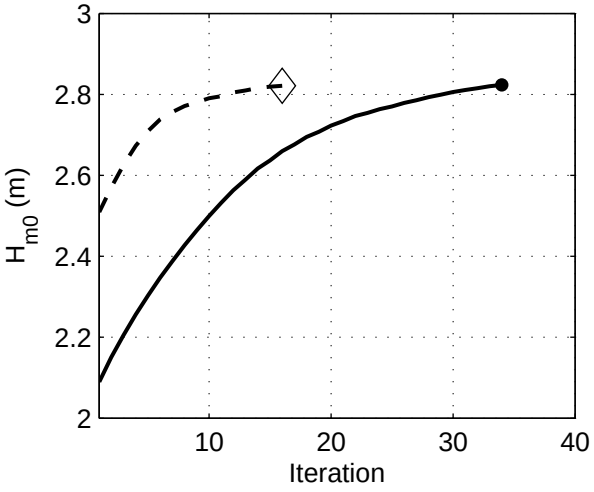

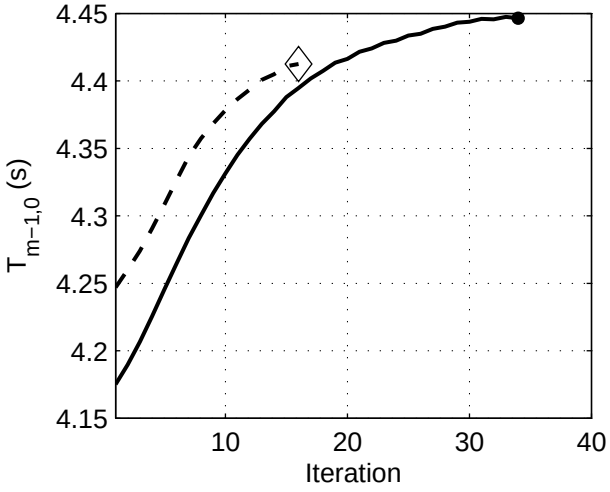

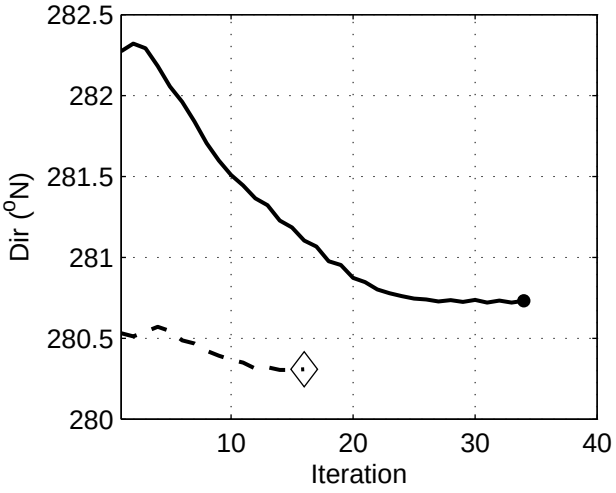

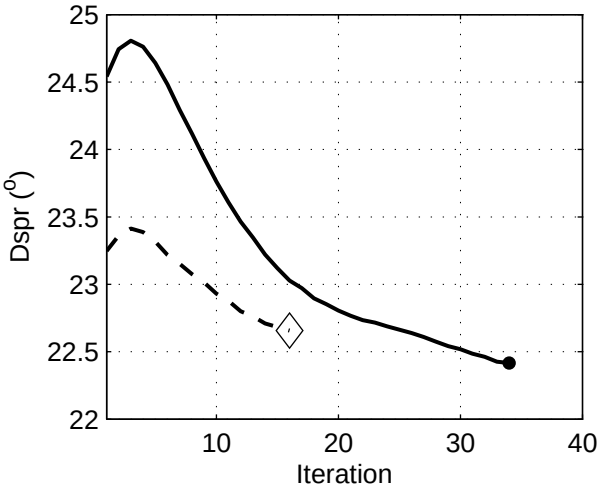

Convergence behaviour of batch file simulation with hotfile for the Amelander Zeegat, case AZG3A 20050102 1200 Wind speed increment runs R_k40_270 and C_k40_270	SWAN	4051A
	Numerical efficiency SWAN	
DELTARES & ALKYON	H5107.46/A2114	Fig. 9.3

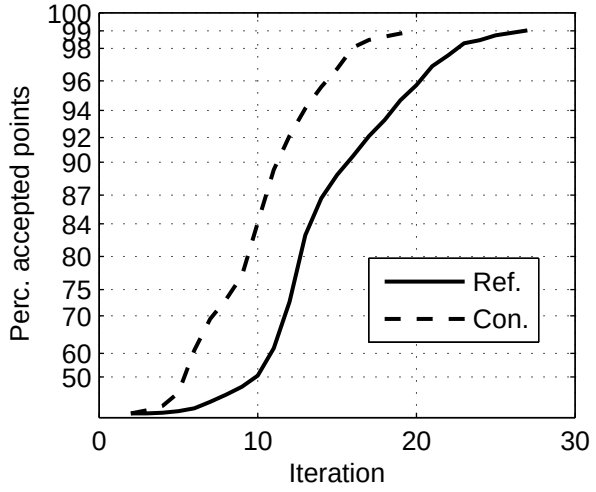

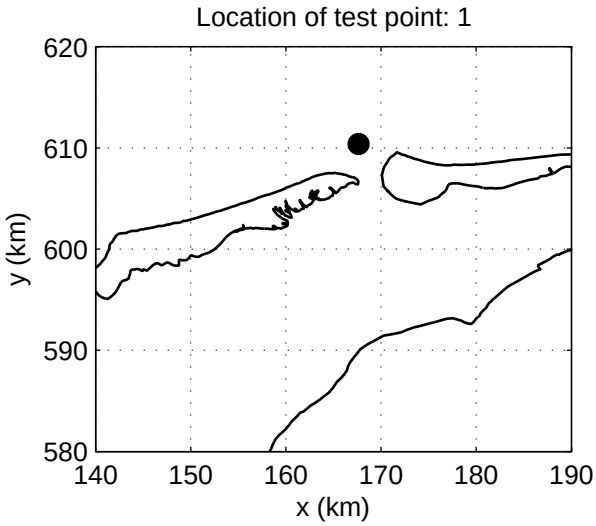

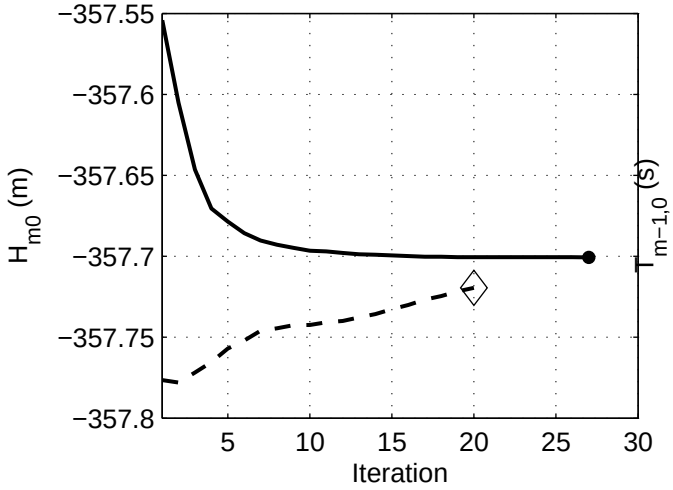

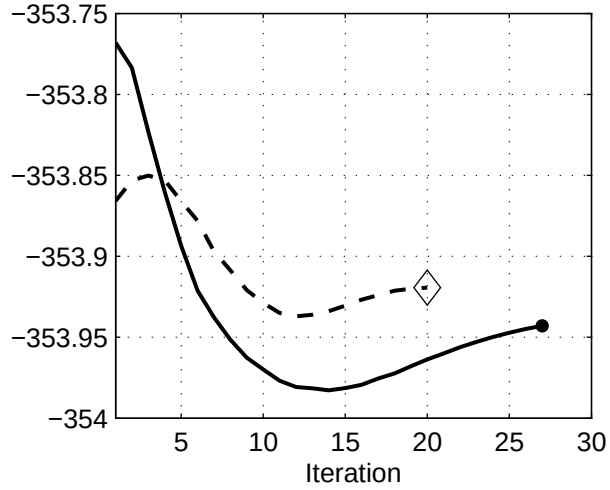

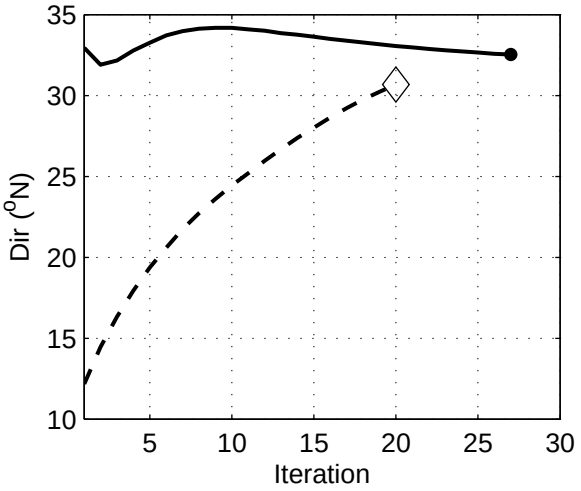

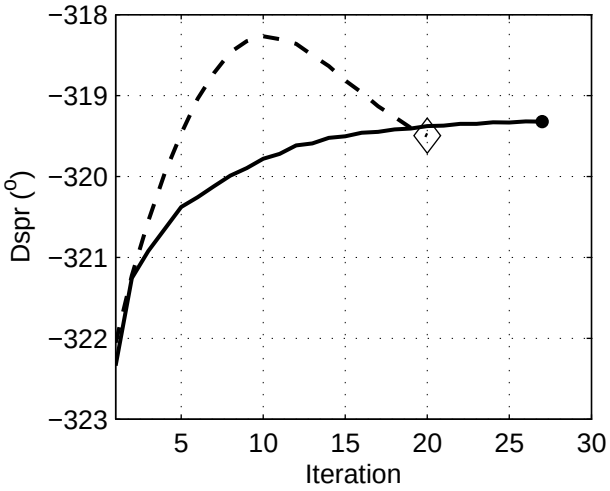

Convergence behaviour of batch file simulation with hotfile for the Amelander Zeegat, case AZG3A 20050102 1200 Wind direction increment runs R_25_d045 and C_25_d045	SWAN	4051A
	Numerical efficiency SWAN	
DELTARES & ALKYON	H5107.46/A2114	Fig. 9.4

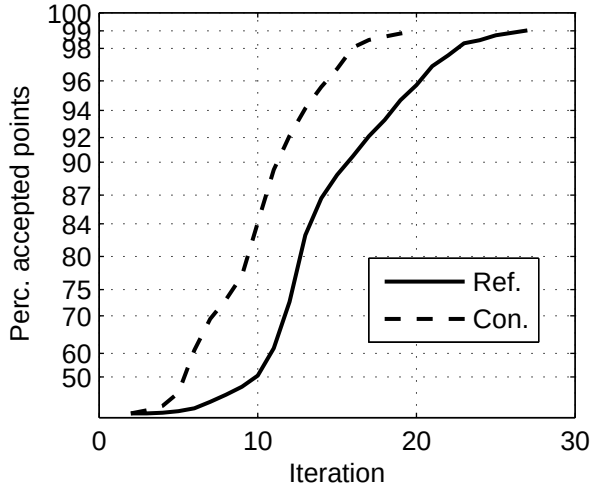

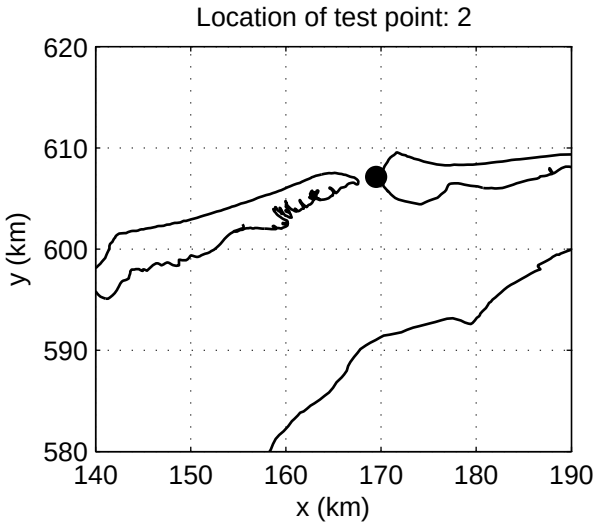

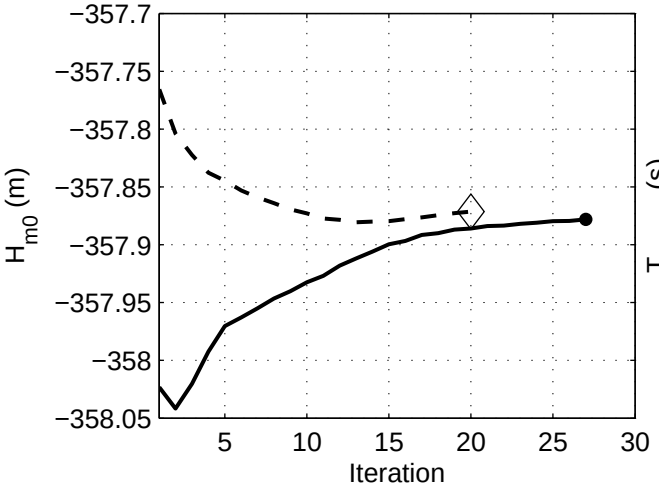

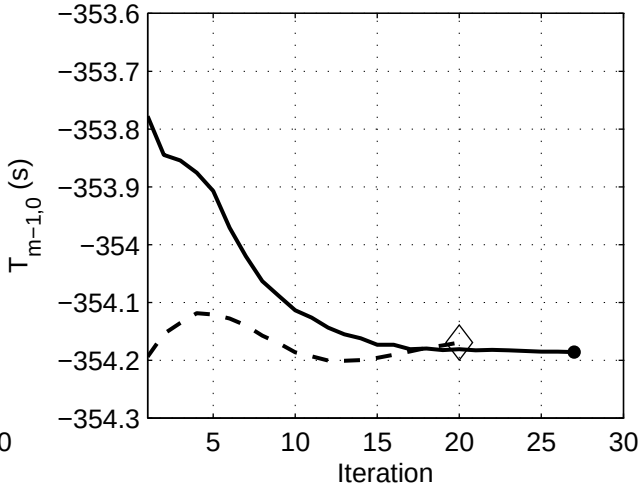

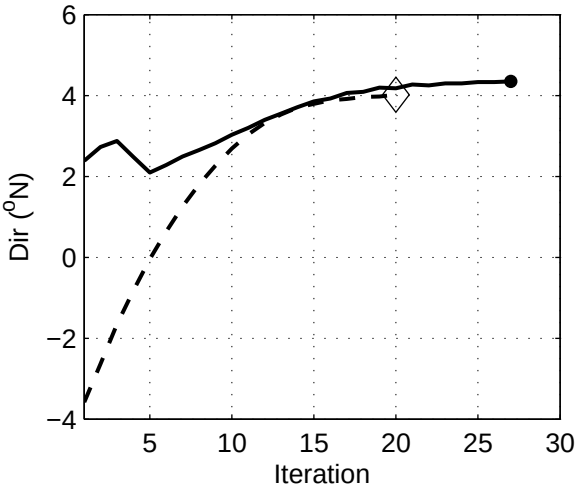

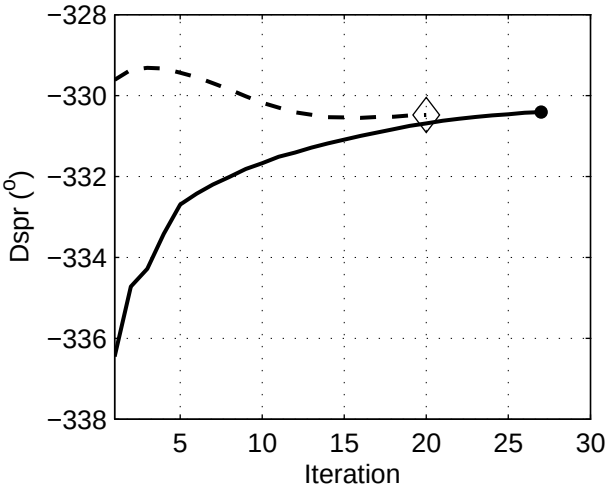

Convergence behaviour of batch file simulation with hotfile for the Amelander Zeegat, case AZG3A 20050102 1200 Wind direction increment runs R_25_d045 and C_25_d045	SWAN	4051A
	Numerical efficiency SWAN	
DELTARES & ALKYON	H5107.46/A2114	Fig. 9.5

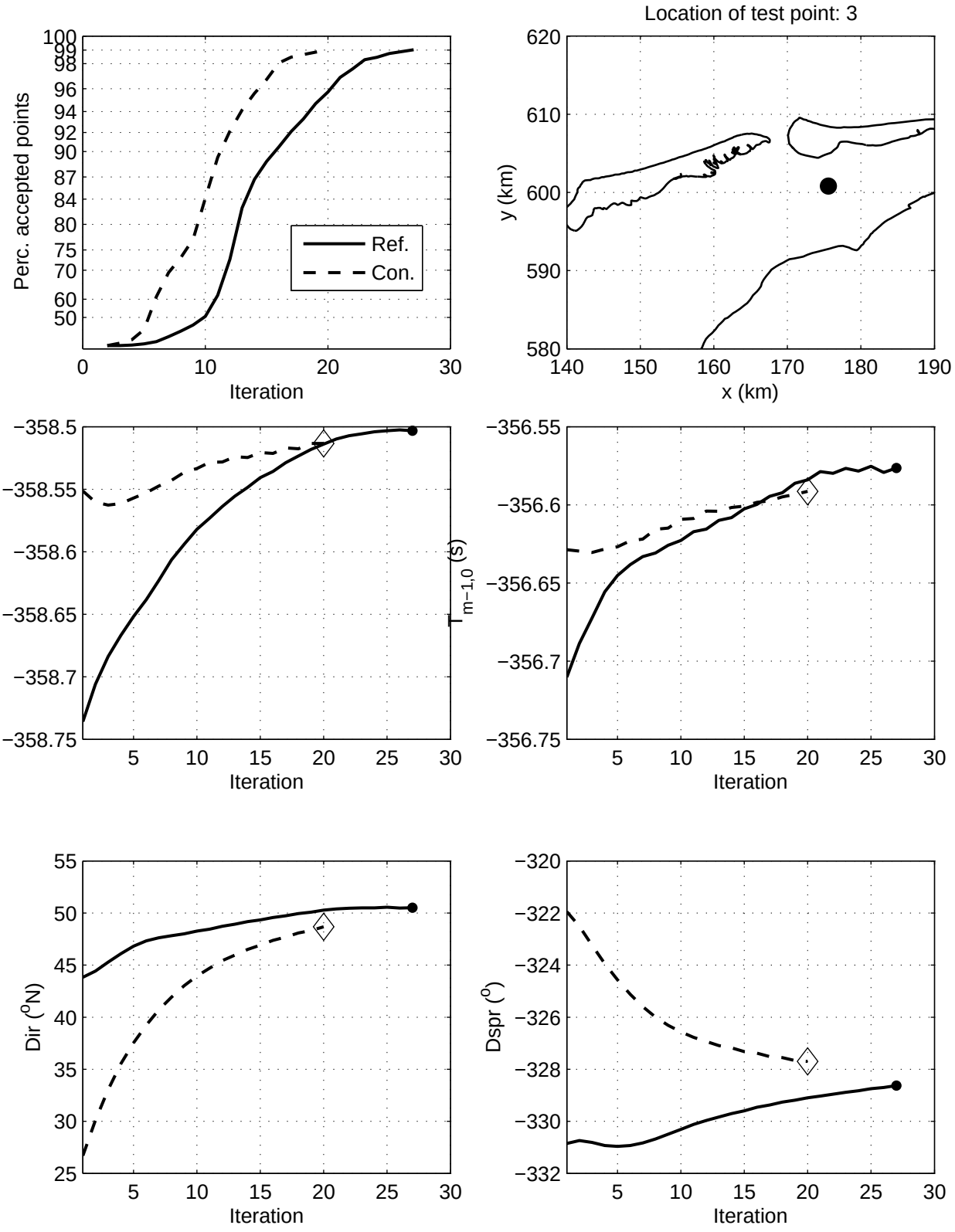

Convergence behaviour of batch file simulation with hotfile for the Amelander Zeegat, case AZG3A 20050102 1200 Wind direction increment runs R_25_d045 and C_25_d045	SWAN	4051A
	Numerical efficiency SWAN	
DELTARES & ALKYON	H5107.46/A2114	Fig. 9.6

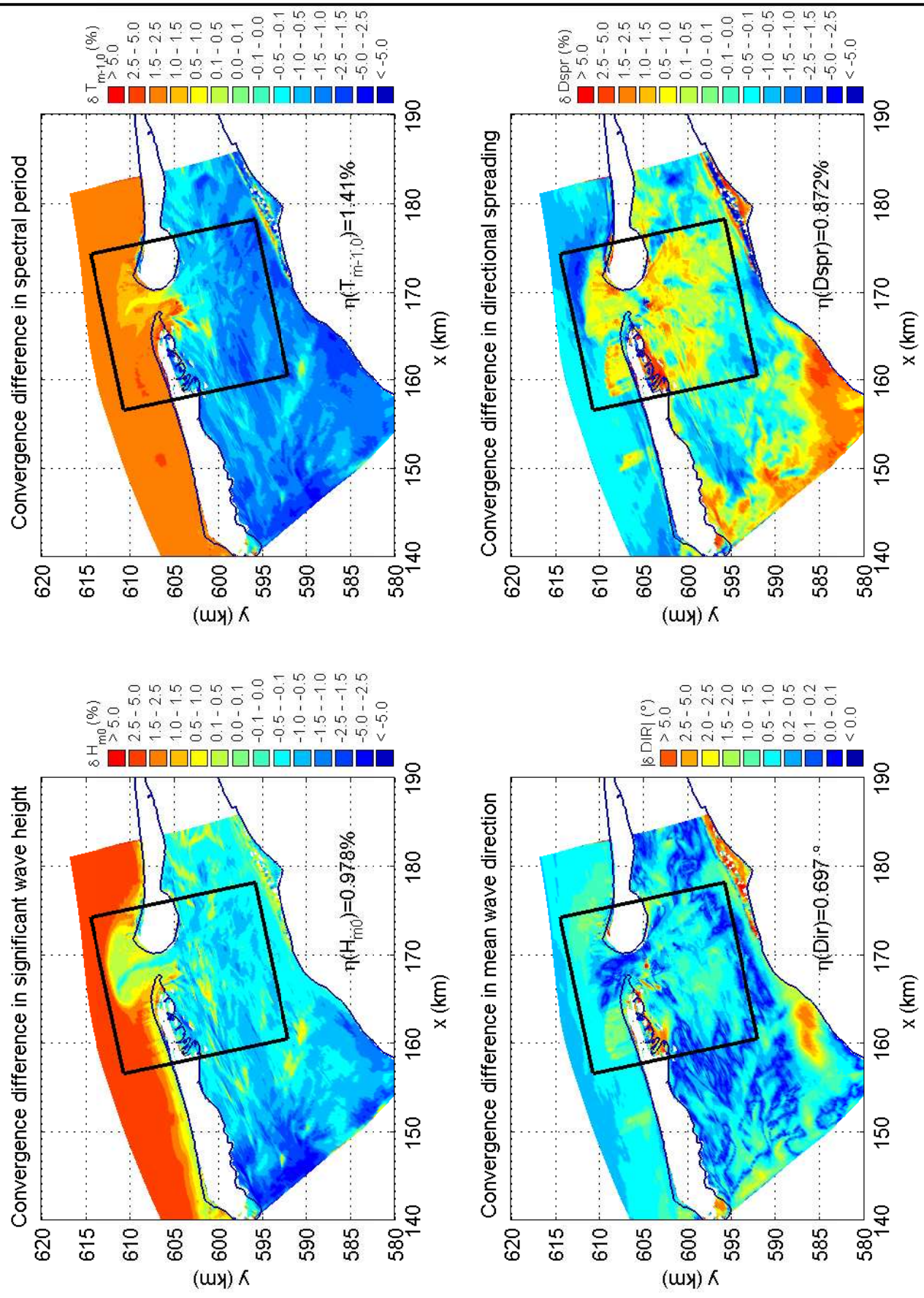

Convergence difference of batch file simulation with hotfile for the Amelander Zeegat, case AZG3A 20050102 1200 Wind speed increment runs R_k20_270 and C_k20_270	SWAN	4051A
	Numerical efficiency SWAN	
DELTARES & ALKYON	H5107.46/A2114	Fig. 9.7

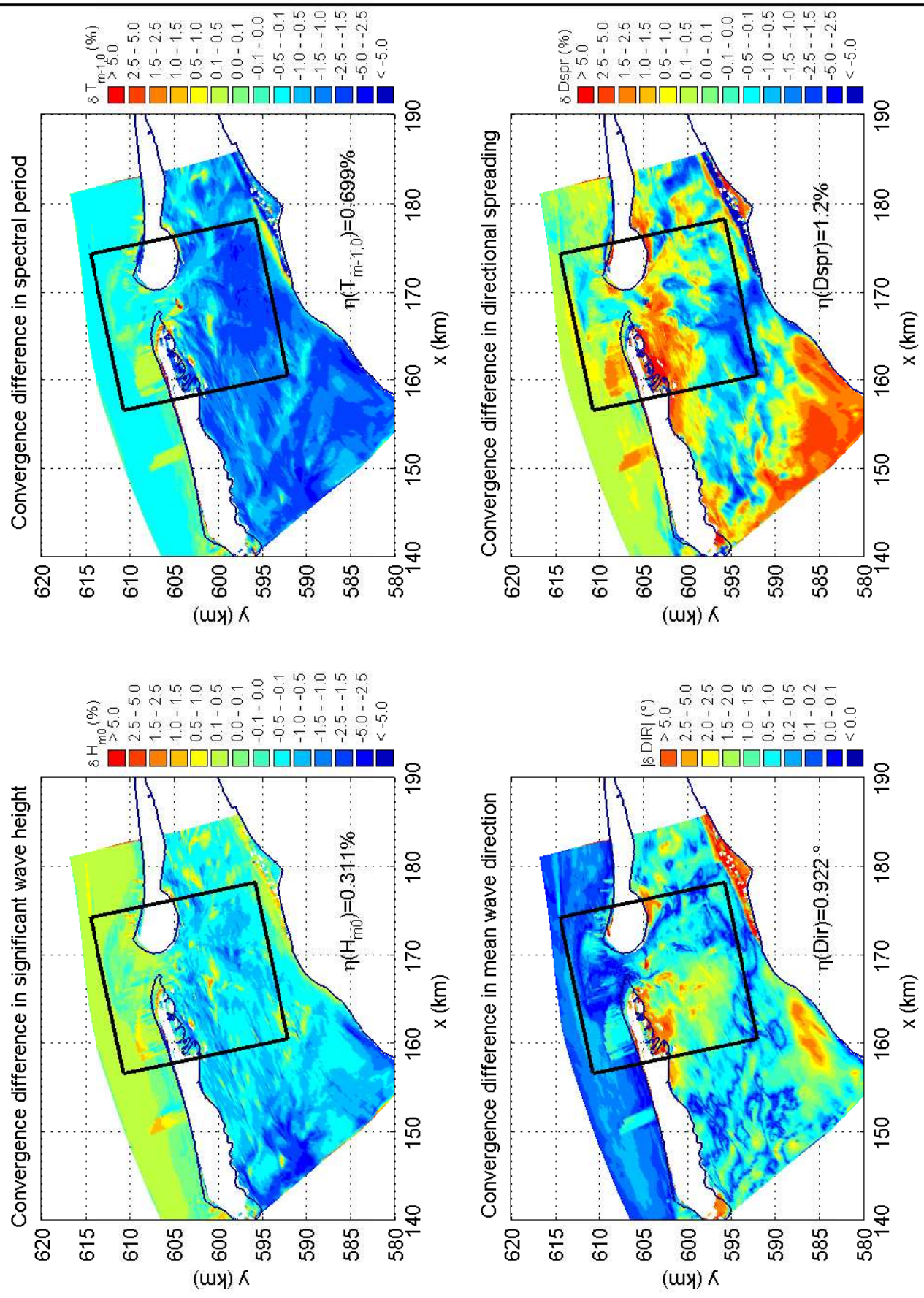

Convergence difference of batch file simulation with hotfile for the Amelander Zeegat, case AZG3A 20050102 1200 Wind speed increment runs R_k25_270 and C_k25_270	SWAN	4051A
	Numerical efficiency SWAN	
DELTARES & ALKYON	H5107.46/A2114	Fig. 9.8

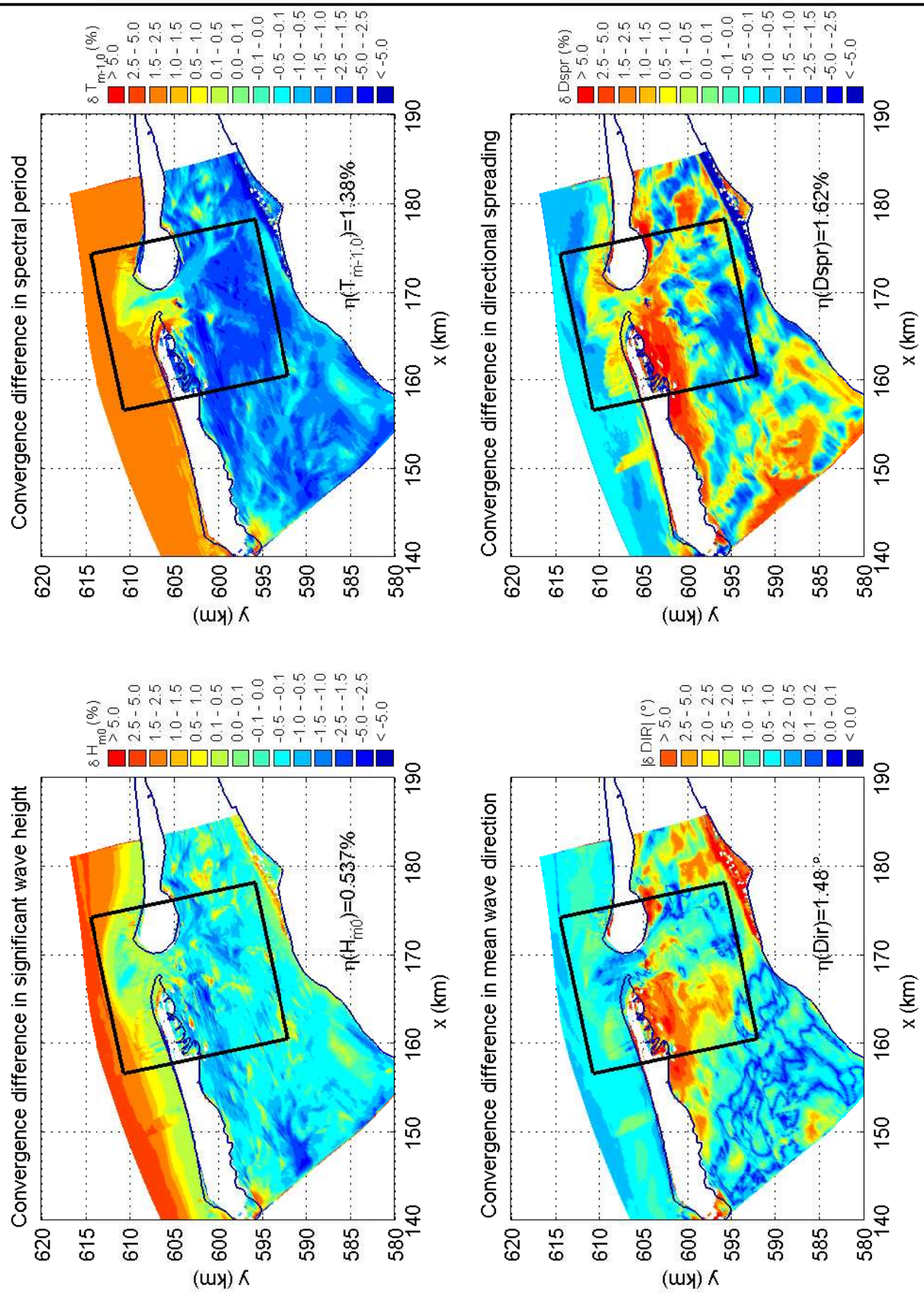

Convergence difference of batch file simulation with hotfile for the Amelander Zeegat, case AZG3A 20050102 1200 Wind speed increment runs R_k30_270 and C_k30_270	SWAN	4051A
	Numerical efficiency SWAN	
DELTARES & ALKYON	H5107.46/A2114	Fig. 9.9

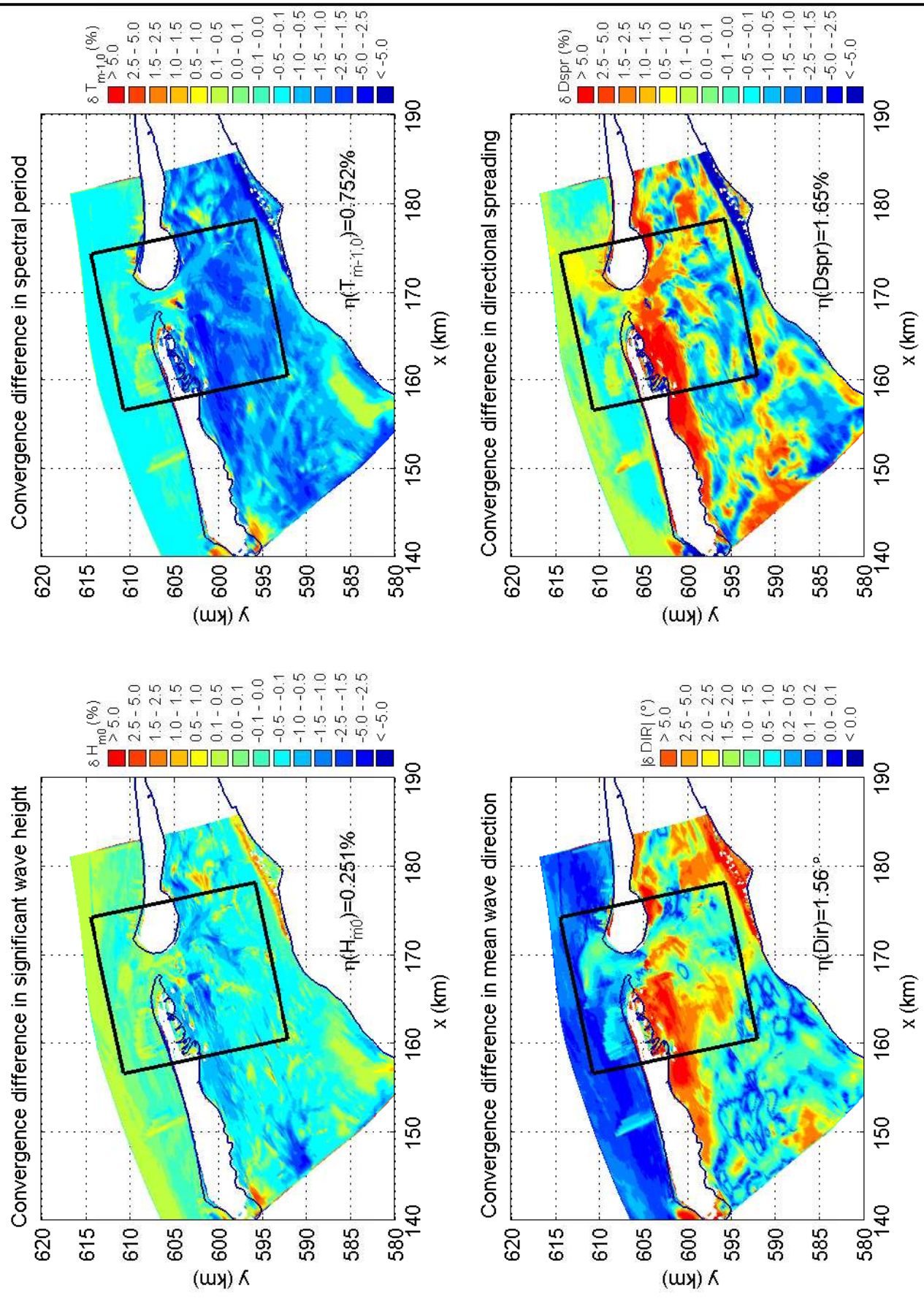

Convergence difference of batch file simulation with hotfile for the Amelander Zeegat, case AZG3A 20050102 1200 Wind speed increment runs R_k35_270 and C_k35_270	SWAN	4051A
	Numerical efficiency SWAN	
DELTARES & ALKYON	H5107.46/A2114	Fig. 9.10

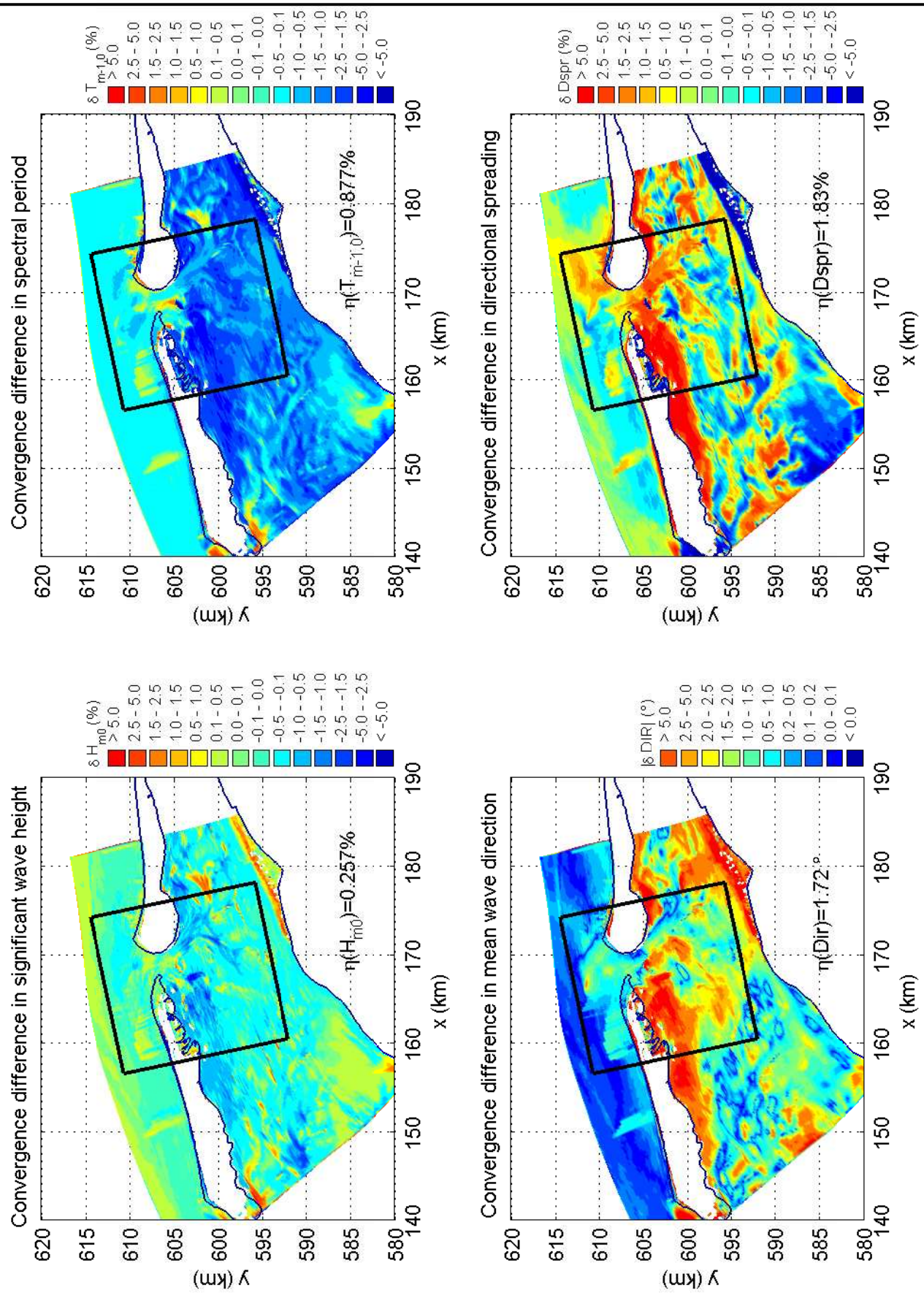

Convergence difference of batch file simulation with hotfile for the Amelander Zeegat, case AZG3A 20050102 1200 Wind speed increment runs R_k40_270 and C_k40_270	SWAN	4051A
	Numerical efficiency SWAN	
DELTARES & ALKYON	H5107.46/A2114	Fig. 9.11

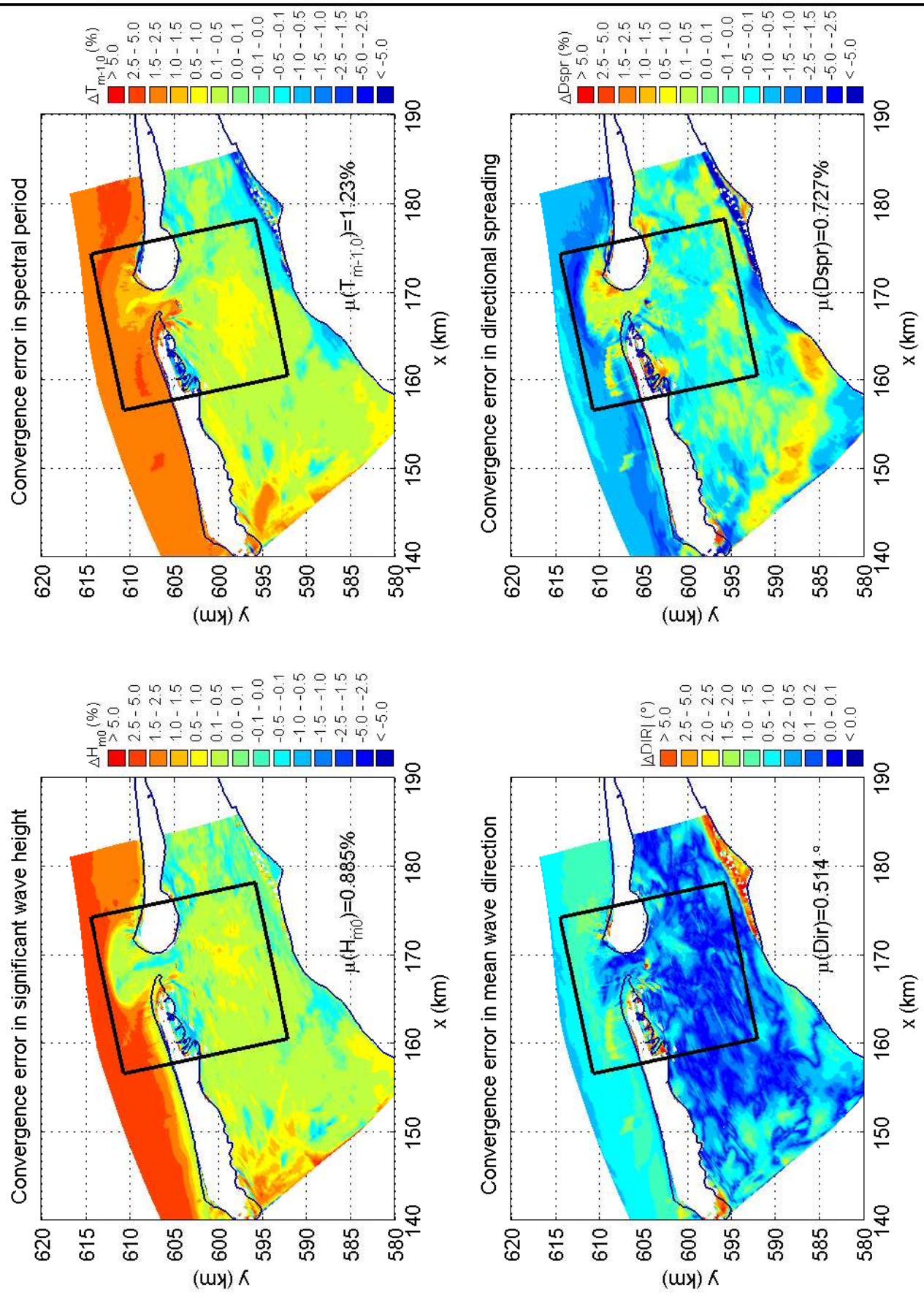

Convergence error of batch file simulation with hotfile for the Amelander Zeegat, case AZG3A 20050102 1200 Wind speed increment runs R_k20_270 and B_k20_270	SWAN	4051A
	Numerical efficiency SWAN	
DELTARES & ALKYON	H5107.46/A2114	Fig. 9.12

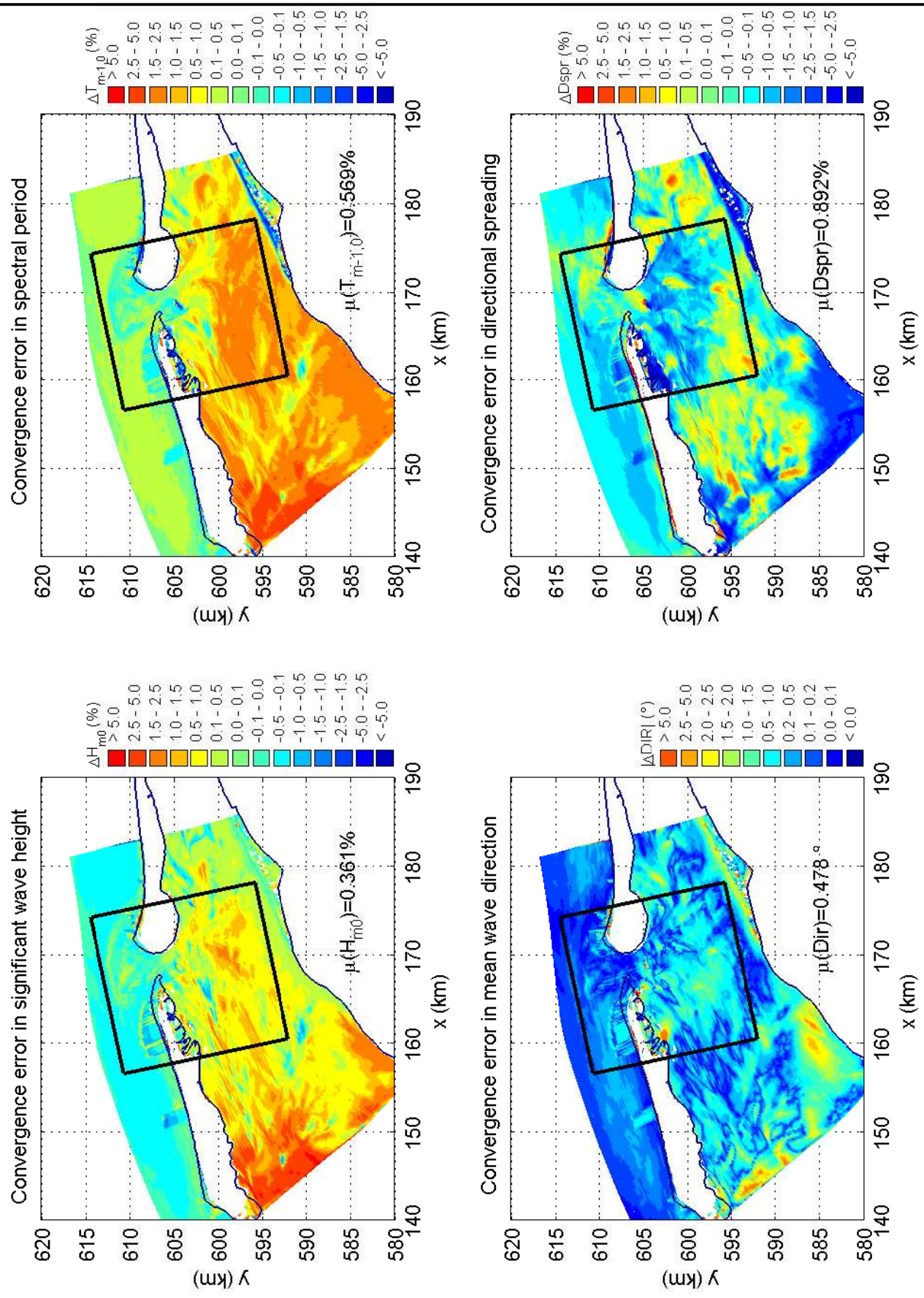

Convergence error of batch file simulation with hotfile for the Amelander Zeegat, case AZG3A 20050102 1200 Wind speed increment runs C_k20_270 and B_k20_270	SWAN	4051A
	Numerical efficiency SWAN	
DELTARES & ALKYON	H5107.46/A2114	Fig. 9.13

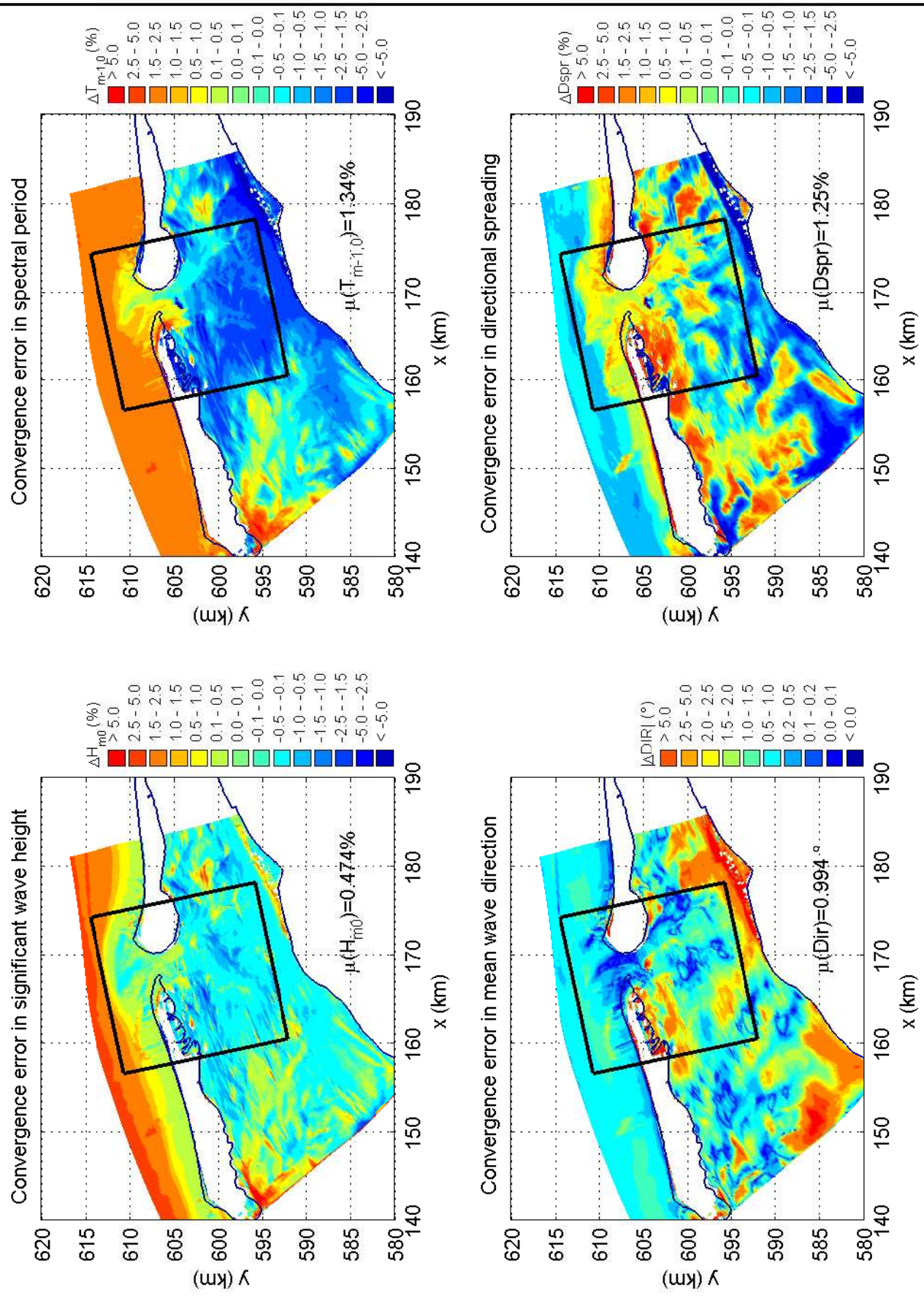

Convergence error of batch file simulation with hotfile for the Amelander Zeegat, case AZG3A 20050102 1200 Wind speed increment runs R_k30_270 and B_k30_270	SWAN	4051A
	Numerical efficiency SWAN	
DELTARES & ALKYON	H5107.46/A2114	Fig. 9.14

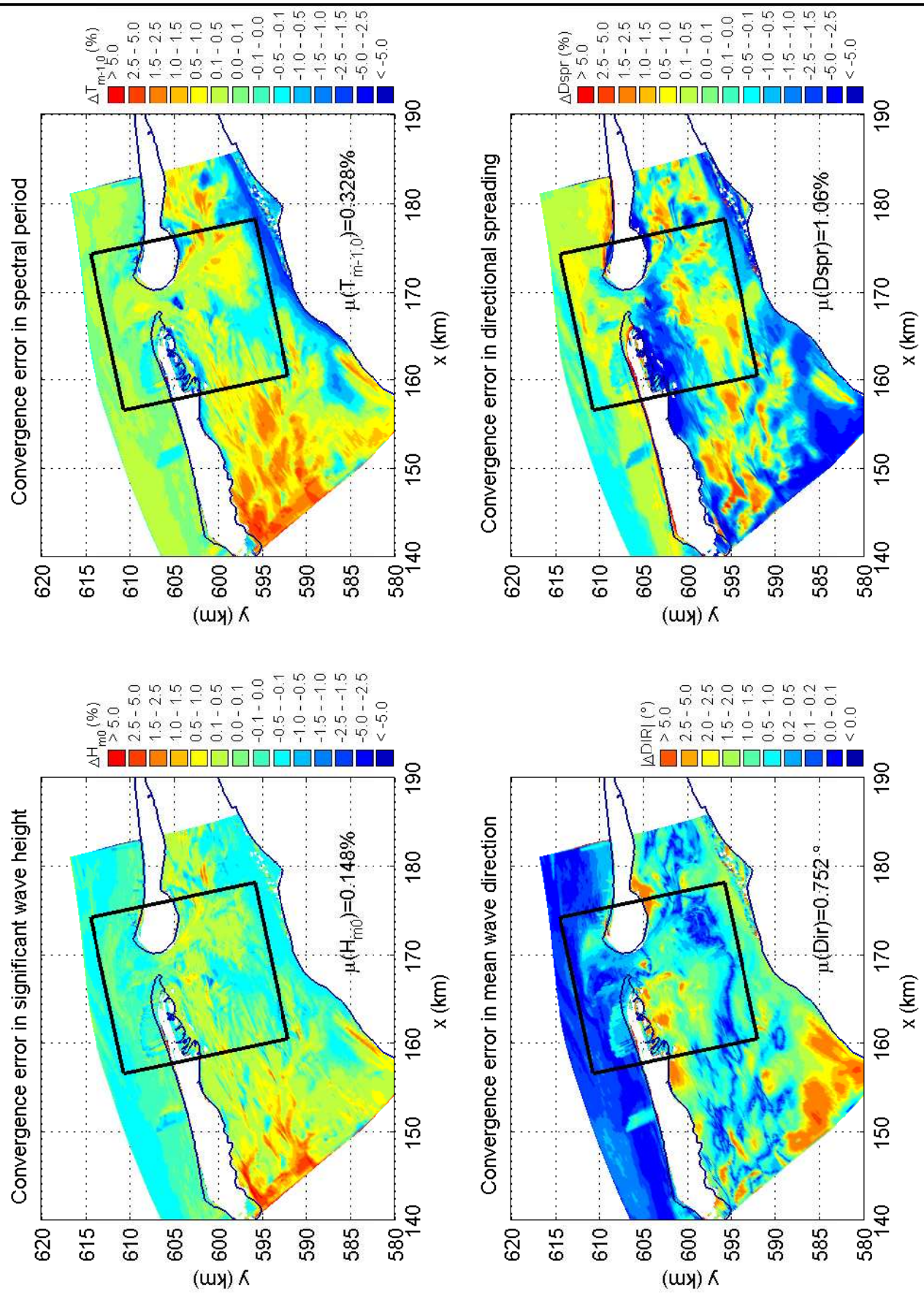

Convergence error of batch file simulation with hotfile for the Amelander Zeegat, case AZG3A 20050102 1200 Wind speed increment runs C_k30_270 and B_k30_270	SWAN	4051A
	Numerical efficiency SWAN	
DELTARES & ALKYON	H5107.46/A2114	Fig. 9.15

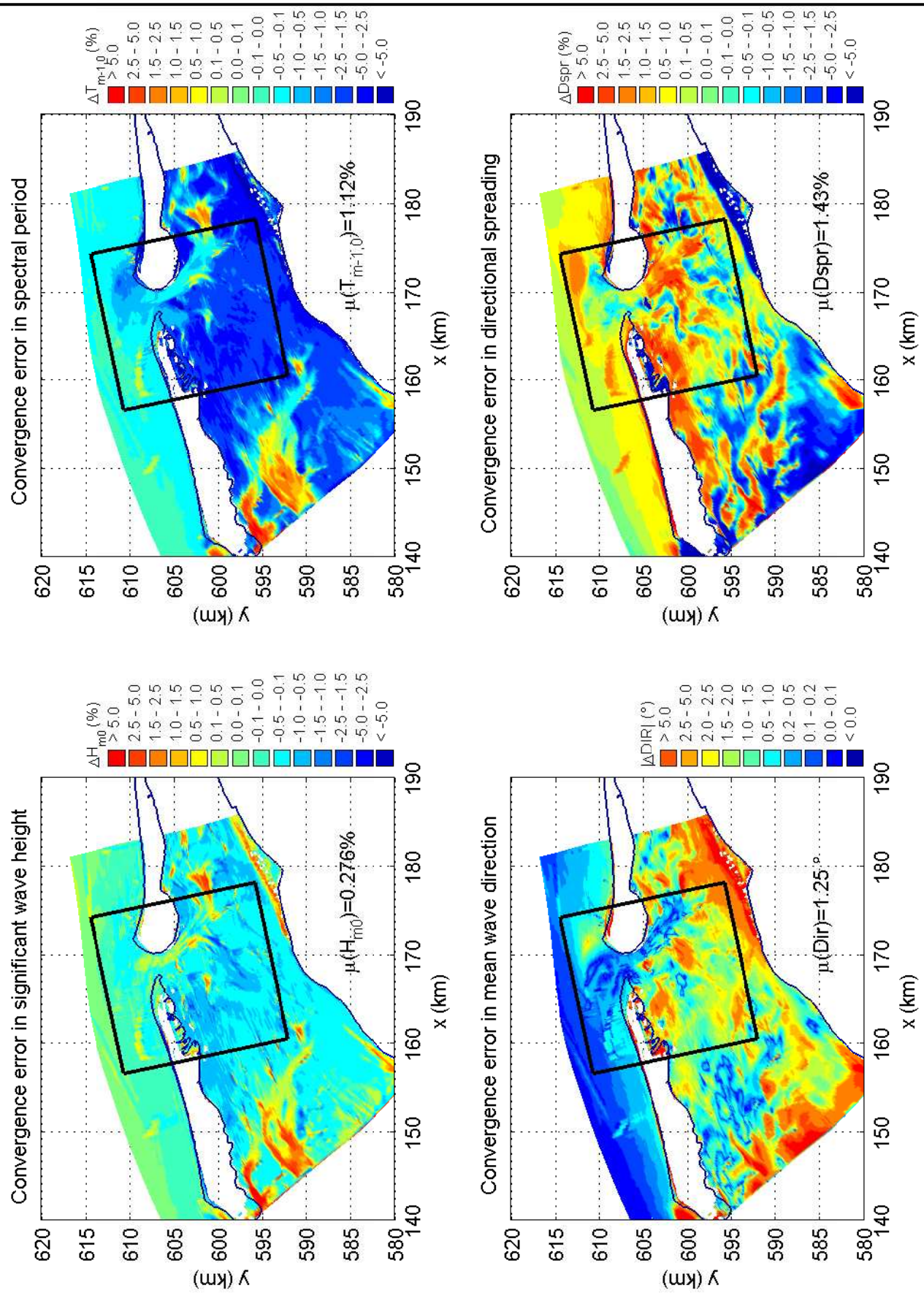

Convergence error of batch file simulation with hotfile for the Amelander Zeegat, case AZG3A 20050102 1200 Wind speed increment runs R_k40_270 and B_k40_270	SWAN	4051A
	Numerical efficiency SWAN	
DELTARES & ALKYON	H5107.46/A2114	Fig. 9.16

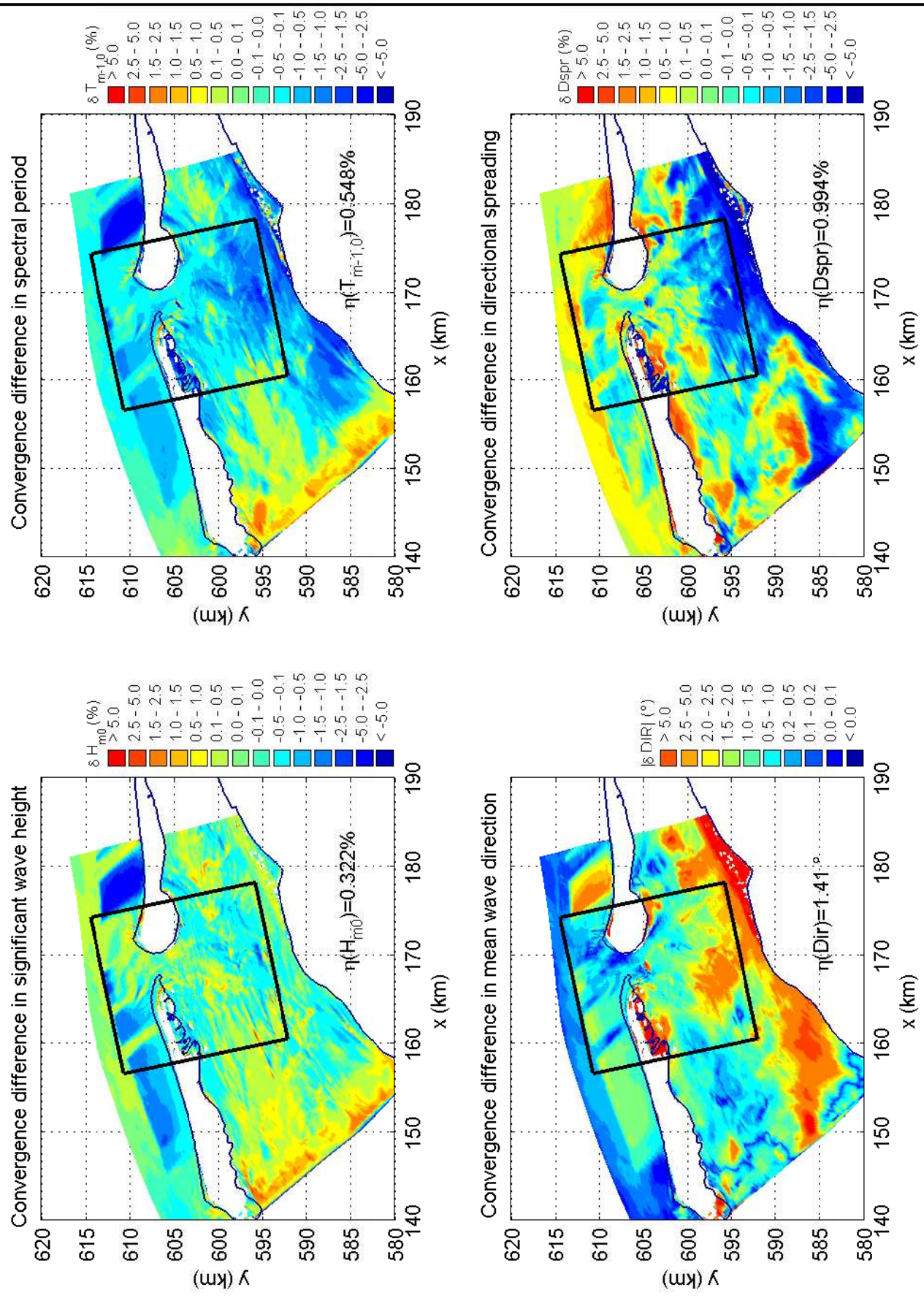

Convergence difference of batch file simulation with hotfile for the Amelander Zeegat, case AZG3A 20050102 1200 Wind direction increment runs R_25d247 and C_25d247	SWAN	4051A
	Numerical efficiency SWAN	
DELTARES & ALKYON	H5107.46/A2114	Fig. 9.17

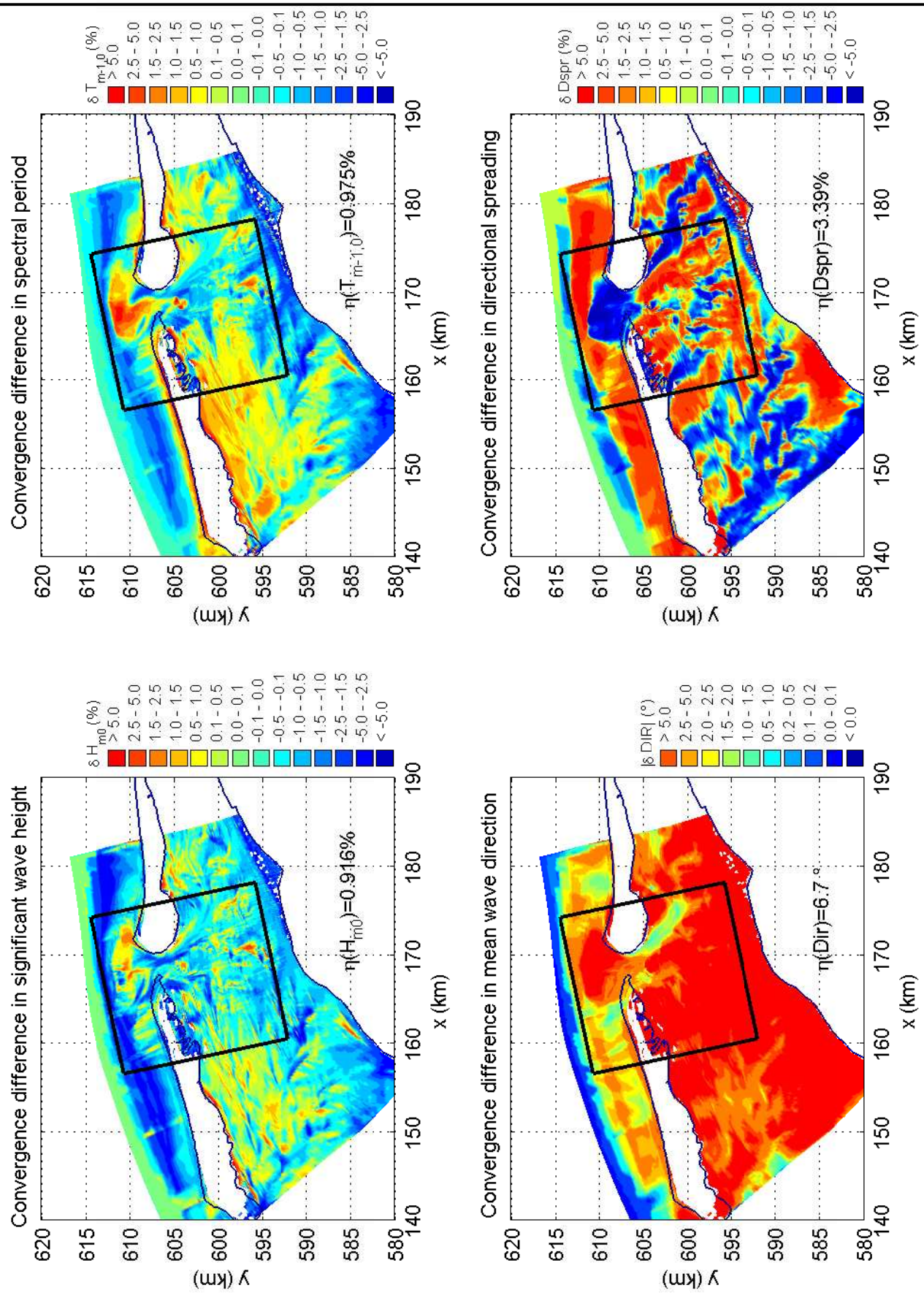

Convergence difference of batch file simulation with hotfile for the Amelander Zeegat, case AZG3A 20050102 1200 Wind direction increment runs R_25d315 and C_25d315	SWAN	4051A
	Numerical efficiency SWAN	
DELTARES & ALKYON	H5107.46/A2114	Fig. 9.18

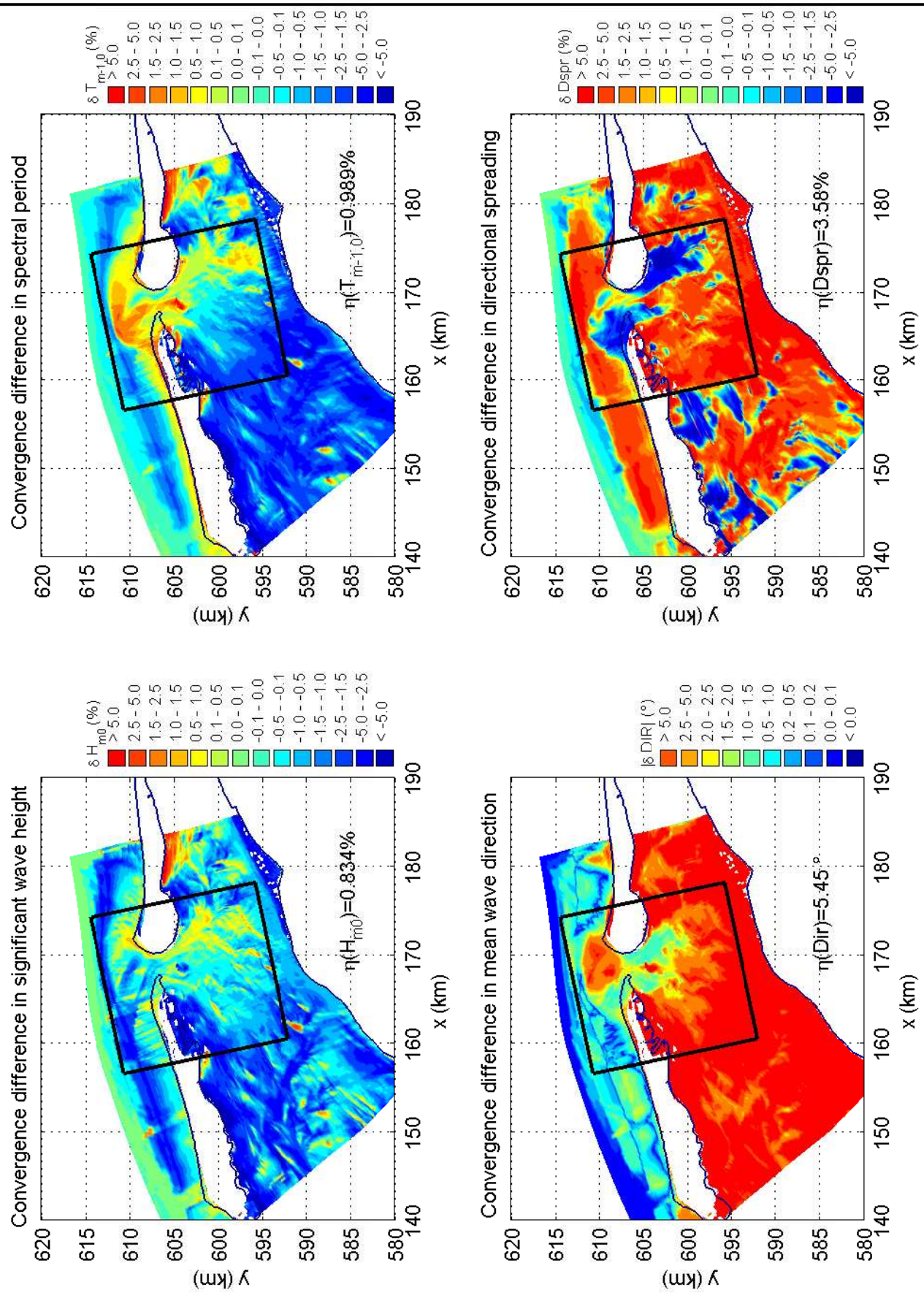

Convergence difference of batch file simulation with hotfile for the Amelander Zeegat, case AZG3A 20050102 1200 Wind direction increment runs R_25d000 and C_25d000	SWAN	4051A
	Numerical efficiency SWAN	
DELTARES & ALKYON	H5107.46/A2114	Fig. 9.19

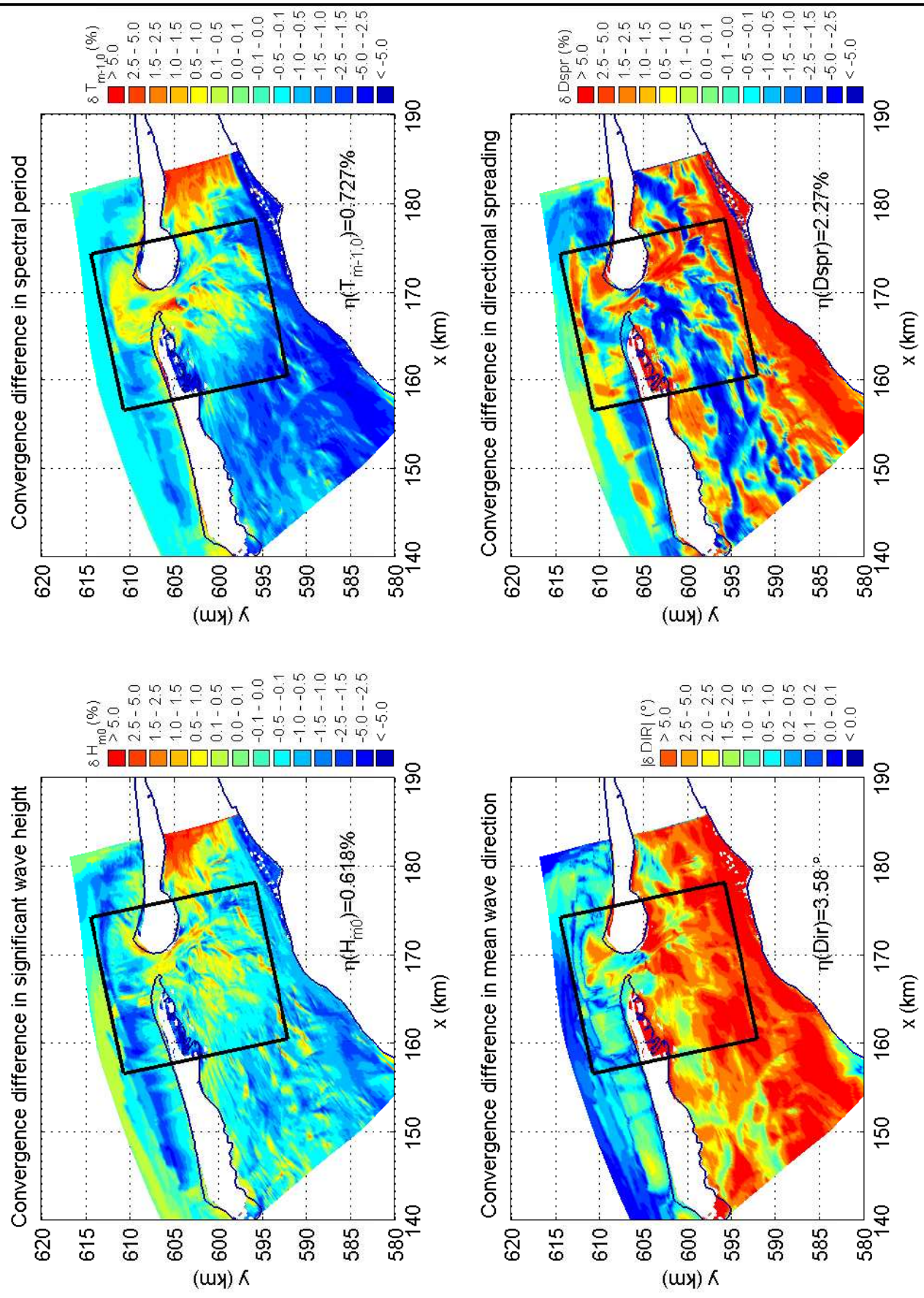

Convergence difference of batch file simulation with hotfile for the Amelander Zeegat, case AZG3A 20050102 1200 Wind direction increment runs R_25d045 and C_25d045	SWAN	4051A
	Numerical efficiency SWAN	
DELTARES & ALKYON	H5107.46/A2114	Fig. 9.20

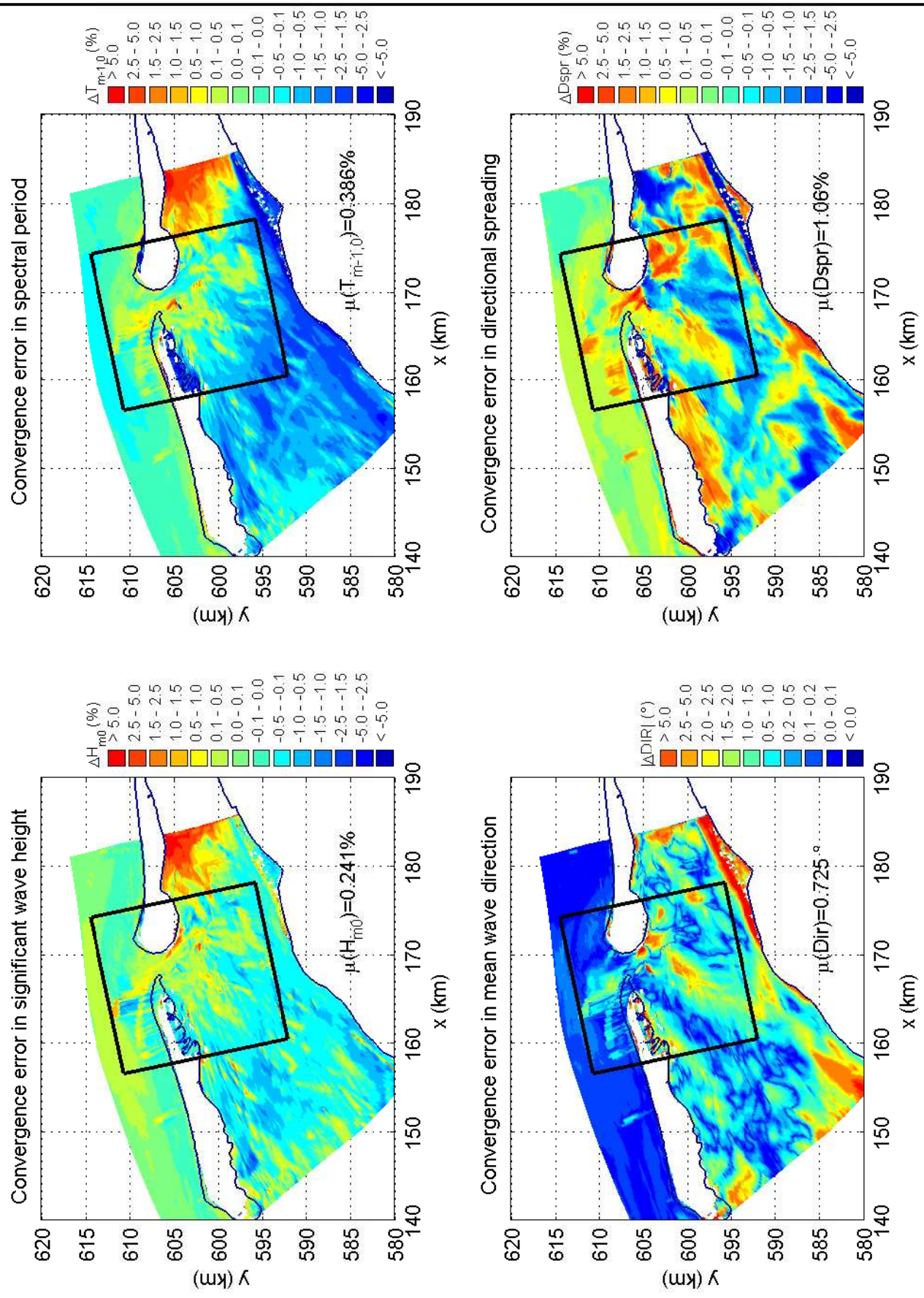

Convergence error of batch file simulation with hotfile for the Amelander Zeegat, case AZG3A 20050102 1200 Wind direction increment runs R_25d045 and B_25d045	SWAN	4051A
	Numerical efficiency SWAN	
DELTARES & ALKYON	H5107.46/A2114	Fig. 9.21

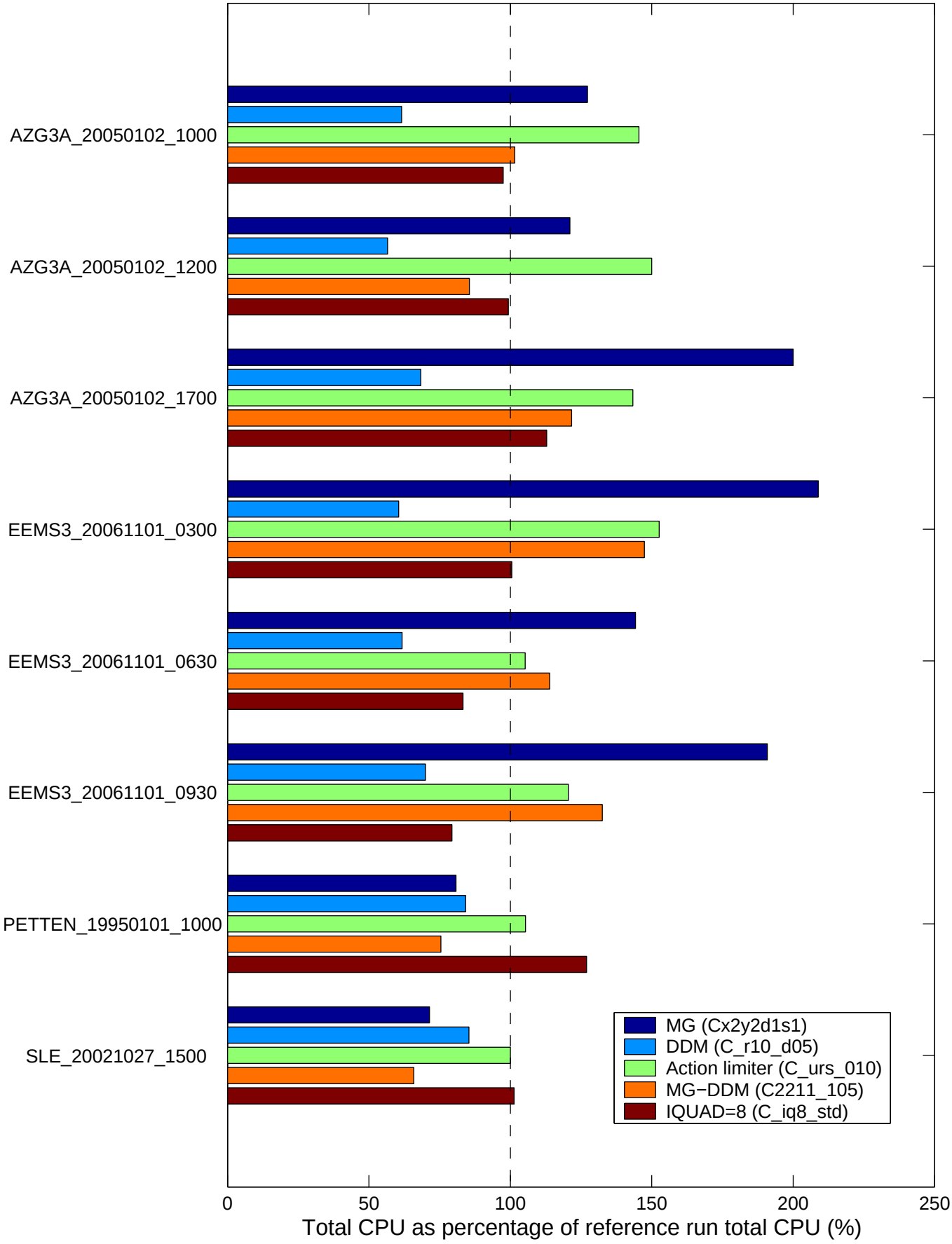

Comparison of total run times of selected numerical methods		SWAN 40.51A
		Numerical efficiency SWAN
DELTARES & ALKYON	H5107.46/A2114	Fig. 10.1

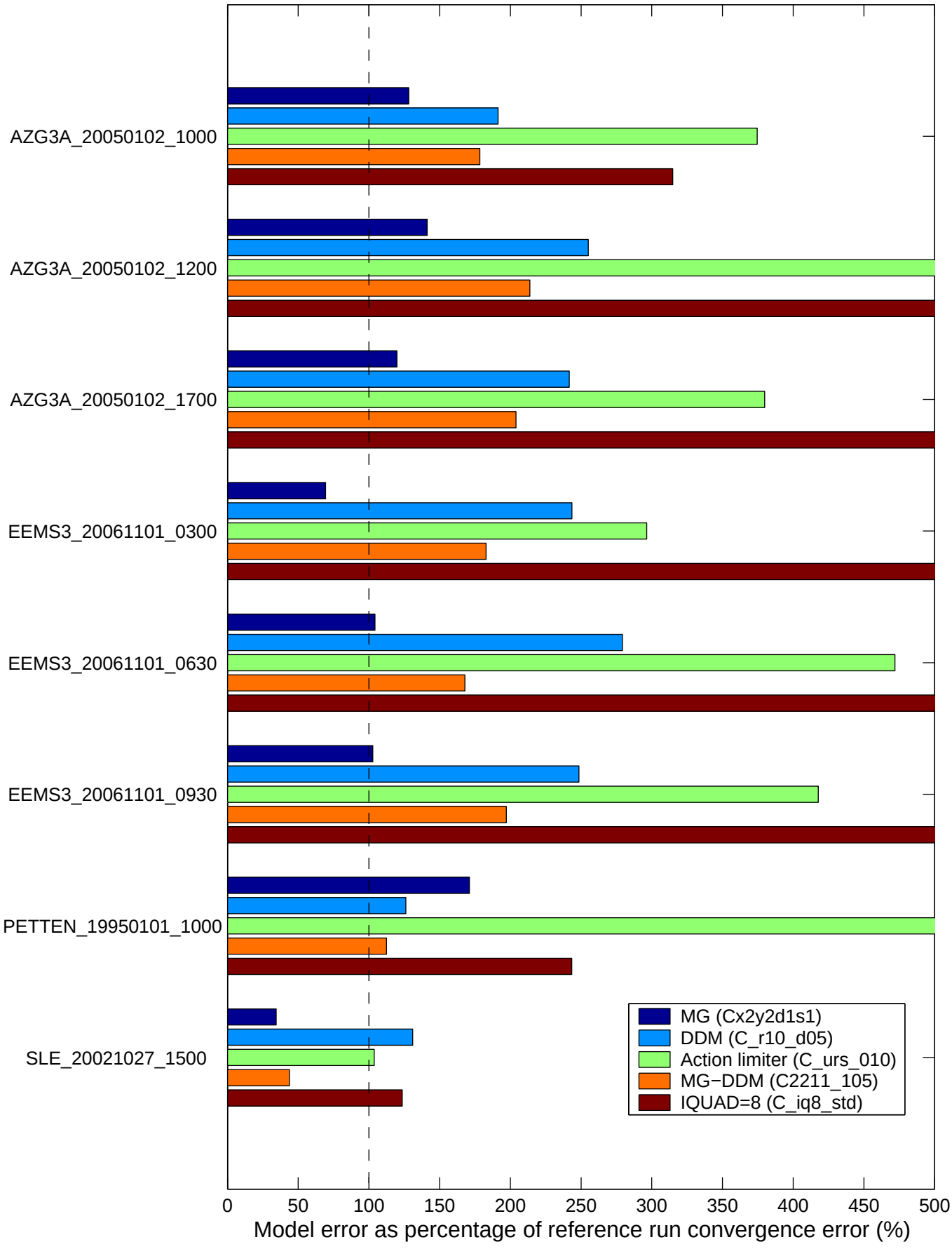

Comparison of model error as percentage of reference run convergence error Mean of all four computed wave parameters		SWAN 40.51A
		Numerical efficiency SWAN
DELTARES & ALKYON	H5107.46/A2114	Fig. 10.2